DESIGN OF SMART POWER GRID RENEWABLE ENERGY SYSTEMS

ALI KEYHANI

A JOHN WILEY & SONS, INC., PUBLICATION

DESIGN OF SMART POWER GRID RENEWABLE ENERGY SYSTEMS

DESIGN OF SMART POWER GRID RENEWABLE ENERGY SYSTEMS

ALI KEYHANI

A JOHN WILEY & SONS, INC., PUBLICATION

Published by John Wiley & Sons, Inc., Hoboken, New Jersey
Published simultaneously in Canada

Library of Congress Cataloging-in-Publication Data is available.

ISBN 978-0470-62761-7

Printed in Singapore

oBook ISBN: 978-1-118-00583-5
ePDF ISBN: 978-1-118-00581-1
ePub ISBN: 978-1-118-00582-8

10 9 8 7 6 5 4 3 2 1

I dedicate this book to my father,
Dr. Mohammed Hossein Keyhani

CONTENTS

FOREWORD

It is an honor for me to add my comments to a very important book by Professor Ali Keyhani, *Design of Smart Grid Renewable Energy Systems*.

The restructuring of the electric power industry was a critical step for individual stakeholders, facilitating their wide participation in the production, delivery, and utilization of energy. The "smart grid" has further offered alternatives to participants looking to enhance the reliability, sustainability, and capability for customer choices in energy systems. The smart grid has made it possible to set up microgrids that could be operated as stand-alone islands in critical operating conditions. Such small installations can enhance the reliability of regional electric power systems when the larger grid is faced with major contingencies. There are several practical examples of microgid installations which have demonstrated that the use of smart switches in distributed power grids could reduce the number and the duration of outages.

In addition, the smart grid allows microgrids to optimize the use of volatile and intermittent renewable energy resources and enhance the sustainability of regional power systems. The applications of solar photovoltaics, which mostly follow the daily load profile for power generation, on-site or local wind energy, along with storage devices for microgrid installations could provide an inexpensive and sustainable means of supplying microgrid loads. The principles of widespread utilization of energy storage can also be found in the emerging market of plug-in electric vehicles, which would utilize wind energy at off-peak hours. Such microgid applications could also eliminate the need for extensive additions of high voltage lines for the transmission of renewable energy across densely populated regions of the world.

However, the evolutions in the electric power industry that I believe will truly revolutionize the way we deliver electricity to individual consumers are

smart grid applications related to real-time pricing, hourly demand response, and the expansion of customer choices for promoting energy efficiency. The use of new smart grid innovations would make it possible for consumers to prioritize their energy use according to their daily schedules, needs, and preferences, taking into account a variable cost of electricity to save money. Smart grid advancements would also enable automated control systems to optimize energy use at home or for businesses, identifying the most appropriate times for device operation to reduce the cost of electricity.

Customer participation will offer a number of incentives for the optimization of electric power operations, including lower operation costs by eliminating the commitment of costly generating units at peak hours, mitigating mandatory system upgrades that are required for responding to a few hundred hours of annual peak loads, and reducing the chance of transmission congestion, which could otherwise operate the power system at a state close to its critical point of collapse. Demand response could also offer a less fluctuating daily profile, which would make it possible to forecast the daily load profile and schedule fuel and hydro consumption more comprehensively and efficiently for power generation.

I believe the content of this book will expose readers to subjects that could potentially alter the paradigm for energy generation, delivery, and utilization in the foreseeable future. I would like to congratulate Professor Keyhani for his keen interest in electric power system innovations and thank him for his efforts on introducing such topics to all of us.

Mohammad Shahidehpour

Bodine Chair Professor and Director
Center for Electricity Innovation
Illinois Institute of Technology
Chicago, Illinois, USA
January 2011

PREFACE

Sustainable energy production and the efficient utilization of available energy resources, thereby reducing or eliminating our carbon footprint, is one of our greatest challenges in the 21st century. This is a particularly perplexing problem for those of us in the discipline of electrical engineering. This book addresses the problem of sustainable energy production as part of the design of microgrid and smart power grid renewable energy systems.

Today the Internet offers vast resources for engineering students; it is our job as teachers to provide a well-defined learning path for utilizing these resources. We should also challenge our students with problems that attract their imagination. This book addresses this task by providing a systems approach to the global application of the presented concepts in sustainable green energy production, as well as analytical tools to aid in the practical design of renewable microgrids. In each chapter, I present a key engineering problem, then formulate a mathematical model of the problem followed by a simulation testbed in MATLAB, highlighting solution steps. A number of solved examples are presented, while problems designed to challenge the student are given at the end of each chapter. Related references are also provided at the end of each chapter.

The book provides an Instructor's *Solution Manual* and PowerPoint lecture notes with animation that can be adapted and changed as instructors deem necessary for their presentation styles. Solutions to the homework problems presented at the end of each chapter are also included in the *Solution Manual*.

The concepts presented in this book integrate three areas of electrical engineering: power systems, power electronics, and electric energy conversion systems. The book also addresses the fundamental design of wind and

photovoltaic (PV) energy microgrids as part of smart bulk power-grid systems. A prerequisite for the book is a basic understanding of electric circuits. The book builds its foundation by introducing phasor systems, three-phase systems, transformers, loads, DC/DC converters, DC/AC inverters, and AC/DC rectifiers, which are all integrated into the design of microgrids for renewable energy as part of bulk interconnected power grids.

In the first chapter, in addition to a historical perspective of energy use, an analysis of fossil fuel use is provided through a series of calculations of our carbon footprint in relation to an entire country's fossil fuel consumption or that of a single household appliance. In Chapter 2, we review the basic principles underlying power systems, single-phase loads, three-phase loads, single- and three-phase transformers, distribution systems, transmission lines, and power system modeling. The generalized per unit system of power system analysis is also introduced. In Chapter 3, the topics include AC/DC rectifiers, DC/AC inverters, DC/DC converters, and pulse width modulation (PWM) methods. The focus is on the utilization of inverters as a three-terminal element of power systems for the integration of wind and PV energy sources; MATLAB simulations of PWM inverters are also provided. In Chapter 4, the fundamental concepts in the design and operation of smart grid power grids are described. The chapter introduces the smart grid elements and their functions from a systems approach, and provides an overview of the complexity of smart power grid operations. Topics covered in the chapter include the basic system concepts of sensing, measurement, integrated communications, and smart meters; real-time pricing; cyber-control of smart grids; high green energy penetration into the bulk interconnected power grids; intermittent generation sources; and the electricity market. We are also introduced to the basic modeling and operation of synchronous generator operations, the limit of power flow on transmission lines, power flow problems, load factor calculations and their impact on the operation of smart grids, real-time pricing, and microgrids. These concepts set the stage for the integration of renewable energy in electric power systems. In Chapter 5, we study PV energy sources. We learn how to compute the energy yield of photovoltaic modules and the angle of inclination for modules with respect to their position to the sun for maximum energy yields. The chapter also presents the modeling of PV modules, the microgrid design of PV power plants, and the maximum power point tracking of PV systems. Chapter 6 introduces wind power generation by describing the modeling of induction generators as part of a microgrid of renewable energy systems. In this chapter, we also study the utilization of doubly-fed induction generators, variable speed permanent magnet generators, brushless generators, and variable-speed wind power conversion from a system's perspective. In Chapter 7, the modeling bus admittance and bus impedance for power grids are presented, as well as a power flow analysis of microgrids as part of interconnected bulk power systems. In Chapter 8, we study the Newton formulation of power flow, the Newton-Raphson solution of a power flow problem, and the fast decoupled solution for power flow studies.

This book provides the fundamental concepts of power grid and microgrid integration using green energy sources, which is a goal of virtually all nations. The design of microgrids is key to the modernization of our infrastructure using green energy sources, power electronics, control and sensor technology, computer technology, and communication systems.

Ali Keyhani

January 2011
Sanibel Island, Florida

ACKNOWLEDGMENTS

For the past 10 years, my research has been supported by the National Science Foundation; this book reflects the work supported by NSF grants.[1] Over the years, many graduate and undergraduate students have also contributed to the material presented in this book, in particular, Abir Chatterjee, a doctoral student, and Adel El Shahat Lotfy Ahmed, Department of Electrical Power and Machines Engineering, Faculty of Engineering, Zagazig University, Egypt.

I thank my wife Maureen Keyhani for her understanding and support.

I would also like to thank Simone Taylor, Director, Editorial Development, and Michael Christian, Editorial Coordinator, at John Wiley & Sons, and Kate McKay of STM Publishing Services.

[1]Some material in this book is based upon work supported by National Science Foundation awards ECCS 0501349, ECCS 0105320 and ECCS 0118080. Any opinion, findings, and conclusions or recommendations expressed in this material are those of the author and do not necessarily reflect the views of the National Science Foundation.

CHAPTER 1

ENERGY AND CIVILIZATION

1.1 INTRODUCTION

Energy technology plays a central role in societal economic and social development. Fossil fuel-based technologies have advanced our quality of life, but at the same time, these advancements have come at a very high price. Fossil fuel sources of energy are the primary cause of environmental pollution and degradation; they have irreversibly destroyed aspects of our environment. Global warming is a result of our fossil fuel consumption. For example, the fish in our lakes and rivers are contaminated with mercury, a byproduct of rapid industrialization. The processing and use of fossil fuels has escalated public health costs: Our health care dollars have been and are being spent to treat environmental pollution-related health problems, such as black lung disease in coal miners. Our relentless search for and need to control these valuable resources have promoted political strife. We are now dependent on an energy source that is unsustainable as our energy needs grow and we deplete our limited resources. As petroleum supplies dwindle, it will become increasingly urgent to find energy alternatives that are sustainable as well as safe for the environment and humanity.

1.2 FOSSIL FUEL

It is estimated that fossil fuels—oil, natural gas, and coal—were produced 300 to 370 million years ago.[1] Over millions of years, the decomposition of the flora

Design of Smart Power Grid Renewable Energy Systems, First Edition. Ali Keyhani.

and fauna remains that lived in the world's oceans produced the first oil. As the oceans receded, these remains were covered by layers of sand and earth, and were subjected to severe climate changes: the Ice Age, volcanic eruption, and drought burying them even deeper in the earth's crust and closer to the earth's core. From such intense heat and pressure, the remains essentially were boiled into oil. If you check the word, "petroleum" in a dictionary, you will find it means "rock oil" or "oil from the earth."

The ancient Sumerians, Assyrians, Persians, and Babylonians found oil on the banks of the Karun and Euphrates Rivers as it seeped above ground. Historically, humans have used oil for many purposes. The ancient Persians and Egyptians used liquid oil as a medicine for wounds. The Zoroastrians of Iran made their fire temples on top of percolating oil from the ground.[1] Native Americans used oil to seal their canoes.[1]

In fact, although our formally recorded history of humanity's energy use is limited, we can project the impact of energy on early civilizations from artifacts and monuments. The legacy of our oldest societies and their use of wood, wood charcoal, wind, and water power can be seen in the pyramids of Egypt, the Parthenon in Greece, the Persepolis in Iran, the Great Wall of China, and the Taj Mahal in India.[2]

1.3 DEPLETION OF ENERGY RESOURCES

Figure 1.1 depicts the time needed to develop various energy sources. Coal, oil, and natural gas take millions of years to form. The oil that was made more

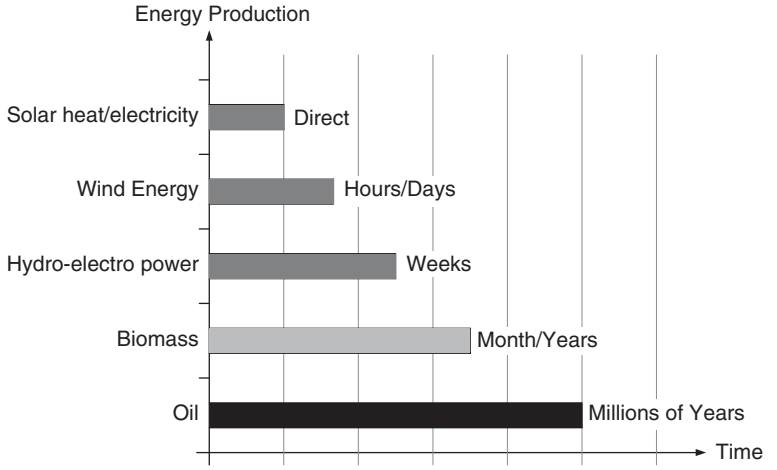

Figure 1.1 The Approximate Time Required for the Production of Various Energy Sources.

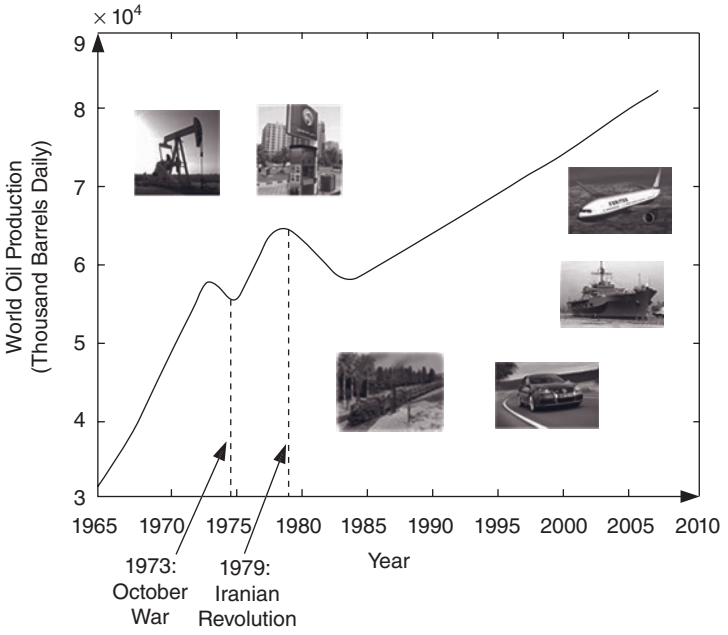

Figure 1.2 The World's Oil Production (Consumption) from 1965–2000 and Estimated from 2005–2009.[3]

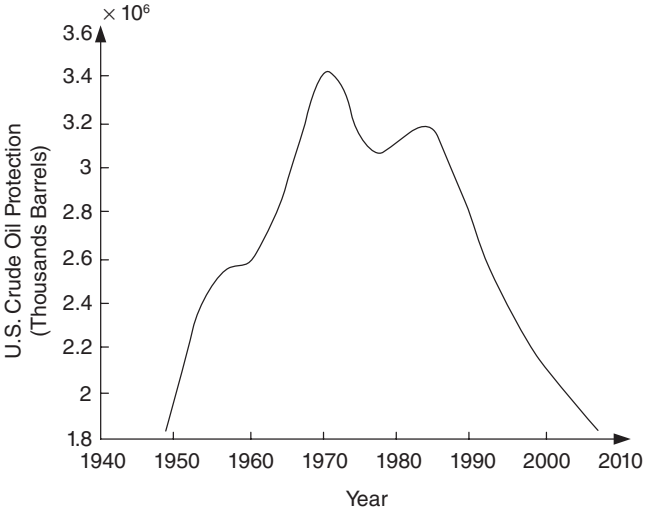

Figure 1.3 U.S. Oil Production/Consumption from 1940–2009.[3]

than a million years ago is being used today.[1] As we look at our energy use over the ages, it becomes clear that our new energy resources are substituting for old resources. Our first energy source was wood. Then coal replaced wood, and oil began to replace some of our coal usage to the point that oil now supplies most of our energy needs.

Since the Industrial Revolution, we have used coal. Since 1800, for approximately 200 years, we have used oil. However, our first energy source was wood and wood charcoal, which we used to cook food. Recorded history shows that humanity has been using wood energy for 5000 of the 100,000 years living on earth. Similarly, we have been using oil for 200 years of the 5000 years of recorded history. In the near future, we will exhaust our oil reserves. Oil is not renewable: we must conserve energy and save our oil—and gas as well.

The Middle East provides more than 50% of the oil imported to the United States. The United States' own oil production peaked around 1970. Europe's oil production is limited except for the North Sea oil reserve; it depends entirely on oil production from other parts of world. In Asia, China, India, Japan, and Korea depend on imported oil. The rapid economic expansion of China, India, and Brazil are also rapidly depleting the world oil reserves.

A closer look at Table 1.1 reveals that if the world reserves are used at the same rate as we do today, oil will run out in 40 years, our natural gas reserves will be depleted in less than 60 years, and our coal reserves will be exhausted in 200 years. No one can predict the future. However, we can empower every

TABLE 1.1 Proven Energy Resources around the World.[3,4]

	Petroleum		Natural Gas		Coal	
Region	2002 Preserved Resources (10^9 bbls)	R/P (Years)	2002 Proved Reserves (10^{12} SCF)	R/P (years)	2002 Preserved Reserves (10^9 tons)	R/P (years)
North America	49.9	10.3	52.4	9.4	257.8	240
South & Central America	98.6	42	250.2	68.8	21.8	404
Europe & Eurasia	97.5	17	2155.8	58.9	355.4	306
Middle East	685.6	92	1979.7	>100	????	>500
Africa	77.4	27.3	418.1	88.9	55.3	247
Asia-Pacific	38.7	13.7	445.3	41.8	292.5	126
World	1047.7	40.6	5501.5	60.7	984.5	204

Note: R/P = Reserves-to-production; bbls = billion barrels; SCF = standard cubic foot. R/P ratios represent the length of time that the remaining reserves would last if production were to continue at the previous year's rate. R/P is calculated by dividing remaining reserves at the end of the year by the production in that year.[4] (Reprinted with permission from the BP Statistical Review of World Energy 2009.)

energy user in a new energy economy based on renewable sources to become an energy producer by conserving energy, reducing carbon footprints, and installing distributed renewable energy sources.

1.4 AN ALTERNATIVE ENERGY SOURCE: NUCLEAR ENERGY

In 1789, Martin Heinrich Klaproth,[5] a German chemist, discovered uranium in the mineral pitchblende. Eugène-Melchior Péligot,[6] a French chemist, was the first person to isolate the metal, but it was Antoine Becquerel,[7] a French physicist, who recognized its radioactive properties almost 100 years later. In 1934, Enrico Fermi[8] used the nuclear fuel to produce steam for the power industry. Later, he participated in building the first nuclear weapon used in World War II. The U.S. Department of Energy[9] estimates worldwide uranium resources are generally considered to be sufficient for at least several decades.

The amount of energy contained in a mass of hydrocarbon fuel such as gasoline is substantially lower in much less mass of nuclear fuel. This higher density of nuclear fission makes it an important source of energy; however, the fusion process causes additional radioactive waste products. The radioactive products will remain for a long time giving rise to a nuclear waste problem. The counterbalance to a low carbon footprint of fission as an energy source is the concern about radioactive nuclear waste accumulation and the potential for nuclear destruction in a politically unstable world.

1.5 GLOBAL WARMING

Figure 1.4 depicts the process of solar radiation incident energy and reflected energy from the earth's surface and the earth atmosphere. Greenhouse gases in the earth's atmosphere emit and absorb radiation. This radiation is within the thermal infrared range. Since the burning of fossil fuel and the start of the Industrial Revolution, the carbon dioxide in the atmosphere has substantially increased as shown in Figures 1.5 and 1.6. The greenhouse gasses are primarily water vapor, carbon dioxide, carbon monoxide, ozone, and a number of other gases. Within the atmosphere of earth, greenhouse gasses are trapped.

The solar radiation incident energy as depicted by circle 1 emitted from the sun and its energy is approximated as 343 W/m^2. Some of the solar radiation, depicted by circle 2 and circle 4, is reflected from the earth's surface and the earth's atmosphere. The total reflected solar radiation is approximated as 103 W per m^2. Approximately 240 W per m^2 of solar radiation, depicted by circle 3, penetrates through the earth's atmosphere. About half of the solar radiation (circle 5), approximately 168 W per m^2, is absorbed by the earth's surface. This radiation (circle 6) is converted into heat energy. This process generates infrared radiation in the form of the emission of a long wave back to earth. A portion of the infrared radiation is absorbed. Then, it is re-emitted

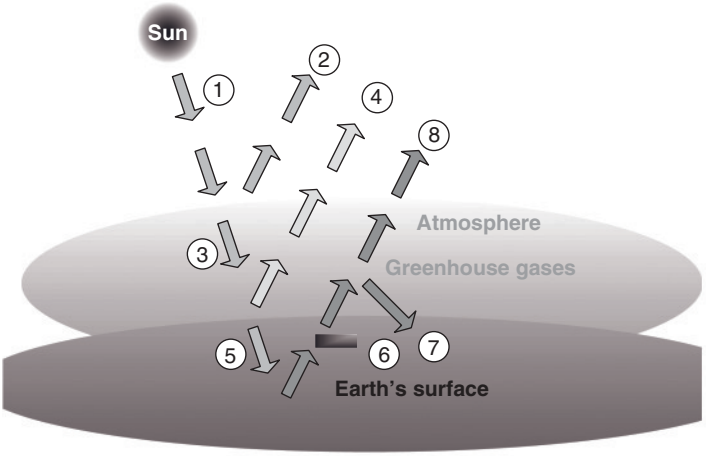

Figure 1.4 The Effects of Sun Radiation on the Surface of the Earth.

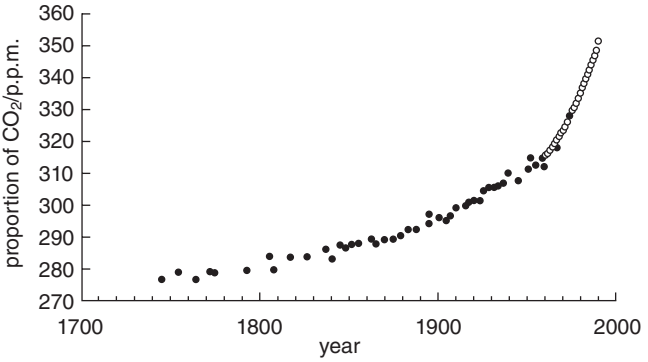

Figure 1.5 The Production of CO_2 since 1700. (Data from the Intergovernmental Panel on Climate Change, IPCC Third Annual Report.[11])

by the greenhouse molecules trapped in the earth's atmosphere. Circle 7 represents the infrared radiation. Finally, some of the infrared radiation (circle 8), passes through the atmosphere and into space. As the use of fossil fuel is accelerated, the carbon dioxide in the earth's atmosphere is also accelerated. The growth of carbon dioxide in our atmosphere is shown in parts per million in Figure 1.5.

The World Meteorological Organization (WMO)[10] is the international body for the monitoring of climate change. The WMO has clearly stated the potential environmental and socioeconomic consequences for the world economy if the current trend continues. In this respect, global warming is an engineering problem, not a moral crusade. Until we take serious steps to reduce our carbon footprints, pollution and the perilous deterioration of our environment will continue.

Figure 1.6 depicts the condition of CO_2 in the upper atmosphere. The Y axis represents the magnitude of response. The X axis is plotted showing the years into future. The Y axis, showing response efforts, does not have units. The CO_2 emission into the atmosphere has peaked during the last 100 years. If concentrated efforts are made to reduce the CO_2 emission and it is reduced over the next few hundred years to a lower level, the earth temperature will still continue to rise, however, then stabilize. Figure 1.7 depicts the stabilization of CO_2 over the subsequent centuries.

The reduction of CO_2 will reduce its impact on the earth atmosphere; nevertheless, the existing CO_2 in the atmosphere will continue to raise the earth's temperature by a few tenths of a degree. The earth's surface temperature will stabilize over a few centuries as shown in Fig. 1.8.

The rise in the temperature due to trapped CO_2 in the earth's atmosphere will impact the thermal expansion of oceans. Consequently, the sea level will rise due to melting of ice sheets as shown in Fig. 1.10.

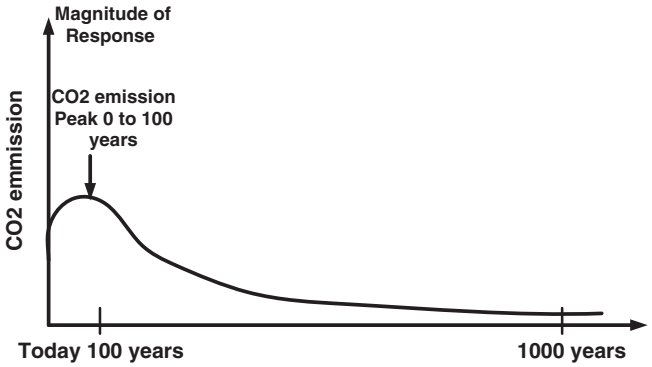

Figure 1.6 The Effect of Carbon Dioxide Concentration on Temperature and Sea Level. (Data from the Intergovernmental Panel on Climate Change, IPCC Third Annual Report.[11])

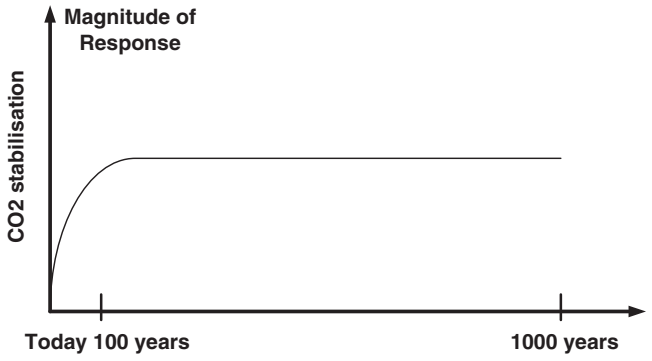

Figure 1.7 CO_2 Stabilization after CO_2 Has Been Reduced. (Data from the Intergovernmental Panel on Climate Change, IPCC Third Annual Report.[11])

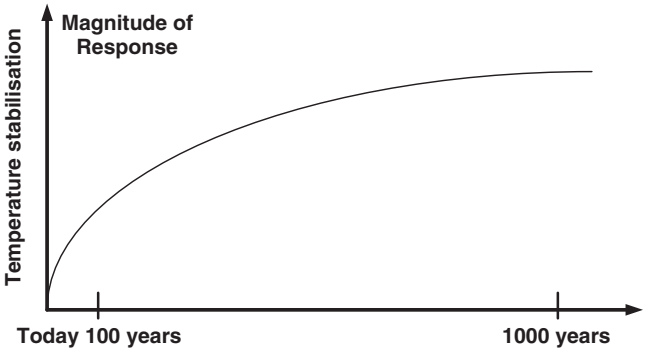

Figure 1.8 Temperature Stabilization after Reduction of CO_2 Emission.

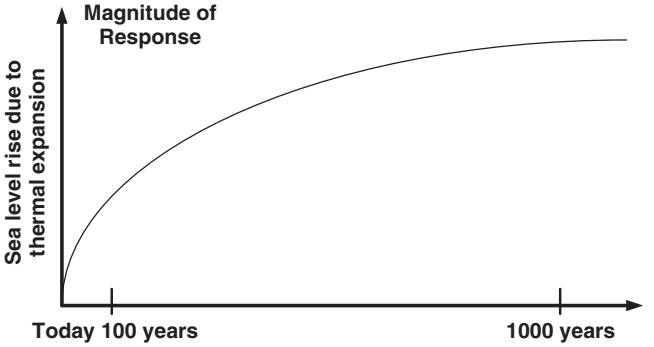

Figure 1.9 The Sea Level Rise after the Reduction of CO_2.

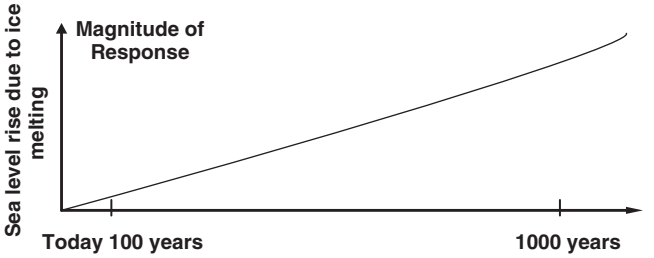

Figure 1.10 The Sea Level Rise after the Reduction of CO_2 in the Atmosphere.

As the ice sheets continue to melt due to rising temperatures over the next few centuries, the sea level will also continue to rise. Figures 1.6 through 1.10 depict the earth's conditions as a function of our level of response. As a direct consequence of trapped CO_2 in the atmosphere, with its melting of the polar ice caps causing increased sea levels that bring coastal flooding, our pattern of life on earth will be changed forever.

1.6 THE AGE OF THE ELECTRIC POWER SYSTEM

Hans Christian Oersted,[12] a Danish physicist and chemist, discovered electromagnetism in 1820. Michael Faraday,[13] an English chemist and physicist, worked for many years to convert electrical force into magnetic force. In 1831, Faraday's many years of effort were rewarded when he discovered electromagnetic induction; later, he invented the first dynamo and the first generator, a simple battery as a source of DC power simple battery. In 1801, an Italian physicist, Antonio Anastasio Volta[14] invented the chemical battery. Another important technological development was the discovery of Faraday's law of induction. Michael Faraday is credited with the discovery of the induction phenomenon in 1831. However, recognition for the induction phenomenon is also accorded to Francesco Zantedeschi,[15] an Italian priest and physicist in 1829, and around the 1830s to Joseph Henry,[16] an American scientist.

Nikola Tesla[17] was the main contributor to the technology on which electric power is based and its use of alternating current. He is also known for his pioneering work in the field of electromagnetism in the late 19th and early 20th centuries. Tesla put world electrification in motion. By the 1920s, electric power production using fossil fuels to generate the electricity, had started around the world. Since then, electric power has been used to power tools and vehicles; to provide heat for residential, commercial, and industrial systems; and to provide our energy needs in our everyday lives. Figure 1.11 shows the U.S. production of electric power from 1920–1999.[18] The International Energy Agency (IEA) forecasts an average annual growth rate of 2.5% for world electricity demand. At the rate around 2.5%, the world electricity demand will double by 2030. The IEA forecasts world carbon dioxide emissions due to power generation will increase by 75% by 2030. In 2009, the world population

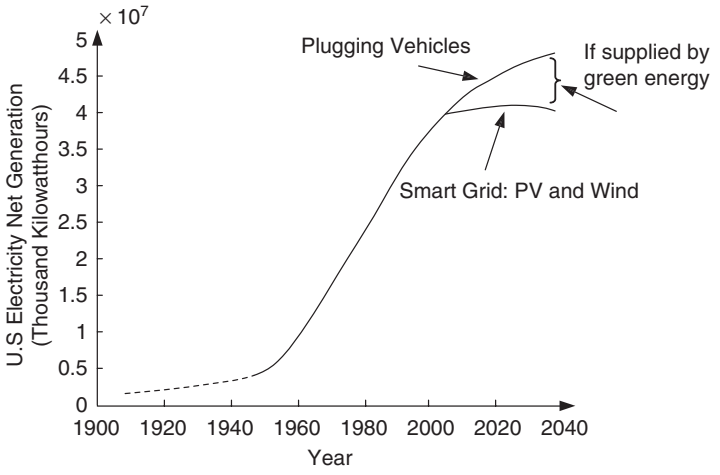

Figure 1.11 The U.S. Production of Electric Power 1920–1999.[19]

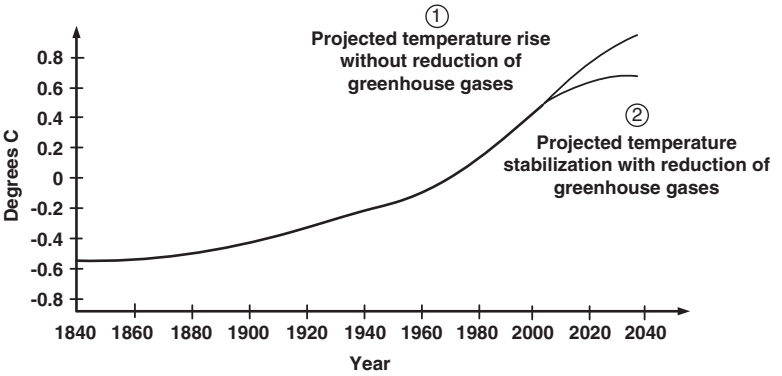

Figure 1.12 The Smooth Average of Published Records of Surface Temperature from 1840–2000.[20]

was approximately 6.8 billion.[19] The United Nations forecasts population growth to 8.2 billion by 2030. Without interventions to contain population growth, another 1.5 billion people will need electric power equivalent to five times the current U.S. rate of electric power consumption.

Figure 1.11 also shows that we can slow the growth of electric power production from fossil fuels by replacing the fossil fuels with renewable sources and integrating the green energy sources in electric power grids. Figure 1.12 shows the mean smooth recorded temperature by the United Nations Environment Programme (UNEP). As more countries such as China, India, Brazil, Indonesia, and others modernize their economy, the rate of CO_2 production will accelerate. We can only hope that we can stop the trend of global warming as presented in Fig. 1.12.

1.7 GREEN AND RENEWABLE ENERGY SOURCES

To meet carbon reduction targets, it is important we begin to use sources of energy that are renewable and sustainable. The need for environmentally friendly methods of transportation and stationary power is urgent. We need to replace traditional fossil-fuel-based vehicles with electric cars, and the stationary power from traditional fuels, coal, gas, and oil, with green sources for sustainable energy fuel for the future.

1.7.1 Hydrogen

Besides renewable sources, such as the wind and the sun, hydrogen (H) is an important source of clean, renewable energy. Hydrogen is abundantly available in the universe. Hydrogen is found in small quantities in the air. It's nontoxic. It's colorless and odorless.

Hydrogen can be used as an energy carrier, stored, and delivered to where it is needed. When hydrogen is used as a source of energy, it gives off only water and heat with no carbon emissions. Hydrogen has three times as much energy for the same quantity of oil.[21,22] A hydrogen fuel cell[21] is fundamentally different from a hydrogen combustion engine. In a hydrogen fuel cell, hydrogen atoms are divided into protons and electrons. The negatively charged electrons from hydrogen atoms create an electrical current with water as a byproduct (H_2O). Hydrogen fuel cells are used to generate electric energy at stationary electric power-generating stations for residential, commercial, and industrial loads. The fuel cell can also be used to provide electric energy for an automotive system, i.e., a hydrogen combustion engine. Hydrogen-based energy has the potential to become a major energy source in the future, but there are many applied technical problems that must be solved; a new infrastructure will also be needed for this technology to take hold.

1.7.2 Solar and Photovoltaic

Solar and photovoltaic (PV) energy are also important renewable energy sources. The sun, the earth's primary source of energy, emits electromagnetic waves. It has invisible infrared (heat) waves, as well as light waves. Infrared (IR) radiation has a wavelength between 0.7 and 300 micrometers (μm) or a frequency range between approximately 1 THz (terahertz; 10 to the power of 12) to the 430 THz.[23] Sunlight is defined by irradiance, meaning radiant energy of light. We define one sun as the brightness to provide an irradiance of about 1 kilowatt (kW) per square meter (m^2) at sea level and 0.8 sun about 800 W/m^2. One sun's energy has 523 watts of IR light, 445 watts of visible light, and 32 watts of ultraviolet (UV) light.

Example 1.1 Compute the area in square meters and square feet needed to generate 5,000 kW of power. Assume the sun irradiant is equivalent to 0.8 sun of energy.

Solution

Power capacity of PV at 0.8 sun = 0.8 kW/m^2

Capacity of 5,000 kW = (1 kW/m^2) · (Required area in m^2)

Required area in m^2 = 5,000/0.8 = 6,250 m^2

1 m^2 = 10.764 ft^2

Required area in ft^2 = (6250) · (10.764) = 67,275 ft^2

Plants, algae, and some species of bacteria capture light energy from the sun and through the process of photosynthesis, they make food (sugar) from carbon dioxide and water. As the thermal IR radiation from the sun reaches the earth, some of the heat is absorbed by earth's surface and some heat is reflected back into space as it can be seen in Figure 1.4. Highly reflective

mirrors can be used to direct thermal radiation from the sun to provide a source of heat energy. The heat energy from the sun—solar thermal energy—can be used to heat water to a high temperature and pressurized in a conventional manner to run a turbine generator.

Solar PV sources are arrays of cells of silicon materials that convert solar radiation into direct current electricity. The cost of a crystalline silicon wafer is very high, but new light-absorbent materials have significantly reduced the cost. The most common materials are amorphous silicon (a-Si), mainly O for p-type Si and C and the transition metals, mainly Fe. Silicon is put into different forms or into polycrystalline materials, such as cadmium telluride (CdTe) and copper indium (gallium) (CIS and CIGS). The front of the PV module is designed to allow maximum light energy to be captured by the Si materials. Each cell generates approximately 0.5 V. Normally, 36 cells are connected together in series to provide a PV module producing 12 V.

Example 1.2 Compute the area in square meters and square feet needed to generate 5,000 kW of power. Assume the sun irradiant is equivalent to 0.8 sun of energy.

Solution

Power capacity of PV at 0.8 sun = 0.8 kW/m^2

Capacity of 5,000 kW = (1 kW/m^2) · (Required area in m^2)

Required area in m^2 = 5,000/0.8 = 6,250 m^2

1 m^2 = 10.764 ft^2

Required area in ft^2 = (6250) · (10.764) = 67,275 ft^2

1.7.3 Geothermal

Renewable geothermal energy refers to the heat produced deep under the earth's surface. It is found in hot springs and geysers that come to the earth's surface or in reservoirs deep beneath the ground. The earth's core is made of iron surrounded by a layer of molten rocks, or magma. Geothermal power plants are built on geothermal reservoirs and the energy is primarily used to heat homes and commercial industry in the area.[24]

1.7.4 Biomass

Biomass is a type of fuel that comes from organic matter like agricultural and forestry residue, municipal solid waste, or industrial waste. The organic matter used may be trees, animal fat, vegetable oil, rotting waste, and sewage. Biofuels, such as biodiesel fuel, are currently mixed with gasoline for fueling cars, or are used to produce heat or as fuel (wood and straw) in power stations to produce electric power. Rotting waste and sewage generate methane gas, which is also a biomass energy source.[25] However, there are a number of controversial issues

surrounding the use of biofuel. Producing biofuel can involve cutting down forests, transforming the organic matter into energy can be expensive with higher carbon footprints, and agricultural products may be redirected instead of being used for food.

1.7.5 Ethanol

Another source of energy is ethanol, which is produced from corn and sugar as well as other means. However, the analysis of the carbon cycle and the use fossil fuels in the production of "agricultural" energy leaves many open questions: per year and unit area solar panels produce 100 times more electricity than corn ethanol.[25]

As we conclude this section, we need always to remember the Royal Society of London's 1662 motto: "Nullius in Verba" (Take Nobody's Word).

1.8 ENERGY UNITS AND CONVERSIONS

To estimate the carbon footprint of different classes of fossil fuels, we need to understand the energy conversion units. Because fossil fuels are supplied from different sources, we need to convert to equivalent energy measuring units to evaluate the use of all sources. The energy content of different fuels is measured in terms of heat that can be generated. One British thermal unit (BTU) requires 252 calories; it is equivalent to 1055 joules. The joule (J) is named after James Prescott Joule[26] (born December 24, 1818), an English physicist and brewer, who discovered the relationship between heat and mechanical work, which led to the fundamental theory of the conservation of energy. One BTU of heat raises one pound of water one degree Fahrenheit (F). To measure the large amount of energy, the term "quad" is used. One quad is equivalent to 1015 BTU.

From your first course in Physics, you may recall that one joule in the metric system is equal to the force of one Newton (N) acting through one meter (m). In terms of dimensions, one joule is equal to one Newton (N) times one meter (m) ($1\ J = 1\ N \times 1\ m$); it is also equal to one watt times one second (sec) ($1\ J = 1\ W \times 1$ sec). Therefore, one joule is the amount of work required to produce one watt of power for one second. Therefore, 1 watt, normally shown as P is 3.41 BTU per hour.

Example 1.3 Compute the amount of energy in watts needed to bring 100 lb of water to 212°F.

Solution

Heat required = (100 lb) · 212°F = 2,1200 BTU

Energy in joules = 21200 BTU/ 1055 = 20.1 J

P (watt) = 3.41 BTU/h

P = 20.1/3.41 = 5.89 W

In engineering, power is defined as

P = I V

where I represents the current through the load and V is the voltage across the load and unit of power, P is in watts if the current is in amperes (amp) and voltage in volts. Therefore, one kilowatt is a thousand watts. The energy use is expressed in kilowatt-hour (kWh) and one kWh is the energy used by a load for one hour. This can also be expressed in joules and one kilowatt-hour (kWh) is equal to 3.6 million joules. Recall from your Introduction to Chemistry course that one calorie (cal) is equal to 4.184 J. Therefore, it follows that hundred thousand BTU is equal to one thousand kWh; it is also equal to 3.41 million BTU. Because power system generators are running on natural gas, oil, or coal, we express the energy from these types of fuel in terms of kilowatts per hour. For example, one thousand cubic feet of gas (Mcf) can produce 301 kWh and one hundred thousand BTU can produce 29.3 KWh of energy.

Example 1.4 Compute the amount of heat in BTU needed to generate 10 kWh.

Solution

One watt = one joule·sec·(j·sec)

1000 watts = 1000 j·sec

1 kWh = 1·60·60·1000 = 3600 kj·sec

10 kWh = 36000 kilo j·sec

One BTU = 1055.058 j·sec

Heat in BTU needed for 10 kWh = 36,000,000/1055.058 = 34,121.3 BTU

The energy content of coal is measured in terms of BTU produced. For example, a ton of coal can generate 25 million BTU: equivalently, it can generate 7325 kWh. Furthermore, one barrel of oil (i.e., 42 gallons) can produce 1700 KWh. Other units of interest are a barrel of liquid natural gas has 1030 BTU and one cubic foot of natural gas has 1030 BTU.

Example 1.5 Compute how many kWh can be produced from 10 tons of coal.

Solution

One ton of coal = 25,000,000 BTU

10 tons of coal = 250,000,000 BTU

1 kWh = 3413 BTU

Energy used in kWh = (250,000,000)/3413 = 73,249.3 kWh

TABLE 1.2 Carbon Footprint of Various Fossil Fuels for Production of 1 kWh of Electric Energy.[27]

Fuel Type	CO_2 Footprint (lb)
Wood	3.306
Coal-fired plant	2.117
Gas-fired plant	1.915
Oil-fired plant	1.314
Combined-cycle gas	0.992

TABLE 1.3 Carbon Footprint of Green and Renewable Sources for Production of 1 kWh of Electric Energy.[27]

Fuel Type	CO_2 Footprint (lb)
Hydroelectric	0.0088
PV	0.2204
Wind	0.03306

Example 1.6 Compute the CO_2 footprint of a residential home using 100 kWh coal for one day.

Solution

1 kWh of electric energy using a coal fire plant has 2.117 lb.

Residential home carbon footprint for 100 kWh = (100) · (2.117) = 211.7 lb of CO_2

The carbon footprint can also be estimated in terms of carbon (C) rather CO_2. The molecular weight of C is 12 and CO_2 is 44. (Add the molecular weight of C, 12 to the molecular weight of O_2, 16 times 2 = 32, to get 44, the molecular weight of CO_2.) The emissions expressed in units of C can be converted to emissions in CO_2. The ratio of CO_2/C is equal to 44/12 = 3.67. Thus, CO_2 = 3.67 C. Conversely, C = 0.2724 CO_2.

Example 1.7 Compute the carbon footprint of 100 kWh of energy if coal is used to produce it.

Solution

C = 0.2724 CO_2

C = (0.2724). 211.7 lb = Antoine Becquerel (Bq) 57.667 lb of C

TABLE 1.4 Fossil Fuel Emission Levels in Pounds per Billion BTU of Energy Input.[27]

Pollutant	Natural Gas	Oil	Coal
Carbon dioxide (CO_2)	117,000	164,000	208,000
Carbon monoxide, CO	40	33	208
Nitrogen oxides	92	448	457
Sulfur dioxide	1	1,122	2,591
Particulates	7	84	2,744
Mercury	0.000	0.007	0.016

The carbon footprints of coal is the highest among fossil fuels. Therefore, coal-fired plants produce the highest output rate of CO_2 per kilowatt-hour. The use of fossil fuels also adds other gasses to the atmosphere per unit of heat energy as shown in Table 1.4.

We can also estimate the carbon footprints for various electrical appliances corresponding to the method used to produce electrical energy. For example, one hour's use of a color television produces 0.64 pounds (lb) of CO_2 if coal is used to produce the electric power. For coal, this coefficient is approximated to be 2.3 lb CO_2/kWh of electricity.

Example 1.8 A light bulb is rated 60 W. If the light bulb is on for 24 hours, how much electric energy is consumed?

Solution
The energy used is given as:

$$\text{Energy consumed} = (60\ \text{W}) \times (24\ \text{h}) / (1000) = 1.44\ \text{kWh}$$

Example 1.9 Estimate the CO_2 footprint of a 60 W bulb on for 24 hours.

Solution

$$\text{Carbon footprint} = (1.44\ \text{kWh}) \times (2.3\ \text{lb}\ CO_2/\text{kWh}) = 3.3\ \text{lb}\ CO_2$$

Large coal-fired power plants are highly economical if their carbon footprints and damage to the environment are overlooked. In general, a unit cost of electricity is an inverse function of the unit size. For example, for a 100 kW unit, the unit cost is \$0.15/kWh for a natural gas turbine and \$.30/kWh for PV energy. Therefore, if the environmental degradation is ignored, the electric energy produced from fossil fuel is cheaper based on the present price of fossil fuel. For a large coal-fired power plant, the unit of electric energy is in the range of \$.04/kWh to \$0.08/kWh. Green energy technology needs supporting

governmental policies to promote electricity generation from green energy sources. Economic development in line with green energy policies will be needed for lessening the ecologic footprint of a developing world.

After thousands of years of burning wood and wood charcoal, CO_2 concentration was at 288 parts per million by volume (ppmv) in 1850 just at the dawn of the Industrial Revolution. By the year of 2000, CO_2 had risen to 369.5 ppmv, an increase of 37.6% over 250 years. The exponential growth of CO_2 is closely related to the production of electric energy (see Figs. 1.4 and 1.6).

1.9 ESTIMATING THE COST OF ENERGY

As we discussed, the cost of electric energy is measured by the power used over time. The power demand of any electrical appliance is inscribed on the appliance and/or included in its documentation or in its nameplate. However, the power consumption of an appliance is also a function of the applied voltage and operating frequency. Therefore, the manufacturers provide on the nameplate of an appliance, the voltage rating, the power rating, and the frequency. For a light bulb, which is purely resistive, the voltage rating and power rating are marked on the light bulb. A light bulb may be rated at 50 W and 120 V. This means that if we apply 120 volts to the light bulb, we will consume 50 watts.

Again, energy consumption can be expressed as follows:

$$P = V \cdot I \tag{1.1}$$

where the unit of power consumption, that is, P is in watts. The unit of V is in volts and unit I is in amperes.

The rate of energy consumption can be written as

$$P = \frac{dW}{dt} \tag{1.2}$$

We can then write the energy consumed by loads (i.e., electrical appliances) as

$$W = P \cdot t \tag{1.3}$$

The above unit of W is in joules or watts-seconds. However, because the unit cost of electrical energy is expressed in dollars per kilowatts, we express the electric power consumption, kilowatts-hour as

$$kWh = kW \times hour \tag{1.4}$$

Therefore, if we let λ represent the cost of electric energy in \$/kWh,
Then the total cost can be expressed as

$$\text{Energy Cost (in dollars)} = kWh \times \lambda \tag{1.5}$$

Example 1.10 Let us assume that you want to buy a computer. You see two computers: brand A is rated as 400 W and 120 V and costs \$1000; brand B is rated as 100 watts and 120 volts and costs \$1010. Your electric company charges \$.09/kWh on your monthly bill. You are interested in the total cost, that is the cost of buying the computer and the operating cost if you use your computer for 3 years at the rate of 8 hours a day.

Solution
At 8 hours a day for 3 years, the total operating time is

$$\text{Operating Time} = 8 \times 365 \times 3 = 8760 \text{ hours.}$$

$$\begin{aligned}\text{Brand A kWh energy consumption} &= \text{Operating Time} \times \text{kW of brand A} \\ &= 8760 \times 400 \times 10^{-3} = 3504\ kWh\end{aligned}$$

$$\begin{aligned}\text{Brand B kWh energy consumption} &= \text{Operating Time} \times \text{kW of brand B} \\ &= 8760 \times 100 \times 10^{-3} = 876\ kWh\end{aligned}$$

$$\begin{aligned}\text{Total cost for brand A} &= \text{Brand A kWh energy consumption} + \text{cost of brand A} \\ &= 3504 \times 0.09 + 1000 = \$1315.36\end{aligned}$$

$$\begin{aligned}\text{Total cost for brand B} &= \text{Brand B kWh energy consumption} + \text{cost of brand B} \\ &= 876 \times 0.09 + 1010 = \$1088.84\end{aligned}$$

Therefore, the total cost of operation and price of brand B is much lower than brand A because the wattage of brand B is much less. Despite the fact that the price of brand A is lower, it is more economical to buy brand B because its operating cost is far lower than that of brand A.

Example 1.11 For Example 1.8, let us assume that the electric energy is produced using coal, what is the amount of CO_2 in pounds that is emitted over 3 years into the environment?
What is your carbon footprint?

Solution
From the Table 1.4, the pounds of CO_2 emission per billion BTU of energy input for coal is 208,000.

$$1 \text{ kWh} = 3.41 \text{ thousand BTU}$$

$$\text{Energy consumed for brand A over 3 years} = 3504 \times 3.41 \times 10^3$$
$$= 11948640 \text{ BTU}$$

$$\text{Therefore, for brand A, pounds of } CO_2 \text{ emitted} = \frac{11948640 \times 208000}{10^9}$$
$$= 2485.32 \text{ lb}$$

$$\text{Energy consumed for brand B over 3 years} = 876 \times 3.41 \times 10^3 = 2987160 \text{ BTU}$$

$$\text{Therefore, for brand B, pounds of } CO_2 \text{ emitted} = \frac{2987160 \times 208000}{10^9}$$
$$= 621.33 \text{ lb}$$

Brand B has a much lower carbon footprint.

Example 1.12 Assume that you have purchased a new high-powered computer with a gaming card and an old CRT (cathode ray tube) monitor. Assume that the power consumption is 500 W and the fuel used to generate electricity is oil. Compute the following:

i) Carbon footprints if you leave them on 24/7.
ii) Carbon footprint if it is turned off 8 hours a day.

Solution

i) Hours in one year $= 24 \times 365 = 8760$ h

$$\text{Energy consumed in one year} = 8760 \times 500 \times 10^{-3} = 4380 \text{ kWh}$$
$$= 4380 \times 3.41 \times 10^3 = 14935800 \text{ BTU}$$

From Table 1.4, pounds of CO_2 emission per billion The BTU of energy input for oil is 164,000.

$$\text{Therefore, the carbon footprint for one year} = \frac{14935800 \times 164000}{10^9}$$
$$= 2449.47 \text{ lb}$$

ii) Carbon footprint in the case of 8 h/day use

$$= \frac{8}{24} \times \text{footprint for use in 24 h}$$
$$= \frac{1}{3} \times 2449.47 = 816.49 \text{ lb}$$

1.10 CONCLUSION

In this chapter, we have studied a brief history of energy sources and their utilization. The development of human civilization is the direct consequence of harnessing the earth's energy sources. We have used the power of the wind, the sun, and wood for thousands of years. However, as new energy sources, such as coal, oil, and gas have been discovered, we have continuously substituted a new source of energy in place of an old source.

Global warming and environmental degradation have forced us to reexamine our energy use and consequent carbon footprints, a topic we also have addressed in this chapter. In the following chapters, we will study the basic concept of power system operation, power system modeling, and the smart power grid system, as well as the design of smart microgrid rentable energy systems.

PROBLEMS

1.1 Writing Assignment. Write a 3000 word report summarizing the Kyoto Protocol. Compute the simple operating margin CO_2 factor for the year 2020 if the system load of 6000 MW is supplied by 10 coal units with a capacity of 100 MW, 10 oil-fired generators with a capacity of 50 MW, and 10 gas-fired generators with a capacity of 50 MW.

i) The system load of 6000 MW supplied from only coal units

ii) The system load of 6000 MW supplied equally from gas units and wind and solar power

1.2 Using the data given in Table 1.4, perform the following:

i) The carbon footprint of 500 W if coal is used to produce the electric power

ii) The carbon footprint of a 500 W bulb if natural gas is used to produce the electric power

iii) The carbon footprint of a 500 W bulb if wind is used to produce the electric power

iv) The carbon footprint of a 500 W bulb if PV energy is used to produce the electric power

1.3 Compute the money saved in one month by using CFL (compact fluorescent light) bulb (18 W) instead of using an incandescent lamp (60 W) if the cost of electricity is $ 0.12 per kWh. Assume the lights are used for 10 hours a day.

1.4 Compute the carbon footprint of the lamps of Problem 1 if natural gas is used as fuel to generate electricity. How much more will the carbon footprint be increased if the fuel used is coal?

1.5 Will an electric oven rated at 240 V and 1200 W provide the same heat if connected to a voltage of 120 V? If not, how much power will it consume now?

1.6 If the emission factor of producing electric power by PV cells is 100 g of CO_2 per kWh, by wind power is 15 g of CO_2 per kWh, and by coal is 1000 g of CO_2 per kWh, then find the ratio of CO_2 emission when (a) 15% of power comes from wind farms, (b) 5% from a PV source, and (c) the rest from coal as opposed to when all power is supplied by coal-run power stations.

1.7 Compute the operating margin of the emission factor of a power plant with three units with the following specifications over one year:

Unit	Generation (MW)	Emission Factor (lb of CO_2/MWh)
1	160	1000
2	200	950
3	210	920

1.8 If the initial cost to set up a thermal power plant of 100 MW is 2 million dollars and that of a PV farm of the same capacity is 300 million dollars, and the running cost of the thermal power plant is \$90 per MWh and that of PV farm is \$12 per MWh then find the time in years needed for the PV farm to become the most economical if 90% of the plant capacity is utilized in each case.

1.9 Consider a feeder that is rated 120 V and serving five light bulbs. Loads are rated 120 V and 120 W. All light loads are connected in parallel. If the feeder voltage is dropped by 20%, compute the following:

i) The power consumption by the loads on the feeder in watts

ii) The percentage of reduction in illumination by the feeders

iii) The amount of carbon footprint if coal is used to produce the energy

1.10 The same as Problem 1.8, except a refrigerator rated 120 V and 120 W is also connected to the feeder and voltage is dropped by 30%.

i) Compute the power consumption by the loads on the feeder in watts

ii) Compute the percentage of reduction in illumination by the feeders

iii) Do you expect any of the loads on the feeder to be damaged?

iv) Compute the amount of carbon footprint if coal is used to produce the energy

(Hint: a 40 W incandescent light bulb produces approximately 500 lumens of light)

1.11 The same as Problem 1.9, except a refrigerator rated 120 W is also connected to the feeder and voltage is raised by 30%.

i) Compute the power consumption by the loads on the feeder in watts

ii) Compute the percentage of reduction in illumination by the feeders

iii) Do you expect any of the loads on the feeder to be damaged?

iv) Compute the amount of carbon footprint if coal is used to produce the energy

1.12 Compute the CO_2 emission factor in pounds of CO_2 per BTU for a unit in a plant that is fueled by coal, oil, and natural gas if 0.3 million tons of coal, 0.1 million barrels of oil, and 0.8 million cubic feet of gas have been consumed over one year. The average power produced over the period was 210 MW. Use the following data and the data of Table 1.4 for computation: a ton of coal has 25 million BTU; a barrel (i.e., 42 gallons) of oil has 5.6 million BTU; a cubic foot of natural gas has 1030 BTU.

REFERENCES

1. California Energy Commission. Energy quest, the energy story. Fossil fuels—coal, oil and natural gas (Chapter 8). Available at http://www.energyquest.ca.gov. Accessed 2010 Sept 26.
2. Durant W. The story of civilization. Available at http://www.archive.org/details/storyofcivilizat035369mbp. Accessed 2010 Nov 9.
3. Brown LR. Mobilizing to save civilization. Available at http://www.earth-policy.org/index.php?/books/pb4/pb4_data. Accessed 2010 Nov 9. (This is part of a supporting dataset for: Brown LR, Plan B 4.0: Mobilizing to Save Civilization. New York: W.W. Norton & Company, 2009. For more information and a free download of the book, go to http://www.earthpolicy.org/datacenter/pdf/book_pb4_ch4-5_all_pdf.pdf.)
4. BP Statistical Review of World Energy—June 2010. Available at http://www.bp.com/liveassets/bp_internet/globalbp/globalbp_uk_english/reports_and_publications/statistical_energy_review_2008/STAGING/local_assets/2010_downloads/statistical_review_of_world_energy_full_report_2010.pdf. Accessed 2009 Sept 20.
5. Encyclopædia Britannica. Martin Heinrich Klaproth. Available at http://www.britannica.com/EBchecked/topic/319885/Martin-Heinrich-Klaproth. Accessed 2010 Nov 9.
6. Encyclopædia Britannica. Eugène-Melchior Péligot. Available at http://www.britannica.com/EBchecked/topic/449213/Eugene-Peligot. Accessed 2010 Nov 9.
7. Encyclopædia Britannica. Antoine-César Becquerel. Available at http://www.britannica.com/EBchecked/topic/58017/Antoine-Cesar-Becquerel. Accessed Nov 9.
8. Encyclopædia Britannica. Enrico Fermi. Available at http://www.britannica.com/EBchecked/topic/204747/Enrico-Fermi. Accessed 2010 Nov 9.

9. Congressional Research Service. Managing the nuclear fuel cycle: policy implications of expanding global access to nuclear power (updated January 30, 2008). Available at http://www.nuclear.energy.gov/pdfFiles/rpt_ManagingtheNuclearFuelCyclePolicy.pdf. Accessed 2010 Nov 9.
10. World Meteorological Organization. Arctic surface-based sea-ice observations: integrated protocols and coordinated data acquisition. Available at http://www.wmo.int/pages/prog/wcrp/documents/CliCASWSreportfinal.pdf. Accessed 2010 Nov 9.
11. Intergovernmental Panel on Climate Change [IPCC]. IPCC Third Annual Report. Available at http://www.grida.no/publications/other/ipcc_tar/?src=/climate/ipcc_tar/vol4/english/index.htm. Accessed 2010 Sept 27.
12. Encyclopædia Britannica. Hans Christian Ørsted. Available at http://www.britannica.com/EBchecked/topic/433282/Hans-Christian-Orsted. Accessed 2010 Nov 9.
13. Encyclopædia Britannica. Michael Faraday. Available at http://www.britannica.com/EBchecked/topic/201705/Michael-Faraday. Accessed 2010 Nov. 9.
14. Available at Conte Alessandro Volta. Available at http://www.britannica.com/EBchecked/topic/632433/Conte-Alessandro-Volta. Accessed 2010 Nov 9.
15. The contribution of Francesco Zantedeschi at the development of the experimental laboratory of physics faculty of the Padua University. Available at http://www.brera.unimi.it/sisfa/atti/1999/Tinazzi.pdf. Accessed 2010 Nov 9.
16. Encyclopædia Britannica. Joseph Henry. Available at http://www.britannica.com/EBchecked/topic/261387/Joseph-Henry. Accessed 2010 Nov 9.
17. Encyclopædia Britannica. Nikola Tesla. Available at http://www.britannica.com/EBchecked/topic/588597/Nikola-Tesla. Accessed 2010 Nov 9.
18. Energy Information Administration. Official Energy Statistics from the US Government. Available at http://www.eia.doe.gov. Accessed 2010 Sept 26.
19. Population Reference Bureau. World population data. Available at http://www.prb.org/pdf10/10wpds_eng.pdf. Accessed 2010 Nov 9.
20. Manitoba Eco Network. Climate change observations. Available at http://www.climatechangeconnection.org/Science/Observations.htm. Accessed 2010 Nov 9.
21. The Open University. The potential of fuel cells to reduce energy demands and pollution from the UK transport sector. Available at http://oro.open.ac.uk/19846/1/pdf76.pdf. Accessed 2010 Oct 9.
22. Stanford University. Hydrogen FQA sustainability. Available at http://www.formal.stanford.edu/jmc/progress/hydrogen.html. Accessed 2010 Nov 9.
23. Hockett RS. Analytical techniques for PV Si feedstock evaluation. Paper presented at the 18th workshop on Crystalline Silicon Solar Cells &Modules: Material and Processes, Vail, CO, August 2008.
24. Earth Policy Institute. Climate, energy, and transportation. Available at http://www.earth-policy.org/data_center/C23. Accessed 2010 Nov 9.
25. Patzek TW. Thermodynamics of the corn-ethanol biofuel cycle. *Critical Reviews in Plant Sciences*, 2004, 23(6), 519–567.
26. Encyclopædia Britannica. James Prescott Joule. Available at http://www.britannica.com/EBchecked/topic/306625/James-Prescott-Joule. Accessed 2010 Nov 9.
27. Low Impact Life Onboard. Carbon footprints. Available at http://www.liloontheweb.org.uk/handbook/carbonfootprint. Accessed 2010 Nov 9.

CHAPTER 2

POWER GRIDS

2.1 INTRODUCTION

A power grid provides electric energy to end users, who use electricity in their homes and businesses. In power grids, any device that consumes electric energy is called a *load*. In residential electrical systems, examples of such loads include air conditioning, lighting, television sets, refrigerators, washing machines, and dishwashers. Industrial loads are composite loads with induction motors forming the bulk of these loads. Commercial loads consist largely of lighting, office computers, copy machines, laser printers, and communication systems. All electrical loads are served at nominal-rated voltages. The nominal-rated voltage of each load is specified by the manufacturer for its safe operation. In power grid analysis, we study how to design the electric power grid network to serve the loads at their rated voltage with a maximum of 5% above or 5% below the nominal-rated values.

In this chapter, we introduce the basic concepts behind power grid loads, single-phase loads, three-phase loads, transformers, distribution systems, energy transmission, and modeling of the power grid using the generalized per unit concept. In the chapters following, we will address smart microgrids and the integration of green and renewable energy sources into interconnected bulk power grids.

Design of Smart Power Grid Renewable Energy Systems, First Edition. Ali Keyhani.

2.2 ELECTRIC POWER GRIDS

2.2.1 Background

Without the planning and design of power plants, the construction of thousands of miles of transmission lines, and the control of generated power to supply the loads on a second-by-second basis, a stable and reliable electric energy system on which we have come to rely would not exist. Our modern industrialized world would not have been developed without the rapid electrification that took place around the world in the early 1900s.[1]

Although we recognize Thomas Edison as a tireless inventor and the designer of the first direct current (DC) generating power plant in 1882,[2–3] it is Nicola Tesla, to whom we owe credit for the invention and design of the power grid. Tesla developed a competing electrical system to Edison's based on alternating current (AC),[2–3] which can be transformed to high voltages and transmitted across great distances. This system is in use today.

Charles Curtis designed the first steam turbine generator in Newport, Rhode Island in 1903.[3–4] However, it was not until 1917, when the first long-distance AC high-voltage transmission line was constructed and then expanded across state lines that the electric power grid became an everyday power grid network in the United States.

Figure 2.1 provides an overview of electric power generation in the 21st century.

According to the U.S. Department of Energy,[3] from 2006 to 2007, the net generation of electric energy increased to 234,157 billion kilowatt-hours (kWh)

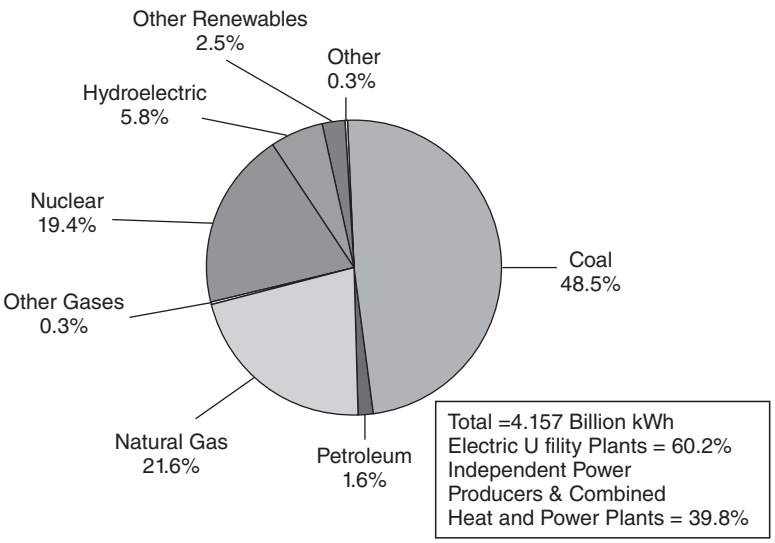

Figure 2.1 U.S. Electric Power Industry Net Generation, 2007.[4] Source: Energy Information Administration, *Electric Power Annual 2007*.

from 4,065 billion kWh. This increase was mostly due to the use of coal, natural gas, and nuclear energy. In 2007, the share of coal-based generation was 2,016 million megawatt hours (MWh), natural gas-based generation was 897 million MWh, and nuclear-based generation was 806 million MWh.[4] The share of renewable energy sources, such as solar energy and wind were around 2.5%.

2.2.2 The Construction of a Power Grid System

A power system grid is a network of transmission and distribution systems for delivering electric power from suppliers to consumers. Power grids use many methods of energy generation, transmission, and distribution. Following the energy crisis of the 1970s, the federal Public Utility Regulatory Policies Act (PURPA)[4–5] of 1978 aimed at improving energy efficiency and increasing the reliability of electric power supplies. PURPA required open access to the power grid network for small, independent power producers. After the deregulation of the power industry, the power generation units of many power grid companies began operating as separate business divisions. New power generation companies entered the power market as independent power producers (IPP): IPPs generate power that is purchased by electric utilities at wholesale prices. Today, power grid generating stations are owned by IPPs, power companies, and municipalities. The end-use customers are connected to the distribution systems of power grid companies who can buy power at a retail price.

Power companies are tied together by transmission lines referred to as *interconnections*. An *interconnected network* is used for power transfer between power companies. Interconnected networks are also used by power companies to support and increase the reliability of the power grid for stable operation and to reduce costs. If one company is short of power due to unforeseen events, it can buy power from its neighbors through the interconnected transmission systems. The construction of a power-generating station with a high capacity, say in the range of 500 MW may take from 5 to 10 years. Before constructing such a power-generating station, a permit must be obtained from the government. Stakeholders, the local power company, and IPPs will have to undertake an economic evaluation to determine the cost of electric energy over the life of the plan as compared with the price of power from the other producers before deciding to build the plant.

Under a deregulated power industry, power grid generation and the cost of electric power are determined by supply and demand. In the United States and most countries around the world, the interconnected network power grid is deregulated and is open for all power producers. The control of an interconnected network is maintained by an independent system operator (ISO). The ISO is mainly concerned with maintaining instantaneous balance of the power grid system load and generation to ensure that the system remains stable. The ISO performs its function by controlling and dispatching the least costly generating units to match power generated with system loads. We will study the operation of a power grid in Chapter 4.

Historically, power plants are located away from heavily populated areas. The plants are constructed where water and fuel (often supplied by coal) are available. Large-capacity power plants are constructed to take advantage of economies of scale. The power is generated in a voltage range of 11 kilovolts (kV) to 20 kV and then the voltage is stepped up to a higher voltage before connection to the interconnected bulk transmission network.

High-voltage (HV) transmission lines are constructed in the range of 138 kV to 765 kV. These lines are mostly overhead. However, in large cities, underground cables are also used. The lines consist of copper or aluminum. A major concern in bulk power transmission is power loss in transmission lines that is dissipated as heat due to the resistance of the conductors. The power capacity is expressed as voltage magnitude multiplied by the current magnitude. High voltages would require less current for the same amount of power and less surface area of conductor, resulting in reduced line loss. The distribution lines are normally considered lines that are rated less than 69 kV.

Bulk power transmission lines are like the interstate highway systems of the energy industry, transferring bulk power along high-voltage lines that are interconnected at strategic locations. High-voltage transmission lines in the range of 110 kV to 132 kV are referred to as *subtransmission lines*. In Fig. 2.2, the subtransmission lines supply power to factories and large industrial plants. The gas turbine power plants supply power to the subtransmission system as shown in Fig. 2.2.

Distribution systems are designed to carry power to the feeder lines and end-use customers. The distribution transformers are connected to the high-voltage side of the transmission or the subtransmission system. The distribution voltages are in the range of 120, 208, 240, 277, and 480 volts. The service voltage of distribution systems depends on the size of service in terms of loads. Higher commercial loads are served at 480 V.

Figure 2.3 depicts a five-bus power system. In this figure, we have two generators that are connected to bus (node) 1 and 2. The step-up transformers that connect the generators to the bulk power network are not shown. Load centers are represented at bus (node) 3, 4, and 5. We use the term *bus* because these points of interconnections are copper bars that connect elements, such as the generator, loads, and lines of the power grid. All buses (nodes) are located in a substation. In Fig. 2.3, we see a generator and a line connected to bus 1.

Power generators are designed to produce a three-phase alternating current (AC). The three sinusoidal distributed windings or coils that carry the same current in a power generator can be seen in Fig. 2.4.

Figure 2.4 represents the sinusoidal voltage (or current) with respect to time. In Fig. 2.4, 0 to 360° (2π radians) is shown along the time axis. Power systems around the world each operate at a fixed frequency of 50 or 60 cycles per second. Based on a universal color-code convention,[6] black is used for one phase of the three-phase system; it denotes the ground as the reference phase with zero-degree angle. Red is used for the second phase, which is 120° out of phase with respect to the black phase. Blue is used for the third phase, which

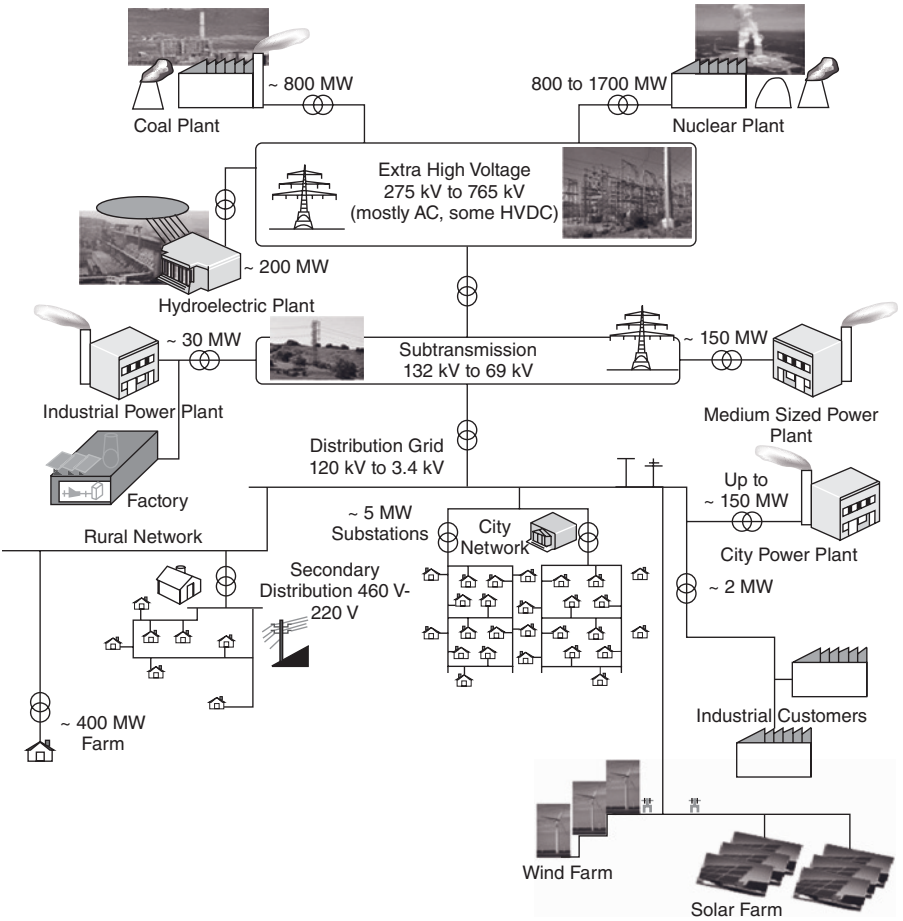

Figure 2.2 A Power System Interconnected Network with High Green Energy Penetration.[6]

is also 120° out of phase with the black phase. Figure 2.4 depicts this color representation as given in each phase.

2.3 THE BASIC CONCEPTS OF POWER GRIDS

2.3.1 Common Terms

First, let us define a few common terms.

- The highest level of current that a conductor can carry defines its *ampacity*: this value is a function of the cross-section area of the conductor.
- Power capacity of an element of power grid is rated in *volt amps* (VA).

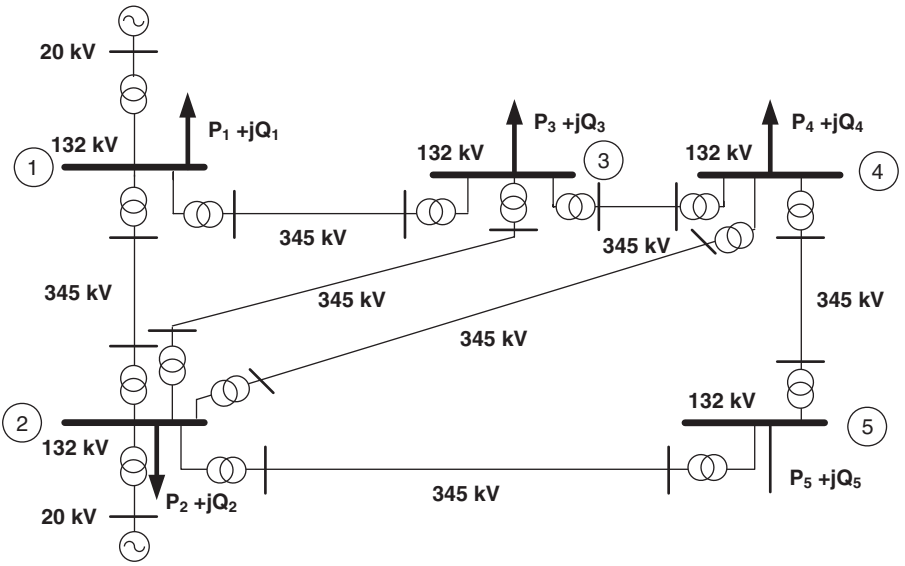

Figure 2.3 A Five-Bus Bulk Power Grid.

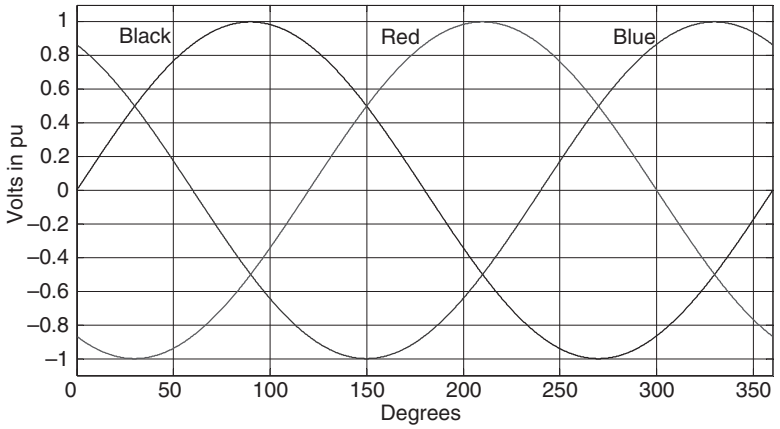

Figure 2.4 Three-Phase Generator Voltage Wave Forms.[7]

- One thousand VA is one *kilovolt amp* (kVA).
- One thousand kVA is one *megavolt amp* (MVA).
- Energy is the use of electric power by loads over time; it is given in *kilowatt-hours* (kWh).
- One thousand kWh is one *megawatt-hours* (MWh).
- One thousand MWh is one *gigawatt-hours* (GWh).

2.3.2 Calculating Power Consumption

The power consumption in a DC circuit can be computed as:

$$P = V \cdot I = \frac{V^2}{R} = I^2 R \tag{2.1}$$

To calculate the power consumption in a single-phase AC circuit, we need to use the complex conjugate of current and multiply it by voltage across the load.

$$S = V \cdot I^* = |V||I| \angle (\theta_V - \theta_I) \tag{2.2}$$

In Equation 2.2, V and I are the root mean square (RMS) values of voltage and currents. The power factor (p.f.) is computed based on the phase angle between the voltage and current where the voltage is the reference phase.

$$\begin{aligned} p.f. &= \cos(\theta_V - \theta_I) \\ Z &= \frac{|V| \angle \theta_V}{|I| \angle \theta_I} \end{aligned} \tag{2.3}$$

In the above equation, $\theta = (\theta_V - \theta_I)$, is also the angle of impedance. The complex power has two components; active power consumption, P and reactive power consumption, Q as shown in Equation 2.4

$$S = |V||I|(\cos\theta + j\sin\theta) = P + jQ \tag{2.4}$$

For complex power, the voltage across the load can also be expressed as: $V = I \cdot Z$

Therefore, we also have the following expression for complex power.

$$S = V \cdot I^* = I \cdot Z \cdot I^* = |I|^2 Z \tag{2.5}$$

$$S = V \cdot I^* = V \left(\frac{V}{Z} \right)^* = \frac{|V|^2}{Z^*} \tag{2.6}$$

Let us review the basic inductive circuit, R–L as given in Fig. 2.5.

In the circuit depicted in Figure 2.5, we are using the standard polarity notation. We mark the polarity of each element by a plus and a negative. These markings facilitate the application of Kirchhoff's law of voltage. The positive terminal indicates the direction of current flow in the circuit. For example, in this circuit, the source voltage rise—from the minus terminal to

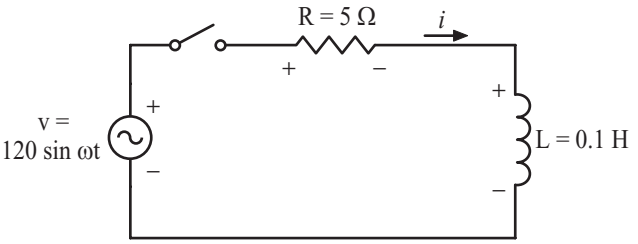

Figure 2.5 An R–L Circuit.

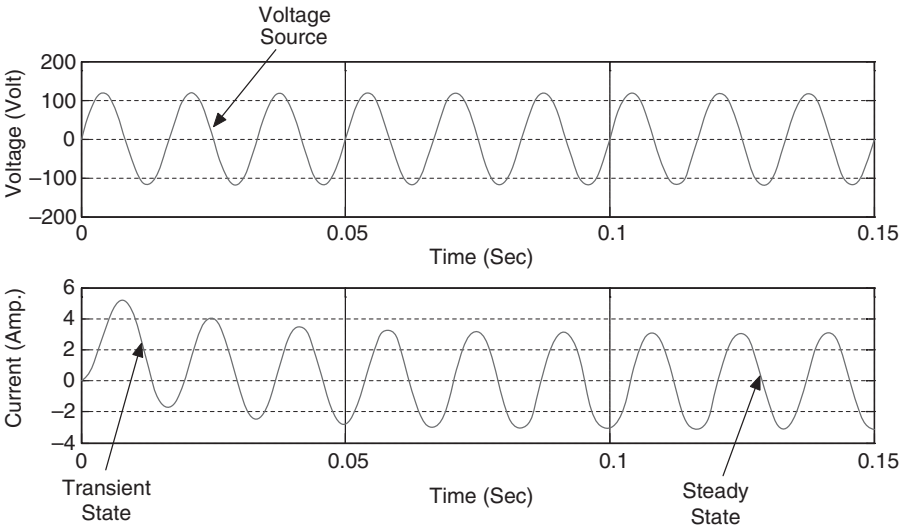

Figure 2.6 The Responses of the Voltage and Current of the Circuit Depicted in Fig. 2.5.

the positive terminal—is equal to the drop across the resistance and inductance in the circuit.

If at $t = 0$, the switch is closed, the response current is given by the differential equation below.

$$v = Ri + L\frac{di}{dt} \tag{2.7}$$

In Equation 2.7, v and i are instantaneous values of voltage and current. After some time, the current reaches steady state. This condition is shown in Fig. 2.6.

At the steady state, v and i can be represented by phasor forms as V and I. In this book, we are interested in the design of a power grid for

steady-state operation. We can express the steady-state operation of an R–L circuit as:

$$V = V_{rms}\angle\theta_V \qquad V_{rms} = \frac{120}{\sqrt{2}}$$

$$I = I_{rms}\angle\theta_I \qquad \theta_I = \omega t + \theta_{I,0}$$

where V is the RMS value and θ_V is the phase angle of V and θ_I is the phase angle of I (RMS) that is determined by θ_V and impedance angle θ ($\theta_I = \theta_V - \theta$), and $\theta_{I,0}$ is the initial angle of current.

$$I = I_{rms}e^{j(\omega t+\theta_{I,0})} \Rightarrow \frac{dI}{dt} = j\omega I_{rms}e^{j(\omega t+\theta_{I,0})} = j\omega I$$

The above differential equation can now be presented in its steady-state forms as:

$$V = (R + j\omega L)I \tag{2.8}$$

Let $X_L = \omega L$ represent the inductor reactance

$$V = (R + jX_L)I \tag{2.9}$$

Let $Z = R + jX_L = |Z|\angle\theta \qquad \theta = \tan^{-1}\left(\frac{X_L}{R}\right) > 0$

We have $\theta_V - \theta_I = \theta$.

Generally, we choose V as the reference voltage, then $\theta_V = 0$

$$V = |V|\angle 0, \qquad I = \frac{V}{Z} = |I|\angle -\theta$$

Therefore, the power supplied by a power source to an inductive load can be expressed as:

$$S = VI^* = |V||I|\cos\theta + j|V||I|\sin\theta = P + jQ. \tag{2.10}$$

As can be seen from the above definition, an inductive load will have a lagging p.f. Therefore, the power source supplies reactive power to the load. The reactive power supplied by the source is consumed by the inductive load. This can also be expressed as:

$$S = VI^* = (R + jX_L)I \cdot I^* = |I|^2 R + j|I|^2 X_L = P + jQ$$

Now let us look at an R–C circuit given in Fig. 2.7 below.

If at $t = 0$ the switch is closed, the system differential equation can be presented as:

$$v = RC\frac{dv_c}{dt} + v_c \tag{2.11}$$

In Equation 2.11 v and v_c are instantaneous values. After some time, the transient response dies out and the voltage across the capacitor reaches steady state. This is shown in Fig. 2.8.

At steady state, the source voltage V and capacitor voltage V_C, can be represented by phasor V and V_C. By now, you should have noticed that we are using capital letters V and I to depict RMS values.

$$V = V_{rms}\angle\theta_V \qquad V_{rms} = \frac{120}{\sqrt{2}}$$

$$V_C = V_{C,rms}\angle\theta_{Vc}$$

$$\frac{dV_C}{dt} = j\omega V_C \qquad I = C\frac{dV_C}{dt} = j\omega C V_C$$

Therefore, we have

$$V_C = I\cdot\left(\frac{1}{j\omega C}\right) = I\cdot\left(-j\frac{1}{\omega C}\right)$$

For the R–C circuit of Fig. 2.7, we have

$$V = \left(R - j\frac{1}{\omega C}\right)\cdot I$$

$$V = (R - jX_C)I$$

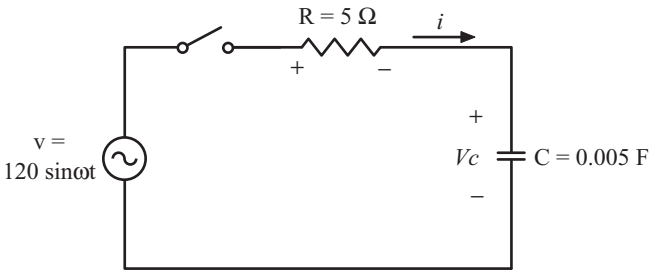

Figure 2.7 An R–C Circuit Supplied by an AC Source.

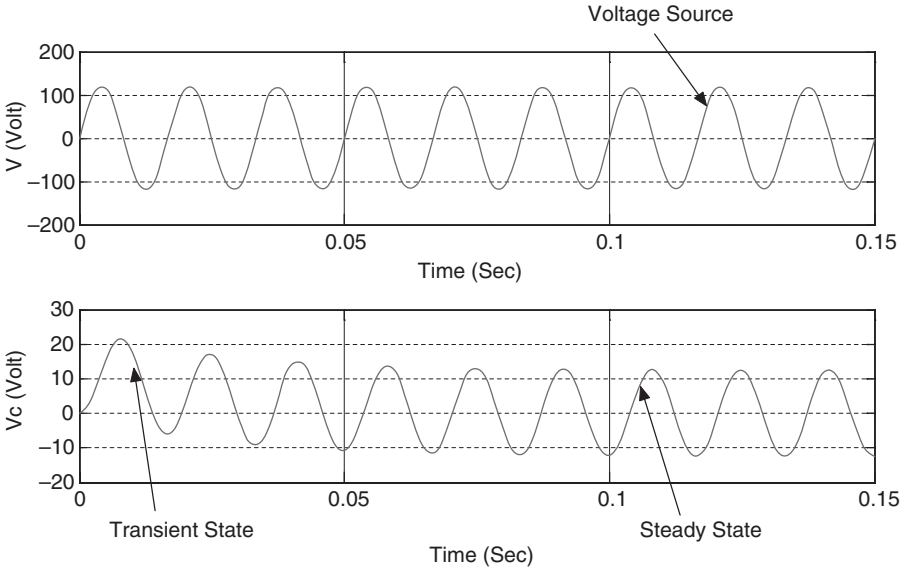

Figure 2.8 The Voltage Response (V) and Capacitor Voltage Response (V_C) of the Circuit Depicted in Fig. 2.7.

where $X_C = \dfrac{1}{\omega C}$ and X_C is the capacitor reactance.

Let $Z = R - jX_C = |Z| \angle -\theta$

Then, $\theta = \tan^{-1}\left(\dfrac{X_C}{R}\right)$

Because we choose the load V as reference, then set θ_V to zero ($\theta_V = 0$) and we have $\theta_V - \theta_I = -\theta$

$$V = |V| \angle 0, \qquad I = \frac{V}{Z} = |I| \angle \theta$$

Therefore, for a capacitor load, the current through the capacitor leads the voltage. The power supplied by the AC source can be expressed as:

$$S = VI^* = |V||I|\cos\theta - j|V||I|\sin\theta = P - jQ \tag{2.12}$$

The capacitive loads will supply reactive power to the source. We can also write the complex power as:

$$S = VI^* = (R - j\,X_C)I \cdot I^* = |I|^2 R - j|I|^2 X_C = P - jQ \tag{2.13}$$

The p.f. is computed based on the angle between the voltage and current where the voltage is in reference phase, and p.f. $= \cos(\theta_V - \theta_I)$ with designation of leading or lagging. That is, for inductive loads, the load current lags the voltage and for the capacitive load, the load current will lead the voltage. Because the impedance is the ratio of voltage over the current flowing through impedance, the impedance of inductive loads has a positive-phase angle and the impedance of capacitive loads has a negative-phase angle.

In a renewable residential system such as a photovoltaic system that is designated as *PV*, we will have a small amount of electric energy production in the range of 5 kVA to 10 kVA. Therefore, we can use a single-phase system to distribute the power to the loads. However, when we are distributing power from PV systems in the MW range, we will need to use three-phase AC systems.

The three-phase AC system can be considered as three single-phase circuits. The first AC generators were single phase. However, it was recognized that the three-phase generators can produce three times as much power. However, the higher phase generators will not produce proportionally more power.[8]

Consider the three-phase four-wire system given in Fig. 2.9.

The balanced three-phase voltages are depicted in Fig. 2.10. In general, three-phase systems[9–10] are designed as balanced systems. Therefore, we use the same structure for generators, distribution lines, and loads. Therefore, we have the following balanced system.

$$\begin{aligned} X_a &= X_b = X_c = X_s \\ Z_{aa} &= Z_{bb} = Z_{cc} = Z_{line} \\ Z_{Ya} &= Z_{Yb} = Z_{Yc} = Z_{load} \\ S_{aa} &= S_{bb} = S_{cc} = P_L + j\,Q_L \end{aligned} \tag{2.14}$$

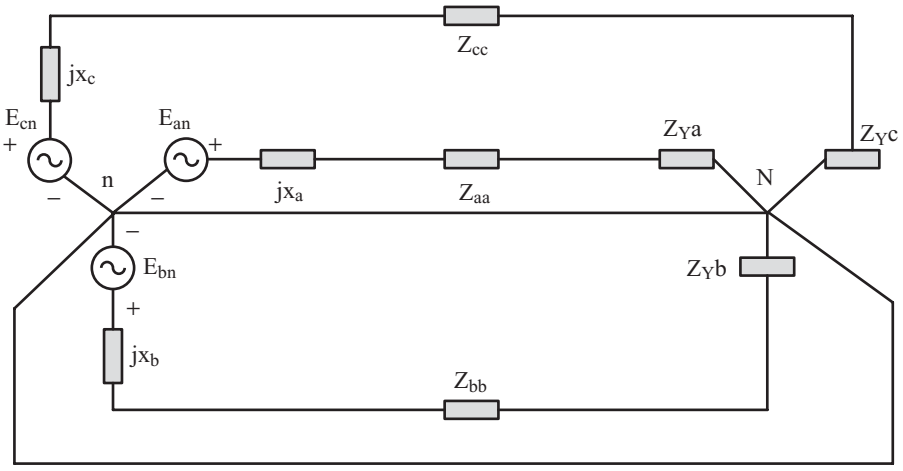

Figure 2.9 The Three-Phase Four-Wire Distribution System.

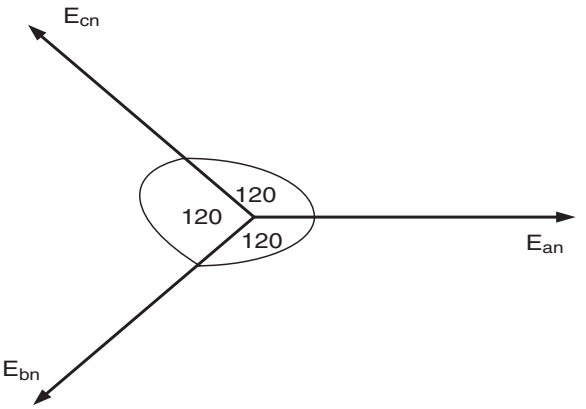

Figure 2.10 The Balanced Three-Phase System.

For balanced generators, we have:

$$\begin{aligned} E_{an} &= E \angle 0 \\ E_{bn} &= E \angle -120 = E \angle 240 \\ E_{cn} &= E \angle 120 = E \angle -240 \end{aligned} \tag{2.15}$$

Therefore, a balanced three-phase system consists of balanced three-phase generators, transmission lines, and loads as shown in Fig. 2.11.

Suppose the loads are pure resistors, i.e., $Z_Y = R_L$ or $S_L = P_L$, and the transmission line impedance is lumped with generator impedance, $Z_{Line} = R_{Line} + j\,X_{Line} + Rgen + j\,Xgen$. Then, we can write the following equations.

$$\begin{aligned} E_{an} &= I_a(Z_{Line} + R_L) \\ E_{bn} &= I_b(Z_{Line} + R_L) \\ E_{cn} &= I_c(Z_{Line} + R_L) \end{aligned} \tag{2.16}$$

$$|I_a| = |I_b| = |I_c| = \frac{|E_{an}|}{|Z_{line} + R_L|} = \frac{|E_{an}|}{|Z \angle \theta|} \tag{2.17}$$

where

$$\begin{aligned} &Z = R_{Line} + j\,X_{Line} + R_L = (R + j\,X) = |Z| \angle \theta \\ &\theta = \tan^{-1}\left(\frac{X}{R}\right) \qquad \text{where} \qquad R = R_{Line} + R \text{ and } X = X_{Line} \\ &I_a = \frac{E}{|Z|} \angle -\theta \text{ and } I_b = \frac{E}{|Z|} \angle -120 - \theta \text{ and } I_c = \frac{E}{|Z|} \angle 120 - \theta \end{aligned} \tag{2.18}$$

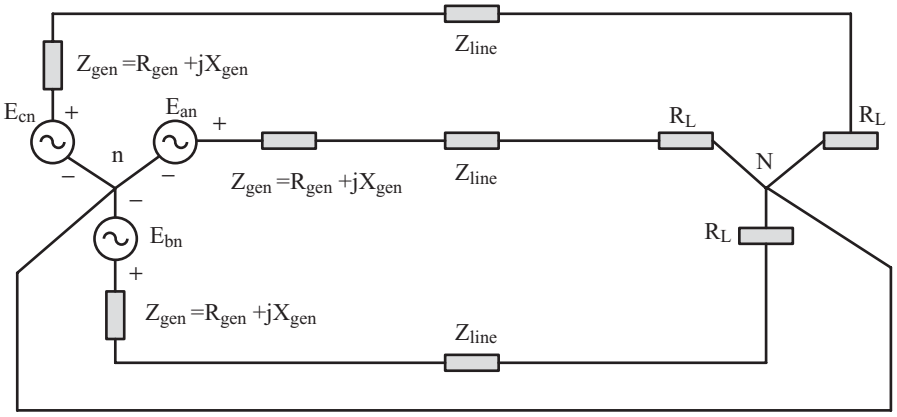

Figure 2.11 A Balanced Three-Phase System.

Therefore, for a balanced three-phase system, the currents are also balanced. We should note that the three-phase voltages are in a plane and they are out of phase by 120° from each other. Therefore, we have:

$$E_{an} + E_{bn} + E_{cn} = 0; \text{ or } E\angle 0 + E\angle -120 + E\angle 120 = 0$$
$$E + j\,0 + E\,(-0.5 - j\,0.866) + E\,(-0.5 + j\,0.866) = 0 \tag{2.19}$$

Similarly, the three-phase currents are in a plane and they are out of phase by 120° from each other. Therefore, we have:

$$I_a + I_b + I_c = I_n \tag{2.20}$$

However, for a balanced three-phase load, the sum of $I_a + I_b + I_c = 0$, therefore $I_n = 0$.

In this case, the neutral conductor does not carry any current so we can omit the neutral conductor. Figure 2.12 shows a three-phase three-wire distribution system.

Consider the three-phase balanced system of Fig. 2.13.

Let us designate the phase voltages and phase currents as shown in Fig. 2.13 by

$$E_{an}, E_{bn}, E_{cn} = \text{line-to-neutral voltages} = \text{phase voltages}$$
$$I_a, I_b, I_c = \text{line currents or phase currents}$$

Let us write a Kirchhoff's voltage law (KVL) for a closed path around the buses *a*, *b*, and *n* for the three-phase system of Fig. 2.14. We have:

$$E_{ab} = E_{an} - E_{bn} \tag{2.21}$$

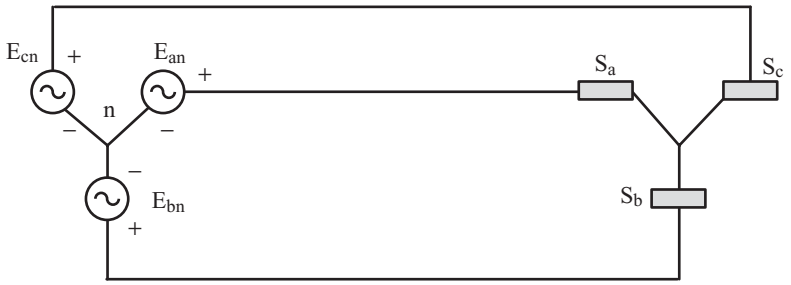

Figure 2.12 A Balanced Three-Phase Three-Wire Distribution System.

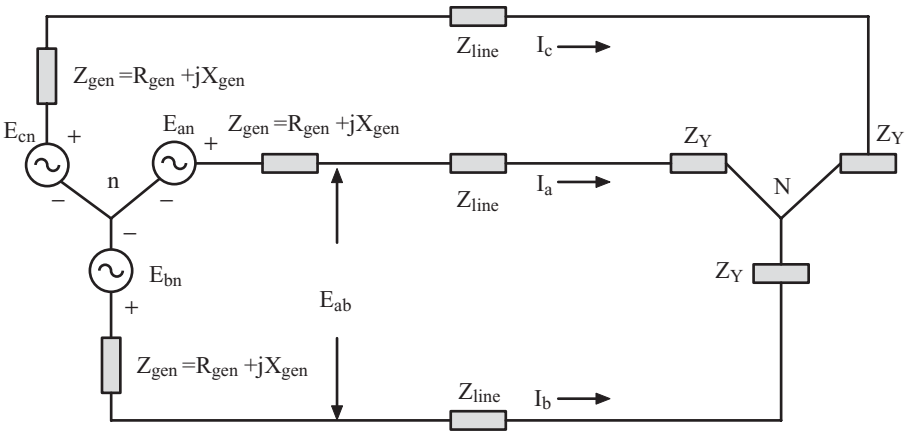

Figure 2.13 A Balanced Three-Phase System.

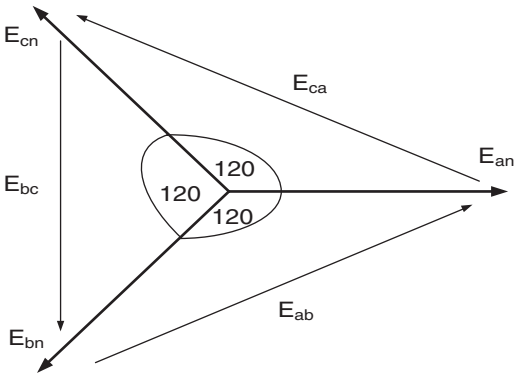

Figure 2.14 Phase Voltages and Line-Line Voltages.

Therefore, for line-line voltages, we have:

$$E_{ab} = E\angle 0 - E\angle -120 = E - E\,(-1 - j\sqrt{3})/2$$
$$E_{ab} = \sqrt{3}\,E\,(\sqrt{3} + j\,1)/2 = \sqrt{3}\,E\angle 30 \text{ volts}$$
$$E_{bc} = E_{bn} - \mathrm{E_{cn}} = \mathrm{E}\angle -120 - \mathrm{E}\angle 120 = \sqrt{3}\,E\angle -90 \tag{2.22}$$

Therefore, we have:

$$E_{ab} + E_{bc} + E_{ca} = 0 \tag{2.23}$$
$$E_{an} + E_{bn} + E_{cn} = 0 \tag{2.24}$$

Let us assume that we have a balanced three-phase system with balanced loads; therefore, we have:

$$I_a = E_{an}/Z_Y,\ I_b = E_{bn}/Z_Y,\ I_c = E_{cn}/Z_Y \tag{2.25}$$

Because the source voltages are balanced and the loads are balanced, the resulting currents are also balanced and we have:

$$I_a + I_b + I_c = 0 \tag{2.26}$$

Let us consider the balanced three-phase Δ loads as given in Fig. 2.15.

We have the following phase currents (Δ currents).

$$I_{AB} = E_{ab}/Z_\Delta$$
$$I_{BC} = E_{bc}/Z_\Delta \tag{2.27}$$
$$I_{CA} = E_{ca}/Z_\Delta$$

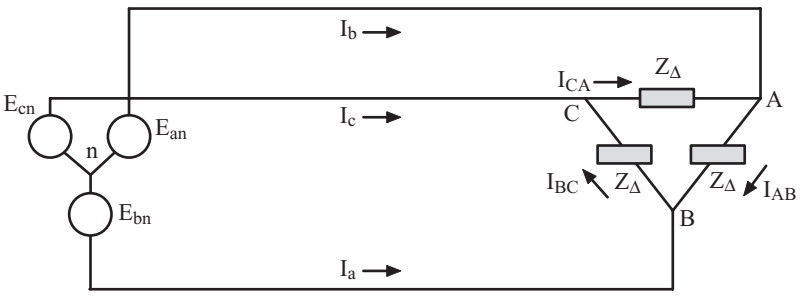

Figure 2.15 A Balanced Δ Load System.

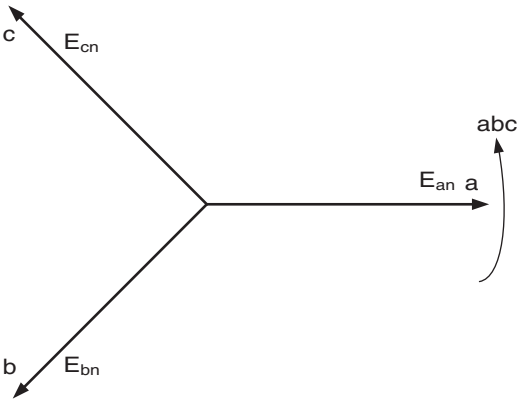

Figure 2.16 A Balanced Three-Phase System.

Recall that the voltages are balanced, therefore

$$E_{an} = E \angle 0$$
$$E_{bn} = E \angle -120$$
$$E_{cn} = E \angle 120$$

or

$$E_{ab} = \sqrt{3}\, E_{an} \angle 30° = \sqrt{3}\, E \angle 30°$$
$$E_{bc} = \sqrt{3}\, E_{bn} \angle (30-120)° = \sqrt{3}\, E \angle -90°$$
$$E_{ca} = \sqrt{3}\, E_{cn} \angle (30+120)° = \sqrt{3}\, \mathrm{E} \angle 150° \qquad (2.28)$$

We designate the phases as shown in Fig. 2.16 as positive sequence voltages. That is, we select phase a as a reference voltage, and it is followed by phase b with 120° out of phase and phase c with 240° out of phase from phase a. The phase currents, I_{AB}, I_{BC}, and I_{CA} are also balanced because the loads are balanced as shown by Equation 2.29.

$$I_{AB} = \sqrt{3}\, E \angle 30° / Z_{\Delta}$$
$$I_{BC} = \sqrt{3}\, E \angle -90° / Z_{\Delta} \qquad (2.29)$$
$$I_{CA} = \sqrt{3}\, E \angle 150° / Z_{\Delta}$$

Let us assume the following data for the system depicted in Fig. 2.15.

$$E = 10\, V, Z_{\Delta} = 5 \angle 30° \, \Omega,$$

Then, we have:

$$I_{AB} = \sqrt{3}\ (2) \angle 0° = 3.464 \angle 0°\ A$$
$$I_{BC} = \sqrt{3}\ (2) \angle -120° = 3.464 \angle -120°\ A$$
$$I_{CA} = \sqrt{3}\ (2) \angle 120° = 3.464 \angle 120°\ A$$

The line currents can be determined by using Kirchhoff's current law at each node of the Δ load.

$$I_a = I_{AB} - I_{CA} = 3.464 \angle 0° - 3.464 \angle 120° = \sqrt{3}\ (3.464 \angle -30°)$$
$$I_b = I_{BC} - I_{AB} = 3.464 \angle -120° - 3.464 \angle 0° = \sqrt{3}\ (3.464 \angle -150°)$$
$$\mathrm{I_c = I_{CA} - I_{BC}} = 3.464 \angle 120° - 3.464 \angle -120° = \sqrt{3}\ (3.464 \angle 90°)$$

Note that the Δ currents, I_{AB}, I_{CA}, I_{BC} are balanced and the line currents, I_a, I_b, and I_c are also balanced. Therefore, $I_{AB} + I_{CA} + I_{BC} = 0$ and the neutral current ($I_a + I_b + I_c = 0$) is always zero for a Δ-connected load.

For a balanced Δ load supplied by a balanced positive sequence source, we have:

$$I_a = \sqrt{3}\ I_{AB} \angle -30°$$
$$I_b = \sqrt{3}\ I_{BC} \angle -30°$$
$$I_c = \sqrt{3}\ I_{CA} \angle -30°$$

$|I_{line}| = (\sqrt{3} I_{\Delta})$ Line currents lag the Δ load currents by 30°.

We can change a Δ-connected load to its Y-equivalent loads as shown in Fig. 2.18.

Assume balanced voltages are applied to two loads so that the line currents are equal.

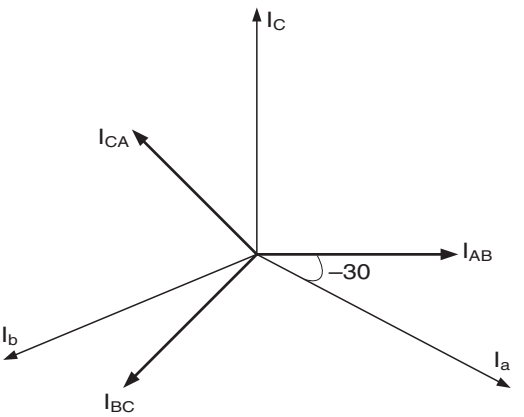

Figure 2.17 The Line and Phase Currents in a Δ-Connected Load.

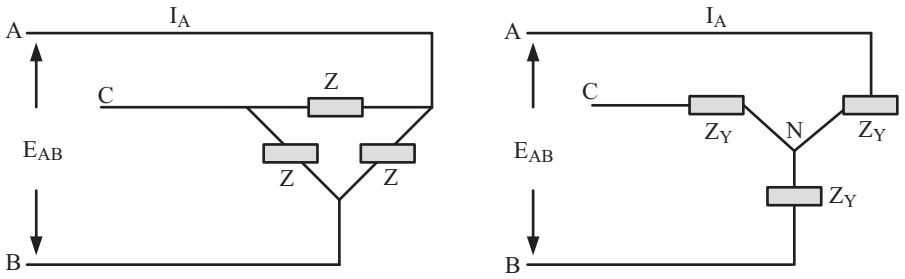

Figure 2.18 Δ-Connected Loads and Equivalent Y-Connected Loads.

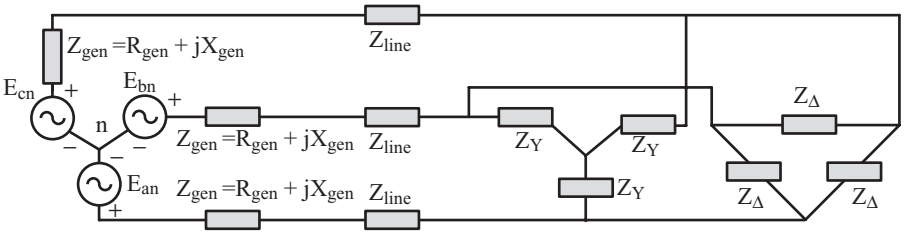

Figure 2.19 A Three-Phase System with Two Loads.

For a Δ-connected load, we have

$$I_A = \sqrt{3}\, I_{AB} \angle -30° = \sqrt{3}\, E_{AB} \angle -30° / Z_\Delta \tag{2.30}$$

For a Y-connected load, we have

$$I_A = E_{AN} / Z_Y = E_{AB} \angle -30° / \sqrt{3}\, Z_Y; \quad \text{Note: } E_{AN} = E_{AB} / \sqrt{3} \tag{2.31}$$

Since $\sqrt{3}\, E_{AB} \angle -30° / Z_\Delta = E_{AB} \angle -30° / \sqrt{3}\, Z_Y$, then we have

$$3\, Z_Y = Z_\Delta \text{ and } Z_Y = Z_\Delta / 3$$

The three-phase system with its three-phase loads can be represented by a one-line diagram. For example, Fig. 2.19 depicts a balanced three-phase system with Y- and Δ-connected loads.

We can represent the system depicted in Fig. 2.19 with a one-line diagram (Fig. 2.20).

In a single-line diagram, the voltages are given as line-to-line voltage and power consumption is specified for all three phases. We can represent the one phase equivalent circuit with line to neutral and power consumption per phase. Figure 2.21 depicts the one-phase equivalent circuit of Figs. 2.19 and 2.20.

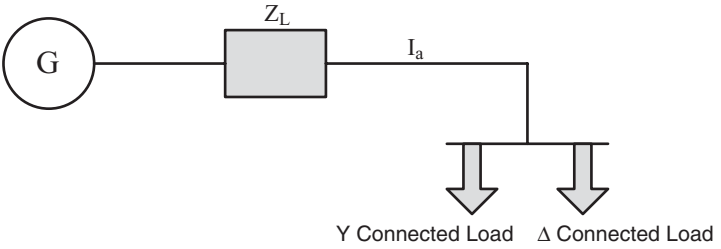

Figure 2.20 A One-Line Diagram of Fig. 2.19.

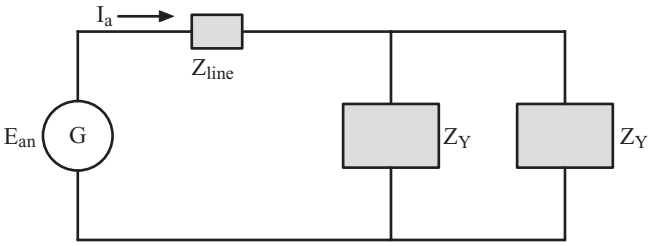

Figure 2.21 One-Phase Equivalent Circuit of Fig. 2.19.

If we closely study the three-phase systems, we recognize that the three-phase systems are three single-phase systems. Therefore, the three-phase systems can distribute three times as much as power as a single-phase system.

$$S_{3\phi} = 3S_{\phi} = 3V_{\phi}I_{\phi}^{*} \tag{2.32}$$

However, because the phase voltage is equal to the line-to-neutral voltage and line-to-line voltage is computed as

$$V_{L-L} = \sqrt{3}V_{L-N} = \sqrt{3}V_{\phi} \tag{2.33}$$

Therefore, the three-phase power can be expressed as

$$S_{3\phi} = \sqrt{3}V_{L-L}I_L^{*} = P_{3\phi} + j\,Q_{3\phi} \tag{2.34}$$

For three-phase Y-connected systems, we have

$$P_{3\phi} = \sqrt{3}V_{L-L}I_L\cos\theta \tag{2.35}$$

$$Q_{3\phi} = \sqrt{3}V_{L-L}I_L\sin\theta \tag{2.36}$$

Also, we can write complex power as

$$S_{3\phi} = \sqrt{(P_{3\phi}^2 + Q_{3\phi}^2)} \tag{2.37}$$

$$P_{3\phi} = S_{3\phi} \cos\theta \tag{2.38}$$

$$Q_{3\phi} = S_{3\phi} \sin\theta \tag{2.39}$$

$$\text{and the p.f. is expressed as p.f.} = \cos\theta\text{, lagging or leading} \tag{2.40}$$

We always need to define the p.f. with its designation of leading or lagging. When we express the *p.f.* as a lagging p.f., we are stating that the current of the load lags the voltage with load voltage as the reference voltage. It also follows that the p.f. can be expressed as

$$\text{p.f.} = \cos\theta = \frac{P}{|S|} \qquad \text{leading or lagging} \tag{2.41}$$

For a lagging p.f. the reactive power, Q, is positive. Therefore, the load consumes reactive power and the phase angle, θ is positive. Similarly, for a leading p.f., the reactive power, Q, is negative. Therefore, the load generates reactive power and the load is a capacitive load, and the angle, θ is negative. In the following examples, we need to use complex number operations. Refer to Appendix A on complex algebra operations.

Example 2.1 Consider a three-phase 480 V, 300 kVA load with p.f. = 0.9 lagging, what is the active, reactive, and complex power of the load?

Solution
We have the following known data:

$$|S| = 300 \text{ kVA}$$

$$\text{p.f.} = \cos\theta = 0.9 \qquad \text{lagging}$$

In this example, we like to compute P, Q, from S.

We know that $S_{3\phi}$ and the p.f.; hence, we can compute $P_{3\phi}$.

$$P_{3\phi} = |S_{3\phi}| \cos\theta = 300 \times 0.9 = 270 \text{ kW}$$

$$Q_{3\phi} = |S_{3\phi}| \sin\theta = 300 \times 0.4359 = 130.77 \text{ kVAr}$$

$Q > 0$ because p.f. is lagging.

$$S = 270 + j\,130.77 = 300 \angle \cos^{-1}(0.9) \text{ kVA}$$

Example 2.2 Consider a three-phase 480 V, 240 kW load with p.f. = 0.8 lagging, what is the active, reactive, and complex power of the load?

Solution
We have the following known data:

$$P = 240 \text{ kW}$$
$$\text{p.f.} = \cos\theta = 0.8 \qquad \text{lagging}$$

We can compute Q and S from P.

$$|S| = P/\cos\theta = 240/0.8 = 300 \text{ kVA}$$
$$Q_{3\phi} = |S_{3\phi}|\sin\theta = 300 \times 0.6 = 180 \text{ kVAr}$$

$Q > 0$ because p.f. is lagging.

$$S = 270 + j\ 180 = 300 \angle \cos^{-1}(0.8) \text{ kVA}$$

Example 2.3 Consider a three-phase 480 V, 180 kVA load with p.f. = 0.0 leading, what is the active, reactive, and complex power of the load?

Solution
We have the following data:

$$|S| = 180 \text{ kVA}$$
$$\text{p.f.} = \cos\theta = 0.0 \text{ leading}$$

To compute: P, Q, from S, we can compute $P_{3\phi}$ as

$$P_{3\phi} = |S_{3\phi}|\cos\theta = 180 \times 0.0 = 0$$
$$Q_{3\phi} = |S_{3\phi}|\sin\theta = 180 \times (-1) = -180 \text{ kVAr}$$

$Q < 0$ because the p.f. is leading.

$$S = 0 - j\ 180 = 180 \angle -90° \text{ kVAr}$$

2.4 LOAD MODELS

We can represent an inductive load by its impedance as shown in Fig. 2.22.

The load impedance, Z_L is an inductive load. Most power system loads are inductive. The majority of industrial, commercial, and residential motors are

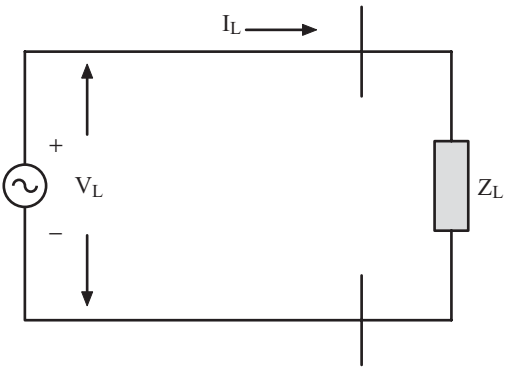

Figure 2.22 The Inductive Impedance Load Model.

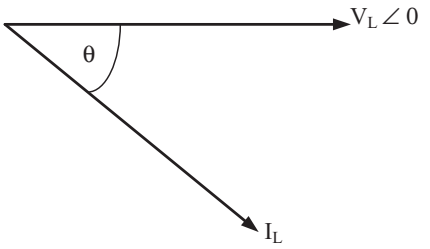

Figure 2.23 The Load Voltage and Its Lagging Load Current for Inductive Load Depicted in Fig. 2.22.

of the induction type. In Fig. 2.22, the load voltage; V_L is a line-to-neutral voltage and I_L is the phase current supplying the load.

$$Z_L = R_L + j\,\omega L = R + j\,X_L = |Z_L|\angle\theta \tag{2.42}$$
$$|Z_L| = \sqrt{R^2 + X_L^2},\ \theta = \tan^{-1}\left(\frac{X_L}{R}\right)$$

The inductive load power representation is expressed by active and reactive power consumption of the load.

$$I_L = \frac{V_L\angle 0}{Z_L\angle\theta} = I_L\angle -\theta,\ I_L = \frac{|V_L|}{|Z_L|}\angle -\theta \tag{2.43}$$

With the load voltage as the reference (i.e., $V_L = |V_L|\angle 0$), the load current lags the voltage as shown in Fig. 2.23.

The complex power absorbed by a load can be expressed as

$$S_L = V_L I_L^* = V_L (I_L \angle -\theta)^* = |V_L||I_L|\cos\theta + j|V_L||I_L|\sin\theta \quad (2.44)$$
$$S_L = |V_L||I_L| \text{ VA}$$
$$P = |V_L||I_L|\cos\theta \text{ W}$$
$$Q = |V_L||I_L|\sin\theta \text{ VAr}$$

And the complex power is expressed as

$$S = P + j\,Q, \text{ where } \theta = \tan^{-1}\frac{Q}{P} \text{ and p.f.} = \cos\theta, \text{ lagging}$$

An inductive load model power representation is shown in Fig. 2.24.

Figure 2.24 depicts inductive load consumption of both active and reactive power.

Figure 2.25 depicts the capacitive impedance load model. Here, again, the load voltage is line-to-neutral and the reference and load current is the phase current supplied to the load.

$$Z_L = R - j\,X_c = |Z_L| \angle -\theta \quad (2.45)$$
$$|Z_L| = \sqrt{R^2 + X_c^2},\ \theta = \tan^{-1}\left(\frac{X_c}{R}\right)$$
$$I_L = \frac{V_L \angle 0}{Z_L \angle -\theta} = I_L \angle \theta, |I_L| = \frac{|V_L|}{|Z_L|} \angle \theta$$

With the load voltage as the reference (i.e., $V_L = |V_L| \angle 0$), the load current leads the voltage as shown in Fig. 2.26.

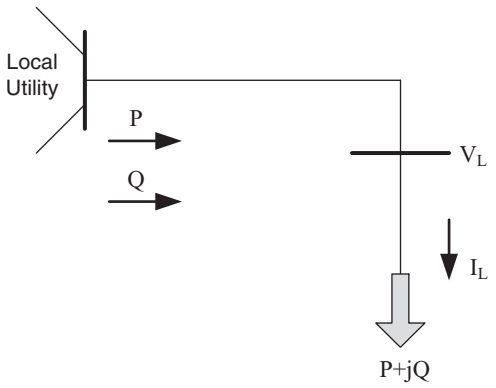

Figure 2.24 The Inductive Load–Power Representation.

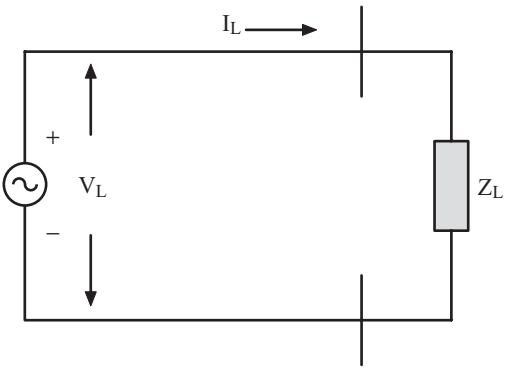

Figure 2.25 The Capacitive Impedance Load Model.

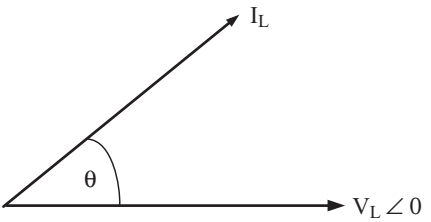

Figure 2.26 The Load Voltage and Current of a Capacitive Load.

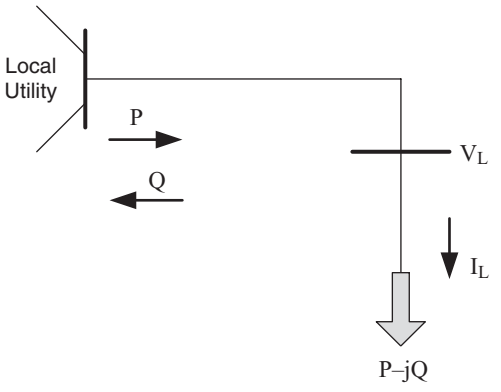

Figure 2.27 The Power Model for a Capacitive Load.

The complex power absorbed by the load is

$$S_L = V_L I_L^* = V_L (I_L \angle \theta)^* = V_L I_L \angle -\theta = |V_L||I_L|\cos\theta - j|V_L||I_L|\sin\theta$$

$$S = P - jQ, \theta = \tan^{-1}\left(\frac{Q}{P}\right) \text{ and power factor p.f.} = \cos\theta, \text{ leading} \qquad (2.46)$$

Therefore, the load model can be represented as

Therefore, the active power is consumed by the load and reactive power is supplied by the capacitive load to the local power network. Recently, more variable-speed drive systems are controlled by power converters, which control many types of motors. In addition, more power electronic loads have penetrated the power systems. These types of loads act as nonlinear loads and can act both as inductive and capacitive loads during their transient and steady state operations. The p.f. correction and voltage control and stability are active areas of research.

Example 2.4 For a single-phase inductive load, given below in Fig. 2.28, compute the line current.

Solution

$$kVA = |V||I_L| \times 10^3$$

$$|I_L| = 40 \times 10^3 / 220 = 181.8$$

$$I_L = 181.8 \angle -25.8° \text{ A}$$

Example 2.5 For a three-phase inductive load given in Fig. 2.29, compute the line current.

Solution

$$kVA_{3\phi} = 2000 \qquad V_{L-L} = 20 \text{ kV}$$

$$kVA = \sqrt{3} V_{L-L} I_L$$

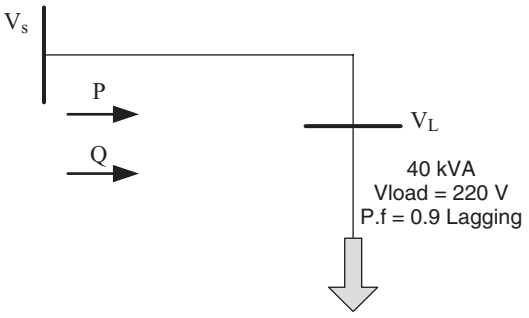

Figure 2.28 The Power Model for Example 2.4.

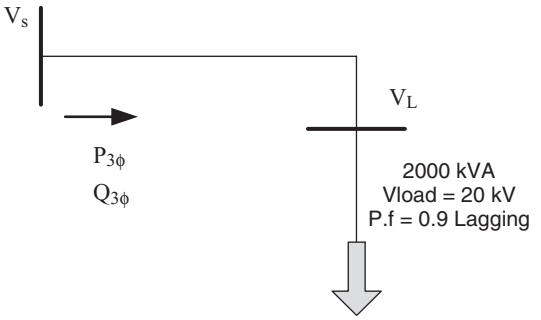

Figure 2.29 The Power Model for Example 2.5.

Figure 2.30 A Generator Operating with a Lagging Power Factor.

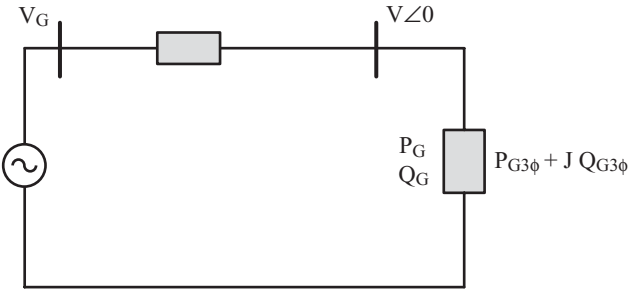

Figure 2.31 The Equivalent Circuit for the Example 2.6.

$$|I_L| = 2000/\sqrt{3} \times 20 = 57.8 \text{ A} \qquad I_L = 57.8\angle -25.8°$$

$$P_{3\phi} = kW = kVA\cos\theta = 2000 \times 0.9 = 1800 \text{ kW}$$

$$Q_{3\phi} = kVar = kVA\sin\theta = 2000 \times \sin(25.8°) = 870.46 \text{ kVAr}$$

Example 2.6 Consider the generator in Fig. 2.30 that is operating with a lagging power factor. Compute the active and reactive power supplied to the system.

Figure 2.31 depicts the equivalent circuit model of Fig. 2.30; Fig. 2.32 presents the generator voltage and the generator current.

$$S_{3\phi} = 3V_G I_G^* = P_{G3\phi} + j\, Q_{G3\phi}$$

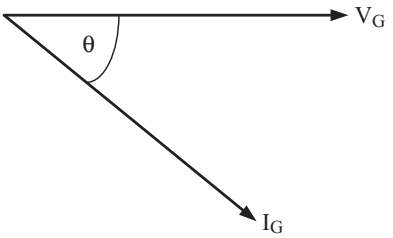

Figure 2.32 The Phasor Relationship of V_G and I_G.

2.5 TRANSFORMERS IN ELECTRIC POWER GRIDS

Two facts are clear by now. The transmitted power is the product of the voltage and the current. Losses in a transmission line are the square of current through the lines multiplied by the line resistance. Therefore, the transmission of a large amount of power at low voltages would have a very large power loss. For high power transmission, we need to raise the voltage and to lower the current. This problem was solved with the invention of transformers.

2.5.1 A Short History of Transformers

In the "War of Currents"[3] in the late 1880s, George Westinghouse[1] (1846–1914) and Thomas Edison (1847–1931) were at odds over Edison's promotion of direct current (DC) for electric power distribution and Westinghouse's advocacy of alternating current (AC), which was also Tesla's choice.[3] Because Edison's design was based on low-voltage DC, power losses in the distribution network were too high. Lucien Gaulard of France and John Gibbs of England[1] demonstrated the first AC power transformer in 1881 in London.[1] This invention attracted the interest of Westinghouse, who then used Gaulard–Gibbs transformers and a Siemens AC generator in his design of an AC network in Pittsburgh. Westinghouse understood that transformers are essential for electric power transmission because they ensure acceptable power losses. By stepping up the voltage and reducing the current, power transmission losses are lessened. Ultimately, Westinghouse established that AC power was more economical for bulk power transmission and started the Westinghouse Company to manufacture AC power equipment.

2.5.2 Transmission Voltage

In early 1890, the power transmission voltage was at 3.3 kV. By 1970, power transmission voltage had reached a level of 765 kV. The standard operating voltages in the secondary distribution system are a low voltage range of 120 to 240 V for single-phase and 208 to 600 V for three-phase. The primary power distribution voltage has a range of 2.4 kV to 20 kV. The subtransmission voltage has a range of 23 kV up to 69 kV. The high-voltage transmission has

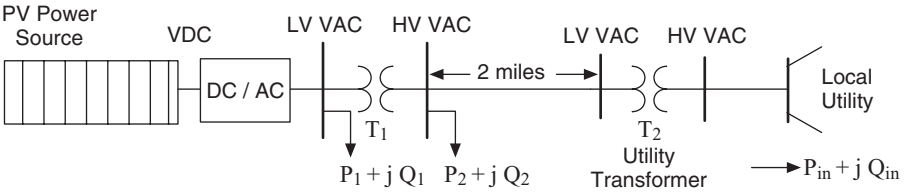

Figure 2.33 A Photovoltaic Power Source Feeding a Radial Distribution System.

a range of 115 kV to 765 kV. The generating voltages are in the range of 3.2 kV to 22 kV. The generating voltage is stepped-up to the high voltage for bulk power transmission, then stepped-down to subtransmission voltage as the power system approaches the load centers of major metropolitan areas. The distribution system is used to distribute the power within the cities. The residential, commercial, and industrial loads are served at 120–600 V voltage levels.[9,10]

Figure 2.33 depicts a typical PV power source feeding a local distributed generation system. The PV panels are like batteries and are the source of DC power. They are connected in series and in parallel. The maximum operating DC voltage is 600 V. With the current DC technology of distribution, megawatts of power distribution are very expensive. If we distribute high DC power of a renewable source such as PV systems at low voltages, power losses through the distribution lines are quite high. We can step-up by using DC/DC converters (i.e., boost converters). However, the costs of associated DC/DC converters and for the protection of a DC system are quite high. In the design of the system shown in Fig. 2.33, the DC power is converted to AC using a DC/AC inverter. We will study the sizing of power converters and the design of a PV system in the next chapter.

In Fig. 2.33, the PV source is in a range of 3 to 5 kVA; it is connected to a 120 V residential system feeding the house loads. We have stepped-up the voltage before transferring the extra power to the local power grid company.

2.5.3 Transformers

A transformer is an element of a power grid that transfers electric power from one voltage level to another through inductively coupled windings. For a single-phase transformer, each winding is wound around a single core. The two windings are magnetically coupled using the same core structure. As in an ideal transformer, the device input power is the same as its output power. This means that the input current multiplied by the input voltage is equal to the product of the output voltage and output current. One of the windings is excited by an AC source. The time-varying magnetic field induces a voltage in the second winding by Faraday's fundamental law of induction.[8–13]

In a transformer, the volt per turn on the secondary winding is the same as in the primary winding. We can select the ratio of turns, to step up the voltage

or to step it down. For high-voltage power transmission, transformers are needed to step up the voltage and therefore to step down the current and reduce the transmission line power losses. Figure 2.34 depicts an ideal transformer. An ideal transformer is assumed to have zero power losses in its core and winding.

$$N_1 I_1 = N_2 I_2 \qquad \text{Ampere} - \text{Turn} \tag{2.47}$$

$$\frac{V_1}{N_1} = \frac{V_2}{N_2} \qquad \text{Volt / Turn} \tag{2.48}$$

In Fig. 2.34, ϕ_m depicts the mutual flux linkage and ϕ_{l1} and ϕ_{l2} the leakage flux on either side of the transformer. The mutual flux linkage will result in the mutual inductance and the leakage flux will result in leakage inductance.

The schematic of an ideal transformer is depicted in Fig. 2.35. Because the power losses in an ideal transformer are assumed to be zero, the input power and output power are the same.

$$S_1 = V_1 I_1^* = S_2 = V_2 I_2^* \tag{2.49}$$

A real transformer has both core and winding losses as shown in Fig. 2.36. These losses are represented by R_1 and R_2. Here, in this representation, R_1 represents the primary-side ohmic loss and R_2 denotes the secondary-side ohmic loss.

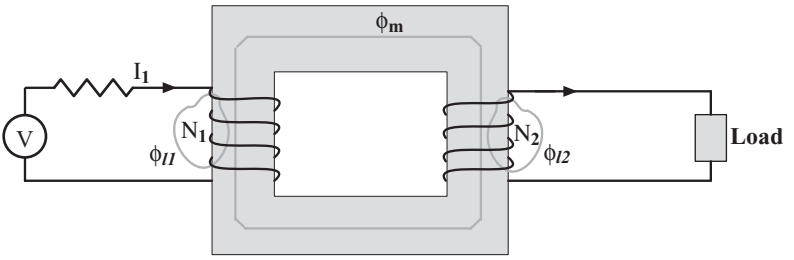

Figure 2.34 An Ideal Single-Phase Transformer.

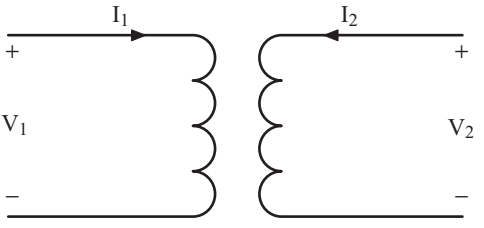

Figure 2.35 The Schematic of an Ideal Transformer.

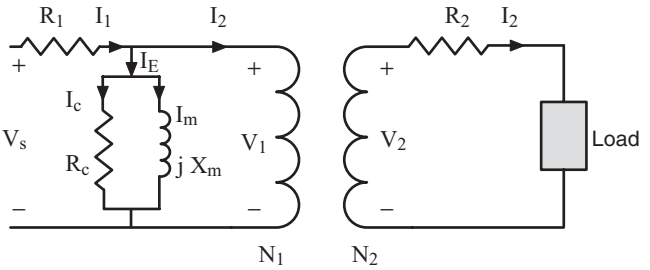

Figure 2.36 The Schematic of a Real Transformer.

It is customary to denote the side that is connected to the source as primary and the side connected to the load as secondary. For simplicity, we will number each side or call each side by their voltage levels, i.e., one side of the transformer is the high-voltage side and the other side is the low-voltage side.

$$I_E = I_m + I_C$$

$$X_m = \omega L_m \tag{2.50}$$

$$N_1 I_2' = N_2 I_2 \tag{2.51}$$

The current I_E is referred to as the excitation current. This current has two components, I_m and I_C. The current I_m is referred to as the magnetizing current and I_c, as the core current. In Equation 2.50, L_m denotes the magnetizing inductance. This inductance is computed from the mutual inductance and the inductance of each coil.

$$V_s = V_m \cos \omega t \tag{2.52}$$

$$\overline{V}_s = \frac{V_m}{\sqrt{2}} \angle 0$$

$$I_m = \frac{V_s \angle 0°}{jX_m} = \frac{V_s}{X_m} \angle -90° \tag{2.53}$$

In AC power distribution, the source voltage can be presented by Equation 2.52. The magnetizing current is computed as presented by Equation 2.53. Figure 2.37 depicts the complete transformer model. In this model, we have shown both sides of the transformer primary resistance and primary leakage reactance and on the secondary side, we have shown the secondary-side leakage reactance and winding resistance. The core losses and magnetizing reactance are represented by the resistance R_C and the reactance X_m and they are shown on the primary side.

$$X_p = \omega_e L_{lp},\ X_s = \omega_e L_{ls} \text{ and } X_m = \omega_e L_m$$

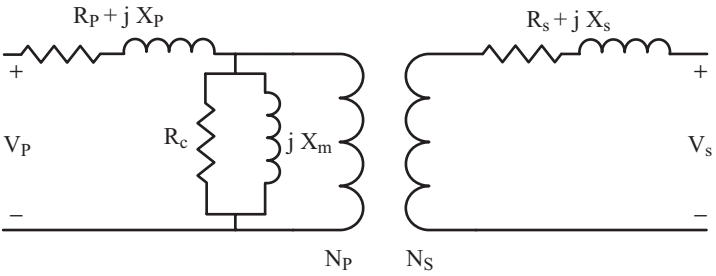

Figure 2.37 The Complete Schematic of a Real Transformer.

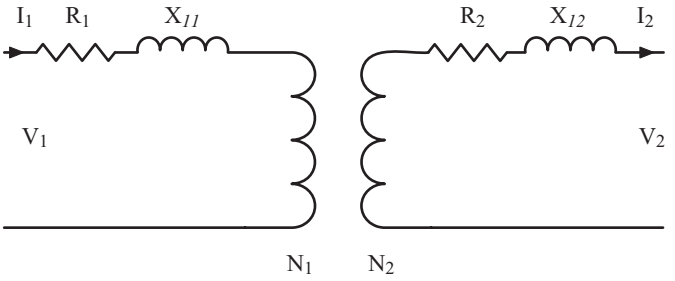

Figure 2.38 The Equivalent Model of a Transformer for Voltage Analysis.

where L_{lp}, L_{ls}, and L_m are referred to as leakage inductance of primary winding, leakage inductance of secondary winding, and the mutual inductance of the transformer, respectively. Because the transformers are designed to have very small exciting current—in the range of 2 to 5% of the load current, the magnetizing shunt elements of transformers are assumed to have very high impedance; therefore, the shunt elements are eliminated in the voltage calculation of transformers. Figure 2.38 depicts the transformer model used in voltage analysis.

In Fig. 2.38, the resistance, R_1, denotes the winding resistance of winding number one and X_{l1} denotes the leakage reactance of the same winding. Similarly, R_2 and X_{l2} denote the resistance and leakage reactance of the winding number 2. In this representation, designation of primary winding and secondary winding are omitted because in general, either side can be connected to the load or source.

Figure 2.39 depicts the equivalent transformer model of Fig. 2.38, where the impedance of both windings is referred to side 1. Let us assume side 1 of a transformer connected to the high voltage side and the side 2 to the low voltage side. Then, Fig. 2.39 can be relabeled as:

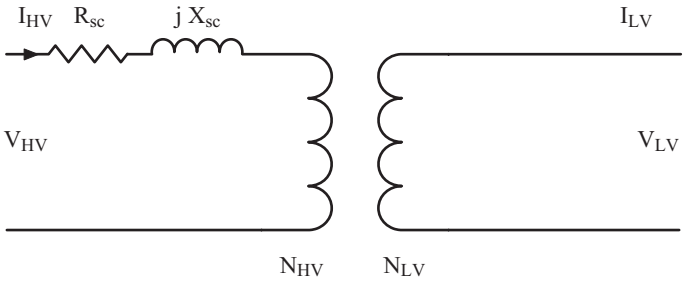

Figure 2.39 The Equivalent Model of a Transformer.

The above equivalent circuit model can be described by the following equations.

$$\frac{V_{HV}}{N_{HV}} = \frac{V_{LV}}{N_{LV}} \qquad \text{Volt per Turn} \tag{2.54}$$

$$N_{HV}\, I_{HV} = N_{LV}\, I_{LV} \qquad \text{Ampere} - \text{Turn} \tag{2.55}$$

The terms R_{sc} and X_{sc} are referred to the short-circuit resistance and the short-circuit reactance of the transformer. These two terms are computed from the short-circuit tests on the transformer. The short-circuit test is performed by shorting one side of the transformer and applying a voltage in the range of 5 to 10% of the rated voltage and measuring the short-circuit current. The applied voltage is adjusted such that the measured short-circuit current is equal to the rated load current. We can think of the short-circuit test as a load test because the test reflects the rated load condition.

$$Z_{sc} = R_{sc} + j\, X_{sc} \tag{2.56}$$

$$R_{sc} = R_1 + a^2\, R_2 \tag{2.57}$$

$$X_{sc} = X_{11} + a^2\, X_{12} \tag{2.58}$$

where $a = \dfrac{V_{HV}}{V_{LV}} = \dfrac{N_{HV}}{N_{LV}}$

2.6 MODELING A MICROGRID SYSTEM

As part of our objective in this chapter, we will now develop a model representing a microgrid system (Fig. 2.40).

In Fig. 2.40(b), we have presented the PV system and DC/AC invert by PV power source. We will discuss the modeling of a PV system and the inverter in later sections.

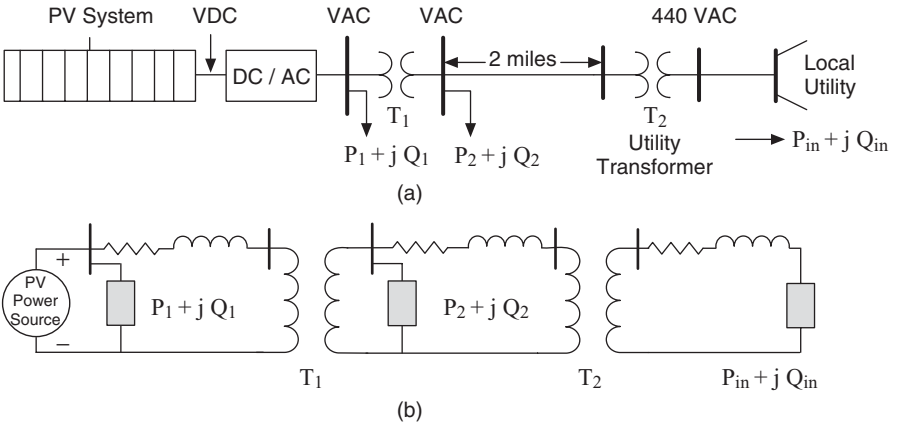

Figure 2.40 (a) One-Line Diagram of a Radial Distribution Feeder. (b) The Impedance Model Diagram for a Radial Microgrid Distribution Feeder.

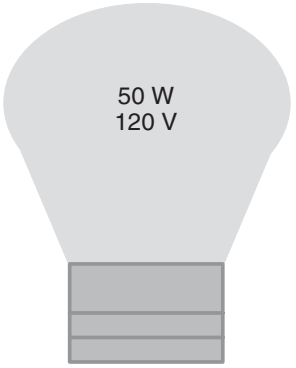

Figure 2.41 The Rated Values of a Light Bulb.

Calculating the voltage at the load using the model shown in Fig. 2.40(b) requires a number of calculations because of the many transformers involved and the need to be aware of which sides of the transformers we are analyzing. First, we need to eliminate the transformers from the above model. To do this, we will normalize the system base on a common base voltage and current. To understand this normalizing method, we present the per unit system.

2.6.1 The Per Unit System

Before we present the concept of the per unit system (p.u), we introduce the concept of the rated values or nominal values.[9,10] To understand the rated values, let us think of a light bulb. For example, consider a 50 W light bulb. The power and voltage ratings are stamped on the light bulb as shown in Fig. 2.41.

The manufacturer of the light bulb is telling us that if we apply 120 volts across the light bulb, we will consume 50 watts. From the above values, we can calculate the impedance of the light bulb.

$$R_{Light\_bulb} = \frac{V^2}{P} = \frac{(120)^2}{50} = \frac{14400}{50} = 288\ \Omega$$

We also know that if we apply 480 volts to the light bulb, which is four times the rated value, then we will have a bright glow and possibly the light bulb will explode. Therefore, the rated values tell us the safe operating condition of an electrical device.

Let us set the following values:

$$P_{base} = 50\ \text{W} = P_{rated}$$
$$V_{base} = 120\ \text{V} = V_{rated}$$

Now let us use these values and normalize the operating condition of the light bulb:

$$P_{p.u} = \frac{P_{actual}}{P_{base}} \tag{2.59}$$

$$V_{p.u} = \frac{V_{actual}}{V_{base}} \tag{2.60}$$

Therefore, for our light bulb we have

$$P_{p.u} = \frac{50}{50} = 1.0\ \text{p.u W}$$

$$V_{p.u} = \frac{120}{120} = 1.0\ \text{p.u V}$$

Therefore, one per unit represents the full load or rated load. Let's assume that we apply 480 V across the light bulb.

$$V_{p.u} = \frac{480}{120} = 4.0\ \text{p.u V}$$

The per unit (p.u) voltage applied to the load is 4 p.u or 4 times the rated voltage.

When we say a device is loaded at half load, the per unit load is 0.5 p.u. If we say the applied voltage is 10% above the rated voltage, we mean 1.10 p.u volts.

In general the per unit system, the voltages, currents, powers, impedances, and other electrical quantities are expressed on a per unit basis.

$$Quantity\ per\ unit = \frac{Actual\ Value}{Base\ Value\ of\ Quantity} \tag{2.61}$$

It is customary to select two base quantities to define a given per unit system. We normally select voltage and power as base quantities.

Let us assume

$$V_b = V_{rated} \tag{2.62}$$

$$S_b = S_{rated} \tag{2.63}$$

Then, base values are computed for currents and impedances:

$$I_b = \frac{S_b}{V_b} \tag{2.64}$$

$$Z_b = \frac{V_b}{I_b} = \frac{V_b^2}{S_b} \tag{2.65}$$

And the per unit system values are

$$V_{p.u} = \frac{V_{actual}}{V_b} \tag{2.66}$$

$$I_{p.u} = \frac{I_{actual}}{I_b} \tag{2.67}$$

$$S_{p.u} = \frac{S_{actual}}{S_b} \tag{2.68}$$

$$Z_{p.u} = \frac{Z_{actual}}{Z_b} \tag{2.69}$$

$$Z\% = Z_{p.u} \times 100\% \qquad \text{Percent of base } Z \tag{2.70}$$

Example 2.7 An electrical lamp is rated 120 volts, 500 watts. Compute the per unit and percent impedance of the lamp. Give the p.u equivalent circuit.

Solution

We compute lamp resistance from the rate power consumption and rated voltage as

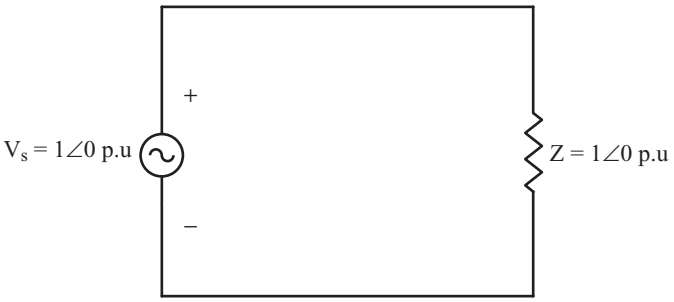

Figure 2.42 The Equivalent Circuit of Example 2.7.

$$P = \frac{V^2}{R} \Rightarrow R = \frac{V^2}{P} = \frac{(120)^2}{500} = 28.8\ \Omega$$

$$\text{p.f.} = 1.0 \qquad Z = 28.8\angle 0\ \Omega$$

Select base quantities as:

$$S_b = 500\ \text{VA}$$
$$V_b = 120\ \text{V}$$

Compute base impedance

$$Z_b = \frac{V_b^2}{S_b} = \frac{(120)^2}{500} = 28.8\ \Omega$$

The per unit impedance is

$$Z_{p.u} = \frac{Z}{Z_b} = \frac{28.8\angle 0}{28.8} = 1\angle 0\ \text{p.u}$$

Percent impedance:

$$\text{Z\%} = 100\%$$

Per unit equivalent circuit is given in Fig. 2.42.

Example 2.8 An electrical lamp is rated 120 volts, 500 watts. If the voltage applied across the lamp is twice the rated value, compute the current that flows through the lamp. Use the per unit method.

Solution

$$V_b = 120 \text{ V}$$

$$V_{p.u} = \frac{V}{V_b} = \frac{240\angle 0}{120} = 2\angle 0 \text{ p.u}$$

$$Z_{p.u} = 1\angle 0 \text{ p.u}$$

The per unit equivalent circuit (see Fig. 2.43) is as follows:

$$I_{p.u} = \frac{V_{p.u}}{Z_{p.u}} = \frac{2\angle 0}{1\angle 0} = 2\angle 0 \text{ p.u A}$$

$$I_b = \frac{S_b}{V_b} = \frac{500}{120} = 4.167 \text{ A}$$

$$I_{actual} = I_{p.u}.I_b = 2\angle 0 \times 4.167 = 8.334\angle 0 \text{ A}.$$

The per unit system for a one-phase circuit is as follows:

$$S_b = S_{1-\phi} = V_\phi \, I_\phi \tag{2.71}$$

where

$$V_\phi = V_{line\text{-}to\text{-}neutral} \tag{2.72}$$

$$I_\phi = I_{line\text{-}current} \tag{2.73}$$

For transformers, we select the bases as

$$V_{bLV} = V_{\phi LV} \qquad V_{bHV} = V_{\phi HV} \tag{2.74}$$

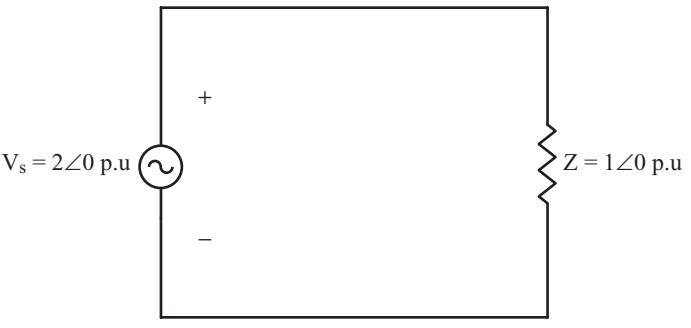

Figure 2.43 The Per Unit Equivalent Circuit of Example 2.8.

$$I_{bLV} = \frac{S_b}{V_{bLV}} \qquad I_{bHV} = \frac{S_b}{V_{bHV}} \tag{2.75}$$

The base impedances on the two sides of transformer are

$$Z_{bLV} = \frac{V_{bLV}}{I_{bLV}} = \frac{(V_{bLV})^2}{S_b} \tag{2.76}$$

$$Z_{bHV} = \frac{V_{bHV}}{I_{bHV}} = \frac{(V_{bHV})^2}{S_b} \tag{2.77}$$

$$S_{p.u} = \frac{S}{S_b} = V_{p.u} I^*_{p.u} \tag{2.78}$$

$$P_{p.u} = \frac{P}{S_b} = V_{p.u} I_{p.u} \cos\theta \tag{2.79}$$

$$Q_{p.u} = \frac{Q}{S_b} = V_{p.u} I_{p.u} \sin\theta \tag{2.80}$$

When we have two or more transformers, we need to normalize the impedance model to a common base. We will make the selections as follows:

Selection 1

$$S_{b1} = S_A \qquad V_{b1} = V_A$$

Then,

$$Z_{b1} = \frac{V_{b1}^2}{S_{b1}} \qquad Z_{pu1} = \frac{Z_L}{Z_{b1}}$$

Selection 2

$$S_{b2} = \mathrm{S_B} \qquad V_{b2} = V_B$$

Then

$$Z_{b2} = \frac{V_{b2}^2}{S_{b2}} \qquad \text{and} \qquad Z_{p.u2} = \frac{Z_L}{Z_{b2}}$$

$$\frac{Z_{p.u2}}{Z_{p.u1}} = \frac{Z_L}{Z_{b2}} \times \frac{Z_{b1}}{Z_L} = \frac{Z_{b1}}{Z_{b2}} = \frac{V_{b1}^2}{S_{b1}} \times \frac{S_{b2}}{V_{b2}^2}$$

$$Z_{p.u2} = Z_{p.u1} \left(\frac{V_{b1}}{V_{b2}}\right)^2 \times \left(\frac{S_{b2}}{S_{b1}}\right) \tag{2.81}$$

In general, the values that are given as nominal values (rated values) are referred to as "old" values and new selection as common base as "new." Using this notation, the transformation between old and new bases can be written as:

$$Z_{p.u,new} = Z_{p.u,old}\left(\frac{V_{b,old}}{V_{b,new}}\right)^2 \times \left(\frac{S_{b,new}}{S_{b,old}}\right) \tag{2.82}$$

We can use the p.u concept and define the p.u model of a transformer. Consider the equivalent circuit of transformer model referred to LV side and HV side as shown in Fig. 2.44 below.

We make the following selection for the transformer bases.

$$V_{b1} = V_{LV,rated} \tag{2.83}$$

$$S_b = S_{rated} \tag{2.84}$$

Then, we can compute the base voltage for the new common base.

$$V_{b2} = \frac{V_{HV}}{V_{LV}} V_{b1} = \frac{1}{a} V_{b1}$$

$$Z_{b1} = \frac{V_{b1}^2}{S_b} \qquad Z_{b2} = \frac{V_{b2}^2}{S_b}$$

$$\frac{Z_{b1}}{Z_{b2}} = \frac{V_{b1}^2}{V_{b2}^2} = \frac{V_{b1}^2}{\left(\frac{1}{a}V_{b1}\right)^2} = a^2$$

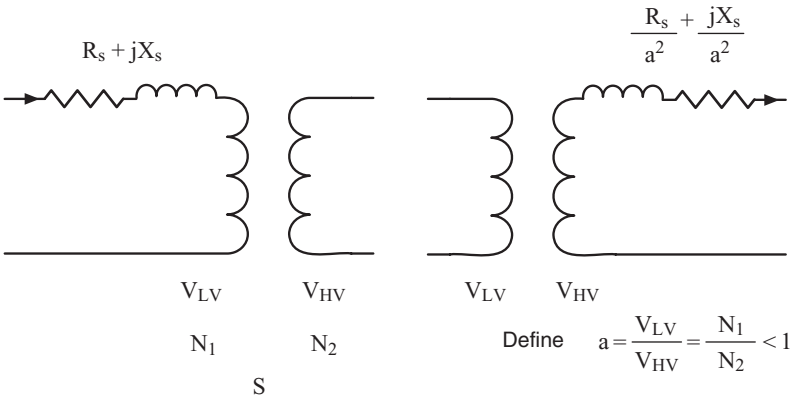

Figure 2.44 The Equivalent Circuit of a One-Phase Transformer.

Per unit impedances are

$$Z_{p.u1} = \frac{R_s + j\,X_s}{Z_{b1}}$$

$$Z_{p.u2} = \frac{\frac{R_s}{a^2} + j\,\frac{X_s}{a^2}}{Z_{b2}} = \frac{\frac{R_s}{a^2} + j\,\frac{X_s}{a^2}}{\frac{Z_{b1}}{a^2}} = \frac{R_s + j\,X_s}{Z_{b1}}$$

From the above, we can see that the p.u impedance of the transformer is identical.

$$Z_{p.u1} = Z_{p.u2}$$

The per phase equivalent of a transformer is given in Fig. 2.45, where R_s and X_s represents the parameters of a transformer referred to on the low-voltage side. $a = V_{LV}/V_{HV} = N_1/N_2 < 1$

The per unit equivalent transformer is depicted in Fig. 2.46.

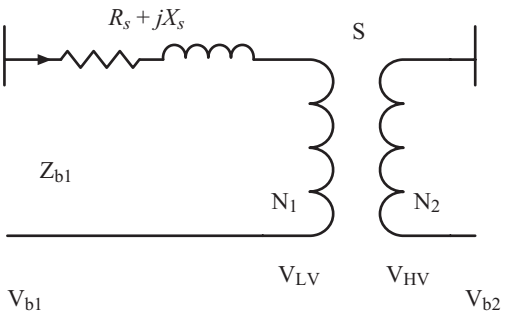

Figure 2.45 The Equivalent Circuit of a Transformer.

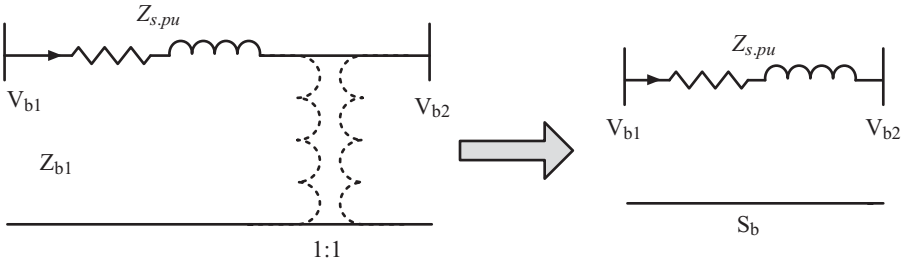

Figure 2.46 The Per Unit Equivalent Circuit of Fig. 2.45.

Example 2.9 A single-phase transformer rated 200 kVA, 200/400 V, and 10% short-circuit reactance. Compute the voltage regulation when the transformer is fully loaded at unity p.f. and rated voltage 400 V.

Solution
Let

$$V_{b2} = 400 \text{ V}$$
$$S_b = 200 \text{ kVA}$$

Then, we have

$$S_{load,p.u} = 1\angle 0 \text{ p.u kVA}$$
$$X_{s,p.u} = j0.1 \text{ p.u}$$

The per unit equivalent model is given in Fig. 2.47.
Rated Voltage:

$$V_{load,p.u} = 1\angle 0 \text{ p.u V}$$
$$I_{load,p.u} = \left(\frac{S_{load,p.u}}{V_{load,p.u}}\right)^* = \left(\frac{1\angle 0}{1\angle 0}\right)^* = 1\angle 0 \text{ p.u A}$$
$$V_{source,p.u} = V_{load,p.u} + I_{p.u}X_{s,p.u}$$
$$= 1.0\angle 0 + 1.0\angle 0 \times j0.1$$
$$= 1 + j0.1 = 1.001\angle 5.7 \text{ p.u V}$$

The p.u load voltage under load is given as

$$V_{pu,full-load} = V_{load,p.u} = 1\angle 0 \text{ p.u V}$$

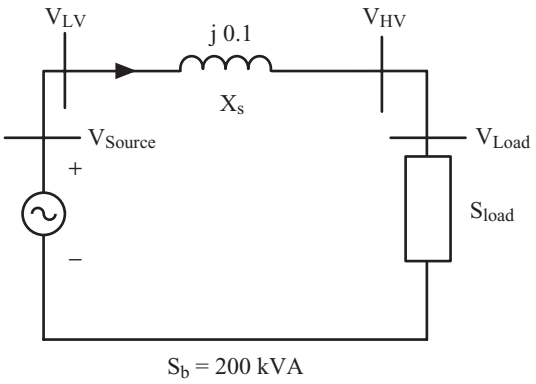

Figure 2.47 Per Unit Equivalent Circuit of Example 2.9.

When we remove the load (no-load) and set the source voltage at $1.001\angle 5.7°$ p.u, the no-load voltage is given as:

$$V_{p\cdot u,no-load} = V_{P,p.u} = 1.001\angle 5.7° \text{ p.u V}$$

Therefore, the voltage regulation (VR) by definition is given as

$$VR = \frac{|V_{p.u,no-load}| - |V_{p.u,full-load}|}{|V_{p.u,full-load}|} \times 100\%$$

And we calculate:

$$VR = \frac{1.001 - 1.0}{1.0} \times 100\% = 0.1\%$$

In the following, we extend the concepts of per unit system to the three-phase system. The extension is very simple. We will look at the three-phase system as three single-phase circuits that are connected as a three-phase system.

For three-phase systems, we select the S_b and V_b the same way as before, except the base values represent the three-phase power and the voltage base is equal to the line-to-line voltage.

$$S_b = S_{three-phase} = 3S_{1phase} \tag{2.85}$$

$$S_b = 3V_\phi I_\phi \tag{2.86}$$

Where the phase voltage is given by:

$$V_\phi = V_{line-to-neutral} = \frac{V_{L(line)}}{\sqrt{3}} \tag{2.87}$$

Therefore, we have

$$V_\phi = \frac{V_L}{\sqrt{3}} \quad \text{and} \quad I_\phi = I_{line.current} = I_L \tag{2.88}$$

From Equations 2.86 and 2.88, we have

$$S_b = 3\frac{V_L}{\sqrt{3}} I_L = \sqrt{3} V_L I_L \tag{2.89}$$

For three-phase transformers, we select the voltage bases for high voltage (HV) and low voltage (LV) as:

$$V_{bLV} = V_{L(LV)} \qquad V_{bHV} = V_{L(HV)} \tag{2.90}$$

Therefore, the base power for the three-phase system can be expressed:

$$S_b = \sqrt{3}V_{b(LV)}I_{b(LV)} = \sqrt{3}V_{b(HV)}I_{b(HV)} \tag{2.91}$$

The current base for the low voltage (LV) and the current base for the high volt (HV) are given as:

$$I_{bLV} = \frac{S_b}{\sqrt{3}V_{b(LV)}} \qquad I_{bHV} = \frac{S_b}{\sqrt{3}V_{b(HV)}} \tag{2.92}$$

As before, we define the Z_b per phase for the three-phase system. Therefore, we have

$$Z_{bLV} = \frac{V_{\phi LV}}{I_{\phi LV}} \tag{2.93}$$

and

$$V_{\phi LV} = \frac{V_{bLV}}{\sqrt{3}} \qquad I_{bLV} = \frac{S_b}{\sqrt{3}V_{b(LV)}}$$

From the above, we have

$$Z_{bLV} = \frac{V_{bLV}}{\sqrt{3}} \times \frac{\sqrt{3}V_{bLV}}{S_b}$$

and finally,

$$Z_{bLV} = \frac{(V_{bLV})^2}{S_b} \tag{2.94}$$

$$Z_{bHV} = \frac{(V_{bHV})^2}{S_b} \tag{2.95}$$

The per unit power is defined as the power of the three-phase system divided by S_b as given

$$S_{p.u} = \frac{S_{3\phi}}{S_b} = \frac{\sqrt{3}V_L I_L^*}{\sqrt{3}V_b I_b} = V_{p.u} I_{p.u}^* \tag{2.96}$$

Again, we restate the base impedance as

$$Z_b = \frac{V_{b\phi}}{I_{b\phi}} = \frac{V_{b\phi}^2}{S_{b\phi}} = \frac{3V_{b\phi}^2}{3S_{b\phi}} = \frac{3V_{b\phi}^2}{S_{b3\phi}}$$

By substituting for the phase voltage in term of line-to-line voltage, we have

$$Z_b = \frac{\left(\frac{V_{bL-L}}{\sqrt{3}}\right)^2}{S_{b\phi}} = \frac{V_{bL-L}^2}{3S_{b\phi}} = \frac{V_{bL-L}^2}{S_{b3\phi}} \tag{2.97}$$

2.7 MODELING THREE-PHASE TRANSFORMERS

The impedance diagram of a three-phase transformer is the same as three single-phase transformers. Let us first discuss how the three-phase transformers are constructed.[9–13]

The three-phase transformers can be constructed from the three single-phase transformers.

Figure 2.48 depicts the description of a three-phase transformer that consists of three single-phase transformers.

In Fig. 2.48, each single-phase transformer is rated at 240 V / 120 V, 100 kVA with short-circuit reactance of 5% based on the rated transformer voltages

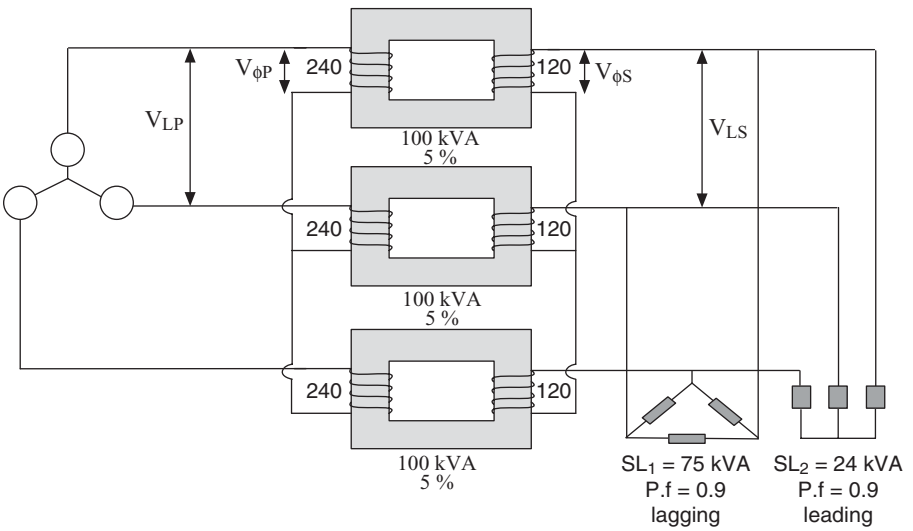

Figure 2.48 The Three Single-Phase Transformers Connected as Three-Phase Y–Y Transformer Bank.

and power rating. The three single-phase transformers are connected as Y–Y and makes a bank of three-phase transformers with rated line-to-line voltages of $\sqrt{3}\times 240$V and $\sqrt{3}\times 120V$, 300 kVA and the short-circuit reactance of 5%. The one-line diagram given in Fig. 2.48 and depicted in Fig. 2.49, where the line-to-line voltages are calculated as

$$V_{LP} = 240\times\sqrt{3} = 415.2 \text{ V}$$
$$V_{LS} = 120\times\sqrt{3} = 207.6 \text{ V}$$

Figure 2.50 depicts the one-phase equivalent circuit for Fig. 2.48. In this figure, the short-circuit reactance is given in actual value in ohms (Ω) on the high-voltage side.

Figure 2.51 depicts the equivalent p.u model of Fig. 2.50. In this figure, the power and voltage bases are given as shown.

Another important type of three-phase transformers is a Y–Δ connection with grounded neutral. Figure 2.52 depicts a Y–Δ connection. The figure shows the coupling windings. For example the winding depicted with N_{p1} is coupled with the winding N_{s1} and similarly N_{p2} with N_{s2} and N_{p3} with N_{s3}.

Figure 2.53 depicts the phase shift in Y–Δ transformers. Because of the phase shift in Y–Δ transformers, they cannot be connected in parallel unless they have proper phase sequence. Therefore, before connecting two Y–Δ transformers, students are urged to study the IEEE standard on transformer

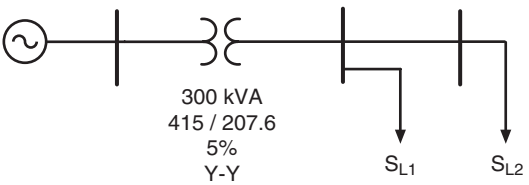

Figure 2.49 One-Line Diagram of Fig. 2.48.

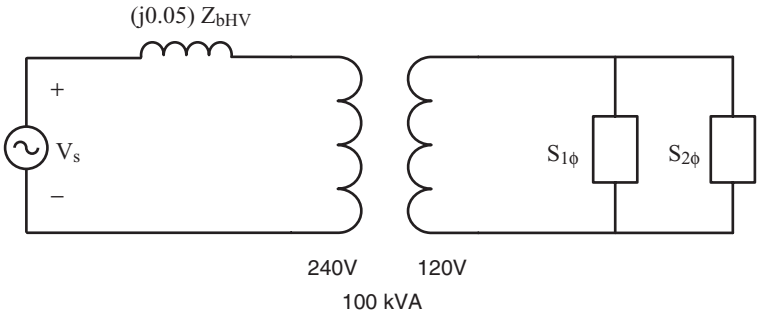

Figure 2.50 One-Phase Equivalent Circuit Model of Fig. 2.48.

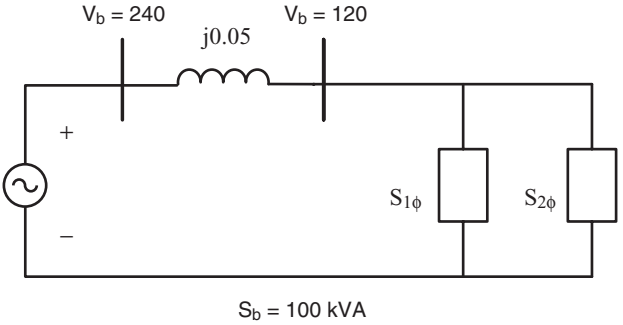

Figure 2.51 The Per Unit Equivalent of Fig. 2.48.

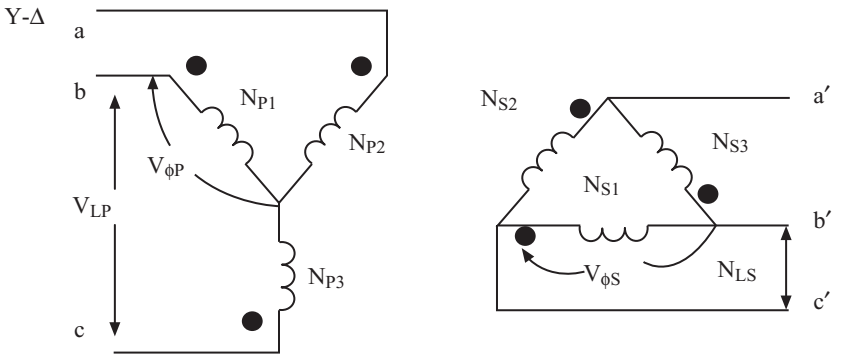

Figure 2.52 A Three-Phase Y–Δ Connection.

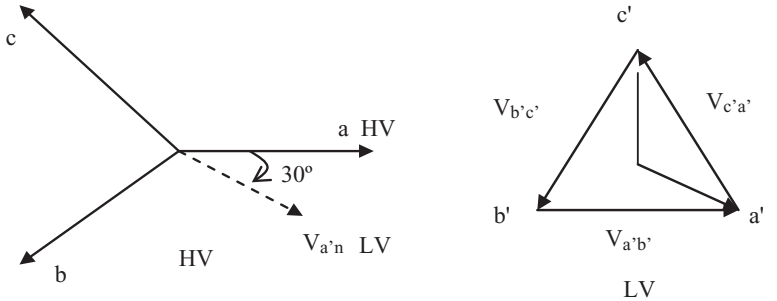

Figure 2.53 A 30° Phase Shift in Y–Δ Transformers.

paralleling or follow industry practice.[12] The large dot in Fig. 2.52 identifies the relative positive terminal of each winding. Students are urged to review the dot notation from their circuit course.

2.8 TAP CHANGING TRANSFORMERS

Figure 2.54 presents a three-phase tap changing transformer. Load tap changing transformers (LTC) are of two types. If the taps are changed under loads, the load tap changing transformer is referred to as tap changing under load (TCUL) or on-load tap changing (OLTC). In off-load tap changing transformers the taps are changed when the loads are not connected.

A tap changing transformer is constructed such that after a few turns a connection point is brought out. The taps can be on one of the windings or both. These types of transformer facilitate voltage regulation.

Voltage stability of a power system is a function of load types. An inductive load draws a lagging current that causes the load voltage to drop. A capacitive load draws a leading current and causes the load voltage to increase. Voltage control elements such as capacitors, reactors, and under load tap changing (ULTC) transformers are used to regulate the power grid bus voltages. If a tap changer is used, tap points are usually made on the high voltage where the current is low because it minimizes the current handling requirements of the contacts. However, a transformer may include a tap changer on both windings.

In distribution networks, step-down transformers have an off-load tap changer on the primary winding and an on-load tap changer on the secondary winding. Normally, the high-voltage tap is controlled and adjusted to match the subtransmission voltage.

We need to define a few terms for LTC transformers. A nominal turns ratio is defined as the condition when all turns of both the primary and secondary windings are carrying currents.

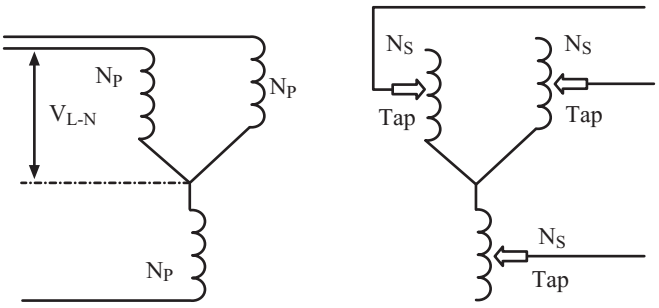

Figure 2.54 A Schematic of a Three-Phase Y–Y Connected Tap Changing Transformer.

$$\frac{V_{HV}}{N_{HV}} = \frac{V_{LV}}{N_{LV}} \text{ or } \frac{V_{HV}}{V_{LV}} = \frac{N_{HV}}{N_{LV}} = a$$

The off-nominal turns ratio refers to when parts of the turns of one or both windings are not carrying currents.

When nominal turns ratio is used, the base voltages are selected as:

$$V_{bHV} = \frac{V_{HV}}{V_{LV}} \times V_{bLV}$$

$$V_{bLV} = \frac{V_{LV}}{V_{HV}} \times V_{bHV}$$

Example 2.10 A single-phase tap changing transformer has 2000 turns on the primary side, and a variable number of turns on the secondary side ($N_{sec\ max}$ = 7300, $N_{sec\ min}$ = 5300) as shown in Fig. 2.55. Compute the minimum and maximum voltage that can be maintained on the secondary voltage. Assume the maximum primary voltage is equal to 36.4 kV.

Solution

$$\frac{V_p}{2000} = \frac{36.4 \times 10^3}{2000} = 18.2\ V/T$$

$$\frac{V_p}{2000} = \frac{V_{\text{sec}}}{N_{\text{sec max}}} = 18.2 = \frac{V_{\text{sec}}}{7300}, \quad V_{\text{sec}} = 132.86\ kV$$

$$\frac{V_p}{2000} = \frac{V_{\text{sec}}}{N_{\text{sec min}}} = 18.2 = \frac{V_{\text{sec}}}{5300}, \quad V_{\text{sec}} = 96.46\ kV$$

Thus, secondary voltage can be changed between 96.46 and 132.86 kV

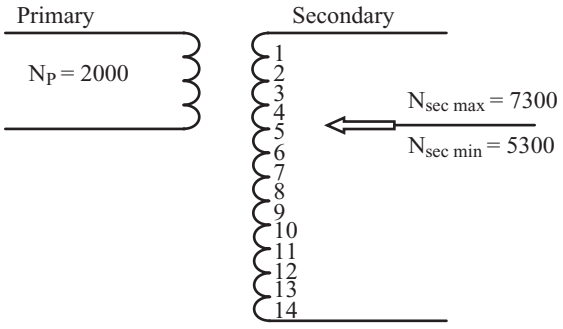

Figure 2.55 A Schematic of a Three-Phase Y–Y Connected Tap Changing Transformer.

2.9 MODELING TRANSMISSION LINES

As we know, electric power is mostly transmitted through three-phase systems.[9–13] The conductor used in each phase has resistance, inductance, and capacitance. In modeling a transmission system, we need to develop a model for the distributed resistance, inductance, and capacitance expressed in miles or kilometers (km) as a lumped model that can be used in the analysis of power grids. A transmission line is designed to carry current and a given designed voltage. The voltage of the transmission line is based on the amount of power, normally in MVA that lines must carry. The current rating is based on the size of the conductor and its thermal rating. Normally, a conductor is sized based on its circular mil area (*CM*), which is a unit denoting the cross-sectional size of a conductor. The circular mil, *CM* is defined as

$$CM = d^2 \tag{2.98}$$

where *d* is the diameter of the conductor. Therefore, 1 mil is equal to 0.001 inch and reversely, 1 inch = 1000 mil and the area A of the conductor is given as:

$$A = d^2 \ cmil$$

The *CM* is also used as a designation for different classes of wires and cables by manufacturers.

The inductance and capacitance of transmission lines are the results of magnetic and electric fields generated from the current and voltage of the conductors. The shunt conductance ($G = 1/R$) is generally very small because the leakage current due to leakage flux that may couple with the ground conductor or an other metallic element around conductors is very small. This conductance is normally ignored. The parameters R, L, and C are needed to construct the transmission line models. The inductance of the line is computed from the flux lines due the current flowing through the conductor. The capacitance of the line is computed from the voltage distribution along conductors.

The inductance of a solid cylindrical conduct has both internal and external inductance.[9.10]

Figure 2.56 depicts a two-wire transmission line. The total inductance is given as

$$L = 410^{-7} \ln \frac{D}{r'} \ H/m \tag{2.99}$$

where: $= r' = re^{-1/4} = 0.7788r$

The term r' is defined as the geometric mean radius (GMR) of a conductor.

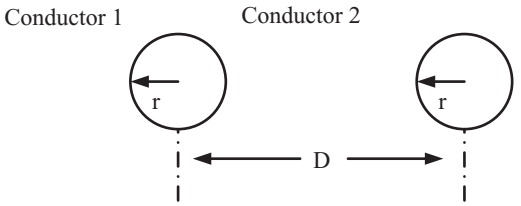

Figure 2.56 Two-Wire Transmission Line.

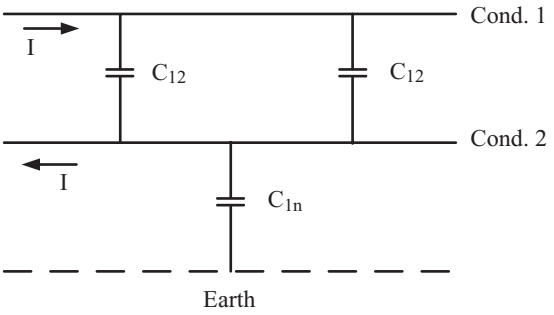

Figure 2.57 Capacitance between Two Conductors and Ground.

As we know, when two charged conductors are at different voltages they act as a charged capacitor. The capacitance can be calculated from the charge on conductors per unit potential difference between two conductors and earth. The neutral conductor is grounded to the earth. However, normally, by grounding the neutral conductor to ground, the earth conductor does not carry current unless a fault occurs, such as when a high-voltage conductor is accidently grounded. From a basic electromagnetic calculation,[8] we can compute the capacitance between two conductors as shown in Fig. 2.57.

$$C_{12} = \frac{0.0388}{2 \cdot \ln \frac{D}{r}} \mu\text{F/mile} \tag{2.100}$$

where D is the distance between the two conductors, μF/mile is F times 10^{-6}, and r is the radius of the conductor.

$$C_{1n} = \frac{0.0388}{\ln \frac{D}{r}} \mu\text{F/mile} \tag{2.101}$$

where C_{12} is the capacitance between the two conductors and C_{in} is the capacitance of one conductor to neutral. In transmission line modeling, we are

interested in equivalent capacitive reactance, X_c. The capacitive reactance in ohms per mile (Ω/mi) to neutral conductor is given as

$$X_C = \frac{1}{2\pi \cdot f \cdot C} = \frac{4.10}{f} \times 10^6 \cdot \log\left(\frac{D}{r}\right) \Omega/\text{mi to neutral} \tag{2.102}$$

where f is the frequency and C is capacitance in F.

Figure 2.58 depicts the inductance of a three-phase line with equilateral spacing.

Figure 2.58 presents a three-phase transmission line. The inductance of the three-phase transmission line is given as

$$L_a = 2 \times 10^{-7} \cdot \ln\left(\frac{D}{r'}\right) \text{H/m} \tag{2.103}$$

$$L_a = 0.7411 \cdot \log\left(\frac{D}{r'}\right) \text{mH/mile} \tag{2.104}$$

due to the symmetry of spacing between the conductors, $L_a = L_b = L_c$.

A three-phase transmission line with bundled conductor lines is used to carry high MVA power using high-voltage lines as depicted in Fig. 2.59.

For bundled conductors, we use equivalent spacing, D_{eq}. Therefore, the inductance L, is given as

$$L = 2 \times 10^{-7} \times \ln \frac{D_{eq}}{D_s^6} \text{H/m} \tag{2.105}$$

where

$$D_{eq} = \sqrt[3]{d_1 \times d_1 \times 2d_1} = d_1 \sqrt[3]{2} \tag{2.106}$$

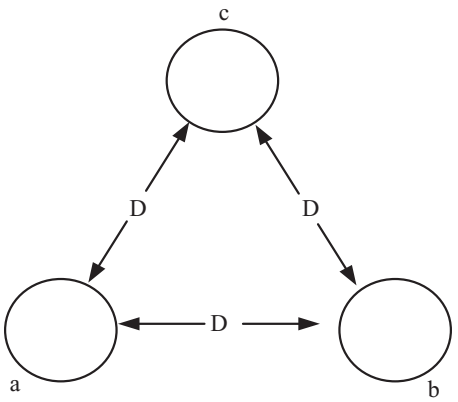

Figure 2.58 The Inductance of a Three-Phase Transmission Line with Equilateral Spacing.

Inductances:

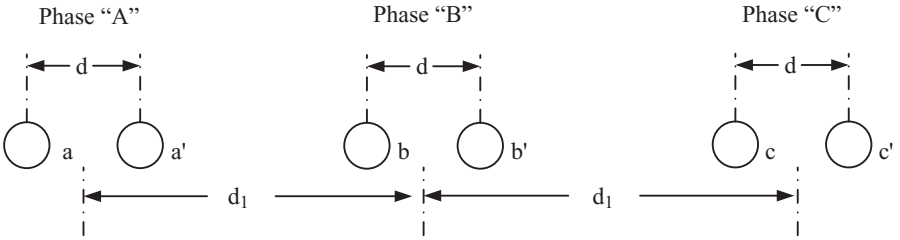

Figure 2.59 Three-Phase Transmission Line with Bundled Conductor Lines.

and

$$D_s^6 = \sqrt[4]{D_{aa} \cdot D_{aa'} \cdot D_{a'a} \cdot D_{a'a'}} \tag{2.107}$$

$$D_s = D_{aa} = 0.7788r \tag{2.108}$$

The term D_s defines the GMR of a bundle of conductors for a phase of a three-phase line.

Normally, in the bundled conductors, the spacing between the conductor of a phase is designated as $D_{a'a'} = D_s$. The value of D_s is given in a tabular form by many manufacturers.

$$D_s^6 = \sqrt[4]{D_s \cdot D_s \cdot d \cdot d} = \sqrt{D_s \cdot d} \tag{2.109}$$

In the above, D_s defines the GMR of a bundle of conductors in a group of bundles in the three-phase line.

The capacitance of the three phase transmission lines can be calculated in the same way:

$$\text{C positive sequence} = C_{12} = \frac{2\pi\varepsilon}{\ln \dfrac{D_{eq}}{D^6_{sc}}} \tag{2.110}$$

$$D_{eq} = \sqrt[3]{d_1 \times d_1 \times 2d_1} = d_1\sqrt[3]{2} \tag{2.111}$$

$$D_{sc}^6 = \sqrt{rd} \tag{2.112}$$

Due to the cost of having equal spacing of the conductors between transmission towers, the transmission lines are constructed with unsymmetrical spacing between the conductors. However, to create approximate spacing between phases, the phases are transposed. This means the position of phases are changed between towers or every few miles in a few towers. Figure 2.60 depicts a transposed three-phase transmission line.

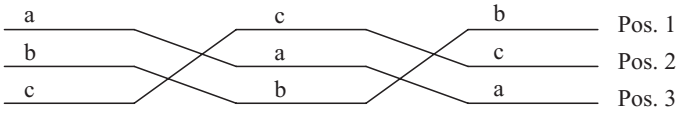

Figure 2.60 The Transposed Three-Phase Transmission Line.

Because the spacing between the phases of the transposed lines is approximately the same, we consider such a three-phase line to have equal resistance, inductance, and capacitance.

$$L_a = L_b = L_c = 2\times10^{-7}\times\log\frac{D_{eq}}{r'}\text{ mH/mile} \tag{2.113}$$

$$L = 2\times10^{-7}\times\ln\frac{D_{eq}}{D_s^6}\text{ H/m} \tag{2.114}$$

$$D_{eq} = \sqrt[3]{D_{12}\times D_{23}\times D_{31}} \tag{2.115}$$

$$X_L = 2\pi\cdot f\cdot L \tag{2.116}$$

The capacitance to neutral for a three-phase line is

$$C_n = \frac{2\pi\varepsilon\cdot\varepsilon_r}{\ln\left(\dfrac{D_{eq}}{D_s}\right)}\text{ F/m to neutral} \tag{2.117}$$

where ε is the permittivity of free space, $\varepsilon = 8.85\times10^{-12}$, and ε_r is the relative permittivity of air which is equal to one.

The X_c at 60 hertz (Hz) is given as

$$X_c = 29.7\times\ln\left(\frac{D_{eq}}{D_s}\right)\text{ k}\Omega\text{/mi to neutral} \tag{2.118}$$

In the calculation of capacitance, D_s is the outside radius of the conductor.

Historically, the transmission line parameters are computed by conductor manufacturers and listed in tabular form for designers to use. However, now software packages are also available to calculate the transmission line parameters for different spacing and design of the lines. Here, we present how we can use a table to select a line parameter reactance and line charging capacitive reactance for design problems in the book.

Generally, most manufacturers use values of GMR for calculating the line parameters in feet and miles or meters and kilometers. The inductive reactance can be calculated as

$$X_L = 2.02f\times10^{-3}\ln\left(\frac{D_{eq}}{D_s}\right)\Omega\text{/mi} \tag{2.119}$$

where D_{eq} is the distance between conductors. The GMR of tables are the same as D_s.

Some conductor manufacturers list the line data in terms of standard spacing of one and spacing of D as given below.

$$X_L = 2.02f \times 10^{-3} \ln\left(\frac{1}{GMR}\right) + 2.02f \times 10^{-3} \ln D \ \Omega/\text{mi} \qquad (2.120)$$

Naturally, both GMR and D must be in feet and f in cycle per second in this formulation. However, because 1 mile is equal to 1.6 km, we can compute the inductive reactance; it can easily be converted to metric system notation. In the above equation, the first term is the inductive reactance for 1 foot and the second term is the inductive reactance for the spacing factor.

As can be expected, the inductance and capacitance are distributed along the line. Therefore, we can assume a distributed model as shown in Fig. 2.61.

In a distributed model of transmission lines, we can define the following:

$z = R + j\omega L$ Ω/m series impedance unit length

$y = G + j\omega C$ shunt admittance per unit length

$\mathrm{Z} = zl\ \Omega$ $\quad l$ = line length in meters

$\mathrm{Y} = yl\ \Omega^{-1}$

Figure 2.62 depicts the lumped model of a transmission line. The parameters of this model can be computed from transmission line data provided by conductor manufacturers.

It should be noted that our discussion here is limited to overhead lines. We have presented very basic concepts related to the selection of overhead conductors and transmission line data for power grid analysis and design. Although this presentation is very brief, students can learn to design a microgrid by recognizing that the design of a microgrid is based on the selection of grid

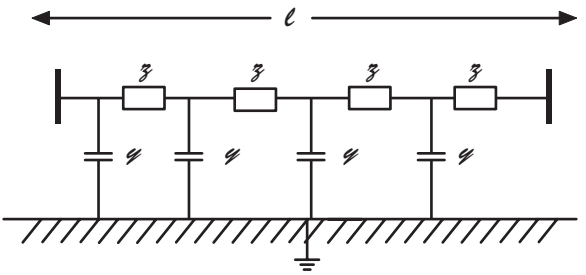

Figure 2.61 A Distributed Model of Transmission Lines.

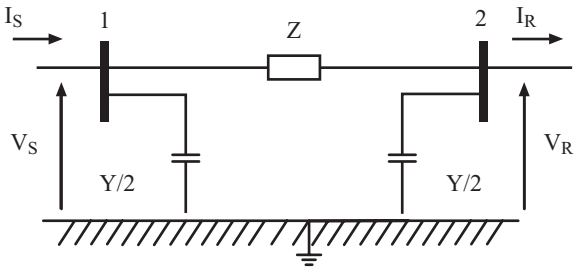

Figure 2.62 A General Model of a Transmission Line.

elements, and then analysis to obtain the desired performance. We will visit this concept in design throughout the book.

Finally, we must note that if we select insulated cables, the selection is more complex. In insulated cables, the heat generated within insulation is a major issue: the cable must be selected based not only on the load current it must carry, it also must be able to operate safely when there is a high transient or fault current due to accidental shorts. This topic will not be addressed further, but students may want to consult other sources.[10]

Appendix B presents typical data for overhead lines. It is important to recognize that the current-carrying capacity is a thermal rating for the conductors. The power that can be transferred is based on the voltage rating of the lines. The voltage rating of the line is determined based on the insulation's requirement and how the spacing between the conductors is designed. Therefore, we need to select the voltage and then compute the power-carrying capacity of the line.

The current flow in the line is given by

$$I_L = \frac{S}{\sqrt{3} \times V_{L-L} \times \text{p.f.}}$$

where S is the power flow, V_{L-L} is the line-to-line voltage and p.f. is the power factor.

The conductor selection is first based on the carrying capacity of the selected line; then we need to address the voltage drop and losses of the line. Therefore, depending on the design requirement, we may select a conductor that may have higher current-carrying capacity.

Example 2.11 A three-phase generator is supplying one MW load operating at 0.9 lagging power factor to a power grid. The generating station is 15 miles from the local power grid. The overhead line data for an aluminum steel conductor reinforced (ASCR) is given in Appendix B.

Perform the following:

i) If the power is transferred at 460 V, select an overhead ASCR conductor to transfer the power. What is the generator voltage if the load voltage is specified at 460 V AC?

ii) If the power is transferred at 3.3 kV, select an overhead ASCR conductor to transfer the power. What is the generator voltage if the load voltage is specified at 3.3 kV AC?

iii) If the power is transferred at 11.3 kV, select an overhead ASCR conductor to transfer the power. What is the generator voltage if the load voltage is specified at 11.3 kV AC?

iv) Compute active and reactive power losses for each design, put your results in a table, and discuss the results.

Solution

The single-phase equivalent diagram of the system is shown in Fig. 2.63.

The load current is given by

$$I_{Load} = \frac{S}{\sqrt{3} \times V_{L-L} \times \text{p.f.}}$$

where S is the power flow, V_{L-L} is the line-to-line voltage of the load and p.f. is the power factor of the load

i) The load current at a load voltage of 460 is

$$I_{Load} = \frac{1 \times 10^6}{\sqrt{3} \times 460 \times 0.9} = 1,394 \text{ A}$$

Because the conductor is carrying 1.39 kA we select the conductor with CM of 1590 kCmil from row 1 of Table B.1 (Appendix B). This conductor has a resistance of is 0.0591 Ω/mi at 25°C as seen from column 4 of Table B.2 (Appendix B).

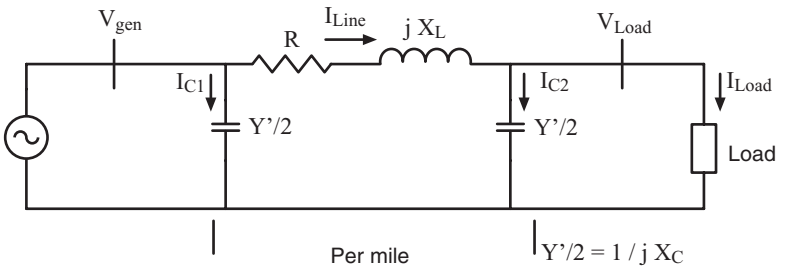

Figure 2.63 Single-Phase Equivalent Diagram of the System in Example 2.11.

The series reactance of the conductor is given in column 6 and row 1 of Table B.2 (Appendix B). The reactance is 0.359 Ω/mi. The capacitive reactance from column 7 and row 1 is 0.0814 MΩ/mi. The half of the above value is used in the equivalent pie model of the transmission lines and is represented with their admittance as $Y'/2 = 1/jX_C$ in Fig. 2.63. Therefore,

$$X_C = \frac{0.0814}{2} = 0.0407 \text{ MΩ/mi}$$

The line charging current as shown in Fig. 2.63 is given by

$$I_{C1} = \frac{V_{Load}}{jX_C} \times distance = \frac{460/\sqrt{3}}{j0.0407 \times 10^6} \times 15 = 97.81.82\angle 90° \; mA$$

It can be seen that the line charging current is in the milli-amp range and is negligible compared to the load current. Therefore, the single-phase equivalent circuit of Fig. 2.63 is reduced as shown in Fig. 2.64. We neglect the line-charging reactances as they are very large compared to the load impedance. It can be seen from Fig. 2.64 that the line current I_{line} is equal to the load current I_{Load}:

$$I_{Line} = I_{Load}$$

In the single-phase equivalent circuit, all the quantities are represented per phase. Wye-connected generator and load is assumed and their phase voltage is found from:

$$V_{ph} = V_{L-L}/\sqrt{3}$$

where V_{ph} is the phase voltage (line-to-neutral) and V_{L-L} is the line-to-line voltage.

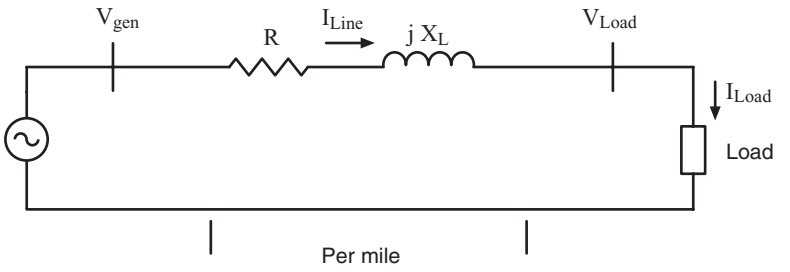

Figure 2.64 Simplified Diagram of Fig. 2.63 by Ignoring the Line-Charging Capacitances.

From Kirchhoff's voltage law and Fig. 2.64, the generator phase voltage is given as

$$\begin{aligned} V_{gen} &= V_{Load} + I_{Line}(R + jX_L) \\ &= \frac{460}{\sqrt{3}} + 1394\angle -\cos^{-1} 0.9 \times 15 \times (.0591 + j0.359) \\ &= 7767\angle 53.21° \text{V} \end{aligned}$$

The generator line voltage is V (line to line) $= \sqrt{3} V_{gen} = \sqrt{3} \times 7763 = 13.4$ kV
The power loss is given by $S_{loss} = 3I_L^2 \cdot Z = 3 \times 1394^2 \times 15 \times (.0591 + j0.359)$

$$S_{loss} = P_{loss} + j\, Q_{loss} = (5.16 + j31.41) \times 10^6$$

Therefore, the active power loss, $P_{loss} = 5.16$ MW

And the reactive power $Q_{loss} = 31.41$ MVAr.

As it can be seen from the above analysis, the power losses are quite high. Next, we select line voltage of 3.3 kV to transfer the power to the load.

ii) The load current at a load voltage of 3.3 kV

$$I_{Load} = \frac{1 \times 10^6}{\sqrt{3} \times 3.3 \times 10^3 \times 0.9} = 194 \text{ A}$$

Because the conductor is carrying 194 A, we select the conductor with CM of 266.8 kCmil from the last row of Table B.2 (Appendix B). This conductor has a resistance of is 0.350 Ω/mi at 25°C as seen from column 4 of Table B.2. The series reactance of the conductor is given in column 6 and the last row of Table B.2. The reactance is 0.465 Ω/mi. The capacitive reactance from column 7 and the last row is 0.1074 MΩ/mi.

Half of the above value is used in the equivalent pie model of the transmission lines and is represented with their admittance as $Y'/2 = 1/jX_C$ in Fig. 2.63. Therefore,

$$X_C = \frac{0.1074}{2} = 0.0537 \text{ MΩ/mi}$$

The line charging current as shown in Fig. 2.63 is given by

$$\begin{aligned} I_{C1} &= \frac{V_{Load}}{jX_C} \times distance \\ &= \frac{3.3 \times 10^3 \times / \sqrt{3}}{j0.0537 \times 10^6} \times 15 = 0.531.82\angle 90° \text{ A} \end{aligned}$$

We can safely neglect the line charging current because it is very small as compared to the load. Applying Kirchhoff's voltage law to the circuit in Fig. 2.64, the generator phase voltage is given as

$$\begin{aligned} V_{gen} &= V_{Load} + I_{Line}\,(R + j\,X_L) \\ &= \frac{3300}{\sqrt{3}} + 194\angle -\cos^{-1} 0.9 \times 15 \times (0.350 + j\,0.465) \\ &= 3.5\angle 53.21^\circ \text{ kV} \end{aligned}$$

The generator line voltage is

$$V_{L\text{-}L} = \sqrt{3} V_{gen} = \sqrt{3} \times 3.5 = 6.06\ kV$$

The power loss is given as

$$\begin{aligned} S_{loss} &= 3I_L^2 \cdot Z = 3 \times 194^2 \times 15 \times (0.350 + j\,0.465) \\ &= (0.57 + j\,0.78) \times 10^6 \\ S_{loss} &= P_{loss} + j\,Q_{loss} \end{aligned}$$

Therefore, the active power loss $P_{loss} = 0.57$ MW and the reactive power loss $Q_{loss} = 0.78$ MVAr.

As we can see by increasing the transmission line, we have reduced the power losses. Next, we evaluate the power losses if the line voltage is selected at 11.3 kV.

iii) The load current at a load voltage of 11.3 kV,

$$I_{Load} = \frac{1 \times 10^6}{\sqrt{3} \times 11.3 \times 10^3 \times 0.9} = 57A$$

The same conductor is selected as in part ii. The resistance of the line from Table B.2 (Appendix B) for 57 A is 0.350 Ω/mi. The series reactance of the line from Table B.2 is 0.465 Ω/mi. The capacitive reactance from column 7 and the last row is 0.1074 MΩ/mi.

Therefore,

$$X_C = \frac{0.1074}{2} = 0.0537 \text{ MΩ/mi}$$

The line charging current as shown in Fig. 2.63 is given by $I_{C1} = V_{Load} / jX_C \times distance = \dfrac{11.3 \times 10^3 / \sqrt{3} \times 15}{0.0537 \times 10^6} = 1.82\angle 90^\circ$ A

In this case, the line charging current is of comparable magnitude to that of the load current. Hence, we do not neglect the line charging reactance. Applying Kirchhoff's current law in Fig. 2.63, the line current is given by:

$$\begin{aligned} I_{Line} &= I_{Load} + I_{C1} \\ &= 57\angle -\cos^{-1} 0.9 + 1.82\angle 90° = 56.2\angle -24.2° \text{ A} \end{aligned}$$

The generator phase voltage is given as

$$\begin{aligned} V_{gen} &= V_{Load} + I_{Line}(R + j\, X_L) \\ &= \frac{11300}{\sqrt{3}} + 56.2\angle -24.2° \times 15 \times (0.350 + j\, 0.465) \\ &= 6.96\angle 1.95° \text{ kV} \end{aligned}$$

The generator line voltage is given as

$$V_{L\text{-}L} = \sqrt{3} V_{gen} = \sqrt{3} \times 6.96 = 12.1\, kV$$

The power loss is given by

$$S_{loss} = 3I_L^2 \cdot Z = 3 \times 56.2^2 \times 15 \times (0.350 + j\, 0.465)$$

$$S_{loss} = P_{loss} + jQ_{loss} = (49.8 + j\, 66) \times 10^3$$

Therefore, the active power loss $P_{loss} = 49.8$ kW and the reactive power loss $Q_{loss} = 66.0$ kVAr.

With line voltage of 11.3 kV, the power losses are quite low.

iv) The active and reactive power loss for each voltage level is shown in Table 2.1.

From Table 2.1 it can be seen that the transmission line losses can be reduced substantially by increasing the transmission voltage.

Example 2.12 If the generator of Example 2.11 is a PV farm and we want to operate the PV bus at unity power factor, how much reactive power will we need to place on the PV bus or load bus if the power is transferred at 3.3 kV?

TABLE 2.1 Active and Reactive Power Losses at Different Line Voltage Levels.

Voltage (kV)	Active Power Loss (MW)	Reactive Power Loss (MVAr)
0.460	5.16	31.41
3.3	0.57	0.78
11.3	0.050	0.066

Solution

In Example 2.11, the load is 1 MW at 0.9 power factor lagging.

Therefore, the power factor angle is $\cos^{-1} 0.9 = 25.84°$

The MVA rating of the load is given as

$$S_{load} = \frac{P}{p.f.} = \frac{1}{0.9} = 1.11 \text{ MVA}$$

Therefore, the reactive power consumption of the load is given as

$$Q = 1.11 \sin 0.9 = 0.48 \text{ MVAr}$$

From Table 2.1, the reactive power loss of transmission line is

$$Q = 0.78 \text{ MVAr}$$

Therefore, the total reactive power consumed

$$Q_{Consumed} = 0.78 + 0.48 = 1.26 \text{ MVAr}$$

The line charging capacitances will supply some reactive power to the system. The reactive power supplied by the line charging reactance is given by (see Fig. 2.63):

$$Q_{produced} = \left(\frac{V_{gen}^2}{X_C} + \frac{V_{Load}^2}{X_C} \right) \times distance = \frac{\left(6.06 \times 10^3\right)^2 + \left(3.3 \times 10^3\right)^2}{0.0537 \times 10^6} \times 15$$
$$= 13.3 \text{ kVAr}$$

The net reactive power supplied by the generator is $Q_{gen} = Q_{consumed} - Q_{produced}$ $= 1.26 - 0.013 = 1.25$ MVAr

Therefore, a reactive power of 1.25 MVAr must be supplied by the PV bus. In other words, a capacitive load of 1.25 MVAr must be connected to the PV bus.

In this chapter, we have learned how to extend the basic knowledge of circuit theory to power system analysis. We have studied the meaning of impedance loads, a power consumption model for loads, the rated values of electrical devices, and the modeling of single- and three-phase transformers. We have also explored the basic concept of the per unit system and have learned how to develop a per unit model—a three-phase systems distribution feeder that can be fed from a renewable energy source.

In the next chapter, we will study the concept of a smart grid system and the design of smart microgrid renewable energy systems.

PROBLEMS

2.1 Assume $a = 120 + j\,100$, $b = 100 + j\,150$ and $c = 50 + j\,80$. Compute the following complex numbers:

i) $(a \times b)/c$

ii) $(a/b) \times c$

iii) $(a-b)/(c-a)$

2.2 If $V = 120\cos(377t + 5°)$. If a voltmeter is used to measure this voltage, what value should the voltmeter read? Express this voltage in polar form.

2.3 The operation of AC machines (in particular, transformers and induction machines) can be studied with the aid of the T-circuit shown in Fig. 2.65 below.

Assume the frequency is 60 Hz. The circuit elements are given in the table below.

	R_1	L_1	R_f	L_m	R_2'	L_2'	R_L	L_L	V_1	V_2	I_1	I_2'	I_f
1	1	0.01	1000	8	1	0.01	Open		480	?	?	?	?
2	1	0.01	1000	8	1	0.01	200	0	480	?	?	?	?
3	0.02	0.00265	Open		0	0	Open		1	?	?	?	?
4	0.02	0.00265	Open		0	0	1	0	1	?	?	?	?
5	0.02	0.00265	Open		0	0	0.707	1.875×10^{-3}	?	1	?	?	?
6	0	0	100	0.1	0.01	106×10^{-6}	1	0	1	?	?	?	?
7	0	0	100	0.01	0.01	106×10^{-6}	1.414	3.75×10^{-3}	1	?	?	?	?
8	0.3	1.33×10^{-3}	Open	3.45×10^{-2}	0.15	0.56×10^{-3}	7.35	0	127	?	?	?	?
9	10	5.2×10^{-2}	Open	0	0	200	0.4	0	500	?	?	?	?
10	0.15	2.54×10^{-3}	Open	1.57	6.24×10^{-3}	98.5	0.178	0	240	?	?	?	?
11	0.3	0.003	1	4.25×10^{-2}	0.2	0.003	10	0	440	?	?	?	?
12	0.3	0.003	0	4.25×10^{-2}	0.2	0.003	1	0	380	?	?	?	?

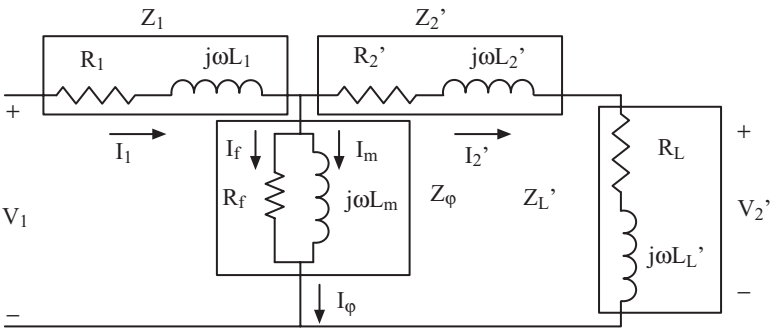

Figure 2.65 Equivalent Circuit for Problem 2.3.

Use the polar form for all complex numbers and solve set 1 through set 12. Show your calculations separately.

2.4 Assume a balanced three-phase load. Each phase load is rated 120 Ω with a phase angle of 10° and the load is connected as a Y bank. A three-phase balance source rated 240 V is applied to this three-phase load. Perform the following:

i) Give the three-phase circuit of this load.

ii) Compute the active and reactive power consumed by this load.

2.5 Assume a single-phase load has inductance of 10 millihenry (mH) and resistance 3.77 Ω and it is connected to a 60 Hz source at 120 V. Compute the active and reactive power consumed or generated by the load.

2.6 Assume a single-phase load has a capacitance of 10 millifarad (mF) and resistance of 2.0 Ω and it is connected to a 60 Hz source at 120 V. Compute active and reactive power consumed or generated by the loads.

2.7 A single-load consumes 10 kW at 0.9 power factor, p.f. lagging at 220 V. What is the magnitude and phase angle of current drawn from the source? If another single-phase load rated at 10 kW and 0.8 leading power factor connected in parallel to the same sources, what is the magnitude of current drawn? What is the current drawn from the source? Give your answer in polar form.

2.8 A single-phase transformer is rated 200 kVA, 120/220 V, 5% reactance. Compute the reactance of the transformer from the high-voltage side. Give the single-phase equivalent circuit.

2.9 Compute the per unit model of Problem 2.7 based on 400 kVA and a base voltage of 440 V.

2.10 Three single-phase transformers are each rated 460 V/ 13.2 kV 400 kVA, 5% short-circuit reactance. The three single-phase transformers are connected as a three-phase Y–Y transformer. Perform the following:

i) Compute the three-phase Y–Y transformer high-voltage-side and low-voltage-side voltage and kVA ratings.

ii) Compute the per unit model of the three-phase transformer.

2.11 A bank of three-phase Y–Y resistive load of 30 Ω is connected to the low-voltage side of the transformer of Problem 2.9 using a feeder with resistance of 1 + j10 Ω. Perform the following:

i) Give the three-phase equivalent model.

ii) Give a one-line diagram.

iii) Compute the per unit model based on the transformer rating.

2.12 Three single transformers are each rated 460 V/ 13.2 kV 400 kVA, 5% short-circuit reactance. The three single-phase transformers are connected as a three-phase Y–Δ transformer. Perform the following:

i) Compute the three-phase Y–Δ transformer high-voltage-side and low-voltage-side voltage and kVA ratings.

ii) Compute the per unit model of the three-phase transformer.

2.13 A bank of three-phase Y–Y resistive load of 30 Ω is connected to the low voltage side of the transformer of Problem 2.11 using a feeder with resistance of 1 + j10 Ω. Perform the following:

i) Give the three-phase equivalent model.

ii) Give the one phase of a Y-connected equivalent circuit.

iii) Give a one-line diagram.

iv) Compute the per unit model based on the transformer rating.

2.14 Three single-phase transformers are each rated 460 V/ 13.2 kV 400 kVA, 5% short-circuit reactance. The three single-phase transformers are connected as a three-phase Δ–Δ transformer. Perform the following:

i) Compute the three-phase Δ–Δ transformer high voltage side and low voltage side voltage and kVA ratings.

ii) Give the three-phase equivalent model.

iii) Give the one-phase of a Y-connected equivalent circuit.

iv) Compute the per unit model based on the transformer rating.

2.15 A bank of three-phase Δ–Δ resistive load of 30 Ω is connected to the low-voltage side of the transformer of Problem 2.13 using a feeder with resistance of 1 + j10 Ω. Perform the following:

i) Give the three-phase equivalent model.

ii) Give the one phase of a Y-connected equivalent circuit.

iii) Give a one-line diagram.

iv) Compute the per unit model based on the transformer rating.

2.16 A balanced three-phase, three wire feeder has three balanced loads as shown in Fig. 2.66.

Each lamp is rated at 100 W and 120 V. The line-to-line voltage on the feeder is 240 V and remains constant under the loads. Find the source current in the feeder lines and the power delivered by the source.

i) Compute the "a," line current in phase a

ii) Compute active and reactive power supplied by the sources.

2.17 Consider a three-phase distribution feeder as shown in Fig. 2.67.

For the three-phase system, all voltages are given line-to-line and the complex power is given as three-phase power.

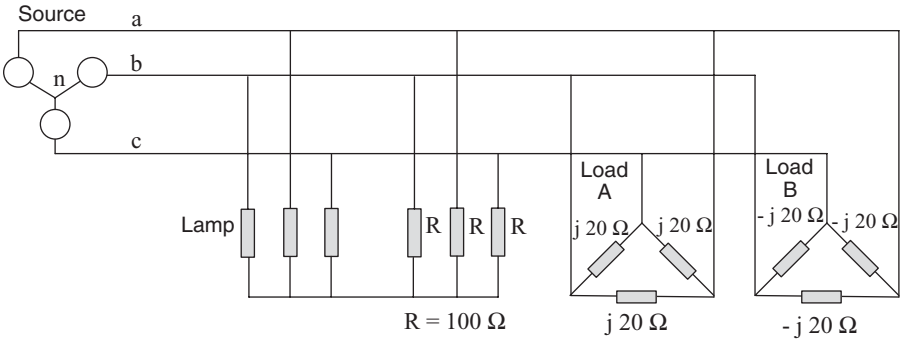

Figure 2.66 The Three-Phase Diagram of Problem 2.15.

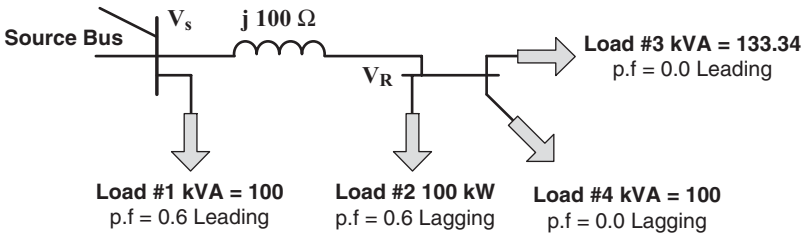

Figure 2.67 The One-Line Diagram of Problem 2.16.

Compute the following:

i) The source voltage Vs, if V_R is to be maintained at 4.4 kV (V_R = 4.4 kV V line value)

ii) The source current and the power factor at the source

iii) The total complex power supplied by the source

iv) How much reactive power should be connected to the source bus to obtain a unity power factor at the source bus?

2.18 Assume a three-phase transformer is Y-grounded on the low-voltage side and Δ-connected winding on the high-voltage side as shown in Fig. 2.68. Each winding of tap-changing winding has 2000 turns on the low-voltage side, and a variable number of turns on the high-voltage winding side. Assume the high-voltage winding side has a maximum number of turns equal to 7300 turns and a minimum number of turns equal to 5300. Compute the minimum and maximum line-to-line voltage that can be maintained on the high-voltage side. Assume the winding voltage across the low-voltage side is set equal to 36.4 kV.

2.19 Write a term paper on the capital cost of a one megawatt solar system and its payback over 25 years. Assume the cost of a coal-fired power

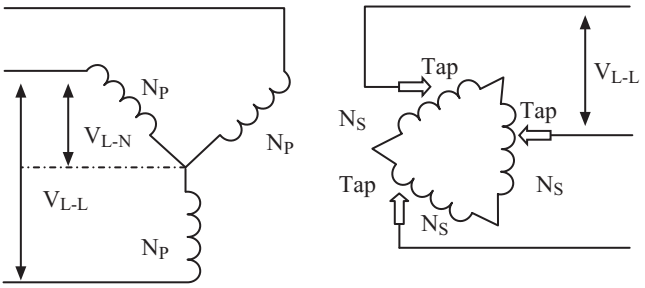

Figure 2.68 Figure for Problem 2.17.

plant is $.10 per kWh and PV, to generate electricity the cost is about $0.25–0.40 per kWh.

2.20 A three-phase generator rated 480 V and 400 kVA connected to a three-phase transformer rated 3.2 kV/480 V, 200 kVA, with reactance of 10% is used to serve a load over a line of 1 + j20 Ω. At the load site, the voltage is stepped down to 220 V from 3.2 kV using a three-phase transformer rated 150 kVA with reactance of 7%. The voltage at the load is to be maintained at 220 V. Perform the following:

i) Give a one-line diagram.

ii) Compute a per unit equivalent circuit based at 200 kVA and 480 V.

iii) Compute the required generator voltage. Is this design viable?

REFERENCES

1. A Century of Innovation-Electrification National Academy of Engineering. Available at http://www.greatachievements.org. Accessed 2009 Sept 18
2. Wikipedia. Nikola Tesla. Available at http://en.wikipedia.org/. Accessed 2009 Sept 28.
3. Wikipedia. War of Currents. Available at *wkipedia.org/wiki/*. Accessed 2009 Jan. 28.
4. U.S. Energy Information Administration. Independent Statistics and Analysis. Available at http://www.eia.doe.gov. Accessed 2009 Sept 18.
5. California Energy Commission. Energy Quest. Glossary of Energy Terms. Available at http://www.energyquest.ca.gov/glossary/glossary-i.html#i. Accessed 2009 April 18.
6. U.S. Environmental Protection Agency. Clean Air Act. Available at http://www.epa.gov/air/caa/. Accessed 2009 Jan 25.
7. 3-Phase Power Resource Site. Available at http://www.3phasepower.org. Accessed 2009 Jan 28.
8. Majmudar H. Electromechanical energy converters. Boston, MA: Allyn & Bacon; 1965.

9. El-Hawary ME. Electric power systems: design and analysis. Reston, VA: Reston Publishing; 1983
10. Grainger J, Stevenson WD. Power systems analysis. New York: McGraw Hill; 2008.
11. Elgerd OI. Electric energy system theory: an introduction. 2nd ed. New York: McGraw-Hill; 1982.
12. IEEE Brown Book. IEEE recommended practice for power system analysis. New York: Wiley-Interscience; 1980.
13. Chapman S. Electric machinery and power system fundamentals. New York: McGraw Hill; 2003.

CHAPTER 3

MODELING CONVERTERS IN MICROGRID POWER SYSTEMS

3.1 INTRODUCTION

A DC/AC inverter converts direct current (DC) power generated by a DC power source to sinusoidal alternating currents (AC). The photovoltaic cells (PV) are sources of DC power. The high-speed microturbine generators are sources of high-frequency AC power. Because these generators are designed for high-speed operation, they are lightweight and low volume. They use natural gas and together with their fuel cells are considered a green energy source because they have a minimal carbon footprint. Variable wind-speed generators have the same operating principle as microturbine generators, except they run at variable speed and generate variable AC power. To utilize the variable frequency AC power sources, the generated power is rectified to DC power using an AC/DC rectifier, DC/AC inverters are used to convert the generator DC power output to AC power at the system operating frequency. This type of wind power is depicted in Fig. 3.1.

In the previous chapter, we studied single-phase loads, three-phase loads, transformers, and modeling of the distributed generation system using the generalized per unit concept. In this chapter, we will study DC/AC inverters, DC/DC converters, rectifiers and their functions in the microgrid of distributed generation. We will also study the modeling of green and renewable energy sources for the design of microgrids as part of an interconnected bulk power grid.

Design of Smart Power Grid Renewable Energy Systems, First Edition. Ali Keyhani.

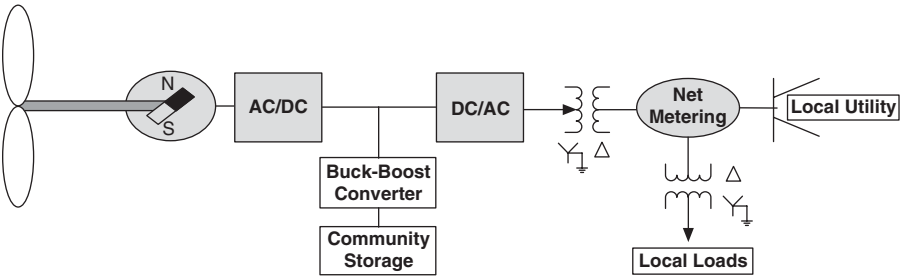

Figure 3.1 A Variable-Speed Permanent Magnet Wind Generator System.[1]

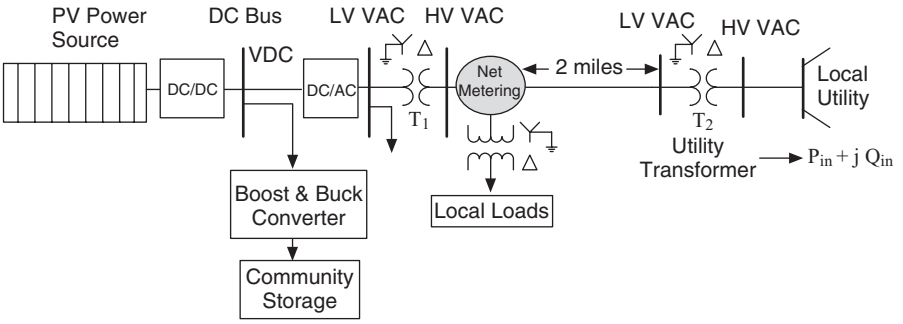

Figure 3.2 A Radial Photovoltaic Microgrid Distributed Generation System.[1]

3.2 SINGLE-PHASE DC/AC INVERTERS WITH TWO SWITCHES

Figure 3.3 depicts a single-phase converter with two switches. In the integration of renewable energy into a power grid, the function of inverters is to convert power from DC to AC at the system frequency of operation. The two-switch single-phase inverter is used for low-power applications and is also referred to as a single-phase half-bridge inverter. The pulse width modulation (PWM) technique is used to achieve an AC voltage with a fundamental frequency of 60 or 50 Hz of the power grid. The two power switches of the single-phase inverter are sequentially turned on and off with antiparallel diodes connected between the DC-link. By turning on the power switches, we can obtain a time-varying voltage at the node a of Fig. 3.3. If the switch SW_1^+ is on, the potential at point a is the same as that of the positive DC bus. On the other hand, if the switch SW_1^- is on, the potential of node a is that of the negative DC bus. To explain the operation of the inverter, let us measure the potential of node a with respect to the point n on the negative DC bus. The potential of the positive DC bus with respect to the point n is $+V_{idc}$. Therefore, if the switch SW_1^+ is on, the voltage V_{an} is $+V_{idc}$ and when SW_1^- is on, V_{an} is zero. To generate a time-varying voltage at point a, a sine wave with the desired frequency is compared with a triangular wave to determine the switching policy. The objective is to sample the DC voltage such that the sample pulse voltage

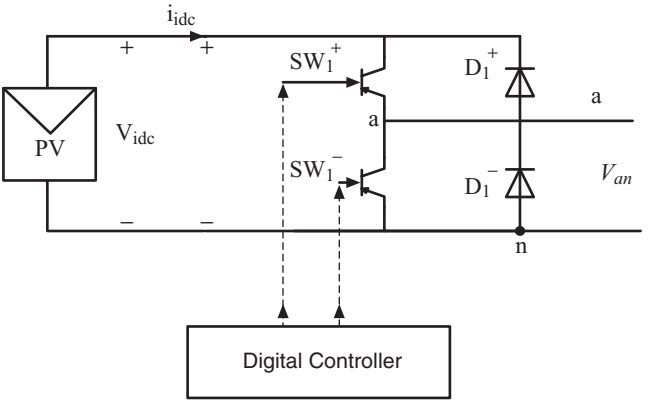

Figure 3.3 A Single-Phase DC/AC Inverter with Two Switches.

will have the same fundamental frequency of the sine wave. The turn on and off sequence of the two switches is decided by the relative value of the sine wave with respect to the triangular wave.

Figure 3.4 shows the waveforms of sine-PWM: two waves are being compared. One is a sine wave, V_c, that is designated as controlled voltage. The second wave is a triangular wave, V_T, with amplitude and frequency higher than the sine wave. The sampling time of time is defined as $T_s = \frac{1}{f_s}$ where f_s is the frequency of the triangular wave. To sample the DC bus voltage such that a pulse-width generated voltage will have the same frequency as the control reference sine wave, the switching policy is based on comparing V_T with V_C. Therefore, by turning on the switch SW_1^+ when V_c is greater than V_T with V_{an} equal to V_{idc} and by turning on the switch SW_1^- when V_c is smaller than V_T with V_{an} equal to zero, the voltage V_{an} is not a pure sinusoid, but it has a DC component, a fundamental AC voltage at the same frequency as the control reference voltage and the harmonic voltages.

Therefore, the switching policy for two power switches is:

i) If $V_c > V_T$ SW_1^+ is *on*; SW_1^- is *off*, and $V_{an} = V_{idc}$ and
ii) If $V_c < V_T$ SW_1^- is *on*, SW_1^+ is *off* and $V_{an} = 0$.

As the magnitude of the sine wave is varied relative to the triangular wave, the fundamental component of V_{an} varies in direct proportion with the relative amplitude of the triangular wave and sine wave. Figure 3.5 shows the waveform when the amplitude of the reference sine wave is reduced. The fundamental component of V_{an} has the same frequency as that of a triangular wave.

The magnitude of the fundamental of AC output voltage is directly proportional to the ratio of the peaks of V_c and V_T. This ratio is defined as the amplitude modulation index, M_a:

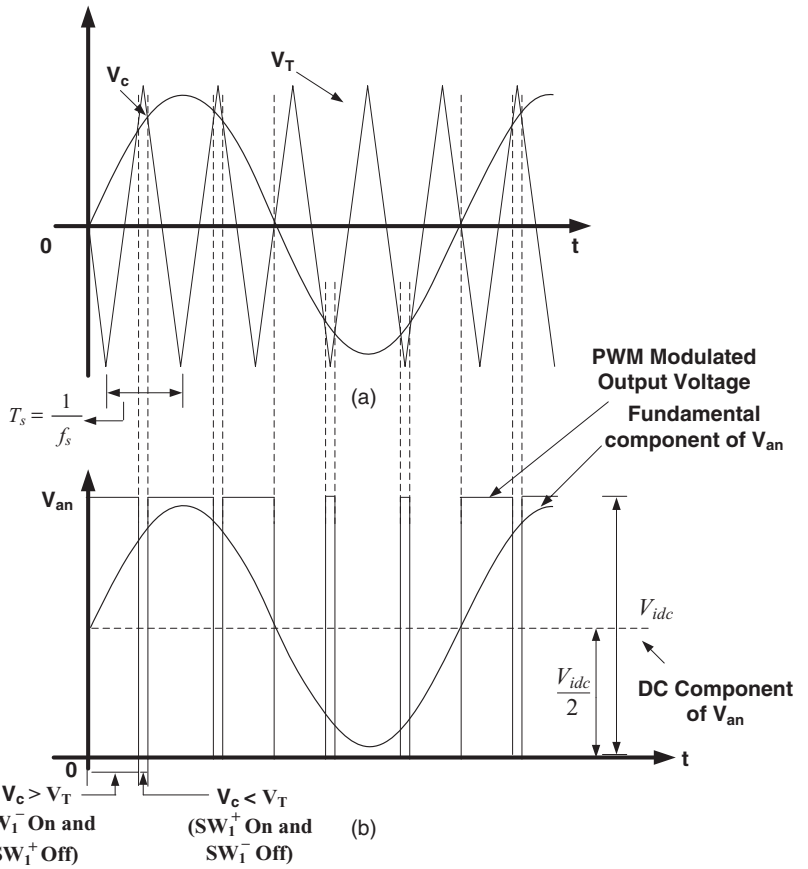

Figure 3.4 A Pulse Width Modulation (PWM) Voltage Waveform of a Single-Phase DC/AC Inverter with Two Switches.

$$M_a = \frac{V_{C(\max)}}{V_{T(\max)}} \tag{3.1}$$

The peak of fundamental component of the output voltage is

$$V_{an,1} = \frac{V_{idc}}{2} M_a \tag{3.2}$$

The instantaneous value of the output voltage will be

$$V_{an} = \frac{V_{idc}}{2} + \frac{V_{idc}}{2} M_a \cdot \sin \omega_e t + harmonics \tag{3.3}$$

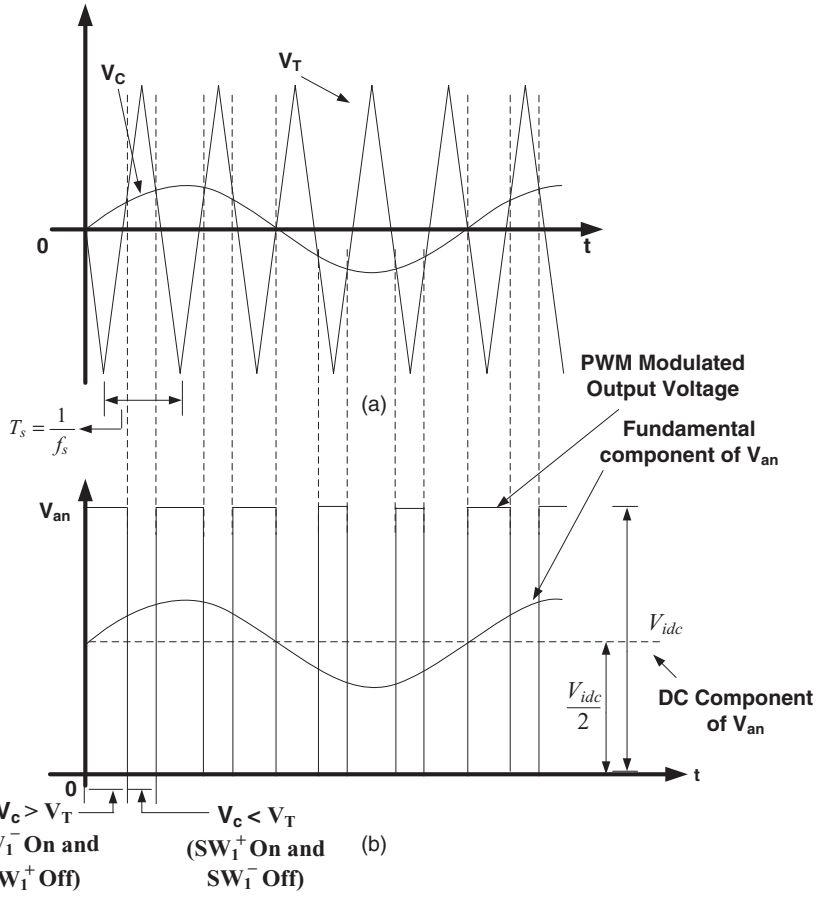

Figure 3.5 A Pulse Width Modulation (PWM) Voltage Waveform of a Single-Phase DC/AC Inverter with Two Switches When the Sine Wave Has Reduced Amplitude.

where the $\omega_e = 2\pi \cdot f_e$ is the frequency of the sine wave in radian per second and f_e is the frequency of the sine wave in Hz.

The output voltage has a DC component of value $V_{idc}/2$ and a fundamental with an amplitude of $M_a \cdot V_{idc}/2$ and harmonics. M_a varies from 0 to 1. The presence of DC components would cause any inductive load to get magnetically saturated. Hence, an inductive load cannot be connected between nodes a and n. However, we can eliminate the DC voltage in the output by connecting loads across the terminal V_{ao}.

Figure 3.6 shows the topology of the inverter having two capacitors with available center tap. The load is connected between node a and the center tap point o. The two capacitors C^+ and C^- are of equal capacitance. Therefore, each has a voltage of $V_{idc}/2$ across it. The potential of the point o is $+V_{idc}/2$ with respect to point n.

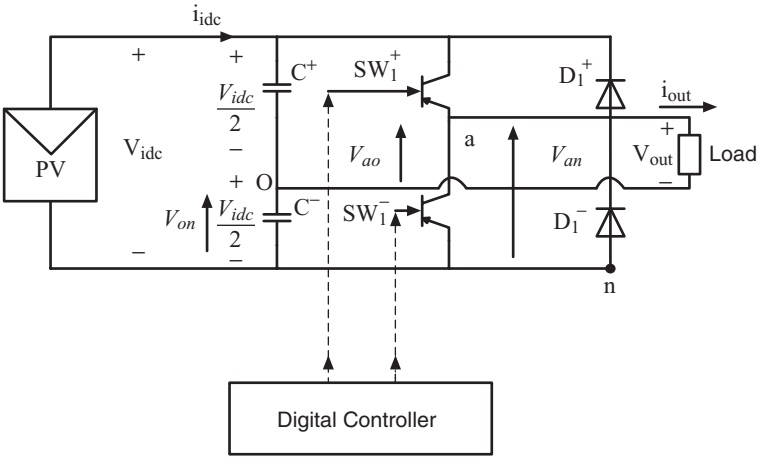

Figure 3.6 A Single-Phase Inverter with Two Switches and Load Connected to the Center Tap Position.

Two capacitors used in this topology with the center tap point o make both the positive and negative voltages available. When SW_1^+ is on, SW_1^- is off, the voltage V_{an} is equal to V_{idc}. Because V_{on} is $+V_{idc}/2$; therefore, V_{ao} $(= V_{an} - V_{on})$ is $+V_{idc}/2$. Similarly, when SW_1^- is on and SW_1^+ is off, then V_{an} is zero and V_{ao} is equal to $-V_{idc}/2$. If the capacitors are sufficiently large, they maintain a constant voltage of $V_{idc}/2$ across them irrespective of the load.

With the center tap point available, the voltage across the load is between positive and negative values of $V_{idc}/2$. The DC component of the output voltage is zero and output voltage V_{ao} can be considered alternating in nature. The logic involved in switching is the same in the previous case. The resulting output voltage is shown in Fig. 3.7.

Figure 3.7(a) depicts the control voltage (V_c) and the triangular wave, (V_T) that samples the control voltage V_c. The sampling of V_c at the sampling frequency of V_T produces the waveform of Fig. 3.7(b) where V_{ao} is output PWM wave voltage and the fundamental of the PWM voltage is shown on Fig. 3.7(b).

The switching policy for two power switches is

i) If $V_c > V_T$ SW_1^+ is on; SW_1^- is off, and $V_{an} = V_{idc}/2$

ii) If $V_c < V_T$ SW_1^- is on; SW_1^+ is off, and $V_{an} = -V_{idc}/2$

Again, the fundamental component of the output voltage can be varied by controlling the amplitude of the sine wave. Figure 3.8 gives the voltage waveforms for a reduced peak value of a sine wave.

Figure 3.8(a) depicts the control voltage (V_c) and the triangular wave, (V_T) that samples the control voltage V_c. However, the amplitude of control voltage

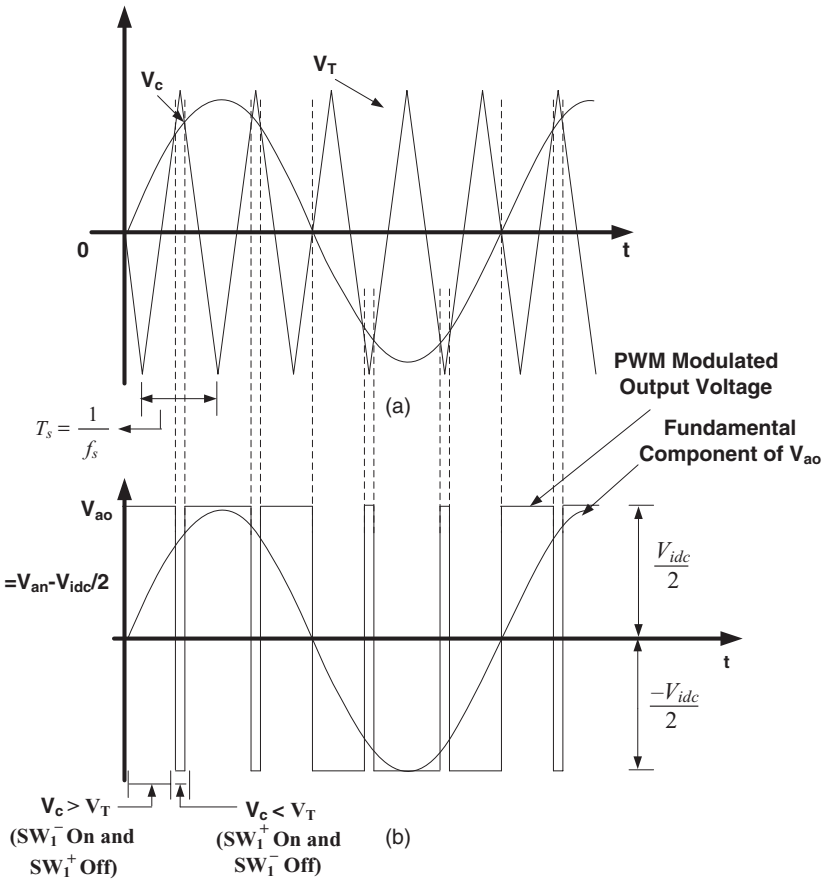

Figure 3.7 The Sine Pulse Width Modulation (PWM) for a Single-Phase Inverter with Two Switches for Load Connected to the Center Tap of the Capacitor.

is half of the control voltage of Fig. 3.7. The sampling of V_c at the sampling frequency of V_T produces the waveform of Fig. 3.8(b) where V_{ao} is output PWM wave voltage and the fundamental of the PWM voltage is shown in Fig. 3.8(b). The output PWM voltage is also half of Fig. 3.7(b).

The output voltage in this case has no DC component. The output voltage is PWM voltage with the fundamental frequency of the reference control voltage and harmonics. The output voltage is given by

$$V_{ao} = \frac{V_{idc}}{2} M_a \cdot \sin \omega_e t + harmonics \tag{3.4}$$

where the $\omega_e = 2\pi \cdot f_e$ is the frequency of the sine wave in radians per second and f_e is the frequency of the sine wave in Hz. When $0 \le M_a \le 1$, the amplitude

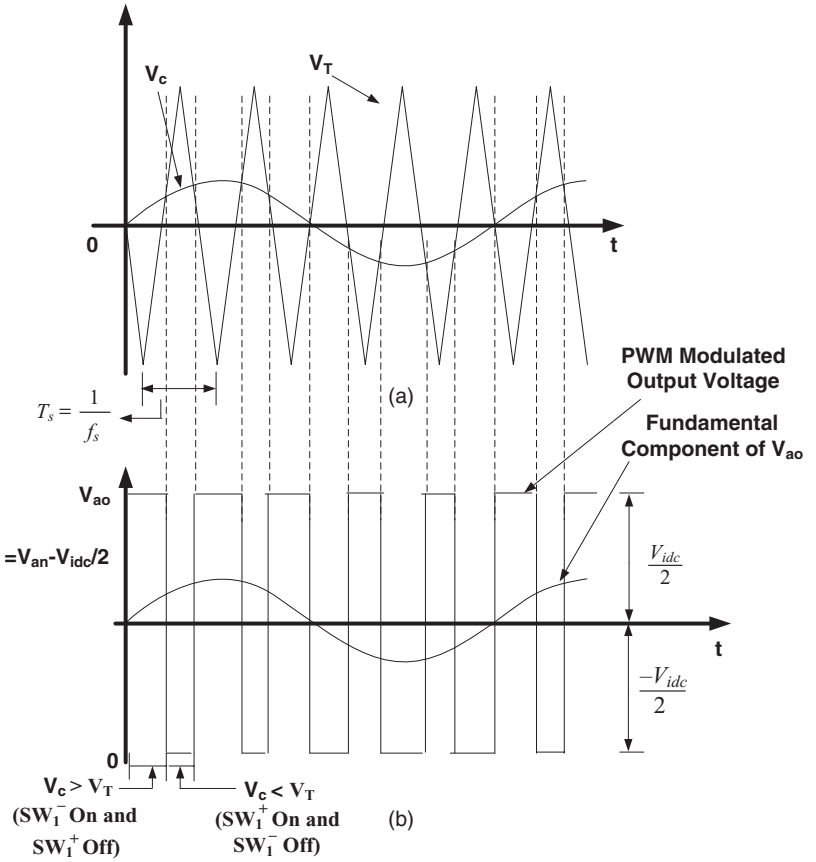

Figure 3.8 The Pulse Width Modulation (PWM) Voltage Waveform of a Single-Phase DC/AC Inverter with Two Switches When the Sine Wave Has Reduced Amplitude.

of the fundamental varies linearly with the amplitude modulation index. When M_a is greater that one, it enters the nonlinear region and as it is increased further, the fundamental output voltage saturates at $\frac{4}{\pi}.\frac{V_{idc}}{2}$ and does not increase with M_a.

The fundamental frequency of the output voltage is the same as the frequency of the sine voltage. Thus, by adjusting the peak of the sine wave, the amplitude of the output voltage can be varied. Similarly, by changing the frequency of the sine wave, the output frequency is varied.

From the point of view of the voltage quality, the output of the inverter should be as close to the sine wave as possible. The harmonic contents in the voltage should be minimized. To achieve low harmonic distortion the frequency of the triangular wave is increased as much as possible relative to the frequency of the sine wave. To measure the effect of higher switching

TABLE 3.1 The Harmonic Content of the Output Voltage for a Different M_f with M_a Fixed at 0.6.

Order of Harmonic	$M_f = 3$ (%)	$M_f = 5$ (%)	$M_f = 7$ (%)	$M_f = 9$ (%)
1	100	100	100	100
3	163	22	0.42	0.05
5	61	168	22	0.38
7	73	25	168	22
9	37	62	22	168

frequency, the frequency modulation index is increased. The frequency of modulation index, M_f is defined as

$$M_f = \frac{f_s}{f_e} \tag{3.5}$$

where f_s is the frequency of the triangular wave and f_e is the frequency of the sine wave.

The amount of harmonics in the output voltage is determined by the frequency modulation index. The amount of harmonics relative to the fundamental for amplitude modulation index of 0.6 and for different frequency modulation indices is tabulated in Table 3.1.

The first column of the Table 3.1 lists the order of the harmonics. The power frequency in the United States is 60 Hz. Therefore, the fundamental will have a frequency of 60 Hz. The third harmonic will have three times the frequency of the fundamental, which is 180 Hz. Similarly, the fifth, seventh, and ninth harmonics will have a frequency of 300 Hz, 420 Hz, and 540 Hz, respectively. The last four columns of Table 3.1, give the harmonic content as a percentage of the fundamental. The order of the harmonic present in the output voltage is a direct consequence of M_f. The third harmonic content when M_f is 3 is 163% of the fundamental. Again, the fifth, seventh, and ninth harmonics are also more than 100% when M_f is 5, 7, and 9, respectively. When M_f is 9, the third and the fifth harmonics are practically absent (0.05% and 0.38%), while the seventh and ninth harmonics are considerable. As M_f is increased, the order of the harmonics, which are a high percentage of the fundamental, also increases. The load on an inverter is usually inductive, which acts like a low-pass filter. Therefore, the higher-order harmonics are easily filtered out. But the low-order harmonics are not. So, if the M_f is high, the low-order harmonic content of the voltage will be very small and the high-order harmonics will be filtered out giving near sinusoidal currents. M_f should be made as high as possible to reduce the harmonic content of the load current. Another consideration is the high switching frequency that increases the switching loss.

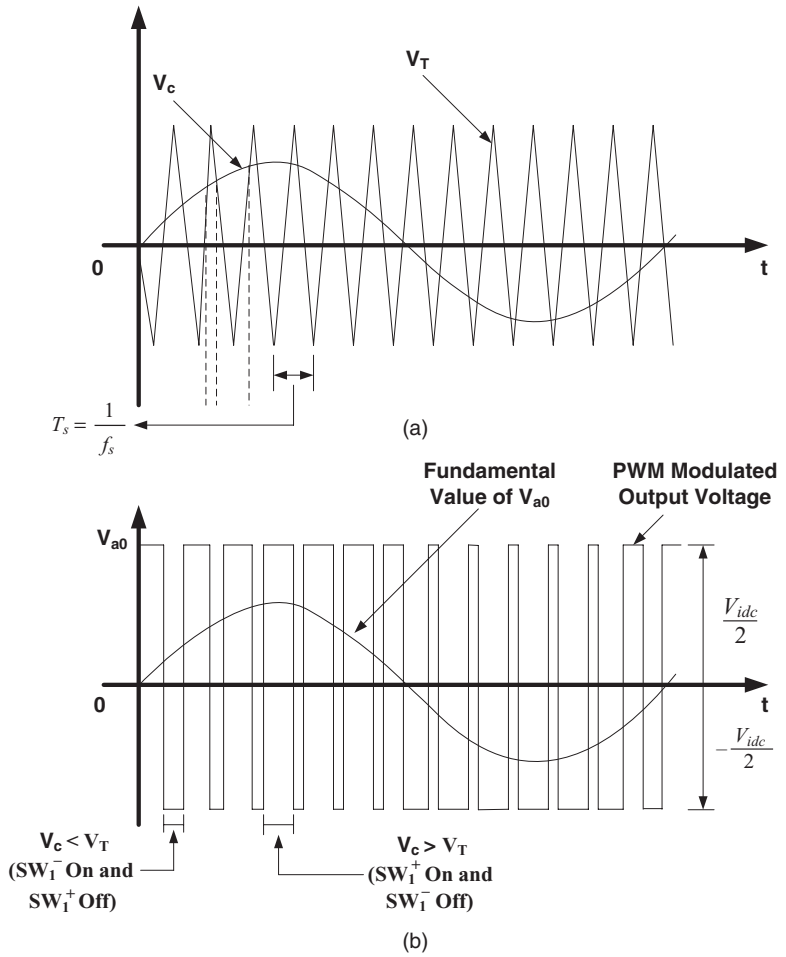

Figure 3.9 The Waveforms of a Single-Phase Inverter with Two Switches with an M_f of 13.

Thus, a tradeoff has to be reached between the switching loss, audible noise, and the harmonic distortion.

Figure 3.9 shows the waveform of the single-phase inverter with two switches when the M_f is increased to 13. The frequency of the triangular wave is 780 Hz, which is 13 times the power frequency. It can be seen from the figure that the switches are turned off and on as shown in Fig. 3.9 in a particular cycle. The higher switching frequency affects the efficiency of the inverter by increasing the switching losses.

Figure 3.10 shows the details of the output voltage and the flow of currents with different switches on when the load is inductive in nature (current lags behind the voltage). The flow of current through the switches depends on the

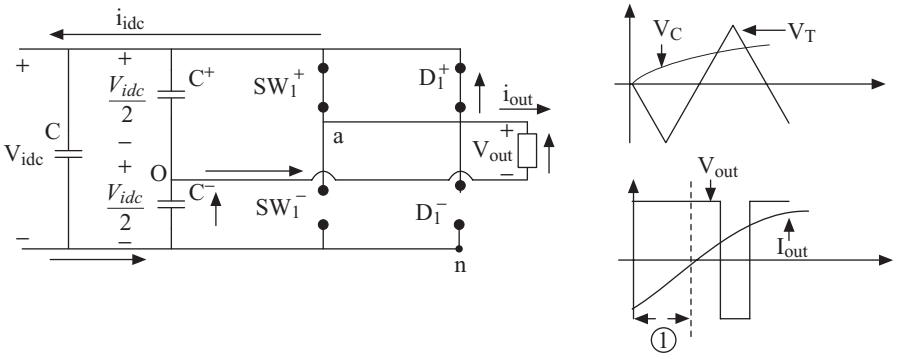

(a) SW_1^+ on, SW_1^- off and D_1^+ conducting, $V_{ao} = +V_{idc}/2$, $i_{out} < 0$

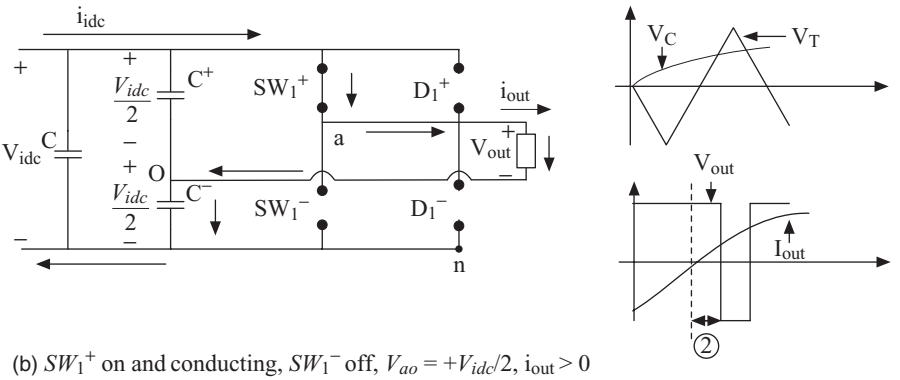

(b) SW_1^+ on and conducting, SW_1^- off, $V_{ao} = +V_{idc}/2$, $i_{out} > 0$

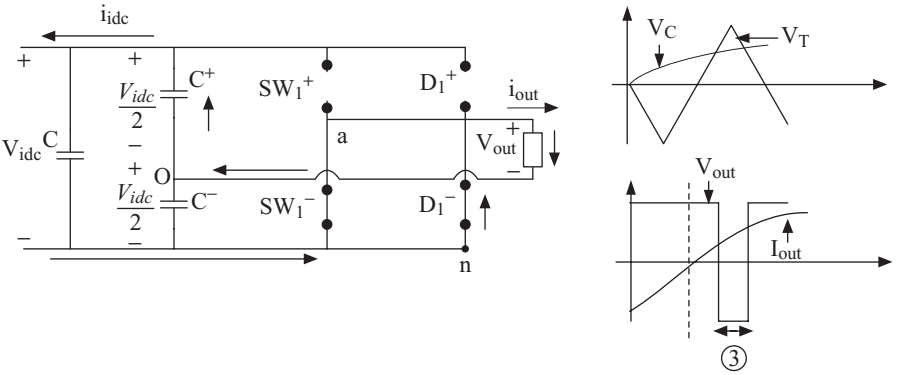

(c) SW_1^- on, SW_1^+ off and D_1^- conducting, $V_{ao} = -V_{idc}/2$, $i_{out} > 0$

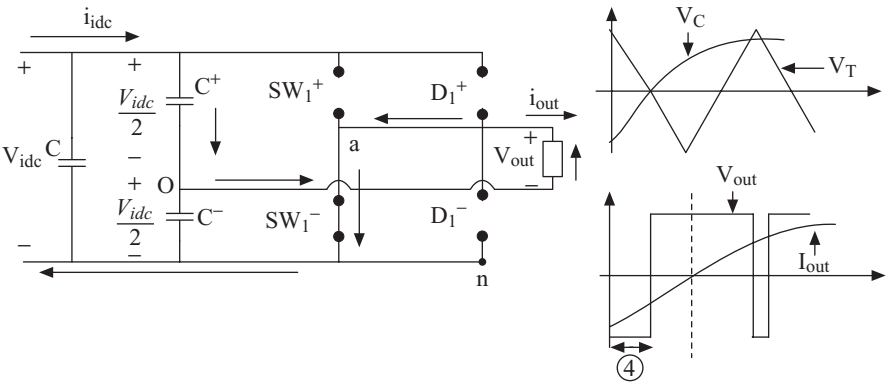

(d) SW_1^- on and conducting, SW_1^+ off, $V_{ao} = -V_{idc}/2$, $i_{out} < 0$

Figure 3.10 (a-d) The Equivalent Circuit of the Single-Phase Inverter with Two Switches for Various Operating Conditions.

direction of current and which switch is on or off. When V_c is greater than V_T, SW_1^+ is turned on by a gate pulse sent to its base. However, the switch SW_1^+ cannot carry current in a negative direction. At this time, the diode D_1^+ is forward biased and conducts the current [see Fig. 3.10(a)]. Now, the potential at point a is that of the positive DC bus. This will reverse bias the diode D_1^-. This condition persists in region 1 as shown in Fig. 3.10(a). After a while, if V_C is still greater than V_T, the current becomes positive, and SW_1^+ is still on, the SW_1^+ conducts current as shown in Fig. 3.10(b). At this stage, the small ohmic voltage drop across SW_1^+ will keep D_1^+ reverse biased and off, while D_1^- is reverse biased by the positive DC bus voltage at point a. This condition exists in region 2 as shown in Fig. 3.10(b). The switch SW_1^+ carries current in a positive direction, while the diode D_1^+ carries current in negative direction. Therefore, the switch as a whole carries current in both directions. However, which component of the switch is carrying current depends of the biased pulse control signals direction of current. Now, when V_c becomes smaller than V_T, SW_1^- is turned on. At this stage, if the current is still positive the current flows through D_1^-. The potential at point a is that of the negative DC bus voltage. The diode D_1^+ is reverse biased by this voltage. This condition is shown in Fig. 3.10(c) in region 3. The last region is the region where the output current is negative, while V_C is smaller than V_T. Now, both voltage and current are negative. This condition is shown in Figure 3.10(d) in region 4. In this region, the current conducts through SW_1^- and the potential at the point a is the same as the negative DC bus. The flow of current through SW_1^- causes a small voltage ohmic drop in which it keeps D_1^- reverse biased. D_1^+ is kept reverse biased by the negative DC bus potential at node a. The path of current for different directions of current is shown in Fig. 3.10(a–d).

Example 3.1 A half-bridge single-phase inverter with load connected to the center tap point of the capacitors, is to provide 60 Hz at its AC output terminal and it is supplied from a PV source with 380 VDC. Assume the switching frequency of 420 Hz (M_f is 7) and amplitude modulation, M_a of 0.9. Write a MATLAB M-file code to present the waveforms of the inverter. Include the sine wave, triangular wave and the output wave V_{ao}.

Solution
Steps followed to write the program are

1. Input DC value (V_{dc}) and the peak values of $V_T(t)$ and V_C (V_{TMax} and V_{Cmax}, respectively) are assigned.
2. The frequencies of $V_T(t)$ and V_C are assigned (f_T and f_C, respectively).
3. T_s, the period of V_T, is calculated as the inverse of f_T.
4. "For loop" is now used to plot V_T, V_C, and V_o by varying k from 0 to 2/60 (two power cycles) in steps of T_s /500.
5. V_T is defined by equations of line.
6. Here, after plotting the wave for one period, it is shifted through integral periods to plot it for the entire time range.
7. V_T is plotted in black color: plot (k, V_T, "k"), where "k" indicates black.
8. V_C is plotted in red color: plot (k, V_T, "r"), where "r" indicates red (V_T and V_C are plotted on the same axis).
9. Value of V_o is decided by considering whether $V_C > V_T$ or $V_C \leq V_T$.
   If $V_C > V_T$
   then $V_{an} = V_{dc}/2$
   else $V_{an} = -V_{dc}/2$
10. V_o is plotted with offset –500 and in blue color indicated by "b":
    plot (k, –500 + V_{an}_new, "b")
11. The points where V_T and V_C intersect are the points of discontinuity for V_O. Here the solid lines and dotted lines are plotted using loops, keeping the x-axis constant and varying the y-axis and using appropriate colors and limits.

The MATLAB coding results are as depicted in Fig. 3.11.

With single-phase inverters with two switches, two capacitors are needed to make the center-tap point available. This makes the inverter bulky. Moreover, the switches are subjected to a voltage equal to the DC link voltage, but the output of the load can be a maximum of half that value. Therefore, the switches are underutilized. We can use four switches and increase the voltage across the load. This topology will be presented next.[1–5]

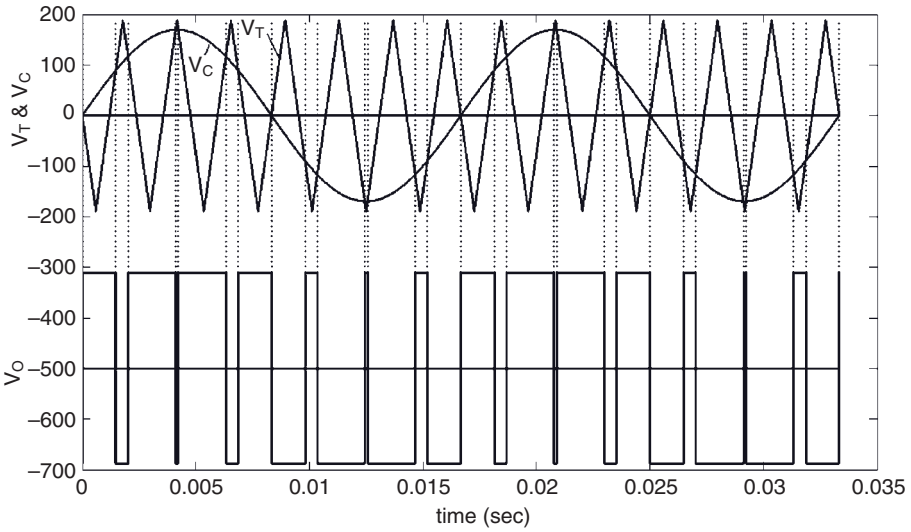

Figure 3.11 The Pulse Width Modulation (PWM) Waveforms of a Single-Phase with Voltage Switching for a Half-Bridge Inverter from MATLAB Coding.

3.3 SINGLE-PHASE DC/AC INVERTERS WITH A FOUR-SWITCH BIPOLAR SWITCHING METHOD

This DC/AC converter topology has two legs. Each leg has two controllable switches and each switch can be turned on by sending a pulse to its base. The operation of each leg is as described before for the half-bridge single-phase converters. For the converter of Fig. 3.12, the SW_1^+ and SW_2^- and SW_1^- and SW_2^+ are switched as pairs. This topology allows the load voltage to vary between $+V_{idc}$ and $-V_{idc}$, which is double the variation available in inverters with two switches. This results in higher voltage and allows more power handling capability of these inverters. When SW_1^+ and SW_2^- are on, the effective voltage across the load terminals is the difference in the voltages at nodes a and b and in this case the voltage is $+V_{idc}$. Again, when SW_2^+ and SW_1^- are on, load voltage is $-V_{idc}$. When sine PWM as shown in Fig. 3.13 is applied, the peak of the fundamental output voltage is given by

$$V_{o,1} = V_{idc} M_a \tag{3.6}$$

Similar logic is followed for an inverter with two switches. If $V_c > V_T$ then the switches SW_1^+ and SW_2^- are on and other switches are off, results V_{an} at V_{idc} and V_{bn} at zero resulting in an output voltage V_{ab} $(= V_{an} - V_{bn})$ of $+V_{idc}$. When $V_c < V_T$ and the switches SW_1^- and SW_2^+ are on, we have V_{an} at zero voltage and V_{bn} at V_{idc} voltage giving an output voltage V_{ab} $(= V_{an} - V_{bn})$ of $-V_{idc}$.

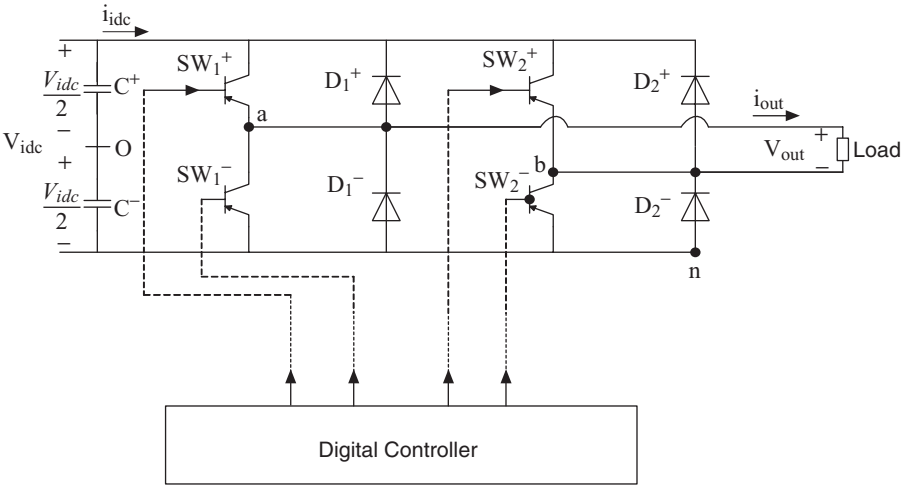

Figure 3.12 A Single-Phase DC/AC Converter with Four Switches.

Therefore, the output voltage varies between the $+V_{idc}$ and $-V_{idc}$ as shown in Fig. 3.13. This modulation technique is known as bipolar sine PWM as the output voltage jumps between positive and negative values.

Therefore, for bipolar output voltage waveform, we have the following switching policy.

If $V_c > V_T$ SW_1^+ and SW_2^- are on, other switches are off and $V_{ab} = V_{idc.}$
If $V_c < V_T$ SW_1^- and SW_2^+ are on, other switches are off and $V_{ab} = -V_{idc}$.

The sequences of switching operations are shown in Fig. 3.14 with the details of the direction of flow of current and the output voltage when different combinations of switches are on.

The output voltage in this case is given by

$$V_{ao} = V_{idc} M_a \cdot \sin \omega_e t + harmonics \tag{3.7}$$

where the $\omega_e = 2\pi \cdot f_e$ is the frequency of the sine wave in radian per second and f_e is the frequency of the sine wave in Hz.

The peak of the fundamental component is $V_{idc} M_a$ with $0 \le M_a \le 1$. When $0 \le M_a \le 1$, the amplitude of the fundamental varies linearly with the amplitude modulation index. When M_a is greater that one, it enters the nonlinear region and as it is increased further, the fundamental output voltage saturates at $\frac{4}{\pi} \cdot V_{idc}$ and does not increase with M_a.

The switching scheme given above results in an output voltage that jumps back and forth between positive and negative DC link voltage because the

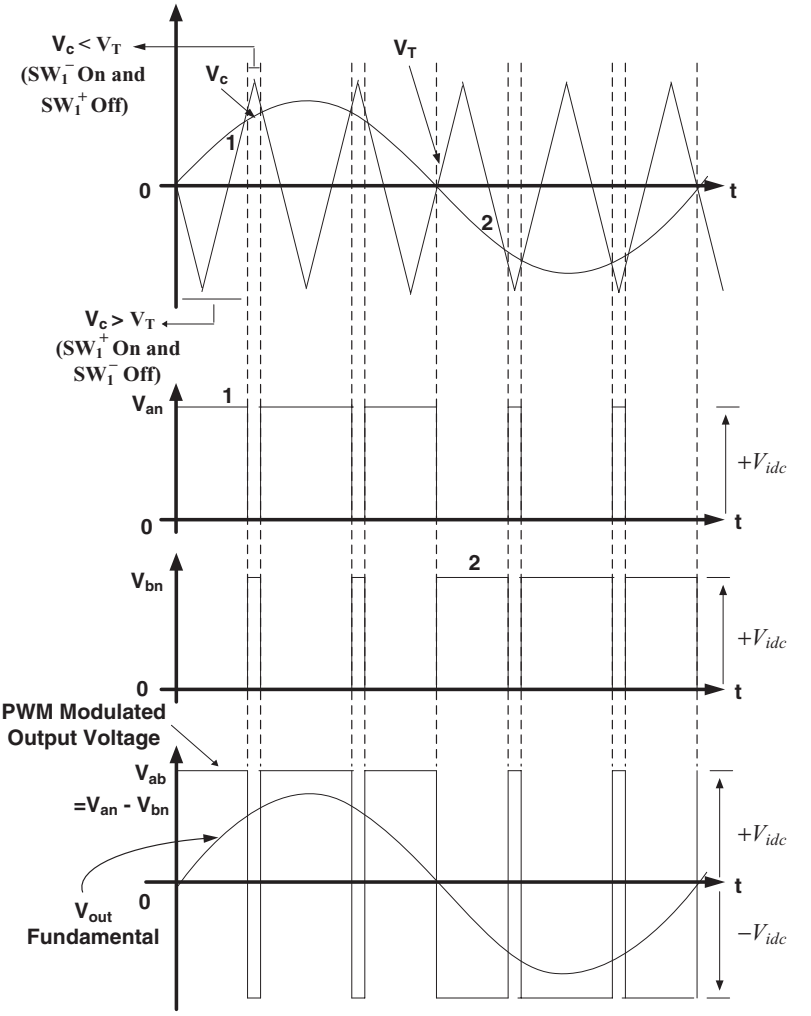

Figure 3.13 Waveforms Showing Sine Pulse Width Modulation (PWM) for Single-Phase Inverter Bipolar Switching.

transition always takes place from positive value to negative value directly, this scheme is called bipolar sine PWM.

The harmonic content of the output voltage in this scheme is the same as that of an inverter with two switches (see Table 3.1). The only difference is that the DC offset voltage in this case is zero.

Like the inverter with two switches, the amplitude of the fundamental component is decided by the sine wave by varying the amplitude modulation index ($M_a = V_{C(Max)} / V_{T(Max)}$). The harmonic content can be reduced by increasing the frequency modulation index ($M_f = f_S / f_e$).[1–5]

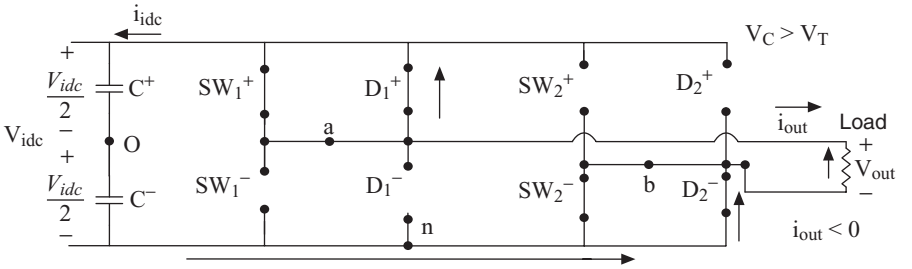

(a) SW_1^+ is on, D_1^+ is on and conducting ($V_{an} = V_{idc}$); SW_2^- is on, D_2^- is on and conducting ($V_{bn} = 0$), $V_{out} = V_{an} - V_{bn} = V_{idc}$, $i_{out} < 0$.

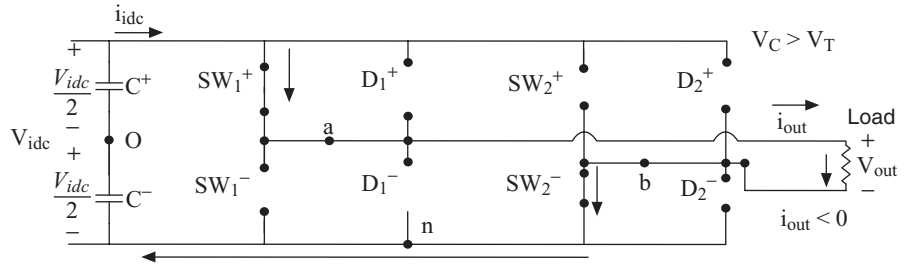

(b) SW_1^+ is on and conducting ($V_{an} = V_{idc}$); SW_2^- is on and conducting ($V_{bn} = 0$), $V_{out} = V_{an} - V_{bn} = V_{idc}$, $i_{out} > 0$.

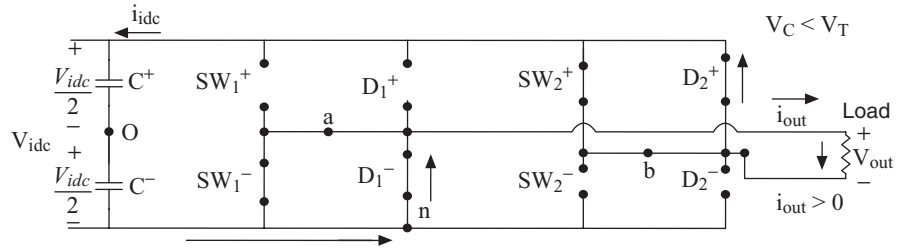

(c) SW_1^- is on, D_1^- is on and conducting ($V_{an} = 0$); SW_2^+ is on, D_2^+ is on and conducting ($V_{bn} = V_{idc}$), $V_{out} = V_{an} - V_{bn} = -V_{idc}$, $i_{out} > 0$.

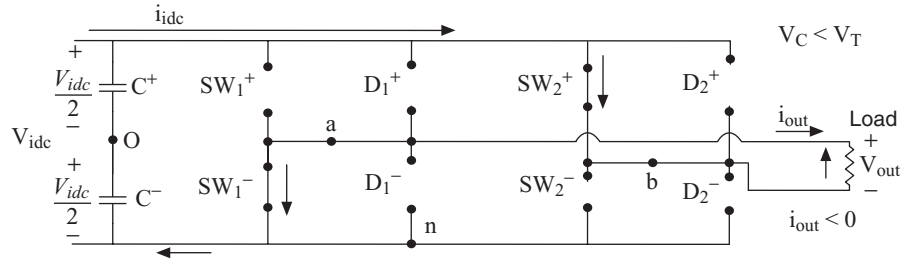

(d) SW_1^- is on and conducting ($V_{an} = 0$); SW_2^+ is on and conducting ($V_{bn} = V_{idc}$), $V_{out} = V_{an} - V_{bn} = -V_{idc}$, $i_{out} < 0$.

Figure 3.14 (a–d) Schematic Representation of Status of Power Switches in a Single-Phase Full-Bridge Inverter.

3.3.1 Pulse Width Modulation with Unipolar Voltage Switching for a Single-Phase Full-Bridge Inverter

In the bipolar PWM scheme, the output PWM voltage jumps between $+V_{idc}$ and $-V_{idc}$. Therefore, the load is subjected to high-voltage fluctuations. The insulations on the load get subject to high stress for this reason. The unipolar PWM method allows the output voltage to jump between $+V_{idc}$ and 0 or $-V_{idc}$ and 0, The switching logic is the same as that for single-phase inverters with two switches, but here there are two legs switched independently with two sine waves. The upper switch of a leg is on when the V_c for that leg is having a greater magnitude than V_T. The same logic is followed for the other leg with its own sine wave, which is 180° apart from the sine wave of the first leg. This results in voltage waveforms shown in Fig. 3.15.

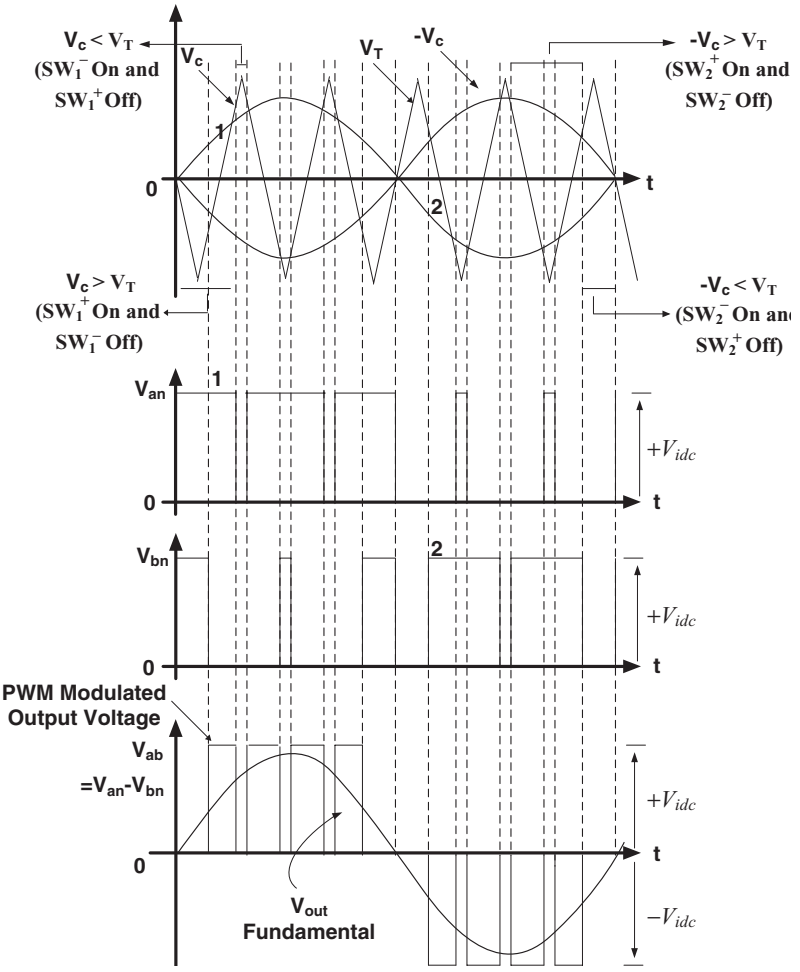

Figure 3.15 Waveforms for the Unipolar Switching Scheme of a Single-Phase Inverter with Four Switches and a Frequency Modulation Index of 5.

The unipolar switching policy can be stated as

If $V_c > V_T$ and $-V_c < V_T$: SW_1^+ and SW_2^- are on, other switches are off and $V_{ab} = V_{idc}$.
If $V_c < V_T$ and $-V_c < V_T$: SW_1^- and SW_2^- are on, other switches are off and $V_{ab} = 0$.
If $V_c < V_T$ and $-V_c > V_T$: SW_1^- and SW_2^+ are on, other switches are off and $V_{ab} = -V_{idc}$.
If $V_c > V_T$ and $-V_c > V_T$: SW_1^+ and SW_2^+ are on, other switches are off and $V_{ab} = 0$.

The output voltage is given by

$$V_{ao} = V_{idc} M_a \cdot \sin \omega_e t + harmonics \tag{3.8}$$

where the $\omega_e = 2\pi \cdot f_e$ is the frequency of the sine wave in radians per second and f_e is the frequency of the sine wave in Hz. Therefore, the peak of the fundamental component has a peak of $V_{idc} M_a$ with $0 \le M_a \le 1$. When $0 \le M_a \le 1$, the amplitude of the fundamental varies linearly with the amplitude modulation index. When M_a is greater that one, it enters the nonlinear region and as it is increased further, the fundamental output voltage saturates at $(4/\pi) \cdot V_{idc}$ and does not increase with M_a.

Similar to the other PWM schemes, here too the frequency and the magnitude of the output voltage is controlled by the reference sine wave and the harmonic content of the output voltage is determined by the frequency modulation index.

Example 3.2 Consider a PV source of 60 V. A single-phase inverter with four switches is used to convert DC to 50 Hz AC using a unipolar scheme. Assume M_a of 0.5 and M_f of 7. Develop a MATLAB program to generate the waveforms of the inverter showing the control voltage and the output voltage.

Solution
The following plots were obtained.

Similar to Table 3.1, Table 3.2 tabulates the harmonic content of the output voltage. Here, it tabulates the output voltage of the unipolar switching scheme. It can be seen from the table that for a frequency modulation index higher than 5, the lower-order harmonics are practically absent. The higher order harmonics in the voltage are not usually a matter of concern because they are filtered out by the low pass characteristics of the inductive loads. The unipolar switching, therefore, has the advantage of reduced harmonics and reduced voltage fluctuations in the load. The number of times a particular switch turns on and off is the same as bipolar switching.[1–5]

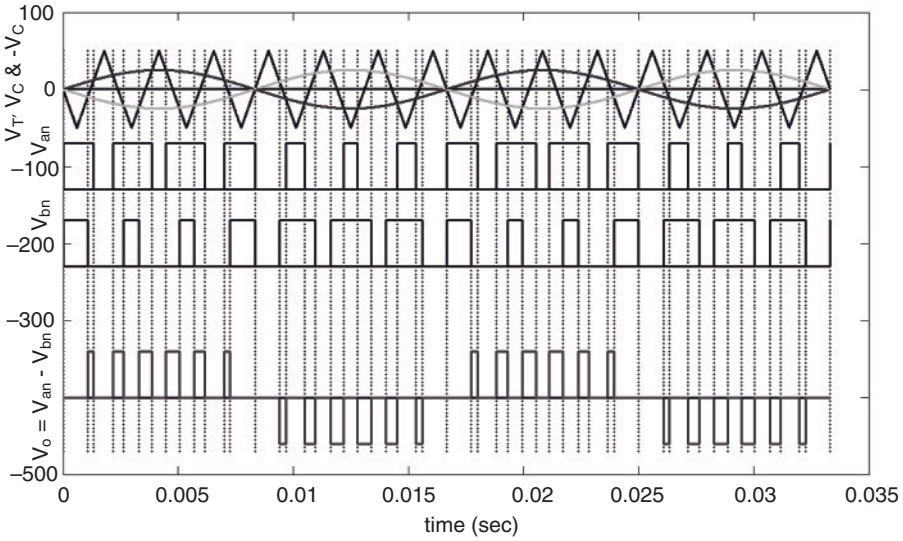

Figure 3.16 A MATLAB Plot of a Unipolar Switching Scheme for a Single-Phase Inverter with Four Switches.

TABLE 3.2 The Harmonic Content of the Output Voltage for a Different M_f with M_a Fixed at 0.6 for a Unipolar Switching Scheme.

Order of Harmonic	$M_f = 3$ (%)	$M_f = 5$ (%)	$M_f = 7$ (%)	$M_f = 9$ (%)
1	100	100	100	100
3	12	0.01	0.01	0.01
5	61	0.55	0.01	0.03
7	67	12	0.03	0.02
9	33	62	0.58	0.01

3.4 THREE-PHASE DC/AC INVERTERS

A three-phase inverter has three legs, one for each phase, as shown in Fig. 3.17. Each inverter leg operates as a single-phase inverter.[2–3] The output voltage of each leg V_{an}, V_{bn}, $V_{cn,}$ where n refers to negative DC bus voltage is computed from the input voltage, V_{idc}, and the switch positions. The inverter has three terminals, two inputs, and one output. The inverter input is DC power that can be supplied from a storage battery system, a PV power source, a fuel cell, or a green energy DC power source such as high-speed generators or variable speed wind generators. The sine wave signal is supplied to a digital signal processor (DSP) controller to control the output AC voltage, power, and frequency. The DSP controller sends a sequence of switching signals to control the six power switches to produce the desired output AC power.[1–5]

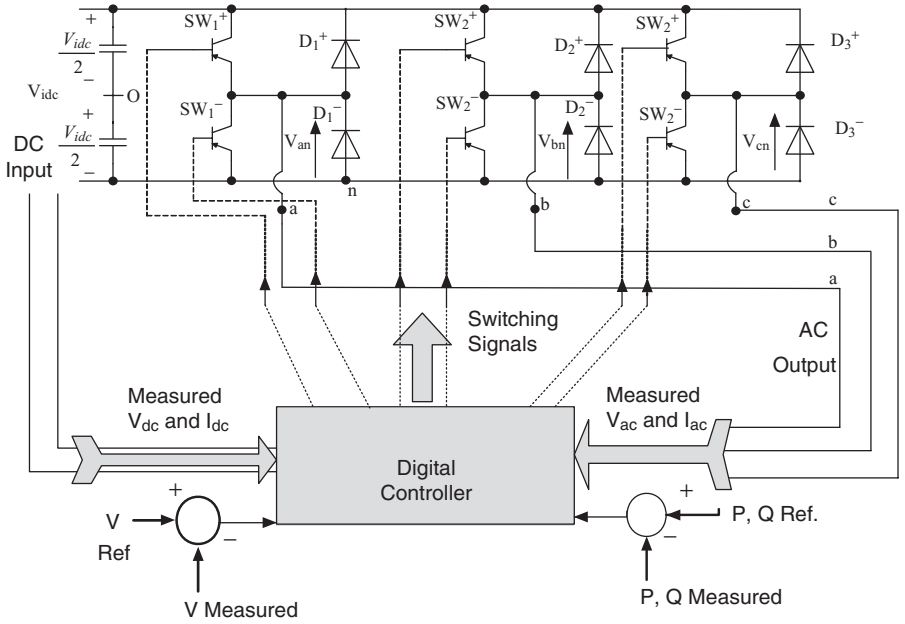

Figure 3.17 The Operation of an Inverter as a Three-Terminal Device.

3.5 PULSE WIDTH MODULATION METHODS

3.5.1 The Triangular Method

The triangular wave can be modeled by equations of lines.

A line can be expressed as

$$Y = mx + b \tag{3.9}$$

where b is the Y-intercept and m is the slope. In Fig. 3.18, the Y-intercept is 0. The slope can be calculated as shown below.

$$\frac{y_2 - y_1}{x_2 - x_1} = \frac{V_{TMax} - 0}{0.25T_s - 0} \tag{3.10}$$

Thus, for $0 < x \le \dfrac{T_s}{4}$, we have

$$Y = \frac{V_{TMax} \cdot x}{0.25 \cdot T_s}. \tag{3.11}$$

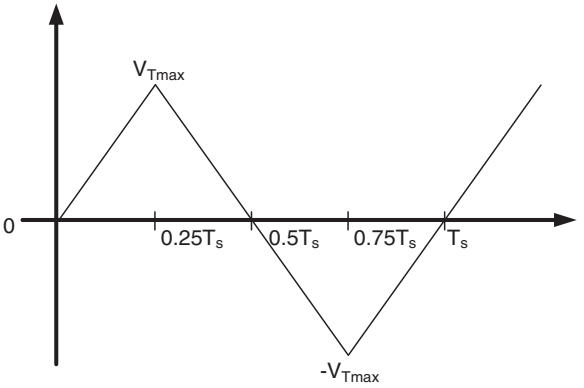

Figure 3.18 Plot of a Triangular Wave.

Here x represents time and Y is amplitude. This process can be repeated for each line segment.

$$m = \frac{y_2 - y_1}{x_2 - x_1} = \frac{0 - V_{TMax}}{0.5T_s - 0.25T_s}, \qquad \text{for} \qquad \frac{T_s}{4} < x \le \frac{T_s}{2} \tag{3.12}$$

The slope m, can be expressed as

$$m = \frac{-V_{TMax}}{0.25 \cdot T_s} \tag{3.13}$$

$$b = Y - m \cdot x, \text{ and therefore, } b = V_{TMax} - \left(-\frac{V_{TMax}}{0.25 \cdot T_S} \right) \cdot 0.25T_S. \tag{3.14}$$

$$Y = \frac{-V_{TMax}}{0.25 \cdot T_S} \cdot x + \left[V_{TMax} - \left(-\frac{V_{TMax}}{0.25 \cdot T_S} \right) \cdot 0.25T_S \right] \tag{3.15}$$

For, $\frac{T_s}{2} < x \le \frac{3T_s}{4}$, the slope m, can be expressed as

$$m = \frac{-V_{TMax} - 0}{0.75 \cdot T_s - 0.5 \cdot T_s} = \frac{-V_{TMax}}{0.25 \cdot T_s} \tag{3.16}$$

$$b = 0 - \left[\frac{-V_{TMax}}{0.25 \cdot T_s} \right] 0.5T_s = \frac{V_{TMax}}{0.25 \cdot T_s} 0.5T_s \tag{3.17}$$

$$Y = \frac{-V_{TMax}}{0.25 \cdot T_s} \cdot x + \left[\frac{V_{TMax}}{0.25 \cdot T_s} 0.5T_s \right] \tag{3.18}$$

for, $\frac{3T_s}{4} < x \le T_s$, the slope m, can be expressed as

$$m = \frac{0-(-V_{TMax})}{T_s - 0.75 \cdot T_s} \quad \text{and} \quad m = \frac{V_{TMax}}{0.25 \cdot T_s} \tag{3.19}$$

$$\text{And } b = -V_{TMax} - \frac{V_{TMax}}{0.25T_s} 0.75T_s \tag{3.20}$$

And the line equation for this time segment can be expressed as

$$Y = \frac{V_{TMax}}{0.25T_s} x + \left[-V_{TMax} - \left(\frac{V_{TMax}}{0.25T_s} 0.75T_s \right) \right] \tag{3.21}$$

The equations above would result in one full period of a triangle wave at the desired frequency, f_s. These equations can now be coded into MATLAB to output the waveform. The MATLAB codes, each period are

$$t_1 = 0\text{: Step size: } T_s/4 \tag{3.22}$$

$$t_2 = T_s/4 + \text{Step size: Step size: } T_s/2 \tag{3.23}$$

$$t_3 = T_s/2 + \text{Step size: Step size: } 3\ T_s/4 \tag{3.24}$$

$$t_4 = 3\ \mathrm{T_s}/4 + \text{Step size: Step size: } T_s \tag{3.25}$$

The step size is user defined. However, it should be reasonably small. To show the operation of a single-phase inverter in a MATLAB simulation, we will put the above into a matrix of one row by multiple columns as shown below.

$$\text{Time} = [t_1\ t_2\ t_3\ t_4]$$

Line equations can then be coded in MATLAB into a matrix form as shown below. One period of the triangular wave can be broken into four regions as mentioned in Equations 3.22–3.25.

Line 1: $\frac{V_{TMax} \cdot t_1}{T_S/4}$

Line 2: $-\frac{V_{TMax} \cdot t_2}{T_S/4} + \left[V_{TMax} - \left(-\frac{V_{TMax}}{T_S/4} \cdot \frac{T_S}{4} \right) \right]$

Line 3: $-\frac{V_{TMax} \cdot t_3}{T_S/4} + \frac{V_{TMax}}{T_S/4} \cdot \frac{T_S}{2}$

Line 4: $\frac{V_{TMax} \cdot t_4}{T_S/4} + \left[-V_{TMax} - \left(\frac{V_{TMax}}{T_S/4} \cdot \frac{3T_S}{4} \right) \right]$

We can write a MATLAB code as

FullLine = [Line1 Line2 Line3 Line4]

Then, the triangular wave can be plotted using the MATLAB code as

plot (Time, Full Line)

The above MATLAB codes can only create one period, which cannot show the operation of the inverter. This can be remedied by restarting the wave back at $t = 0$. After a full period has been completed, this is just a reference wave and remains constant.[1–5]

Example 3.3 Assume a single-phase full-bridge inverter is to provide 120 V, 60 Hz, 2 kW at its AC output terminal, and is supplied from a PV source under 600 VDC. In practice, the sampling frequency is generally in the range of 5 kHz or above 20 kHz out of the sensitive audio frequency range. However, here it has been selected to be much lower than that so that the waveforms can be seen clearly. Assume the switching frequency of 420 Hz and amplitude modulation, M_a of 0.9. Define the simulation steps and develop a MATLAB program using the triangular method.

The steps are

1. Input the DC value (V_{dc}) and assign the peak values of $V_T(t)$ and V_C (V_{TMax} and V_{Cmax}, respectively).
2. The sampling frequency of $V_T(t)$ is designated as f_S and the sampling frequency of V_C is designated as are assigned sampling f_C.
3. T_s, the period of V_T, is calculated as the inverse of f_S.
4. "For loop" is now used to plot V_T, V_C, and V_o by varying k from 0 to 2/60 (two power cycles) in steps of T_s/500
5. V_T is defined by equations of line for triangular method:

$$V_T = -V_{TMax} \cdot \frac{remainder\ of\ (k/T_S)}{T_S/4}$$

$$\text{for} \quad 0 \le remainder\ of \left(\frac{k}{T_S}\right) < \frac{T_S}{4}$$

$$= V_{TMax} \cdot \frac{remainder\ of\ (k/T_S) - 0.5 \cdot T_S}{T_S/4}$$

$$\text{for} \quad \frac{T_S}{4} \le remainder\ of \left(\frac{k}{T_S}\right) < \frac{3 \cdot T_S}{4}$$

$$= -V_{TMax} \cdot \frac{remainder\ of\ (k/T_S) - \cdot T_S}{T_S/4}$$

6. Here, after plotting the wave for one period, it is shifted through integral periods to plot it for the entire time range.
7. V_T is plotted in black color: plot (k, V_T, "k"), where "k" indicates black
8. V_C is plotted in red color: plot (k, V_T, "r"), where "r" indicates red (V_T and V_C are plotted on the same axis).
9. The value of V_o is decided by considering whether $V_C > V_T$ or $V_C < V_T$
   If $V_C > V_T$
   then $V_{an} = V_{dc}$
   else $V_{an} = -V_{dc}$
10. V_o is plotted with offset –500, and in blue color indicated by "b":
    plot (k, –500 + V_{an}_new, "b");
11. The points where V_T and V_C intersect are the points of discontinuity for V_O. Here the solid lines and dotted lines are plotted using loops to keep the x-axis constant and by varying the y-axis and using appropriate colors and limits.

```
MATLAB Program
VCMax=120*sqrt(2);          %maximum value of VC
VTMax=VCMax/0.9;            %maximum value of VT
Vdc=VTMax;                  %input dc value
fC=60;                      %frequency of VC
fT=420;                     %frequency of VT
Ts=1/fT;                    %time period of VT
Vo_new=0;
for k=0:Ts/500:2/60         % to plot from 0 to 0.04 sec
                            in steps of Ts/500
  plot (k,0,'k');
  plot (k,-500,'k');        % the 2 time-axes are plotted
                            at different offsets
  if(rem(k,Ts)<Ts/4)        % VT is defined using
                            equations of line
    VT=-VTMax*rem(k,Ts)/0.25/Ts;
  elseif(rem(k,Ts)>=Ts/4 && rem(k,Ts)<3*Ts/4)
    VT=VTMax*(rem(k,Ts)-0.5*Ts)/0.25/Ts;
  else
    VT=-VTMax*(rem(k,Ts)-Ts)/0.25/Ts;
  end                       %VT is defined using
                            identity mapping
  VC=VCMax*sin(2*pi*fC*k); % VC is defined
  plot (k,VT,'k');          %VT is plotted in black ('k')
  hold on
  plot (k,VC,'r');          %VC is plotted in red ('r')
                            on the same axis as VT
```

```
  hold on
%ploting Von
  if (VC>VT) %Vo is decided depending on VC>VT and
value assigned in Vo_new
    Vo_old=Vo_new;
    Vo_new=Vdc;
  else
    Vo_old=Vo_new;
    Vo_new=-Vdc;
  end
  plot (k,-500+Vo_new,'b');          %Van is plotted in
                                     blue ('b') with offset
                                     of -500
  hold on
  if(Vo_new ~= Vo_old)               %The points of
                                     discontinuity in Van
                                     are found out
    for j = -500-Vdc:30:VTMax        %dotted lines plotted
      plot (k,j);
      hold on
    end
    for j = -500-Vdc:.2:-500+Vdc     %continuous lines
                                     plotted between the
                                     upper & lower lines
                                     %of Vo=Va - Vb
      plot (k,j);
      hold on
    end
  end
end
```

Figure 3.19 depicts the results of the simulation of Method 1.

3.5.2 The Identity Method

This method uses identity mapping by assigning a number x to the same number x. If y (x) is equal to x, then if

$$x = 1 \text{ then } y = 1,$$
$$x = 2 \text{ then } y = 2, \text{ etc.} \tag{3.26}$$

The function that accomplishes this for a triangle wave can be expressed as

$$F(x) = \sin^{-1}(\sin x) \tag{3.27}$$

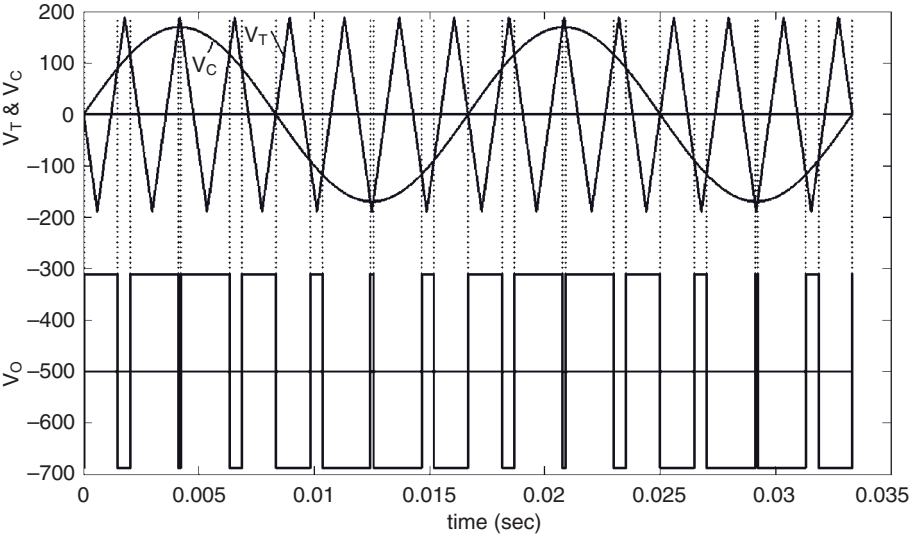

Figure 3.19 Plot of $V_T(t)$ and $Vc(t)$ and V_o for Example 3.3 Using the Equation of Line of Triangular Method.

Substituting in any numbers for x, it will result $F(x) = x$. Thus, as the sine wave propagates, the arcsine will cause $F(x)$ to look like a triangular wave not a sine wave. Because MATLAB works in radians, this equation needs to be multiplied by $2/\pi$. Then when the sine wave hits its max of $\pi/2$ and $-\pi/2$ it will become

$$F(x) = A \cdot \frac{2}{\pi} \cdot \sin^{-1}(\sin x) \tag{3.28}$$

Example 3.4 Repeat Example 3.3 by plotting the triangular wave using identity mapping.

Solution
The same procedure is followed as in the triangular method. The only difference is that the V_T is defined differently: $V_T = V_{TMax} \cdot \frac{2}{\pi} \cdot a\sin(\sin(2\pi \cdot f_s \cdot t))$. The result obtained is the same as that obtained in the triangular method.

3.6 ANALYSIS OF DC/AC THREE-PHASE INVERTERS

The three-phase inverters have six switches and six diodes as shown in Fig. 3.20. A switch is formed by the pair SW_i and D_i ($i = a, b, c$), which can conduct current in both directions. The three-phase inverter consists of three limbs that lie between the DC links, with each limb having two switches. By

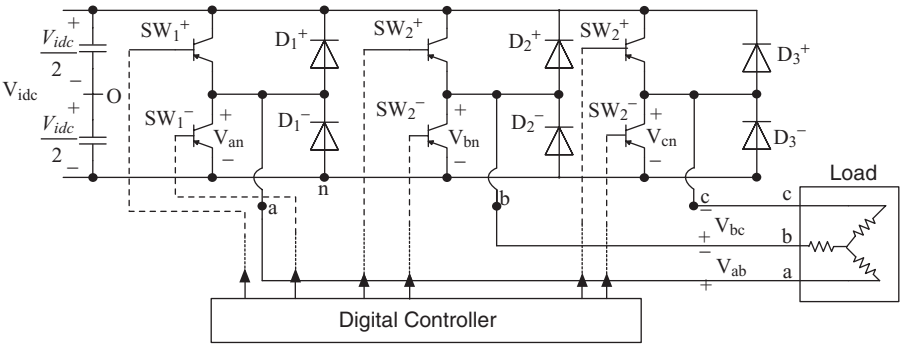

Figure 3.20 Three-Phase Inverter Topology.

turning on the upper switch, the output node (a, b, or c) acquires a voltage of the upper DC line. Conversely, when the lower switch of a limb is on, the output node of that limb attains a voltage of the lower DC line. By alternately turning on the upper and lower switch, the node voltage oscillates between the upper and lower DC line voltages.

$$V_{L-L,rms} = M_a \cdot \sqrt{\frac{3}{2}} \cdot \frac{V_{idc}}{2} \tag{3.29}$$

The above can be approximated as

$$V_{L-L,rms} = 0.612\, V_{idc}$$

where $V_{L-L,rms}$ denotes the root mean square (RMS) value of the fundamental of output line voltage.

Therefore, as was stated for single-phase inverters, the switching frequency is decided by the triangular wave, V_T and the output voltage is decided by the reference control voltage V_C, modulating wave. The modulated output voltage of each leg has the same waveform of a single-phase converter. The frequency modulation index determines the harmonic content in the output voltage waveform. The standard frequency is 60 Hz for the United States and 50 Hz in most other countries. It is generally desirable that the frequency of the triangular wave be very high to make a high-frequency modulation index that will result in low harmonics in output voltage and the load currents. However, with an increase of the triangular frequency, the switching frequency increases and the high switching frequency results in high switching losses.

Several other factors affect the selection of switching frequency; it is also desirable to use high switching frequency due to the relative ease of filtering harmonic voltages. In addition, if the switching frequency is too high, the switches may fail to turn on and off properly; this may result in a short-circuit of the DC link buses and damage the switches. In a residential and commercial

system, the switching frequency selected has to be out of the audible frequency range to reduce the high-pitch audible noise. Therefore, for most applications the switching frequency is selected to be below 6 kHz or above 20 kHz. For most applications in a residential system, the switching frequency is selected below 6 kHz.

To develop a simulation model for the above converter operation, we need to express the above waveforms by mathematical expressions.

Let us assume that V_C (Phase a) can be expressed as

$$V_{C(a)} = M_a \sin(\omega_e t) \tag{3.30}$$

where $\omega_e = \dfrac{2\pi}{T_e} t$, $T_e = \dfrac{1}{f_e}$ and f_e is the frequency of desired controlled voltage and

$$M_a = \frac{V_{C(\max)}}{V_{T(\max)}}.$$

The expression for the triangular waveform is given by

$$x_1 = -1 + \frac{T_s}{2} t \qquad \text{for} \qquad 0 \le t < \frac{T_s}{2}$$

Expressing the unit of time t in radian and recalling $f_s = M_a f_e$

The above can be rewritten as

$$x_1 = -1 + \frac{2N}{\pi} \cdot \omega_e t \qquad \text{for} \qquad 0 \le \omega_e t < \frac{\omega_e T_s}{2} \tag{3.31}$$

where $N = 1,2,3$ and so on. In this formulation, M_f can be selected as a variable of the simulation.

We can rewrite the above as

$$x_1(t) = -1 + \frac{2N}{\pi} \cdot \omega_e t \qquad \text{for} \qquad 0 \le \omega_e < \frac{\pi}{M_f} \tag{3.32}$$

Similarly,

$$x_2(t) = 3 - \frac{2M_f}{\pi} \omega_e t \qquad \text{for} \qquad \frac{\pi}{N} \le \omega_e t < \frac{2\pi}{M_f} \tag{3.33}$$

The triangular waveform $V_T(t)$ can be modeled by Equations 3.32 and 3.33.

To develop a simulation testbed, let us express V_C (for Phase a), V_C (for Phase b), and V_C (for Phase c) as

$$V_C(a) = M_a \sin \omega_e t \tag{3.34}$$

$$V_C(b) = M_a \sin\left(\omega_e t - \frac{2\pi}{3}\right) \tag{3.35}$$

$$V_C(c) = M_a \sin\left(\omega_e t - \frac{4\pi}{3}\right) \tag{3.36}$$

And the triangular wave of $V_T(t)$ as

$$x_1(t) = -1 + 2N\frac{\omega_e t}{\pi} \quad \text{for} \quad 0 \le \omega_e t < \frac{\pi}{N} \tag{3.37}$$

$$x_2(t) = 3 - 2N\frac{\omega_e t}{\pi} \quad \text{for} \quad \frac{\pi}{N} \le \omega_e t < \frac{2\pi}{N} \tag{3.38}$$

Therefore, the algorithm PWM voltage generation steps are as follows.

$$\text{If } V_c(a) \ge x_1(t) \text{ or } x_2(t), \text{ then } V_{an} = V_{idc} \tag{3.39}$$

Similarly,

$$\text{If } V_c(\text{b}) \ge x_1(t) \text{ or } x_2(t), \text{ then } V_{bn} = V_{idc} \tag{3.40}$$

$$\text{If } V_c(\text{c}) \ge x_1(t) \text{ or } x_2(t), \text{ then } V_{cn} = V_{idc} \tag{3.41}$$

$$\text{Otherwise, } V_{an} = 0;\ V_{bn} = 0 \text{ and } V_{cn} = 0 \tag{3.42}$$

The i_{idc} can be computed as:

$$i_{idc} = i_a \times SW_1^+ + i_b \times SW_2^+ + i_c \times SW_3^+ \tag{3.43}$$

As discussed in the operation of a single-phase converter, one switch is on in each leg of the three-phase converter. A sequence of switching operation for one cycle of inverter operation is shown in Fig. 3.22. For example, in phase a, V_{an} with respect to the negative DC bus depends on V_{idc} and the switch status SW_1^+ and SW_1^-. This is depicted by Fig. 3.22a.

The control objective is the same as discussed for a single-phase converter, that is the PWM seeks to control the modulated output voltage of each phase such that the magnitude and frequency of the fundamental inverter output voltage is the same as the control voltage. The PWM samples the DC bus voltage and the sampled voltage is the inverter output voltage.

Example 3.5 Compute the minimum DC input voltage if the switching frequency is set at 5 kHz. Assume the inverter is rated 207.6 V AC, 60 Hz, 100 kVA.

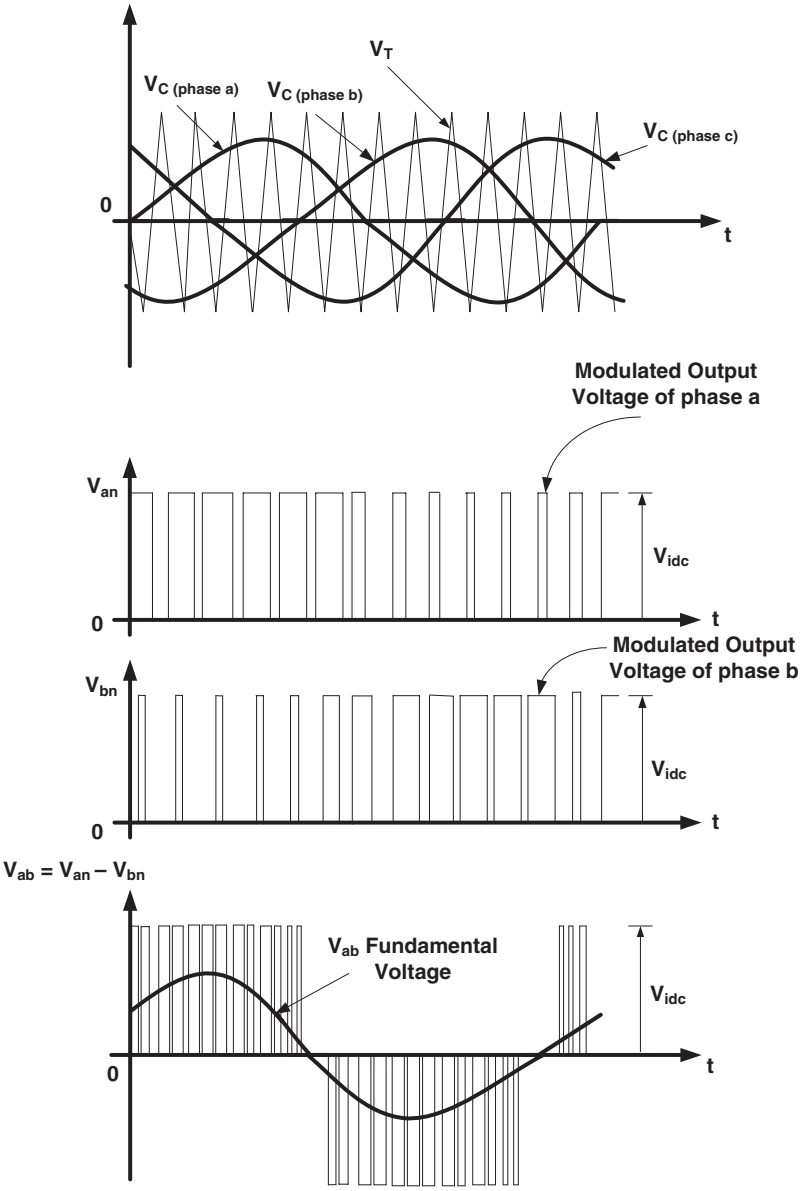

Figure 3.21 A Pulse Width Modulation (PWM) Operation of a Three-Phase Converter.

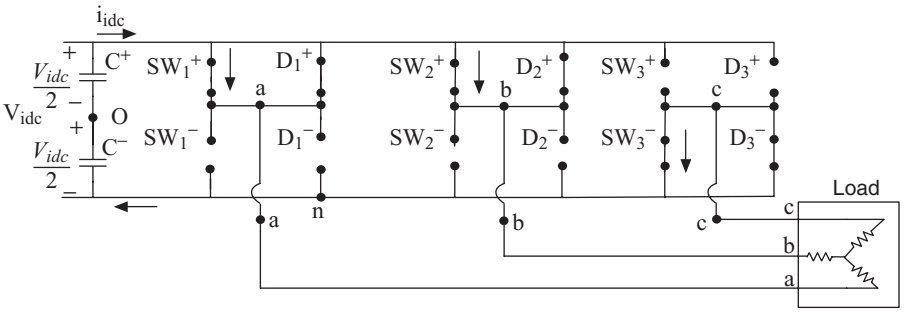

(a) V_{an}, $V_{bn} = V_{idc}$, $V_{cn} = 0$. I_a, $I_b > 0$, $I_c < 0$, SW_1^+ on, SW_2^+ on, SW_3^- on

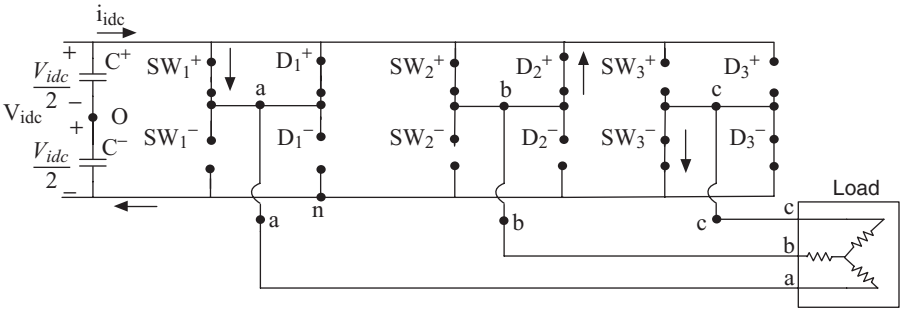

(b) V_{an}, $V_{bn} = V_{idc}$, $V_{cn} = 0$. $I_a > 0$, I_b, $I_c < 0$, SW_1^+ on, D_2^+ on, SW_3^- on

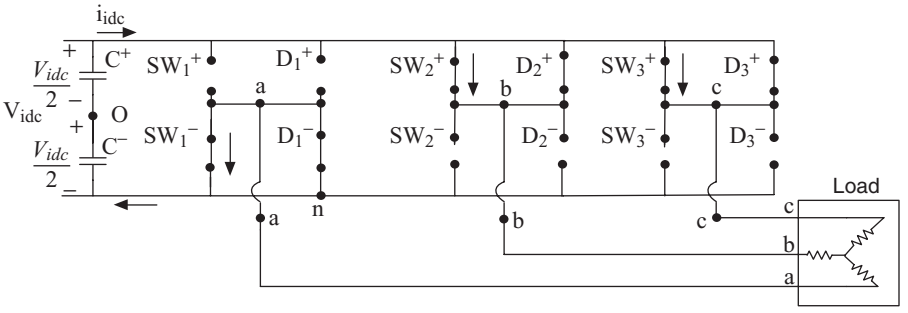

(c) $V_{an} = 0$, $V_{bn} = V_{cn} = V_{idc}$, $I_a < 0$, I_b, $I_c > 0$, SW_1^- on, SW_2^+ on, SW_3^+ on

Solution

$$V_{rated} = 207.6 \text{ V, kVAr} = 100 \text{ kVA}, f = 60 \text{ Hz}$$

The AC-side voltage of the inverter is given as

$$V_{peak} \sin(2 \cdot \pi \cdot f \cdot t) = 207.6\sqrt{2} \cdot \sin(2 \cdot \pi \cdot 60 \cdot t) = 293.59 \sin(2 \cdot \pi \cdot 60 \cdot t)$$

Here, $V_{peak} = 293.59$ V

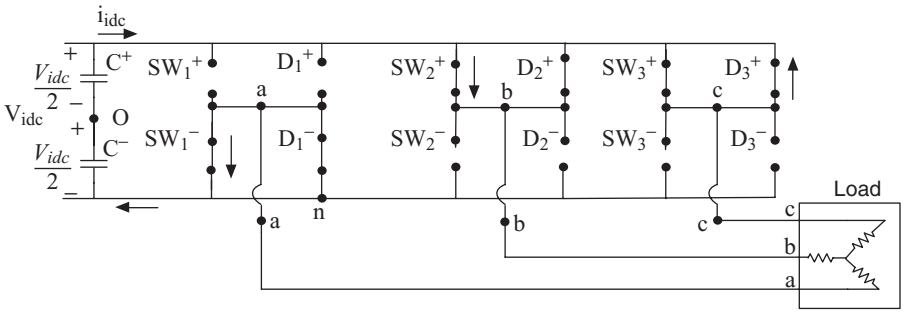

(d) V_{an}= 0, $V_{bn} = V_{cn} = V_{idc}$, I_a, $I_c < 0$, $I_b > 0$, SW_1^- on, SW_2^+ on, D_3^+ on

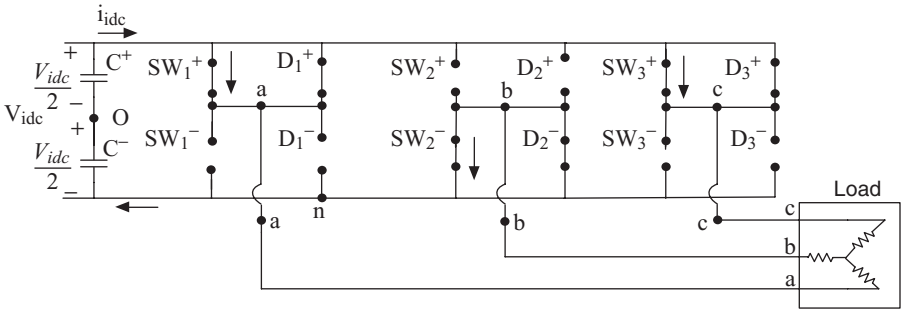

(e) $V_{an} = V_{cn} = V_{idc}$, $V_{bn} = 0$, I_a, $I_c > 0$, $I_b < 0$, SW_1^+ on, SW_2^- on, SW_3^+ on

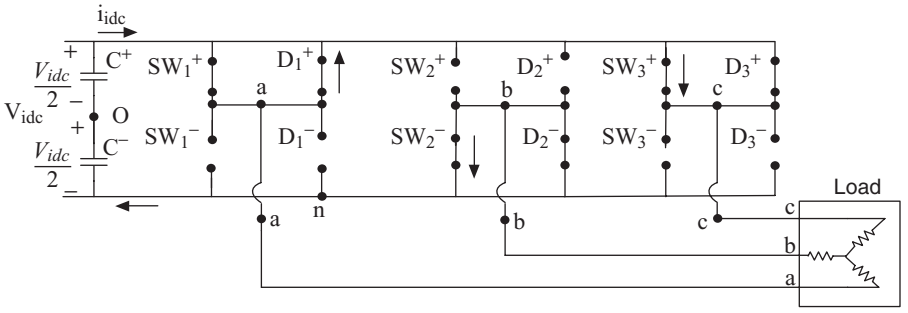

(f) $V_{an} = V_{cn} = V_{idc}$, $V_{bn} = 0$, I_a, $I_b < 0$, $I_c > 0$, D_1^+ on, SW_2^- on, SW_3^+ on

Figure 3.22 (a-f) Operation of the Switching Sequence of a Three-Phase Inverter.

For the three-phase inverter using sine PWM, the line-line peak voltage is given as $V_{L-L,peak} = M_a \cdot \sqrt{3} \cdot \frac{V_{dc}}{2}$

Therefore,

$$V_{dc} = \frac{2}{\sqrt{3}} \cdot \frac{V_{L-L,peak}}{M_a}$$

For the inverter to operate at maximum value of M_a is 1, the minimum DC voltage is given as

$$V_{dc,\min} = \frac{2}{\sqrt{3}} \cdot \frac{V_{L-L,peak}}{M_{a,\max}} = \frac{2}{\sqrt{3}} \cdot \frac{293.59}{1} = 339.01 \text{ V}$$

Therefore, the minimum $V_{dc} = 339.01$ V

Example 3.6 Consider the three-phase radial PV distribution system given below.

Assume Load 1 is a three-phase load of 5 kW at a power factor of 0.85 leading and Load 2 is a three-phase load of 10 kW at a power factor of 0.9 lagging at rated voltage of 110 volts with a 10% voltage variation. Assume a PV source voltage is rated 120 V DC. Compute the transformer ratings. Assume an ideal transformer.

If the amplitude modulation index, M_a, can be controlled from 0.7 to 0.9 in steps of 0.05, compute the following:

i) The transformer low-voltage-side rating (LV)
ii) The transformer high-voltage-side rating (HV)
iii) The PV system per unit model if the transformer ratings are selected as the base values
iv) The per unit model of this PV system

Solution
For the DC/AC inverter:

$$V_{L-L,rms} = \frac{\sqrt{3}}{\sqrt{2}} \cdot M_a \frac{V_{dc}}{2}$$

Let us vary the modulation index from 0.7 to 0.9 to find the suitable voltage.

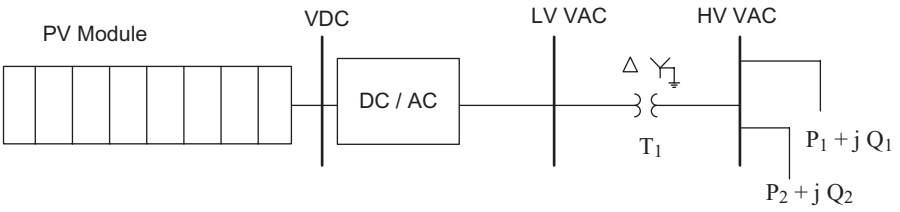

Figure 3.23 A Microgrid Stand-Alone Photovoltaic System.

TABLE 3.3 Variation of AC-Bus Voltage with Modulation Index.

$V_{dc} = 120$ V		
Modulation Index, M_a	AC-Bus Voltage (Low-Voltage Side)	AC-Bus Voltage (High-Voltage Side)
0.70	51.4 V	110 V
0.75	55.1 V	110 V
0.80	58.8 V	110 V
0.85	62.5 V	110 V
0.90	66.1 V	110 V

From the Table 3.3, we see that the modulation index of 0.9 is most suitable. Therefore,

$$V_{L-l,rms} = \frac{\sqrt{3}}{\sqrt{2}} \cdot M_a \frac{V_{dc}}{2} = \frac{\sqrt{3}}{\sqrt{2}} \times 0.9 \times \frac{120}{2} = 66.13\,V$$

$$\text{kVA for Load 1} = \frac{kW_1}{p.f._{\cdot 1}} = \frac{5}{0.85} = 5.88\,\text{kVA}$$

$$\text{p.f. angle} = \cos^{-1} 0.85 = 31.78^o, \text{ leading}$$

$$\text{kVA for Load 1} = \frac{kW_1}{p.f._{\cdot 1}} = \frac{10}{0.9} = 11.11\,\text{kVA}$$

$$\text{p.f. angle} = \cos^{-1} 0.9 = 25.84^o, \text{ lagging}$$

Let an ideal transformer be selected. It is rated at 70/110. The kVA of the transformer should be greater than or equal to the total load it supplies. A 20 kVA has adequate capacity.

$$\text{therefore, the p.u value of load 1} = S_{p.u,1} = \frac{kVA_1}{kVA_{base}} = \frac{5.88}{20} = 0.29\angle 31.78^o$$

$$\text{therefore, the p.u value of load 2} = S_{p.u,2} = \frac{kVA_2}{kVA_{base}} = \frac{11.11}{20} = 0.556\angle -25.84^o$$

Now, for the DC/AC inverter:

$$\text{The base value of the DC side is} = \frac{DC\ side\ voltage}{AC\ side\ voltage} \times base\ voltage\ of\ AC\ side$$

$$= \frac{120}{66.13} \times 70 = 127.02\,V$$

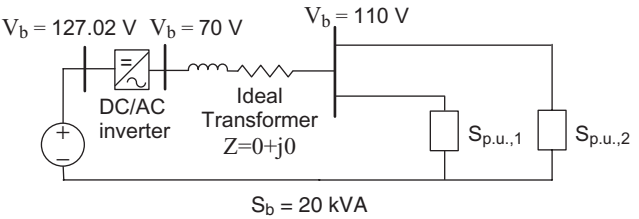

Figure 3.24 Per Unit Model of Fig. 3.23.

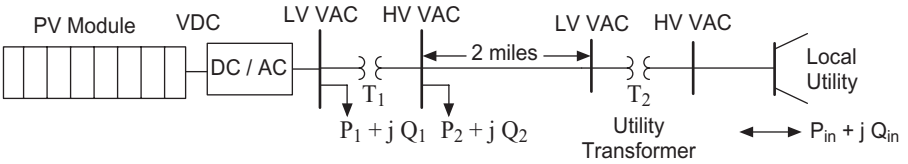

Figure 3.25 A Radial Microgrid Photovoltaic System Operating in Parallel with the Local Utility.

$$\text{Therefore, the p.u value of the DC side of inverter} = \frac{120}{127.02} = 0.94 \text{ p.u}$$

$$\text{Therefore, the p.u value of the AC side of inverter} = \frac{66.13}{70} = 0.94 \text{ p.u}$$

Example 3.7 Consider the three-phase radial microgrid PV given below.

Assume a PV is providing power to two submersible pumps on a farm. The Load 1 is rated at 5 kVA at 120 V AC and Load 2 is rated at 7 kVA at 240 V AC. Assume a load voltage variation of 10%, and an amplitude modulation index of 0.9. The distribution line has impedance of 0.04 Ω and reactance of 0.8 Ω per mile. Assume a utility voltage of 460 V.

Compute the following:

i) The transformer T_1 rating at the (LV) voltage side
ii) The transformer T_2 rating at the high (HV) voltage side
iii) The PV system per unit model with the transformer T_2 ratings selected as the base values and assuming the transformers have an impedance of 10% based on selected ratings

Solution

The transformer T_2 is selected as base with voltage of 240/460 V. It must supply the loads on the low-voltage side and must have a kVA rating greater

than the loads connected to it. We choose a transformer of rating 15 kVA (>5 + 7 = 12) and select this rating as the base.

The base on the transmission line side is 240 V and 15 kVA.

The impedance of the transmission line is equal to its length times the impedance per unit length.

$$Z_{line} = 2 \times (0.04 + j0.8) = 0.08 + j1.6\ \Omega$$

The base impedance for the transmission line is

$$Z_{b,trans} = \frac{V_{base}^2}{VA_{base}} = \frac{240^2}{15 \times 10^3} = 3.84$$

The p.u value of the transmission line is equal to

$$Z_{pu,trans} = \frac{Z_{trans}}{Z_{b,trans}} = \frac{0.08 + j1.6}{3.84} = 0.02 + j0.42 \text{ p.u } \Omega$$

The p.u value of Load 2 is given as

$$\mathrm{S}_2 = \frac{kVA_2}{kVA_{base}} = \frac{7}{15} = 0.467 \text{ p.u kVA}$$

Let us select a transformer T_1 of 120/240 V, 15 kVA. The base on the low-voltage side of T_1 is 120 V.

Therefore, the p.u value of the AC side of inverter $= \frac{120}{120} = 1$ p.u V

and the p.u value of Load 1 is given as

$$\mathrm{S}_1 = \frac{kVA_1}{kVA_{base}} = \frac{5}{15} = 0.33 \text{ p.u kVA}$$

The transformer impedances are as given: j0.10 p.u Ω

For the DC/AC inverter:

$$V_{L,rms} = \frac{\sqrt{3}}{\sqrt{2}} \cdot M_a \frac{V_{dc}}{2}$$

Let us select a modulation index of 0.9.

$$V_{dc} = \frac{\sqrt{2}}{\sqrt{3}} \cdot \frac{2 \cdot V_{L,rms}}{M_a} = \frac{\sqrt{2}}{\sqrt{3}} \cdot \frac{2 \times 120}{0.9} = 217.7\ V$$

$$\text{The base value of the DC side is} = \frac{DC\ side\ voltage}{AC\ side\ voltage} \times base\ voltage\ of\ AC\ side$$

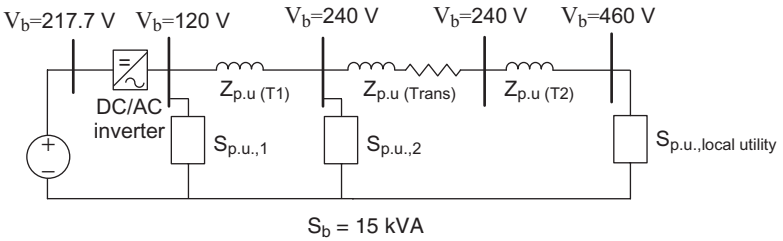

Figure 3.26 Per Unit Model of Fig. 3.25.

$$\text{V base DC side} = \frac{217.7}{120} \times 120 = 217.7\ V$$

$$\text{Therefore the p.u value of the DC side of inverter} = \frac{217.7}{217.7} = 1 \text{ p.u V}$$

3.7 MICROGRID OF RENEWABLE ENERGY SYSTEMS

Figure 3.27 depicts a community microgrid system operating in parallel with the local utility system. The transformer T_1 voltage is in the range of 240 VAC/ 600 VAC and the transformer T_2 that connects the PV system to the utility bus system is rated to step-up the voltage to the utility local AC bus substation.

Example 3.8 Consider a microgrid that is fed from a PV generating station with AC bus voltage of 120 V as shown in Fig. 3.28.

The modulation index for the inverter is 0.9.

Compute the following:

i) The per unit value of line impedance

ii) The per unit impedance of transformers T_1 and T_2

iii) The per unit model of the load

iv) The per unit equivalent impedance and give the impedance diagram. Assume the base voltage, V_b of 240 V in the load circuit and the S_b of 500 kVA.

Solution

We select the voltage base and power base as specified. For the utility side, we have

$$V_b = 240\ V \qquad S_b = 500 \text{ kVA}$$

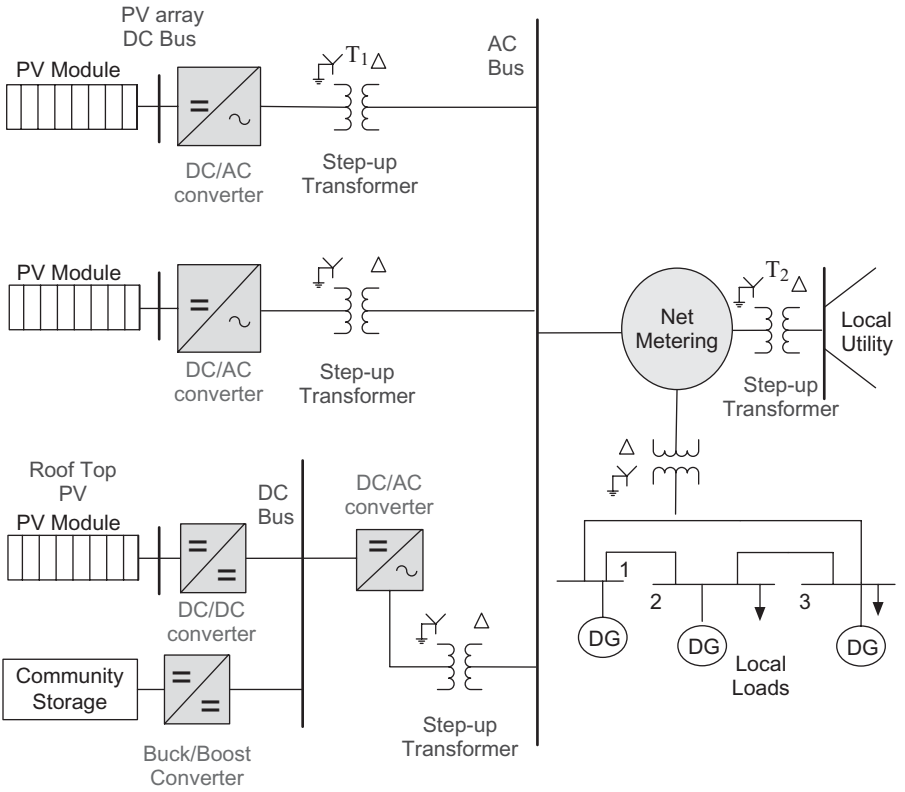

Figure 3.27 One-Line Diagram for a Community Microgrid Distribution System Connected to a Local Utility Power Grid.

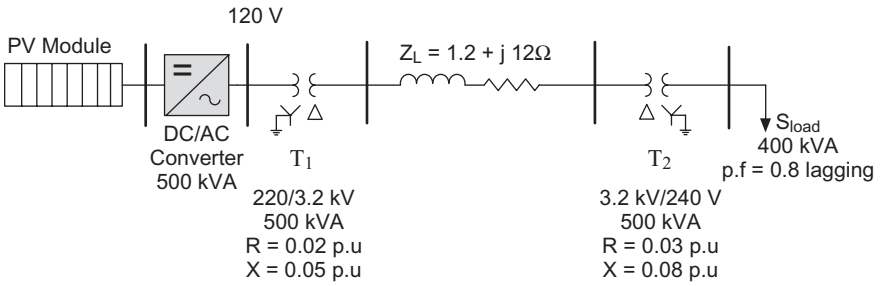

Figure 3.28 The Microgrid of Example 3.8.

The p.u load, $S_{p.u(Load)} = \frac{400}{500}\angle -\cos^{-1} 0.8 = 0.8\angle -36.87°$ p.u kVA

The p.u impedance of T_2 will remain the same as its rated value of $0.03 + j\ 0.08$.

The base impedance of the transmission line can be computed as

$$Z_{b\_3200} = \frac{V_b^2}{S_b} = \frac{(3200)^2}{500 \times 10^3} = 20.48\ \Omega$$

The per unit transmission line impedance can be computed as

$$Z_{trans.line,p.u} = \frac{Z_{tran.actual}}{Z_{b\_3200V}} = \frac{1.2 + j12}{20.48} = 0.058 + j0.586 \text{ p.u } \Omega$$

The p.u impedance of T_1 is at its rated value also will remain the same as $0.02 + j\ 0.05$.

For the inverter:

$$V_{L,rms} = \frac{\sqrt{3}}{\sqrt{2}} \cdot M_a \frac{V_{dc}}{2}$$

$$V_{dc} = \frac{\sqrt{2}}{\sqrt{3}} \cdot \frac{2 \cdot V_{L,rms}}{M_a} = \frac{\sqrt{2}}{\sqrt{3}} \cdot \frac{2 \times 120}{0.9} = 217.7\ V$$

The base value of the DC value is $= \frac{DC\ side\ voltage}{AC\ side\ voltage} \times base\ voltage\ of\ AC\ side$

$$= \frac{217.17}{120} \times 120 = 217.17\ V$$

$$\text{Therefore, the p.u value of the DC side of inverter} = \frac{217.17}{217.17} = 1\text{p.u}$$

The per unit impedance diagram is given as

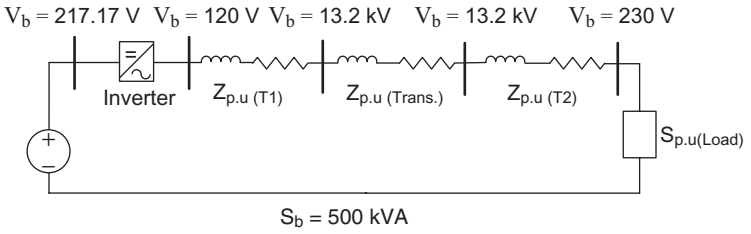

Figure 3.29 The Per Unit Model of Fig. 3.28.

3.8 THE DC/DC CONVERTERS IN GREEN ENERGY SYSTEMS

The block diagram of a DC/DC converter is depicted by Fig. 3.30. The DC/DC converter is a three-terminal device. The input voltage is converted to a higher or lower output voltage as the switching frequency is controlled. Therefore, a DC/DC converter is an electronic transformer similar to tap-changing transformers. The Duty Cycle D defines the relationships between the input voltage and output voltage. A switching signal (See Fig. 3.30) provides the command to the switch of converter, which can be used to vary the value of Duty Cycle D. Depending on whether the output voltage is lower or higher than the input value, the converter is called a *buck* or *boost* or *buck–boost* converter.

The components of DC/DC converters are an inductor L, a capacitor C, a controllable semiconductor switch S, a diode D, and load resistance R. The power electronic switches are the key element for stepping up the input DC voltage to a higher level of DC voltage in the case of a boost converter and to step down the voltage for a buck converter. The exchange of energy between an inductor and a capacitor is used for designing DC/DC converters.[4] The current slew rate through a power switch is limited by an inductor. The inductor stores the magnetic energy for the next cycle of transferring the energy to the capacitor. The slew rate is defined to describe how quickly a circuit variable changes with respect to time. The high transient switching current is damped by the switching resistance due to switching losses. The stored energy is expressed in Joules as a function of the current by Equation 3.44.

$$\text{Energy stored in inductor} = \frac{1}{2} L \cdot i_L^2$$

$$\text{Energy stored in capacitor} = \frac{1}{2} C \cdot v_C^2 \tag{3.44}$$

where i_L is the inductor current and v_c is the voltage across the capacitor.

The stored energy in an inductor is recovered by a capacitor. The capacitor provides a new level of controlled output DC voltage.

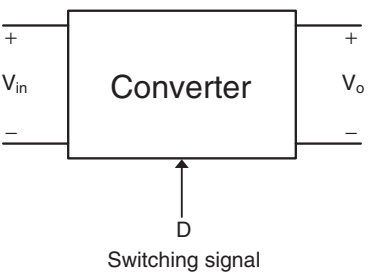

Figure 3.30 Block Diagram of a DC/DC Converter.

The fundamental voltage and current equations are

$$v_L = L\frac{di_L}{dt} \tag{3.45}$$

$$i_C = C\frac{dv_C}{dt} \tag{3.46}$$

The power switch is used to charge the inductor upon closing the switch. However, because the current and voltage are related by Equations 3.45 and 3.46, the energy stored in the inductor is transferred to the capacitor in the discharge phase of the switching cycle. The basic elements of the circuit topology can be reconfigured to reduce the output voltage or to increase the output voltage.

3.8.1 The Step-Up Converter

A PV module is a variable DC power source. Its output increases as the sun rises and it has its maximum output at noon when the maximum solar energy can be captured by the solar module. The same is true for a variable-speed wind energy source. When the wind speed is low, a limited mechanical energy is converted to variable frequency electrical power; in turn, the rectified variable AC power provides a low-voltage DC power source. A DC/DC boost converter allows capturing a wider range of DC power by boosting the DC voltage. The higher DC voltage will be in a range that can be converted to AC power at a system operating frequency by DC/AC inverters.

A step-up converter is called a boost converter; it consists of an inductor *L*, capacitor *C*, controllable semiconductor switch *S*, diode *D*, and load resistance *R* as depicted by Fig. 3.31.

The inductor draws energy from the source and stores it as a magnetic field when the switch *S* is on. When the switch is turned off that energy is transferred to the capacitor. When steady state is reached, the output voltage will be higher than the input voltage and the magnitude depends on the duty ratio of the switch.

To explain how the boost converter operates, let us assume that the inductor is charged in the previous cycle of operation and the converter is at steady-state operation. Let us start the cycle with the power switch *S* open. This condition is depicted in Fig. 3.32(a). Because the inductor is fully charged in the

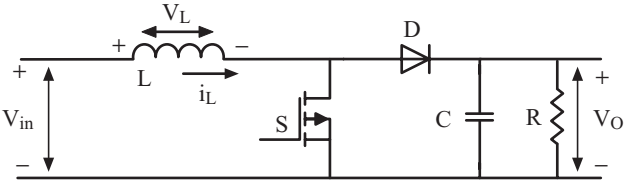

Figure 3.31 A Boost Converter Circuit.

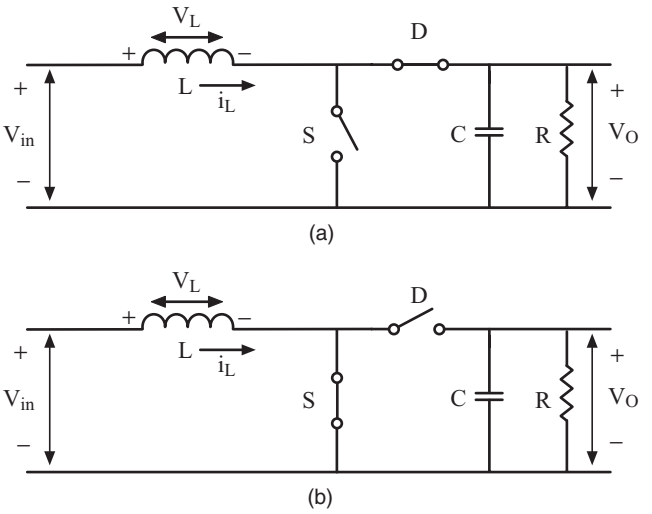

Figure 3.32 The Equivalent Circuit of Boost Converter When the Switch S Is (a) Open, and (b) Closed.

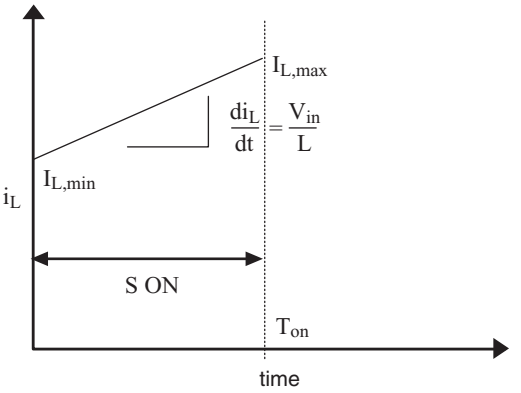

Figure 3.33 Charging Phase: When the Switch Is Closed, the Current Ramps Up through the Inductor.

previous cycle, it will continue to force its current through the diode *D* to the output circuit and charge the capacitor. Let us assume that in the next cycle, the power switch, *S* is closed. Now, the diode will be reverse-biased by the capacitor voltage; hence, it will act as open. The equivalent circuit is shown in Fig. 3.32(b). Now the voltage across the inductor is equal the input voltage, $+V_{in}$. Therefore, by Equation 3.45, the current in the inductor starts to rise from its initial value with a slope V_{in} / L. The output voltage now is supplied by the charged capacitor alone. The inductor current i_L, is shown in Fig. 3.33.

Let us look at the next cycle, when the power switch *S* is open again. Now, the energy stored in the inductor is transferred to the capacitor. The equivalent

circuit is given in Fig. 3.32(a). At the instant when the switch is opened, the inductor has an existing current of $I_{L,max}$, as shown in Fig. 3.33. This current was flowing through the switch S before it was opened. When the switch is opened, the inductor, which acts like a current source, tries to maintain its current, but the path through the switch is no longer available. Therefore, the inductor forces its current through the diode D and the diode starts conducting, boosting the voltage up across the capacitor. The equivalent circuit of Fig. 3.32(a) shows that the voltage across the inductor is now the difference of input and output voltages. Because the output voltage is more than the input voltage, the inductor voltage is negative. From Equation 3.45, the inductor current now starts to decrease with a slope $(V_{in} - V_o)/L$ starting from $I_{L,max}$. During steady state, the inductor current must go back to its value, which it had, at the beginning of the switching cycle ($I_{L,min}$) when the switching cycle ends. The current waveform when the switch S is opened is shown in Fig. 3.34.

Figure 3.35 shows the steady-state current and voltage waveforms of the inductor for a few cycles of operation. In steady state, the average inductor

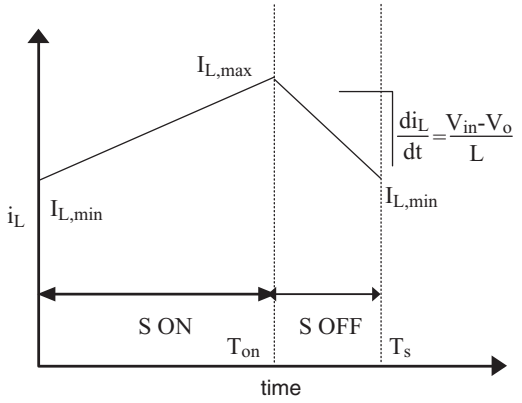

Figure 3.34 Discharging Phase: When the Switch Opens, Current Ramps Down through the Inductor.

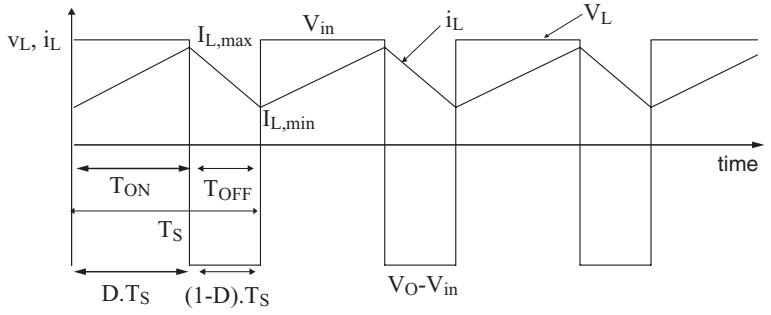

Figure 3.35 The Steady-State Voltage and Current Waveform of a Boost Converter.

voltage is zero. Therefore, in the steady state operation, as expected, the inductor current is constant. If the average voltage of the inductor had not been zero, the average value of the inductor current would have continued to rise or fall depending on the polarity of the inductor voltage. For this case, the inductor current would not have returned to the value it started from, when the cycle began, at the end of the switching period according to Equation 3.45.

The waveforms of a boost converter in steady state are shown in Fig. 3.35.

If the initial voltage of the capacitor is zero, the inductor current slowly charges up the capacitor over several cycles. The output voltage across the capacitor rises over each cycle until a steady state is reached.

Let us analyze the operation of boost converter depicted by Fig. 3.31. The variable D in Fig. 3.35 is defined as a duty ratio of the switch and i_L and v_L are the inductor voltage and current with direction and polarity as indicated in Figs. 3.31 and 3.32. The current flows from the DC source through the inductor L when the switch S is on. Then, the current flows through the switch S and back to the source. In Fig. 3.32(b), the diode is reverse biased by the output voltage across the capacitor. As shown in Fig. 3.35, during the time $D \cdot T_S$, energy is stored in the inductor and the voltage across the inductor has a value of V_{in}. When the switch is turned off, the inductor forces the current through the diode and charges the capacitor and builds the output voltage through the diode during the time $(1 - D)$. T_S, the voltage across the inductor is $-(V_O - V_{in})$, which is negative because $V_O > V_{in}$. At the end of time T_S, the capacitor is fully charged and the energy of inductor is transferred to the capacitor.

For steady-state operation, the average voltage across the inductor is zero. Equating the average voltage of the inductor to zero, that is, $V_L = 0$, we have

$$\frac{1}{T_S} \cdot [V_{in} \cdot DT_S - (V_O - V_{in}) \cdot (1-D) \cdot T_S] = 0$$

$$\text{or} \quad V_o = \frac{V_{in}}{1-D} \tag{3.47}$$

where f_s is switching frequency and T_S is defined as $T_S = 1/f_S$ and $T_S = T_{on} + T_{off}$ (see Fig. 3.35) is defined as the switching period. The duty ratio is defined as

$$D = \frac{T_{on}}{T_S} = \frac{T_{on}}{T_{on} + T_{off}} \tag{3.48}$$

Again,

$$T_{off} = T_S - T_{on} = (1 - T_{on}/T_S)T_S = (1-D)T_S \tag{3.49}$$

We know that the value of D is less than one. Therefore, the output voltage is always more than the input voltage. With the expression of the output voltage derived, the expression of the input current can be obtained from power

balance. Because the input and output power must be balanced for a lossless system, we can calculate the output current.

$$V_{in} \cdot I_{in} = V_O \cdot I_O \tag{3.50}$$

where I_{in} and I_O are the average input and output currents, respectively, we can compute:

$$I_{in} = I_L = \frac{V_O}{V_{in}} \cdot I_O \tag{3.51}$$

$$I_{in} = \frac{I_O}{1-D} \tag{3.52}$$

Here, I_L is the average value of inductor current. As can be seen from Fig. 3.31, the input current and the inductor current are the same.

The ripple in the inductor current, ΔI_L, is the difference in its maximum and minimum values in steady state. It can be derived from Equation 3.45, knowing how much time the inductor is exposed to what voltage. From the Fig. 3.32(b), it is seen that the inductor voltage is $+V_{in}$ for a time $D \cdot T_S$. Therefore, from Equation 3.45 and Fig. 3.35,

$$\Delta I_L = I_{L,Max} - I_{L,Min} = \frac{V_{in}}{L} \cdot DT_S. \tag{3.53}$$

The maximum and minimum values of the inductor current can determined from its average values and the ripple as shown in Equation 3.67.

$$I_{L,Max} = I_L + \frac{\Delta I_L}{2}, I_{L,Min} = I_L - \frac{\Delta I_L}{2} \tag{3.54}$$

It will take several cycles to reach the steady state. Initially, the capacitor voltage will be zero—and it remains zero when the switch is first closed. The inductor current flows through the switch S and the capacitor remains cutoff from the input for time T_{on} [see an equivalent circuit in Fig. 3.32(b)]. The capacitor will start receiving a charge only when the switch S is open at the end of time T_{on}. The equivalent circuit is shown in Fig. 3.32(a). Using Kirchhoff's voltage law, we have

$$V_{in} = L\frac{di_L}{dt} + v_C \tag{3.55}$$

The capacitor current is given by Equation 3.46. In the circuit of Fig. 3.32(a), the capacitor and inductor currents are the same for no load. By putting $i_C = i_L$ in Equation 3.46 and using it in Equation 3.55 we get:

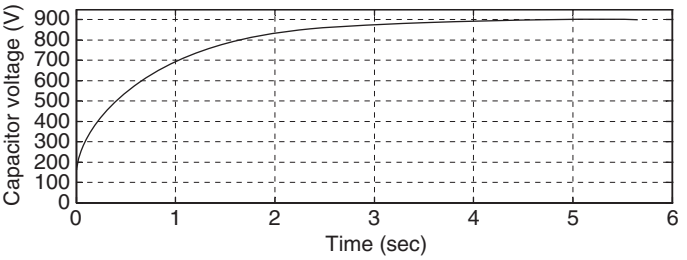

Figure 3.36 No-Load Output Voltage Build-Up of a Boost Converter with a Supply Voltage of 40 V and a Duty Ratio of 50%.

$$V_{in} = LC\frac{d^2 v_C}{dt^2} + v_C \tag{3.56}$$

Putting $1/LC = \omega_0^2$ in Equation 3.56 and solving the differential equations with an initial condition we have

$$v_C(t) = \frac{I_{Ton}}{C\omega_0}\sin\omega_0(t - T_{on}) - V_{in}\cos\omega_0(t - T_{on}) + V_{in} \tag{3.57}$$

At the end of the switching period, T_s, the capacitor voltage will be given by putting $t = T_S$ in Equation 3.57. By using $T_{off} = T_S - T_{on}$ we get:

$$v_C(T_S) = \frac{I_{Ton}}{C\omega_0}\sin\omega_0 T_{off} - V_{in}\cos\omega_0 T_{off} + V_{in} \tag{3.58}$$

Again, at the end of one switching period T_s, the switch S is the cutoff from the output side and its voltage remains constant at the above value. In the next cycle, when switch S is turned off again, the capacitor voltage starts to rise again. Ideally, at no load, the voltage across the capacitor will continue to rise without reaching the steady state. However, in practice the resistance in the snubber circuits of the diode and the switch will cause the voltage of the capacitor to settle down at a particular value. The time taken by the capacitor voltage to reach the steady state increases as the value of the capacitance is increased. Figure 3.36 shows the rise of the capacitor voltage for a boost converter supplied by a source of 40 V with an inductance of 1 mH and a capacitance of 100 μF, operating at a 50% duty ratio.

Example 3.9 Consider the microgrid of Fig. 3.37. Assume the PV generating station can produce 175 kW of power, transformer T_1 is rated 5% impedance, 240 V/120 V and 75 kVA, and transformer T_2 is rated at 10% impedance, 240 V/460 V, and 150 kVA. Assume the power base of 1000 kVA and the voltage base of 460 V in transformer T_2. Assume the three-phase inverter has a modulation index of 0.8 and the boost converter has a duty ratio of 0.6.

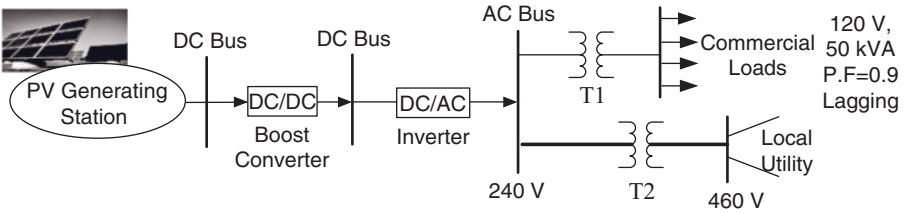

Figure 3.37 One-Line Diagram of Example 3.9.

Compute the following:

i) The per unit value of transformers T_1 and T_2, and per unit model of the load

ii) The per unit equivalent impedance and give the impedance diagram

Solution

The power base is selected as 1000 kVA and voltage base on the utility side is selected as 460 V.

We have

$$V_{bnew} = 460 \text{ V} \qquad S_{bnew} = 1000 \text{ kVA}$$

Therefore, the new impedance base on the 460 V is given as

$$Z_{b460V} = \frac{V_b^2}{S_b} = \frac{(460)^2}{1000 \times 10^3} = 0.2116\ \Omega$$

For the new base, the transformer T_2, we have

$$Z_{p.u\_new} = Z_{p.u\_old} \times \left(\frac{V_{b\_old}}{V_{b\_new}}\right)^2 \frac{S_{b\_new}}{S_{b\_old}}$$

$$Z_{p.u\_new-\text{T2}} = 0.1 \times \left(\frac{460}{460}\right)^2 \times \frac{1000}{150} = 0.67 \text{ p.u } \Omega$$

The old values of the transformer T_1 are given on its nameplate rating. We recalculate the new per unit impedance of T_1 based on the new selected bases.

For the transformer T_1, we have

$$Z_{p.u\_new-T1} = 0.05 \times \left(\frac{240}{240}\right)^2 \times \frac{1000}{75} = 0.67 \text{ p.u } \Omega$$

The base voltage on the low side of the T_1 transformer is given by the ratio of the old base voltage to the new base voltage (i.e., both on the LV side or HV side).

$$V_{b\_new(LV)} = \frac{V_{b\_new(HV)}}{V_{b\_old(HV)}} V_{b\_old(LV)}$$

Using the transformer, T_1, nameplate ratings and the new base voltage on the transmission can be computed as

$$V_{b\_new(LV)} = \left(\frac{240}{240}\right)(120) = 120 \text{ V}$$

The per unit load can be calculated as

$$S_{p.u(Load)} = \frac{50}{1000} \angle -\cos^{-1} 0.9 = 0.05 \angle -25.84° \text{ p.u kVA}$$

For the inverter:

$$V_{L,rms} = \frac{\sqrt{3}}{\sqrt{2}} \cdot M_a \frac{V_{dc}}{2}$$

$$V_{dc} = \frac{\sqrt{2}}{\sqrt{3}} \cdot \frac{2 \cdot V_{L,rms}}{M_a} = \frac{\sqrt{2}}{\sqrt{3}} \cdot \frac{2 \times 240}{0.8} = 489.9\ V$$

$$\text{The base value of the DC side is} = \frac{DC\ side\ voltage}{AC\ side\ voltage} \times base\ voltage\ of\ AC\ side$$

$$= \frac{489.9}{240} \times 240 = 489.9\ V$$

$$\text{Therefore, the p.u value of the DC side of the inverter} = \frac{489.9}{489.9} = 1. \text{ p.u V}$$

Now, for the DC/DC converter:

$$V_o = \frac{V_{in}}{1 - duty\ ratio}$$

$$V_{in} = (1 - duty\ ratio) \times V_o = (1 - 0.6) \times 489.9 = 195.96 \text{ V}$$

The base value of the low-voltage side is given as

$$\text{V base on DC side} = \frac{low\ voltage\ side}{high\ voltage\ side} \times base\ voltage\ of\ high\ voltage\ side$$

$$\text{V base on DC side} = \frac{195.96}{489.9} \times 489.9 = 195.96\ V$$

$$\text{Therefore, the p.u value of the DC side of the inverter} = \frac{195.96}{195.96} = 1 \text{ p.u V}$$

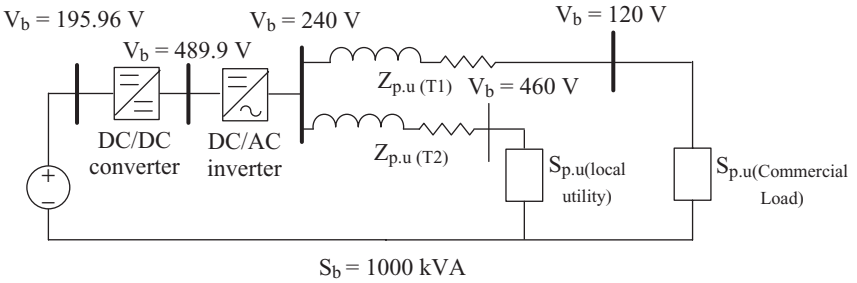

Figure 3.38 The Per Unit Model of Fig. 3.37.

Example 3.10 Write a MATLAB code to generate the voltage and current waveform of the boost converter with an input of 120 V and operating at the duty ratio of 0.75. The capacitance value used is 100 μF. Plot the inductor voltage and current waveforms in steady state.

Solution

```
% Boost Converter
clc; clear all;
Vin=120;                %input dc value
D=0.75;                 %duty ratio
L=1e-3;                 %inductor value
R=20;                   %load resistance
f=5e3;                  %switching frequency

T=1/f;                  %switching time period
Vo=Vin/(1-D);           %output voltage is defined
Io=Vo/R;
Iin=Io/(1-D);
I_Lavg=Iin;
dI_L=Vin/L*D*T;         %inductor ripple current
I_Lmin=I_Lavg-dI_L/2;   %minimum inductor current
I_Lmax=I_Lavg+dI_L/2;   %maximum inductor current
V_L=0;
V_Lp=Vin;               %positive voltage of inductor
V_Ln=Vin-Vo;            %negative voltage of inductor

for k=0:T/500:5*T       % to plot from 0 to 0.04 sec in
                        steps of Ts/500
  plot (k,0,'k');
  V_L_old=V_L;
  if(rem(k,T)<D*T)      % V_L is defined using equations
                        of line
    V_L=V_Lp;
  else
```

```
    V_L=V_Ln;
  end
  if(rem(k,T)<D*T)      % I_L is defined using equations
                        of line
    I_L=I_Lmin+(I_Lmax-I_Lmin)/D/T*rem(k,T);
  else
    I_L=I_Lmax-(I_Lmax-I_Lmin)/(1-D)/T*(rem(k,T)-D*T);
  end

  plot (k,V_L,'k');     %V_L is plotted in black ('k')
  hold on;
  %the points of discontinuities are joined by a
vertical line
  if V_L_old~= V_L
    for j= V_Ln :.1:V_Lp
      plot(k,j,'k')
    end
  end

  plot(k,I_L,'r');      %I_L is plotted in black 'r'
  hold on;
end
grid on;
xlabel('time (sec)');
ylabel('Inductor voltage (V) and current (Amp)');
title('Steady state voltage and current plot');
```

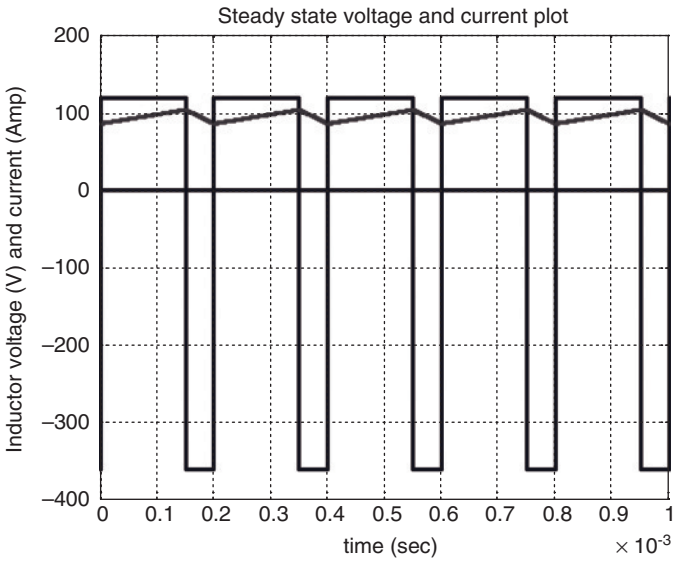

Figure 3.39 Inductor Voltage and Current for Example 3.10.

3.8.2 The Step-Down Converter

The buck and boost converters are used in a green energy microgrid to lower DC bus voltage or step up the DC bus voltage. To charge a battery, the DC bus voltage is stepped down to battery bus voltage. To use the DC power stored in storage system, the storage system DC bus voltage is stepped up using a boost DC/DC converter.

At present, the storage battery in residential and commercial systems is rated at 6 V and 12 V DC. Three 12 V DC batteries can be used in series to create a 36 V DC bus voltage for a community storage system. To obtain higher kilowatts of storage, a number of 36 V DC bus systems can be connected in parallel. The storage systems with high kilowatts and DC voltage are used as community storage systems that are placed in substations of utilities.

A step-down converter is a basic converter and is known as a buck converter. As inferred from its name, the main function of this converter is to convert the input DC voltage level to another and lower voltage level. The main components in a buck converter are a semiconductor switch *S*, diode *D*, inductor filter *L*, and capacitor filter *C* as shown in Fig. 3.40.

The operating cycle of the converter can be explained starting from the closing of the switch *S*. During this time, the diode *D* is reverse biased by the input voltage and is open. The equivalent circuit is shown in Fig. 3.41.

As can be seen in Fig. 3.41, the voltage across the inductor is $V_{in} - V_o$. Because the input voltage is more than the output voltage, the voltage across the inductor is positive and the inductor is being charged. The current in the inductor can determined from Equation 3.45. Because v_L is positive, di_L / dt is positive and the current rises from its initial value. This phase of the operation takes place as long as the switch *S* is on, during the time T_{on} as shown in

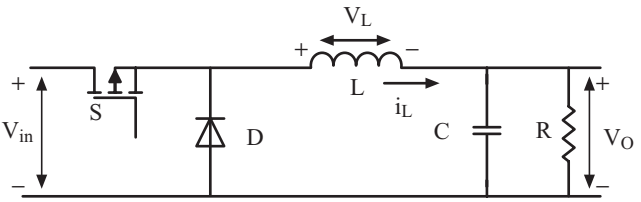

Figure 3.40 A Buck Converter Circuit.

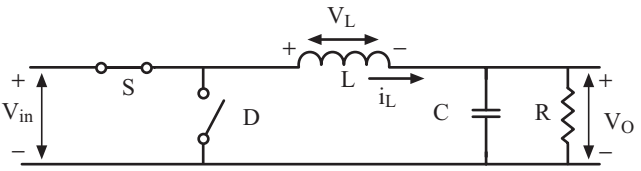

Figure 3.41 The Equivalent Circuit of a Step-Down Converter When the Switch *S* Is Closed.

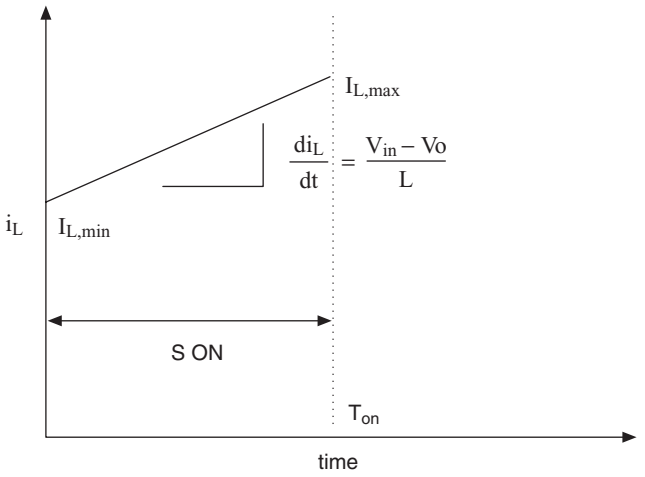

Figure 3.42 The Charging Phase of the Inductor for a Buck Converter.

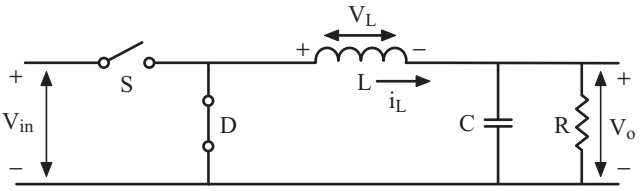

Figure 3.43 The Equivalent Circuit When *S* Acts as Open and *D* Acts as a Closed Switch.

Fig. 3.42. Here, the inductor continues to be charged and stores energy in it as magnetic field energy, which is released in the next phase of operation to the capacitor.

At the end of time T_{on}, the switch *S* is opened and the next phase of operation starts. The inductor current needs to maintain itself. The only path for that occurs when the switch is off and the inductor forces the diode into conduction. In the next phase of operation, the switch *S* is opened and the diode *D* starts to conduct. The equivalent circuit is shown in Fig. 3.43.

The voltage across the inductor is now $-V_o$ as shown in Fig. 3.43. In this phase, the current in the inductor decreases obeying Equation 3.58. Because the voltage across it is negative, the value of di_L / dt is negative and the current decreases from its initial value. Now the inductor is cutoff from the source and it delivers its energy to the output capacitor *C* and the load. This phase continues until the switch *S* is closed at the end of switching period. The current waveform for this phase is shown in Fig. 3.44.

Therefore, we see that the inductor plays the role of energy transfer from the input to the output circuit. When the switch is closed (see Fig. 3.41), the

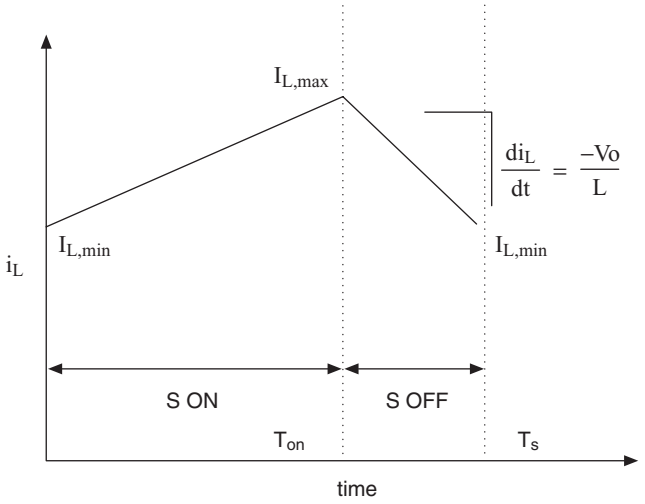

Figure 3.44 The Discharging Phase of the Inductor for a Buck Converter.

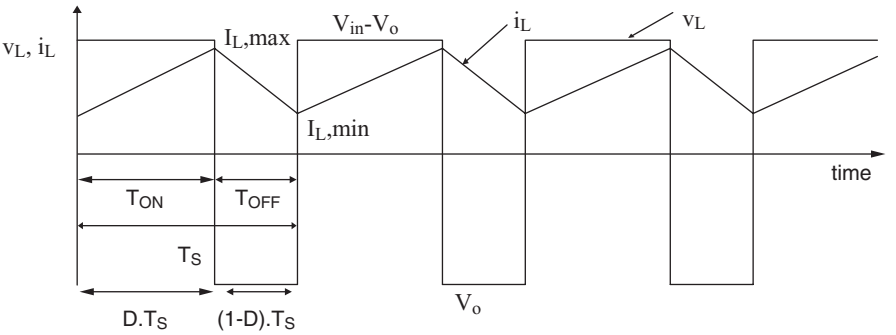

Figure 3.45 The Voltage and Current Waveform of the Buck Converter.

inductor is charged from the source, then when the switch is open (see Fig. 3.43), it delivers that energy to the output capacitor and load. When the converter reaches steady state at the end of the cycle, the current in the inductor must return to the value it started from at the beginning of the cycle. The steady-state operation of a buck converter is shown in Fig. 3.45.

To derive the input–output voltage relationship, a continuous conduction mode is assumed. The average voltage across the inductor must be zero over a switching period at steady state. Therefore, we have

$$\frac{(V_{in}-V_o)\times D\times T_S - V_o\times(1-D)\times T_S}{T_S} = 0 \tag{3.59}$$

$$\text{or } V_o = D\cdot V_{in} \tag{3.60}$$

where D is the duty ratio, f_s is the switching frequency, and T_S it defined as $T_S = 1/f_S$, the switching period. The duty ratio is defined as

$$D = \frac{T_{on}}{T_S} \quad \text{and} \quad 1 - D = \frac{T_{off}}{T_S}, \tag{3.61}$$

Because the input and output power must be balanced for a lossless system, we can calculate the input current.

$$V_{in} \cdot I_{in} = V_O \cdot I_O$$

where, I_{in} and I_O are the average input and output currents, respectively. We can compute

$$I_{in} = \frac{V_o}{V_{in}} \cdot I_o = DI_o \tag{3.62}$$

Similar to the boost converter, the ripple in the inductor current ΔI_L is the difference in its maximum and minimum values in steady state. From Equation 3.45,

$$\Delta I_L = I_{L,Max} - I_{L,Min} = \frac{V_o}{L} \cdot (1 - D)T_S \tag{3.63}$$

$$I_{L,Max} = I_L + \frac{\Delta I_L}{2}, I_{L,Min} = I_L - \frac{\Delta I_L}{2} \tag{3.64}$$

where I_L is the average value of inductor current. The average capacitor current is zero at steady state; therefore, the inductor current is equal to the output current.

$$I_L = I_O \tag{3.65}$$

Example 3.11 Assume a PV system with DC bus voltage of 120 V DC. A DC/DC buck converter, which has a duty ratio of the switch of 0.75 with a switching frequency of 5 kHz, is supplied by the PV system DC bus. If the value of the inductor L is 1 mH, the capacitor C is 100 μF and the battery system is assumed to act as a load resistance of 4 Ω.

Compute the following:

i) The output voltage
ii) The minimum and maximum inductor current
iii) The rating of the switch S and diode D

Solution

i) The output voltage is given as

$$V_o = D \cdot V_{in}$$

$$\mathrm{V_o} = 0.75 \times 120 = 90\ V$$

ii) The output current is

$$I_o = \frac{V_o}{R} = \frac{90}{4} = 22.5\ A$$

The average inductor current can be computed as

$$I_L = I_o = 22.5 = 22.5\ A$$

$$\Delta I_L = \frac{V_o}{L} \cdot (1-D) T_S = \frac{V_o}{L} \cdot (1-D) \frac{1}{f} = \frac{90}{0.001} \times (1-0.75) \times \frac{1}{5000} = 4.5\ \mathrm{A}$$

The maximum inductor current is

$$I_{L,Max} = I_L + \frac{\Delta I_L}{2} = 22.5 + \frac{4.5}{2} = 24.75\ \mathrm{A}$$

The minimum inductor current is

$$I_{L,Min} = I_L - \frac{\Delta I_L}{2} = 22.5 - \frac{4.5}{2} = 20.25\ \mathrm{A}$$

iii) The switch S is being subjected to the input voltage when it is off. Therefore, the voltage rating of the switch should be more than 120 V. The maximum current flowing through the switch is $I_{L,Max} = 24.75$. Hence, the current rating should be 25 A.

Similarly, the diode is also subjected to a maximum voltage equal to input voltage and maximum current of inductor maximum current. Hence, the diode should also have a rating of 120 V and 25 A.

Example 3.12 Write a MATLAB code to generate the voltage and current waveform of the buck converter in Example 3.11.

The MATLAB code:

```
% Buck Converter
clc; clear all;
Vin=120;                %input dc value
D=0.75;                 %duty ratio
L=1e-3;                 %inductor value
R=4;                    %load resistance
f=5e3;                  %switching frequency
```

```
T=1/f;                  %switching time period
Vo=D*Vin;               %out put voltage is defined
Io=Vo/R;
I_Lavg=Io;
dI_L=Vo/L*(1-D)*T;      %inductor ripple current
I_Lmin=I_Lavg-dI_L/2;   %minimum inductor current
I_Lmax=I_Lavg+dI_L/2;   %maximum inductor current
V_L=0;
V_Lp=Vin-Vo;            %positive voltage of inductor
V_Ln=-Vo;               %negative voltage of inductor
for k= 0:T/500:5*T      % to plot from 0 to 0.04 sec in
                        steps of Ts/500
  plot (k,0,'k');
  V_L_old=V_L;
  if(rem(k,T)<D*T)      % V_L is defined using equations
                        of line
    V_L=V_Lp;
  else
    V_L=V_Ln;
  end
  if(rem(k,T)<D*T)      % I_L is defined using equations
                        of line
    I_L=I_Lmin+(I_Lmax-I_Lmin)/D/T*rem(k,T);
  else
    I_L=I_Lmax-(I_Lmax-I_Lmin)/(1-D)/T*(rem(k,T)-D*T);
  end

  plot (k,V_L,'k');     %V_L is plotted in black ('k')
  hold on;

  %the points of discontinuities are joined by a vertical
line
  if V_L_old~= V_L
    for j= V_Ln :.1 :V_Lp
      plot(k,j,'k')
    end
  end

  plot(k,I_L,'r');      %I_L is plotted in black 'r'
  hold on;
end
grid on;
xlabel('time (sec)');
ylabel('Inductor voltage (V) and current (Amp)');
title('Steady state voltage and current plot');
```

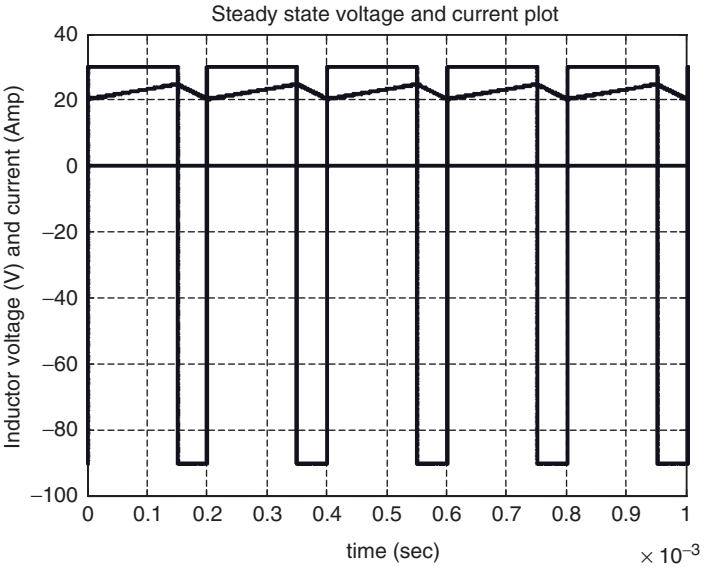

Figure 3.46 The Inductor Voltage and Current for Example 3.12.

Just like a boost converter, the buck converter will also take several cycles to reach the steady state. The capacitor voltage is initially zero and as the inductor transfers its energy to the capacitor over several cycles, the capacitor voltage picks up and attains a steady value depending on the duty ratio D. If the converter is not loaded—in other words, the output terminal is open instead of having a resistance connected—the capacitor voltage stays at its state value determined by the duty ratio.

3.8.3 The Buck-Boost Converter

A buck-boost converter, which consists of input voltage V_{in}, inductor L, capacitor C, load R, and controllable switch S, is shown in the Fig. 3.47.

The operation of the buck-boost converter is explained starting from the closing of the switch S. When the switch S is closed, the diode D is reverse biased both by the input and output voltages (the voltage at the upper output DC bus is negative), and the input voltage is impressed across the inductor. The equivalent circuit is shown in Fig. 3.48. The inductor voltage being positive, the current in the inductor starts to rise from its initial value following Equation 3.45. During this time, the inductor starts to increase its stored energy.

The inductor current wave is shown in Fig. 3.49. The inductor current rises with a slope of V_{in} / L as long as the switch S is closed.

At the end of the duty period, the switch is turned off; the diode is forced to conduct the inductor current and it becomes on. The equivalent circuit is shown in Fig. 3.50.

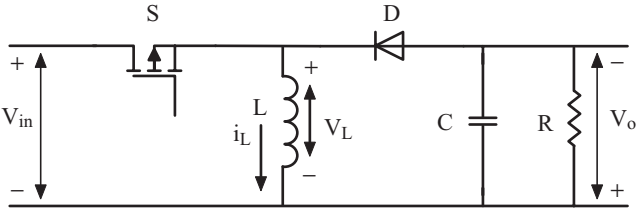

Figure 3.47 A Buck-Boost Converter Circuit.

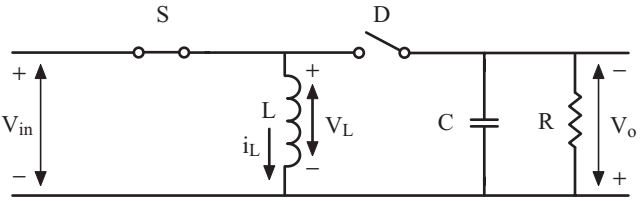

Figure 3.48 An Equivalent Circuit of a Buck-Boost Converter When Switch *S* Is Closed.

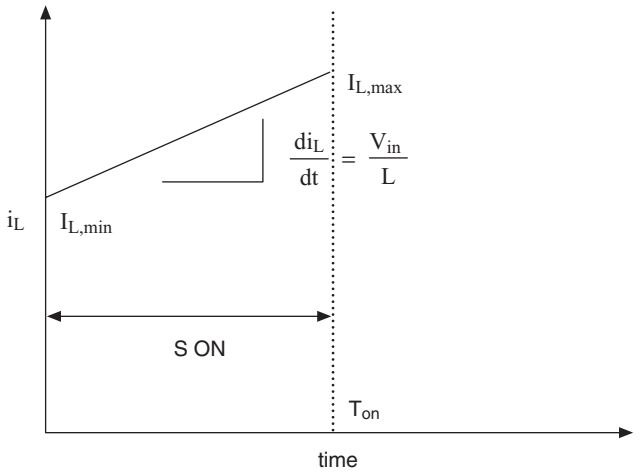

Figure 3.49 The Inductor Current When the Switch Is Closed.

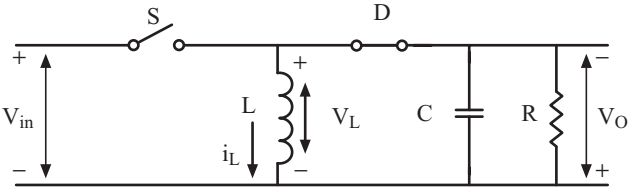

Figure 3.50 An Equivalent Circuit of a Buck-Boost Converter When Switch *S* Is Open.

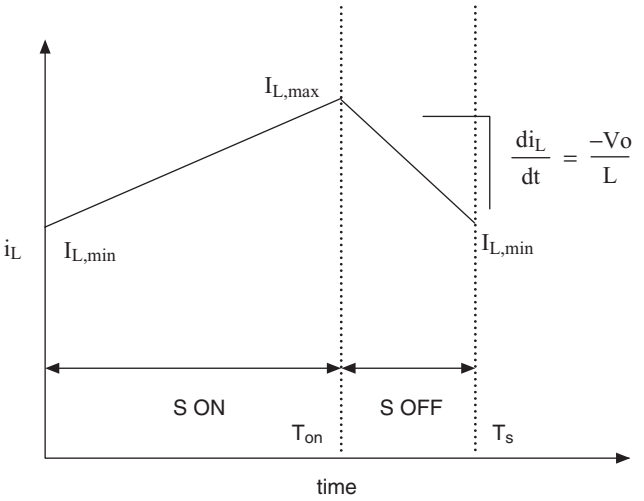

Figure 3.51 The Inductor Current When the Switch Is Open.

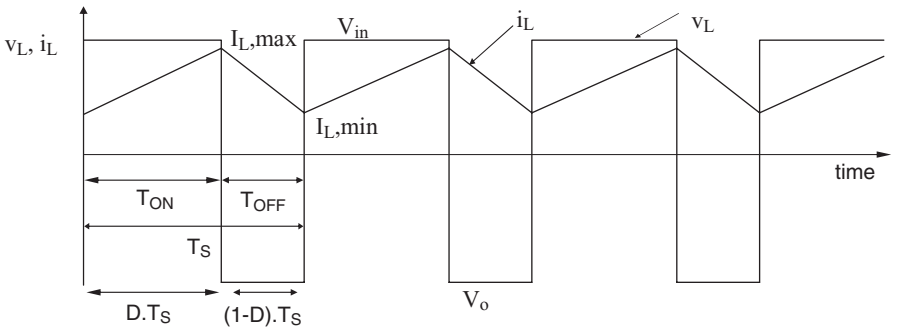

Figure 3.52 The Voltage and Current Waveform of the Buck-Boost Converter.

Now, the stored energy in the inductor is transferred to the capacitor *C*. The current waveform of the inductor is shown in Fig. 3.51.

At steady state, the inductor current must return to the value it started from at the end of the cycle. The steady-state waveforms are shown in Fig. 3.52.

Like other converters, we equate the average value of inductor voltage to zero:

$$\frac{V_{in} \cdot DT_S - V_O \cdot (1-D) \cdot T_S}{T_S} = 0 \tag{3.66}$$

From this equation, it is found that the transfer ratio for the input–output relation will be

$$V_o = \frac{D \cdot V_{in}}{1 - D} \tag{3.67}$$

where f_s is switching frequency and T_S it defined as $T_S = 1/f_S$, the switching period.

The duty ratio is defined as

$$D = \frac{T_{on}}{T_S} = \frac{T_{on}}{T_{on} + T_{off}} \tag{3.68}$$

The value of the output voltage depends on the duty ratio of the switch. If D is less than half, the converter steps the voltage down, and if it is more than half, it boosts the voltage.

From an input–output energy balance,

$$V_{in} \cdot I_{in} = V_O \cdot I_O \tag{3.69}$$

where I_{in} and I_O are the average input and output currents, respectively. We can compute:

$$I_{in} = \frac{V_O}{V_{in}} \cdot I_O = \frac{D \cdot I_O}{1 - D} \tag{3.70}$$

Now, from Fig. 3.53 assuming that the average input current is (area of the trapezium divided by the time):

$$I_{in} = \frac{1}{T_S} \cdot \left(\frac{I_{L,Max} + I_{L,Min}}{2} \right) \cdot D \cdot T_S = D \cdot \frac{I_{L,Max} + I_{L,Min}}{2} \tag{3.71}$$

Again, from Fig. 3.53, the average inductor current is

$$\begin{aligned} I_L &= \frac{1}{T_S} \left[\left(\frac{I_{L,Max} + I_{L,Min}}{2} \right) \cdot D T_S + \left(\frac{I_{L,Max} + I_{L,Min}}{2} \right) \cdot (1 - D) T_S \right] \\ &= \frac{I_{L,Max} + I_{L,Min}}{2} \end{aligned} \tag{3.72}$$

From Equations 3.71 and 3.72,

$$\text{or } I_{in} = D \cdot I_L \tag{3.73}$$

The ripple in the inductor current, ΔI_L, is the difference in its maximum and minimum values in steady state.

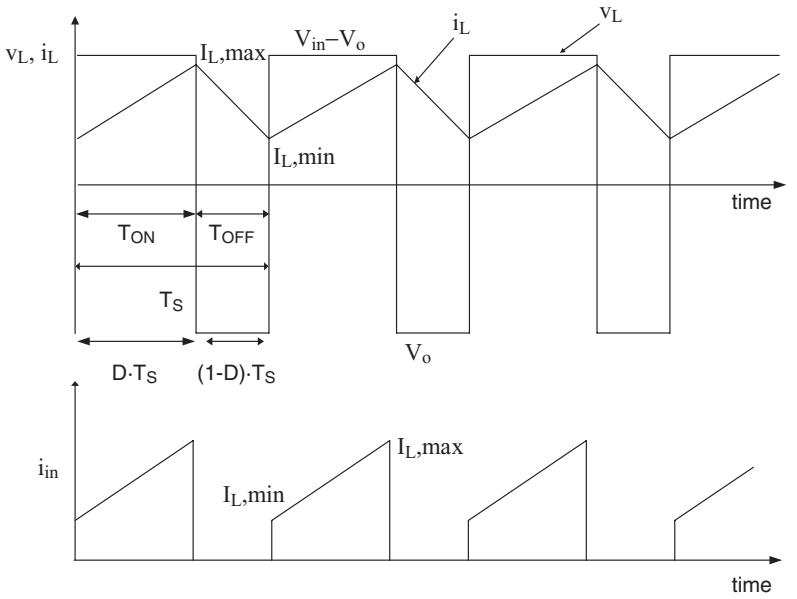

Figure 3.53 The Input Current Waveform of a Buck-Boost Converter.

$$\Delta I_L = I_{L,Max} - I_{L,Min} = \frac{V_{in}}{L} \cdot DT \tag{3.74}$$

$$I_{L,Max} = I_L + \frac{\Delta I_L}{2}, I_{L,Min} = I_L - \frac{\Delta I_L}{2} \tag{3.75}$$

For all three converters, we have assumed that the output voltage is constant and stiff. However, in practice, the capacitor voltage has a small ripple on top of the average value. The quality of the output voltage is determined by the amount of ripple in it. The smaller the ripples the better the quality of the output voltage is. The ripples in the output voltage can be reduced by increasing the capacitance C or by increasing the switching frequency f_s. But increasing the capacitance increases the size of the capacitor, which increases the cost and size of the converter. Again, by increasing the switching frequency, the switching losses would increase, decreasing the efficiency of the converter. Hence, a tradeoff is reached between the quality of output voltage and the size of capacitor and switching frequency. The inductor current should be maintained at a positive value. A minimum value of inductance is needed for this purpose. Moreover, if the ripple in inductor current is high, the maximum current in the switches will increase, increasing their rating and cost. However, to limit the ripple in the inductor current, the inductance should be as high as possible; however, the size and cost of the converter increases with higher size inductor.

So a tradeoff must be reached between the size of the inductor, capacitor, switching frequency, and the cost and size of the converter and its efficiency.

Example 3.13 Design a buck-boost converter that is supplied from a PV source whose voltage varies from 80 V to 140 V—depending on the available sun irradiant energy—and supplies a load of 10 kW at fixed 120 V DC. Give the range of duty ratio needed to supply the load at the rated voltage.

Solution
The output voltage is given as

$$V_o = 120\ V$$

The power rating is specified as

$$P = 10\ kW$$

Therefore, the output current rating can be computed as

$$I_o = \frac{10 \times 10^3}{120} = 83.33\ \text{A}$$

The maximum average input current rating is

$$I_{ave} = I_{in} = \frac{10 \times 10^3}{80} = 125\ A$$

The duty ratio for an input voltage of 80 V can be computed as

$$D = \frac{V_o}{V_{in} + V_o} = \frac{120}{80 + 120} = 0.6$$

The duty ratio for an input voltage 140 V can be computed as

$$D = \frac{V_o}{V_{in} + V_o} = \frac{120}{140 + 120} = 0.46$$

Therefore, $0.46 \le D \le 0.6$.

3.9 RECTIFIERS

A rectifier is a power converter that converts AC voltage into DC.[2–3] A three-phase diode bridge rectifier consists of six diodes arranged in three branches as shown in Fig. 3.54. The input voltage to the rectifier is three-phase AC

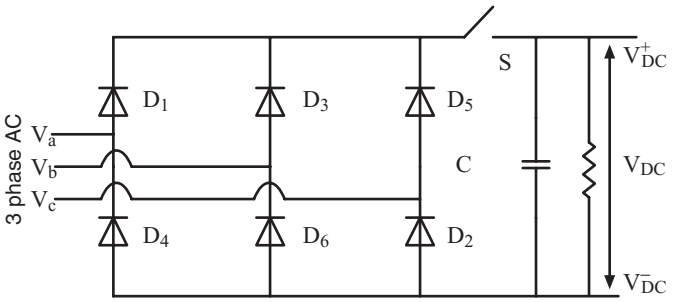

Figure 3.54 A Three-Phase Rectifier.

voltage and the output is DC voltage. The instantaneous output voltage of the rectifier is the same as the input line voltage. When the incoming AC voltage is positive, a diode in each branch is self-commuted, which is forward biased, and the input AC is rectified into DC voltage. This process of commutation is called *line commutation*. When the incoming AC voltage is negative, the diode will be reverse biased and act as an open circuit device.

Let us assume the following voltages are supplied to the three-phase rectifier of Fig. 3.54.

$$\begin{aligned} V_a &= \sqrt{2}V \cdot \sin(2\pi f \cdot t) \\ V_b &= \sqrt{2}V \cdot \sin(2\pi f \cdot t - 2\pi/3) \\ V_c &= \sqrt{2}V \cdot \sin(2\pi f \cdot t - 4\pi/3) \end{aligned} \tag{3.76}$$

where V is the RMS voltage of each phase in volt F is the frequency of the voltage in Hertz, and t is the time in seconds.

The line line-to-line voltages as shown Fig. 3.55 can be expressed as

$$\begin{aligned} V_{ab} &= V_a - V_b \\ V_{bc} &= V_b - V_c \\ V_{ca} &= V_c - V_a \\ V_{ba} &= -V_{ab} \\ V_{cb} &= -V_{bc} \\ V_{ac} &= -V_{ca} \end{aligned}$$

The input line-to-line voltages to the rectifier and its output voltage are shown in Fig. 3.55. The input voltage consists of three alternating voltages at 60 Hz, which is rectified by the rectifier to give a unipolar voltage at the output terminals. The input voltages and the diodes that conduct during

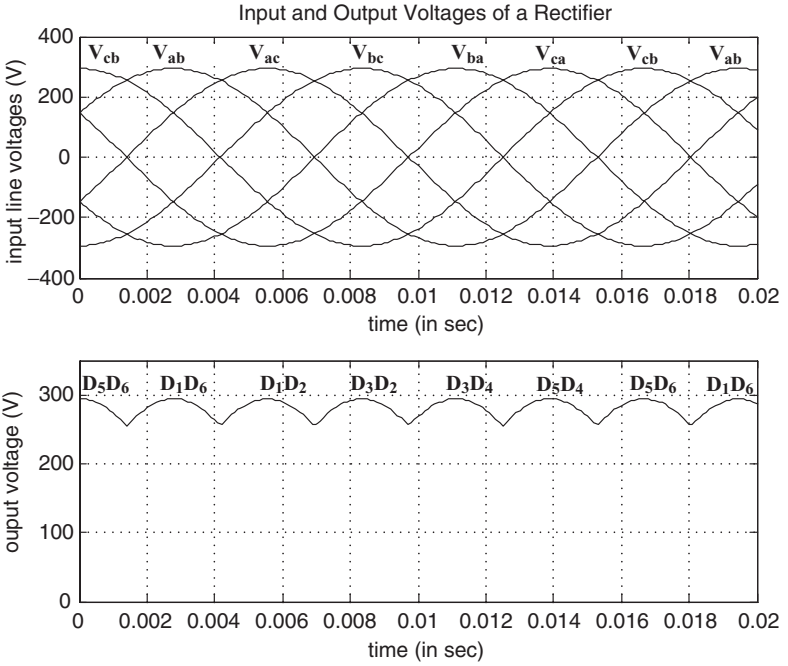

Figure 3.55 The Input Line-to-Line Voltage and the Output Voltage of a Three-Phase Rectifier with the Switch into the Conduction Shown.

each instant are marked on the figure. At any given moment, two diodes will be conducting: one from a branch at the upper side and the other from another branch at the lower side. Which of the two diodes conducts depends on which of the available line voltages has the highest positive value at that instant.

To explain the operation of the rectifier, let us start from the time $t = 0$. At this time, it is seen from Fig. 3.55, that V_{cb} has the maximum positive value. Therefore, the diodes that conduct are D_5 and D_6 (see Fig. 3.55). Because the frequency of the input voltage is 60 Hz, the period of input voltage is 16.667 ms ($T = 1/f$). Therefore, for 1.38 ms later, the voltage V_{ab} has the maximum positive value. The diode D_1 comes into conduction due to forward bias by V_{ac} (as it becomes positive and is applied across D_1 and D_5). At this time, D_5 is reverse biased and D_5 is turned off. D_1 and D_6 continue to conduct as long as V_{ab} has the maximum positive value. After a one-sixth cycle at 4.16 ms, the voltage V_{ac} becomes more positive than V_{ab}. D_2 is forward biased by voltage V_{bc}, which becomes positive at that instant. At the same time, D_6 is reverse biased (see Fig. 3.55) and turned off. The output voltage becomes V_{ac} (D_1 and D_2 conduct). The same thing is repeated a sixth of a cycle later

when D_1 is turned off and D_3 comes into conduction with an output voltage of V_{bc}. Then sequentially, the output voltage is V_{bc}, V_{ba}, V_{ca}, V_{cb}, and V_{ab}. With diodes $D_3 D_2$, $D_3 D_4$, $D_5 D_4$, $D_5 D_6$, and $D_1 D_6$ conducting in each case, respectively (see Fig. 3.55).

When the diodes are forward biased, the output voltage of the rectifier is shown in Fig. 3.55. When the rectifier is simulated, the output voltage can be recorded during these intervals.

From Fig. 3.55, we see that the output voltage is a pulsating DC wave with ripples. The average value of the output DC voltage can be computed as

$$V_{idc} = \frac{3\sqrt{2}}{\pi} V_{ab,rms} \tag{3.77}$$

This is the output voltage that appears across the output terminals of the rectifier when the switch S as shown in Fig. 3.54 is open (no load). This voltage has a DC component and ripple superimposed on it. To smooth out the ripple at the load terminal, a capacitor C is connected across the load terminals. This capacitor filters out the ripples and makes the voltage uniform. If the switch S is closed and there is no load connected across the output terminals, the voltage across the terminals is the peak of the line-to-line voltage ($V_{idc} = \sqrt{2} \cdot V_{ab,rms}$). The average value of this voltage reduces with the load and depends on the nature and magnitude of the load current.

Example 3.14 Write a MATLAB testbed for a diode-bridge three-phase rectifier. In your MATLAB simulation testbed, assume the input AC voltage of 120 V RMS (line to neutral), perform the following:

i) Plot the input line voltages
ii) Plot the output DC voltage
iii) Show that the instantaneous output voltage is same as the maximum of the input voltages

Solution

The steps to write the codes:

1. The input phase voltages are defined.
2. From the input phase voltages, the line voltages are defined.
3. The three-line voltages and their negatives are plotted.
4. The instantaneous output voltage is the maximum positive value among the input line voltages at that instant.
5. The output voltage is plotted.

The MATLAB program testbed codes are

```
% Rectification
clc;
f=60;
V=120;              % rms value of input line-
                    to-neutral voltage
t=0:0.0001:40e-3;
Va=V*sqrt(2)*
sin(2*pi*f*t);      % instantaneous input voltages defined
Vb=V*sqrt(2)*sin(2*pi*f*(t-1/f*2/3));
Vc=V*sqrt(2)*sin(2*pi*f*(t-1/f*4/3));
Vab=Va-Vb;          % the line-to-line voltages found out
Vbc=Vb-Vc;
Vca=Vc-Va;
Vba=-Vab;
Vcb=-Vbc;
Vac=-Vca;
subplot(2,1,1)      % input voltages are plotted
plot(t,Vab,t,Vbc,t,Vca,t,Vba,t,Vcb,t,Vac);
grid on;
xlabel('time (in sec)');
ylabel('input line voltages (V)');
title('Input and Output Voltages of a Rectifier')
Vx1=max(Vab,Vbc); % the maximum instantaneous voltage
                    is found out
Vx2=max(Vx1,Vca);
Vx3=max(Vx2,Vba);
Vx4=max(Vx3,Vcb);
Vx5=max(Vx4,Vac);
Vmax=Vx5;
Vdc=Vmax;
subplot(2,1,2)
plot(t,Vdc);        % the output voltage is plotted
grid on;
axis([0 40e-3 0 350])
xlabel('time (in sec)');
ylabel('ouput voltage(V)');
```

The result is given in Fig. 3.56.

The diode bridge rectifier can only carry current from the positive DC bus to the negative DC bus. Thus, power only flows from the AC side to the DC side making it a unidirectional converter. In rectifiers with controllable switches, where the switches can be turned on at any desired moment, the rectifiers can be made to feed back power from the DC side to the AC side, making them bidirectional.

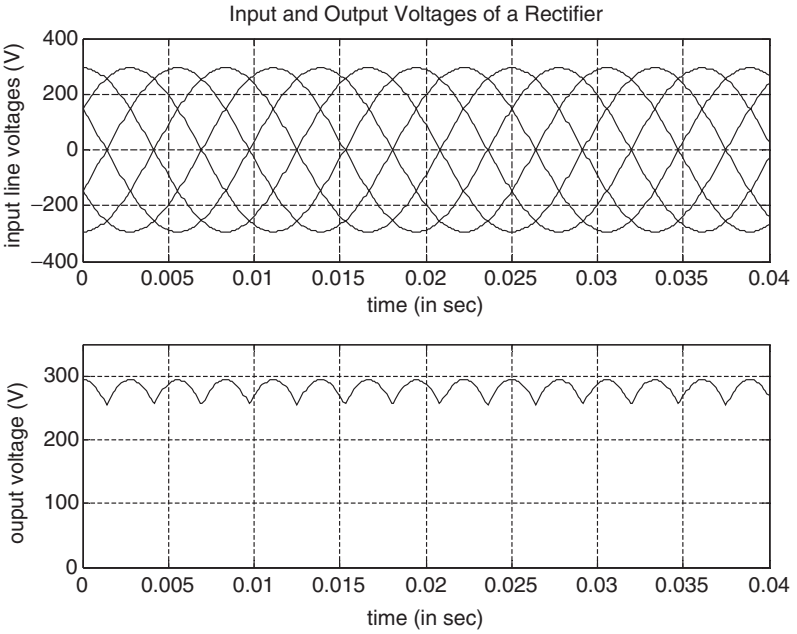

Figure 3.56 The Result of the Simulation.

3.10 PULSE WIDTH MODULATION RECTIFIERS

PWM rectifiers are widely used in three-phase AC/DC/AC systems due to their capability in DC voltage boost and regulation, input power factor correction, and input current harmonic control. In general, the DC link voltage contains a significant second-order harmonic component, which affects the voltage loop of the rectifier controller, especially when the control gain is high. Three-phase AC/DC/AC voltage stiff systems consisting of a front-end rectifier, a DC link with a capacitor, and an inverter are widely used in motor driven, on-line uninterruptible power supplies (UPS), and distributed generation systems. The rectifier controllers have two feedback loops: an outer voltage loop and an inner current loop, where the voltage regulator generates current command, which regulates current and power factor control. Under normal operating conditions, as a source of DC power in the distributed generation, steady-state DC bus voltage needs to be kept within its rating plus an acceptable variation as supported by the DC bus storage system. However, once the inverter output power changes in response to the load cycle variation or not balanced, the output power is no longer a constant, which leads to fluctuation of the DC link voltage. Two control problems must be addressed. The first problem is the storage system must keep the DC bus voltage within an acceptable range. The second problem is to control the inverter to provide

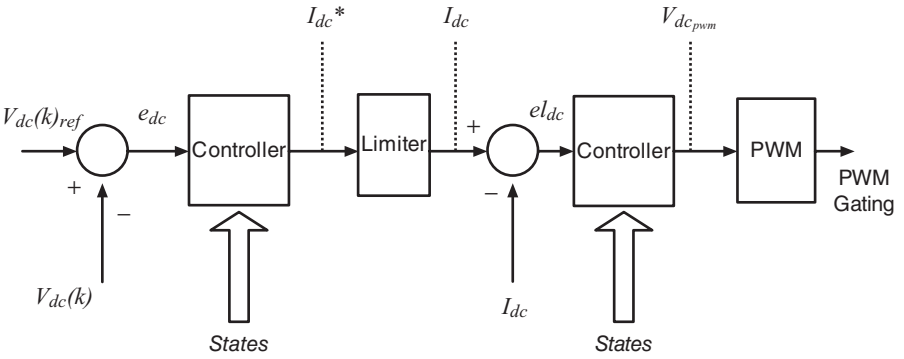

Figure 3.57 The Control Diagram of DC Bus Voltage Regulation Using a Rectifier System.

active and reactive power to the power grid. Figure 3.57 depicts the block diagram of rectifier control of DC bus voltage.

The first control goal is to minimize the DC link voltage. The second control goal is to improve instantaneous power balance between the input and output of a rectifier-inverter system and minimizing the DC coupling capacitance to reduce the cost. A lower DC coupling capacitance provides a better instantaneous power balance. However, this is only desirable under a balanced load. Once the inverter load is unbalanced, it is apparent that the steady-state inverter output power is no longer a constant, and neither is the inverter input DC power. Due to the existence of the DC link capacitor, the rectifier side steady-state power can be decoupled from the inverter side and controlled to within a range without being affected by the power fluctuation on the inverter side, which will lead to balanced front-end three-phase input currents.

A microgrid distribution generation (DG) system is depicted in Fig. 3.58. In this DG system, it is assumed that the variable frequency power is generated by a wind farm or a high-speed microturbine. The resulting AC power is rectified and stored in a high-power density capacitor or a storage device.

The DG control objective is to eliminate the effects of an unbalanced three-phase inverter load on the front-end input current and still guarantee unity power factor and fast DC bus voltage regulation against load disturbances.

3.11 A THREE-PHASE VOLTAGE SOURCE RECTIFIER UTILIZING SINUSOIDAL PWM SWITCHING

The analysis of the rectifier mode of operation is presented on a per-phase basis. The fundamental frequency component of $V_{PWM,a}$ is shown in Fig. 3.59. The AC/DC converter operates in a rectifier mode if the converter voltage $V_{PWM,a}$ is made to lag the supply voltage V_{AN} by an angle of δ. This causes the power to flow from the AC side to the DC side, as shown in the simplified

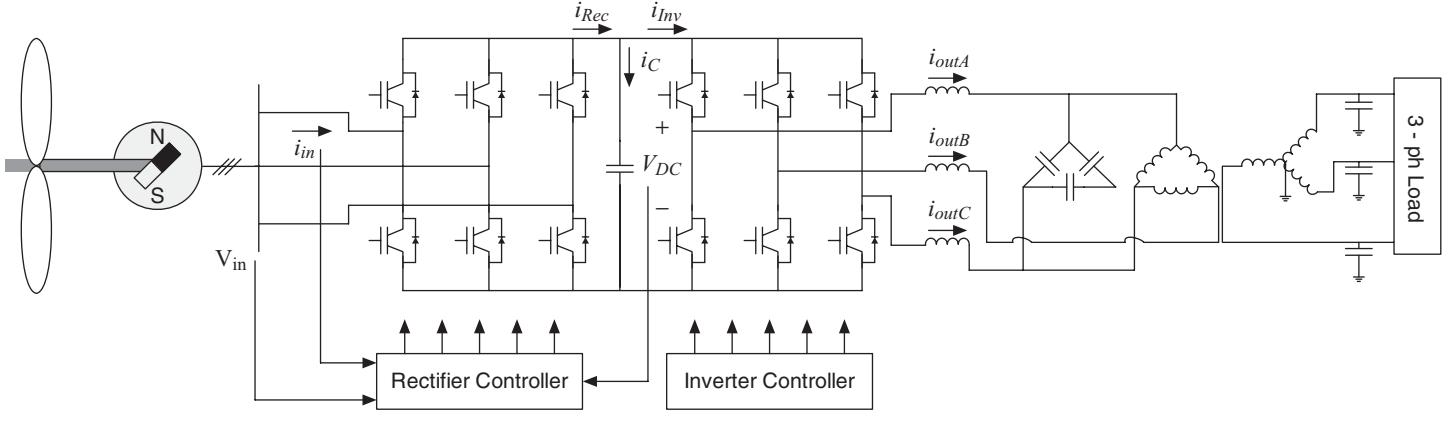

Figure 3.58 The Three-Phase AC/DC/AC System Topology Using a Wind Generator.

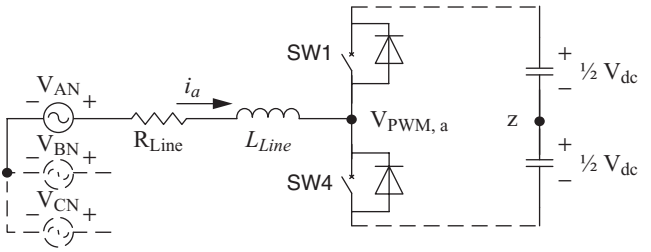

Figure 3.59 A One-Leg Model of a Three-Phase Pulse Width Modulation (PWM) Rectifier.

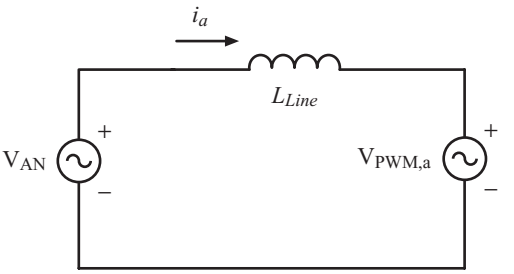

Figure 3.60 The Steady State Per-Phase Equivalent Circuit at Steady State for Fundamental Frequency Voltage.

equivalent circuit in Fig. 3.60, which allows the use of a simple AC power-transfer formula

$$P = \frac{V_{AN} \cdot V_{PWMa}}{X} \sin\delta \tag{3.78}$$

where the symbol V denotes the RMS value of the fundamental frequency voltage. The control of power angle δ is achieved by controlling the phase displacement of the command sinusoidal waveforms. For example, when the reference voltage is set to lag the AC source voltage by the fundamental component of $V_{PWM,a,}$ it will lag the source voltage by the same angle. Equation 3.78 states the condition for transfer of power to the DC bus from the AC source. The magnitude of $V_{PWM,a}$ is controllable by controlling the amplitude modulation index.

The phasor-diagram shown in Fig. 3.61 describes the rectifier mode of operation. The control of the input power factor angle θ of the rectifier can also be controlled by the angle δ. To achieve a unity power factor, the angle δ should be controlled such that the phase current is in-phase with the input voltage V_{AN} as shown in Figure 3.62.

The AC supply voltage and the supply current are shown in Fig. 3.63. The supply current is magnified 10 times in the figure. Figure 3.64 depicts the DC output voltage and Fig. 3.65 depicts one leg to neutral, $V_{PWM,a}$, the PWM voltage.

In Fig. 3.63 the input current is in-phase with the voltage. In this mode of operation, the rectifier operates at unity power factor.

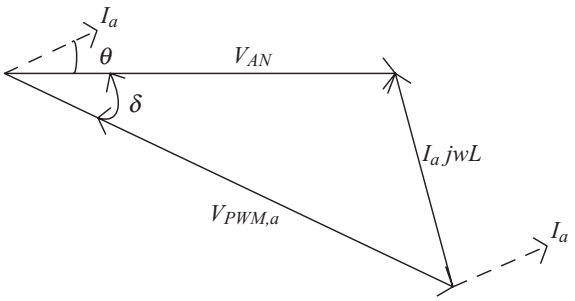

Figure 3.61 A Phasor Diagram for a Fundamental Frequency Rectifier Operation Mode.

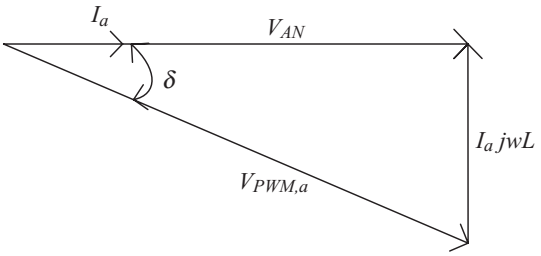

Figure 3.62 A Rectifier Mode for a Fundamental Frequency at a Unity Input Power Factor.

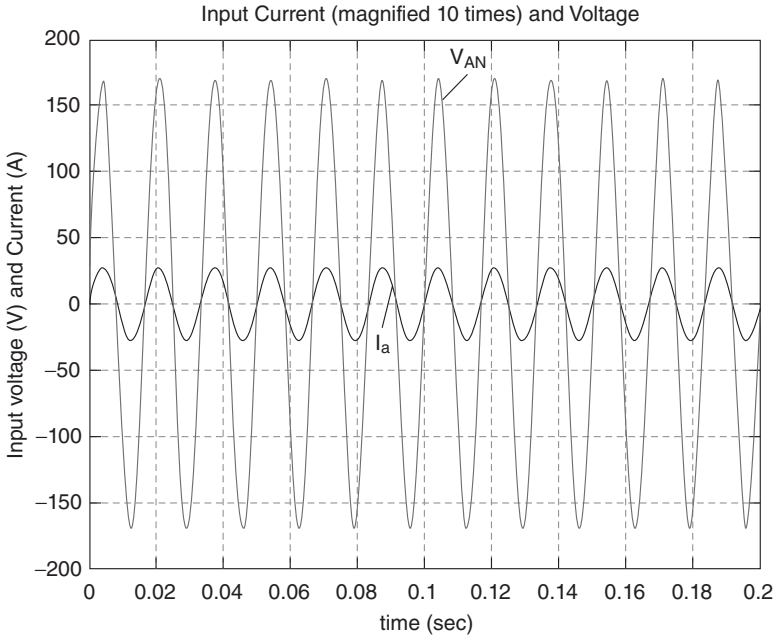

Figure 3.63 The AC Input Fundamental Voltage and Current Waveforms for the Rectifier (Waveforms of Example 3.15).

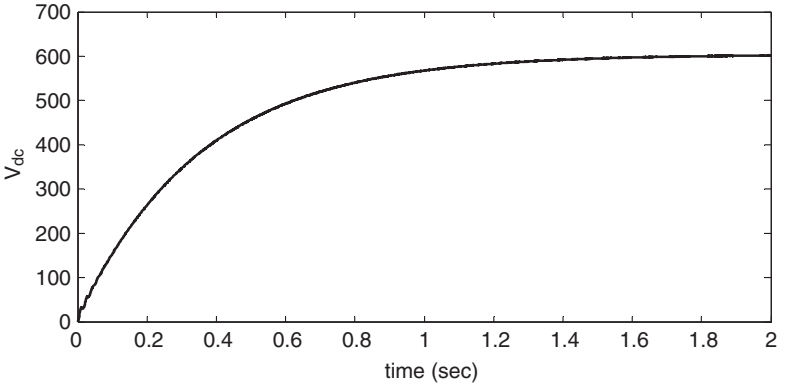

Figure 3.64 The DC Output Voltage.

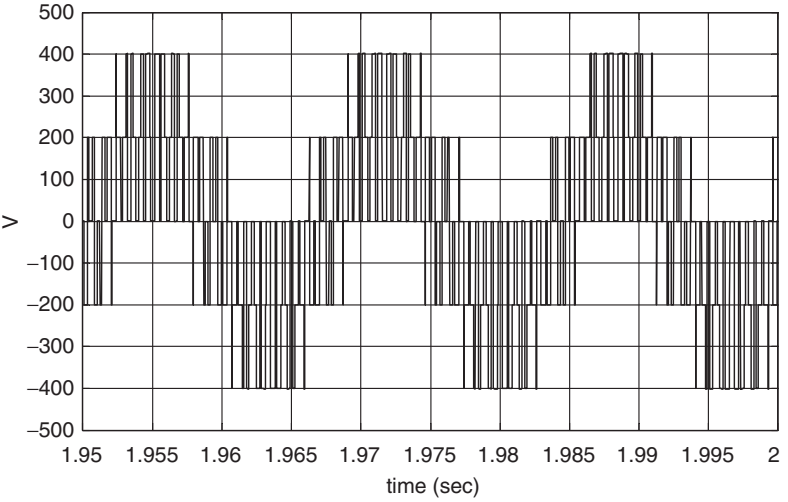

Figure 3.65 One Leg to Neutral Pulse Width Modulation (PWM) Voltage ($V_{PWM,a}$).

The value of $V_{PWM,a,1}$, the Rms value of the fundamental component of the voltage at the AC terminal of the rectifier depends on the value of V_{AN}, the AC supply voltage, and the current drawn from it as well as the value of the reactance, X present between them. The relationship between $V_{PWM,a,1}$ and V_{AN} is given by:

$$V_{PWMa} = V_{AN} - I_a X \tag{3.79}$$

For a given AC input voltage, current, power factor, and reactance, the value of $V_{PWM,a,1}$ can be determined. The value of the DC link voltage is determined by the modulation index and $V_{PWM,a,1.}$ For a three-phase rectifier, it is given by:

TABLE 3.4 The Values of M_a, V_{dc}, and the AC Voltage at the Rectifier Input Terminal.

V_{dc}	$V_{PWM,a,1}$	M_a
604 V	128.2 V RMS	0.6

TABLE 3.5 Data for Example 3.15.

V_{AN}	f_1	P	X	p.f.	M_a
120 V RMS	60 Hz	720 W	11 Ω	1	0.8

$$V_{dc} = \frac{2\sqrt{2} \cdot V_{PWMa,L-n}}{M_a} \tag{3.80}$$

Example 3.15 Consider a rectifier mode of operation for the following system data of a three-phase rectifier. Assume the data presented in Table 3.5.

Find the angle δ and the DC link voltage neglecting the harmonics.

Solution

The three-phase power is given by

$$P = 3 \cdot V_{AN} \cdot I_a \cdot \cos\theta$$

Therefore, the phase current,

$$I_a = \frac{P}{3 \cdot V_{AN} \cdot \cos\theta} = \frac{720}{3 \times 120 \times 1} = 2\angle 0 \text{ A}$$

The PWM voltage of the rectifier input is given by

$$V_{PWMa} = V_{AN} - I_a X$$
$$V_{PWMa} = 120 - 2\angle 0 \times 11\angle 90 = 122\angle -10.39 \text{ V}$$

Hence, the angle $\delta = 10.39$ degrees.

The line to neutral voltage of the input of the rectifier is given by

$$V_{L-N,rms} = \frac{M_a}{\sqrt{2}} \frac{V_{dc}}{2}$$

Hence, the rectified voltage is

$$V_{dc} = \frac{2\sqrt{2} \cdot V_{PWMa}}{M_a} = \frac{2\sqrt{2} \times 122}{0.8} = 431.3 \text{ V}$$

3.12 THE SIZING OF AN INVERTER FOR MICROGRID OPERATION

As stated before for sinusoidal-triangle PWM, we can control the magnitude of the output voltage, by controlling the amplitude modulation index.

In a microgrid system, three-phase inverters are used. The input of the inverter is a DC source that can be obtained from a PV source, a fuel cell, or variable frequency AC voltage from a variable-speed wind generator, which is rectified into DC. The DC voltage is typically converted into AC by employing sine PWM. The output AC voltage is obtained by comparing a triangular wave and a sine wave. The magnitude of the fundamental component of the output AC voltage depends on the amplitude modulation index, M_a that is defined as the ratio of the amplitude of the reference sine wave and the triangular wave. The frequency of the output voltage is the same as the reference sine wave. The harmonic content is decided by the frequency modulation index M_f that is defined as the ratio of the frequencies of the triangular wave and the reference sine wave. The harmonic content of the voltage should be as low as possible. To reduce the harmonics, the frequency modulation index should be high. The value of the fundamental component of the output AC line-to-line voltage is given by:

$$V_{PWM,ab} = \frac{\sqrt{3}}{\sqrt{2}} \cdot \frac{V_{dc}}{2} M_a \tag{3.81}$$

Table 3.6 illustrates the variation of amplitude modulation index required to generate a fixed-amplitude AC voltage from the DC bus voltage. The switches of the inverter should be rated at the voltage of the DC link and should be able to carry current for the rated condition. The frequency modulation index should be chosen from the commutation characteristics of the switches used.

Although the amplitude modulation index decides the magnitude of the output voltage, the frequency modulation index decides the harmonic content. The amplitude modulation index plays a minor role in the harmonic content. Table 3.7 gives the harmonic content in terms of per unit of the fundamental.

TABLE 3.6 The Values of Modulation Index Required to Keep the AC Voltage (Line-to-Line) Fixed for a Three-Phase Inverter.

V_{ac} = 120 V	
V_{DC} (V)	M_a
200	0.98
250	0.78
300	0.65

TABLE 3.7 The Per Unit Harmonic Content of the Output-Phase Voltage.

Order of Harmonic	$M_a = 1$	$M_a = 0.9$	$M_a = 0.8$	$M_a = 0.7$	$M_a = 0.6$
1	1.000	1.000	1.000	1.000	1.000
$1 \cdot M_f \pm 2$	0.318	0.298	0.275	0.248	0.218
$2 \cdot M_f \pm 1$	0.181	0.283	0.393	0.506	0.617

The second column of the table shows that if the fundamental of the voltage wave has a magnitude of 1, for $M_a = 1$, then the magnitude of the harmonic of order $1 \cdot M_f \pm 2$ is 0.318 or 31.8% of the fundamental (M_f is the frequency modulation index). For example, if the frequency modulation index is chosen as 50 (switching frequency of 3 kHz with a power frequency of 60 Hz), then from $1 \cdot M_f \pm 2$, the order of the harmonics that will be significant are 48 and 52. In other words, harmonics of $48 \times 60 = 2.88$ kHz and $52 \times 60 = 3.12$ kHz will have magnitudes comparable to the fundamental. Similarly, the harmonic of order $2 \cdot M_f \pm 1$ is 18.1% of the fundamental. Which means the 99th and 101st harmonics will have significant amplitudes. These harmonics will have frequencies 99 and 101 times the fundamental frequency, respectively (5.94 kHz and 6.06 kHz). Next, the third column gives the harmonic contents as a fraction of the fundamental if the amplitude modulation index is 0.9. This means that if M_a is 0.9, then the 48th and 52nd harmonics will be 29.8% of the fundamental. The subsequent columns show the harmonic content for different amplitude modulation indices.

In general, the orders of the harmonics that are significant or comparable to the fundamental are $N \cdot M_f \pm M$ where N and M are integers such that their sum results in an odd integer. Most electrical circuits consist of R-L structures. The impedance of the inductance is directly proportional to the frequency ($X_{L,1} = L \cdot 2 \cdot \pi \cdot f$). As the order of the harmonic voltage increases, its frequency also increases. The harmonic impedance offered by the inductor becomes $X_{L,n} = L \cdot 2 \cdot \pi \cdot n \cdot f = n \cdot X_{L,1}$. In other words, the harmonic impedance becomes the order of the harmonic times the fundamental impedance. Therefore, the higher the order of the harmonic the more is the harmonic impedance and less is the current. Therefore, with a higher M_f the more is the order of harmonic and less is the harmonic current. If the harmonic content of the current is less, the closer is the current to the desired sinusoidal wave. Hence, it is always desired to have a higher frequency modulation index. However, there is some practical constraint to it. If the sampling frequency is high, then the number of turn on and offs of the switch per second increases and the switching losses increase. Moreover, if the sampling frequency is too high, the switches may fail to turn on and off properly. Therefore, a tradeoff is reached between harmonic content and the switching loss to determine the sampling frequency. Furthermore, the sampling frequency is selected out of audio range.

3.13 THE SIZING OF A RECTIFIER FOR MICROGRID OPERATION

For a diode bridge rectifier, the open-circuit DC voltage is directly proportional to the input AC voltage. These rectifiers are used only when the frequency at the AC side is not important and when no control is required for the DC voltage. The DC voltage is directly proportional to the AC input voltage. A capacitor may be connected across the DC link to stabilize the DC voltage. The open circuit voltage with no capacitor is given by:

$$V_{dc} = \frac{3\sqrt{6} \cdot V_{PWMa}}{\pi} \tag{3.82}$$

In applications where the frequency of the AC side is to be maintained at a particular value, PWM rectifiers are employed. The DC output voltage of the three-phase sine-triangle PWM rectifier is determined not only by amplitude modulation index, but also the power angle δ discussed before. The rectifier is usually supplied from an AC source with a reactance between the rectifier and the AC source. The current drawn by the rectifier causes a voltage drop; as a result, the AC voltage at the rectifier terminal is different from that of the AC source. The rectified voltage V_{DC} is directly proportional to the AC voltage at the rectifier terminal and is inversely proportional to the modulation index:

$$V_{dc} = \frac{2\sqrt{2} \cdot V_{PWMa}}{\sqrt{3} \cdot M_a} \tag{3.83}$$

The switches of the rectifier should be rated at least at the DC link voltage and the frequency modulation index is determined from the commutation time of the switches. Similar to the inverter, the harmonic content of the current is less if the sampling frequency is high. However, a higher sampling frequency results in higher switching losses and may cause commutation of the switches too. Hence, a tradeoff is reached between the switching loss and the harmonic content to decide upon the sampling frequency.

3.14 THE SIZING OF DC/DC CONVERTERS FOR MICROGRID OPERATION

The DC/DC converters are used to connect the battery to the microgrid. The type of converter is chosen based on the application: a boost converter to step the voltage up, a buck converter to step it down, whereas a buck-boost converter is used for both stepping up and down. The output of the converters is given in Equation 3.84. As, seen from the equation, the output voltage depends on the duty ratio of the switch. The switch should have a rating equal to that of the high voltage side for buck converter and boost converter. For a

buck-boost converter, the switch should be rated to a voltage level higher than the sum of the input and output voltages. The current rating of the converter should be such that the converter is able to charge and discharge the battery with required current.

$$\begin{aligned} V_o &= \frac{V_{in}}{1-D} \text{ : boost converter} \\ V_o &= D \cdot V_{in} \text{ : buck converter} \\ V_o &= \frac{D \cdot V_{in}}{1-D} \text{ : buck-boost converter} \end{aligned} \tag{3.84}$$

The output voltage of the DC/DC converter is not constant in the strictest sense of the word. It has small ripples about an average value. Ideally, for a stiff voltage source, the ripple should be zero. Practically, there is some ripple present in the output voltage depending on the load, the output capacitance, and the switching frequency. A higher value of capacitor and a higher switching frequency is required to keep the ripple small for a given load. Like an inverter, the switching frequency is decided by considering the switching losses and the turn-on and turn-off time of the switch used. A tradeoff is reached between the ripple in the output voltage and the switching loss. Again, the size and cost of the converter increases with the size of the inductor and the capacitor. So, a tradeoff is reached between the ripple of the output voltage and the inductor current and the size and cost of the converter while designing it.

PROBLEMS

3.1 Consider the microgrid of Figure 3.66. A three-phase transformer, T1, is rated 500 kVA, 220/440, transformer with the reactance of 3.5%. The microgrid is supplied from an AC bus of a PV generating station with its DC bus rated at 540 V. The distribution line is 10 miles long and has a series impedance of $0.1 + j\ 1.0\ \Omega$ per mile and local load of 100 kVA at 440 V. The microgrid is connected to the local power grid using a three-phase transformer T2, rated at 440 V/13.2 kV with the reactance

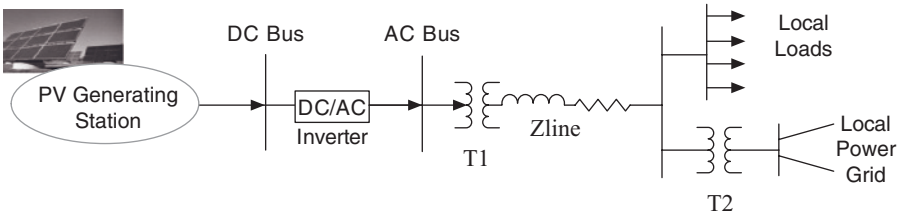

Figure 3.66 A One-Line Diagram for Problem 3.1.

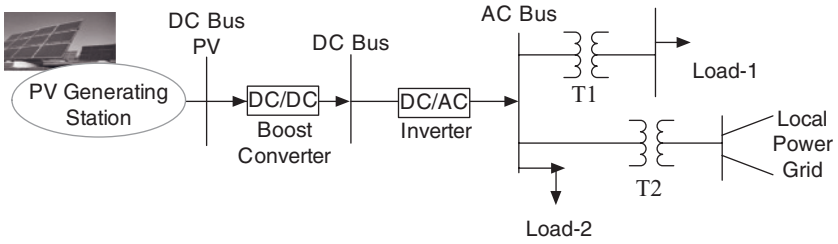

Figure 3.67 A One-Line Diagram of Problem 3.2.

of 8%. Compute the per unit impedance diagram of the microgrid system. Assume the voltage base of 13.2 kV on the local power grid side and kVA base of 500.

3.2 Consider the microgrid of Figure 3.67. Assume the inverter AC bus voltage of 240 V and transformer T1 is rated 5% impedance, 240 V/120 V and 150 kVA. The transformer T2 is rated at 10% impedance, 240 V/3.2 kV and 500 kVA. The local loads are rated at 100 kVA and a power factor of 0.9 lagging. The inverter modulation index is 0.9.
Compute the following:

i) The DC bus voltage and inverter rating

ii) The boost converter PV bus input voltage and input current ratings for the required DC bus voltage of the inverter

iii) The size of the microgrid PV station

iv) The per unit model of the microgrid

3.3 For Problem 3.2 depicted in Figure 3.67, assume the DC bus voltage of inverter is equal to 800 V DC. The transformer T1 is rated 9% impedance, 400 V/220 V and 250 kVA. The transformer T2 is rated at 10% impedance, 400 V/13.2 kV and 500 kVA. The Load 1 is rated at 150 kVA with a power factor of 0.85 lagging. The Load 2 is rated at 270 kVA with a power factor of .95 leading.
Compute the following:

i) The modulation index and inverter rating.

ii) The boost converter PV bus voltage and input current for the required DC bus voltage of the inverter.

iii) The minimum size of the microgrid PV station.

3.4 For Problem 3.3 depicted in Figure 3.67, assume transformer T1 is rated at 5% impedance, 440 V/120 V and 150 kVA. The transformer T2 is rated at 10% impedance, 240 V/3.2 kV and 500 kVA. The inverter modulation index is 0.9. Select the power base of 500 kVA and the voltage base of 600 V. The local power grid internal reactance is 0.2 per unit base on 10 MVA and 3.2 kV. Assume the microgrid is not loaded.

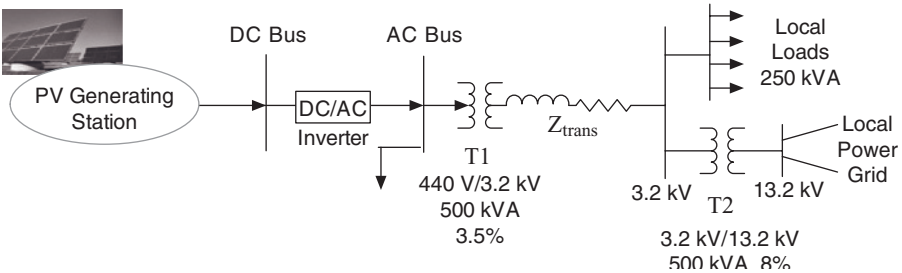

Figure 3.68 A One-Line Diagram of Problem 3.5.

Compute the following:

i) The per unit equivalent impedance model

ii) The fault current if a balance three-phase fault occurs on the inverter bus

3.5 Consider the microgrid of Figure 3.68. A three-phase 500 kVA, 440/3.2 kV transformer with the per unit reactance of 3.5% feeds from an AC source of a PV generating station. The distribution line is 10 miles long and has a series impedance of $0.01 + j\ 0.09\ \Omega$ per mile. The local load is 250 kVA. Balance of power can be injected into the local utility using a 3.2/ 13.2 kV transformer and with the per unit reactance of 8%. Assume the voltage base of 13.8 kV on the local power grid side, kVA base of 500, and the DC bus voltage of 800 V.

Compute the following:

i) The inverter and the PV generating station ratings

ii) The per unit impedance diagram of the microgrid

3.6 Consider the microgrid of Figure 3.68 and the data of Problem 3.5. The local power grid net input reactance can be approximated as 9% based on the voltage base of 13.2 kV and 500 kVA base. Assume DC bus voltage of 880 V.

Compute the following:

i) The inverter modulation index and inverter rating

ii) The short-circuit current of AC bus if a three-phase short-circuit occurs on the AC bus of the inverter; ignore the PV station fault current contribution

iii) The same as part (i), except assume that the internal reactance of PV generating station and its inverter can be approximated as 1 per unit based on inverter rating

3.7 Consider a three-phase DC/AC inverter with a DC bus voltage rate at 600 V. Assume the DC bus voltage can drop during a discharge cycle to 350 V DC. Determine the AC bus voltage range and its corresponding the modulation index.

TABLE 3.8 Data for Problem 3.8.

V_{AN}	f_1	P	X	p.f.	M_a
120 V RMS	60 Hz	1500 W	15 Ω	1	0.85

3.8 Consider a rectifier mode of operation for the following system data of a three-phase rectifier. Assume the data given in Table 3.8.
Perform the following:

i) Find the angle δ and the DC link voltage. Ignore the resulting harmonics.

ii) Write a MATLAB program to simulate the rectifier operation to plot the current I_a and the voltage V_{AN} considering V_{PWMa} and δ are known and have values same as the result of Part i). Assume the PWM voltage is calculated from the incoming AC power. Ignore the resulting harmonics.

3.9 For a three-phase rectifier with the supply-phase voltage of 120 V and the reactance between the AC source and the rectifier is 11 Ω. Write a MATLAB program to plot the modulation index necessary to keep the V_{DC} constant at 1200 V when the input power factor angle is varied from –60° to 60°. Assume that the active power supplied by the system remains fixed at 5.5 kW.

3.10 Develop a MATLAB testbed and compute the triangular wave V_T using the Fourier series. Assume the following specifications: peak 48 V, frequency 1 kHz, and order of harmonics ≤30. Plot the waveform.
Hint: $V_T(t)$ can be constructed using the Fourier series of a triangle wave. An advantage to this method is that you can create the waveform over a long period. The equation and solution of a Fourier series can be found in many sites online. It should be quickly noticed that the triangle waveform has an odd symmetry, thus $a_0 = 0$ and $a_k = 0$.

The Fourier equation becomes

$$F(t) = a_0 + \sum_{k=1}^{\infty} a_k \cdot \cos(k \cdot \omega t) + b_k \cdot \sin(k \cdot \omega t)$$

$$F(t) = \sum_{k=1}^{\infty} b_k \cdot \sin(k \cdot \omega t)$$

b_k is all that needs to be solved for. The triangle function can then be split into sections, somewhat like the first method, to find b_k.

The equation to form a triangular wave has been discussed in section 3.5.1.

$$b_k = \frac{-8 \cdot (-1)^k}{k^2 \cdot \pi^2} \sin\left(k \cdot \frac{\pi}{2}\right)$$

Now, we will substitute substitution and we will obtain the equations for the triangle wave as shown by equation:

$$F(t) = A \cdot \sum_{k=1,3,5}^{\infty} \frac{-8 \cdot (-1)^k}{k^2 \cdot \pi^2} \sin\left(k \cdot \frac{\pi}{2}\right) \cdot \sin(k \cdot \omega t)$$

where A is amplitude. This equation can then be put into MATLAB.

We can use this equation to describe the operation of a converter in a MATLAB simulation.

For example, let us define the frequency, sampling time, and amplitude as

$$f_s = 5000;\ T_s = 1/f_s;\ V_{TMax} = 48$$

To see the full waveform, the step size should be at least half of T_s and a power of 10 smaller to create enough points.

$$t = 0 : T_s / 20 : 10$$

the above MATLAB codes will create a waveform 10 seconds long. We can use a loop to iterate the equation constantly adding it to itself as needed by a series $\sum_{k=1,3,5}^{\infty}$.

3.11 Develop a MATLAB testbed and compute the triangular wave for PWM using the identity mapping method. Assume a peak value of 48 and a frequency of 1 kHz. Plot the wave form.

3.12 Develop a MATLAB testbed for the DC/AC inverter given below. Assume V_{idc} is equal to 560 V (DC), $V_{C\ (max)}$ is equal to 220 V, f_e is equal to 60 Hz and modulation index of $5 \le M_a \le 1.0$, and change M_f from 2 to 20.

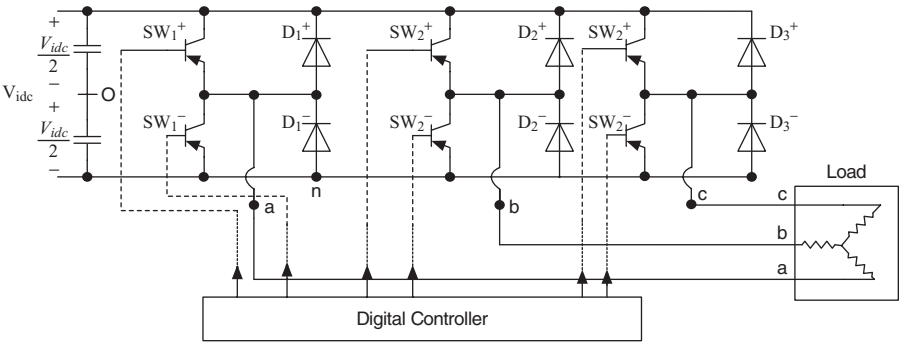

Figure 3.69 The Linear and Overmodulated Operation of a Three-Phase Converter.

Perform the following:

i) The ratio of the fundamental–frequency of the line–line (RMS) to the input DC voltage, V_{idc}, ($V_{(lin–line\ (RMS))} / V_{idc}$.)

ii) Plot the $V_{(lin–line\ (RMS))}/V_{idc}$ as a function of M_a for $M_f = 2$ and $M_f = 20$.

3.13 Consider a PV source of 60 V. A single-phase inverter with four switches is used to convert DC to 50 Hz AC using a unipolar scheme. Select the following modulation indices:

a. $M_a = 0.5$ and $M_f = 7$

b. $M_a = 0.5$ and $M_f = 10$

c. $M_a = 0.9$ and $M_f = 4$

Write a MATLAB program to generate the waveforms of the inverter showing V_{an}, V_{bn}, V_{cn} voltages. Make tables and discuss your results.

REFERENCES

1. Keyhani A, Marwali MN, Dai M. Integration of green and renewable energy in electric power systems. Hoboken, NJ: Wiley; 2010.
2. Mohan N, Undeland T, Robbins W. Power electronics. New York: Wiley; 1995.
3. Rashid MH. *Power electronics, circuits,* devices and applications. 3rd ed. Englewood Cliffs, NJ: Pearson Prentice Hall; 2003.
4. Enjeti P. An advanced PWM strategy to improve efficiency and voltage transfer ratio of three-phase isolated boost dc/dc converter. Paper presented at: 2008 Twenty-Third Annual IEEE Applied Power Electronics; Feb 24–28, 2010; Austin, TX.
5. Dowell LJ, Drozda M, Henderson DB, Loose VW, Marathe MV, Roberts DJ. ELISIMS: comprehensive detailed simulation of the electric power industry. Los Alamos National Laboratory, Technical Rep. No. LA-UR-98-1739. Los Alamos, NM: Los Alamos National Laboratory.

CHAPTER 4

SMART POWER GRID SYSTEMS

4.1 INTRODUCTION

Initially designed in the early 1900s, today's power grid has evolved to become a large interconnected network that connects thousands of generating stations and load centers through a system of power transmission lines.[1–3] A power grid system is designed based on the long-term load forecast of the power grid load centers that are developed according to the anticipated needs of the community it serves. Then, an analytical model of the system is developed to project the grid's real-time operation. In a smart power grid system, a large number of microgrids operate as part of an interconnected power grid. For example, a photovoltaic- (PV-) based residential system with its local storage system and load would be one of the smallest microgrids in the smart power grid system.[4] To understand the new paradigm of tomorrow's smart power grid design and operation, we need to understand today's electric power grid operation and costs of design.[4–5]

In this chapter, we introduce the basic system concepts of sensing, measurement, integrated communications, smart meters, and high green energy penetration of intermittent generation sources. We also introduce the basic concepts of generator operation, power flow, the limit of power flow on transmission lines, and load factor calculation and its impact on the operation of a smart grid and microgrids. A basic understanding of a power grid's operation will facilitate how to design a microgrid to operate as a standalone system when it is separated from its local power grid. These concepts set the stage for

Design of Smart Power Grid Renewable Energy Systems, First Edition. Ali Keyhani.

the design of green energy microgrids that will be presented in the chapters that follow.

4.2 POWER GRID OPERATION

The operational objectives of a power grid are to provide continuous quality service at an acceptable voltage and frequency with adequate security, reliability, and an acceptable impact upon the environment—without damage to the power grid equipment—all at a minimum cost.[5–6]

In Fig. 4.1, the direction of the arrows indicates the priority in which the objectives are implemented. Quality service that is environmentally acceptable, secure, and reliable, and entails minimum cost is the main objective in power grid system operations. However, during emergency conditions, the system may be operated without regard for economy and environmental restriction such as the use of a high polluting energy source, instead concentrating on the security and reliability of the service for energy users, while maintaining power grid stability.

The term *continuous service* means "secure and reliable service." The term *secure*, as it is used here, means that upon occurrence of a contingency, the power grid could recover to its original state and supply the same quality electric energy as before.

For example, if in the power grid of Fig. 4.2, the line connecting bus 2 and bus 4 is out of service, the power grid is *secur*e if it still can serve all loads. However, the power grid is *reliable* if it has adequate reserves to face increased load demands. In addition, the power grid of Fig. 4.2 is reliable if when it is subjected to scheduled or unscheduled energy source outages, it is still able to supply quality electric energy to the users.

To ensure security and reliability, power plant facilities and resources must first be planned then managed effectively. A large power grid is comprised of many elements including generating units, transmission lines, transformers, and circuit breakers. As new green energy sources are adopted into the power grid and a smart power grid is put in place, additional equipment such as DC/DC converters and DC/ AC converters must be integrated and scheduled for power grid operation. In addition, market structure and real-time pricing[5–6] of energy need to be evaluated.

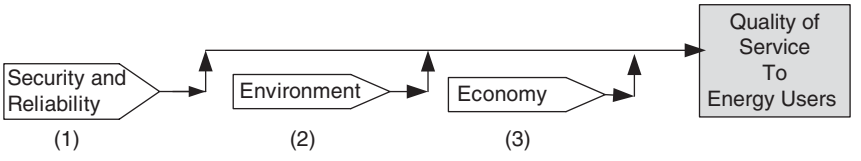

Figure 4.1 The Interrelated Objectives of Operation of a Power System.

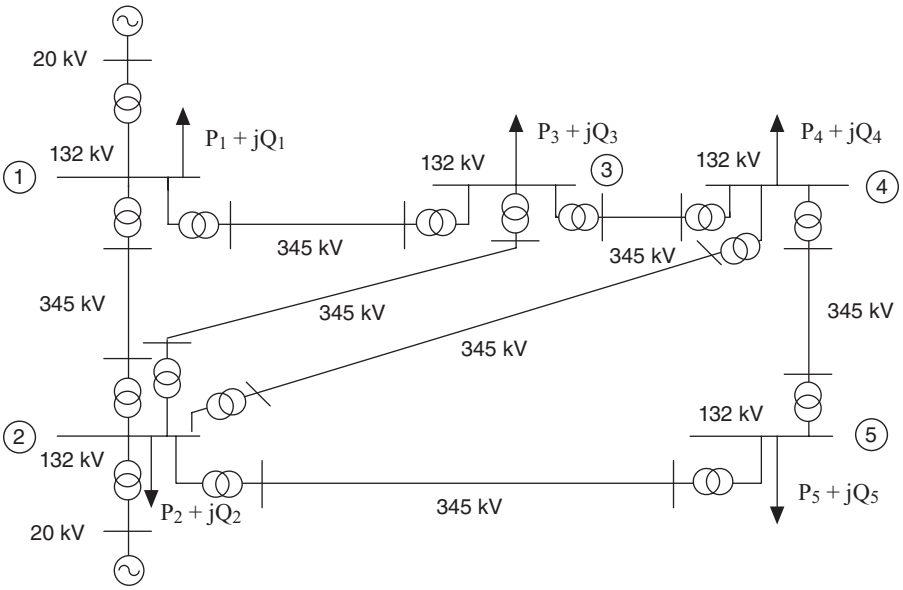

Figure 4.2 A Five-Bus Power System.

At the outset, we need to schedule power generation to supply the system loads for every second of the system's operation.[6–8] The energy resources of a large power system consist of hydro and nuclear energy, fossil fuel, renewable energy sources such as wind and solar energy, as well as green energy sources such as fuel cells, combined heat and power (CHP; also known as cogeneration), and microturbines. These resources must be managed and synchronized to satisfy the load demand of the power grid. The load demand of a power grid is cyclic in nature and has a daily peak demand over a week, a weekly peak demand over a month, and a monthly peak demand over a year. Energy resources must be optimized to satisfy the peak demand of each load cycle, such that the total cost of production and distribution of electric energy is minimized.

Figure 4.3 depicts a 24-hour load variation sampled every 5 minutes. From Fig. 4.3, it can be seen that peak demand is twice the minimum power demand. Figure 4.4 shows that the peak power demand occurs on Monday and the minimum power demand occurs on Sunday. The power system operator must plan the power grid energy resources and facilities to satisfy the varying load conditions.

Operations planning is divided into three tasks—long-, medium-, and short-term operations—as shown in Fig. 4.5. Operations control deals with controlling the system as it is operated minute by minute. An operations accounting system records the events occurring on a grid system and by analyzing recorded

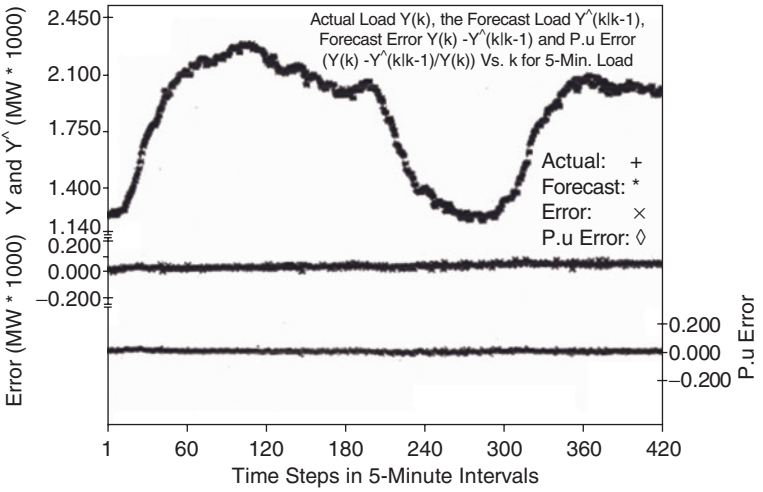

Figure 4.3 A 24-Hour Load Variation Sampled Every 5 Minutes.[7]

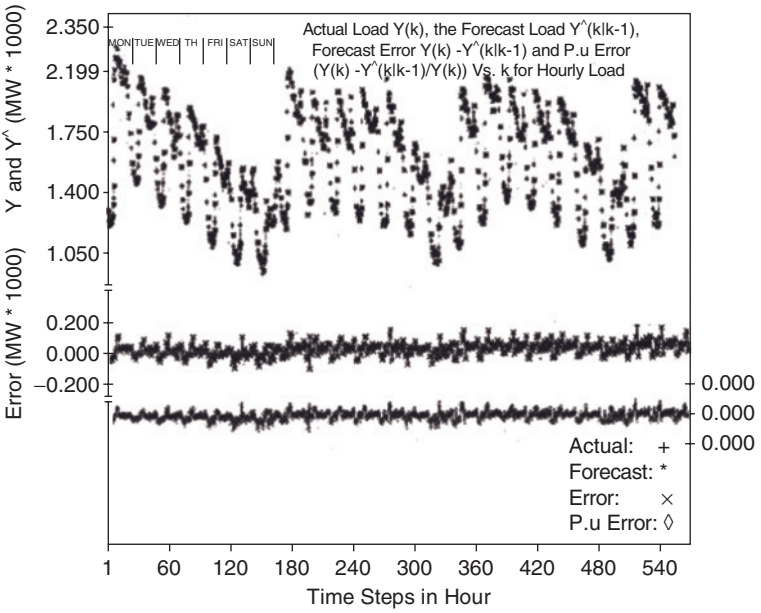

Figure 4.4 A Weekly Load Variation Sampled Hourly.

data attempts to account for various events that affected the grid. Operations accounting data is also used in the planning of future power grids.

The decision time involved in operations planning and control of the power grid is depicted in Fig. 4.6. The vertical axis of Fig. 4.6 shows the decision time for implementing a function. The horizontal axis indicates where the control

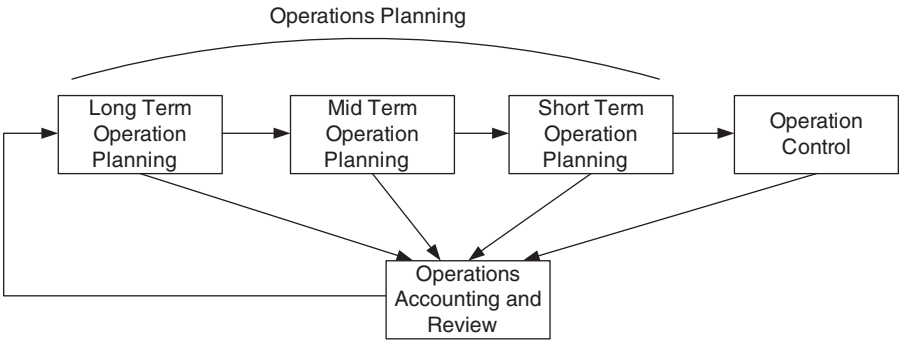

Figure 4.5 The Interrelated Tasks of Planned Scheduling Operation.[7]

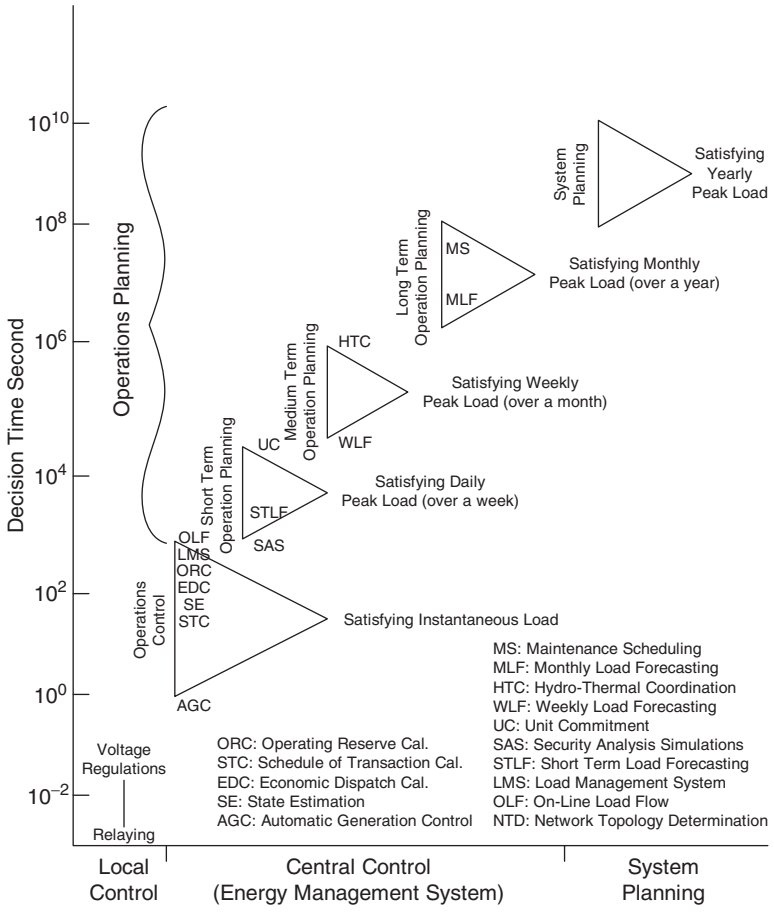

Figure 4.6 Energy Management System and Its Functions versus Decision Time.

of a function takes place. These functions are programmed into the computer software. The hardware for implementing these functions includes two computers, one operating in real-time in charge of the grid; the second is on-line as a backup if the first computer encounters problems. The computer system is referred to as an energy management system (EMS) or the energy control center.

The Supervisory Control and Data Acquisition (SCADA) system consists of data acquisition and control hardware and software, man–machine and interface software systems, and dual computer systems with real-time operating systems. Therefore, the EMS consists of a SCADA system plus the application functions used to operate and control the power grid. The primary functions of SCADA are (1) to collect information throughout the power grid, (2) to send the collected data through the power grid communication system to the control center, and (3) to display the data in the control center for power grid operators to use for decision making and in the determination of the application function for grid operation. As part of the smart power grid design, additional data concerning the energy resources such as wind, solar, PV energy sources, and real-time pricing from the power market must be incorporated into the SCADA system. Distributed over a wide area, the smart power grid must be optimized for its efficient and stable operation—yet another task for the SCADA system.

The problems of operations planning can be broken down into four different tasks. The first task is (1) to schedule all resources and facilities yearly, (2) on a monthly basis for satisfying the forecasted monthly peak load, (3) then utilizing the weekly results to produce a daily schedule, and (4) finally using the daily schedule to prepare a feasible and secure hourly schedule.

The long-term operation planning consists of two functions: a monthly load-forecasting program and a maintenance scheduling program based on estimates of the peak load demand of every month. The maintenance scheduling program schedules units for maintenance according to many criteria, e.g., the manufacturer's maintenance recommendations, experience with particular equipment such as generators, transformers, transmission lines, etc., such that the peak load demand of every month is satisfied within a reasonable risk.

The scheduling of resources and facilities on a weekly basis is accomplished through medium-term operation planning. This task consists of two functions: a weekly load forecasting program and a hydrothermal coordination program. The weekly load-forecasting program estimates the peak demand of every week over a month. The hydrothermal coordination program determines the best schedule of operation of the hydro and thermal units such that the amount of fuel consumed in the thermal units is minimized, and the weekly load demand of the system is satisfied. As renewable energy sources are increasingly used in the power grid, the operation planning will become highly complex due to the intermittent nature of renewable energy sources. Furthermore, as real-time pricing is put into effect,[8] the task of operation planning will become more complex as energy users react to daily hourly pricing.

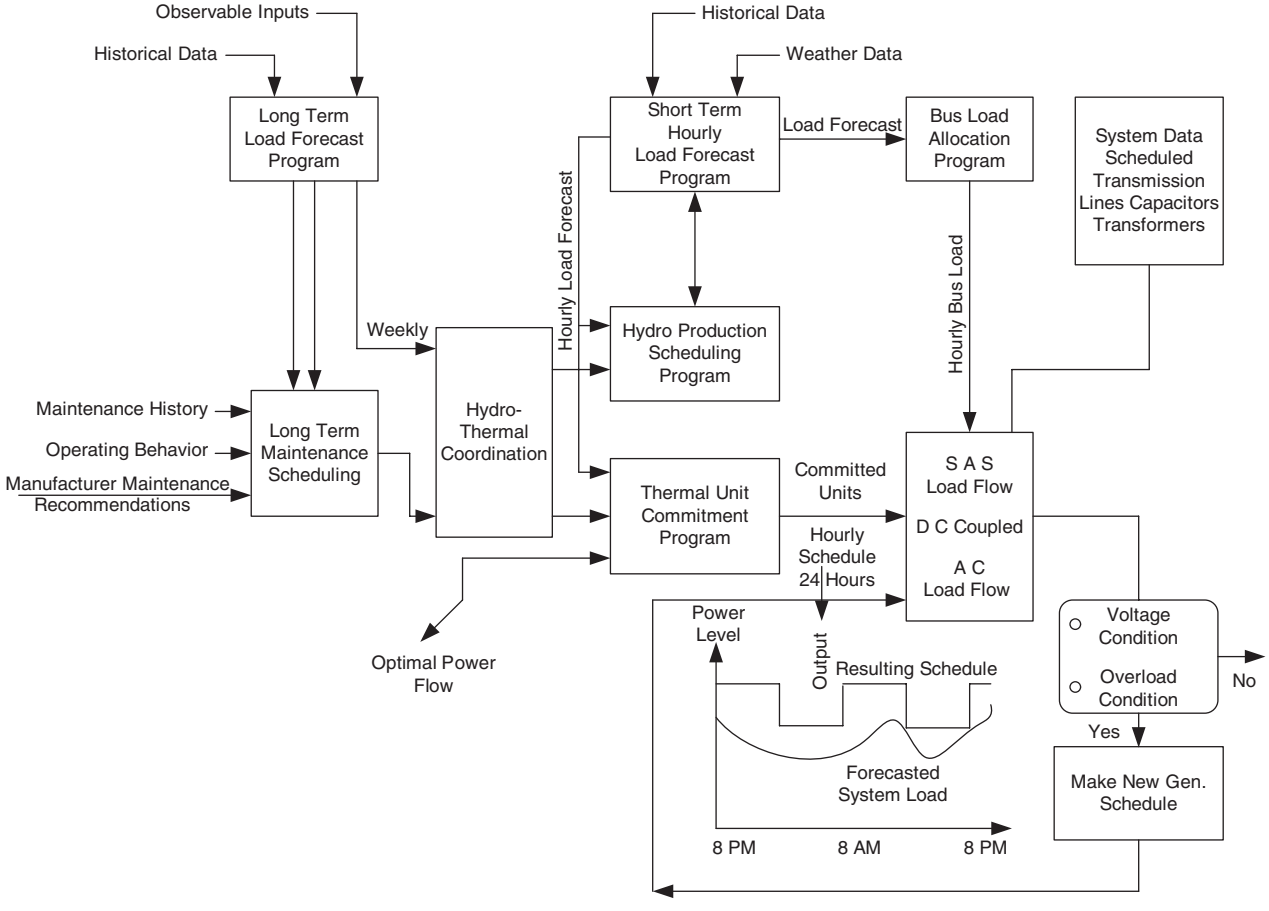

Figure 4.7 The Interrelated Tasks of a Planned Scheduling Operation.

These problems are being addressed in the planned operation of a smart power grid.

The weekly scheduling of facilities and resources on a daily basis is performed by short-term operation planning, which consists of a short-term load-forecasting program, a security analysis simulations program, and a unit commitment program. The short-term load-forecasting estimates the hourly load demands of the next 168 hours. The unit commitment or economic generation scheduling, which is also referred to as the ordering method or predispatching, determines the generating units to be committed to system operation based on the availability of different units, as specified by long- and medium-term operation planning so that the hourly forecasted load for the next 24 to 168 hours is satisfied. In addition, the unit commitment function makes a sequence of decisions leading to the starting and stopping of thermal units to assure an adequate but not excessive amount of generating capacity is available to meet the hourly forecasted grid load. It should be mentioned that due to uncertainty in the load forecast, it is customary to plan for additional capacity either synchronized or ready to be synchronized within a short period. This excess capacity is called the operating reserve, which we will discuss later. The security analysis simulation function is a set of dispatcher-oriented, interactive programs that are used to compute the system bus-load voltages. The last activity of short-term operation planning is a security analysis simulation function. The security analysis simulation function computes the system bus voltages based on the hourly generation schedule from the unit commitment program and an hourly bus-load forecast. If for the expected hourly loading, generation scheduling, and the expected or scheduled system configuration, the resulting operation condition is not acceptable, then changes in the system configuration (e.g., changing the tap setting of the transformers or the scheduled generation) will be made and the computation will be repeated. Once a feasible economical hourly schedule of generation is determined, the planned operation of the system will be passed to operations control, which will attempt to satisfy the minute-to-minute demands of the system as was described in the preceding section. Bus-load voltage calculation is important in power grid planning and operation; it is called power flow or load flow. We will discuss this function in Chapter 7.

In the deregulated power market, many contracts are executed between buyers and sellers in advance. For example, the day-ahead market is developed based on the forecasted load demands of the system to supply electrical power at least 24 hours before delivery to buyers and end-users.[9–10]

4.3 THE VERTICALLY AND MARKET-STRUCTURED UTILITY

Figure 4.8 depicts a vertically integrated power grid, which dates back to Thomas Edison.[1,2] It is essentially a network structure, with a large power station located where coal or hydropower were available. The electric energy

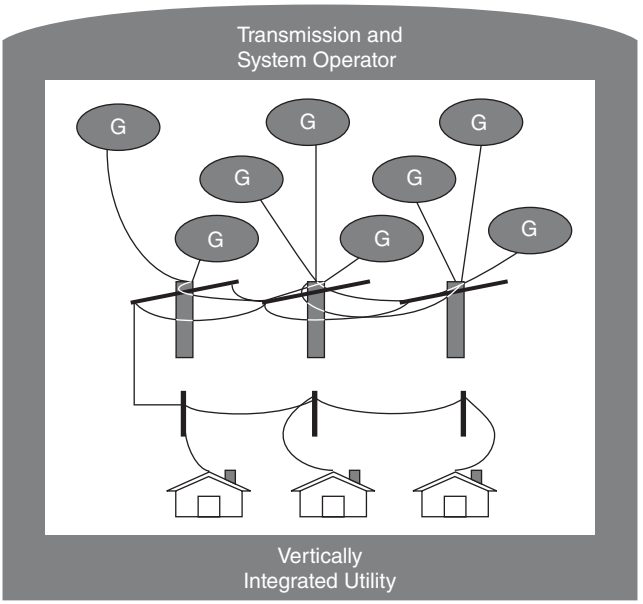

Figure 4.8 A Vertically Integrated Power Grid.

users were first served at large cities and then through a radial distribution system to the rural areas. In today's power grid, energy flows one way—essentially, from power stations to the residential, commercial, and industrial users. Because most power stations are remotely located where coal resources and hydropower sources are available, the power must be transmitted through high-voltage transmission systems and subtransmission systems to end users. The power losses to the load during transmission can be estimated by studying the power flow through the system. For the United States, in 2004, the losses were estimated to be approximately over 265,180,000,000 million kWh.[3]

If a power grid is subject to a sudden outage at a power generating station or the loss of a critical line carrying large megawatts of power from generating stations to the load centers, such a loss creates a sudden deficiency of generating power. With the result that system operators cannot match energy production to energy demand; hence, the power grid is subject to power oscillation. If the system operators are not able to match energy production to energy consumption, the power grid becomes unstable, and protective relays remove the equipment from service prompting a blackout.

Figure 4.9 depicts a market-operated power grid. In this structure, the independent system operator (ISO) is in charge of power grid operation. ISO energy-management computer systems compute the operating reserve that is necessary to maintain reliable interconnected power grid operation.[7–9] The ISO operators operate the power grid based on the North American Electric Reliability Council (NERC)[9–10] Policy 1 generation control and performance

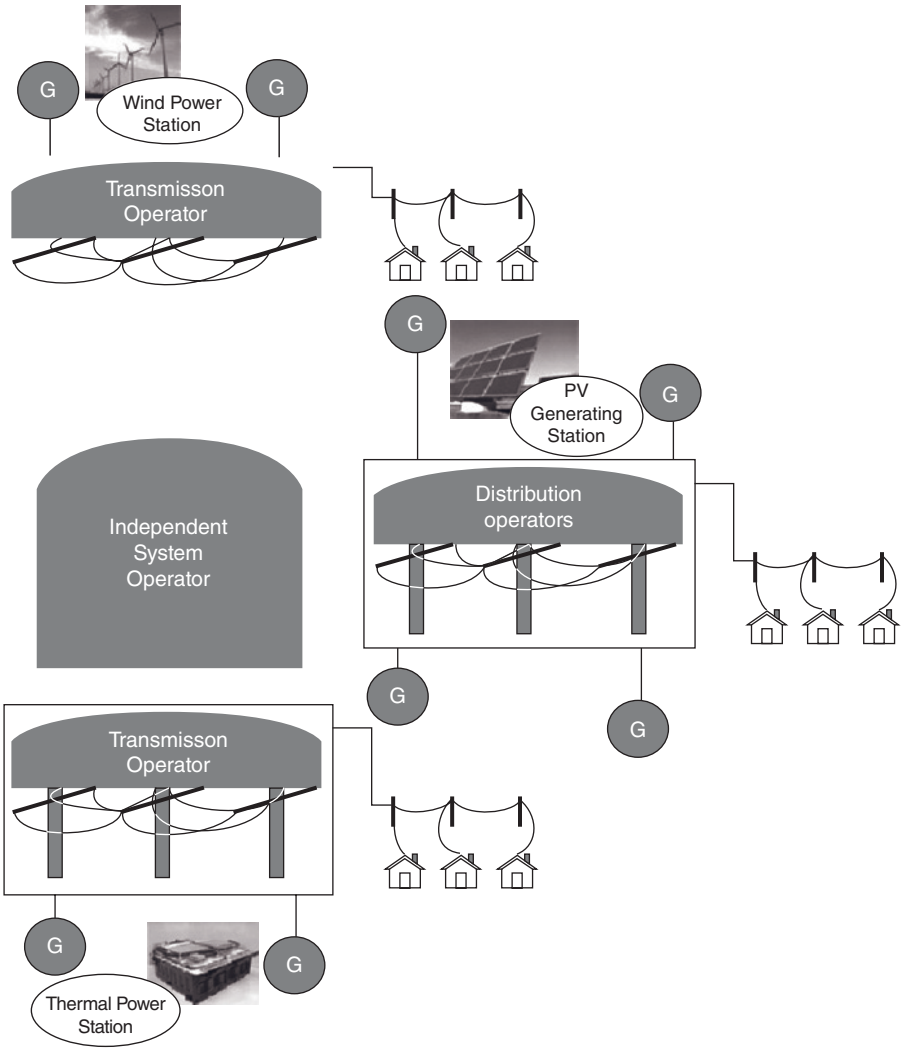

Figure 4.9 A Market-Structured Power Grid.

standard. This document specifies the operating reserves requirements.[11–19] According to NERC, "Each control area shall operate its power resources to provide for a level of operating reserve sufficient to account for such factors as errors in forecasting, generation and transmission equipment unavailability, number and size of generating units, system equipment forced outage rates, maintenance schedules, regulating requirements, and regional and system load diversity."[2] Following loss of resources or loads, the ISO operator takes appropriate steps to stabilize the power grid. The additional generation is in the form of a spinning reserve.[7–9] The spinning reserve is defined as synchronized power

that is ready to be dispatched by the system operator. The spinning reserve is normally from a 5- to 10-minute reserve. The reserve power can also be in the form of standby off-line reserves, and contracted customer-interrupted loads.

A close look at the operation of a power grid makes it apparent that the end-energy users are collectively controlling the system load. When we, as customers turn on or turn off power devices, we are impacting the system. When a load is turned on, the system generators are loaded and the speed of the system generators drop. The drop in system speed reduces the system frequency. When a load is turned off, the speed of the system increases and in turn, the system frequency increases. The system operator controls the system frequency and system voltage. This control action is referred to as load following. To elaborate further, we can say that the system operator reacts to the changing loads by monitoring the system frequency. This control action takes place under load-frequency control (LFC).[11]

In a market-structured power grid system, the ISO has the responsibility of controlling the power grid. All stakeholders, power grid companies, independent power producers, municipal power companies and so on, are operating under power market rules; still, all stakeholders must study the system load profile and expected demand to position themselves for maximum profit. However, the ISO still operates the power grid such that its stability is assured, while it provides efficient utilization of power in the power market.

In this book, we will only present the functions that are important for the understanding of a smart power grid consisting of many microgrids where every bus (node) of the system has both load and generation. To understand this concept, we need to understand the operation control of a power grid in more detail.

4.4 POWER GRID OPERATIONS CONTROL

The primary functions of operations control are satisfying the instantaneous load on a second-to-second and minute-to-minute basis.[6–8] Some of these functions are

1. Load frequency control (LFC)
2. Automatic-generation control (AGC)
3. Network topology determination (NTD)
4. State estimation (SE)
5. On-line load flow and contingency studies
6. Schedule of transactions (ST)
7. Economic dispatch calculation (EDC)
8. Operating reserve calculation (ORC)
9. Load management system (LMS)

The decision time of operations control is from dynamic response in a fraction of a cycle in LFC, to 1–10 seconds for automatic-generation control, to 5–10 minutes for economic-dispatch calculations, and from a second up to 30 minutes for a load management system.[8–10] However, with the implementation of a smart grid system with a high penetration of renewable green energy sources and a smart metering system, we will have a more-complex power system. In the following sections, we will study the function of LFC and automatic-generation control. Later in the book, we will study network topology determination, and power flow (load flow) studies in detail. Other functions are left for students to study on their own using the reference section at the end of this chapter and Internet resources.[1–4]

4.5 LOAD-FREQUENCY CONTROL

LFC is also referred to as the governor response control loop as shown in Fig. 4.10. As the load demand of the power system increases, the speed of the generators decreases and this reduces the system frequency. Similarly, as the system load-demand decreases, the speed of the system generators increase and this increases the system frequency. The power system-frequency control must be maintained for the power grid to remain stable.

In the AC power grids, all generating sources are operating in parallel and all (inject) supply power to the power grid. This means that all power sources are operating at the same system frequency. The system operating frequency in the United States is 60 Hz and at 50 Hz in the rest of the world. The generators are operating at the system frequency; they are all synchronized and

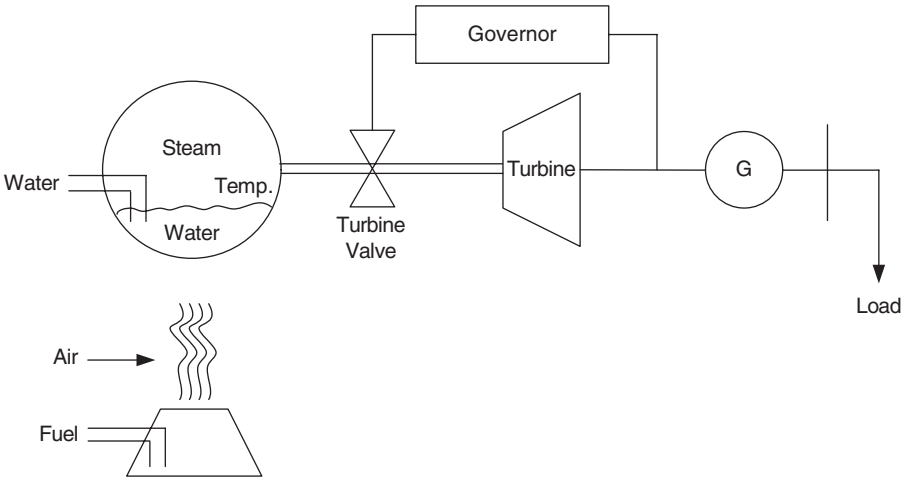

Figure 4.10 The Governor Control System.[11]

operating at the same synchronized speed: all are supplying (injecting) power to the power grid. The synchronized speed can be computed as

$$\omega_{syn} = \frac{2}{P}\omega_s \tag{4.1}$$

where $\omega_s = 2\pi f_s$ and f_s is the system frequency. In revolutions per minute (rpm), we have

$$n_{syn} = \frac{120 f_s}{P} \text{ rev/min} - \text{rpm} \tag{4.2}$$

In the above equation, P is the number of poles and f_s is the generator frequency. Therefore, for a two-pole machine, operating at 60 Hz ($f = 60$ Hz), the shaft of the machine is rotating at 3600 rpm. If the prime mover power has a slower speed, such as the hydropower unit, the generator has more poles. For example, if $P = 12$, the prime mover speed is 600 rpm and still the unit operates at 60 Hz.

Synchronized operation means that all generators of the power grid are operating at the same frequency and all generating sources are operating in parallel. This also means that all generating units are operating at the system frequency regardless of the speed of each prime mover. In AC systems, the energy cannot be stored; it can only be exchanged between inductors and capacitors of the system and is consumed by loads. Therefore, for an AC system to operate at a stable frequency, the power generated by AC sources must be equal to the system loads. However, the loads on the system are controlled by the energy users, i.e., when we turn off a light, we reduce the system load; when we turn on a light on, we increase the system load. In response to load changes, the energy is supplied from the inertia energy stored in the massive mass of a rotor. However, at every instant, the balance between energy supplied to the grid and the energy consumed by loads plus losses are maintained. This concept can be expressed as

$$\sum_{i=1}^{n_1} P_{G_i} = \sum_{i=1}^{n_2} P_{L_i} + P_{losses} \tag{4.3}$$

where P_{G_i} is the power generated by generator I, P_{L_i} is the power consumed by load i and the n_1 is the number of the system generators and n_2 is the number of the system loads. The transmission line losses are designated by P_{losses}.

As can be expected, as the system load demand at time t increases, we should expect that the system frequency decreases because the power system at that instant has more loads than at the instant $t - k$ where k is the time step. In fact, this is precisely what happens at first. However, the system has a feedback loop that is called the load-speed control and as the system frequency

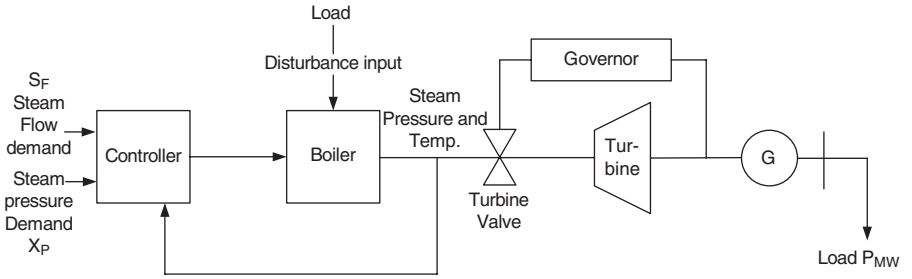

Figure 4.11 A Boiler Control System.[11]

drops, i.e., the prime mover shaft speed decreases, the feedback loop increases the input power to match the system generation with the system load. This is called governing system control: the governor opens the turbine valves to increase the input power that in turn speeds up the shaft of the generator. However, with an increase in the system loads, the additional power generated matches the system generation to the system load and the system will operate at the system synchronized speed.

The governor control keeps the turbine shaft speed constant at the desired synchronized speed to generate power at a synchronized system frequency. To ensure the safety of the boiler and turbine, the boiler control system controls the condition of steam that is expressed by steam pressure and steam temperature. The boiler control system controls the turbine valve in the desired position such that the steam pressure and temperature are within their specified range. Figure 4.11 depicts the boiler control system. The governor control feedback controls the turbine shaft speed—as the system load changes; the governor feedback opens or closes the turbine valves. However, the opening and closing turbine valves are dependent on steam conditions. The turbine valves can be opened or closed as long as the boiler steam conditions are within the desired range.

To match the system generation to the system load, two control methods are implemented. These methods are turbine-following control and boiler follow-up control. In the turbine-following control, the turbine generator is assigned the responsibility of throttle pressure. The turbine valves are controlled within a specified range that ensures that steam conditions, steam pressure, and temperature are within the safe range. The MW load demand corresponds to steam flow demand and it is controlled by the boiler. When the step increase in load control command is issued, the control command is sent to the boiler. The boiler control system then increases the fuel rate, feed water, and airflow, which increases the throttle pressure. The change in the throttle pressure is measured by the turbine control system. The turbine valves are controlled by the turbine control system. The turbine valves are opened to increase the steam flow and MW output of the generator. Note that when the steam flow increases due to the opening of the turbine valves, the turbine shaft

accelerates. However, because the generator is synchronized to the power grid and the system load has increased, then the MW power generated is injected into the power system and a new balance between the system load and generation is established. Therefore, the system frequency is maintained and all connected generator operate at a synchronized speed.

In boiler follow-up control,[11] the boiler is assigned the responsibility of throttle pressure. The MW load demand is controlled by the turbine generator. In this mode of operation, a step increase in generation due to a step change in load demand goes directly to the turbine valves. The load demand increases, the turbine valves open, and hence the steam flow and MW output of the generator increases. However, the boiler is controlling the throttle pressure, and if the pressure drops out of the range assigned to the boiler, the boiler control system overrules the turbine control action to maintain the pressure. Both the proposed control systems can provide satisfactory control. The boiler follow-up control has a faster response and is widely used. The turbine control system has a slower response; however, it protects the boiler and ensures that steam is conditioned before energy is extracted from the boiler.

For the stable operation of a power system, in addition to frequency control, we must also control the terminal voltages of generators and power factors. Figure 4.12 depicts the voltage regulator for a steam turbine-generator. As we indicated, the governor controls the main steam valves of the turbine and controls the steam flow to the turbine. The steam flow to the turbine is the primary mechanical power on the shaft of the generator. In Fig. 4.12, we have

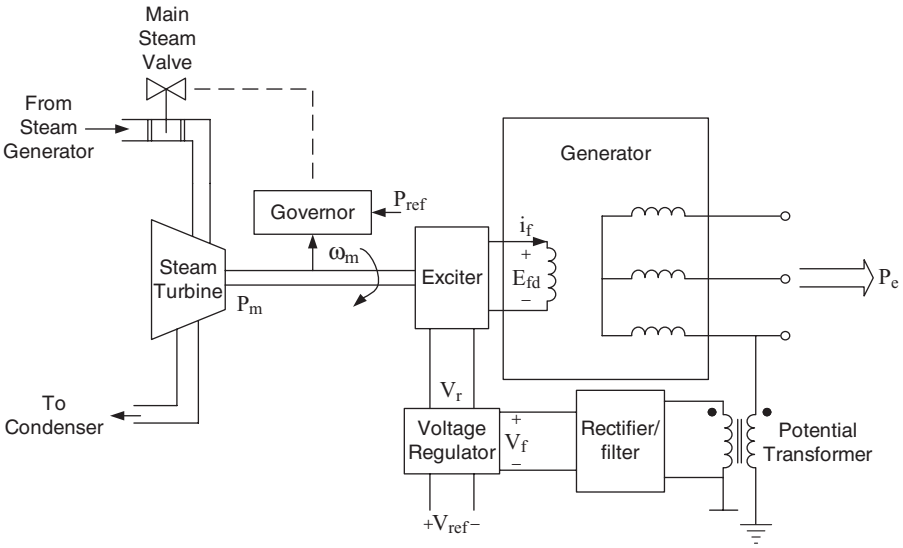

Figure 4.12 Voltage Regulator and Turbine-Governor Controls for a Steam Turbine-Generator.

also shown the generator excitation system that is located on the rotor of the machine. The generator's terminal voltage is controlled by the voltage regulator. The field voltage is applied to the generator excitation winding based on the regulator set point (V_{ref}).

By applying the mechanical power to the rotor winding that is supplied with DC current, a time-varying field is established in the air gap of the machine. Based on Faraday's law of induction, the voltage is included on the stator windings. Again, because the generator is synchronized to the power grid, the power is injected into the system. Figure 4.13 depicts the main concepts that we must understand from the operation of a steam power plant. A power generator is a three-terminal device. We set the field current of the generator to set the generator's terminal voltage.

$$E = K \cdot I_f \cdot \omega \tag{4.4}$$

The open-circuit-induced voltage, E is a function of the machine dimensions that are given by the constant K and field current, I_f and shaft speed, ω.

By adjusting the field current, a generator can operate at leading or lagging power factor. We will study this concept later in this chapter. However, the reactive power, Q_G generated by machines must be equal to the total reactive loads and transmission lines' reactive losses,

$$\sum_{i=1}^{n_1} Q_{Gi} = \sum_{i=1}^{n_2} Q_{Li} + Q_{losses} \tag{4.5}$$

where Q_G is the reactive power generated, Q_L is the reactive power of load, Q_{losses} is the reactive power loss.

Let us formally introduce two important analysis studies in power system planning, design, and operation.

1. Power Flow Studies. Given the schedule system generation, system load, and schedule system elements such as transmission lines and transformers, etc., we compute the system bus voltages and power flow on transmission lines. These conditions are expressed by Equations 4.3 and 4.5. We often refer to bus voltages as system states that represent the voltage magnitude and phase angle at each bus. For power flow studies, we are interested in the system injection model: we do not include the generator impedance in the power grid injection model that describes the injected power at the terminal of the generator into the network model of the transmission system.
2. Short-Circuit Studies. Given the system model, the bus voltages, and load, we compute balanced and unbalanced fault currents that can flow on the system if a fault happens. Based on this study, we calculate the short-circuit currents that the breakers may experience upon occurrence of a

fault. This study also provides the level of fault current throughout the system for setting relays of the protection system. In the short-circuit studies, the internal input impedance of generating sources must be included because they limit the fault current as it happens upon occurrence of a fault. Without internal input impedance of generating sources, the fault current would be infinite; this is unrealistic because the source would catch fire before an extremely high current is reached.

Let us return to the operation of a generator. In the second terminal of Fig. 4.13, we supply the mechanical power to the generator shaft, and in turn, we set up a time-varying flux in the air gap of the generator that will couple the windings located on the stator of the generator and produces the terminal voltage. The output power of the generator is injected into the power system network. The injected power and its power factor are controlled by controlling the field current and the terminal voltage. We will discuss this point later in this chapter.

The dynamic range of a power system operation starts from start up—a transient condition to the steady-state operation. The dynamic duration of a power grid can be from a few cycles to several minutes. The generator excitation-control system can be subjected to dynamic perturbation from a few cycles to a few seconds as the field current of the generator is changed to

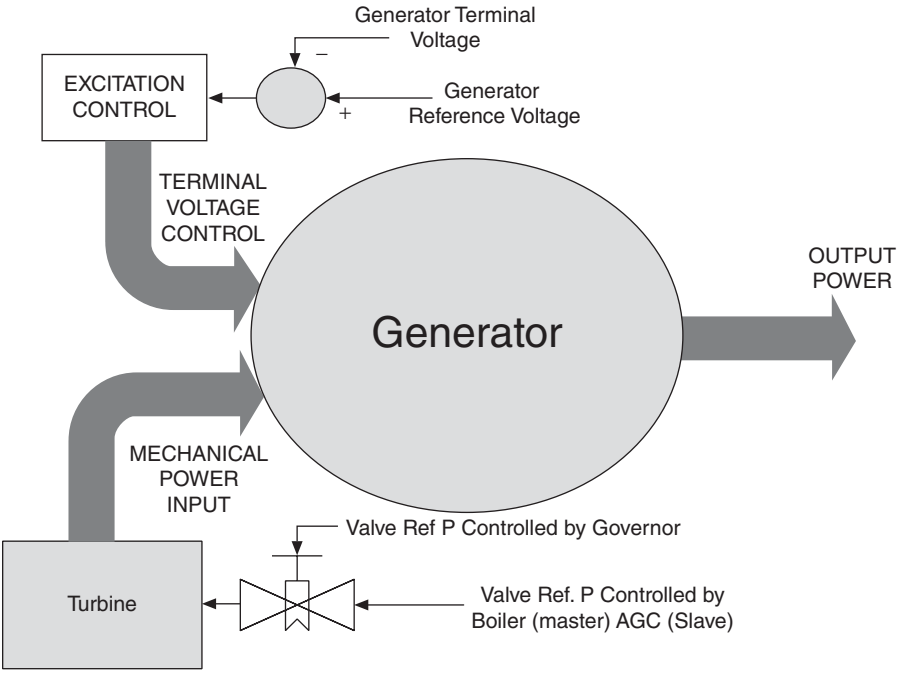

Figure 4.13 A Generator as a Three-Terminal Device.

a new voltage setting. When a power grid is subjected to an outage from the loss of a generator, the power grid will be subjected to the dynamic stability problem that can be stabilized if the power grid can provide the power needed to balance the system generation to the system load. For example, for a generator outage, the governors of all units within the power grid will react to a deficiency in needed power (that is a drop in the system frequency) and will inject additional power into the grid to match the generation to the system load. We can identify different dynamic problems that can affect a power grid:

1. Electrical dynamics and excitation controls may have a duration of several cycles to a few seconds.
2. Governing and LFC may have a dynamic duration of several seconds to a few minutes.
3. A prime-mover and an energy supply control system may have a dynamic duration of several minutes. A prime-mover is a steam-generating power system.

4.6 AUTOMATIC GENERATION CONTROL

In the preceding sections, we defined the function of a boiler and a governor in the LFC. As we pointed out, as the load changes, the supply of power to the system must be adjusted such that at all times, the system-generated power balances the system loads and losses to keep the system operating at rated voltages and rated frequency.

The system load has a general pattern of increasing slowly during the day and then decreasing at night. The cost of generated power is not the same for all generating units. Therefore, more power generation is assigned to the least costly units. In addition, a few lines connect one power grid to another neighboring power grid. These lines are referred to as tie lines. Tie lines are controlled to import or export power according to set agreed contracts. When power is exported from a power system to a neighboring power system through the tie lines, the exported power is considered as load; conversely when imported, it is considered as power generation. The control of the power flow through these lines is prespecified on agreed schedules and they are based on secure operation and economic transactions. To control both the power flow through transmission tie lines and the system frequency, the concept of area control error (ACE) is defined as

$$ACE = \Delta P_{TL} - \beta \Delta f \tag{4.6}$$

where

$$\begin{aligned} \Delta P_{TL} &= P_{Sch} - P_{Actual} \\ \Delta f &= f_S - f_{Actual} \end{aligned} \tag{4.7}$$

P_{Sch}: The scheduled power flow between two power networks
P_{Actual}: The actual power flow between two power networks
f_s: The reference frequency, i.e., the rated frequency
f_{actual}: The actual measured system frequency
β: The frequency bias

The AGC software control is designed to accomplish the following objectives:

1. Match area generation to area load, i.e., match the tie-line interchanges with the schedules and control the system frequency.
2. Distribute the changing loads among generators to minimize the operating costs.

The above condition is also subject to additional constraints that might be introduced by power grid security considerations such as loss of a line or a generating station.

The first objective involves the supplementary controller and the concept of tie-line bias. The term β is defined as bias and it is a tuning factor that is set when AGC is implemented. A small change in the system load produces proportional changes in the system frequency. Hence, the area control error ($ACE = \Delta P_{TL} - \beta\Delta f$) provides each area with approximate knowledge of the load change and directs the supplementary controller for the area to manipulate the turbine valves of the regulating units. To obtain a meaningful regulation (i.e., reducing the ACE to zero), the load demands of the system are sampled every few seconds. The second objective is met by sampling the load every few minutes (1–5 minutes) and allocating the changing load among different units to minimize the operating costs. This assumes the load demand remains constant during each period of economic dispatch. To implement the above objectives, nearly all AGC software is based on unit control. For unit i, the desired generation at time instant K is normally sampled every 2 or 4 seconds and is given by Equation 4.8,

$$P_D^i(K) = P_E^i(K) + P_R^i(K) + P_{EA}^i(K) \tag{4.8}$$

where $P_E^i(K), P_R^i(K), and\ P_{EA}^i(K)$ are the economic, regulating, and emergency assist components of desired generation for unit i at time instant K, respectively.

Figure 4.15(b) depicts the concept of stored inertia energy and the energy management time scale of power grid control. The stored inertia energy in the rotor of generating units provides energy to the high-frequency load changes. The high-frequency loads are shown in Fig. 4.3. Simply, when an energy user turns off a light, the load drop creates a high-frequency load fluctuation. Of course, when a large number of energy users turn their lights off, they create high- and low-frequency load fluctuations. The low-frequency load fluctuation

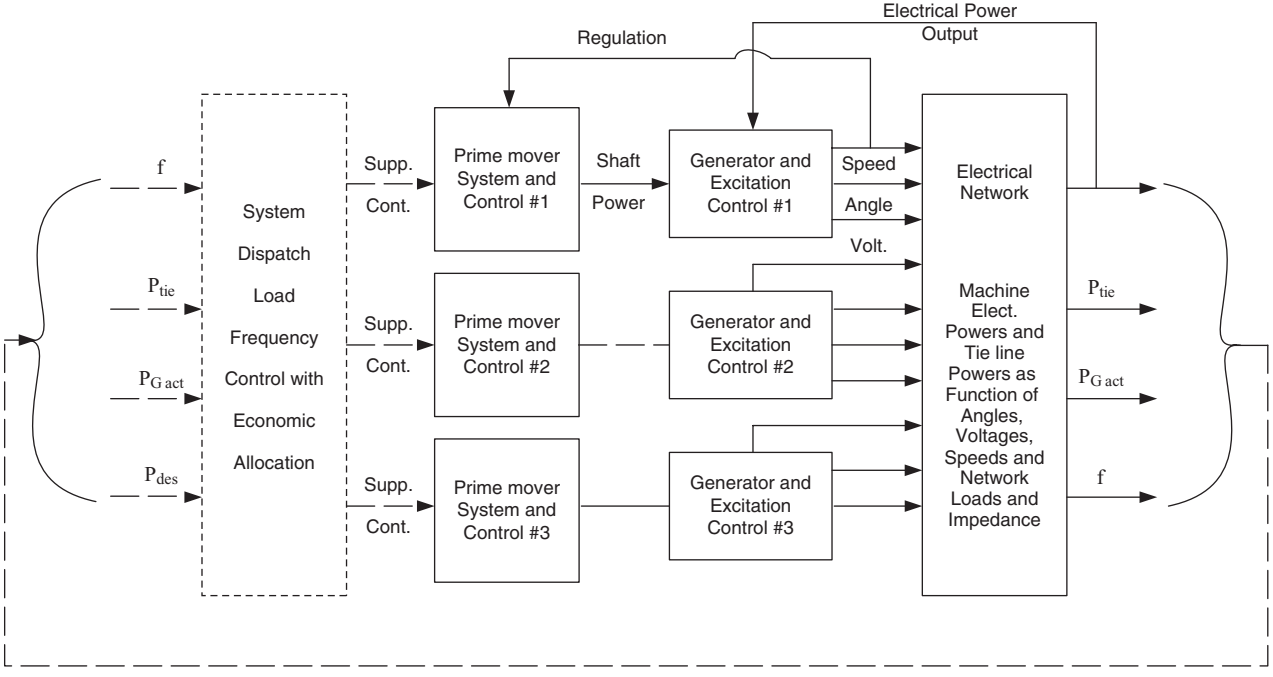

Figure 4.14 The Automatic Generation Control (AGC).

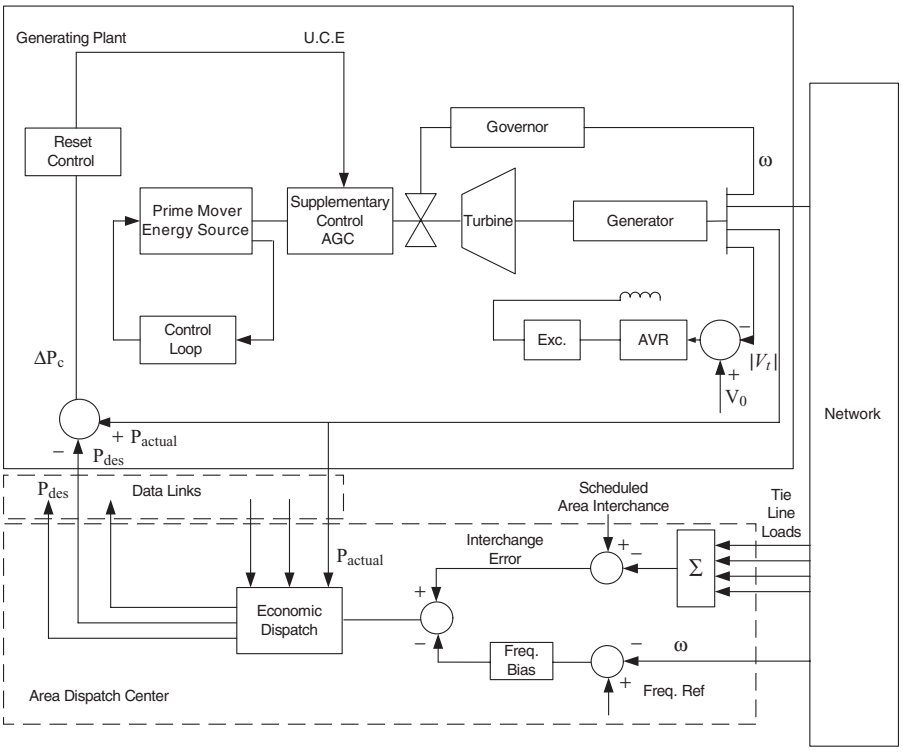

(a)

Figure 4.15 (a) Schematic Diagram of Load–Frequency Control System with Economic Dispatch.

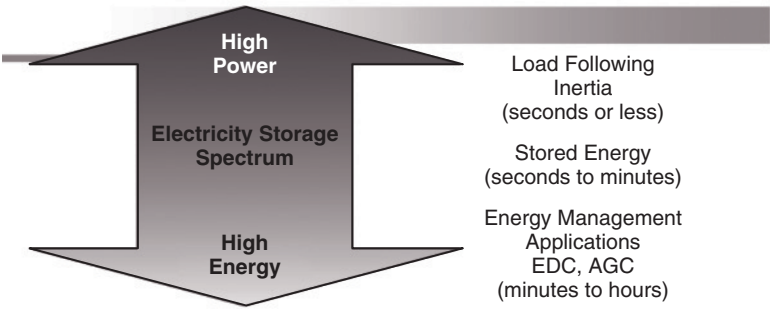

(b)

Figure 4.15 (b) The Energy Management Time Scale of Power Grid Control.[12]

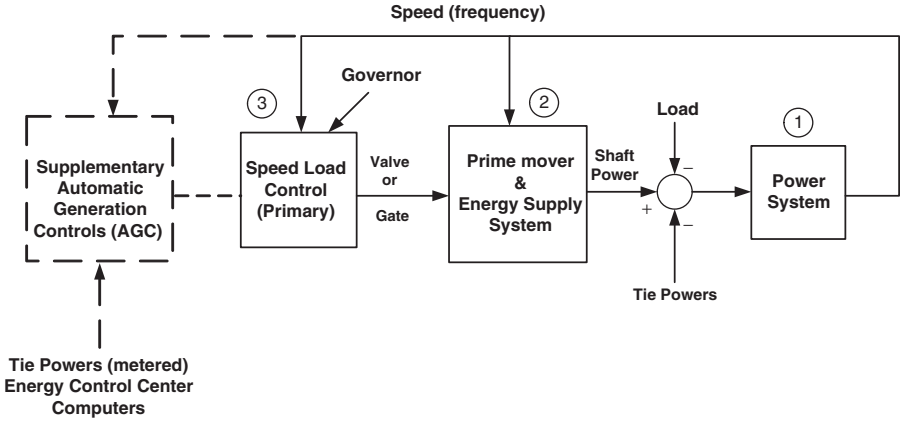

(c)

Figure 4.15(c) The Automatic Generation Control (AGC) Block Diagram.

has a clear load rise or a load drop trend. This change of load is controlled by AGC as shown in Fig. 4.15(c). The AGC and the system operator follow the grid load. However, the AGC controls the input energy into the power grid in response to load changes.

The AGC also controls the connected microgrids in a large interconnected power grid. The microgrid concept assumes a cluster of loads and its microsources, such as photovoltaic, wind, and combined heat and power (CHP) are operating as a single controllable power grid. To the local power grid, this cluster becomes a single dispatchable load. When a microgrid power grid is connected to a power grid, the microgrid bus voltage is controlled by the local power grid. Furthermore, the power grid frequency is controlled by the power grid operator. The microgrid cannot change the power grid bus voltage and the power grid frequency. Therefore, when a microgrid is connected to a local power grid, it becomes part of the power grid network, and is subject to power grid disturbances. To understand why this is the case, we need to understand the control system that is used by power grid operators. Figure 4.15(a) depicts the prime mover, energy supply (steam or gas turbine), and governor (speed load control) system. These systems are located in the power-generating station. The supplementary controls and AGC are part of the EMS of the local power grid. The LFC system is designed to follow the system load fluctuation. As stated before, when the load changes, let's say as the load increases in the microgrids connected to the local power grid, then the inertia energy stored in the system supplies the deficiency in energy, to balance the load to generation. This energy is supplied by prime movers (stored energy in rotors) as depicted by Fig. 4.15(b). The balance between load and generation must be maintained for the local power grid to remain stable. When the balance between generation and load is disturbed, the dynamics of the generators and loads can cause the system frequency and/or voltages to vary, and if this oscil-

lation persists, it will lead to system collapse of the local power grid and connected microgrids. If the load increases rapidly and the power grid frequency drops, then steam units open the steam valves and hydro unit control loops will open the hydro gates, to supply energy to stabilize the system frequency. This action takes place regardless of the cost of energy from generating units. All units that are under LFC participate in the regulation of the power system frequency. This is called the governor speed control, as shown in Fig. 4.15(c). Every 1 to 2 minutes, the supplementary control loop, under AGC, will economically dispatch all units to match load to generation, and at the same time, minimize the total operating cost. Therefore, the AGC will change the set points of the generators under its control. This timing of the cycle can fall within one to several minutes. In Fig. 4.15(c), the dotted line section encompasses the AGC, which is located at the local power grid energy-control center. However, when a microgrid is disconnected from the local power grid, the microgrid must be designed to control its voltage and frequency.

A smart grid system and smart metering will facilitate load control. We will discuss the basic concepts of a smart power grid design and operation in later chapters.

4.7 OPERATING RESERVE CALCULATION

As discussed, the power grid operation remains stable as long as a balance exists between the system loads and system generation. The operating reserve decision is made based on the security and the necessary reliability. A stable frequency response is essential to stabilize the operation of an interconnected system upon the loss of load or generation outage.[9–10]

The spinning reserve is the amount of additional power that is distributed in the form of a few megawatts among many generators operating in the power grid. These units are under AGC control and can dispatch power to ensure the balance of system loads and system generation. The cost of additional power will add to the cost of proving electric energy services. The real-time pricing and smart meters will empower many energy end users to participate in proving the spinning reserves in the future operation of power systems, increasing overall efficiency, and reducing the cost of operation of power grids.

4.8 THE BASIC CONCEPTS OF A SMART POWER GRID

In a classical power grid, a fixed price is charged to energy users. However, the cost of energy is highest during the daily peak load operation.[15–16] The classical power system operation has no control over the loads except in an emergency situation when a portion of the loads can be dropped as needed to balance the power grid generation with its loads. Therefore, much equipment is used for a short time during the peak power demand but it remains idle during daily operations.

For an efficient smart power grid system design and operation, substantial infrastructure investment in the form of a communication system, cyber network, sensors, and smart meters must be installed to curtail the system peak loads when the cost of electric energy is highest. The smart power grid introduces a sensing, monitoring, and control system that provides end users with the cost of energy at any moment through real-time pricing. In addition, the advanced control systems of smart metering provide the energy users with the ability to respond to real-time pricing. Furthermore, the smart power grid supplies the platform for the use of renewable green energy sources and adequate emergency power for major metropolitan load centers. It safeguards against a complete blackout of the interconnected power grids due to man-made events or environmental calamity. It also allows for the break-up of the interconnected power grid into smaller, regional clusters. In addition, the smart power grid enables every energy user to become an energy producer by giving the user the choice of PV or wind energy, fuel cells, and combined heat and power (CHP) energy sources and to participate in the energy market by buying or selling energy through the smart meter connection.

The bulk power grid of the United States and many other countries are already operating as a large interconnected network. The mission of the North American Electric Reliability Corporation (NERC)[9] is to ensure the reliability and security of the America's bulk power grid. Figure 4.16 depicts the North American electric reliability centers.

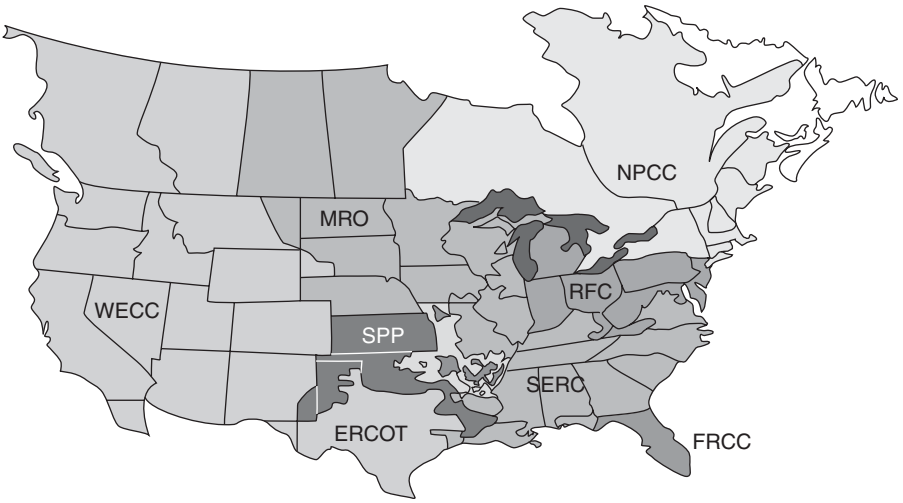

Figure 4.16 North American Electric Reliability Centers (NERC). ERCOT, Electric Reliability Council of Texas; FRCC, Florida Reliability Coordinating Council; MRO, Midwest Reliability Organization; NPCC, Northeast Power Coordinating Council, Inc.; RFC, Reliability First Corporation; SERC, SERC Reliability Corporation; SPP, Southwest Power Pool, Inc.; WECC, Western Electricity Coordinating Council.[1–3]

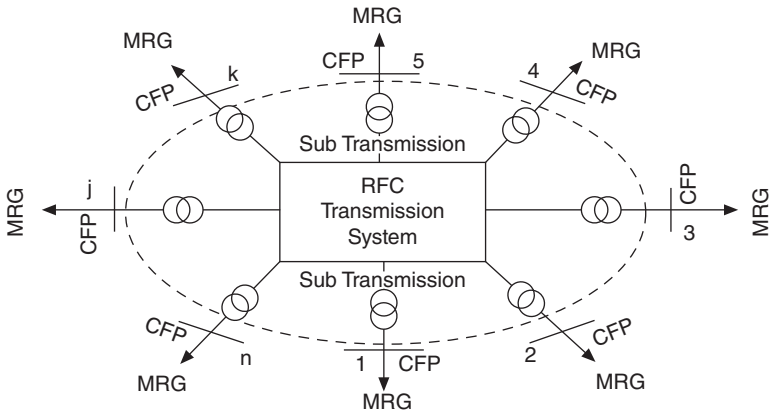

CFP: Cyber Fusion Point
MRG: Microgrid Renewable Green Energy System

Figure 4.17 A Cyber-Controlled Smart Grid.

Similarly, it is natural to expect that future cyber-controlled smart grid systems will be developed for the NERC-mandated reliability centers of the U.S. grid. A future cyber controlled system is depicted in Fig. 4.17.

The cyber-fusion point (CFP) represents a node of the smart grid system where the renewable green energy system is connected to large-scale interconnected systems. The U.S. interconnected system has eight regional reliability centers as shown in Fig. 4.16. It is expected that renewable microgrids will be connections of regional reliability centers such as Reliability *First* Corporation (RFC) transmission systems. The CFP is the node in the system that receives data from upstream, i.e., from the interconnected network, and downstream, i.e., from the microgrid renewable green energy (MRG) system and its associated smart metering systems. The CFP node is the smart node of the system where the status of the network is evaluated and controlled, and where economic decisions are made as to how to operate the local MRG system. A CFP also evaluates whether its MRG system should be operated as an independent grid system or as a grid system separate from the large interconnected system. A cyber system is the backbone of the communication system for the collection of data on the status of the interconnected network system. The security of the cyber network is essential for the security of the grid. Figure 4.17 illustrates such a future cyber-instrumented power grid.

Two-way communication is a key characteristic of the smart power grid energy system. It enables end users to adjust the time of their energy usage for nonessential activities based on the expected real-time price of energy. The knowledge gained from smart meters permits the power grid operators to spot power outages more quickly and smooth demand in response to real-time pricing as the cost of power varies during the day.[10–15]

The cyber control of a smart grid is the subject of research by many disciplines in electrical and computer engineering. It requires a control system that analyzes the performance of the power grid using distributed, autonomous, and intelligent controllers. The cyber system will learn on-line from the sensors, the smart grid, and microgrid states. The control system analyzes the system for possible impeding failure. By sensor measurements and monitoring, the cyber control system governs grid behavior based on real-time data in the face of ever-changing operating conditions and new equipment. The system uses electronic switches that control multiple MRG systems with varying costs of generation and reliability.

As a result, a cyber-controlled smart grid requires consumers to pay the real-time price of produced electric power. Table 4.1 presents the cost of electric energy as of 2009 from different sources.[3]

Figure 4.18 shows that the feeder maximum load and minimum load is changing by a factor of 2 over 24 hours. As we have learned in the previous chapter, the local power company must use many types of electric power sources to match the system generation to the system load.

The power flow into this load center is supplied by 345 kV and 138 kV transmission systems. The area load demands are satisfied by the secondary and tertiary windings of transformers rated at 138/69/12. Industrial loads are served at 138/69/23 kV. The bus load is the power flowing into the primary windings of the transformers connected to 23 kV. The power flows from higher voltage systems to lower voltage systems. Therefore, the bus load can be defined as 138 kV and/ or 345 kV transformer loads.

TABLE 4.1 The Cost of Electric Energy in 2009.[3]

Energy Source	Cost per Kilowatt Hour (Cents)	Typical Uses	Typical Installation Size
Solar energy (photovoltaics)	20–40	Base load power source	1–10,000 kW
Microturbines	10–15	Can be used in base load, peaking or cogeneration applications	30–300 kW
Fuel cells	10–15	Rural (off-grid) power Transportation appropriate for base load applications	1–200 kW
Wind turbines	5–10		5–10 MW
Internal combustion engines	1.5–3.5	Well-established, long history as back up or in peaking applications	50 kW–5 MW
Central power generation	1.7–3.7	Base load/peaking electricity generation	500–3000 MW

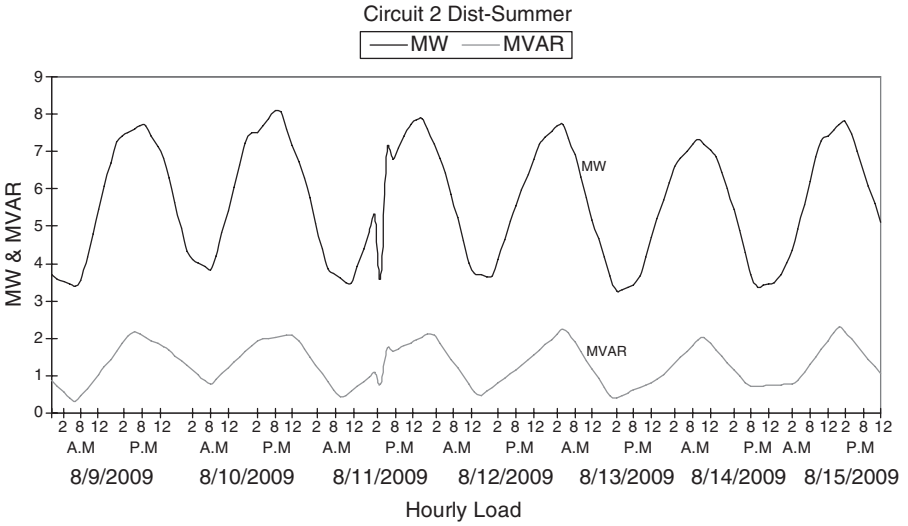

Figure 4.18 The Hourly Loads of a Distribution Feeder of a Midwestern Power Company.[7]

An important factor affecting the load demands and real-time pricing is the effect of weather and its ensuing rapid increase in load demands. To separate weather-induced bus load, we use the average bus load when weather conditions are normal and subtract when weather conditions are above normal. In Fig. 4.19, a composite hourly load sequence was generated by a midwestern power grid company.[16] The recursive mean and variance of {Y(.)} can be computed based on Equations 4.9 and 4.10.

$$\bar{Y}(K+1) = \bar{Y}(K) + \frac{Y(K+1) - \bar{Y}(K)}{K+1} \tag{4.9}$$

$$\sigma y^2(K+1) = \frac{K}{K+1}\sigma y^2(K) + \frac{[Y(K+1) - \bar{Y}(K+1)]^2}{K} \tag{4.10}$$

The weather effect on the load sequence, holidays, and unforeseen conditions, which cause the load demand sequence to be higher or lower than a given nominal mean load profile, is subtracted from the recorded data. By removing the component of $\{Y_R(.)\}$, weather-induced load demand due to the weather effect, we generate a new sequence designated as the nominal load sequence $\{Y_N(.)\}$. The effect of weather conditions on the load depends on temperature, humidity, wind speed, and illumination. However, to demonstrate the basic concept, only the weighted average, maximum and minimum temperature that were recorded, were used. Therefore, the effect of weather condition on the load is expressed in terms of temperature. A weather-sensitive load is present

when the daily temperature, T, is outside of the comfort range of $T_{min} < T < T_{max}$ where T_{min} and T_{max} are the lower and upper limits of the comfort range. This suggests that the nominal nonweather sensitive load sequence $\{Y_N(.)\}$ is assumed to be equal to the sequence $\{Y_R(.)\}$ when the temperature is within the comfort range, and sudden load changes due to outages or special events have not occurred.

Figure 4.19(a–d) shows the plots of $\{Y_R(.)\}$ and $\{Y_N(.)\}$ load sequences for week 10, 11, 12, and 13 bus loads. It can be seen that the general weekly profile of weather-sensitive load sequence $\{Y_R(.)\}$ and nominal load (nonweather-

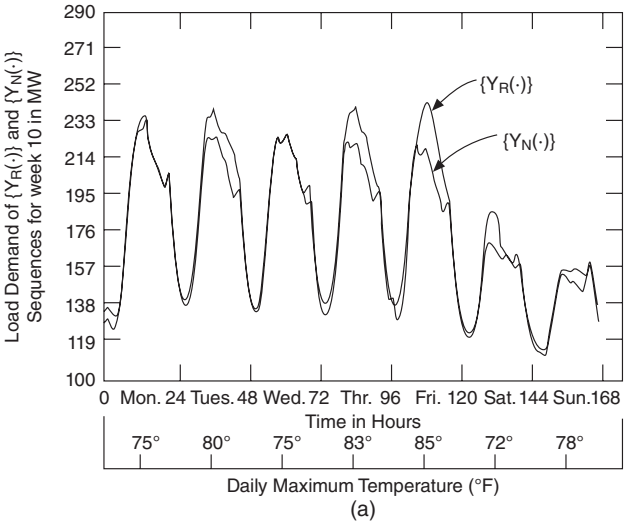

(a)

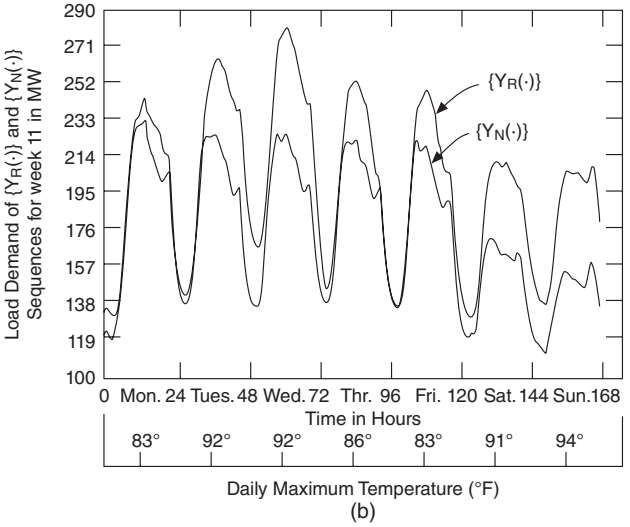

(b)

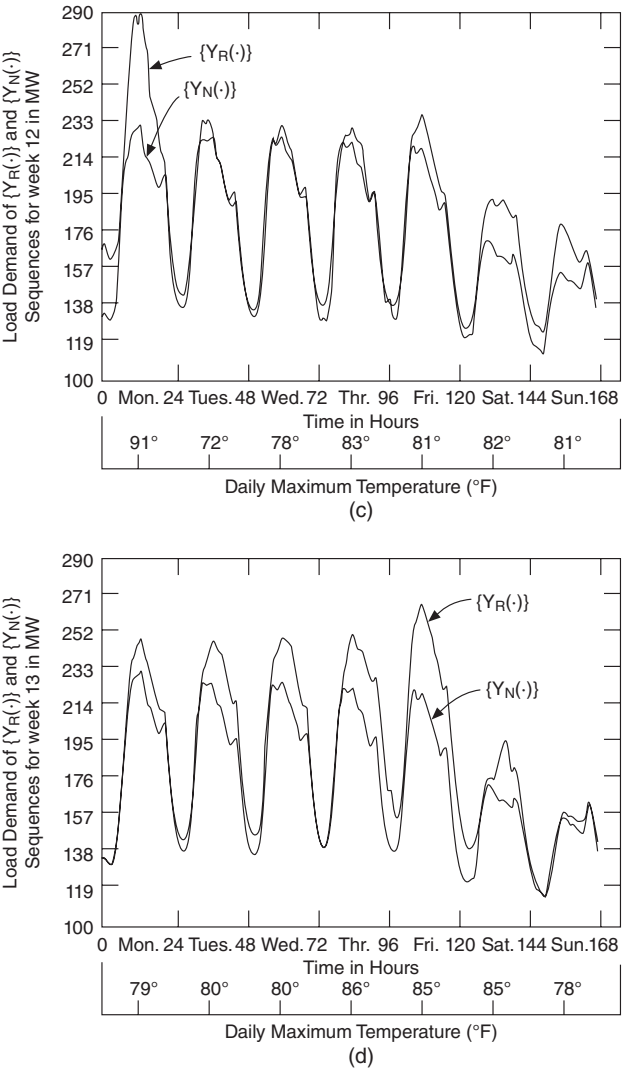

Figure 4.19 (a–d) Plot of $\{Y_R(.)\}$ and $\{Y_N(.)\}$ for Weeks 10, 11, 12, and 13.[16]

sensitive) sequence $\{Y_N(.)\}$ are essentially the same when the daily temperature is normal. However, when the daily temperature is high, a weather-induced load is superimposed on the $\{Y_N(.)\}$ sequence.

The procedure is based on computing an average relationship between the temperature and the pure weather-induced component of the load, which is designated as Y_{PW}. The sequence $\{Y_{PW}(.)\}$ is generated where each member of $\{Y_{PW}(.)\}$ is a mean value of the pure weather-sensitive component of the load at a given temperature.

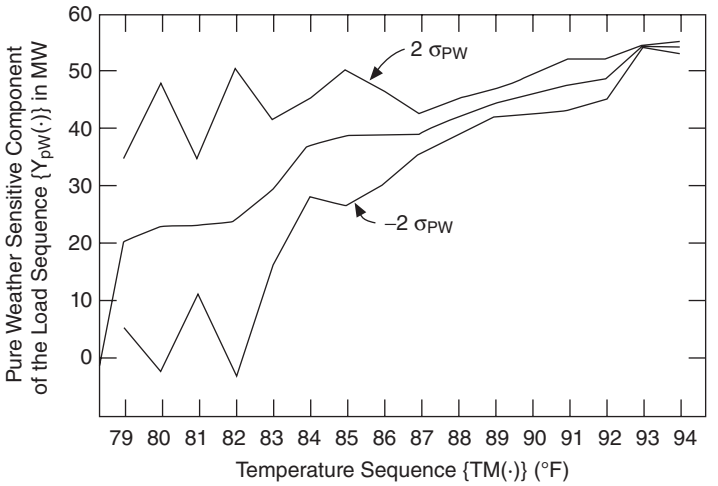

Figure 4.20 The Mean and Standard Deviation of a Pure Weather-Sensitive Load versus Temperature.[7]

Figure 4.20 shows the mean and standard deviation ($\pm 2\sigma_{PW}$) of the pure weather-induced component of the load at different temperatures.

Figure 4.20 also depicts the pure weather-sensitive component of the load. The weather-sensitive load sequence has saturated at 80°–82°, 84°–87°, and above 93° Fahrenheit.

Historically, power grid companies have operated the power system as a public service. They have provided reliable electric power at a constant price regardless of changing conditions. Their systems used additional spinning reserve units to serve the unexpected loading and outages due to the loss of equipment. However, in an age of global climate change, this kind of service cannot be provided without severe environmental degradation.[5]

A power grid operator has to schedule generation sources based on the cost of energy. However, the weather-sensitive load component adds substantial uncertainties in planning load–generation balance. As can be expected, the least costly units are scheduled to satisfy the base loads. The more costly units are scheduled to satisfy the time-changing loads. Therefore, the price of electric energy is continuously changing as load demands are changing. If real-time pricing is implemented, the variable electric rates must be used for the privilege of reliable electrical service during high-demand conditions.

4.9 THE LOAD FACTOR

The load factor is one of the key factors that determines the price of electricity. The load factor is the ratio of a customer's average power demand to its peak demand. As has been observed, the daily load demands have a daily variation.

The cost of peak power demand is substantially higher than the average power demand. Therefore, the cost of power demand changes with the time of day. The term "real-time pricing" refers to the minute-by-minute price of electric power as the energy control center commits the scheduled generators to the production of electric power. The load factor as defined below defines the price of power in an electric power grid.

$$Load\ factor\ (\%) = \frac{Average\ Power}{Peak\ Power} \times 100 \tag{4.11}$$

The average power is defined as the amount of power consumption during a period. The peak power is defined as the amount of maximum power consumption during the same period. The load factor can be calculated based on daily, monthly, or yearly cycle. For system planning, the load factor is calculated on a monthly or annual basis. The facility investments must be made so that the system can handle the maximum demand. Therefore, it is desirable to have a low maximum demand. On the other hand, because revenues are generated in proportion to the average demand, it is desirable to have a high average demand. Therefore, a desirable load factor is close to one, so that peak demand and average demand are close to each other.

We should understand the difference between "power factor" and "load factor." As we know, the load power factor determines the active and reactive power consumption of the load. However, induction motors that are widely used in a power grid have lagging power factors. The load factor is power consumption in kW divided by the worst-case consumption over a period. Therefore, the load factor defines the cost to the supplier per unit of energy delivered in that period. In other words, the load factor indicates how efficiently the power grid is operating.

Example 4.1 An industrial site has a constant power demand of 100 kW over a year of energy consumption. Compute the customer load factor over one year of providing energy to this site.

Solution

$$\text{Total energy} = 8760\ \text{h/yr} \times 100\ \text{kW} = 876{,}000\ \text{kWh/yr}$$

Because the power demand is constant the average and peak is the same. Therefore, the load factor of this customer is 100%.

Example 4.2 A commercial site has peak demand of 200 kW during 12 hours a day and an average demand of 50 kW demand the rest of a day. Compute the customer load factor over one year of providing energy to this site. Explain the associated cost of providing energy to the industrial site (Example 4.1) and the commercial site.

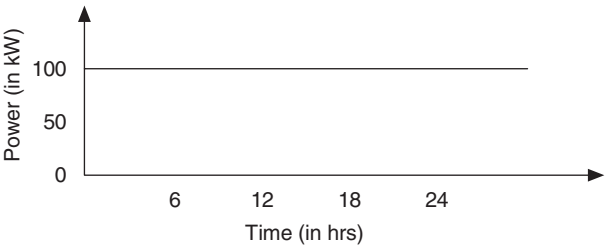

Figure 4.21 The Load for 24 Hours for Example 4.1.

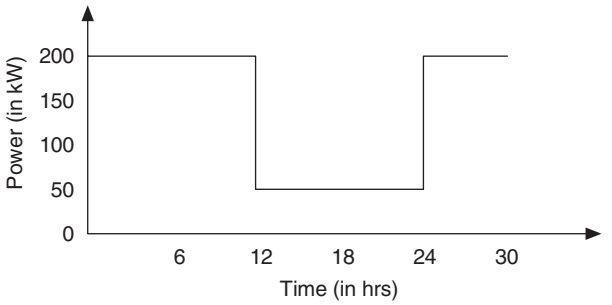

Figure 4.22 The Load for 24 Hours for Example 4.2.

Solution

$$The\ average\ power = \frac{\sum power_i \times time_i}{\sum time_i} = \frac{200 \times 12 + 50 \times 12}{12 + 12} = 125\ \text{kW}$$

$$Load\ factor = \frac{average\ power}{peak\ power} = \frac{125}{200} \times 100 = 62.5\%$$

When the load factor is close to unity (100%), the generating plant is efficiently used. The cost of supplying power to the load is more when the load factor is low.

At a commercial site with a low load factor, say in the range of 50%, the power grid would need twice as much installed equipment and resources to serve the site. The lower load factor means that the price must be adjusted to recuperate the extra costs. Because the industrial site and commercial site use the same amount of kW, the same price is charged the two sites. However, the smart meter, in conjunction with real-time pricing can provide an incentive for efficiency and load demand control. The users as stakeholders would be encouraged to control the loads during peak power demands by shifting

the usage at times when prices are favorable. Furthermore, the end users have a high incentive to participate by installing local green energy sources such as wind and PV.

4.9.1 The Load Factor and Real-Time Pricing

Real-time pricing was introduced by F. Schweppes[8] in July 1978 during an energy crisis. A simple analysis of the cost to the supplier per unit of energy delivered explains the relationship between cost and plant utilization. The real-time price of electricity is a function of load factor, load demand, and unexpected events. The first cost is the utilization of a power plant and its operating costs. To build a large plant, many issues must be addressed. In a regulated market, large plants take years to build and are located far away from load centers; electric power is transferred by long transmission lines. Normally, coal-fired power plants are built close to a coal mine. From an operational viewpoint, the sudden loss of a large plant creates instant real-time price change in the power market because the allocated real-time reserve is limited due to cost. Small power plants are normally gas-fired; they are built over a short time and their construction costs can be accurately estimated. Gas-fired plants can be placed close to load centers because these plants need limited space. Furthermore, when plants are close to load centers and their power does not need to be shipped over long-distance transmission lines, these plants have lower system losses. These plants also tend to have good system security and are generally more reliable and have fewer adverse consequences when they are subjected to sudden outage. Combined cycle units are highly desirable because of their high efficiency. Cogeneration facilities are also attractive because they typically have lower ratings. Plants fueled by renewable energy sources are attractive as well because of their low operating cost. Due to many sources of power and their associated cost, the cost of real-time power is a variable and needs to be determined as sources of electric energy to supply the system load changes.

Example 4.3 Suppose a PV plant of 1000 kW capacity is constructed for $500 per kW. Compute the cost of energy per kWh to the end users for one year of operation at full capacity if the total cost on investment is to be recovered in 2 years when the PV plant operates 6 hours a day on the average for 2 years and the cost of production is negligible.

Solution

$$\text{The energy consumed in 1 year} = \textit{power capacity} \times \textit{time in hours}$$
$$= 1000 \times 365 \times 6 = 2{,}190 \text{ MWh}$$

$$\text{Let the price of 1 kWh of energy be} = \$\, x \textit{ per kWh}$$

$$\text{The investment cost} = \textit{capacity} \times \textit{cost per unit capacity} = 1000 \times 500 = 500{,}000$$

Therefore, the energy consumed for 2 years $2{,}190 \times 2 = 4{,}380$ MWh

$$4{,}380 \times 10^3 \times x = 500{,}000$$

$$x = \frac{500{,}000}{4{,}380 \times 10^3} = \$0.1142 \text{ kWh}$$

Let us introduce the cost of fuel, labor, and maintenance in a load factor calculation.

$$EUC = VC + \frac{amortized\ fixed\ cost}{LF} \tag{4.12}$$

In Equation 4.12, the term VC defines variable cost associated with fuel and other cost of plant operation and EUC represents the energy unit cost in cents per kWh.

Example 4.4 Suppose a natural gas plant of 1000 kW capacity is constructed for \$300 per kW. Assume the variable cost, VC, is 2 cents per kWh. Perform the following:

i) Compute the cost of electric energy to end users if the 100% of installed capacity is used 24 hours a day over 5 years.
ii) Compute the cost of electric energy to end users if the 100% of installed capacity is used 12 hours and 50% of installed capacity is used for the rest of a day over 5 years.
iii) Plot the energy unit cost versus the load factor, *LF* from 0 to 1.

Solution

$$\text{The investment cost} = capacity \times cost \cdot per\ unit\ capacity$$
$$= 1000 \times 300 = \$300{,}000$$

$$\text{Energy consumed over a period of 5 years at full capacity} = 1000 \times 24 \times 365 \times 5$$
$$= 43{,}800 \text{ MWh}$$

If this cost is distributed over 5 years, the amortized fixed cost

$$= \frac{300{,}000}{43{,}800 \times 10^3} = 0.007$$

i) Load factor = 1

$$EUC = VC + \frac{amortized\ fixed\ cost}{LF}$$

$$EUC = 0.02 + \frac{0.007}{1} = \$0.027/\text{kWh}$$

ii)

$$\text{The average power} = \frac{\sum power_i \times time_i}{\sum time_i}$$

$$= \frac{1000 \times 1 \times 12 + 1000 \times 0.5 \times 12}{12 + 12} = 750 \text{ kW}$$

$$\text{Load factor} = \frac{average\ power}{peak\ power} = \frac{750}{1000} \times 100 = 75\%$$

$$EUC = 0.02 + \frac{0.007}{0.75} = \$0.029 \text{ kWh}$$

iii) To compute the energy unit cost versus the load factor, *LF* from 0 to 1, a MATLAB M-file is developed as presented below:

```
% PLOT OF EUC
clc; clear all;
LF = 0.01:.01:1;              % defining the range of
                              load factor
VC = 0.02;                    % variable cost
A_FC = 0.007;                 % amortized fixed cost
EUC = VC + A_FC./LF;          % defining EUC in $/kWh
EUC = EUC*100;                % converting into
                              cents/kWh
plot(LF,EUC)
grid on;                      % labeling the axes
xlabel('Load Factor');
ylabel('EUC(in cent/kWh)');
title('EUC vs Load Factor');
```

Plot:

From the solution and plot, it can be seen that the EUC increases rapidly as the load factor is decreased. This is because the capacity of the plant is under-utilized when the load factor is small. The real-timing pricing takes into account the power grid load factors and the cost of spinning reserve that are sitting on-line to keep the system operating at stable operating conditions if the system is subjected to contingencies.

4.10 A CYBER-CONTROLLED SMART GRID

A cyber-controlled smart grid consists of many distributed generation stations in the form of microgrids. The microgrids incorporate intelligent load control

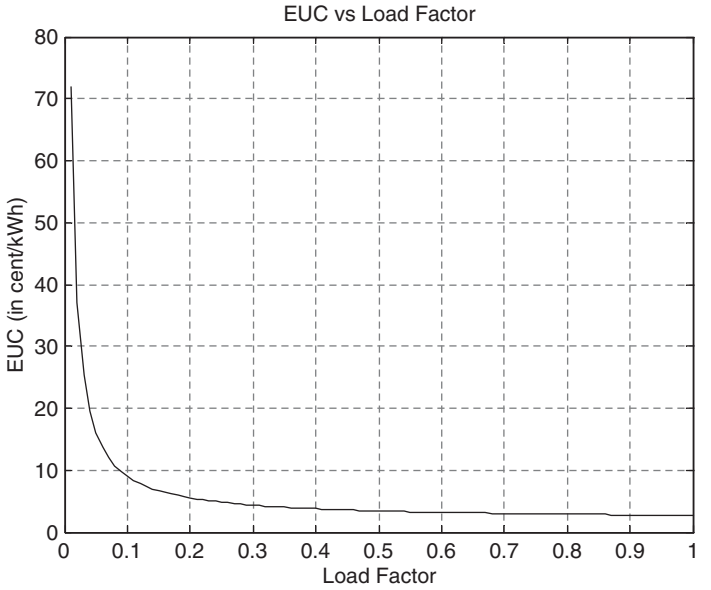

Figure 4.23 The Cost in Cents per kWh as a Function of Load Factor.

equipment in its design, operation, and communication.[13–14] This enables the energy end users and the microgrids serving them to better control energy usage. Smart appliances such as refrigerators, washing machines, dishwashers, and microwaves can be turned off if the energy end user elects to reduce energy use. This is done by connecting the smart appliances to the energy management systems in smart buildings. This technology will enable the energy end users to control their energy costs. Advanced communications capabilities in conjunction with smart meters and smart appliances enable the energy end users with the tools to take advantage of real-time electricity pricing and incentive-based load control. Furthermore, the emergency load reduction can be achieved by turning off millions of air conditioners on a rotation basis for a few minutes. With real-time pricing, the energy end users would have a very high incentive to become energy producers and install green energy sources. As real-time prices take hold, commercial and industry units are expected to generate their own energy and sell their extra power back to the power grid.

Cyber-controlled smart grid technology has three important elements: sensing and measurement tools, a smart transducer, and an integrated communication system.[13–14] These elements monitor the state of the power system by measuring line flows, bus voltages, magnitude, and phase angle using phasor measurement technology[15–16] and state estimation.[17] The technology is based on advanced digital technology such as microcontrollers/digital signal processors. The digital technology facilitates wide-area monitoring systems, real-time

line rating, and temperature monitoring combined with real-time thermal rating systems.

Transducers are sensors and actuators play a central role in automatic computerized data acquisition and monitoring of smart grid power systems. A smart transducer is a device that combines a digital sensor, a processing unit, and a communication interface. The smart/controller transducer accepts standardized commands and issues control signals. The smart transducer/controller is also able to locally implement the control action based on feedback at the transducer interface. The utilization of low-cost smart transducers is rapidly increasing in embedded control systems in smart grid monitoring and control.

Real-time, two-way communication is enabling a new paradigm in the smart grid system. It enables the end users to install green energy sources and to sell energy back to the grid through net metering. The customers can sign up for different classes of service. Smart meters facilitate the communication between the customers by providing the real-price by the supplier. The customers can track energy use via Internet accounts, where the expected price of energy can be announced a day ahead for planning purposes and the real-time price of energy can be provided to end users so they may be aware of the savings that can be realized by curtailing their energy use when the energy system is under stress.[16–17]

A smart meter allows the system operator to control the system loads. Load control ultimately provides new markets for local generation in the form of renewable green energy sources. With the installation of smart meters (i.e., a net metering system), end users can produce their own electric power from renewable sources and sell their extra power to their local power grid.

As more customers use a net metering system, a substantial change in energy demand will result. Residential, commercial, and industrial concerns will install PV systems, use wind farm and micro-generation technologies and store energy as independent power producers.[18] The energy management systems of smart buildings with their own renewable power sources and CHP is likely the trend of the future. With the installation of an advanced net metering system, every node of the system will be able to buy and sell electric power. The use of real-time prices will facilitate the control of frequency and tie-line deviations in a smart grid electric power system. Under the grid emergency operation, the real-time pricing will provide a feedback signal as the basis of an economic load/shedding policy to assist the direct stabilizing control for a smart grid. Real-time pricing can be integrated with demand response to match the system load demand and generation in real-time. This will facilitate coordinating demand to flatten a sudden change in energy use. If the sudden surge in demand is not satisfied, it will result in the cascading collapse of the power grid. In demand response control, these spikes can be eliminated without the cost of adding spinning reserve generators. It will also reduce maintenance and extend the life of equipment. Energy users can reduce their energy bills by using their smart meters to program and operate their low-priority household appliances only when energy is at its cheapest.

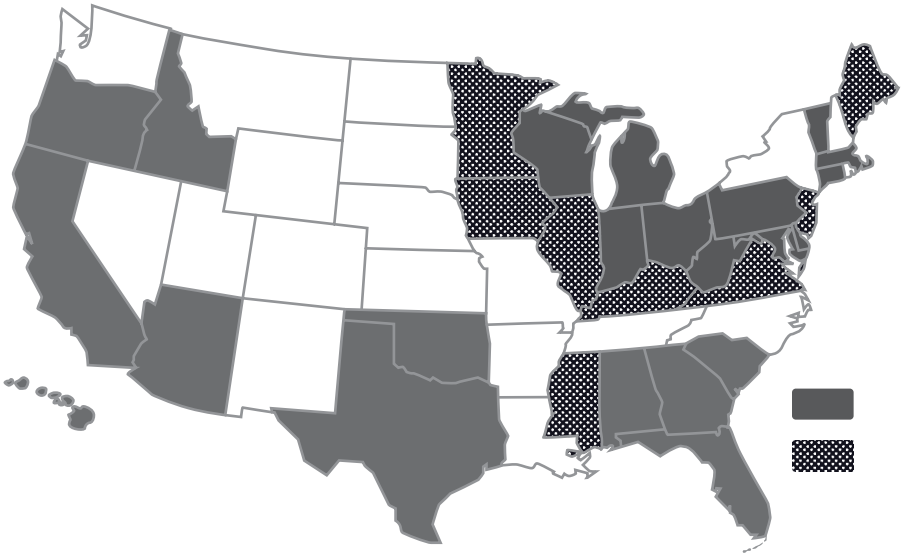

Figure 4.24 The Above Map Represents Smart Meter Deployments, Planned Deployments, and Proposed Deployments by Investor-Owned Utilities and Some Public Power Utilities (http://www.edisonfoundation.net/IEE; as of this writing, approximately 60 million customers have been equipped with a smart meter[1]). The gray area indicates that deployment is for more than 50% of end users. The dotted area indicates that deployment is for less than 50% of end users.

Figure 4.24 shows the state of smart metering installation in the United States as of April 2009.

Figure 4.17 depicts the MRG system. The MRG system's energy management system (EMS) communicates with individual smart meters located at residential, commercial, and industrial customer sites. Smart meters control loads, such as air-conditioning systems, electric ranges, electric water heaters, electric space heaters, refrigerators, washers, and dryers using Ethernet TCP/IP sensors, transducers, and communication protocol, as shown in Fig. 4.25.

The intelligence nodule of the EMS of the MRG system receives information on the status of connected loads from local smart meters. The EMS of the MRG system controls various customer loads, based on real-time pricing signals and normal, alert, or emergency grid signals. In general, the EMS takes information from the power grid and the open access same-time information system (OASIS).[1–6] Based on real-time pricing, smart meters are programmed to control loads on the customer's sites. The EMS's control of loads depends on input signals from its EMS and the customer's preestablished contract criteria. The EMS of the MRG microgrids has the capability to shed customer load and respond to local power grid operating conditions.

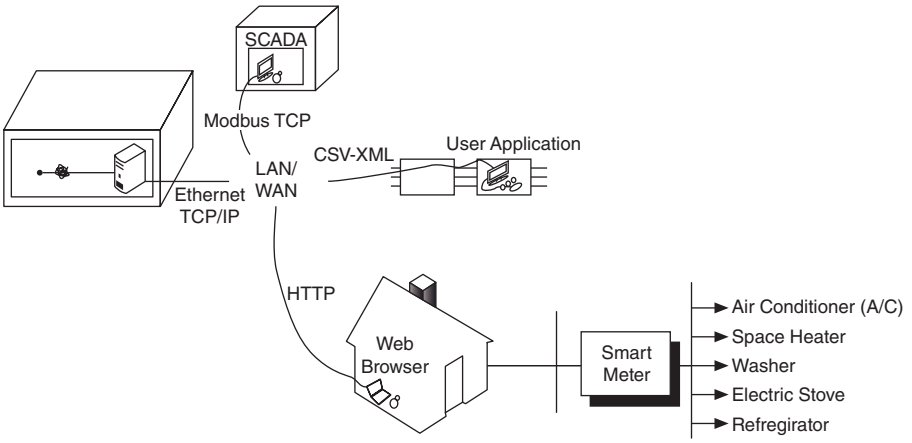

Figure 4.25 Ethernet TCP/IP Sensors, Transducers, and Communication Protocol for Load Control.

Smart microgrid systems are comprised of renewable green energy sources with their associated power converters, efficient transformers, and storage systems.[18]

4.11 SMART GRID DEVELOPMENT

Global warming and the environmental impact of coal-based power generation are changing the design and operation of the power grid. The industry is experiencing a gradual transformation that will have a long-term effect on the development of the infrastructure for generating, transmitting, and distributing power. This fundamental change will incorporate renewable green energy sources in a new distributed generation program based on increased levels of distributed monitoring, automation, and control as well as new sensors. Power grid control will rely on data and information collected on each microgrid for decentralized control. In return, the microgrids and interconnected power grid will be able to operate as a more reliable, efficient, and secure energy supplier.

The technology of the power grid and microgrids has a number of key elements. Adaptive and autonomous decentralized controls respond to changing conditions. Predictive algorithms capture the power grid state (phasor measurements)[16] for a wide area and are able to identify potential outages. The system also provides market structure for real-time pricing and interaction between customers, grid networks, and power markets. Furthermore, the smart grid provides a platform to maximize reliability, availability, efficiency, economic performance, and higher security from attack and naturally occurring power disruptions.

TABLE 4.2 A Comparison of the Current Grid and the Smart Grid.

	Current Grid	Smart Grid
System communications	Limited to power companies	Expanded, real-time
Interaction with energy users	Limited to large energy users	Extensive two-way communications
Operation & maintenance	Manual and dispatching	Distributed monitoring and diagnostics, predictive
Generation	Centralized	Centralized and distributed, substantial renewable resources, energy storage
Power flow control	Limited	More extensive
Reliability	Based on static, off-line models and simulations	Proactive, real-time predictions, more actual system data
Restoration	Manual	Decentralized control
Topology	Mainly radial	Network

The implementation of an advanced metering infrastructure provides real-time pricing to the energy end users. In parallel, the penetration of renewable energy sources is providing a platform for autonomous control or local control of connected microgrids to the local power grid. A distributed autonomous control will provide reliability through fault detection, isolation, and restoration. The autonomous control and real-time pricing also delivers efficiency in feeder voltage to minimize feeder losses and to reduce feeder peak demand of plug-in electric vehicles. The maturing storage technology will provide community energy storage, which becomes yet another important element for microgrid control and allows the energy user to become an energy producer. These interrelated technologies require a coordinated modeling, simulation, and analysis system to achieve the benefits of a smart power grid.

4.12 SMART MICROGRID RENEWABLE GREEN ENERGY SYSTEMS

Figures 4.26 and 4.27 present the DC and AC architectures of MRG systems. The MRG systems will also include cyber communication systems consisting of smart sensors for monitoring, controlling, and tracking the normal, alert, emergency, and restorative states of systems.

The smart meters of a MRG system are connected to a large interconnected power grid (see Fig. 4.17). The MRG system is also designed to provide an intelligent grid optimization manager that would allow control of various customer loads based on pricing signals and grid stress. Smart meters control devices at the customer's location by changing their use of power. Smart meters have the ability to shed customer load and allow distributed generation to come on-line, when the price of power is above a specified level. The EMS

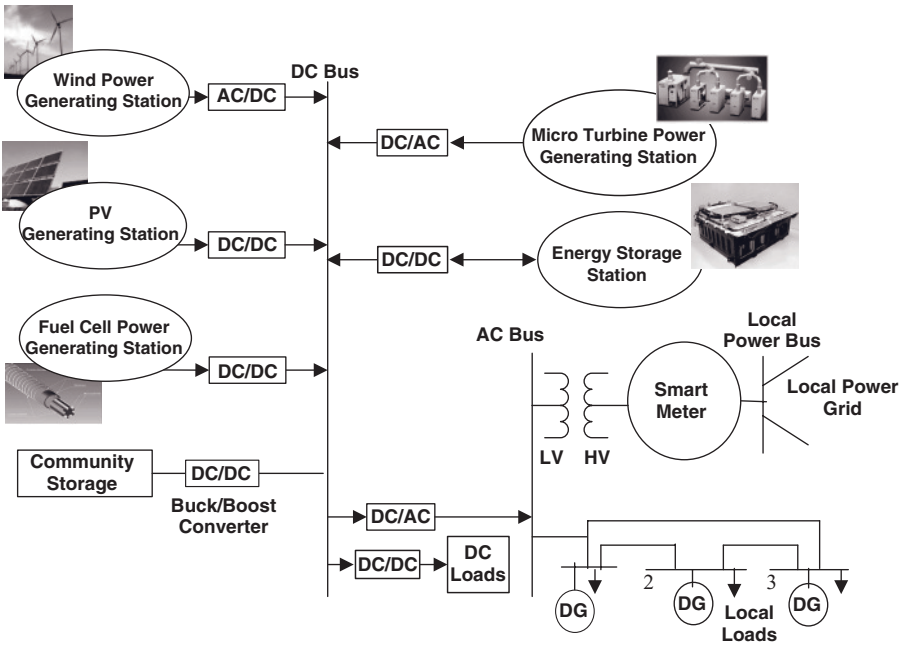

Figure 4.26 The DC Architecture of a Microgrid Renewable Green Energy (MRG) Distributed Generation (DG) System.

has two-way communication with the smart meters under its control. The EMS of a microgrid receives status and power signals from all of the modules (loads and generating sources). The EMS is able to control power flow into and out of the microgrid system from its host local power grid based on variables such as weather forecasts, load forecasts, unit availability, and power sales transactions.

The MRG systems provide a new paradigm for defining the operation of distributed generation (DG). MRG systems are designed as clusters of loads and microsources, operating as a single controllable system. To the local power grid, this cluster becomes a single dispatchable load, which can respond in seconds. The point of interconnection in the smart microgrid is represented by a node where the microgrid is connected to the local power grid, as shown in Figs. 4.26 and 4.27. This node is referred to as the locational marginal pricing (LMP),[5–6] where the node price (cost) represents the locational value of energy. Power grids (energy serving entities) try to provide reliable supplies of electric energy to their energy users. Maximum benefits require low cost, sufficient supply, and stable operation. The architectures shown in Figs. 4.26 and 4.27 are of interest to smart grid technology because they facilitate "plug and play" capabilities. In these architectures, green energy sources, such as fuel cells, microturbines, or renewable sources, such as PV-generating stations and wind farms, can be connected to a DC bus or an AC bus, using uniform

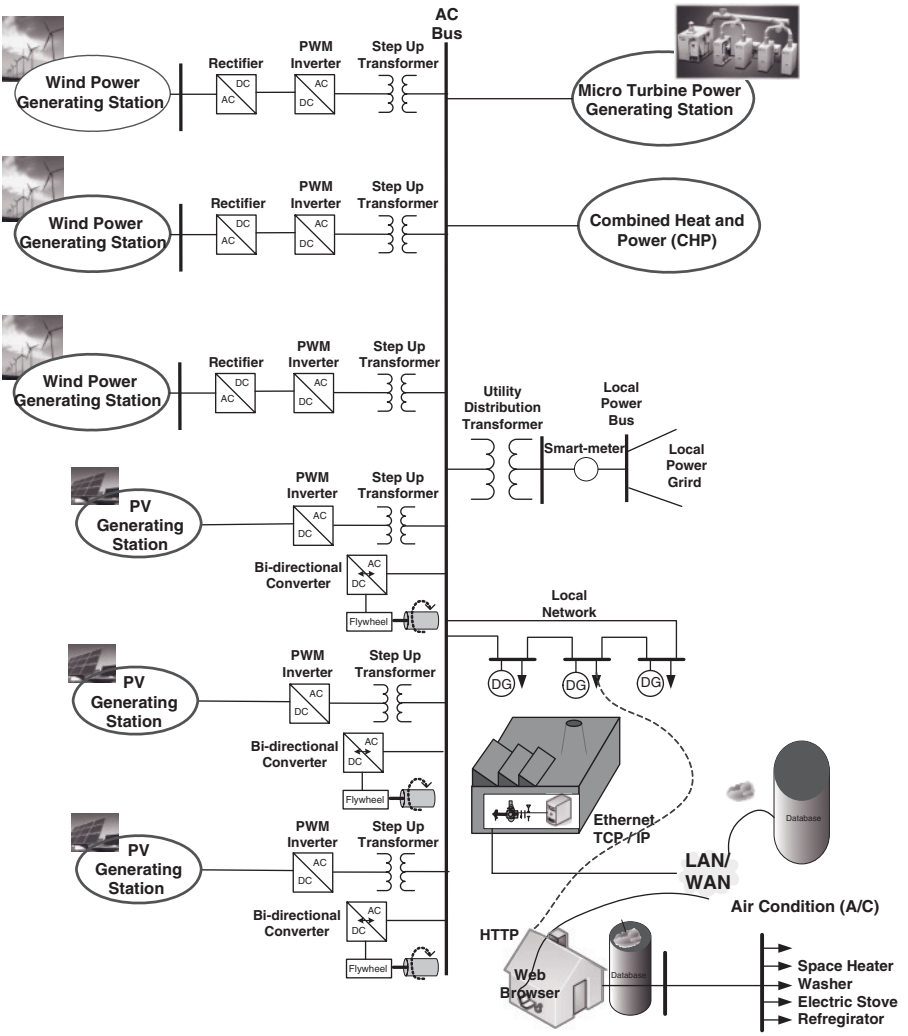

Figure 4.27 The AC Architecture of a Microgrid Renewable Green Energy (MRG) Distributed Generation (DG) System.

interchangeable converters. The MRG systems must be able to operate in two modes of operation: (1) in synchronized operation with the local power grid system, and (2) in the island mode of operation, upon the loss of the power grid system. In the island mode of operation, the MRG operates as an autonomous microgrid controlling its frequency and bus voltage. When a MRG system is connected to a power grid, the MRG system operates using a master- and slave-control technology. The master referred to is the EMS of the local power grid and the slave is the MRG microgrid. If the MRG system is suddenly separated from its local power grid and MRG stability is maintained,

then the slave controller takes over LFC and voltage control. For MRG systems with high power capacity, there is a purchasing agreement between the power grid and MRG systems, regarding active and reactive power transfer. The MRG system can control its loads and accept a "price signal" and/or an "emergency operation signal" from its local power grid to adjust its active and reactive power generation. The MRG system has hardware in place to shed loads in response to a price signal, and it can rotate nonessential loads to keep on critical loads. However, because disturbances in a local power grid cannot be predicted with current technology, it is quite possible upon the loss of the local power grid that an MRG system would not be rapidly disconnected from the local power grid; hence, the stability of the MRG systems would not be maintained. Future research in cyber-monitoring and control MRG systems is being conducted to provide predictive models to track states in the system and to provide distributed intelligence control technology.

In Figs. 4.26 and 4.27, the EMS controls the infinite bus voltage and the system frequency. The slave controller controls the AC bus voltage of the inverter and the inverter current. Therefore, the slave controller of the MRG system inverter must be able to control active and reactive power, at leading or lagging power factor, or operate at the unity power factor. In small, renewable energy systems, the inverter is controlled at the unity power factor, and it leaves the voltage control, that is, the reactive power (VArs) control, to the EMS of the local power grid.

The MRG system of Fig. 4.26 and Fig. 4.27 has a number of distribution generation sources such as wind-generating stations and PV-generating stations. The power capacity of such a system is in a range of 1–10 MW. We are using step-up transformers to step up the AC voltage to reduce the power losses. Depending on the size of distributed generators (DGs), we will step up the voltage to a range of 34.5 kV–69 kV, before injecting the power into the local power grid network. As shown in Fig. 4.28, the storage system facilitates storing the renewable energy. The stored energy can be used as load demand fluctuates during the daily load cycle of 24 hours. Because the investment in developing a power grid is quite high and its construction takes many years, the power system is planned years in advance. However, if renewable green energy sources are installed in the distribution system, the lead-time is from a few months to a few years depending on the size of facilities to be installed.

The residential MRG system depicted in Fig. 4.28 consists of rooftop photovoltaics with a capacity in the range of 5–25 kVA depending on the available roof surface area. A DC/DC boost converter is used to boost the voltage of the DC bus. The maximum power point tracking (MPPT) system is designed to track and operate the PV power generator at the maximum power point. The DC/AC inverter converts the DC bus voltage to AC voltage at the operating frequency and rated residential voltage. The MRG system of Fig. 4.28 is connected to the local power grid by stepping up the voltage to the local distribution voltage. The MRG system can also store DC power during the day for use during the night.

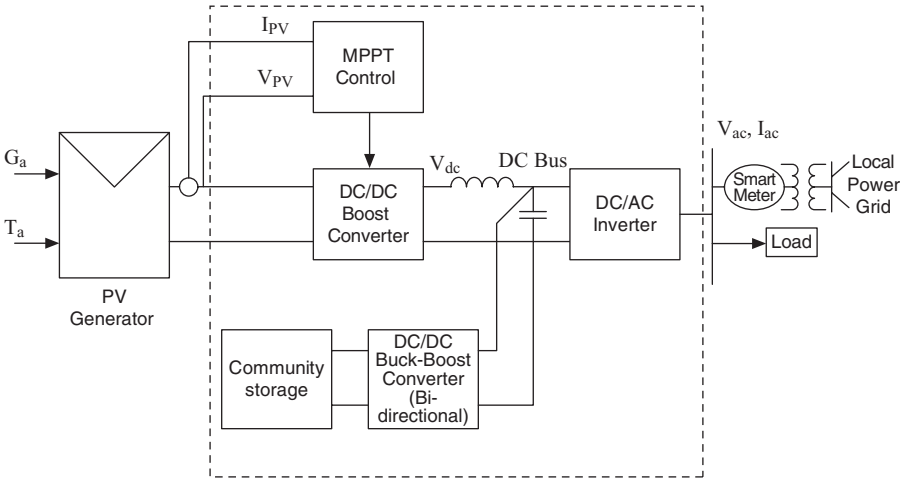

Figure 4.28 A Residential Microgrid Renewable Green Energy (MRG) System with a Local Storage System.

Figure 4.27 depicts the injection of electric energy into the network at all voltage levels in interconnected power grid systems. These injection nodes are part of an MRG system of a cyber-controlled smart grid as shown in Fig. 4.17. The loads are under the control of smart meters. Therefore, every node in the cyber-controlled power grid is price sensitive.

The high penetration of renewable energy sources can be placed at all voltage levels as shown in Fig. 4.29. Many states have mandated the use of renewable energy. It requires that investor-owned utilities obtain 25% of their electricity from renewable and advanced energy sources by 2025. In some states, a 0.5% set aside has been put in for solar PV energy sources. There are penalties of $450 per MWh for noncompliance with solar benchmarks and $45 per MWh for noncompliance with other benchmarks that began in 2009. These benchmarks can be met by purchasing renewable energy credits (REC) each equal to 1 MWh of renewable energy. Purchasers of the product could sell RECs into the REC market. As of this writing, their current value is around $37.50. It is expected that solar RECs will probably sell at much higher rates.[1–5]

There are a number of advantages to smart MRG systems. It empowers the individual to provide his or her own energy needs. This participation by energy end users has been called the "democratization of energy." This allows matching the characteristics' of loads to their generators. This makes these types of microgrids independent from the interconnected grid power failures. Smart MRG technologies have the ability to identify a potential stability problem. Real-time information enables MRG systems to separate themselves from the interconnected grid and operate as an "island." During normal synchronized operation, the interconnected smart grid with its smart monitoring of power

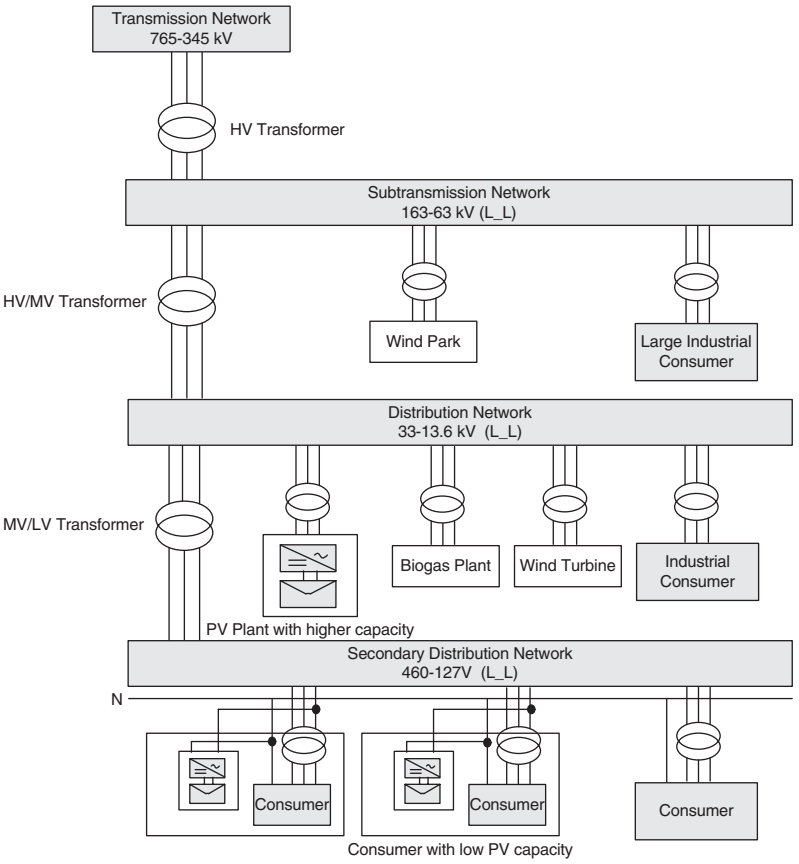

Figure 4.29 A Smart Grid with High Penetration of Renewable Energy Sources.

grids can control and manage the interconnected power grid to control the system loads and avoid system-wide blackout.

When a smart microgrid DG is connected to a power grid, then the smart microgrid DG generating station should operate using a master- and slave-control technology. The master is the EMS of the power grid system. The EMS controls the infinite bus voltage located at the connection node of one microgrid to its local power grid. In Fig. 4.27 the smart grid DG is connected to the power grid system by a transformer. The slave controller controls the AC bus voltage of the microgrid inverter (bus voltage magnitude and phase angle) and the inverter current. Therefore, the slave controller of the microgrid DG inverter also controls active and reactive power. The microgrid inverter is designed to operate as a unity power factor and to leave the voltage control, that is, the reactive power (VArs) control, to the EMS of the power grid system. Or, the inverter of DG operates with a leading power factor, a lagging power factor. If

the smart grid is suddenly separated from its local power grid and system stability is maintained, then the slave controller takes over LFC and voltage control.

The word "smart" refers to the requirement that a microgrid controls its loads, and that it accepts the "price signal" and/or the "emergency operation signal" from its local power grid to adjust its active and reactive power generation. Other designs are also possible such as a net smart metering communication between the EMS of the local power grid and the EMS of the microgrid system. Smart microgrids should have hardware in place to shed loads, in response to the price signal, or to rotate nonessential loads and to supply power critical loads. However, because disturbances in a power grid system cannot be predicted, the DG microgrid system should be designed to rapidly disconnect from its power grid system to maintain the stability of the microgrid DG systems. To ensure stable operation, the storage system of the microgrid, with its inverter, has to be able to participate in the ancillary market.[5] The architecture of Fig. 4.27 is of interest to distributed generation technology because it facilitates plug and play capabilities. In this architecture, green energy sources, such as fuel cells, microturbines, or renewable sources, such as PV-generating stations and wind farms, can be connected to a DC bus, using uniform interchangeable converters. The architecture of Fig. 4.27 satisfies the "Renewable Portfolio" laws that have been mandated by many states. This architecture allows for the selling of and buying of energy to and from local utilities. Note that the microgrid can offer real-time pricing or a tariff-based contract by facilitating load control through a cyber-controlled smart meter or net metering, if a customer has local generation at the customer site to control loads. The smart meter and its cyber control are also shown in Fig. 4.27. In addition, the microgrid can participate in system control at a bulk power level, through its own smart metering that is interfaced with its local power grid EMS.

The microgrid DG system is designed so that upon separation from the local power grid, the microgrid DG system is restored by shedding noncritical loads if there has been a generation deficiency, so the local microgrid is able to return to normal operation. This problem of stability is a function of how strongly a microgrid DG system is connected to a power grid system. This problem must be addressed as system parameters are defined, and as the level of connecting a microgrid DG system to a local power grid is defined. It also requires the microgrid DG system to have other green energy sources, such as CHP and microturbines, to ensure quality and stable service if some power sources have forced outage.

As presented in Chapter 2, the classical interconnected power network is designed for one-way flow of power. However, when the subtransmission and distribution and residential systems have the ability to generate more electric power that can reverse the flow of power from low voltages to higher voltages and create reverse power flow, it can raise safety and reliability issues. These protection problems of a smart grid are another important topic of current research.

The design of a power grid requires major investment. However, a smart grid can minimize costs of operations and maintenance by the rational pricing of electric power. The optimized generation and transmission lines planning facilitate efficient power flows that will reduce power losses and promote the efficient use of lowest-cost generators. Currently, the interconnected power networks have a number of communication systems within control systems for their generating plants, transmission lines, substations, and major load centers. The energy flow is directed from generators to the load centers. The power system operators, through metering of power flows and measurement of bus voltages and frequency, monitor the system. The system demands are met through load frequency and AGC. When the system demands are not met, the system frequency drops and a brownout, a rolling blackout, or an uncontrolled blackout may occur. The total amount of power demand by the users can vary widely as a function of environmental conditions. The spinning reserve at spare generating plants is kept in standby mode on-line to respond to the fluctuating power demands. The smart grid with its independent MRG system eliminates the cost of a spinning reserve because its operating system is based on real-time pricing.

4.13 A POWER GRID STEAM GENERATOR

We have presented the basic system concept of a smart grid and microgrids of MRG systems. However, there are a few basic analysis concepts that are needed in both the interconnected smart grid and microgrids of MRG systems: the modeling of power generators, the limit of stable power transfer in transmission systems, and the modeling of the smart grid and power flow.

A three-phase synchronous generator depicted by Fig. 4.30 is a three-terminal device.[19–20] The mechanical power is input from a prime energy source such as hydropower or mechanical power from a thermal unit that drives the shaft of the generator. The field winding of the generator is located on the rotor of the machine. The field winding is energized by DC current through the excitation system of the generator through a slip ring or by placing the excitation on the rotor of machines. The three-phase balanced windings are located on the stator of the machine. As the names stator and rotor imply, the stator is stationary and rotor is the rotating element of the machine. The space between the stator and rotor is referred to as the air gap of the machine. The air gap length is in millimeters and the rotor is supported by a well-designed bearing system to keep the air gap as small as possible yet keep the rotor from having contact with the stator (i.e., rubbing). Because the air gap length is designed to be as small as possible, the maximum flux lines cross the air gap and link to the stator of the machine. By rotating the field winding in the air gap of the machine, the time varying flux is generated. The time-changing flux lines link the three-phase winding located on the stator of the machine. Two types of time-changing flux are produced. One is the linking flux that crosses the air gap of the machine and the second flux is the leakage flux that leaks

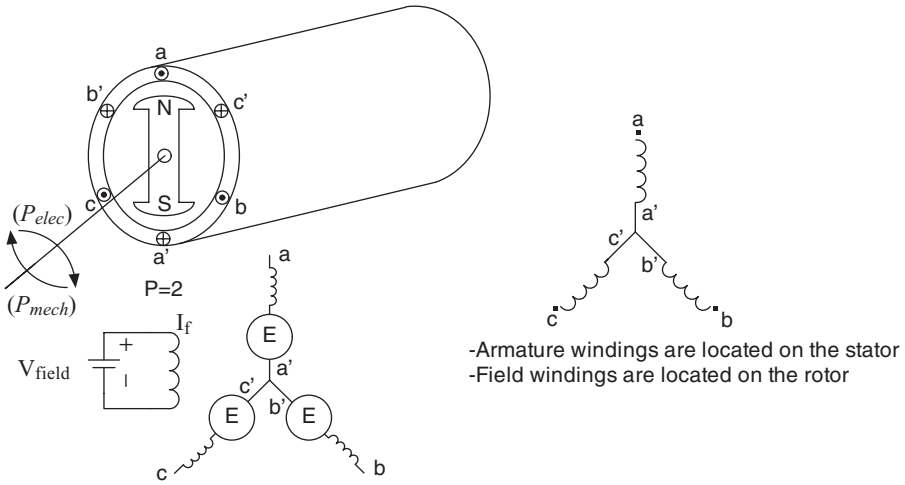

Figure 4.30 A Three-Phase Synchronous Generator.

through the air. The linkage flux gives rise to the magnetizing inductance and to leakage inductance. Because the induced voltage and current is produced on the stator windings, the stator windings are referred to as armature windings.

The operating frequency of the generator is a function of shaft speed as described below.

$$\frac{d\theta_{elec}}{dt} = \frac{p}{2}\frac{d\theta_{mech}}{dt} \tag{4.13}$$

$$\omega_{elec} = \frac{P}{2}\omega_{mech} \tag{4.14}$$

$$2\pi f_{elec} = \frac{P}{2}\omega_{mech} \tag{4.15}$$

$$\omega_{mech} = n\frac{2\pi}{60} \tag{4.16}$$

$$f = \frac{P}{2}\frac{n}{2\pi}\frac{2\pi}{60} = \frac{Pn_{syn}}{120} \tag{4.17}$$

$$\text{where } n_{syn} = (120f/P) \text{ Hz}$$

P is the number of poles, θ_{elec} and θ_{mech} represent the electrical and mechanical angle in radians. ω_{elec} and ω_{mech} represent electrical and mechanical speed in radian per second. Finally, n is revolution per minute (rpm), f is cycle per second, and n_{syn} is the synchronized speed in rpm.

$$E = K \cdot I_f \cdot \omega \tag{4.18}$$

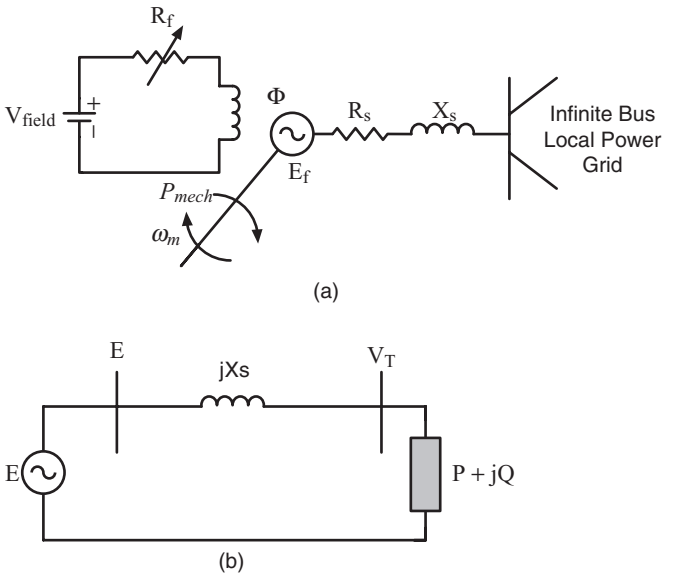

Figure 4.31 **(a)** One-Machine Generator Connected to the Local Power Grid Bus. **(b)** A One-Phase Equivalent Circuit Model of a Three-Phase Generator.

The open-circuit induced voltage, E is a function of machine dimensions, which is given by constant K and field current, I_f and shaft speed, ω. Figure 4.31(a) depicts the one-line diagram of a generator connected to a local power grid. Figure 4.31(b) depicts the circuit model of a three-phase generator where the induced voltage is represented by E and the generator terminal voltage is shown by V_T. The magnetizing inductance of the machine is not shown in the above circuit model. The generator is designed to draw a small amount of current to be magnetized. The leakage inductance is shown by X_s as synchronized reactance because it is computed using the steady-state synchronized operation. The power supplied by the generator is shown as active and reactive power P and Q.

There are a number of commonly used exciters. In the DC generator commutator exciter, the excitation energy is derived from a DC generator. The exciter includes a DC generator with its commutator and brushes to inject DC field current into the field winding of the generator. It is exclusive of input control elements. This exciter may be driven by a motor, prime mover, or the shaft of the synchronous machine. The generator rectifier exciter derives its energy from an generator and is converted to DC by a rectifier system. This type of exciter includes a generator and power rectifiers that may be either noncontrolled or controlled. The generator may be driven by a motor, prime mover, or the shaft of the synchronous machine. The rectifier may be stationary or rotating with the generator shaft. A compound rectifier exciter derives its

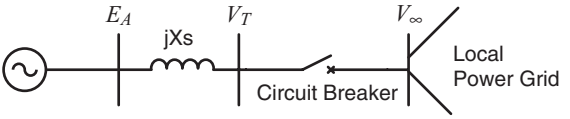

Figure 4.32 The Generator Operation before Synchronization.

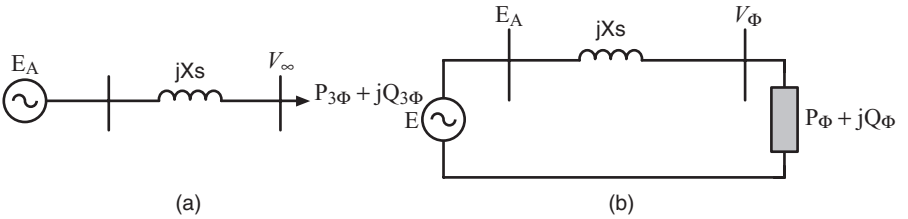

Figure 4.33 The Operation of the Generator in Parallel with the Power System. **(a)** One-Line Diagram. **(b)** One-Phase Equivalent Circuit Model.

electric power from the terminals of the synchronous machine and then it is converted to DC by rectifier systems.[22]

Let us study the operation of a generator in parallel with an interconnected power network as shown in Fig. 4.32.

For synchronous operation, the following conditions are necessary:

1. The electrical speed of the synchronous generator should be equal to the electrical speed of the power system generators.
2. The terminal voltage of the generator should be equal to the V_∞ bus and they must be in the same a-b-c sequence.

When the above conditions are satisfied, the circuit breaker can be closed. Synchronous operation means the parallel operation of synchronous generators. The notation, V_∞ bus, has a special meaning. We call a bus voltage as an infinite bus to signify that its voltage is constant and cannot be changed by external events. This means that an infinite bus acts as an ideal voltage source.

Let us now study the operation of a synchronous generator when it is synchronized with an interconnected power system as shown in Fig. 4.33(a). Because the power system has many power sources, we can consider the power system bus that we will connect the generator as an "infinite bus."

Let us assume that all power losses in the operation of the generator are neglected and we have the reference phase angles that are given below:

$$V_{\infty,L-N} = V\angle 0,$$
$$E_{A,L-N} = E_A\angle\delta \tag{4.19}$$

We can use the equivalent circuit of Fig. 4.33(b) to calculate the current supplied to the load.

$$I_L = \frac{E\angle\delta - V}{jX_s} \quad \text{and} \quad I_L^* = \frac{E\angle -\delta - V}{-jX_s} \tag{4.20}$$

The complex power generated and supplied to the load (per phase), i.e., injected into the power system, can be computed as

$$S_\phi = j\frac{E^2{}_A\angle 0}{X_s} - j\frac{E_A V\cos\delta}{X_s} + \frac{E_A V\sin\delta}{X_s} = P_\phi + jQ_\phi$$
$$P_\phi = \frac{E_A V}{X_S}\sin\delta \quad \text{and} \quad Q_\phi = \frac{E_A^2}{X_s} - \frac{E_A V}{X_S}\cos\delta \tag{4.21}$$

Because we have assumed that losses are neglected, then the mechanical power supplied to the generator shaft can be expressed as

$$P_{mech} = 3P_\phi = 3\frac{E_{A(L-N)}V_{\infty(L-N)}}{X_s}\sin\delta = \frac{E_{A(L-L)}V_{\infty(L-L)}}{X_s}\sin\delta \tag{4.22}$$

To understand how a generator can be operated with leading or lagging power factors, we need to study the relationship between phase angle δ and the excitation voltage, E_A.

Consider a synchronous generator of Fig. 4.34:

Let us assume the mechanical power supplied to the generator shaft is constant and losses are ignored. Therefore, the mechanical power supplied, P_{mech} is equal to the electrical power injected into the local power grid as expressed by Equation 4.22.

If we adjust, the field current to a value as $I_f = I_{f0}$, then the excitation voltage will be equal to $E_A = E_A\angle\delta_0$, where designation of subscript "0" signifies this condition.

These conditions can be expressed as $P_{elec} = 3\frac{E_A V_\infty}{X}\sin\delta$ when $E_A = E_A\angle\delta_0$; $I_f = I_{f0}$

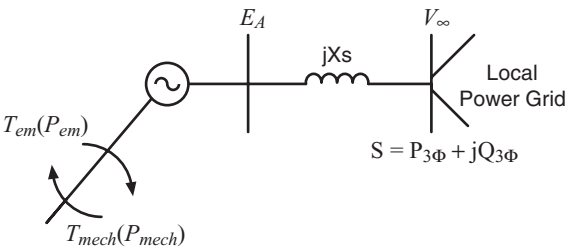

Figure 4.34 The Operation of a Generator Injecting Power into a Local Power Grid.

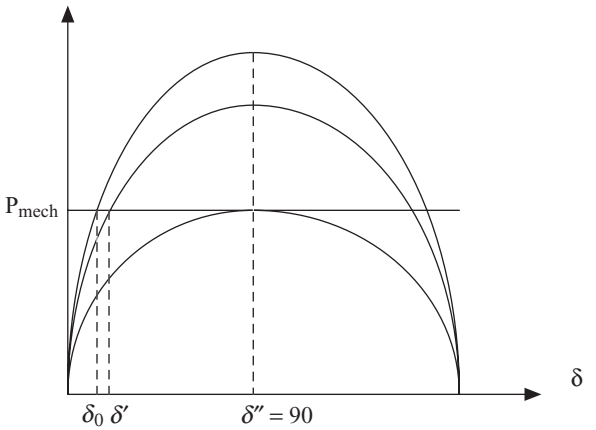

Figure 4.35 The Plot of P_{mech} versus the Power Angle for Different Values of E_A.

and

$$P_{elec} = 3\frac{E_A V_\infty}{X_s}\sin\delta = P_{mech} \tag{4.23}$$

Figure 4.35 depicts the power angle as a function of excitation voltage, E_A. If we reduce I_f to a new value of I_f', then E_A reduces to a new value of E_A'. However, if we continue to keep P_{mech} constant, and continue to reduce I_f, we can still generate the same amount of electrical power, therefore, as the value of E_A decreases to a new value of E_A'', the angle, δ, keeps increasing to generate the same amount of electrical power, until it δ reaches 90°.

$$p_{elec} = 3\frac{E_A'' \cdot V_\infty}{X}\sin 90° = P_{mech} \tag{4.24}$$

This is maximum power generated and is called *pull-out power*. If we continue to reduce I_f further, P_{elec} decreases and δ increases. The machine loses synchronization when $\delta > 90°$. This means power cannot be injected, and the local power system will drive the machine as a motor. The angle, δ is called the power angle or torque angle.[22]

Consider a generator supplying power at a lagging power factor to a local power grid. As we discussed before, the AGC will ensure that the balance of generation and loads will be maintained. This condition is shown in Fig. 4.36.

$$\sum_{i=1}^{6} P_{Gi} = \sum_{i=1}^{6} P_{Li} + P_{losses} \tag{4.25}$$

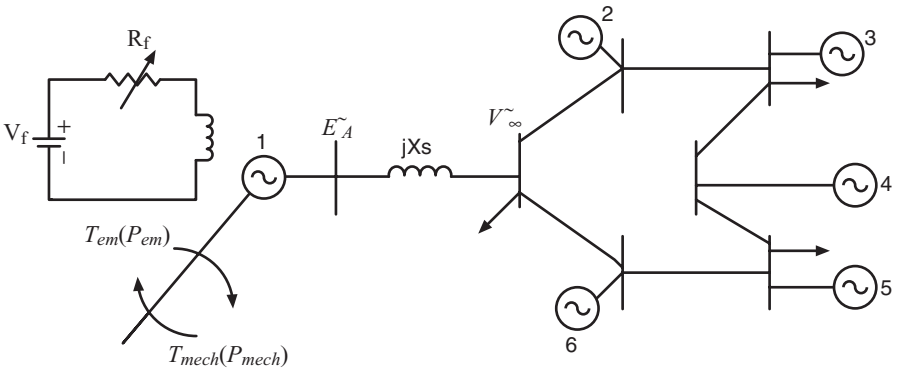

Figure 4.36 The Operation of a Generator Injecting Power with a Lagging Power Factor into a Local Power Grid.

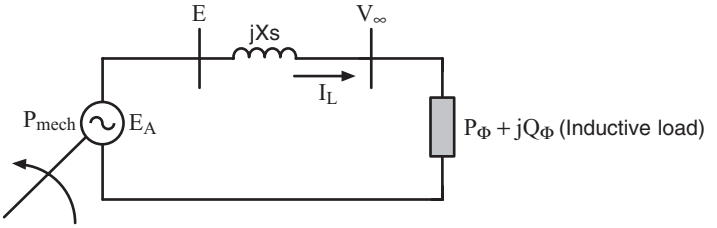

Figure 4.37 The Equivalent Circuit Model of a Generator Injecting Power with a Lagging Power Factor into a Local Power Grid.

$$\sum_{i=1}^{6} Q_{Gi} = \sum_{i=1}^{6} Q_{Li} + Q_{losses} \tag{4.26}$$

Consider the equivalent circuit model of Fig. 4.37. Let us neglect power losses and assume that $V_{\infty(L-N)} = V\angle 0$, $E_{A(L-N)} = E\angle\delta$ and the following operating conditions: $P_{mech} = const, |E_A| = const$ (i.e., ω_m = const, I_f = const). However, the field current, I_f is adjusted such that $|E_A| > V_\infty$.

$$\tilde{E}_A = jX_s I_L + \tilde{V}_\infty$$

$$P_{mech} = 3\frac{E_{A(L-N)}V_{\infty(L-N)}}{X_s}\sin\delta = \frac{E_{A(L-L)}V_{\infty(L-L)}}{X_s}\sin\delta$$

$$P_{mech} = P_{3\phi} = 3\frac{E_{A(L-N)}V_{\infty(L-N)}}{X_s}\sin\delta = 3V_{\infty(L-N)}I_L\cos\theta \tag{4.27}$$

Figure 4.38 depicts the operation of a generator with a lagging power factor. This operating condition is designated as an overexcited generator when the

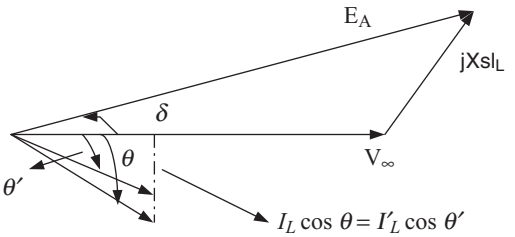

Figure 4.38 The Phasor Diagram of a Generator Injecting Power with a Lagging Power Factor into a Local Power Grid.

magnitude of excitation voltage is greater than the magnitude of terminal voltage (i.e., $|E_A| > V_\infty$).

To change the power factor of the generator, we keep the supplied mechanical power constant: $P_{mech} = const$ and the shaft speed is also constant, i.e., $\omega_m = const$.

By reducing the field current from a value of I_f to a new lower value of I'_f, the excitation voltage, E_A, reduces to a new lower value of E'_A. However, because the supplied mechanical power remains constant, the electric power generated by the generator must also remain constant. Therefore, the angle, δ increases to a higher value of δ. This condition can be expressed as

$$P_{mech} = 3P_\phi = 3\frac{E_{A(L-N)}V_{\infty(L-N)}}{X_s}\sin\delta = 3\frac{E'_{A(L-N)}V_{\infty(L-N)}}{X_s}\sin\delta' \tag{4.28}$$

$$P_{mech} = P_{3\phi} = 3\cdot V_{\infty(L-N)}I_L\cos\theta = 3\cdot V_{\infty(L-N)}I'_L\cos\theta' \tag{4.29}$$

The balance of power is maintained and $|I_L|$ reduces to a new lower value of $|I'_L|$, and θ reduces to new lower value θ'.

However, because $I_L\cos\theta = I'_L\cos\theta'$, the active power generated remains the same.

$$Q_{3\phi} = 3\cdot V_{\infty(L-N)}I_L\sin\theta \quad Q'_{3\phi} = 3\cdot V_{\infty(L-N)}I'_L\sin\theta' \tag{4.30}$$

We can conclude that by reducing I_f, the reactive power generated by the synchronous generator is reduced. However, the active power generated by the generator remains the same and we can have a new operating condition where $Q_{3\phi} < Q'_{3\phi}$ and at the same time the balance of generations and load is maintained.

$$\sum_{i=1}^{6} P_{Gi} = \sum_{i=1}^{6} P_{Li} + P_{losses} \tag{4.31}$$

$$\sum_{i=1}^{6} Q_{Gi} = \sum_{i=1}^{6} Q_{Li} + Q_{losses} \tag{4.32}$$

Suppose we decide to operate the generator at unity power factor. To obtain the unity power factor, we can reduce the field current, I_f such that the power factor angle, θ (i.e., the angle between V and I) reduces to zero.

$$P_{mech} = P_{3\phi} = 3\frac{E''_{A(L-N)}V_{\infty(L-N)}}{X_s}\sin\delta'' = 3V_{\infty(L-N)}I''_L\cos(\theta'' = 0) \tag{4.33}$$

Figure 4.39 depicts the operation of a generator with unity power factor. We conclude that by reducing I_f, we can operate the machine with unity power factor while generating the same active power. However, the reactive power generated by the machine is reduced to zero.

Suppose we continue to reduce the field current, I_f such that $\theta > 0$, i.e., I_L would lead V_∞. This operating condition is depicted by Fig. 4.40.

$$P_{mech} = P_{3\phi} = 3\frac{E'''_{A(L-N)}V_{\infty(L-N)}}{X_s}\sin\delta''' = 3V_{\infty(L-N)}I'''_L\cos\theta''' \tag{4.34}$$

$$Q_{3\phi} = -3V_{\infty(L-N)}I'''_L\sin\theta''' \tag{4.35}$$

Now, the generator is operating with a leading power factor as shown by Fig. 4.40.

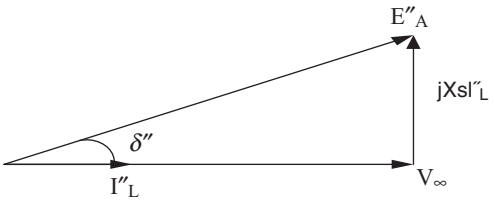

Figure 4.39 The Phasor Diagram of a Generator Injecting Only Active Power (i.e., A Unity Power Factor) into a Local Power Grid.

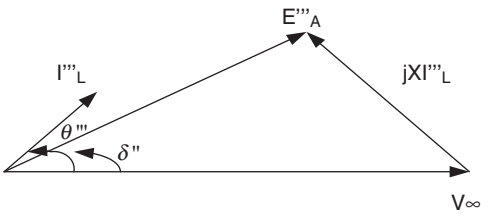

Figure 4.40 The Phasor Diagram of a Generator Operating with a Leading Power Factor.

Example 4.5 For a 440 V generator with a synchronous reactance of 0.1 Ω, and supplying a load of 2 kW at unity power factor, find

i) The field current, if k = 0.25 V sec/rad/A ($E_f = k \cdot \omega_s \cdot I_f$).
ii) The field current if the power factor of the load is 0.85 lagging. Assume the machine has four poles.

Solution

i) The phase current $= I_L = \dfrac{P}{\sqrt{3} \cdot V_L \cdot \cos\theta} = \dfrac{2000}{\sqrt{3} \times 440 \times 1} = 2.62$ A

The electromagnetic field (emf) excitation is given as

$$\text{emf} = E_f = V_{ph} + I_{ph} \cdot X_s = \frac{440}{\sqrt{3}} \angle 0 + 2.62 \angle 0 \times 0.8 \angle 90 = 254.04 \angle 0.47 \text{ V}$$

$$\omega_s = 2 \cdot \pi \cdot \frac{2f}{P} = 2 \cdot \pi \times \frac{2 \times 60}{4} = 188.5 \text{ rad/sec}$$

$$\text{The field current} = I_f = \frac{E_f}{k \cdot \omega_s} = \frac{254.04}{0.25 \times 188.5} = 5.39 \text{ A}$$

ii) The phase current $= I_L = \dfrac{P}{\sqrt{3} \cdot V_L \cdot \cos\theta} = \dfrac{2000}{\sqrt{3} \times 440 \times .85} = 3.08$ A

The excitation emf $= E_f = V_{ph} + I_{ph} \cdot X_s$

$$= \frac{440}{\sqrt{3}} \angle 0 + 3.08 \angle \left(-\cos^{-1} 0.85\right) \times 0.8 \angle 90 = 255.34 \angle 0.47$$

$$\text{The field current} = I_f = \frac{E_f}{k \cdot \omega_s} = \frac{255.34}{0.25 \times 188.5} = 5.42 \text{ A}$$

It can be seen that the field current needs to be increased to supply lagging power factor load (overexcitation).

Example 4.6 For the generator of Example 4.5, the field current is reduced to 5.093 A without disturbing the mechanical energy input to the generator. Find the power factor angle of the load.

Solution
Because the mechanical input remains the same, the value of active power is unaltered.

$$\text{The excitation emf} = E_f = k \cdot \omega_s \cdot I_f = 0.25 \times 188.5 \times 5.093 = 240 \text{ V}$$

$$P = \frac{3 \cdot |E_f| \cdot |V_{ph}| \cdot \sin\delta}{|X_s|}$$

$$\Rightarrow \delta = \sin^{-1}\left(\frac{P \cdot |X_s|}{3 \cdot |E_f| \cdot |V_{ph}|}\right) = \sin^{-1}\left(\frac{2000 \times 0.8}{3 \times 240 \times 440/\sqrt{3}}\right) = 0.50^o$$

$$E_f = V_{ph} + I_{ph} \cdot X_s$$

$$\Rightarrow 240\angle 0.5 = \frac{440}{\sqrt{3}}\angle 0 + I_{ph}\angle \cos^{-1}\theta \times 0.8\angle 90$$

$$\Rightarrow I_{ph}\angle \cos^{-1}\theta = \frac{1}{0.8\angle 90}\left(240\angle 0.5 - \frac{440}{\sqrt{3}}\angle 0\right) = 17.74\angle 81.51^o \text{ A}$$

Example 4.6 illustrates that a reduction of field current from that for the unity power factor (underexcitation) results in the leading power factor.

We conclude that by reducing the field current, I_f, the supplied current would lead the voltage and we can operate the generator with the leading power factor while generating the same active power.

As we can see from the above presentation, a generator of a smart grid is a three-terminal device. The mechanical power is supplied to the generator; the excitation voltage is controlled by the voltage regulator—the field current is set for the power factor of the generator. These conditions determine the active and reactive power supplied by the generator. We should also keep in mind that we can reset the power supplied by the generators during the operation because the AGC maintains the balance of loads and generation as given by Equations 4.36 and 4.37 and depicted by Fig. 4.41.

$$\sum_{i=1}^{6} P_{Gi} = \sum_{i=1}^{6} P_{Li} + P_{losses} \tag{4.36}$$

$$\sum_{i=1}^{6} Q_{Gi} = \sum_{i=1}^{6} Q_{Li} + Q_{losses} \tag{4.37}$$

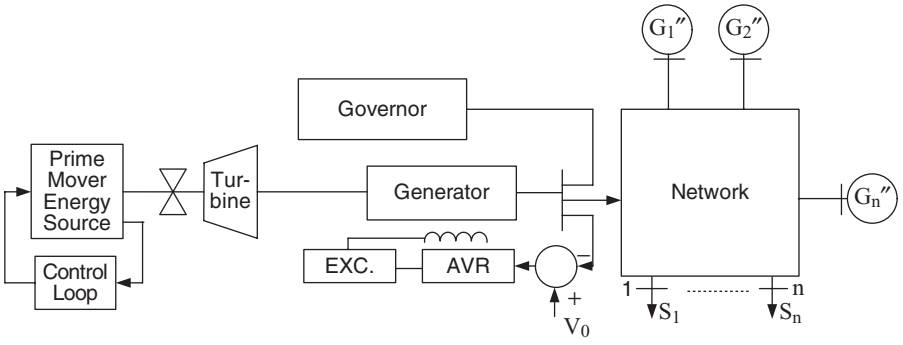

Figure 4.41 A Generator Operation as Part of an Interconnected Power Network.[11]

Let us review the fundamental objectives of the design of a smart grid system: (1) To provide quality power at a minimum price, and (2) to ensure the continuity of service by keeping the power grid stable. The issue of stability of the power grid is complex and we need to study how to construct dynamic models for each element of the power grid and then to define the time duration of study. However, we have discussed some aspects of steady-state stability through the AGC and LFC. The power system transient stability studies require more in depth modeling of a power system by representing the dynamics of energy sources. The design of a smart grid for studying how to provide rated voltage to loads of the system requires the steady-state model of power systems using the balanced system model. However, so far, we have studied how to develop a per unit model for transformers, loads, and generators. We will use these models to construct the system model.

4.14 POWER GRID MODELING

To construct a smart power grid, we need to represent the elements of a power grid in a per unit system.[21] Every element of a grid has its own voltage, power, and impedance ratings. The ratings give the users information on the safe utilization of that element. Then, we need to select a common system power base and convert all elements of the power grid to the same common base.[19–20]

The power grid models are needed for two fundamental engineering design problems. These design problems are power flow studies and short-circuit studies. For power flow studies, all energy sources are scheduled to inject electric power into the power grid network to satisfy the scheduled system loads. The objective of power flow studies is to compute the bus voltages. For short-circuit studies, we have already solved the power flow problem and the bus voltages are known. The bus loads are replaced by their load impedance models. The objective of short-circuit studies is to study the "if then condition" for calculating the fault currents and circuit-breaker short-circuit current capacity for a fault anywhere in the power grid system. The scheduled generation may be supplied from conventional power plants and renewable energy sources such as wind or solar sources or green energy sources such as fuel cells, biomass, or microturbines. For power flow studies, the power sources are represented as power injection points. The internal impedance of the energy source is not used in voltage computation. There are a number of generator models that are used in power flow studies. The basic models are (1) A constant P_G and Q_G, and (2) a constant P and V model. In the constant P and Q model, the injected power into the power network is given and the bus voltage magnitude and phase angle are computed. We will discuss the modeling of a power grid network for power flow studies in Chapter 7.

Figure 4.42 depicts an eight-bus power grid system. As can be seen the transformers of PV and wind generators are grounded through a grounding reactance. The grounding reactance function is to limit ground current if a single line to ground fault happens to occur in the system and to detect ground current. The Δ–Y transformers are used to step up the voltage to the voltage level of transmission lines. The circuit breakers are located to isolate one section of the system during maintenance and unforeseen faults. The Δ–Y transformers, T_1 and T_2, are also providing isolation and limit the ground current flow in the system. The transformer Δ–Y, T_3, provides lower voltage as the power is transferred to the loads. In addition, the transformer, T_3 is grounded Δ–Y to provide a grounded system on the load side.

The impedance diagram for the power grid system of Fig. 4.42 is shown by Fig. 4.43. This impedance diagram depicts the balanced operation of the system. Because the system is balanced, the sum of the voltages at the neutral point is zero and no ground current will flow in this system. However, if there is a single line to ground fault on the system, we need to model the unbalanced system. The modeling of unbalanced system will be addressed in Chapter 8.

For short-circuit studies, we use the bus voltage and the bus load active and reactive power consumption to calculate the load current. The load impedance model is given by the ratio of bus voltage and bus load current shown by Equation 4.38:

$$\begin{aligned} S &= V \cdot I^* \\ I &= (S/V)^* \\ Z_{Load} &= V/I \end{aligned} \tag{4.38}$$

The impedance diagram of Fig. 4.43 cannot be used for power flow studies because the bus voltages are unknown and the load impedance cannot be computed. However, for short-circuit studies, we are interested in the computation of fault currents. The internal impedance of generators, motors, and loads should be included in the power grid model because the internal impedance limits the fault current flow. For power flow studies, we need to represent the generators and load as injection power models.

Example 4.7 Consider the microgrid given in Fig. 4.44.

The impedances of the transmission line are given in Fig. 4.44.

The system data are:

PV generating station: 2 MW, 460 V DC, 7% reactance

Gas turbine generating station: 10 MVA, 3.2 kV, 10% reactance

Transformer T_1: 10 MVA, 460 V/13.2 kV, 7% reactance

Transformer T_2: 25 MVA, 13.2 kV/69 kV, 9% reactance

Transformer T_3: 20 MVA, 13.2 kV/3.2 kV, 8% reactance

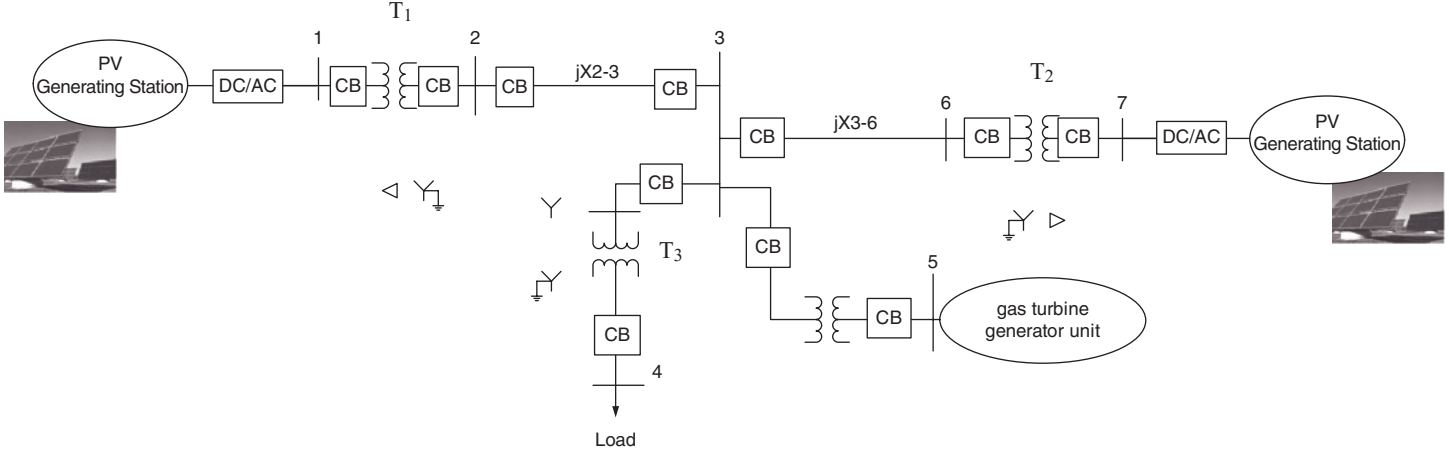

Figure 4.42 An Eight-Bus Power Grid System.

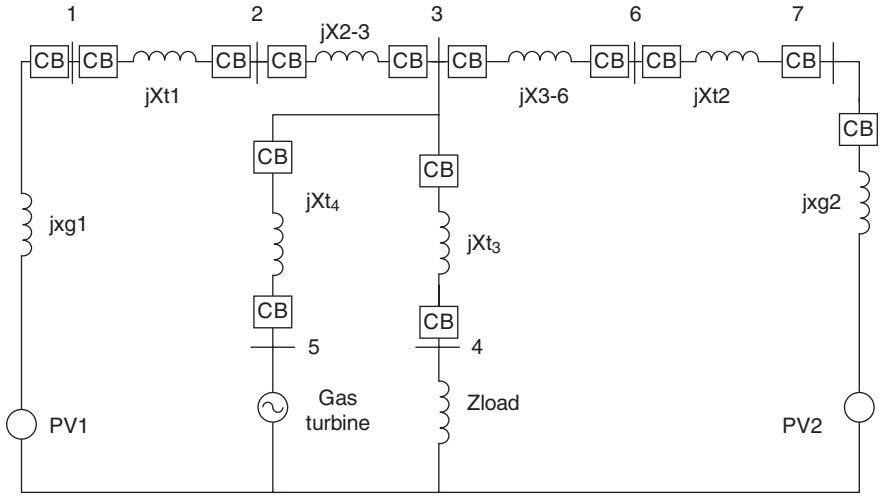

Figure 4.43 The Impedance Diagram of Figure 4.42.

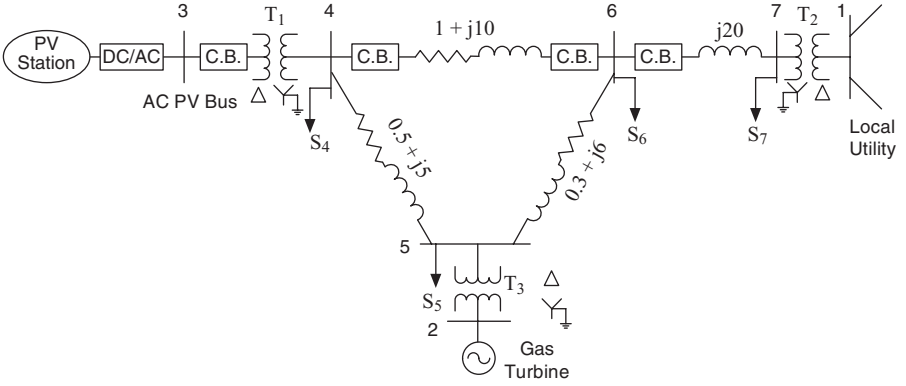

Figure 4.44 One-Line Diagram for Example 4.7.

Load S_4: 4 MW at 0.9 lagging power factor
Load S_5: 8 MW at 0.9 lagging power factor
Load S_6: 10 MVA at 0.9 leading power factor
Load S_7: 5 MVA at 0.85 lagging power factor

Assume the local power internal reactance is equal to 10 Ω and negligible internal resistance. Select the transformer T_2 rating as base.

Develop the following:

i) Per unit impedance model for power flow studies

ii) Per unit impedance model for short-circuit studies

Solution
Selecting the rating of transformer T_2 as base, the power base is

$$S_b = 25 \text{ MVA}$$

The voltage base on the PV generator side $V_b = 460$ V. Therefore, the voltage base on the transmission line side is $V_b = 13.2$ kV.

The base impedance is given by

$$Z_b = \frac{V_b^2}{S_b} = \frac{13.2^2}{25} = 6.97\ \Omega$$

i) The per unit impedance at a new base is given by

$$Z_{p.u.,new} = Z_{p.u.,old} \times \frac{S_{b,new}}{S_{b,old}} \times \left(\frac{V_{b,old}}{V_{b,new}} \right)^2$$

Hence, the new per unit impedance of transformer T_1 is

$$\mathcal{Z}_{3-4} = jX_{pu} = j0.07 \times \frac{25}{10} \times \left(\frac{13.2}{13.2} \right)^2$$
$$= j0.175 \text{ p.u } \Omega$$

Because the ratings of transformer T_2 is chosen as base, its p.u impedance remains at

$$\mathcal{Z}_{1-7} = j0.09 \text{ p.u } \Omega$$

Hence, the new p.u impedance of transformer T_3 is

$$\mathcal{Z}_{2-5} = jX_{pu} = j0.08 \times \frac{25}{20} \times \left(\frac{13.2}{13.2} \right)^2$$
$$= j0.1 \text{ p.u } \Omega$$

Table 4.3 gives the values of per unit impedances of the transformers.

TABLE 4.3 Per Unit Impedance of the Transformers.

Transformer	Impedance	Per Unit Impedance
1	$\mathcal{Z}_{3\text{-}4}$	$j0.175$
2	$\mathcal{Z}_{1\text{-}7}$	$j0.09$
3	$\mathcal{Z}_{2\text{-}5}$	$j0.1$

TABLE 4.4 Per Unit Impedance of the Transmission Lines.

Line	Impedance (Ω)	Per Unit Impedance
4-5	$\mathcal{Z}_{4-5} = 0.5 + j5$	$0.072 + j717$
4-6	$\mathcal{Z}_{4-6} = 1 + j10$	$0.143 + j1.434$
5-6	$\mathcal{Z}_{5-6} = 0.3 + j6$	$0.043 + j0.861$

TABLE 4.5 Per Unit Loads.

Bus	Load (MVA)	Per Unit Load
4	$S_4 = -4 - j1.94$	$-0.16 - j0.078$
5	$S_5 = -8 - j3.87$	$-0.32 - j0.155$
6	$S_6 = -10 + j4.84$	$-0.40 + j0.194$
7	$S_7 = -5 - j3.10$	$-0.20 - j0.124$

The per unit values of the line impedances is given by

$$Z_{pu} = \frac{Z}{Z_b}$$

Table 4.4 gives the values of per unit impedances of the transmission line.

The per unit loads of the system are given by

$$S_{pu} = \frac{S}{S_b}$$

Table 4.5 gives the values of per unit loads.

Figure 4.45 gives the per unit model of the system of Example 4.7 for power flow studies.

ii) For short-circuit studies, the internal impedances of the generators are also included in the model.

The p.u impedance of PV station at the new base is

$$\mathcal{Z}_{3'-3} = jX_{pu} = j0.07 \times \frac{25}{2} \times \left(\frac{13.2}{13.2}\right)^2$$
$$= j0.875 \text{ p.u } \Omega$$

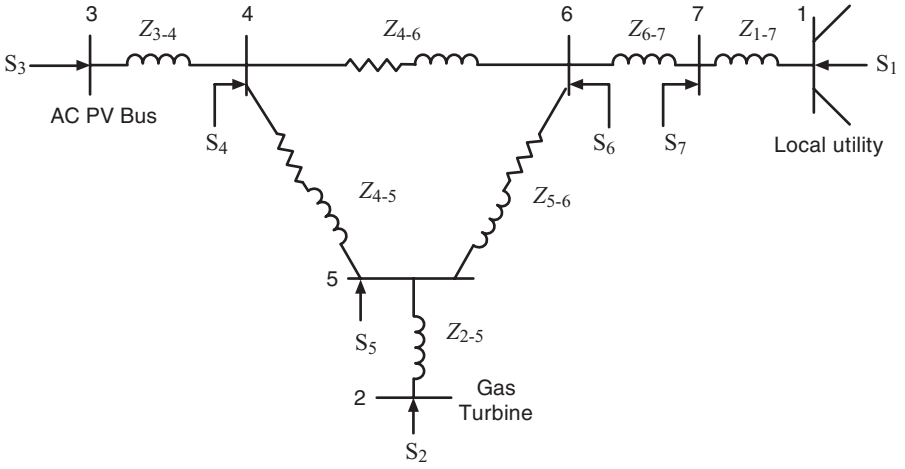

Figure 4.45 Model for Power Flow Studies.

TABLE 4.6 Per Unit Values of the Internal Impedance of the Generators.

Generator	Impedance	Per Unit Impedance
Local power grid	$\mathcal{Z}_{1\text{-}1}$	$j1.43$
Gas turbine	$\mathcal{Z}_{2\text{-}2}$	$j0.25$
PV	$\mathcal{Z}_{3\text{-}3}$	$j0.875$

The new p.u impedance of the gas turbine generator is

$$\mathcal{Z}_{2'-2} = jX_{pu} = j0.1 \times \frac{25}{10} \times \left(\frac{13.2}{13.2}\right)^2$$
$$= j0.25 \text{ p.u } \Omega$$

The new p.u impedance of the local power grid is

$$\mathcal{Z}_{1'-1} = Z_{pu} = \frac{Z}{Z_b} = \frac{j10}{6.97} = j1.43 \text{ p.u } \Omega$$

Table 4.6 gives the values of p.u internal impedances of the generators.

The p.u model for short-circuit studies is given in Fig. 4.47. The p.u impedance of transformers and the transmission lines are as given in Tables 4.3 and 4.4, respectively.

In this chapter, we have learned about the fundamental operation of a power grid and how to model the power grid for the analysis and design of a smart grid. We have also presented the important elements of a smart grid and

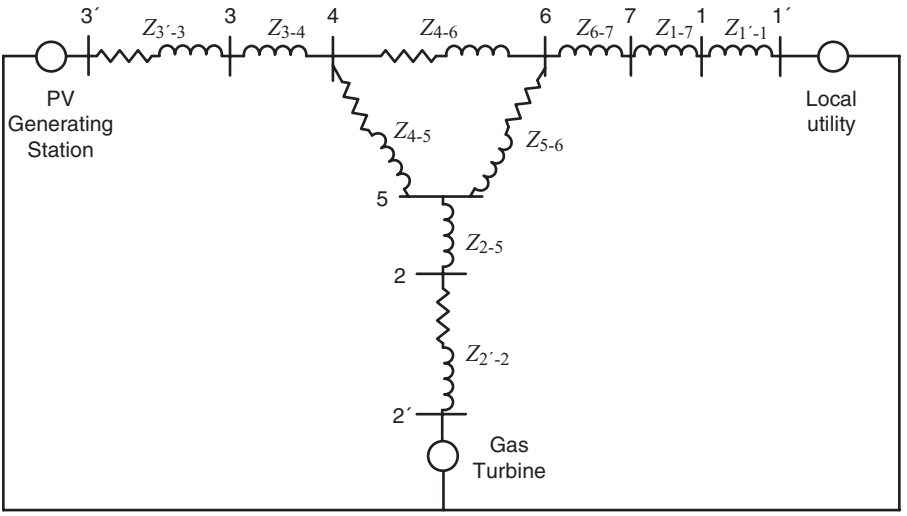

Figure 4.46 Model for Short-Circuit Studies.

load dynamics including how load variation during daily operation affects the price of electric energy. The importance of generator and motor internal impedance for limiting fault current power grid network was emphasized. Finally, the problems of power flow studies and short-circuit studies for design of a power grid were presented. In the following chapter, we will study the design of smart microgrid renewable energy systems.

PROBLEMS

4.1 A three-phase generator rated 440 V, 20 kVA is connected through a cable with impedance of 4 + j15 Ω to two loads:

a. A three-phase, Y-connected motor load rated 440 V, 8 kVA, p.f. of 0.9 lagging

b. A three-phase, Δ-connected motor load rated 440 V, 6 kVA, p.f. of 0.85 lagging

If the motor load voltage is to be 440 V, find the required generator voltage.

4.2 A generator is rated at 100 MVA, 20 kV, 60 Hz, 0.8 p.f. lagging and reactance of 10%. Compute the following:

i) The generator per unit model if it is loaded at 50%

ii) The generator per unit model if it is loaded at 100%

iii) The number of poles in the generators if the shaft power is supplied at 120 rpm

4.3 Develop a table showing the speed of magnetic field rotation in AC machines with two, four, and six poles operating at frequencies 50, 60, and 400 Hz.

4.4 A 20 MVA machine-rated 20 kV, three-phase, 60 Hz generator is supplying power to the local power grid at rated machine voltage. The machine is delivering the rate power to the local power grid. The machine synchronous reactance is equal to 8 Ω with negligible resistance. Compute the following:

i) The machine excitation voltage when the machine is operating at 0.85 lagging power factor

ii) The machine excitation voltage when the machine is operating at 0.85 leading power factor

iii) The machine excitation voltage when the machine is operating at unity power factor.

iv) The maximum power the machine can deliver for *i*, *ii*, and *iii*.

4.5 For Problem 4.4, assume the load is equal to 5000 W at unity p.f. Compute the p.u equivalent circuit. Assume S_b = 100 MV A, V_b = 345 kV.

4.6 A two-pole, Y-connected generator rated at 13.8 kV, 20 MVA, 0.8 p.f. leading is running at 1800 rpm. The generator has a synchronous reactance of 8 Ω per phase (at 60 Hz) and a negligible armature resistance per phase. The generator is operated in parallel with an interconnected power network.

i) What is the torque angle of the generator at rated conditions?

ii) What is the maximum power possible out of this generator?

4.7 A three-phase, eight pole, 220 MVA, 13.2 kV, 0.9 leading power factor, Y-connected synchronous generator is running at 1200 rpm. Its synchronous reactance is 0.8 Ω per phase at 60 Hz. The generator is fully loaded and supplies power to a network at rated voltage. Compute the generator voltage regulation.

4.8 The one-line diagram of a power grid is depicted by Fig. 4.47. The data for the system are as follows:

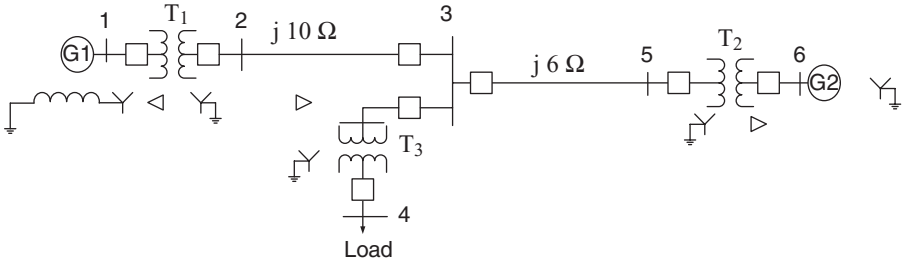

Figure 4.47 The System for Problem 4.8.

Transmission line between bus 2 and bus 3 is j10 Ω and between bus 3 and bus 5 is j6 Ω

G1 wind generating system	25 MVA, 13.2 kV, and reactance of 0.20 per unit
G2 gas turbine generating system	50 MVA, 20 kV, and reactance 0.20 per unit
Transformer $T_{.1}$	100 MVA, 220 Y/13.8 Δ kV, and reactance of 10%
Transformer T_2	200 MVA, 220/20 kV, and reactance of 10%
Transformer T_3	100 MVA, 220 Y/22Y kV, and reactance of 10%

Develop the following:

i) Per unit impedance model for short-circuit studies

ii) Per unit impedance model for power flow studies

4.9 The one-line diagram of a power grid is depicted by Fig. 4.48. The data for the grid are given in the figure.
Assume an MVA base of 100 and base voltage of 13.2 kV; also assume the input reactance of local power grid is 10% based on the transformer T_1. The input reactance of all the sources is 7% with a base same as their rating.
The system data are

Transformer T_1: 20 MVA, 33 /13.2 kV, and 10% reactance

Transformer T_2: 20 MVA, 13.2 / 3.3 kV, and 12% reactance

Transformer T_3: 5 MVA, 3.3 / 460 V, and 6.5% reactance

Transformer T_4, T_5, and T_6: 2 MVA, 3.3 / 460 V, and 6.5% reactance

Transformer T_7: 5 MVA, 3.3 / 460 V, and 6% reactance

Transmission line impedance is given in Table 4.7.

The local loads are 1 MVA at 0.85 power factor lagging.

Develop the following:

i) Per unit model for power flow studies

ii) Per unit model for short-circuit studies

TABLE 4.7 Transmission Line Data for Problem 4.9.

Line	Resistance (Ω)	Series Reactance (Ω)
8–9	0.05	0.5
9–10	0.04	0.4
9–11	0.04	0.51
11–12	0.04	0.5
11–13	0.01	0.12
13–14	0.03	0.32
14–15	0.04	0.45

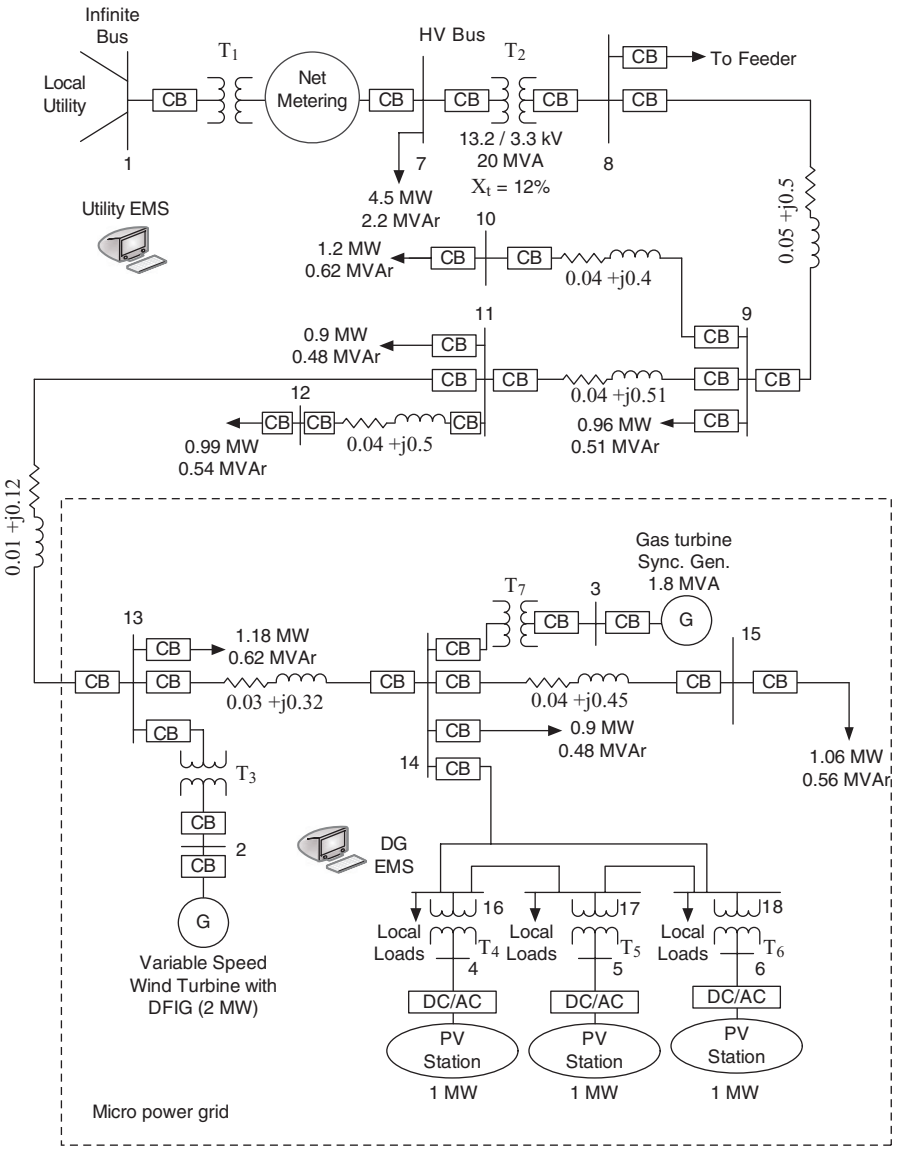

Figure 4.48 The System for Problem 4.9.

4.10 Consider the microgrid given in Fig. 4.49.
Assume the following data:

a. Transformers connected to the PV-generating station are rated at 460 V Y-grounded/13.2 kV Δ, have 10% reactance, and 10 MVA capacity. The transformer connected to the power grid is 13.2 / 63 kV, 10 MVA, 10% reactance.

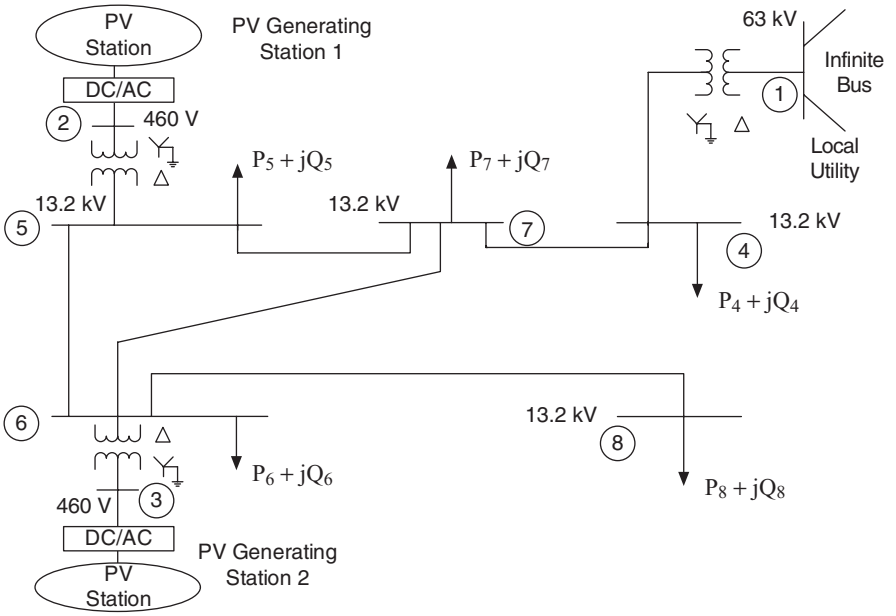

Figure 4.49 Photovoltaic (PV) Microgrid of Problem 4.10.

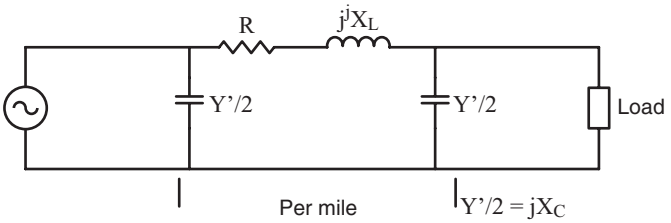

Figure 4.50 A Transmission Line Pie Model.

b. Assume the load on bus 4 is 1.5 MW at a power factor of 0.9 lagging, on bus 5 is 2.5 MW at a power factor of 0.9 lagging, on bus 6 is 1.0 MW at a power factor of 0.95 lagging, on bus 7 is 2 MW at a power factor of 0.95 leading, and on bus 8 is 1.0 MW and a power factor of 0.9 lagging.

c. Transmission line has a resistance of 0.0685 Ω/mile, reactance of 0.40 Ω/mile and half of line charging admittance (Y′/2) of $11 \times 10^{-6}\ \Omega^{-1}$/mile. The line 4–7 is 5 miles, 5–6 is 3 miles, 5–7 is 2 miles, 6–7 is 2 miles, and 6–8 is 4 miles long. The transmission line model is given by Fig. 4.50.

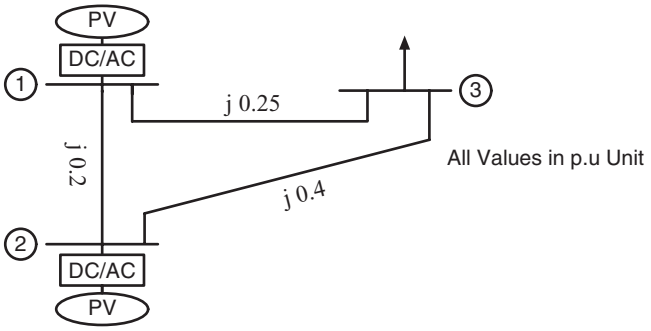

Figure 4.51 A One-Line Diagram of Problem 4.11.

d. Assume a PV-generating station 1 is rated at 0.75 MW and PV-generating station 2 is rated at 3 MW. Assume PV-generating stations are operating at unity power factors.
e. Assume S_{base} of 10 MVA and a voltage base of 460 V in PV generator number. Assume the local power grid bus voltage has 5% tolerance.

Develop the following:

i) Per unit model for power flow studies
ii) Per unit model for short-circuit studies

4.11 Consider the PV power grid given by Fig. 4.51 below. The PV_1 has an internal reactance of 0.8 p.u and injects one per unit power into the grid; PV_2 has an internal impedance of 0.4 p.u and injects 0.5 p.u power into the grid. The load is one p.u active and one p.u reactive power.
Develop the following:

i) Per unit model for short-circuit studies
ii) Per unit model for power flow studies

4.12 Compute the load factor for a feeder assuming that the maximum load is 8 MW and the average power is 6 MW.

4.13 Compute the load factor for a feeder for daily operation for one month assuming the same daily profile. Assume the average power is 170 MW and the peak is 240 MW.

4.14 If the feeder of Example 4.13 is supplied from a wind source rated 80 MW and central power-generating station rated 500 MW, assume the capital cost of wind power is $500 per KW and the central station $100 per KW. Compute the EUC if the maintenance cost for the wind source is free, except maintenance is 1 cent per kWh and the central power-generating station fuel and maintenance cost is 3.2 cents per kWh. Give a figure for EUC from zero load factors to unity over 5 year's utilization.

4.15 If the feeder of Example 4.13 is supplied from 10 fuel cell sources rated for a total of 2 MW and 20 microturbines rated for total of 6 MW, assume the capital cost of fuel cell is $1000 per kW and microturbine is $200 per kW. Compute the fuel source EUC if the variable cost for the fuel cell is 15 cents per kWh and the microturbine is 2.2 cents per kWh, assume 5 years of operation. Show EUC as a function of time from zero load factors to unity in a figure.

REFERENCES

1. Institute for Electric Energy. Homepage. Available at http://www.edisonfoundation.net/IEE. Accessed 2010 Oct 7.
2. MISO-MAPP Tariff Administration. Transition guide. Available at http://toinfo.oasis.mapp.org/oasisinfo/MMTA_Transition_Plan_V2_3.pdf. Accessed 2010 Jan 12.
3. Energy Information Administration. Official Energy Statistics from the US Government. Available at http://www.eia.doe.gov. Accessed 2010 Oct 29.
4. Carbon dioxide Information Analysis Center. Frequently asked global change questions. Available at http://www.cdiac.ornl.gov/pns/faq.html. Accessed 2009 Sept 29.
5. Shahidehpour M, Yamin H. Market operations in electric power systems: forecasting, scheduling, and risk management. New York/Piscataway, NJ: Wiley/IEEE; 2002.
6. Hirst E, Kirby B. Technical and market issues for operating reserves. Available at http://www.ornl.gov/sci/btc/apps/Restructuring/Operating_Reserves.pdf. Accessed 2009 Jan 10.
7. Keyhani A, Miri SM. On-line weather-sensitive and industrial group bus load forecasting for microprocessor-based applications. IEEE Transactions on Power Apparatus and Systems 1983; 102(12):3868–3876.
8. Schweppe, FC. Power systems 2000: hierarchical control strategies. IEEE Spectrum, 1978; 15(7): 42–47.
9. North American Electric Reliability Council. NERC 2008 Long Term Reliability Assessment 2008–2017. Available at http://www.nerc.com/files/LTRA2008.pdf. Accessed 2010 Oct 8.
10. Wood AJ, Wollenberg, BF. Power generation, operation, and control. New York: Wiley; 1996.
11. Babcock & Wilcox Company. Steam its generation & use. 38th ed. Charlotte, NC: Babcock & Wilcox; 1975.
12. Nourai A, Schafer C. Changing the electricity game. IEEE Power and Energy Magazine 2009; 7(4):42–47.
13. Ko WH, Fung CD. VLSI and intelligent transducers. Sensors and Actuators 1982; 2:239–250.
14. De Almeida AT, Vine, EL. Advanced monitoring technologies for the evaluation of demand-side management programs. IEEE Transactions on Power Systems 1994; 9(3):1691–1697.

15. Adamiak M. Phasor measurement overview. Available at http://phasors.pnl.gov/Meetings/2004%20January/Phasor%20Measurement%20Overview.pdf. Accessed 2010 Oct 24.
16. Phadke, AG. Computer applications in power. IEEE Power & Energy Society 1993; 1(2):10–15.
17. Schweppe FC, Wildes J. Power system static-state estimation, part I: exact model power apparatus and systems. IEEE Transactions on Volume 1970; PAS-89(1): 120–125.
18. Ducey R, Chapman R, Edwards S. The U. S. Army Yuma Proving Ground 900-kVA Photovoltaic Power Station. Available at http://photovoltaics.sandia.gov/docs/PDF/YUMADOC.PDF. Accessed 2010 Oct 10.
19. Grainger J, Stevenson WD. Power systems analysis. New York: McGraw Hill; 2008.
20. Gross AC. Power system analysis. New York: Wiley; 1986.
21. Keyhani A, Marwali M, Dai M. Integration of green and renewable energy in electric power systems. Hoboken, NJ: Wiley; 2010.
22. Majmudar H. Electromechanical energy converters. Boston: Allyn and Bacon; 1965.

ADDITIONAL RESOURCES

Anderson PM, Fouad AA. Power system control and stability. 1st ed. Ames, IA: Iowa State University Press; 1977.

Anderson R, Boulanger A, Johnson JA, Kressner A. Computer-aided load management for the energy industry. Tulsa, OK: Pennwell; 2008. p 333.

Berger AW, Schweppe FC. Real time pricing to assist in load frequency control. IEEE Transactions on Power Systems 1989; 4(3):920–926.

Bohn R, Caramanis M, Schweppe F. Optimal pricing in electrical networks over space and time. Rand Journal on Economics 1984; 18(3):360–376.

Caramanis M, Bohn R, Schweppe F, Optimal spot pricing: practice & theory. IEEE Transactions on Power Apparatus and Systems 1982; PAS-101(9):3234–3245.

Chapman S. Electric machinery and power system fundamentals. New York: McGraw Hill; 2003.

Dowell LJ, Drozda M, Henderson DB, Loose VW, Marathe MV, Roberts, DJ. ELISIMS: comprehensive detailed simulation of the electric power industry. Available from: Los Alamos National Laboratory, Los Alamos, NM; Tech. Rep. No. LA-UR-98-1739.

Electricity Storage Association. Technologies & Applications: Flywheels. Available at http://electricitystorage.org/tech/technologies_technologies_flywheels.htm. Accessed 2010. Oct 10.

Elgerd OI. Electric energy system theory: an introduction. 2d ed. New York: McGraw-Hill; 1982.

El-Hawary, ME. Electric power systems: design and analysis. Reston, VA: Reston Publishing; 1983.

IEEE Brown Book. IEEE recommended practice for power system analysis. New York: Wiley-Interscience; 1980.

Institute of Electrical and Electronics Engineers, Inc. IEEE Std 1451.1-1999, standard for a smart transducer interface for sensors and actuators–network capable application processor (NCAP) Information Model. Piscataway, NJ: IEEE; 1999.

Masters GM. Renewable and efficient electric power systems. New York: Wiley; 2004.

Nourai A. Large-scale electricity storage technologies for energy management. In: Proceedings of the Power Engineering Society Summer Meeting, Vol. 1; July 25, 2002; Chicago, IL. Piscataway, NJ: IEEE; 2002. p 310–315.

Schweppe F, Caramanis M, Tabors R, Bohn R. Spot pricing of electricity. Alphen aan den Rijn, the Netherlands: Kluwer; 1988.

Schweppe F, Tabors R, Kirtley J, Outhred H, Pickel F, Cox A. Homeostatic utility control. IEEE Transactions on Power Applications and Systems 1980; PAS-99(3): 1151–1163.

CHAPTER 5

MICROGRID SOLAR ENERGY SYSTEMS

5.1 INTRODUCTION

From the beginning of recorded history, humans have worshipped the sun. The first king of Egypt was Ra, the sun god. The sun god of justice for Mesopotamia was Shamash. In Hinduism, the sun god, Surya, is believed to be the progenitor of mankind. Apollo and Helios were the two sun divinities of Ancient Greece. The sun also figured prominently in the religious traditions of Zoroastrianism (Iran) and Buddhism (Asia), as well as in the Aztec (Mexico) and Inca (Peru) cultures.[1]

The sun's energy is the primary source of energy for life on our planet. When the sun disappears from our universe, we will cease to exist.[2] Solar energy is a readily available renewable energy; it reaches earth in the form of electromagnetic waves (radiation). Many factors affect the amount of radiation received at a given location on earth. These factors include location, season, humidity, temperature, air mass, and the hour of day. *Insolation* refers to exposure to the rays of the sun, i.e., the word insolation has been used to denote the solar radiation energy received at a given location at a given time. The phrase *incident solar radiation* is also used; it expresses the average irradiance in watts per square meter (W/m^2) or kilowatt per square meter (kW/m^2).

The surface of the earth is coordinated with imaginary lines of latitude and longitude as shown in Fig. 5.1(a). Latitudes on the surface of the earth are

Design of Smart Power Grid Renewable Energy Systems, First Edition. Ali Keyhani.

imaginary parallel lines measured in degrees. The lines subtend to the plane of the equator. The latitudes vary from 90° south (S) and 90° north (N). The longitudes are imaginary lines that vary from 180° east (E) to 180° west (W). The longitudes converge at the poles (90° north and 90° south). The radiation of the sun on the earth varies with the location based on the latitudes. Approximately, the region between 30° S and 30° N has the highest irradiance as depicted in Fig. 5.1. The latitude on which the sun shines directly overhead between these two latitudes depends on the time of the year. If the sun lies directly above the northern hemisphere, it is summer in the north and winter in the southern hemisphere. If it is above the southern hemisphere, it is summer in the southern hemisphere and winter in the north.

Figure 5.1(b) is a plot showing the irradiance at different locations on the earth marked by its latitude and longitude. The latitude varies from –90° to 90°, which is 90° N and 90° S, respectively. Similarly, the longitudes vary from –180° to 180°, which is 180° W and 180° E, respectively. The z-axis of the plot gives the irradiance in kWh/m^2. The points on the z-axis convey the amount of irradiance. The colors on the plot represent the intensity of the irradiance as given in Fig. 5.1(b).

The sun's position as seen from earth between latitudes 15°N and 35°N is the region with the most solar energy. This semiarid region, as shown in Fig. 5.1(b) and Fig. 5.1(c), is mostly located in Africa, the Western United States, the Middle East, and India. These locations have over 3,000 hours of intense sunlight radiation per year. The region with the second largest amount of solar energy radiation lies between 15°N latitude and the equator and has approximately 2,500 hours of solar energy per year. The belt between latitude 35°N and 45°N has limited solar energy. However, typical sunlight radiation is roughly about the same as the other two regions, although there are clear seasonal differences in both solar intensity and daily hours. As winter approaches, the solar radiation decreases; by midwinter, it is at its lowest level. The 45°N latitude and the region beyond experience approximately half of the solar radiation as diffused radiation. The energy of sunlight received by the earth can be approximated to equal 10,000 times the world's energy requirements.[3]

The sun's radiation is in the form of ultraviolet, visible, and infrared energy as depicted in Fig. 5.2. The majority of the energy is in the form of a short wave that is used in the planet's heat cycle, weather cycle, wind, and waves. A small fraction of the energy is utilized for photosynthesis in plants and the rest of the solar energy is emitted back into space.

The solar energy reaching the atmosphere is constant; hence the term *solar constant*. The solar constant is computed to be in the range of 1.4 kW/m^2, or 2.0 $cal/cm^2/min$. Sunlight's shorter wavelengths scatter over a wider area than the longer wavelengths of light. The scattering may be due to gas molecules, pollution, and haze. The blue and violet light have the maximum atmospheric scattering at sunrise and sunset without affecting the red rays of sunlight.

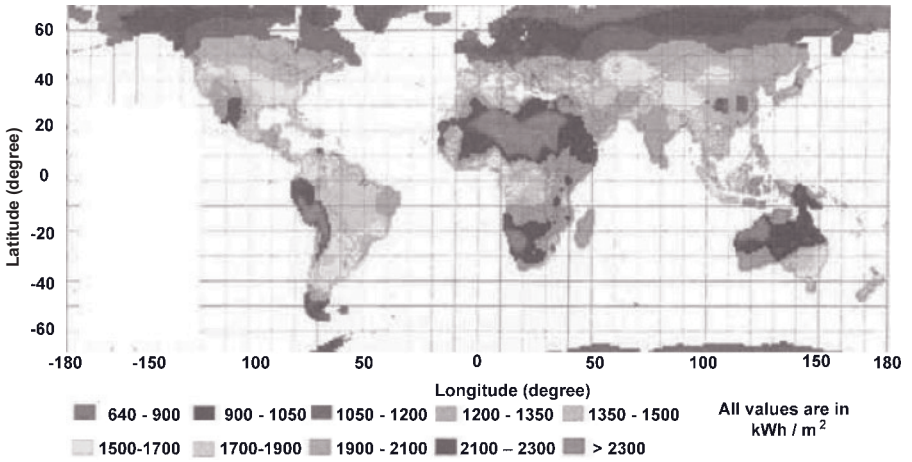
Latitude (degree)
60
40
20
0
-20
-40
-60
-180
-150
100
50
0
50
100
150
180
Longitude (degree)
640 - 900
900 - 1050
1050 - 1200
1200 - 1350
1350 - 1500
1500-1700
1700-1900
1900 - 2100
2100 – 2300
> 2300
All values are in kWh / m 2

(a)

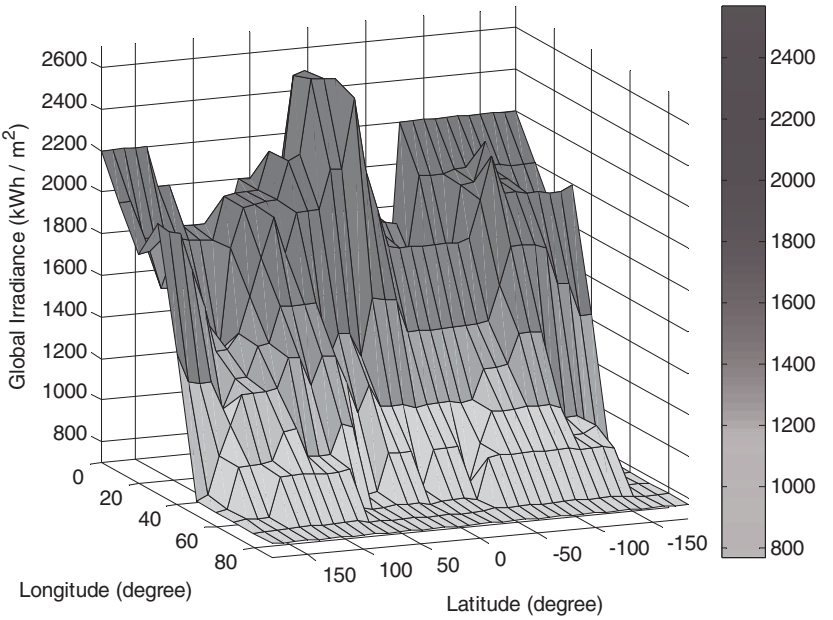
Global Irradiance (kWh / m2)
2600
2400
2200
2000
1800
1600
1400
1200
1000
800
0
20
40
60
80
Longitude (degree)
150
100
50
0
-50
-100
-150
Latitude (degree)
2400
2200
2000
1800
1600
1400
1200
1000
800

(b)

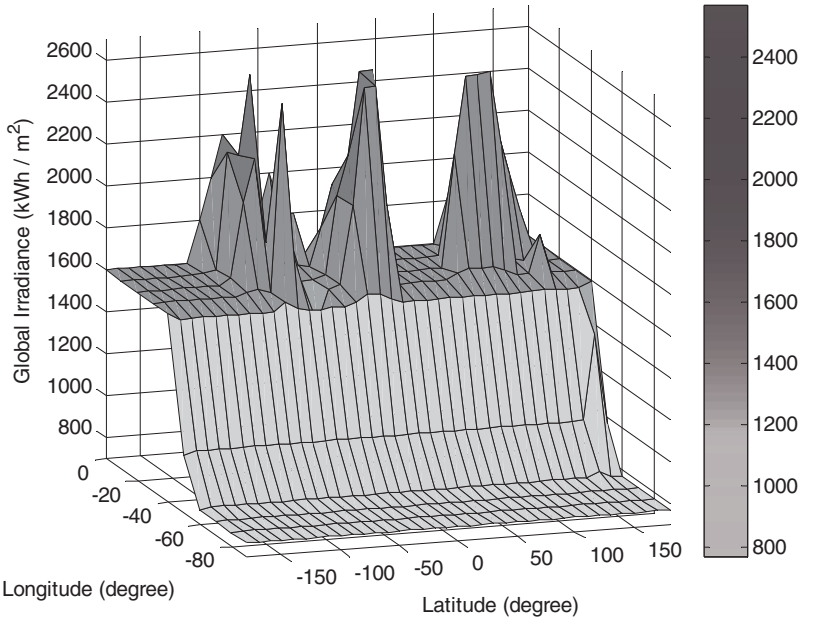

(c)

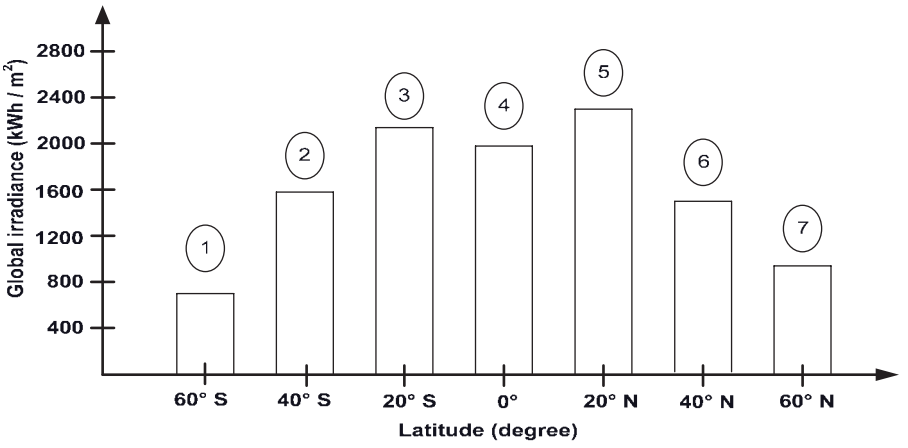

(d)

Figure 5.1 **(a)** The Global Irradiation Values for the World (kWh/m^2).[2,3] **(b)** The Average Northern Hemisphere Global Irradiation Source by Longitude and Latitude.[4,9] **(c)** The Average Southern Hemisphere Global Irradiation Source by Longitude and Latitude. **(d)** The Average World Global Irradiation Source by Regions.[4,9] Region 1: Argentina, Chile; Region 2: Argentina, Chile; Region 3: Brazil, South Africa, Peru, Australia, Mozambique; Region 4: Indonesia, Brazil, Nigeria, Columbia, Kenya, Malaysia; Region 5: India, Pakistan, Bangladesh, Mexico, Egypt, Turkey, Iran, Algeria, Iraq, Saudi Arabia; Region 6: China, United States, Japan, Germany, France, United Kingdom, South Korea; Region 7: Russia, Canada, Sweden, Norway.

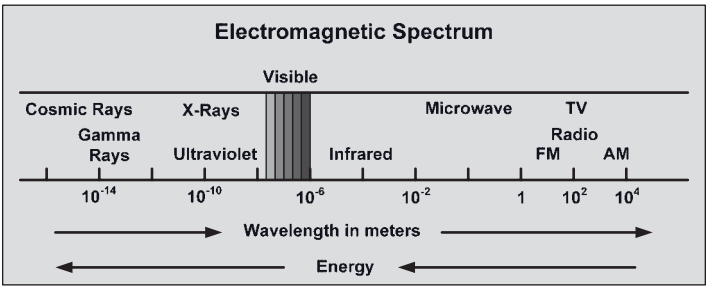

Figure 5.2 The Electromagnetic Spectrum.[1,2]

5.2 THE SOLAR ENERGY CONVERSION PROCESS: THERMAL POWER PLANTS

Auguste Mouchout constructed a parabolic mirror to channel the sun's energy to power a steam engine in 1866.[5] Todays' thermal solar electric power plant also uses the sun's heat energy to generate steam power for running the turbines.

Concentrating solar power (CSP) systems have locating lenses designed for concentrating the sunlight into the receiver, which acts as a boiler to generate steam. The system uses a tracking control system for maximum efficiency. A number of concentrating technologies exists; a parabolic mirror that uses materials that are silver-based or of polished aluminum is often used. Figure 5.3 depicts the CSP system located in the Mojave Desert in California, which uses a parabolic mirror.

Solar power towers (see Fig. 5.4) generate steam power by creating intense concentrated solar energy that is directed via a tower heat processing system.[2] The system uses a large number of sun-tracking mirrors, or parabolic reflectors. The number of mirrors depends on the system capacity. Another type of mirror used is called a heliostat (from *Helios*, the Greek word for sun). Earlier power towers used water/steam as the heat-transfer fluid. More recent advanced designs have used molten nitrate salt.

A French physicist, Augustin-Jean Fresnel (1788–1827),[7] developed the Fresnel lens, which has a large aperture and short focal length. Its construction requires less material than a conventional lens, and it allows for more light to pass through.

The compact linear Fresnel reflector (CLFR) is used in solar power plants. The CLFR system uses Fresnel lens and reflectors that are located on a single axis to concentrate the solar energy to generate steam. The CLFR uses a number of thin mirror strips to focus high-intensity sunlight into a heat-processing system. Flat mirrors are much cheaper to produce than parabolic ones and they facilitate a greater number of reflectors for use in steam generation. Figure 5.5 depicts a CLFR power generating station.

Figure 5.3 The Concentrated Parabolic Trough Solar Power System.[6] (Photo courtesy of the California Energy Commission)

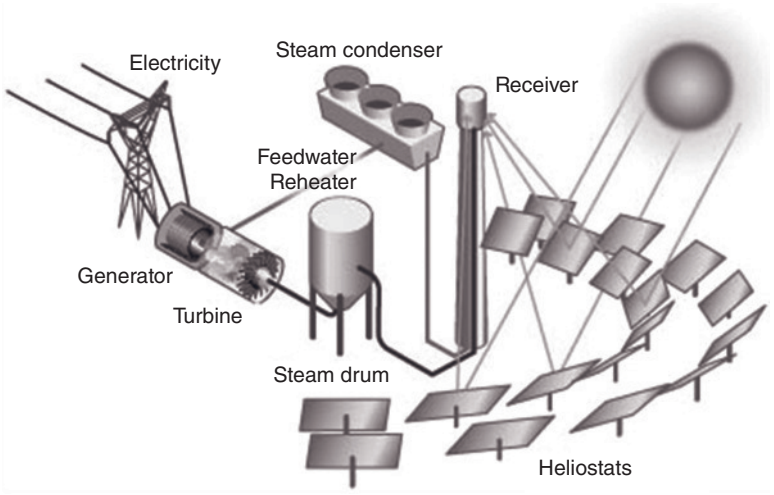

Figure 5.4 A Steam Solar Power Generating Station.[1]

Another type of solar heat engine is the Stirling engine.[1] It operates by cyclic compression with expansion of the working fluid such as air or other gas. It uses two different temperature levels in its thermodynamic process converting heat energy into mechanical work. The Stirling solar dish engine system is an active area of research.[4]

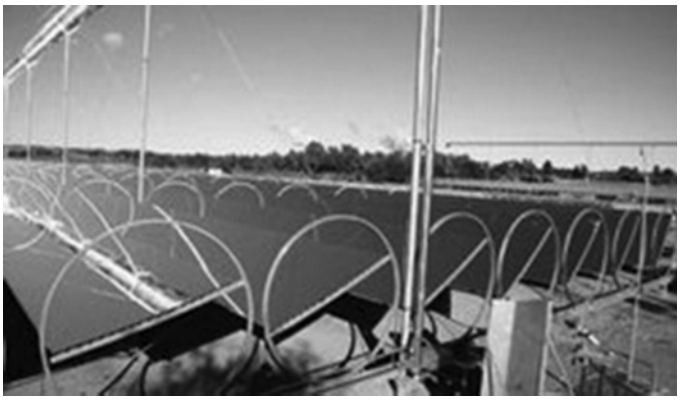

Figure 5.5 A Linear Fresnel Reflector (CLFR) Concentrating Solar Power (CSP) Technology.[2]

5.3 PHOTOVOLTAIC POWER CONVERSION

Solar cells convert the radiation energy directly to electric energy. Solar cells, also called photovoltaic (PV) cells, were developed by Carlson and Wronski in 1976.[8] A PV module consists of a number of PV cells. When sunlight strikes the PV cell, electrons are freed from their atoms. The freed electrons are directed toward the front surface of the solar cell. This process creates a current flow that occurs between the negative and positive sides. The PV photon cell charge offers a voltage of 1.1 up to 1.75 electron volt[2] (eV^2) with a high optical absorption. Figure 5.6 depicts a solar cell structure.[2]

Figure 5.6 depicts a photovoltaic (PV) cell structure. A photovoltaic (PV) module connects a number cell of PV cells in series. You may think of a PV cell as a number of capacitors that are charged by photon energy of light. Figure 5.7 depicts how the irradiance energy of the sun is converted to electric energy using PV cells.

5.4 PHOTOVOLTAIC MATERIALS

The manufacture of PV cells is based on two different types of material: (1) a semiconductor material that absorbs light and converts it into electron–hole pairs, and (2) a semiconductor material with junctions that separate photo-generated carriers into electrons and electron holes. The contacts on the front and back of the cells allow the current to the external circuit. Crystalline silicon cells (c-Si) are used for absorbing light energy in most semiconductors used in solar cells. Crystalline silicon cells are poor absorbers of light energy[6]; they have an efficiency in the range of 11 to 18% of that of solar cells. The most-efficient monocrystalline c-Si cell uses laser-grooved, buried grid contacts, which allow for maximum light absorption and current collection.[6] Each

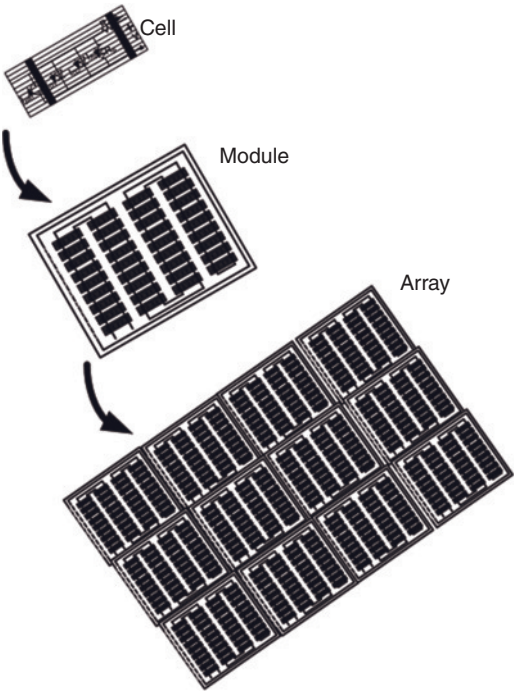

Figure 5.6 A Solar Cell or Photovoltaic Cell Structure.[9]

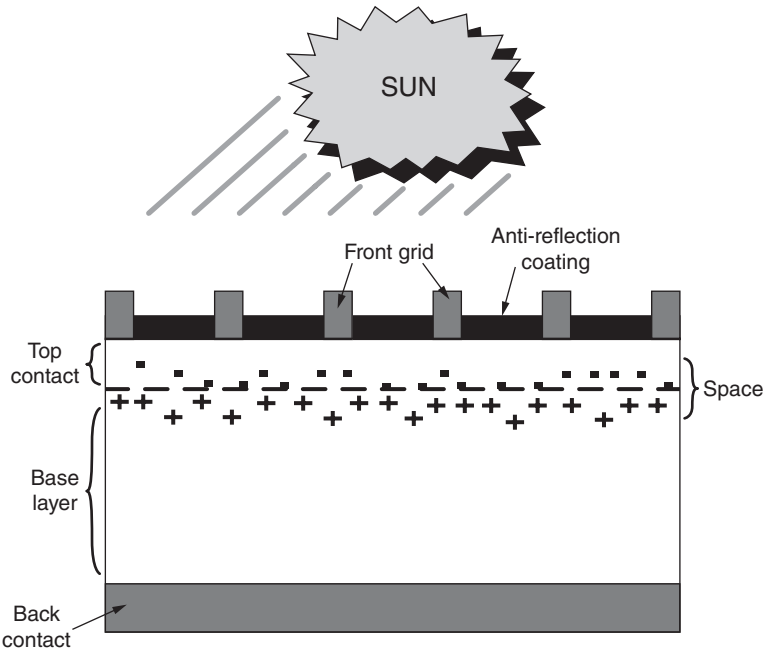

Figure 5.7 The Structure of a Photovoltaic Cell.[2]

of the c-Si cells produces approximately 0.5 V. When 36 cells are connected in series, it creates an 18 volt module. In the thin-film solar cell, the crystalline silicon wafer has a very high cost. Other common materials are amorphous silicon (a-Si), and cadmium telluride and gallium, which are another class of polycrystalline materials.[6] The thin-film solar cell technology uses a-Si and a p-i-n single-sequence layer, where "p" is for positive and "n" for negative, and "i" for the interface of a corresponding p- and n-type semiconductor.[10] Thin-film solar cells are constructed using lamination techniques, which promote their use under harsh weather conditions: they are environmentally robust modules. Due to the basic properties of c-Si devices, they may stay as the dominant PV technology for years to come. However, thin-film technologies are making rapid progress and a new material or process may replace the use of c-Si cells.[8]

Here we briefly introduce PV technology as it exists today. But as an evolving technology, students and engineers should recognize that these advances will come from basic research in material engineering and read the *IEEE Spectrum* to keep up with the developments in PV technology. Below we continue our discussion on how to develop models to study the integration of PV sources into the smart power grid system.

5.5 PHOTOVOLTAIC CHARACTERISTICS

As sun irradiance energy is captured by a PV module, the open-circuit voltage of the module increases.[1,4] This point is shown in Fig. 5.8 by V_{oc} with

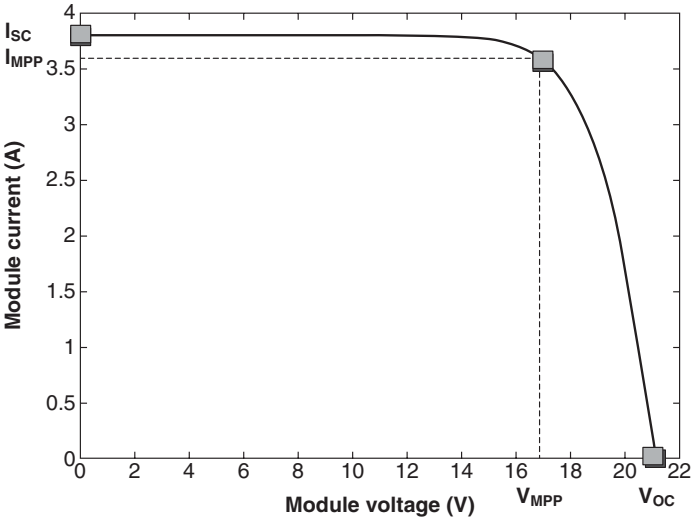

Figure 5.8 The Operating Characteristics of a Photovoltaic Module.[9]

TABLE 5.1 Voltage and Current Characteristics of Typical Photovoltaic Modules.

Module	Type 1	Type 2	Type 3	Type 4
Power (Max), W	190	200	170	87
Voltage at maximum power point (MPP), V	54.8	26.3	28.7	17.4
Current at MPP, A	3.47	7.6	5.93	5.02
V_{OC} (open-circuit voltage), V	67.5	32.9	35.8	21.7
I_{SC} (short-circuit current), A	3.75	8.1	6.62	5.34
Efficiency	16.40%	13.10%	16.80%	>16%
Cost	$870.00	$695.00	$550.00	$397.00
Width	34.6″	38.6″	38.3″	25.7″
Length	51.9″	58.5″	63.8″	39.6″
Thickness	1.8″	1.4″	1.56″	2.3″
Weight	33.07 lbs	39 lbs	40.7 lbs	18.3 lbs

TABLE 5.2 Cell Temperature Characteristics of a Typical Photovoltaic Module.

Typical Cell Temperature Coefficient		
Power	$T_k(P_p)$	–0.47%/°C
Open-circuit voltage	$T_k(V_{oc})$	–0.38%/°C
Short-circuit current	$T_k(I_{sc})$	0.1%/°C

TABLE 5.3 Maximum Operating Characteristics of a Typical Photovoltaic Module.

Limits	
Maximum system voltage	600 V DC
Operating module temperature	–40°C to 90°C
Equivalent wind resistance	Wind speed: 120 mph

zero-input current. If the module is short-circuited, the maximum short-circuit current can be measured. This point is shown in Fig. 5.8 by I_{SC} with zero-output voltage. The point on the I versus V characteristic where maximum power (P_{MPP}) can be extracted lies at a current I_{MPP} and the corresponding voltage point, V_{MPP}. Typical data for a number of PV modules are given in Table 5.1. This information is used to design PV strings and PV-generating power sources.

PV module selection criteria are based on a number of factors[11]: (1) the performance warranty, (2) module replacement ease, and (3) compliance with natural electrical and building codes. A typical silicon module has a power of 300 W with 2.43 m^2 surface area; a typical thin film has a power of 69.3 W with

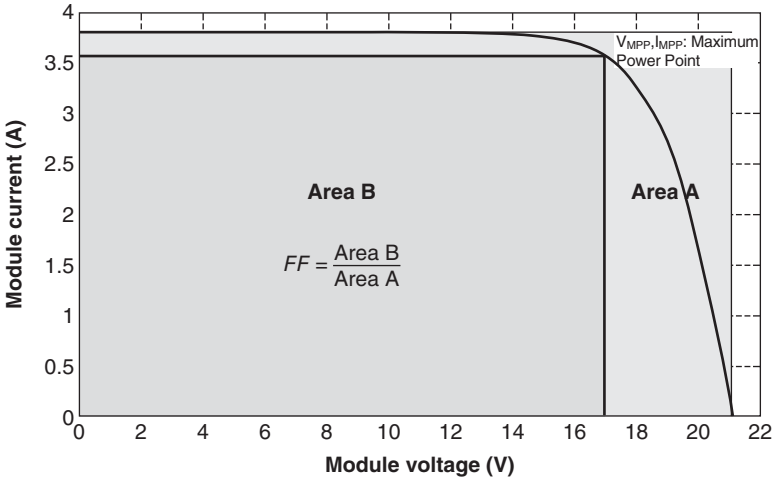

Figure 5.9 Photovoltaic Module Fill Factor.

an area of 0.72 m^2. Hence, the land required by a silicon module is almost 35% less. Typical electrical data apply to standard test considerations (STC). For example, under STC, the irradiance is defined for a module with a typical value such as 1000 W/m^2, spectrum air mass (AM) 1.5, and a cell temperature of 25°C.

The PV fill factor (*FF*), as shown in Fig. 5.9, is defined as a measure of how much solar energy is captured. This term is defined by PV module open circuit voltage (V_{oc}), and PV module short-circuit current (I_{sc}).

$$FF = \frac{V_{MPP} I_{MPP}}{V_{OC} I_{SC}} \tag{5.1}$$

And

$$P_{\max} = FF \cdot V_{OC} I_{SC} = V_{MPP} I_{MPP} \tag{5.2}$$

As seen in Fig. 5.9, the maximum value for FF is unity. However, this value can never be attained. Some PV modules have a high fill factor. In the design of PV system a PV module with a high FF would be used. For high-quality PV modules, FFs can be over 0.85. For typical commercial PV modules, the value lies around 0.60. Figure 5.10 depicts a three-dimensional display of a typical PV module and the fixed irradiance energy received by the module. As shown, a typical PV module characteristic is not only a function of irradiance energy, but it is also a function of temperature.

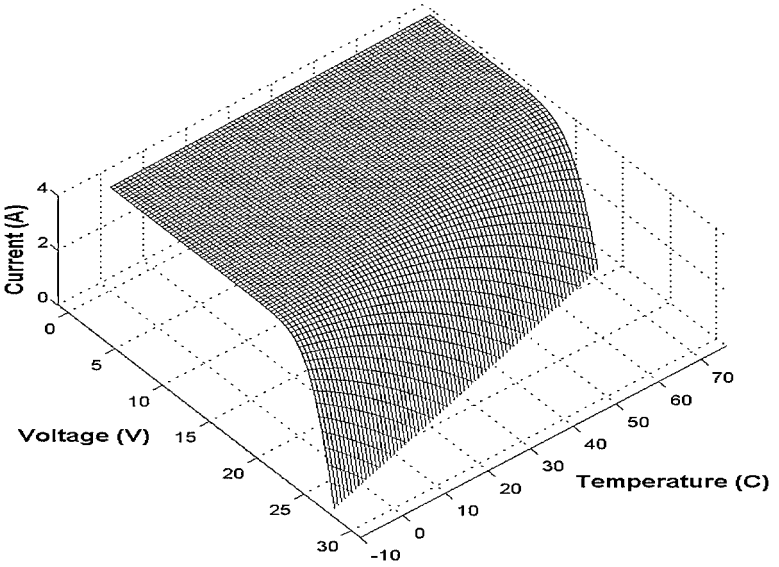

Figure 5.10 Three-Dimensional I–V Curve and Temperature for a Typical Photovoltaic Module.

5.6 PHOTOVOLTAIC EFFICIENCY

The PV module efficiency, η is defined as:

$$\eta = \frac{V_{MPP} I_{MPP}}{P_S} \tag{5.3}$$

where $V_{MPP} I_{MPP}$ is the maximum power output, P_{mpp} and P_S is the surface area of the module. The PV efficiency can be also defined as:

$$\eta = FF \cdot \frac{V_{OC} I_{SC}}{\int_0^{\infty} P(\lambda) \cdot d\lambda} \tag{5.4}$$

where $P(\lambda)$ is the solar power density at wavelength λ.

Figure 5.11 depicts a PV module consisting of 36 PV cells. If each cell is rated at 1.5 V, the module rated voltage is 54 V.

A string is designed by connecting a number of PV modules in series. A number of strings connected in parallel make an array. Two general designs of PV systems can be envisioned. Figure 5.13 depicts a PV design based on a central inverter. Figure 5.14 depicts the utilization of multiple inverters.

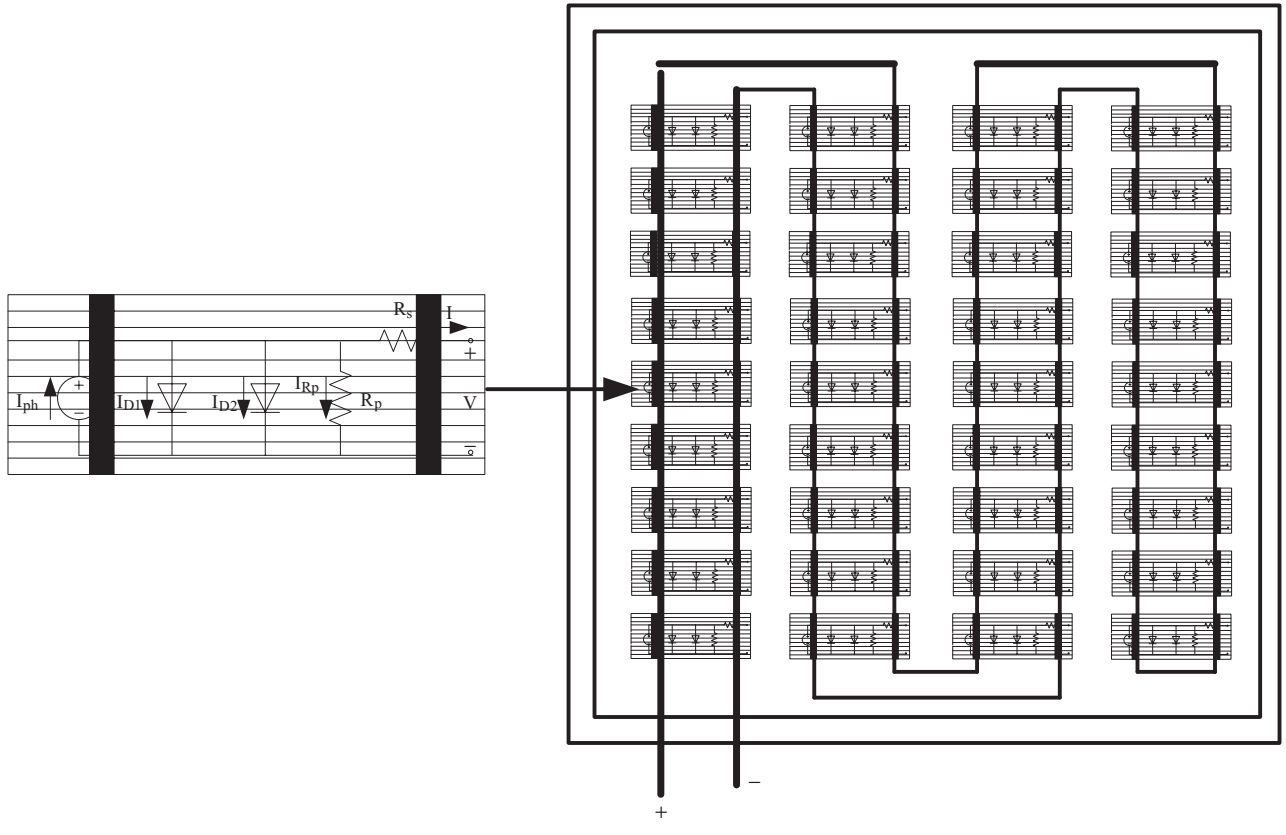

Figure 5.11 A Photovoltaic Module Consisting of 36 Photovoltaic Cells.

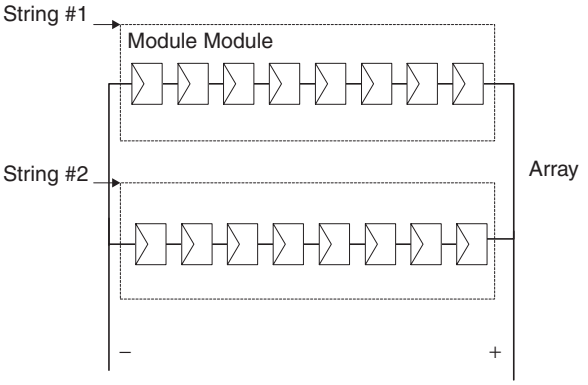

Figure 5.12 Basic Configuration Showing Modules, Strings, and an Array.

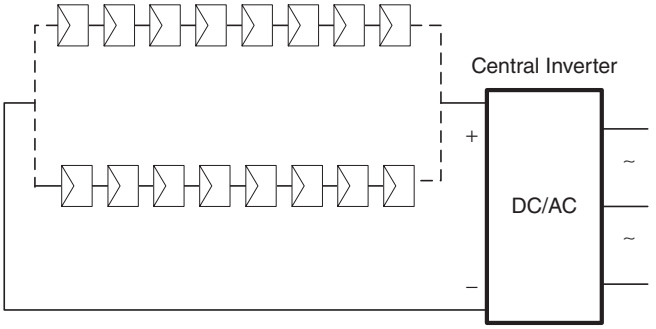

Figure 5.13 Central Inverter for a Large-Scale Photovoltaic Power Configuration.

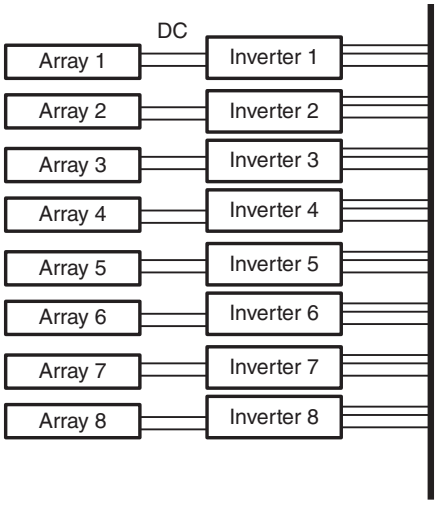

Figure 5.14 General Structure of Photovoltaic Arrays with Inverters.

Basically, to provide a higher DC operating voltage, modules are connected in series. To provide a higher operating current, the modules are connected in parallel.

$$\text{V (series connected)} = \sum_{j=1}^{n} V_j; \; n\text{: number of series connected panels} \quad (5.5)$$

For parallel connected panels,

$$\text{I (parallel connected)} = \sum_{j=1}^{m} I_j; \; m\text{: number of parallel connected panels} \quad (5.6)$$

In a PV system consisting of a number of arrays, all arrays must have equal exposure to sunlight: the design should place the modules of a PV system such that some of them will not be shaded. Otherwise, unequal voltages will result in some strings with unequal circulating current and internal heating producing power loss and lower efficiency. Bypass diodes are usually used between modules to avoid damage. Most new modules have bypass diodes in them as shown in Fig. 5.15 to ensure longer life. However, it is very difficult to replace built-in diodes if a diode fails in a panel.

The photovoltaic (PV) industry, the International Society for Testing and Materials (ASTM)[8], and the U.S. Department of Energy have established a standard for terrestrial solar spectral irradiance distribution. The irradiance of a location is measured by an instrument called a pyranometer.[9] Figure 5.16 depicts irradiance in W/m^2 per nanometer (nm) as a function of wavelength in nanometers (nm).

The solar spectrum is the plot of the irradiance from the sun received at a particular location at a given temperature and air mass flow. The intensity (W/m^2/nm) of the radiation is plotted as a function of wavelength (nm). The

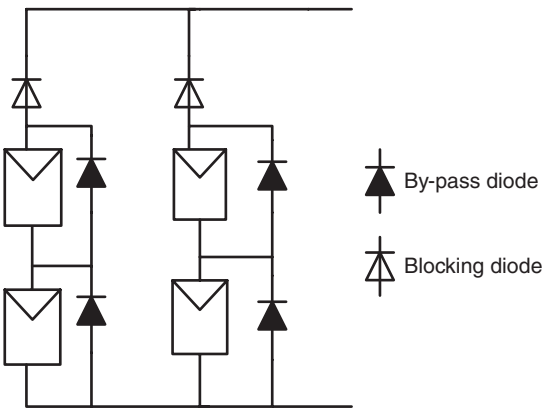

Figure 5.15 Bypass and Blocking Diodes in a Photovoltaic Array.

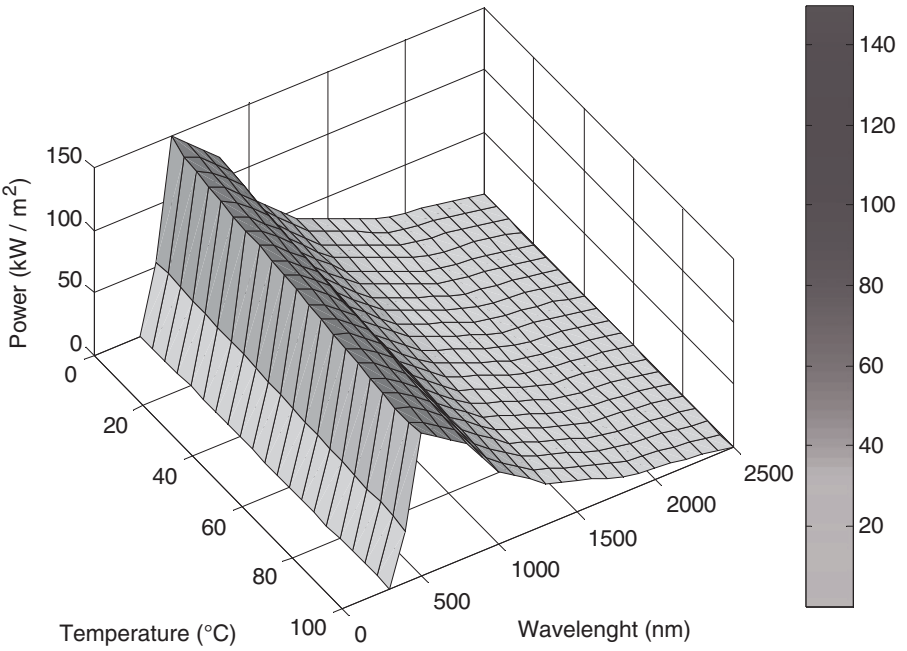

Figure 5.16 Spectra for Photovoltaic Performance Evaluation.[12,15]

photovoltaic modules convert the radiation energy to electrical energy. The amount of energy produced by the PV module is directly proportional to the area of the module. The kW/m^2 /nm of the PV module is plotted as a function of wavelength and estimated temperature from the solar spectrum. The above curve is plotted with an air mass of 1.5.

The PV modules are tested under a nominal temperature (NT). The NT is used to estimate the cell temperature based on the ambient temperature as shown below.

$$T_c = T_a + \left(\frac{NT - 20}{Kc}\right) \cdot S \tag{5.7}$$

The cell temperature, T_c and the ambient temperature, T_a are in degrees centigrade. The operating nominal temperature, NT designates the cell temperature as tested by manufacturers; S is the solar insolation (kW/m^2). Kc is a constant empirically computed from test data; it is in the range of 0.7 to 0.8.

5.7 THE DESIGN OF PHOTOVOLTAIC SYSTEMS

The design of engineering systems is based on trial and error. Nevertheless, the design must demonstrate a clear understanding of the scientific and

engineering principles behind the proposed design. In this sense, "trial and error" is for fine-tuning the final design. However, all engineering systems must be based on the underlying physical process.

In concrete terms, if we are designing a PV-generating system, we are using manufactured PV modules that have certain characteristics. However, in defining the overall objective of the PV systems we are putting into place, then some PV modules may satisfy those objectives and some may not. Therefore, we need to test available PV modules against our design specifications.

For a PV-generating system, the first specification is the power requirement in kW or MW that we intend to produce. If the PV system is to operate as an independent power generating station, the rated load voltage is specified. For example, for a residential PV system, we may install from a few kilowatts of power to serve the residential loads at a nominal voltage of 120 V and 207.8 V. If the residential PV is connected to the local utility, then the interconnection voltage must be specified for the design of such a system. Other design restrictions may also apply to a particular design. Again, consider the case of designing a residential PV system. We already know that a PV module generates a DC voltage source and DC power. How high a DC voltage is safe in a residential system is determined by the electric codes of a particular locality. In principle, we may want to design the residential PV system at a lower DC voltage and higher PV DC voltage for more-involved power systems at commercial and industrial sites. Another design consideration for residential users may be the weight and surface area needed for a PV system. Finally, it is understood that the PV designer always seeks to design a PV system to satisfy site constraints at the lowest installed and operating costs.

Table 5.4 defines a few terms that we have discussed in this chapter. We will use these terms to introduce the design of PV systems.

We know that all PV-generating stations are designed based on connecting PV modules to generate the required power (the terms PV module and PV panel are used interchangeably). One PV module has a limited power rating; therefore, to design a higher power rating, we construct a string by connecting a number of PV modules in series.

$$SV = NM \times V_{OC} \tag{5.8}$$

where SV defines, the string voltage and V_{oc} is the open circuit voltage of a module.

As an example, if the number of modules is five and the open-circuit voltage of the module is 50 V, we have:

$$SV = 5 \times 50 = 250\ V \text{ DC}$$

This may be a high voltage in a residential PV system. We can think of a PV cell, a module, or an array as a charged capacitor. The amount of charge of a

TABLE 5.4 Photovoltaic Design Terms.

Terms	Abbreviations	Descriptions
String voltage	SV	String voltage for series-connected modules
Power of a module	PM	Power produced by a module
String power	SP	Power that can be generated in one string
Number of strings	NS	Number of strings per array
Number of arrays	NA	Number of arrays in a design
Surface area of a module	SM	Surface area of a module
Total surface area	TS	Total surface area
Array power	AP	Array power is generated by connecting a number of strings in parallel
Number of modules	NM	Number of modules per string
Total number of modules	TNM	Total number of modules in all arrays put together
Array voltage for maximum power point tracking	V_{AMPP}	The operating voltage for maximum power point tracking of an array
Array current for maximum power point tracking	I_{AMPP}	The operating current for maximum power point tracking of an array
Array maximum power point	P_{AMPP}	The maximum operating power of an array
Number of converters	NC	Total number of DC/DC converters
Number of rectifiers	NR	Total number of AC/DC rectifiers
Number of inverters	NI	Total number of inverters

PV system is a function of sun irradiance. At full sun, the highest amount of charge is stored that will generate the highest open-circuit voltage for a PV system. In general, the open-circuit voltage of a PV panel for a residential system might be set at a voltage lower than 250 V DC. The rated open-circuit voltage is governed by local electric codes. In general, the open-circuit string voltage is less than 600 V DC for a commercial and industrial system at this time. However, higher DC voltage designs of PV systems are considered for higher power PV sites.

The string power, *SP*, is the power that can be produced by one string.

$$SP = NM \times PM \tag{5.9}$$

where *NM* is the number of modules and *PM* is the power produced by a module.

For example, if a design uses four PV modules, each rated 50 W, then the total power produced by the string is given as

$$SP = 4 \times 50 = 200 \text{ W}$$

As we discussed, for producing higher rated power from a PV-generating station, we can increase the string voltage. In addition, we can connect a number of strings in parallel and create an array. Therefore, the array power, AP is equal the number of string times the string power.

$$AP = NS \times SP \tag{5.10}$$

If the number of strings is 10 and each string is producing 200 W, we have:

$$AP = 10 \times 200 = 2000 \text{ W}$$

The DC power produced by an array is the function of the sun's position and irradiance energy received by the array. An array can be located on roofs or free-standing structures. The array power is processed by a converter to extract maximum power from the sun's irradiance energy. Because the transfer of DC power over a cable at low voltages results in high power losses, the array power is either converted to AC power by using a DC/AC inverter or in some applications, the array power is converted to a higher DC voltage power to produce higher AC voltage and to process higher rated power.

To obtain the maximum power out of an array, the maximum power point (MPP) tracking method is used. The MPP tracking method locates the point on the trajectory of power produced by an array where the array voltage and array current are at its maximum point and the maximum power output for the array.

The array MPP is defined as

$$P_{MPP} = V_{AMPP} \times I_{AMPP} \tag{5.11}$$

where V_{AMPP} is the array voltage at MPP tracking and I_{AMPP} is the array current at its maximum power point tracking (MPPT).

An array is connected to either an inverter or a boost converter and the control system operates the array at its MPP tracking.

The final design of a PV system is based on the MPP operation of a PV array generating station. Keeping in mind, however, the converter control system is designed to locate the maximum operating point based on generated array voltage and array current, thus accommodating the changing irradiance energy received by an array as the sun's position changes during the day.

The inverter output voltage is controlled by controlling the inverter amplitude modulation index. To process the maximum power by an inverter, the amplitude modulation index, M_a should be set at maximum value without producing the unwanted harmonic distortion. The value of M_a is set less than one and in the range of 0.95 to produce the highest AC output voltage.

Example 5.1 Design a PV system to process 10 kW of power at 230 V, 60 Hz single-phase AC. Determine the following:

i) Number of modules in a string and number of strings in an array
ii) Inverter specification and one-line diagram

The PV module data is given below.

Solution
The load voltage is specified as 230 V single-phase AC. To acquire maximum power from the PV array, we select a modulation index of $M_a = 0.9$. The inverter input voltage is given by

$$V_{idc} = \frac{\sqrt{2}V_{ac}}{M_a}$$

$$V_{idc} = \frac{\sqrt{2} \times 230}{0.9} = 361.4\ V \tag{5.12}$$

The inverter is designed to operate at the MPPT of PV array. Therefore, the number of modules to be connected in series in a string is given by

$$NM = \frac{V_{idc}}{V_{MPP}} \tag{5.13}$$

where V_{MPP} is the voltage at the MPP of PV of the module.

$$NM = \frac{361.4}{50.6} \approx 7$$

The string voltage is given as

$$SV = NM \times V_{MPP} \tag{5.14}$$

Using this module, string voltage (see Table 5.5) for this design is

$$SV = 7 \times 50.6 = 354.2\ V$$

i) The power generated by one string is given by:

$$SP = NM \times P_{MPP}$$

where P_{MPP} is the nominal power generated at the MPP tracking.

TABLE 5.5 The Voltage and Current Characteristics of a Typical Photovoltaic Module.

Power (max)	300 W
Maximum voltage, P_{MPP}	
Voltage at maximum power point (MPP), V_{MPP}	50.6 V
Current at MPP, I_{MPP}	5.9 A
V_{oc} (open-circuit voltage)	63.2 V
I_{sc} (short-circuit current)	6.5 A

TABLE 5.6 Photovoltaic Specifications for 10 kW Generation.

Modules per String	Strings per Array	Number of Arrays	String Voltage (V)
7	5	1	354.2

The power generated by a string for this design is given as

$$\text{kW per string} = 7 \times 300 = 2100\ W$$

To calculate the number of strings for a 10 kW PV system, we divide the PV power rating by power per string

$$NS = \frac{AP}{SP} \tag{5.15}$$

where NS is the number of strings and AP is the array power and SP is the string power. For this design we have:

$$NS = \frac{10 \times 10^3}{2100} = 5$$

Therefore, we have five strings and one array to generate 10 kW of power.

ii) In the final design, the inverter should be rated such that it is able to process generation of 10 kW and supply the load at 230 V AC from its array at its MPPT. Based on the PV module of Table 5.5, the string voltage is specified as

$$V_{idc} = 354.2\ V$$

TABLE 5.7 Inverter Specifications.

Input Voltage V_{idc} (V)	Power Rating (kW)	Output Voltage, V_{AC} (V)	Amplitude Modulation Index, M_a	Frequency Modulation Index, M_f
354.2	10	230	0.92	100

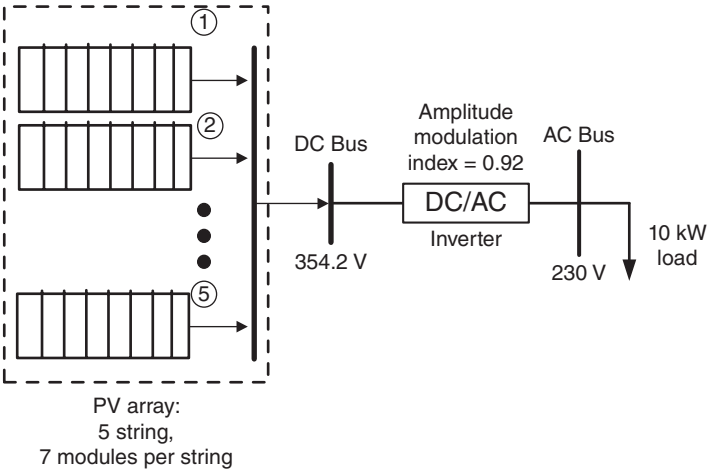

Figure 5.17 The One-Line Diagram of Example 5.1.

and the modulation index is given as follows:

$$M_a = \frac{\sqrt{2}V_{ac}}{V_{idc}}$$

$$\mathrm{M_a} = \frac{\sqrt{2} \times 230}{354.2} = 0.92$$

Let us select a switching frequency of 6 kHz. Therefore, the frequency modulation index is given by

$$M_f = \frac{f_S}{f_e} = \frac{6000}{60} = 100$$

The one-line diagram is given in Fig. 5.17.

Example 5.2 Design a PV system to process 500 kW of power at 460 V, 60 Hz, three-phase AC, and using PV data of Example 5.1. Determine the following:

i) Number of modules in a string and number of strings in an array
ii) Inverter and boost specification
iii) The output voltage as a function and total harmonic distortion
iv) The one-line diagram of this system

Solution
The load is 500 kW rated at 460 V AC. Based on the voltage of the load and an amplitude modulation index of 0.9, we have the following input DC voltage for a three-phase inverter:

$$V_{idc} = \frac{2\sqrt{2}V_{LL}}{\sqrt{3}M_a} = \frac{2\sqrt{2}\times 460}{\sqrt{3}\times 0.9} = 835\,V \tag{5.16}$$

We will limit the maximum string voltage to 600 V DC. Therefore, we can use a boost converter to boost the string voltage to 835 V.

If we select an approximate string voltage of 550 V, we have:

i) The number of modules in a string is given by

$$\frac{V_{string}}{V_{MPP}} = \frac{550}{50.6} \approx 11$$

where V_{MPP} is the voltage of a module at MPPT.

The string power, SP can be computed as

$$SP = NM \times P_{MPP}$$

Using a module rated at 300 W, we have:

$$SP = 11\times 300 = 3300\,W$$

The string voltage is given as:

$$SV = NM \times V_{MPP}$$

Therefore, the string voltage, SV, for this design is

$$SV = 11\times 50.6 = 556.6\,V$$

TABLE 5.8 Photovoltaic Specifications.

Modules per String	Strings per Array	Number of Arrays	String Voltage (V)
11	6	25	556.6

If we design each array to generate a power of 20 kW, then the number of strings, *NS*, in an array is given by:

$$NS = \frac{power\ of\ one\ array}{power\ of\ one\ string}$$

$$NS = \frac{20}{3.3} = 6$$

The number of array, *NA*, for total power generation is

$$NA = \frac{PV\ generation}{power\ of\ one\ array} \tag{5.17}$$

Therefore, $NA = \frac{500 \cdot kW}{20 \cdot kW} = 25$

ii) The inverters should be rated to withstand the output voltage of a boost converter and should be able to supply the required power. The inverter is rated at 100 kW with input voltage of 835 V DC and the amplitude modulation index of 0.9. The output voltage of inverter is 460 V AC.

The number of inverters, *NI*, needed to process a generation of 500 kW is given by

$$NI = \frac{PV\ generation}{power\ of\ one\ inverter} \tag{5.18}$$

Therefore, $NI = \frac{500}{100} = 5$

Hence, we need to connect five inverters in parallel to supply the load of 500 kW, if a switching frequency is set at 5.04 kHz.

Therefore, the frequency modulation index, M_f, is given by

$$M_f = \frac{f_S}{f_e} = \frac{5040}{60} = 84$$

TABLE 5.9 Inverter Specifications.

Number of Inverters	Input Voltage V_{idc} (V)	Power Rating (kW)	Output Voltage, V_{AC} (V)	Amplitude Modulation Index, M_a	Frequency Modulation Index, M_f
5	835	100	460	0.90	84

TABLE 5.10 Boost Converter Specifications for a Generation of 500 kW.

Number of Boost Converters	Input Voltage, V_i (V)	Power Rating (kW)	Output Voltage, V_o (V)	Duty Ratio, D
25	556.6	20	835	0.33

TABLE 5.11 Harmonic Content of Line-to-Neutral Voltage Relative to the Fundamental.

3rd Harmonic	5th Harmonic	7th Harmonic	9th Harmonic
0.01%	0.02%	0	0.03%

The number of boost converters needed is the same as the number of arrays, which is 25, and the power rating of each boost converter is 20 kW.

The boost converter input voltage is equal to the string voltage:

$$V_i = 556.6\ V$$

The output voltage of the boost converter is equal to the inverter input voltage:

$$V_{idc} = V_o = 835\ V$$

The duty ratio of the boost converter is given by

$$D = 1 - \frac{V_i}{V_o}$$

$$D = 1 - \frac{556.6}{835} = 0.33$$

iii) With a frequency modulation of 84, the harmonic content of the output voltage was computed from a simulation testbed using a fast Fourier method; it is tabulated below.

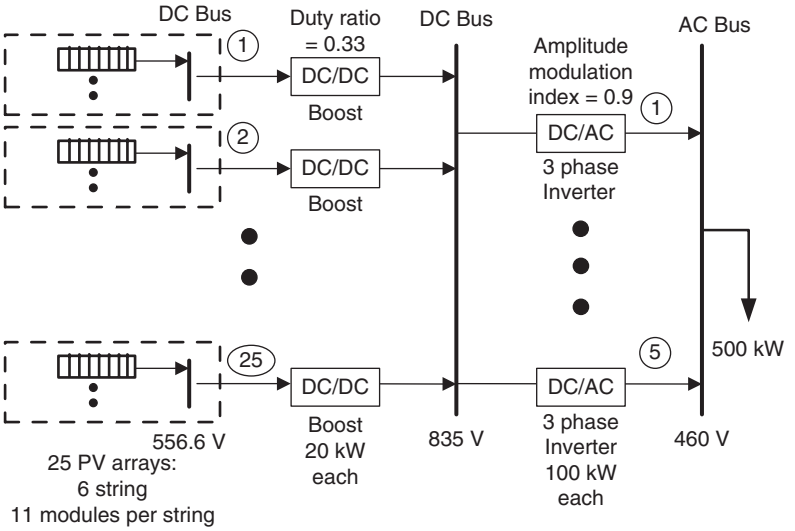

Figure 5.18 The One-Line Diagram of Example 5.2.

The output line-to-neutral voltage as a function of time is

$$\begin{aligned} V_{ac} &= \frac{460\sqrt{2}}{\sqrt{3}} \cdot \sin(2\pi 60 \cdot t) + \frac{0.01}{100} \times \frac{460\sqrt{2}}{\sqrt{3}} \cdot \sin(2\pi \times 3 \times 60 \cdot t) \\ &\quad + \frac{0.02}{100} \times \frac{460\sqrt{2}}{\sqrt{3}} \cdot \sin(2\pi \times 5 \times 60 \cdot t) + \frac{0}{100} \times \frac{460\sqrt{2}}{\sqrt{3}} \cdot \sin(2\pi \times 7 \times 60 \cdot t) \\ &\quad + \frac{0.03}{100} \times \frac{460\sqrt{2}}{\sqrt{3}} \cdot \sin(2\pi \times 9 \times 60 \cdot t) \\ &= 376\sin(2\pi 60 \cdot t) + 0.037\sin(6\pi 60 \cdot t) + 0.075\sin(10\pi 60 \cdot t) \\ &\quad + 0.113\sin(18\pi 60 \cdot t) \end{aligned}$$

The total harmonic distortion is given by

$$THD = \sqrt{\sum (\%harmonic)^2} = \sqrt{0.01^2 + 0.02^2 + 0^2 + 0.03^2} = 0.04\%$$

iv) The one-line diagram is given in Fig. 5.18

Example 5.3 Design a PV system to process 1000 kW of power at 460 V, 60 Hz three-phase AC using the PV data given in Table 5.12. Determine the following:

i) Number of modules in a string, number of strings in an array, number of arrays, surface area for PV, weight of PV, and cost

TABLE 5.12 Photovoltaic Data for Example 5.3.

Module	Type 1
Power (Max), W	190
Voltage at MPP, V	54.8
Current at MPP, A	3.47
V_{OC} (open-circuit voltage), V	67.5
I_{SC} (short-circuit current), A	3.75
Efficiency	16.40%
Cost	$870.00
Width	34.6″
Length	51.9″
Thickness	1.8″
Weight	33.07 lbs

ii) DC/AC Inverter and boost converter specifications and the one-line diagram of the system

Solution
The load is 1000 kW rated at 460 V AC. Based on the voltage of the load and an amplitude modulation index of 0.85, the input DC voltage for a three-phase inverter is:

$$V_{idc} = \frac{2\sqrt{2}V_{LL}}{\sqrt{3}M_a} = \frac{2\sqrt{2}\times 460}{\sqrt{3}\times 0.85} = 884\ V$$

We will limit the maximum voltage that a string is allowed to have to 600 V. Therefore, we use a boost converter to boost the string voltage to 884 V.

i) If we select string approximate voltage of 550 V, the number of modules in a string, NM, is given as

$$NM = \frac{V_{string}}{V_{MPP}} = \frac{550}{54.8} \approx 10$$

where V_{MPP} is the voltage at MPP of the PV module.

$$SP = NM \times P_{MPP}$$

where P_{MPP} is the power generated by a PV module at MPP.

$$SP = 10 \times 190 = 1900\ W$$

And the string voltage, SV, is

$$SV = NM \times V_{MPP}$$

Therefore, the string voltage, SV, for this design is

$$SV = 10 \times 54.8 = 548\ V$$

If each array is to have a rating of 20 kW, the number of strings, NS, in an array is

$$NS = \frac{AP}{SP}$$

$$NS = \frac{20}{1.9} = 11$$

The number of arrays, NA, for this design is

$$NA = \frac{PV\ generation}{power\ of\ one\ array}$$

$$NA = \frac{1000}{20} = 50$$

The total number of PV modules, TNM, is given by the product of the number of modules per string, the number of strings per array, and the number of arrays:

$$TNM = NM \times NS \times NS$$

$$TNM = 10 \times 11 \times 50 = 5{,}500 \tag{5.19}$$

The surface area of one module, SM, is given by the product of its length and width.

$$SM = \frac{34.6 \times 51.9}{144} = 12.5\ ft^2$$

The total surface area, TS, is therefore given by the total number of modules and the surface area of each module.

$$TS = 5500 \times 12.5 = 68{,}750\ ft^2 = \frac{68{,}750}{43{,}560} = 1.57\ acre$$

The total cost of PV modules is given by the product of the number of PV modules and the cost of one module.

$$\text{The total cost} = 5500 \times 870 = \$4.78 \; million$$

The total weight of PV modules is given by the product of the number of PV modules and the weight of one module.

$$\text{The total weight} = 5500 \times 33.07 = 181{,}885 \; lb$$

ii) The inverters should be rated to withstand the output voltage of the boost converter and should be able to supply the required power. Selecting an inverter rated at 250 kW, we have the number of inverters, *NI*, needed to process the generation of 1000 kW as given by

$$NI = \frac{PV \; generation}{power \; of \; one \; inverter}$$

$$NI = \frac{1000}{250} = 4$$

Hence, we need to connect four inverters in parallel to supply the load of 1000 kW.

Selecting a switching frequency of 5.40 kHz, the frequency modulation index is given by

$$M_f = \frac{f_S}{f_e} = \frac{5400}{60} = 90$$

TABLE 5.13 Photovoltaic Specifications for 1000 kW Generation.

Modules per String	Strings per Array	Number of Arrays	String Voltage (V)	Total Area (ft^2)	Total Weight (lbs)	Total Cost (million $)
10	11	50	548	68,750	181,885	4.78

TABLE 5.14 Inverter Specifications.

Number of Inverters	Input Voltage V_{idc} (V)	Power Rating (kW)	Output Voltage, V_{AC} (V)	Amplitude Modulation Index, M_a	Frequency Modulation Index, M_f
4	884	250	460	0.85	90

TABLE 5.15 Boost Converter Specifications.

Number of Boost Converters	Input Voltage V_i (V)	Power Rating (kW)	Output Voltage, V_o (V)	Duty Ratio, D
50	548	20	884	0.38

The number of boost converters needed is the same as the number of arrays, which is 50. Selecting a boost converter rating of 20 kW and the boost converter input voltage to be equal to the string voltage:

$$V_i = 548\ V$$

The output voltage of the boost converter is equal to the inverter input voltage:

$$V_{idc} = V_o = 884\ V$$

The duty ratio of the boost converter is given by

$$D = 1 - \frac{V_i}{V_o}$$

$$\mathrm{D} = 1 - \frac{548}{884} = 0.38$$

The one-line diagram is given in Fig. 5.19.

5.8 THE MODELING OF A PHOTOVOLTAIC MODULE

As we discussed, a commercial PV module is constructed from a number of PV cells. A PV cell is constructed from a p-n homojunction material. This is when a p-type doped semiconductor is joined with an n-type doped semiconductor, and a p-n junction is formed. If the p-and the n-type semiconductors have the same bandgap energy, a homojunction is formed. The homojunction is a semiconductor interface, a phenomenon that takes place between layers of similar semiconductor material. These types of semiconductors have equal band gaps and they normally have different doping. The absorption of photons of energy generates DC power.

A PV cell is shown in Fig. 5.20. As irradiance energy of sun is received by the module, it is charged with electric energy. The model of a PV cell is similar to that of a diode and can be expressed by the well-known Shockley-Read equation.

The PV module can be modeled by a single exponential model. The model is presented in Fig. 5.21. The current is expressed in terms of voltage, current, and temperature as shown in Equation 5.20.

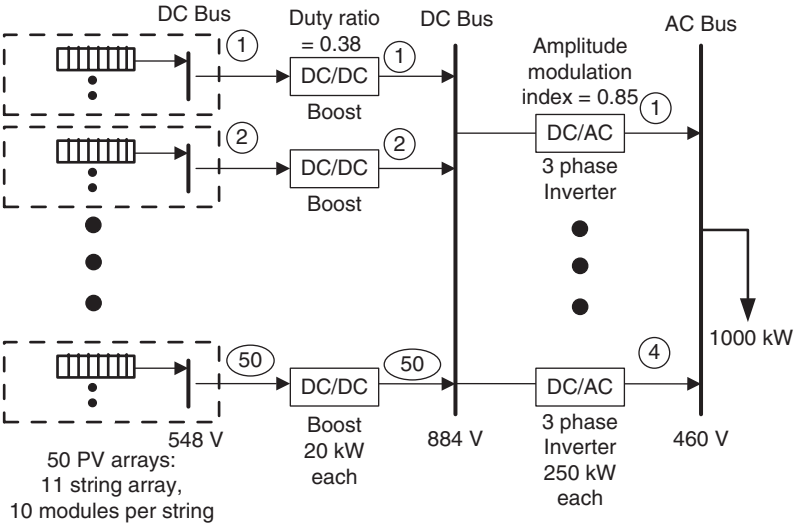

Figure 5.19 The One-Line Diagram of Example 5.3.

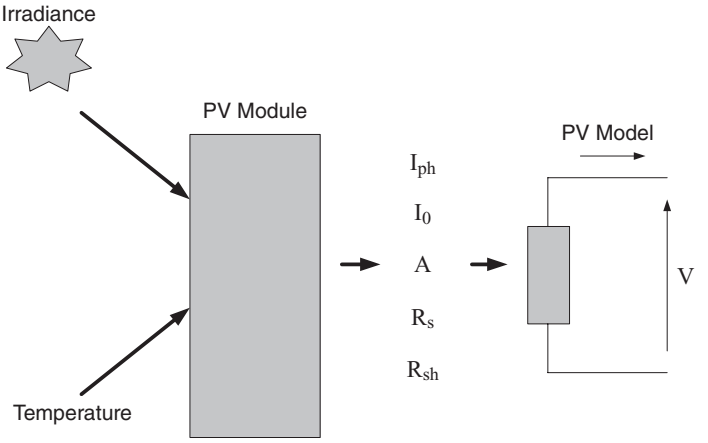

Figure 5.20 The Modeling of a Photovoltaic Module.

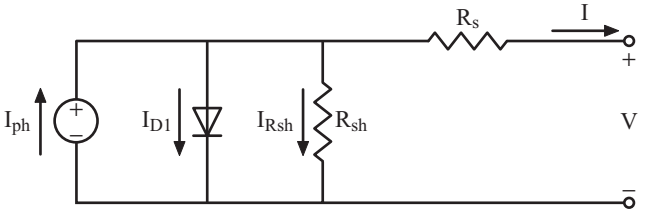

Figure 5.21 The Single Exponential Model of a Photovoltaic Module.

In the above model, the PV module is represented by a current source I_{ph} in parallel with the shunt resistance R_{sh}. The current flowing through the shunt resistance is designated as I_{Rsh}. The output DC voltage, V is in series with the internal resistance R_S. The PV model shown in Fig. 5.21 also depicts the power loss through current, I_{D1} circulating through the diode. The single exponential model is given by Equation 5.20.

$$I = I_{ph} - I_0\left\{\exp\left[\frac{q(V + IR_s)}{n_c AkT}\right] - 1\right\} - \frac{V + IR_s}{R_{sh}} \tag{5.20}$$

Other parameters are the diode quality factor (A), n_c is the number of cells in the module, Boltzmann's constant (k), 1.38×10^{-23} J/K; the electronic charge (q), 1.6×10^{-19} C, and the ambient temperature (T) in Kelvin**.**

Equation 5.20 is nonlinear and its parameters I_{ph}, I_o, R_s, R_{sh}, and A are functions of temperature, irradiance and manufacturing tolerance. We can use numerical methods and curve fitting to estimate the parameters from test data provided by manufacturers. The estimation of a PV array model is quite involved. We will present the formulation of this problem at the end of this chapter.

5.9 THE MEASUREMENT OF PHOTOVOLTAIC PERFORMANCE

A PV module at a maximum constant level of irradiance can produce 1000 W/m^2. 1000 W/m^2 is also termed as one sun. The power output of the PV module is calibrated in relation to exposure to the sun. Table 5.16 depicts the irradiance in W/m^2.

The sun irradiance energy is calibrated for a PV array system based on the angle of incident. This data is used to operate the PV array at its MPP. In the next section, we will discuss how the power converters use digital controllers to operate a PV-generating station at its MPP.

TABLE 5.16 Sun Performance versus Incident Irradiance.

Sun Performance	Incident Irradiance
One Sun	1000 W/m^2
0.8 Sun	800 W/m^2
0.6 Sun	600 W/m^2
0.4 Sun	400 W/m^2
0.2 Sun	200 W/m^2

5.10 THE MAXIMUM POWER POINT OF A PHOTOVOLTAIC ARRAY

First, let us review the maximum power transfer in a resistive circuit. Consider the circuit of Fig. 5.23. Assume a voltage source with an input resistance, R_{in}. This source is connected to a load resistance, R_L.

The current supplied to the load is

$$I = \frac{V}{R_{in} + R_L} \tag{5.21}$$

The power delivered to the load R_L is

$$P = I^2 R_L \tag{5.22}$$

$$P = V^2 \frac{R_L}{(R_{in} + R_L)^2} \tag{5.23}$$

Differentiating with respect to R_L:

$$\frac{dP}{dR_L} = V^2 \frac{(R_{in} + R_L)^2 \frac{dR_L}{dR_L} - R_L \frac{d(R_{in} + R_L)^2}{dR_L}}{(R_{in} + R_L)^4}$$

$$\frac{dP}{dR_L} = V^2 \frac{R_{in} - R_L}{(R_{in} + R_L)^3} \tag{5.24}$$

Setting the above to zero, we can calculate the operating point for the maximum power. The MPP can be delivered to the load when, $R_L = R_{in}$.

A PV module output power is the function of irradiance solar energy. Figure 5.22 depicts the output power in W/m^2 at various irradiances as a function of module current and output voltage.

The PV system should be operated to extract the maximum power from its PV array as the environmental conditions change in relation to the position of the sun, cloud cover, and daily temperature variations. The equivalent circuit model of a PV array depicted in Fig. 5.21 can be presented during its power transfer mode to a load R_L as shown in Fig. 5.24.

Figure 5.24 presents the circuit model for a PV source by a current source that has a shunt resistance, R_{sh} and series resistance, R_s.[20] The shunt resistance has a large value and series resistance is very small. The load resistance is represented by R_L. In Fig. 5.24, R_L is the reflected load because in practice the load is connected to the converter side if the PV operates as a standalone. When the PV is connected to the power grid, the load is based on the injected power to the power grid. The equivalent voltage source circuit model of current source model is depicted by Fig. 5.25.

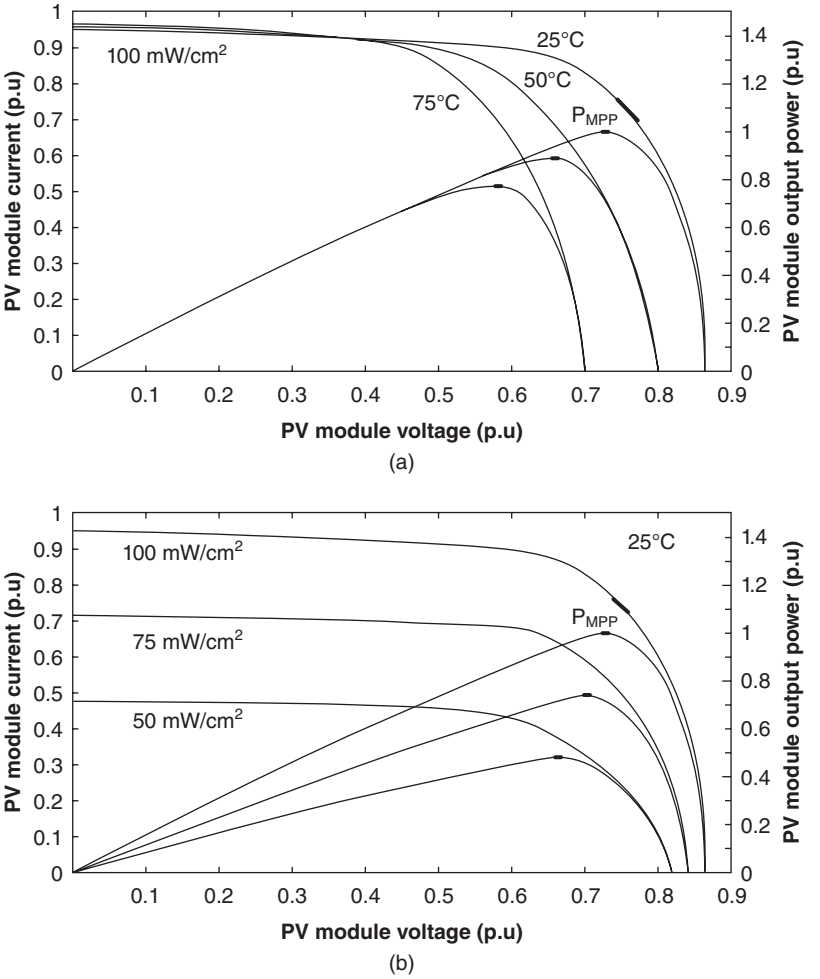

Figure 5.22 (a)The PV Output Current versus Output Voltage and Output Power as a Function of Temperture Variation. (b) The Output power in W/m^2 at Various Irradiances as a Function of Module Current and Output Voltage.[10]

As can be seen in Fig. 5.22, the characteristics of a PV module are highly nonlinear. The input impedance of a PV array is affected by irradiance variation and temperature. The corresponding output power is also shown in Fig. 5.22.

Figure 5.26 depicts the PV energy processing system using a boost converter to step up the voltage and an inverter to convert the DC power to AC. To achieve maximum power transfer from the PV array, the input impedance of the PV generator must match the load. The MPPT control algorithm seeks to operate the boost converter at a point on the PV array current and voltage characteristics where the maximum output power can be obtained. For a PV

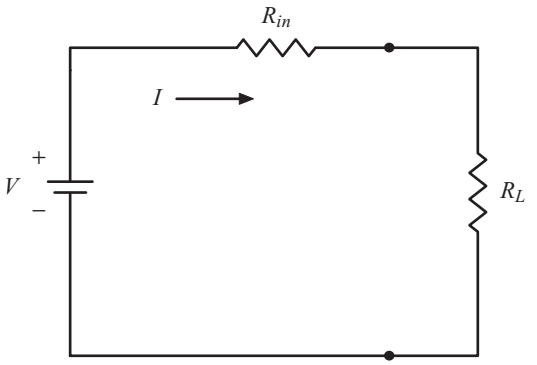

Figure 5.23 A DC Source with a Resistive Load.

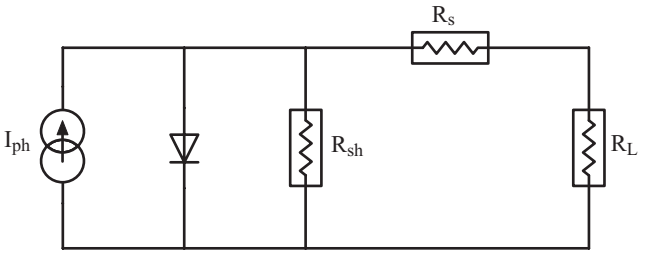

Figure 5.24 A Photovoltaic Model and Its Load.

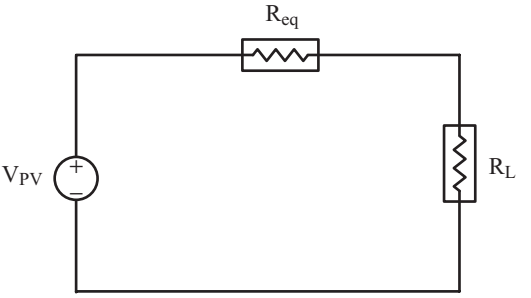

Figure 5.25 A Simple Voltage Source Equivalent Circuit Model of a Photovoltaic Array.

power generating station, the control algorithm computes the dP/dV > 0 and dP/dV < 0 to identify if the pick power has been obtained. Figure 5.27 depicts the control algorithm. If the PV system is to supply power to DC loads, then a DC/AC inverter is not needed.

Depending on application, a number of designs of a PV system can be proposed. When the PV system is to charge a battery storage system, the PV

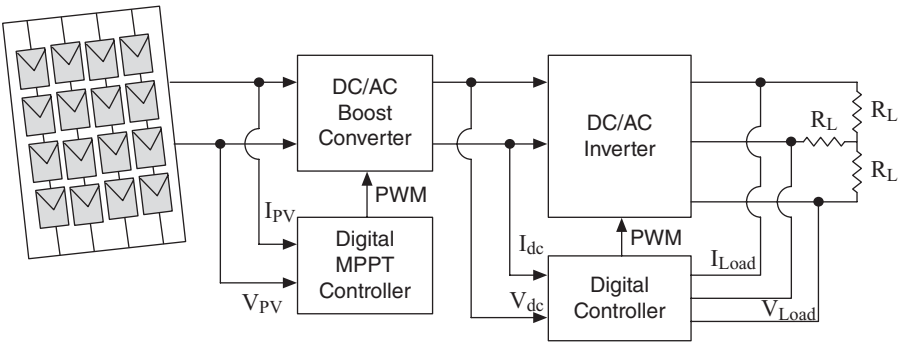

Figure 5.26 A Photovoltaic Energy Processing Using a Boost Converter to Step Up the Voltage and an Inverter.

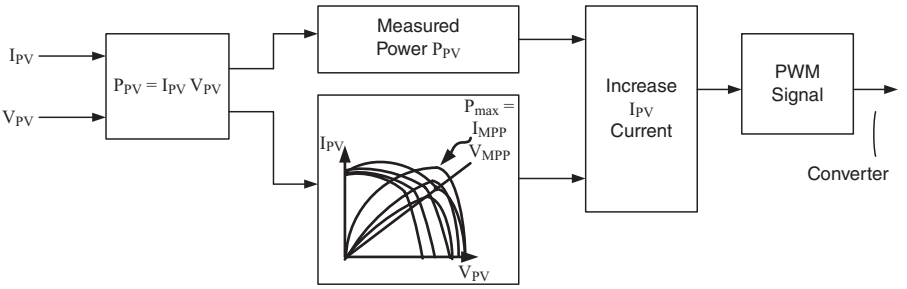

Figure 5.27 A Maximum Power Point Tracking Control Algorithm.

system can be designed as depicted by Fig. 5.28 using a boost converter or as in Fig. 5.29 using a buck converter. In this design again, the MPPT is accomplished using an MPPT control algorithm depicted by Fig. 5.27.

Figure 5.30 depicts the design of a PV-generating system and MPPT using an inverter when the PV-generating station is connected to a local utility. Again, the digital controller tracks the PV station output voltage and current and computes the MPPT point according to the control algorithm of Fig. 5.27. The control algorithm issues the PWM switching policy to control inverter current such that the PV station operates at its MPP. However, the resulting control algorithm may not result in minimum total harmonic distortion. The design presented by Fig. 5.27 has two control loops. The first control loop is designed to control DC/DC converter and the second control loop can control the total harmonic distortion and output voltage.

When the MPPT control is performed as part of the inverter as shown in Fig. 5.30, the tracking of MPPT may not be optimum. In this type of MPPT the current to the inverter flows though all modules in the string. However, the I-V curves may not be the same and some strings will not operate at their MPPT. Therefore, the resulting energy capture may not be as high and some energy will be lost in such systems.

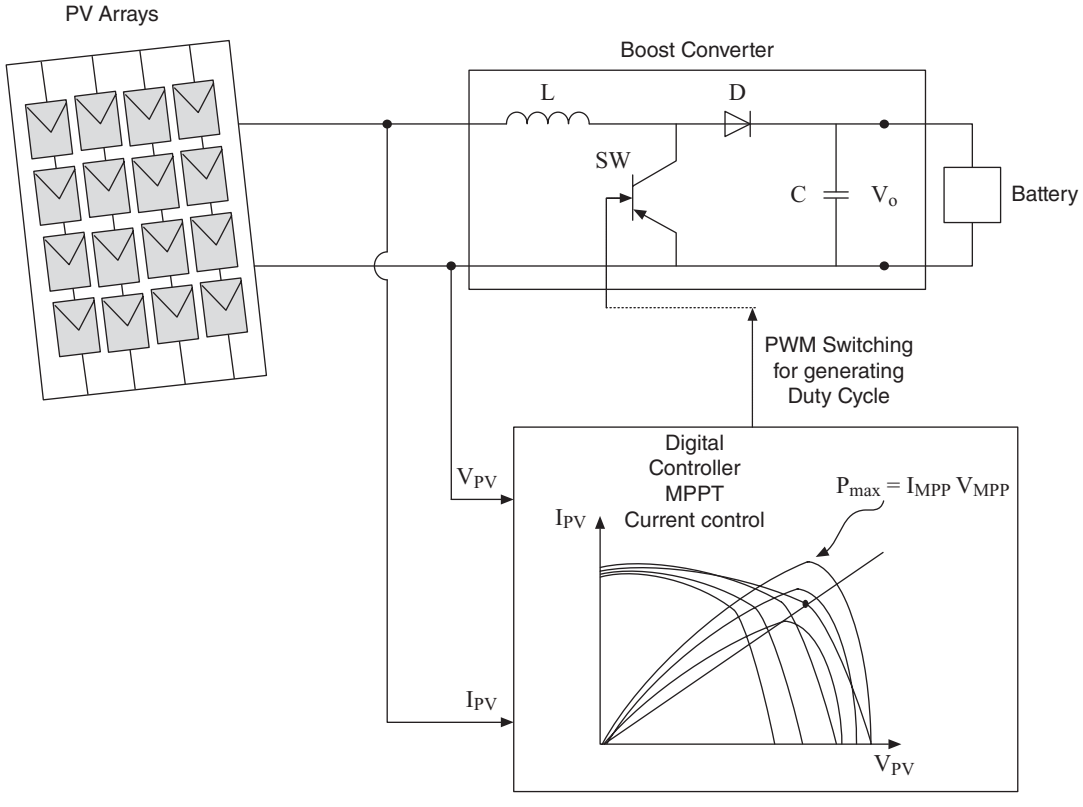

Figure 5.28 Maximum Power Point Tracking Using Only a Boost Converter.

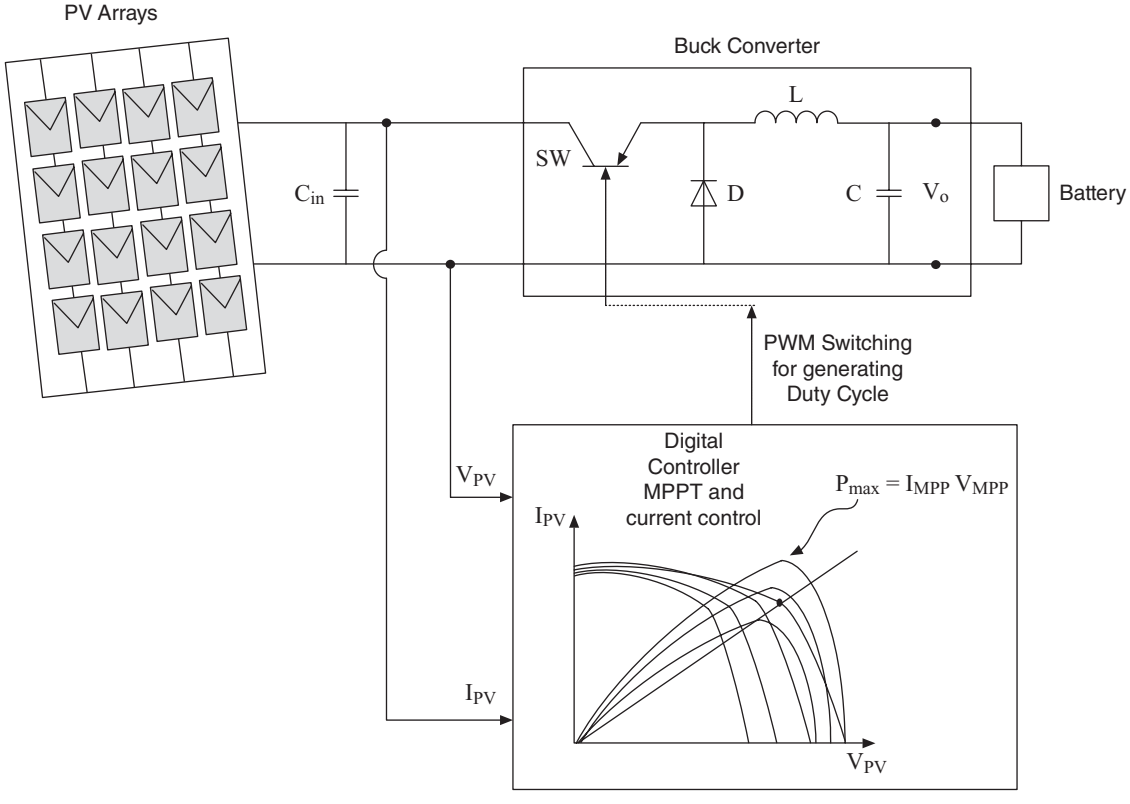

Figure 5.29 Maximum Power Point Tracking Using a Buck Converter.

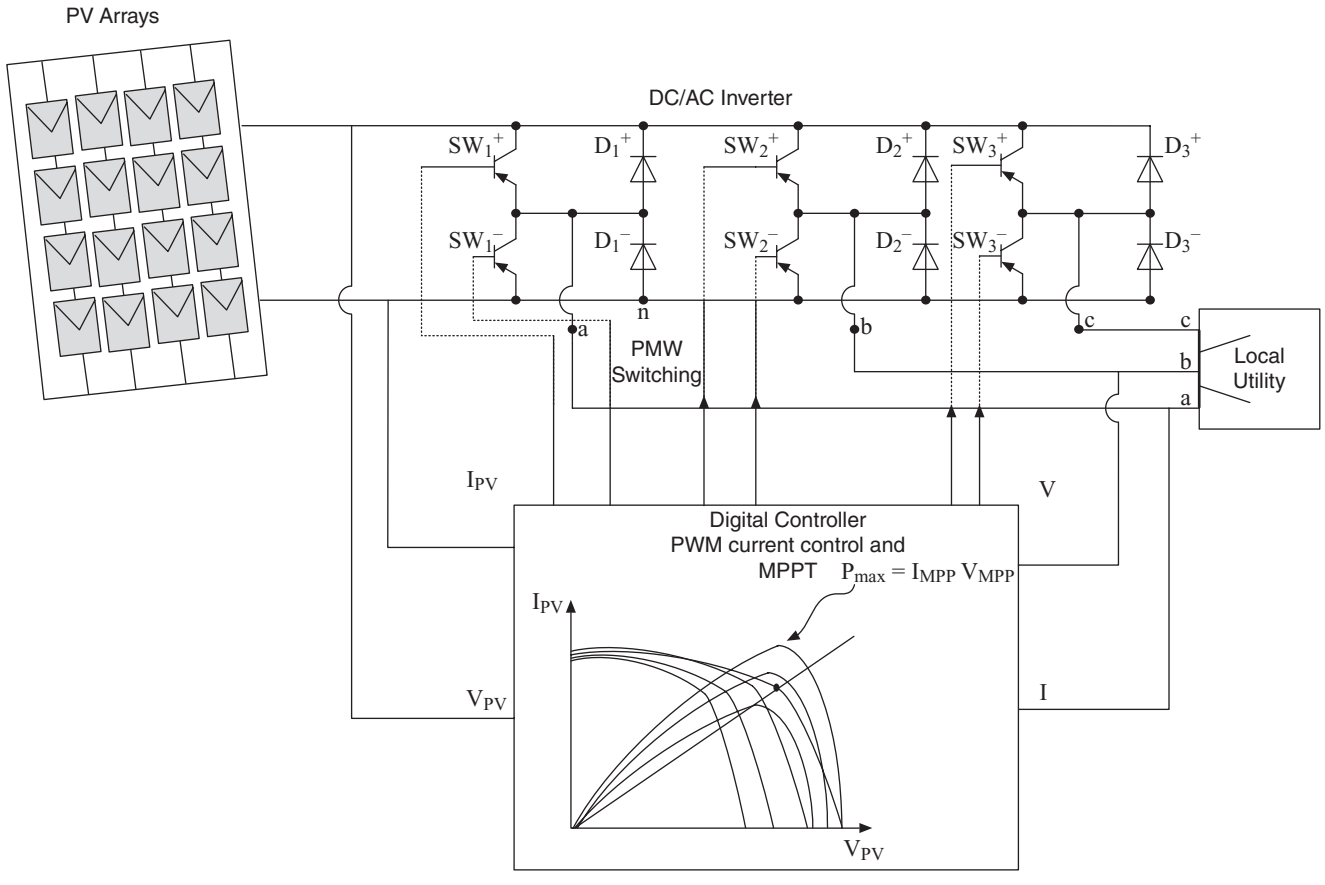

Figure 5.30 A Photovoltaic Generating Station Operating at Maximum Power Point Tracking when the Photovoltaic System Is Connected to a Local Power Grid.

Figure 5.31 depicts a PV-generating station with a battery storage system when the PV system is connected to the local utility. The DC/DC converter and its MPPT are referred to a charger controller. The charger controllers have a number of functions. Some charger controllers are used to detect the variations in the current-voltage characteristics of a PV array. MPPT controllers are necessary for a PV system to operate at voltage close to MPP to draw maximum available power as shown in Fig. 5.27. The charger controllers also perform battery power management. For normal operation, the controllers control the battery voltage, which varies between the acceptable maximum and minimum values. When the battery voltage reaches a critical value, the charge controller function is to charge the battery and protect the battery from an overcharge. This control is accomplished by two different voltage thresholds, namely, battery voltage and PV module voltage.

At lower voltage, typically 11.5 V, a controller switches the load off and charges the battery storage system. At higher voltage, usually 12.5 V for a 12 V battery storage system charge, a controller switches the load to the battery. The control algorithm adjusts the two voltage thresholds depending on the battery storage system.

DC/DC MPPT PV charger controllers facilitate standardization of integration of PV system for use in a local storage system. The system of Fig. 5.31 also can be used as a standalone microgrid that can deliver high-quality power for an uninterruptible power supply (UPS).

Example 5.4 Design a microgrid of PV system rated at 50 kW of power at 220 V, 60 Hz single-phase AC using a boost converter and single-phase DC/AC inverter. Use the data given in Table 5.17 for your design.

Determine the following:

i) Number of modules in a string for each PV type, number of strings in an array for each PV type, number of arrays and surface area, weight and cost for each PV type

ii) Boost converter and inverter specifications and the one-line diagram of this system

Solution

The load is 50 kW rated at 220 V AC. Based on the voltage of the load and an amplitude modulation index of 0.9, the input DC voltage for the inverter is

$$V_{idc} = \frac{\sqrt{2}V_{ac}}{M_a} = \frac{\sqrt{2} \times 220}{0.9} = 345\ V$$

i) If we select string voltage, SV of 250 V, the number of modules is

$$NM = \frac{string\ voltage}{V_{MPP}}$$

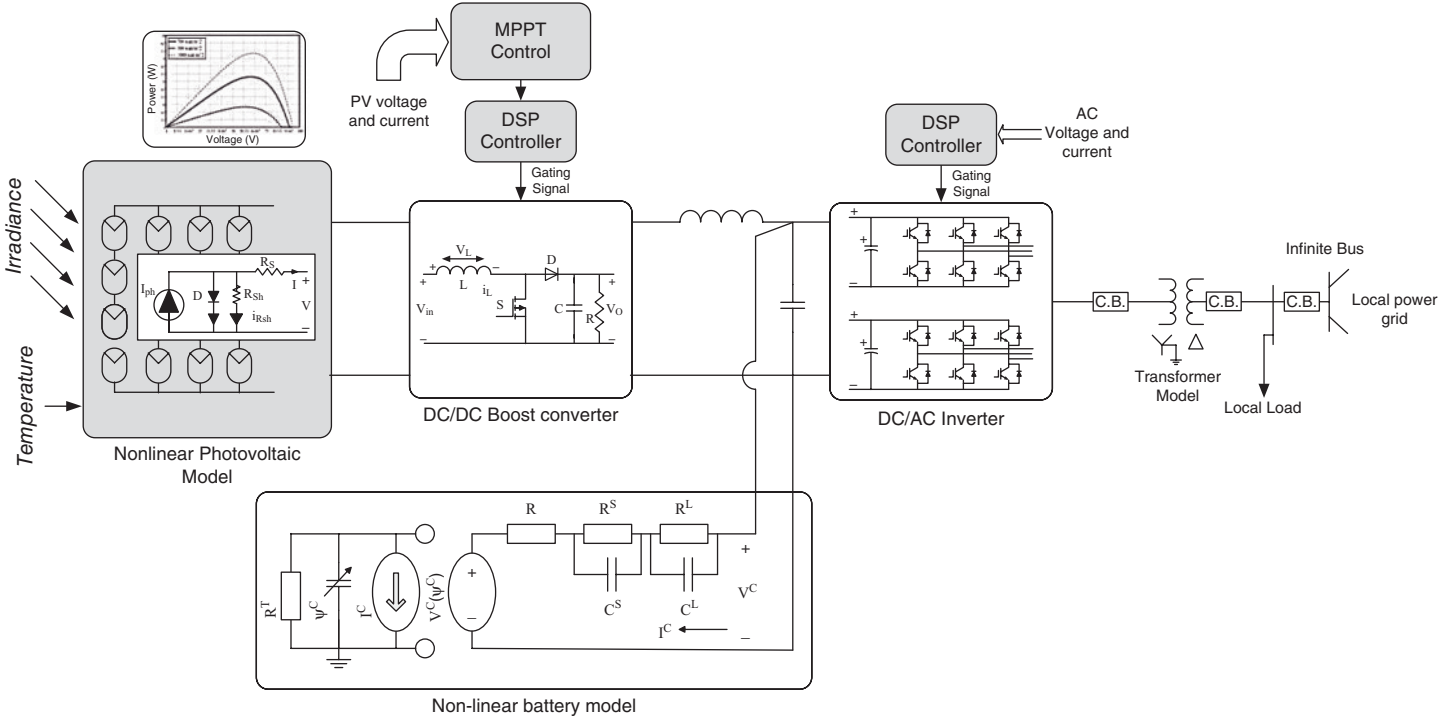

Figure 5.31 A Photovoltaic Generating Station Operating at Maximum Power Point Tracking with a Battery Storage System when the Photovoltaic System Is Connected to a Local Power Grid.

TABLE 5.17 Typical Photovoltaic Modules.

Module	Type 1	Type 2	Type 3	Type 4
Power (Max), W	190	200	170	87
Voltage at max. power point (MPP), V	54.8	26.3	28.7	17.4
Current at MPP, A	3.47	7.6	5.93	5.02
V_{OC} (open-circuit voltage), V	67.5	32.9	35.8	21.7
I_{SC} (short-circuit current), A	3.75	8.1	6.62	5.34
Efficiency	16.40%	13.10%	16.80%	>16%
Cost	$870.00	$695.00	$550.00	$397.00
Width	34.6″	38.6″	38.3″	25.7″
Length	51.9″	58.5″	63.8″	39.6″
Thickness	1.8″	1.4″	1.56″	2.3″
Weight	33.07 lbs	39 lbs	40.7 lbs	18.3 lbs

TABLE 5.18 Single-Phase Inverter Data.

Inverter	Type 1	Type 2	Type 3	Type 3
Power	500 W	5 kW	15 kW	4.7 kW
Input voltage DC	500 V	500 V max	500 V	500 V
Output voltage AC	230 VAC/60 Hz @ 2.17 A	230 VAC/ 60 Hz @ 27 A	220 VAC/ 60 Hz@ 68 A	230 VAC/ 60 Hz @ 17.4 A
Efficiency	Min. 78% @ full load	97.60%	>94%	96%
Length	15.5″	315 mm	625 mm	550 mm
Width	5″	540 mm	340 mm	300 mm
Height	5.3″	191 mm	720 mm	130 mm
Weight	9 lbs	23 lbs	170 kg	21 kg

TABLE 5.19 Typical Boost Converters.

Input Voltage (V)	Output Voltage (V)	Power (kW)
24–46	26–48	9.2
24–61	26–63	12.2
24–78	26–80	11.23
24–78	26–80	13.1
24–98	26–100	12.5
80–158	82–160	15.2
80–198	82–200	14.2
80–298	82–300	9.5
200–600	700–1000	20.0

where V_{MPP} is the voltage at MPP of the PV module.

$$NM = \frac{250}{54.8} \approx 5 \quad \text{type 1}$$
$$= \frac{250}{26.3} \approx 10 \quad \text{for type 2}$$
$$= \frac{250}{28.7} \approx 9 \quad \text{for type 3}$$
$$= \frac{250}{17.4} \approx 15 \quad \text{for type 4}$$

The string voltage, SV is given as:

$$SV = NM \times V_{MPP}$$

Therefore, the string voltage, SV for this design is:

$$SV = 5 \times 54.8 = 274\,V \quad \text{for type 1}$$
$$= 10 \times 26.3 = 263\,V \quad \text{for type 2}$$
$$= 9 \times 28.7 = 258.3\,V \quad \text{for type 3}$$
$$= 15 \times 17.4 = 261\,V \quad \text{for type 4}$$

Selecting the 15.2 kW boost converter from Table 5.19, the number of boost converters, NC, is

$$NC = \frac{PV\ generation}{boost\ converter\ power\ rating}$$

$$NC = \frac{50}{15.2} \approx 4$$

Therefore, the design should have four arrays: each with its boost converter. The array power, AP is

$$AP = \frac{PV\ generation}{number\ of\ arrays}$$

$$AP = 50/4 = 12.5\ \text{kW}.$$

String power, SP is given as

$$SP = NM \times P_{MPP}$$

where P_{MPP} is the power generated by the PV module at MPP.

$$\begin{aligned} SP &= 5 \times 190 = 0.95\,\text{kW} && \text{for type 1} \\ &= 10 \times 200 = 2.0\,\text{kW} && \text{for type 2} \\ &= 9 \times 170 = 1.53\,kW && \text{for type 3} \\ &= 15 \times 87 = 1.305\,kW && \text{for type 4} \end{aligned}$$

The number of strings, NS is given by

$$NS = \frac{power\ per\ array}{power\ per\ string}$$

$$\begin{aligned} NS &= \frac{12.5}{0.95} = 14 && \text{for type 1} \\ &= \frac{12.5}{2} = 7 && \text{for type 2} \\ &= \frac{12.5}{1.53} = 9 && \text{for type 3} \\ &= \frac{12.5}{1.305} = 10 && \text{for type 4} \end{aligned}$$

The total number of modules, TNM is given by:

$$TNM = NM \times NS \times NA$$

$$\begin{aligned} TNM &= 5 \times 14 \times 4 = 280 && \text{for type 1} \\ &= 10 \times 7 \times 4 = 280 && \text{for type 2} \\ &= 9 \times 9 \times 4 = 324 && \text{for type 3} \\ &= 15 \times 10 \times 4 = 600 && \text{for type 4} \end{aligned}$$

The surface area, TS needed by each PV type is given by the product of the total number of modules, and the length and the width of one PV module:

$$\begin{aligned} TS &= \frac{280 \times 34.6 \times 51.9}{144} = 3492\ sq\ ft && \text{for type 1} \\ &= \frac{280 \times 38.6 \times 58.5}{144} = 4391\ sq\ ft && \text{for type 2} \\ &= \frac{324 \times 38.3 \times 63.8}{144} = 5498\ sq\ ft && \text{for type 3} \\ &= \frac{600 \times 25.7 \times 39.6}{144} = 4241\ sq\ ft && \text{for type 4} \end{aligned}$$

TABLE 5.20 The Photovoltaic Specifications for Each Photovoltaic Type.

PV Type	Number of Modules per String	Number of Strings per Array	Number of Arrays	String Voltage (V)	Total Area of the PV (ft^2)	Total Weight of the PV (lb)	Total Cost of the PV ($)
1	5	14	4	274	3,492	9,260	243,600
2	10	7	4	263	4,391	10,920	194,600
3	9	9	4	258.3	5,498	13,187	178,200
4	15	10	4	261	4,241	11,040	238,200

The total weight needed for each PV type is the product of the number of modules and the weight of one module:

$$\begin{aligned}\text{The total weight} &= 280 \times 33.07 = 9260\ lb \quad \text{for type 1}\\ &= 280 \times 39.00 = 10920\ lb \quad \text{for type 2}\\ &= 324 \times 40.70 = 13187\ lb \quad \text{for type 3}\\ &= 600 \times 18.40 = 11040\ lb \quad \text{for type 4}\end{aligned}$$

The total cost for each PV type is the product of the number of modules and the cost of one module:

$$\begin{aligned}\text{The total cost} &= 280 \times 870 = \$243{,}600 \quad \text{for type 1}\\ &= 280 \times 695 = \$194{,}600 \quad \text{for type 2}\\ &= 324 \times 550 = \$178{,}200 \quad \text{for type 3}\\ &= 600 \times 397 = \$238{,}200 \quad \text{for type 4}\end{aligned}$$

ii) The boost converter rating is

$$\text{The boost converter power rating} = \frac{PV\ generation}{number\ of\ converters}$$

$$\text{The boost converter rating} = \frac{50}{4} = 12.5\,kW$$

Selecting the boost converter output voltage of $V_{idc} = V_o = 345\,V$ and input voltage equal to string voltage:

$V_i = 274\,V$ for type 1, $V_i = 263\,V$ for type 2, $V_i = 258.3\,V$ for type 3 and $V_i = 261\,V$ for type 4

TABLE 5.21 Boost Converter Specifications.

PV Type	Number of Boost Converters	Input Voltage V_i (V)	Power Rating (kW)	Output Voltage, V_o (V)	Duty Ratio, D
1	4	274	12.5	345	0.205
2	4	263	12.5	345	0.237
3	4	258.3	12.5	345	0.251
4	4	261	12.5	345	0.243

The duty ratio of the boost converter is given by

$$D = 1 - \frac{V_i}{V_o}$$

$$\mathrm{D} = 1 - \frac{274}{345} = 0.205 \qquad \text{for type 1 PV}$$

$$= 1 - \frac{263}{345} = 0.237 \qquad \text{for type 2 PV}$$

$$= 1 - \frac{258.3}{345} = 0.251 \qquad \text{for type 3 PV}$$

$$= 1 - \frac{261}{345} = 0.243 \qquad \text{for type 2 PV}$$

The inverters should be rated to withstand the output voltage of the boost converter and should be able to supply the required power. Let each inverter have a rating of 10 kW.

The input voltage of the inverter is $V_{idc} = 345\,V$ with an amplitude modulation index of 0.90. The output voltage of the inverter is at 220 V AC

The number of inverters, *NI*, to process a generation of 50 kW is given by

$$NI = \frac{PV\ generation}{power\ of\ one\ inverter}$$

$$NI = \frac{50}{10} = 5$$

Hence, we need to connect five inverters in parallel to supply the load of 50 kW. Of course, we can also use one inverter with a higher rating to convert the DC power to AC. Naturally, many other designs are also possible.

Selecting a switching frequency of 5.1 kHz, the frequency modulation index will be given as

$$M_f = \frac{f_S}{f_e} = \frac{5100}{60} = 85$$

TABLE 5.22 Inverter Specifications.

Number of Inverters	Input Voltage V_{idc} (V)	Power Rating (kW)	Output Voltage, V_{AC} (V)	Amplitude Modulation Index, M_a	Frequency Modulation Index, M_f
5	345	10	220	0.90	85

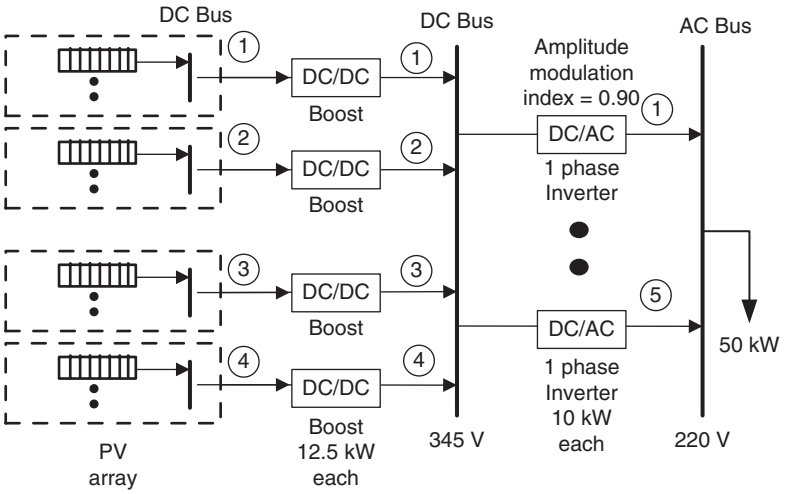

Figure 5.32 The One-Line Diagram of Example 5.4.

Students can compute the total harmonic distortion.

The one-line diagram of the system is shown in Fig. 5.32.

The selection of the type of PV system may be based on the weight and cost of the system. For residential and commercial systems with existing roof structures, the PV modules that have minimum weight are normally selected.

The selection of the boost converter is based on the power rating of the boost converter and its output voltage. The boost converter must be rated at the minimum output voltage of the PV system and the required DC input voltage of the inverter. The amplitude modulation index is selected to be less than one, but close to one for processing the maximum power of the DC source to the AC power. The frequency modulation index selected is based on the highest sampling time recommended by the manufacturer of the inverter to limit the total harmonic distortion. The number of strings and the number of modules in the string is based on the rating of the input voltage of the boost converter. The number of boost converters and inverters is based on the required output power of the PV-generating station.

5.11 A BATTERY STORAGE SYSTEM

The capacity of a battery is rated in ampere-hours (Ah). The Ah measures the capacity of a battery to hold energy: 1 Ah means that a battery can deliver one amp for 1 hour. Based on the same concept, a 110 Ah battery has a capacity to deliver 10 amps for 11 hours. However, after a battery is discharged for an hour, the battery will need to be charged longer than one hour. It is estimated it will take 1.25 Ah to restore the battery to the same state of charge. Battery performance also varies with temperature, battery type, and age. Lead-acid battery technology is well established and is a widely adopted energy source for various power industries.

Recent advances in the design of the deep-cycle lead-acid battery have promoted the use of battery storage systems when rapid discharge and charging are required. For example, if the load requires a 900 Ah bank, a number of battery storage systems can be designed. As a first design, three parallel strings of deep-cycle batteries rated 300 Ah can be implemented. The second design can be based on two strings of deep-cycle 450 Ah batteries. Finally, the design can be based on a single large industrial battery. Lead-acid batteries are designed to have approximately 2.14 V per cell. For an off-the-shelf 12 V battery the voltage rating is about 12.6 to 12.8 V.

The fundamental problem is that if a single cell in a string fails, the entire storage bank will rapidly discharge beyond the required discharge level; this will permanently destroy the bank.

It is industry practice not to install more than three parallel battery strings. Each string is monitored to ensure equal charging and discharging rates. If a storage bank loses its equalization, it will result in accelerated failure of any weak cells and the entire storage bank. The battery characteristics change with age and charging and discharging rates. It is industry practice not to enlarge an old battery bank by adding new battery strings. As the battery ages, the aging is not uniform for all cells. Some cells will establish current flow to the surrounding cells and this current will be difficult to detect. If one cell fails, changing the resistance in one battery string, the life of the entire string can be reduced substantially. Therefore, the storage system will fail. By paralleling several strings, the chances of unequal voltages across the strings increases; therefore, for optimized battery storage systems, the system should be designed using a single series of cells that are sized for their loads.

The battery capacity can be estimated for a given time duration by multiplying the rated load power consumption in watts by the number of hours that the load is scheduled to operate. This results in energy consumption in watt hours (or kilowatt hours [kWh]), stated as

$$\text{kWh} = \text{kV} \cdot \text{Ah} \tag{5.25}$$

For example, a 60-W light bulb operating for one hour uses 60 watt-hours. However, if the same light bulb is supplied by a 12-V battery, the light it will

TABLE 5.23 Typical Battery Storage Systems.

Class 1	34–40 Ah	12 V
Class 2	70–85 Ah	12 V
Class 3	85–105 Ah	12 V
Class 4	95–125 Ah	12 V
Class 5	180–215 Ah	12 V
Class 6	225–255 Ah	12 V
Class 7	180–225 Ah	6 V
Class 8	340–415 Ah	6 V

consume 5 amp-hours. Therefore, to compute Ah storage required for a given load, the average daily usage in W should be divided by the battery voltage. As another example, if a load consumes 5 kWh per day from a 48-V battery storage system, we can determine the required Ah by dividing the watt-hours by the battery voltage. For this example, we will need 105 Ah. However, because we do not want to discharge the battery more than 50%, the battery storage needed should be 210 Ah. If this load has to operate for 4 days, the required capacity is 840 Ah. If the battery cabling is not properly insulated from earth, the capacitive coupling from the DC system with earth can cause stray current flow from the DC system to underground metallic facilities, which will corrode the underground metallic structure.

Battery energy storage is still expensive for large-scale stationary power applications under the current electric energy rate. However, the battery storage system is an important technology for the efficient utilization of an intermittent renewable energy system such as wind or PV in the integration of the renewable energy in electric power systems. Utility companies are interested in the large-scale integration of a battery storage system in their substations as community storage to capture the high penetration of solar energy and wind in their distribution system. The community storage system with the ramping capability of at least an hour can be utilized in power system control. This is an important consideration for utility companies because the installed energy storage system can be used as spinning reserve.

The storage system must be effectively and efficiently scheduled for the charging, discharging, and rest time of each string. Therefore, the battery storage system requires extensive monitoring and control. These issues are currently being studied.[13,14]

5.12 A STORAGE SYSTEM BASED ON A SINGLE-CELL BATTERY

The rapid electrification of the automotive industry has a large impact on storage technology and its use in stationary power. At present, nickel metal hydride (NiMH) batteries are used in most electric and hybrid electric vehicles available to the public. Lithium-ion batteries have the best performance of the

available batteries. The cost of energy storage for grid-level renewable energy storage at present is approximately around $300–$500 per kWh. The price is rapidly decreasing as more companies are developing new technologies.

The large battery storage system is constructed from single-cell batteries[13–15] and is considered a multicell storage system. The performance of multicell storage is a function of output voltage, internal resistance, cell connections, the discharge current rate, and cell aging.[13–15]

Single-cell battery technology is rapidly making new advances, e.g., a new lithium-ion battery is being developed. The price of a single-cell battery has also been dropping dramatically. In comparison to the regular lead-acid battery where 12 cells are internally connected in a 12-V battery, the single-cell batteries can be individually connected and reconfigured. Also, because the individual single-cell's rate of charging and discharging can be monitored, the health and performance of all cells in a string can be evaluated. Figure 5.33 depicts three single cells in a string.

Figure 5.34 depicts a battery storage system consisting of two strings of three single cells that are connected in parallel making an array.

Table 5.24 presents the energy densities and power density of two single-cell batteries.

Table 5.25 presents the energy density and the cost of a storage system of lead-acid batteries as compared with single-cell batteries. In all batteries, the

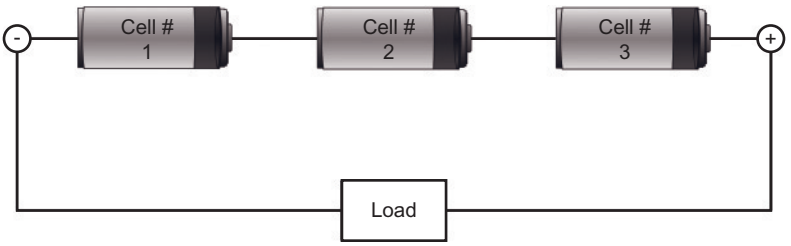

Figure 5.33 Three Single Cells in a String.

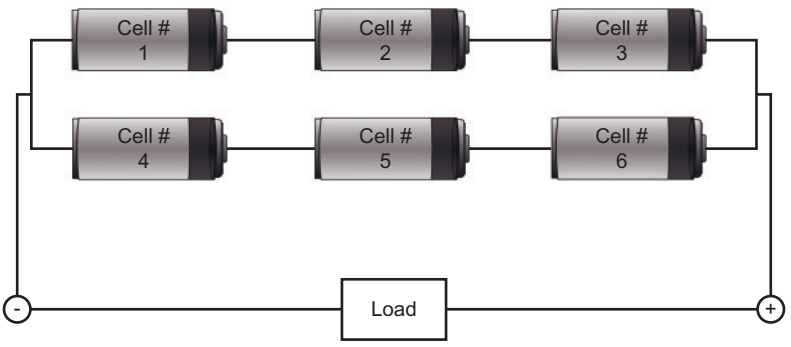

Figure 5.34 Two Strings of Three Single Cells Connected in Parallel.

TABLE 5.24 Comparison of Battery Energy Density and Power Density.[15]

Application/ Battery Type	Energy Density (Wh/kg)	Energy Stored (kWh)	Fraction of Usable Energy (%)
NiMH hydride	65	40–50	80
Lithium-ion	130	40–50	80

TABLE 5.25 The Energy Density and the Cost of a Storage System.

Type	Wh/kg	Wh	Weight Kg (1)	$/kg	$/kWh	$/kW
Standard	25	1875	75	2.5	100	9.35
Thin-film	20	1000	50	4.0	200	10.0
NiMH hydride	45	1800	40	22.5	500	45.0
Lithium-ion	65	1170	18	45	700	41.0

performance will change with repeated charging at the discharge current rates. As expected, the higher the discharge current rate is the lower will be the remaining capacity and output voltage and the higher the internal resistance. However, the reduced capacity as the result of a higher discharge current rate will be recovered after the battery system is allowed to rest before the next discharge cycle.

Therefore, the design and optimization of a multicell storage system require an understanding of the storage system's discharge performance under various operation conditions. Furthermore, if the battery storage system is to be used as a community storage system in a power grid distribution system, dynamic models of the battery systems are needed. The dynamic model of a storage system will facilitate dispatching power from intermittent green energy sources.

Example 5.5 Design a microgrid with the load of 1000 kW rated at 460 V AC and connected to the local power grid at 13.2 kV using a transformer rated 2 MVA, 460 V/13.2 kV and 10% reactance. To support the emergency loads, the microgrid needs a 200 kWh storage system to be used for 8 hours a day. Data for a three-phase inverter is given in Table 5.26. The data for the PV system is given in Example 5.4.

Determine the following:

i) The ratings of PV arrays, converters, inverters, storage systems and a single-line diagram of this design based on the minimum surface area. Also, compute the cost, weight, and square feet area of each PV type and give the results in a table.

ii) Per unit model for the design

TABLE 5.26 Three-Phase Inverter Data.

Inverter	Type 1	Type 2	Type 3	Type 3
Power	100 kW	250 kW	500 kW	1 MW
Input voltage DC	900 V	900 V max	900 V	900 V
Output voltage AC	660 VAC/ 60 Hz	660 VAC/ 60 Hz	480 VAC/ 60 Hz	480 VAC/ 60 Hz
Efficiency	Peak efficiency 96.7%	Peak efficiency 97.0%	Peak efficiency 97.6%	Peak efficiency 96.0%
Depth	30.84″	38.2″	43.1″	71.3″
Width	57″	115.1″	138.8″	138.6″
Height	80″	89.2″	92.6″	92.5″
Weight	2350 lbs	2350 lbs	5900 lbs	12000 lbs

TABLE 5.27 Inverter Specifications.

Number of Inverters	Input Voltage V_{idc} (V)	Power Rating (kW)	Output Voltage, V_{AC} (V)	Amplitude Modulation Index, M_a	Frequency Modulation Index, M_f
4	835	250	460	0.90	84

Solution

i) The load is 1000 kW rated at 460 V AC. Based on the voltage of the load and an amplitude modulation index of 0.9, we have the following input DC voltage for the inverter:

$$V_{idc} = \frac{2\sqrt{2}V_{LL}}{\sqrt{3}\cdot M_a} = \frac{2\sqrt{2}\times 460}{\sqrt{3}\times 0.9} = 835\,V$$

Selecting an inverter rated 250 kW, the total number of inverters, *NI*, for the processing of 1000 kW is given as

$$NI = \frac{PV\ generation}{rating\ of\ inverters}$$

$$NI = \frac{1000}{250} = 4$$

For this design, four inverters should be connected in parallel. If we select a switching frequency of 5.04 kHz, the frequency modulation index is

$$M_f = \frac{f_S}{f_e} = \frac{5040}{60} = 84$$

TABLE 5.28 A Photovoltaic System Design Based on Photovoltaic Type.

PV Type	Surface Area of One Module (ft^2)	Power Rating (W)	Area per Unit Power (ft^2/W)
1	12.47	190	0.066
2	15.68	200	0.078
3	16.97	170	0.100
4	7.07	87	0.081

Students should recognize that other designs are also possible. The input DC voltage of PV specifies the output AC voltage of inverters. Table 5.28 gives the data for each PV type.

As noted in Table 5.28, the PV module of type 1 requires minimum surface area. Selecting PV type 1 and string open circuit voltage of 550 V DC, the number of modules, *NM* is

$$NM = \frac{string\ voltage}{V_{MPP}}$$

where V_{MPP} is the voltage at MPP of the PV module from the PV data.

$$NM = \frac{550}{54.8} \approx 10 \quad \text{for type 1 PV}$$

The string voltage, *SV*, under load is given as:

$$SV = \mathrm{NM} \times V_{MPP}$$
$$SV = 10 \times 54.8 = 548\ V$$

The string power, *SP*, is given as

$$SP = NM \times P_{MPP}$$

where P_{MPP} is the power generated by the PV module at MPP.

$$SP = 10 \times 190 = 1.9\ kW \quad \text{for type 1}$$

If we design each array to generate a power of 20 kW, then the number of strings, *NS*, is given by:

$$NS = \frac{power\ of\ one\ array}{power\ of\ one\ string}$$

$$NS = \frac{20}{1.9} = 11$$

The number of arrays, NA, is given by

$$NA = \frac{PV\ generation}{power\ of\ one\ array}$$

$$NA = \frac{1000}{20} = 50$$

The total number of PV modules, TNM, in an array is given by

$$TNM = NM \times NS \times NA$$

where NM is number of modules in a string, NS is the number of strings, and NA is the number of arrays in a PV station.

$$NA = 10 \times 11 \times 50 = 5500 \quad \text{for PV module of type 1}$$

The total surface area needed, TS for type 1 PV module is as

$$TS = \frac{5500 \times 34.6 \times 51.9}{144} = 68{,}586\ ft^2 = 1.57\ acre$$

The total weight, TW, needed for a type 1 PV module is the product of the number of modules and the weight of each module.

$$TW = 5500 \times 33.07 = 181{,}885\ lb$$

The total cost for a PV module is the product of the number of modules and the cost of each module.

$$\text{Total cost} = 5500 \times 870 = \$4.78\ million \quad \text{for PV module type 1}$$

TABLE 5.29 The Photovoltaic Specifications.

PV Type	Number of Modules per String	Number of Strings per Array	Number of Arrays	String Voltage (V)	Total Area of the PV (ft^2)	Total Weight of the PV (lb)	Total Cost of the PV (Million $)
1	10	11	50	548	68,586	181,885	4.78

TABLE 5.30 Boost Converter Specifications.

Number of Boost Converters	Input Voltage V_i (V)	Power Rating (kW)	Output Voltage, V_o (V)	Duty Ratio, D
50	548	20	835	0.34

The output voltage of the boost converter, V_o, is the same as the input voltage, of the inverter, V_{idc}.

$$V_o = V_{idc} = 835\,V$$

The boost input voltage, V_i, is same as the string voltage, $SV = V_i = 548$ V

The duty ratio of the boost converter is given by

$$D = 1 - \frac{V_i}{V_o}$$

For this design, it is,

$$D = 1 - \frac{548}{835} = 0.34$$

We need one boost converter for each array. Therefore, the number of boost converters is 50 and each is rated 20 kW.

Table 5.23 presents a number of batteries for storing 200 kWh of energy. In storage design, we need to limit the number of batteries in a string and limit the number of arrays to three. These limitations are imposed on lead-acid-type batteries to extend the life of the storage system. We select the Class 6 batteries that are rated at 255 Ah at 12 V. In this design, three batteries per string and three strings in each array are used. The string voltage, *SV*, of the storage system is

$$SV = 3 \times 12 = 36\,V$$

The string energy stored, *SES*, in each battery is given by the product of the Ah and the battery voltage.

$$SES = 255 \times 12 = 3.06\,kWh$$

Each array has nine batteries. Therefore, the array energy stored, *AES*, is given as:

$$AES = 9 \times 3.06 = 27.54\,kWh$$

TABLE 5.31 Battery Array Specifications.

Battery Class	Number of Batteries per String	Number of Strings per Array	Number of Arrays	String Voltage (V)	Energy Stored per Array (kWh)
6	3	3	8	36	27.54

The number of arrays, NA, needed to store 200 kWh is given by

$$NA = \frac{total\ energy}{energy\ in\ each\ array}$$

$$NA = \frac{200}{27.54} \approx 8$$

Because we have eight storage arrays, we use one buck–boost converter for each array storage system. We need a total of eight buck-boost converters. The buck–boost converters are used to charge-discharge the battery storage system.

In this design, the buck–boost converter input is 835 V of the DC bus and its output must be 36 V DC to charge the battery storage system. If the storage systems are to be used for 8 hours, they can be discharged to 50% of their capacity. Therefore, they can be used to supply 100 kWh. The power, P, supplied by the storage system is given by

$$P = \frac{kWh}{hour}$$

$$P = \frac{100}{8} = 12.5\ kW$$

The array power, AP, rating is given by

$$AP = \frac{power}{number\ of\ arrays}$$

$$AP = \frac{12.5}{8} = 1.56\ kW$$

Let us select a buck–boost converter rated at 1.56 kW. The duty ratio is given by

$$D = \frac{V_o}{V_i + V_o}$$

TABLE 5.32 Buck–Boost Converter Specifications.

Number of Buck-Boost Converters	Input Voltage V_i (V)	Power Rating (kW)	Output Voltage, V_o (V)	Duty Ratio, D
8	835	1.56	36	0.04

$$D = \frac{36}{835 + 36} = 0.04$$

Figure 5.35 depicts the one-line diagram of the PV system.

ii) To compute the per unit system, we let the base volt-ampere be $S_b = 1\,MVA$. The base values for the system of Fig. 5.35 are:
The base value of watt-hours is therefore, $E_b = 1\,MWh$
The base voltage on the utility side is 13.2 kV.
The base voltage on the low-voltage side of the transformer is 460 V.
The new p.u reactance of the transformer on the new 1-MVA base is given by:

$$X_{p.u\,trans(new)} = X_{p.u\,trans(old)} \times \frac{S_{b(new)}}{S_{b(old)}} \times \left(\frac{V_{b(old)}}{V_{b(new)}}\right)^2$$

$$X_{p.u\,trans(new)} = 0.1 \times \frac{1}{2} \times \left(\frac{13.2}{13.2}\right)^2 = 0.05 \text{ p.u}$$

The per unit power, $P_{p.u}$, rating of the inverters is given by

$$P_{p.u} = \frac{power\ rating}{S_b}$$

$$P_{p.u\text{-}inverter} = \frac{250 \times 10^3}{1 \times 10^6} = 0.25\ p.u$$

And, the per unit power rating of the boost converters

$$P_{p.u\,boost} = \frac{20 \times 10^3}{1 \times 10^6} = 0.020\ p.u$$

The base voltage of the DC side of the inverter is 835 V. Therefore, the p.u voltage of the DC side, V p.u, of the inverter is

$$V_{p.u} = \frac{835}{835} = 1\ p.u$$

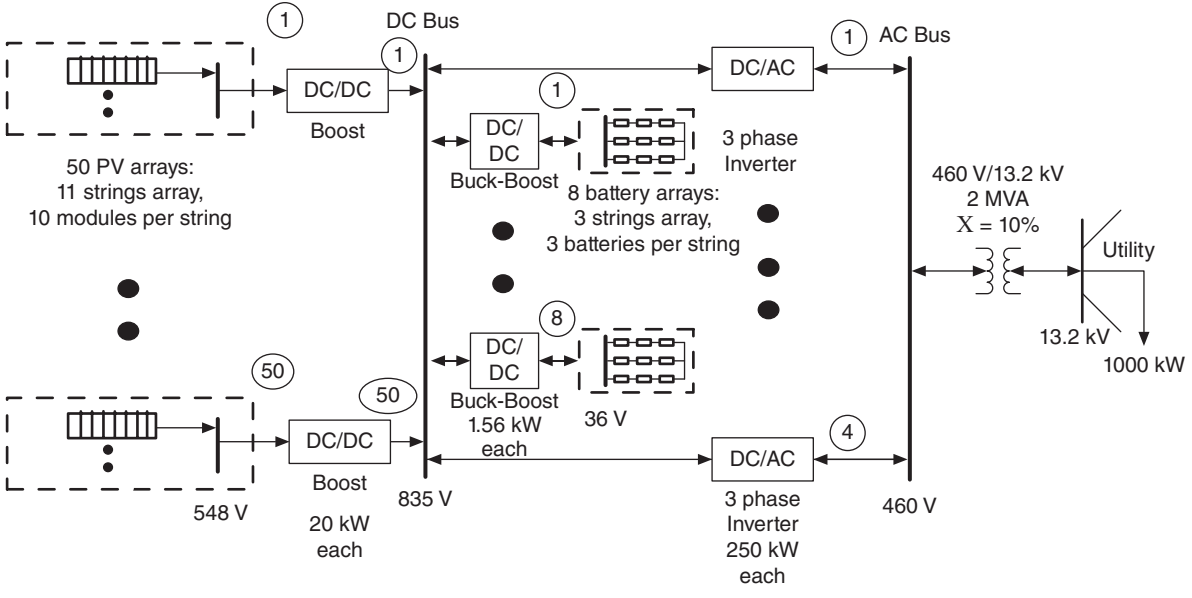

Figure 5.35 The One-Line Diagram of Example 5.5.

Because the base voltage of the low-voltage side of the boost converter is the same as the rated voltage, the per unit value is 1 p.u. The same is true for the storage system.

Similarly, the per unit power for the buck–boost and the energy storage system can be computed.

$$P_{p.u\ buck-boost} = \frac{1.56 \times 10^3}{1 \times 10^6} = 0.001\ p.u$$

$$\text{Energy stored} = \frac{27.54 \times 10^3}{1 \times 10^6} = 0.027\ p.u$$

The p.u model of the system is shown in Fig. 5.36.

Example 5.6 Design a microgrid of PV system using the data in Table 5.17, assume the total load is 500 kW at 460 V, 60 Hz three-phase AC.

For each type of PV system, determine the following:

i) The number of modules in a string, number of strings in an array, number of arrays, weight, and surface area

ii) The boost converter and inverter specifications, and the one-line diagram.

Solution

The load is 500 kW rated at 460 V AC. Based on the voltage of the load and an amplitude modulation index of 0.9, the input DC voltage for the three-phase inverter from Equation 5.16 is:

$$\frac{2\sqrt{2} \times 460}{\sqrt{3} \times 0.9} = 835\ V$$

i) Limiting the maximum voltage for a string to 600 V DC, a boost converter has to be used to boost the string voltage.

If we select string voltage, SV, to 550 V, the number of modules, NM from Equation 5.13 is

$$\begin{aligned} \text{NM} &= \frac{550}{54.8} \approx 10 \quad \text{for type 1} \\ &= \frac{550}{26.3} \approx 21 \quad \text{for type 2} \\ &= \frac{550}{28.7} \approx 20 \quad \text{for type 3} \\ &= \frac{550}{17.4} \approx 32 \quad \text{for type 4} \end{aligned}$$

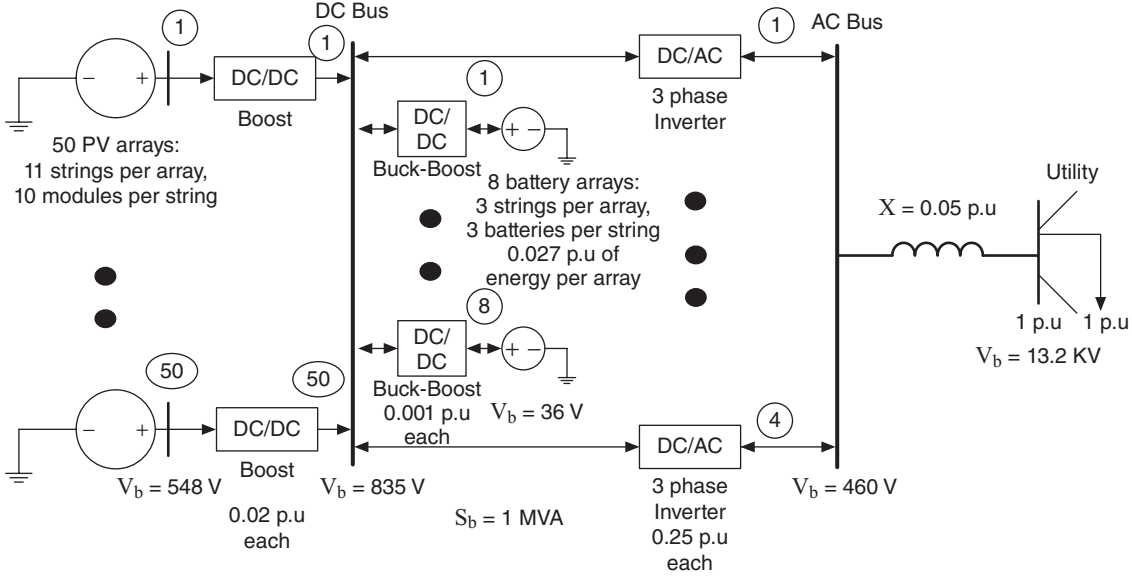

Figure 5.36 The Per Unit Model of the System Outlined in Example 5.5.

The string voltage, SV, from Equation 5.14 is

$$\begin{aligned} SV &= 10 \times 54.8 = 548\ V \quad \text{for type 1} \\ &= 21 \times 26.3 = 552\ V \quad \text{for type 2} \\ &= 20 \times 28.7 = 574\ V \quad \text{for type 3} \\ &= 32 \times 17.4 = 557\ V \quad \text{for type 4} \end{aligned}$$

String power from Equation 5.9:

$$\begin{aligned} \text{SP} &= 10 \times 190 = 1.9\ kW \quad \text{for type 1} \\ &= 21 \times 200 = 4.2\ kW \quad \text{for type 2} \\ &= 20 \times 170 = 3.4\ kW \quad \text{for type 3} \\ &= 32 \times 87 = 2.784\ kW \quad \text{for type 4} \end{aligned}$$

If we design each array to generate power of 20 kW, then the number of strings, *NS*, from Equation 5.15 is

$$\begin{aligned} NS &= \frac{20}{1.9} = 11 \quad \text{for type 1} \\ &= \frac{20}{4.2} = 5 \quad \text{for type 2} \\ &= \frac{20}{3.4} = 6 \quad \text{for type 3} \\ &= \frac{20}{2.784} = 8 \quad \text{for type 4} \end{aligned}$$

The number of arrays, *NA*, is given by Equation 5.17:

$$NA = \frac{500}{20} = 25$$

The total number of PV modules, *TNM* as given by Equation 5.19:

$$\begin{aligned} TNM &= 10 \times 11 \times 25 = 2750 \quad \text{for type 1} \\ &= 21 \times 5 \times 25 = 2625 \quad \text{for type 2} \\ &= 20 \times 6 \times 25 = 3000 \quad \text{for type 3} \\ &= 32 \times 8 \times 25 = 6400 \quad \text{for type 4} \end{aligned}$$

The total surface area, *TS*, needed by each PV type can be computed from the number of modules and each module's area in square feet.

$$TS = \frac{2750 \times 34.6 \times 51.9}{144} = 34{,}294\ ft^2 = 0.787\ acre \quad \text{for type 1}$$
$$= \frac{2625 \times 38.6 \times 58.5}{144} = 41{,}164\ ft^2 = 0.944\ acre \quad \text{for type 2}$$
$$= \frac{3000 \times 38.3 \times 63.8}{144} = 50{,}907\ ft^2 = 1.169\ acre \quad \text{for type 3}$$
$$= \frac{6400 \times 25.7 \times 39.6}{144} = 45{,}232\ ft^2 = 1.038\ acre \quad \text{for type 4}$$

The total weight is

$$\text{Total weight} = 2750 \times 33.07 = 90{,}943\ lb \quad \text{for type 1}$$
$$= 2625 \times 39.00 = 102{,}375\ lb \quad \text{for type 2}$$
$$= 3000 \times 40.70 = 122{,}100\ lb \quad \text{for type 3}$$
$$= 6400 \times 18.40 = 117{,}760\ lb \quad \text{for type 4}$$

The total cost for each design is

$$\text{Total cost} = 2750 \times 870 = \$2.39\ million \quad \text{for type 1}$$
$$= 2625 \times 695 = \$1.82\ million \quad \text{for type 2}$$
$$= 3000 \times 550 = \$2.09\ million \quad \text{for type 3}$$
$$= 6400 \times 397 = \$2.54\ million \quad \text{for type 4}$$

ii) We need to use one boost converter for each array. The total number of converters is 25—each can be selected with 20 kW rating. The nominal output voltage of the boost converter is the same as the input of the inverter.

$$V_{idc} = V_o = 835\ V$$

TABLE 5.33 The Photovoltaic Specifications for Each Photovoltaic Type.

PV Type	Number of Modules per String	Number of Strings per Array	Number of Arrays	String Voltage (V)	Total Area of the PV (ft^2)	Total Weight of the PV (lb)	Total Cost of the PV (Million $)
1	10	11	25	548	34,294	90,943	2.39
2	21	5	25	552	41,164	102,375	1.82
3	20	6	25	574	50,907	122,100	2.09
4	32	8	25	557	45,232	117,760	2.54

The input voltage, V_i, of the boost converter is equal to the string voltage.

$$V_i = 548\ V \quad \text{for type 1}$$
$$V_i = 552\ V \quad \text{for type 2}$$
$$V_i = 574\ V \quad \text{for type 3}$$
$$V_i = 557\ V \quad \text{for type 4}$$

The duty ratio of the boost converter is given by

$$D = 1 - \frac{V_i}{V_o}$$

$$D = 1 - \frac{548}{835} = 0.34 \quad \text{for type 1 PV}$$
$$= 1 - \frac{552}{835} = 0.34 \quad \text{for type 2 PV}$$
$$= 1 - \frac{574}{835} = 0.31 \quad \text{for type 3 PV}$$
$$= 1 - \frac{557}{835} = 0.33 \quad \text{for type 2 PV}$$

The inverters should be rated to withstand the output voltage of the boost converter and should be able to supply the required power. We can select each inverter having a rating of 100 kW, the input voltage of the inverter to be $V_{idc} = 835\ V$ with amplitude modulation index of 0.9 and output voltage of the inverter at 460 V AC.

The number of inverters, NI, from Equation 5.18, needed to process a generation of 500 kW is given by

$$NI = \frac{500}{100} = 5$$

TABLE 5.34 Boost Converter Specifications.

PV Type	Number of Boost Converters	Input Voltage, V_i (V)	Power Rating (kW)	Output Voltage, V_o (V)	Duty Ratio, D
1	25	548	20	835	0.34
2	25	552	20	835	0.34
3	25	574	20	835	0.31
4	25	557	20	835	0.33

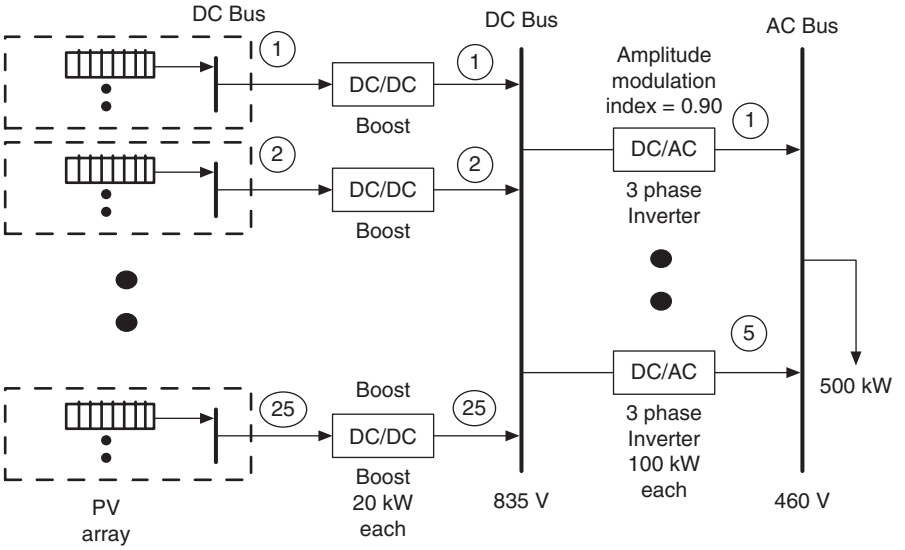

Figure 5.37 The One-Line Diagram of Example 5.6.

TABLE 5.35 Inverter Specifications.

Number of Inverters	Input Voltage, V_{idc} (V)	Power Rating (kW)	Output Voltage, V_{AC} (V)	Amplitude Modulation Index, M_a	Frequency Modulation Index, M_f
5	835	100	460	0.90	166.67

Hence, we need to connect five inverters in parallel to supply the load of 500 kW

Selecting a switching frequency of 10 kHz to limit the total harmonic distortion, the frequency modulation index is given by

$$M_f = \frac{f_S}{f_e} = \frac{10000}{60} = 166.67$$

The one-line diagram of the system is shown in Fig. 5.37.

Example 5.7 Assume a residential house total load is 7.5 kW from 11 P.M.–8 A.M. and 15 kW for the remaining 24 hours. Determine the following:

i) Plot load cycle for 24 hours
ii) Total kWh energy consumption for 24 hours
iii) If the sun irradiance is 0.5 sun for 8 hours daily, what is the roof space needed to generate adequate kWh for 24 hours operation?

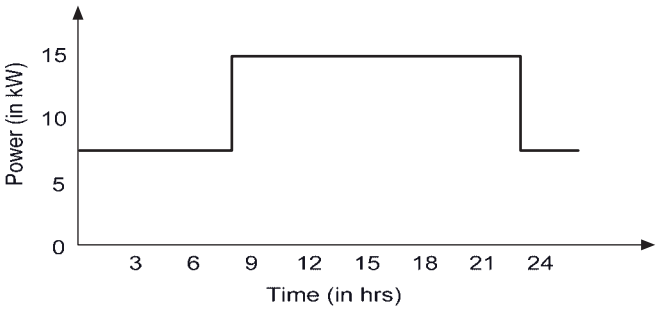

Figure 5.38 Plot of the Daily Load Cycle for Example 5.7.

iv) Assume the maximum kWh to be used during the night is 40% of the total daily load. Search the Internet to select a battery storage system and give your design data.

Solution

i) The load is 7.5 kW for 9 hours (11:00 P.M. to 8:00 A.M.) and 15 kW for 15 hours (8:00 A.M.–11:00 P.M.). The load cycle is as given in Fig. 5.38.

ii) The total kWh energy consumption for 24 hours is the area under the curve of the daily load cycle and is given by kWh = kW × hours.

Therefore, the energy consumption $= 7.5 \times 9 + 15 \times 15 = 292.5\ kWh$

iii) The type 1 PV is selected because it needs the minimum area per unit power produced.

The amount of power produced by type 1 PV (See Table 5.17) is equal to 190 W per module for 1 Sun. Therefore, the energy produced for 0.5 sun for 8 hours is given by: $0.5 \times 190 \times 8 = 0.76\ kWh$

The number of modules, *NM*, needed is given by

$$NM = \frac{total\ energy\ demand}{energy\ of\ one\ panel}$$

$$NM = \frac{292.5}{0.76} \approx 385$$

The surface area, *SM*, of one module is given by $width \times length$

$$SM = 34.6 \times 51.9 / 144 = 12.47\ ft^2$$

The total area, *TS*, for 292.5 kWh is given by the product of the number of modules and the area of one module:

$$TS = 385 \times 12.47 = 4801.11\ ft^2$$

iv) The energy used during the night is 40% of the total energy. Therefore, the energy demand for one night $= 0.4 \times 292.5 = 117\ kWh$.

From Table 5.23, a Class 6 battery storage system is chosen to store the kWh needed for the night. For battery storage conservation, the batteries should not be discharged more than 50% of their capacity.

The energy stored per battery is given by amp-hours × voltage (Ah × V). Therefore, the energy stored in one battery $= 255 \times 12 = 3.06\ kWh$. The number of batteries, *NB*, needed is given by

$$NB = \frac{2 \times energy\ demand}{energy\ stored\ per\ battery}$$

$$NB = \frac{2 \times 117}{3.06} = 77.$$

We can use three batteries in a string; the maximum number of strings in an array is three. Therefore, the maximum number of batteries in the array is $3 \times 3 = 9$.

The number of arrays of battery is given by

$$NA = \frac{total\ number\ of\ batteries}{number\ of\ batteries\ per\ array}$$

$$NA = \frac{77}{9} = 8$$

Example 5.8 Consider a microgrid with 2 MW. The system operates as part of a microgrid connected to the local utility at 13.2 KV.

The local utility uses the following design data:

a) The transformer specifications are 13.2 kV/460 V, 2 MVA, and 10% reactance; 460 V/220 V, 20 kVA, and 5% reactance.
b) The data for the PV system are given in Table 5.17.

Determine the following:

i) The number of modules in a string, number of strings, number of arrays, surface area, weight, and cost
ii) The inverter specification and the one-line diagram

Solution

A three-phase inverter rated at AC voltage 220 V can process approximately 20 kW. Based on 20 kW three-phase inverter and 220 volts AC output and the modulation index of 0.9, the input DC voltage is as given by Equation 5.16.

TABLE 5.36 Weight Per Unit Power.

PV Type	Surface Area of One Module (ft^2)	Power Rating (W)	Weight per Unit Power (lb per W)
1	33.07	190	0.174
2	39.00	200	0.195
3	40.70	170	0.239
4	18.30	87	0.210

$$V_{idc} = \frac{2\sqrt{2} \times 220}{\sqrt{3} \times 0.9} = 399\ V$$

i) Table 5.36, tabulates the data for each of the four types of PV modules.

Table 5.36 shows the PV module type 1 has the minimum weight per unit power; hence, our choice. The string voltage, SV of the PV system should be close to the rated inverter input voltage, V_{idc}.

Using string voltage, SV of 400, from Equation 5.13, we have

$$NM = \frac{399}{54.8} \approx 7$$

Using seven modules, string voltage, *SV*, as given by Equation 5.14 is

$$SV = 7 \times 54.8 = 384\ V$$

The string power, *SP*, from Equation 5.9 is

$$SP = 7 \times 190 = 1.33\ kW$$

Designing an array to generate 20 kW, the number of strings, *NS*, in an array is as given by Equation 5.15:

$$NS = \frac{20}{1.33} = 15$$

The number of arrays, *NA*, needed for this design is given by Equation 5.17:

$$NA = \frac{2000}{20} = 100$$

And, the total number of PV modules from Equation 5.19, $TNM = 7 \times 15 \times 100 = 10,500$

TABLE 5.37 The Photovoltaic Specifications for 2000 kW.

PV Type	Number of Modules per String	Number of Strings per Array	Number of Arrays	String Voltage (V)	Power per String (kW)	Total Area of the PV (ft^2)	Total Weight of the PV (lb)	Total Cost of the PV (million $)
1	7	15	100	384	1.33	130,940	347,235	9.14

The total surface area, *TS*, needed by the type 1 PV module is computed from the area of one module and the total the number of modules.

$$TS = \frac{10{,}500 \times 34.6 \times 51.9}{144} = 130{,}940\ ft^2 = 3\ acre$$

The total weight, *TW*, for the type 1 PV module can be computed in a similar manner as

$$TW = 10{,}500 \times 33.07 = 347{,}235\ lb$$

The total cost for the type 1 PV module is the product of the number of modules and the cost of each module as given below.

$$\text{Total cost of PV modules} = 10{,}500 \times 870 = \$9.14\ million$$

ii) We will use one inverter for each array. Hence, the rating of each inverter will also be 20 kW.

The number of inverters, *NI*, needed for a generation of 2000 kW as from Equation 5.18

$$NI = \frac{2000}{20} = 100$$

For 2000 kW PV-generating station, we need 100 inverters to operate in parallel. Other designs using higher rating inverters are also possible. For this design, the final input DC voltage of the inverter is specified by the string voltage as

$$V_{idc} = V_{string} = 384\ V$$

With nominal DC input, the voltage of the inverter is selected, the amplitude modulation index, M_a is given as

$$M_a = \frac{2\sqrt{2} \times 220}{\sqrt{3} \times 384} = 0.93\ V$$

If the switching frequency is selected at 10 kHz, the frequency modulation index, M_f is given as

$$M_f = \frac{f_S}{f_e} = \frac{10000}{60} = 166.67$$

The one-line diagram of the system is given in Fig. 5.39. We will use 100 transformers of 20 kVA and 5% reactance, which are connected to the inverters to step the voltage up from 220 V to 460 V. Finally, one transformer of 460 /13.2 kV and 10% reactance of 2 MVA is used to connect the system to the local power grid.

Again, students should recognize that many designs are possible. Each design specification has its own limitation that must be taken into account. The above analysis can be altered as needed to satisfy any design requirements.

TABLE 5.38 Inverter Specifications.

Number of Inverters	Input Voltage V_{idc} (V)	Power Rating (kW)	Output Voltage, V_{AC} (V)	Amplitude Modulation Index, M_a	Frequency Modulation Index, M_f
100	384	20	220	0.93	166.67

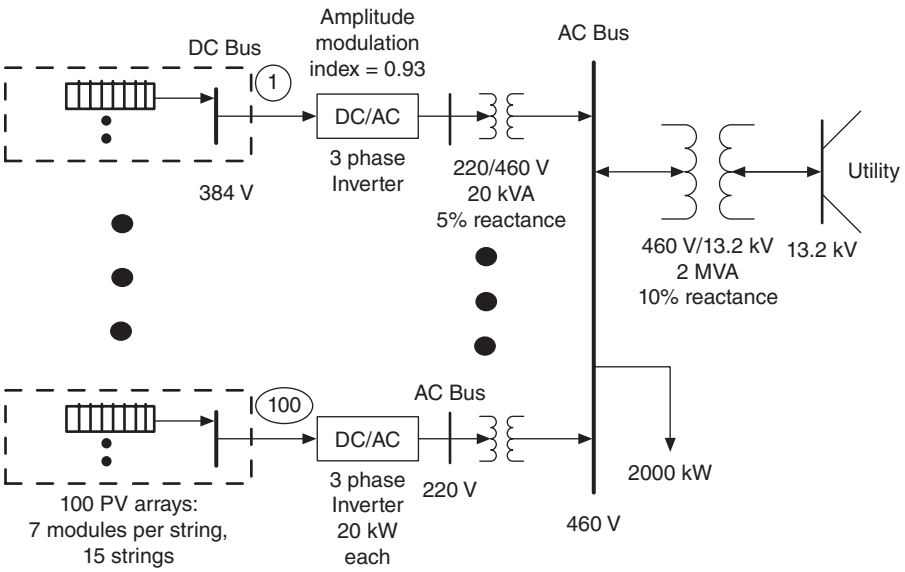

Figure 5.39 The One-Line Diagram of the System of Example 5.8.

Example 5.9 Design a microgrid of a PV system of 1000 kW that is connected to the local utility bus at 13.2 kV by a 220V/13.2kV, 500 kVA, 5% reactance transformer. A local load of 500 kW is supplied at 220 V. A battery storage system of 100 kWh is fed from an AC bus of a PV system using a bidirectional rectifier that is used 8 hours a day.

Solution
Figure 5.40 depicts the microgrid of Example 5.9. We can select a type 1 PV module that has the most minimum weight among the four PV types as shown in Table 5.36. The number of modules can be specified, based on the selection of string voltage, *SV*, as given by Equation 5.13.

$$NM = \frac{400}{54.8} \approx 7$$

If the *NM* is equal to 7, then, the SV, from Equation 5.14 is

$$SV = 7 \times 54.8 = 384\ V$$

The string power, *SP*, from Equation 5.9 is

$$SP = 7 \times 190 = 1.33\ kW$$

If we design based on 20 kW in an array, then the number of strings, *NS*, in an array from Equation 5.15 is

$$NS = \frac{20}{1.33} = 15$$

We can compute the number of arrays, *NA*, from Equation 5.17 as

$$NA = \frac{1000}{20} = 50$$

The total number of PV modules, the *TNM* from Equation 5.19 is

$$TNM = 7 \times 15 \times 50 = 5,250$$

The surface area, *TS* for type 1 PV modules is

$$TS = \frac{5,250 \times 34.6 \times 51.9}{144} = 65,470\ sq\ ft = 1.50\ acre$$

In a similar manner, we can compute the total weight and total cost.

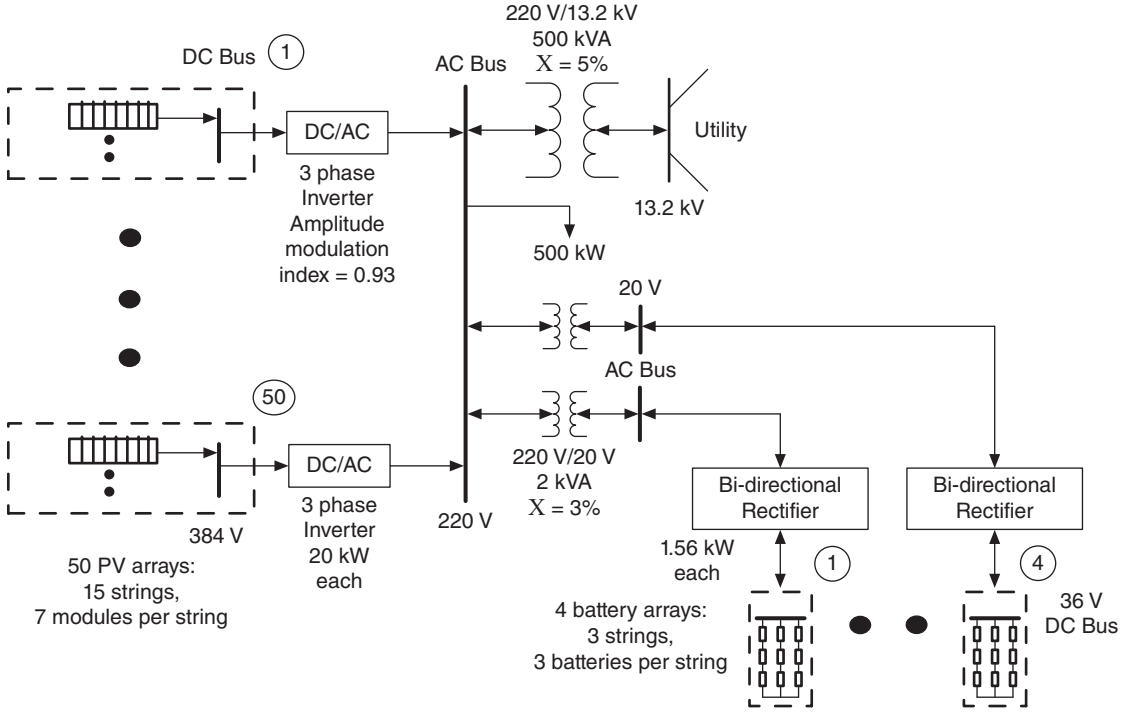

Figure 5.40 The One-Line Diagram of the PV System for Example 5.9.

TABLE 5.39 The Photovoltaic Specifications for 1000 kW.

PV Type	Number of Modules per String	Number of Strings per Array	Number of Arrays	String Voltage (V)	Total Area of the PV (ft^2)	Total Weight of the PV (lb)	Total Cost of the PV (Million $)
1	7	15	50	384	65,470	173,618	4.56

TABLE 5.40 Inverter Specifications.

Number of Inverters	Input Voltage, V_{idc} (V)	Power Rating (kW)	Output Voltage, V_{AC} (V)	Amplitude Modulation Index, M_a	Frequency Modulation Index, M_f
50	384	20	220	0.93	84

$$\text{Total weight} = 5{,}250 \times 33.07 = 173{,}618\ lb$$

$$\text{Total cost} = 5{,}250 \times 870 = \$4.56\ million$$

The rating of each inverter should be the same as the power generated by each array—20 kW. Because the input DC of the inverter is 384 V DC and output AC voltage of the inverter is 220 V AC, the amplitude modulation index, M_a of the inverter is given by

$$M_a = \frac{2\sqrt{2} \times 220}{\sqrt{3} \times 384} = 0.93$$

The number of inverters, *NI*, for a 1000 kW PV system from Equation 5.18 is

$$NI = \frac{1000}{20} = 50$$

Therefore, we need to connect 50 inverters, one for each array for generation of 1000 kW.

Let us select a switching frequency of 5.04 kHz. Therefore, the frequency modulation index is given by

$$M_f = \frac{f_S}{f_e} = \frac{5040}{60} = 84$$

One design choice for storing 100 kWh of energy is to use Class 6 batteries from Table 5.23.

TABLE 5.41 The Battery Storage Array Specification for 100 kWh.

Battery Class	Number of Batteries per String	Number of Strings per Array	Number of Arrays	String Voltage (V)	Energy Stored per Array (kWh)
6	3	3	4	36	27.54

These batteries are rated at 255 Ah at 12 V. Using three batteries per string and three strings in each array, we will have a battery storage system consisting of nine batteries in an array.

The string voltage, *SV*, for the battery storage system is given below.

$$SV = 3 \times 12 = 36\ V$$

The energy stored, *ES*, is

$$ES = Amp\text{-}hours \times Voltage$$
$$ES = 255 \times 12 = 3.06\ kWh$$

The energy stored in an array, *ESA*, is given by

$$ESA = number\ of\ batteries \times kWh\ of\ one\ battery$$
$$ESA = 9 \times 3.06 = 27.54\ kWh$$

The number of arrays, *NA*, needed to store 100 kWh is given by

$$NA = \frac{total\ energy}{energy\ in\ each\ array}$$
$$NA = \frac{100}{27.54} \approx 4$$

If the battery storage system is to supply PV loads for 8 hours, the battery storage system should be designed to discharge to 50% of capacity. Therefore, the power supplied by the battery storage system is 50% of the storage system capacity. For this design, using 50 kWh:

$$Storage\ kW = \frac{50}{8} = 6.25\ kW$$

And each array needs to supply one fourth of the total kW or 1.56 kW.

TABLE 5.42 Bidirectional Rectifier Specifications for Charging the Storage System.

Number of Bidirectional Rectifiers	Input Voltage (V) AC	Power Rating (kW)	Output Voltage (V) DC	Amplitude Modulation Index
4	20	1.56	36	0.9

A bidirectional rectifier can be used to charge and discharge the stored energy system from the AC bus of a PV-generating station (see Example 5.9). One bidirectional rectifier is used for each array of the battery storage system.

A bidirectional rectifier with an amplitude modulation index of 0.9 with the output DC voltage equal to that of the battery array is selected. The AC input of the rectifier for an output of 36 V, with a modulation index of 0.9 is given by

$$V_{L-L} = \frac{\sqrt{3} \times M_a \times V_{odc}}{2\sqrt{2}}$$

$$= \frac{\sqrt{3} \times 0.9 \times 36}{2\sqrt{2}} = 20\ V\ AC$$

One rectifier is connected to each of the battery arrays and each rectifier is designed to be rated at the same power rating of the battery array.

The total power rating of all the rectifiers together is $= 4 \times 1.56 = 6.24\ kW$.

The bus voltage at the inverter output terminals is 220 V. One transformer of 220/20 V, 3% reactance, 2 kVA is used to step down the voltage from 220 V to 20 V for each of the bidirectional rectifiers.

A 500 kVA, 220 V/13.2 kV, 5% reactance transformer is used to connect the system with the local power grid.

5.13 THE ENERGY YIELD OF A PHOTOVOLTAIC MODULE AND THE ANGLE OF INCIDENCE

To estimate the energy yield of a photovoltaic module, the angle of inclination for a module with respect to the position of the sun must be determined. The angle of inclination is defined as the position that a magnetic needle makes with the horizontal plane at any specific location. The magnetic inclination is 0° at the magnetic equator and 90° at each of the magnetic poles. The irradiance is defined as the density of radiation incident on a given surface expressed in W/m^2 or W/ft^2. When the sun rotates, the angle at which the rays of sun reach a PV module change. The PV energy yield at a location as a function the PV module inclination angle is given in Appendix C.

5.14 THE STATE OF PHOTOVOLTAIC GENERATION TECHNOLOGY

In recent years, the shift towards the development and installation of PV sources of energy has resulted in an explosion of growth in the research, development, and manufacture of PV systems. Specifically, as of 2008, 13.4 GW of PV capacity has been installed in Western countries, which is an annual growth rate of 71%, with Germany leading in terms of installed capacity, followed by Spain. Importantly, in recent years, this growth has been fueled by an increase in grid-connected systems. Today, 35% of the share of grid-connected cumulative installed capacity is comprised of grid-PV-connected centralized applications. This further highlights the growing relevance of PV systems in fulfilling the ever-increasing energy demands of the 21st century.

The current PV modules have about 12–16% efficiency. However, there are modules in production with 36% efficiency that would change the panels from 300 W to 900 W in the same footprint. Research into the development of more efficient PV modules is ongoing worldwide. The theoretical limit for a PV module constructed from multilayered cells is 60%. In the future, we can expect PV panes rated 1,500 W; concentrated solar PV has the potential to go up to 200 suns today.

The technology of high power inverters is reaching into the 2 MW class. Solar panels are being designed at 600 V bus voltage. In Italy, the Rende installation uses one MW inverter and produces 1.4 GWh per year.[16] This design uses 180 W panels. Five or 10 years from now, we can envision a scalable design of a rooftop solar PV system that can produce 2 MW. It won't take much to get there from the PV side. Students are urged to search the Internet for up-to-date developments in PV systems.[1–6]

5.15 THE ESTIMATION OF PHOTOVOLTAIC MODULE MODEL PARAMETERS

Recall the equivalent circuit of a single-diode model of a PV cell.

The model of Figure 5.41 presents the current-voltage characteristics for a single cell of a PV module.[17–20] The model of a module consisting of a number of cells, n_c can be presented as:

$$I = I_{ph} - I_o\left(e^{\frac{V+IR_s}{n_c V_t}} - 1\right) - \frac{V + IR_s}{R_{sh}} \tag{5.26}$$

In Equation 5.26, V_t, the junction thermal voltage, is given as:

$$V_t = \frac{AkT_{stc}}{q} \tag{5.27}$$

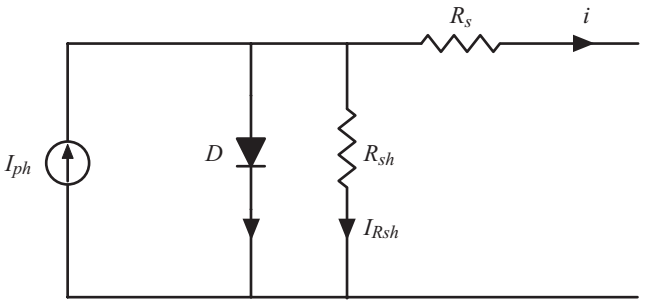

Figure 5.41 The Single Exponential Model of a PV Module.[17]

TABLE 5.43 The Photovoltaic Module Parameters of a Single Diode Model.

I_{ph}	Photo-generated current at STC
I_o	Dark saturation current at STC
R_s	Panel series resistance
R_{sh}	Panel parallel (shunt) resistance
n_c	Number of cells in the panel connected in series
V_t	Junction thermal voltage
A	Diode quality (ideality) factor
k	Boltzmann's constant
T_{stc}	Temperature at STC in Kelvin
q	Charge of the electron

It is helpful to express the equations in terms of V_t rather than A. The value of A can be determined easily if V_t is found, by simply rearranging the terms of Equation 5.27, we have:

$$A = \frac{qV_t}{kT_{stc}} \tag{5.28}$$

Table 5.43 features a description of the variables used in modeling a module presented by Equation 5.26.

The term STC denotes the standard conditions used to measure the nominal output power of photovoltaic cells. The cell junction temperature at STC is 25°C, the irradiance level is 1000 W/m^2, and the reference air mass is 1.5 solar spectral irradiance distributions. In Equation 5.26, the term "-1" is much smaller than the exponential term and it is generally ignored.

The problem of estimating the model parameters is to determine the five parameters, I_{ph}, I_o, R_s, R_{sh}, and A from the data sheet provided by the manufacturer of the PV module measured under STC. Because A can be expressed

TABLE 5.44 The Measured Data Used in Model Estimation.

I_{SC}	Short-circuit current at STC
V_{OC}	Open-circuit voltage at STC
V_{mmp}	Voltage at the maximum power point (MPP) at STC
I_{mpp}	Current at the MPP at STC

easily in terms of V_t, q, k, and T_{stc}, of which only the former is unknown, the approach will be to first obtain V_t, and then solve Equation 5.27 for A.

The V-I characteristic will be employed to estimate the model parameters. These characteristics are the short-circuit current, the open-circuited voltage, and the MPP. Table 5.44 summarizes the measured data at STC used for model development.

The model of Equation 5.26 is evaluated at the measured data points as defined in Table 5.44.

$$I_{sc} = I_{ph} - I_o e^{\frac{I_{sc}R_s}{n_c V_t}} - \frac{I_{sc}R_s}{R_{sh}} \tag{5.29}$$

$$I_{mpp} = I_{ph} = I_o e^{\frac{V_{MPP}+I_{MPP}R_s}{n_c V_t}} - \frac{V_{MPP}+I_{MPP}R_s}{R_{sh}} \tag{5.30}$$

$$I_{oc} = 0 = I_{ph} - I_o e^{\frac{V_{oc}}{n_c V_t}} - \frac{V_{oc}}{R_{sh}} \tag{5.31}$$

Because the MPP corresponds to the point where the power is maximum on the V-I characteristic, we have:

$$\left.\frac{dP}{dV}\right|_{\substack{V=V_{MPP}\\ I=I_{MPP}}} = 0 \tag{5.32}$$

We are estimating five parameters; therefore, a fifth equation is still needed. The derivative of the current with the voltage at short-circuit is given as the negative of the reciprocal of R_{sho},

$$\left.\frac{dI}{dV}\right|_{I=I_{sc}} = -\frac{1}{R_{sho}} \tag{5.33}$$

Hence, five equations with five variables have been established. The detailed derivation of five parameters from five equations are given in references 17–19.

In this chapter, we studied solar energy systems, specifically the development and design of a PV system with PV microgrid modeling. We also learned how to estimate the energy yield of a photovoltaic module based on the angle of inclination for a PV string with respect to the position of the sun. The irradiance was defined as the density of radiation incident on a given surface expressed in W/m^2 or W/ft^2. Finally, we developed an estimation method to construct a model for a PV module.

PROBLEMS

5.1 Search the Internet and specify four PV modules. Give a table as shown below (Table 5.45) and compare the rated voltage, cost, width, length, and weight.

5.2 Search the Internet to find the voltage-current characteristic of four PV modules. Make a table of input impedances as current varies for each operating temperature. Develop a plot of input impedance as a function of PV load current for each operating temperature.

5.3 Design a microgrid of PV rated at 100 kW of power at 230 V AC using a PV module with the following voltage and current characteristics. Determine the following:

i) Number of modules in a string for each PV type
ii) Number of strings in an array for each PV type
iii) Number of arrays
iv) Inverter specifications
v) One-line diagram of this system

5.4 Design a microgrid of a PV system rated at 600 kW of power at 460 V AC using a PV module with the data given in Table 5.46.

TABLE 5.45 Voltage and Current Characteristics of a Typical PV Module.

Power (max)
Voltage at maximum power point (MPP)
Current at MPP
V_{oc} (open-circuit voltage)
I_{sc} (short-circuit current)
Efficiency
Cost
List five operating temperatures for V_{oc} vs. I_{sc}
Width
Length
Height
Weight

TABLE 5.46 Photovoltaic Module Data for Problem 5.3.

Power (max)	400 W
Voltage at Maximum Power Point (MPP)	52.6 V
Current at MPP	6.1 A
V_{oc} (open-circuit voltage)	63.2 V
I_{sc} (short-circuit current)	7.0 A

Determine the following:

i) Number of modules in a string for each PV type
ii) Number of strings in an array for each PV type
iii) Number of arrays
iv) Inverter specifications
v) One-line diagram of this system

5.5 Search the Internet for four single-phase inverters and summarize the operating conditions in a table and discuss the results.

5.6 Search the Internet for DC/DC boost converters and DC/AC inverters and create a table summarizing the operating conditions of four DC/DC boost converters and DC/AC inverters and discuss the results and operations.

5.7 Design a microgrid of 50 kW, rated at 230 V AC. Use the PV module of Problem 5.3 and the converters of Problem 5.5. The design should use the least number of converters and inverters. Determine the following:

i) Number of modules in a string for each PV type
ii) Number of strings in an array for each PV type
iii) Number of arrays
iv) Converter and inverter specifications
v) One-line diagram of this system

5.8 Design a microgrid of 600 kW of power rated at 230 V AC. Use the PV module of Problem 5.3. The design should use the least number of converters and inverters. Determine the following:

i) Number of modules in a string for each PV type
ii) Number of strings in an array for each PV type
iii) Number of arrays
iv) Converter and inverter specifications
v) One-line diagram of this system

5.9 Design a microgrid of a PV system rated at 2 MW and connected through a smart net metering to the local utility at 13.2 kV. The local loads consists of 100 kW of lighting loads rated at 120 V and 500 kW

TABLE 5.47 Photovoltaic Module Data.

Panel	Type 1	Type 2	Type 3	Type 4
Power (Max), W	190	200	170	87
Voltage at max. power point (MPP), V	54.8	26.3	28.7	17.4
Current at MPP, A	3.47	7.6	5.93	5.02
V_{OC} (open-circuit voltage), V	67.5	32.9	35.8	21.7
I_{SC} (short-circuit current, A	3.75	8.1	6.62	5.34
Efficiency	16.40%	13.10%	16.80%	>16%
Cost	$870.00	$695.00	$550.00	$397.00
Width	34.6″	38.6″	38.3″	25.7″
Length	51.9″	58.5″	63.8″	39.6″
Thickness	1.8″	1.4″	1.56″	2.3″
Weight	33.07 lbs	39 lbs	40.7 lbs	18.3 lbs

of AC load rated at 220 V. The system has a 700 kWh storage system. Local transformer specifications are 13.2 kV/460 V, 2 MVA, and 10% reactance; 460 V/230 V, 250 kVA, and 7% reactance; and 230V/120 V, 150 kVA, and 5% reactance. The data for this problem are given in Table 5.47.

i) Search the Internet for four DC/DC boost converters, rectifier, and inverters and create a table. Summarize the operating conditions in a table and discuss the results and operations as they relate to this design problem. Develop a MATLAB testbed to perform the following:

ii) Select a boost converter, bidirectional rectifier, and inverters for the design of a microgrid from commercially available converters. If commercial converters are not available, specify the data for a new design of a boost converter, bidirectional rectifier, and inverters.

iii) Give the one-line diagram of your design. Make tables and give the number of modules in a string for each PV type, number of strings in an array for each PV type, number of arrays, converters, weight and surface area required for each PV module type.

iv) Design a 1700 kWh storage system. Search online and select a deep-cycle battery storage system. Give the step in your design and including the dimension and weight of the storage system.

v) Develop a per unit model of the PV microgrid system

5.10 Design a PV microgrid system operating at voltage of 400 V DC serving a load of 50 kW and at 220 V AC. Use the data sets given in Tables 5.48 and 5.50. Perform the following:

i) Select a deep-cycle battery to store 100 kWh

ii) Select a boost converter, bidirectional rectifier, and inverters for the design of a microgrid from commercially available converters

TABLE 5.48 Typical Deep-Cycle Battery Data.

Part Number	Volts	Overall Dimensions			Unit Wtlbs (kg)	Capacity Ampere-Hours							
		Length (mm)	Weight (mm)	Height (mm)		1-H Rate	2-H Rate	4-H Rate	8-H Rate	24-H Rate	48-H Rate	72-H Rate	120-H Rate
PVX-340T	12	7.71 (196)	5.18 (132)	6.89 (175)	25 (11.4)	21	27	28	30	34	36	37	38
PVX-420T	12	7.71 (196)	5.18 (132)	8.05 (204)	30 (13.6)	26	33	34	36	42	43	43	45
PVX-490T	12	8.99 (228)	5.45 (138)	8.82 (224)	36 (16.4)	31	39	40	43	49	52	53	55
PVX-560T	12	8.99 (228)	5.45 (138)	8.82 (224)	40 (18.2)	36	45	46	49	56	60	62	63
PVX-690T	12	10.22 (260)	6.60 (168)	8.93 (277)	51 (23.2)	42	53	55	60	69	73	76	79
PVX-840T	12	10.22 (260)	6.60 (168)	8.93 (277)	57 (25.9)	52	66	68	74	84	90	94	97
PVX-1080T	12	12.90 (328)	6.75 (172)	8.96 (228)	70 (31.8)	68	86	88	97	108	118	122	126
PVX-1040T	12	12.03 (306)	6.77 (172)	8.93 (227)	66 (30.0)	65	82	85	93	104	112	116	120
PVX-890T	12	12.90 (328)	6.75 (172)	8.96 (228)	62 (28.2)	55	70	72	79	89	95	98	102

TABLE 5.49 Boost Converters.

Input Voltage (V)	Output Voltage (V)	Power (kW)
24–46	26–48	9.2
24–61	26–63	12.2
24–78	26–80	11.23
24–78	26–80	11.23
24–78	26–80	13.1
24–98	26–100	12.5
80–158	82–160	15.2
80–198	82–200	14.2
80–298	82–300	9.5

TABLE 5.50 Single-Phase Inverter Data.

Inverter	Type 1	Type 2	Type 3	Type 3
Power	500 W	5 kW	15 kW	4.7 kW
Input Voltage DC	500 V	500 V max	500 V	500 V
Output Voltage AC	230 VAC/60 Hz @ 2.17 A	230 VAC/ 60 Hz @ 27 A	220 VAC/ 60 Hz @ 68 A	230 VAC/ 60 Hz @ 17.4 A
Efficiency	Min. 78% @ full load	97.60%	> 94%	96%
Length	15.5″	315 mm	625 mm	550 mm
Width	5″	540 mm	340 mm	300 mm
Height	5.3″	191 mm	720 mm	130 mm
Weight	9 lbs	23 lbs	170 kg	20 lbs

(see data in Tables 5.48–5.50). If commercial converters are not available, specify the data for the new design of a boost converter, bidirectional rectifier, and inverters.

iii) Give the one-line diagram of your design. Make tables and give the number of modules in a string for each PV type; number of strings in an array for each PV type; number of arrays, converters, weight, and surface area required for each PV module type.

5.11 Write a MATLAB testbed for the design of a PV system with minimum weight and minimum number of inverters using the data of Tables 5.47–5.51.

Perform the following:

i) PV system for 5000 kW at 3.2 kV AC: Specify the inverter operating condition

TABLE 5.51 Three-Phase Inverter Data.

Inverter	Type 1	Type 2	Type 3	Type 3
Power	100 kW	250 kW	500 kW	1 MW
Input voltage DC	900 V	900 V max	900 V	900 V
Output voltage AC	660 VAC/60 Hz	660 VAC/ 60 Hz	480 VAC/ 60 Hz	480 VAC/ 60 Hz
Efficiency	Peak efficiency 96.7%	Peak efficiency 97.0%	Peak efficiency 97.6%	Peak efficiency 96.0%
Depth	30.84″	38.2″	43.1″	71.3″
Width	57″	115.1″	138.8″	138.6″
Height	80″	89.2″	92.6″	92.5″
Weight	2350 lbs	2350 lbs	5900 lbs	12000 lbs

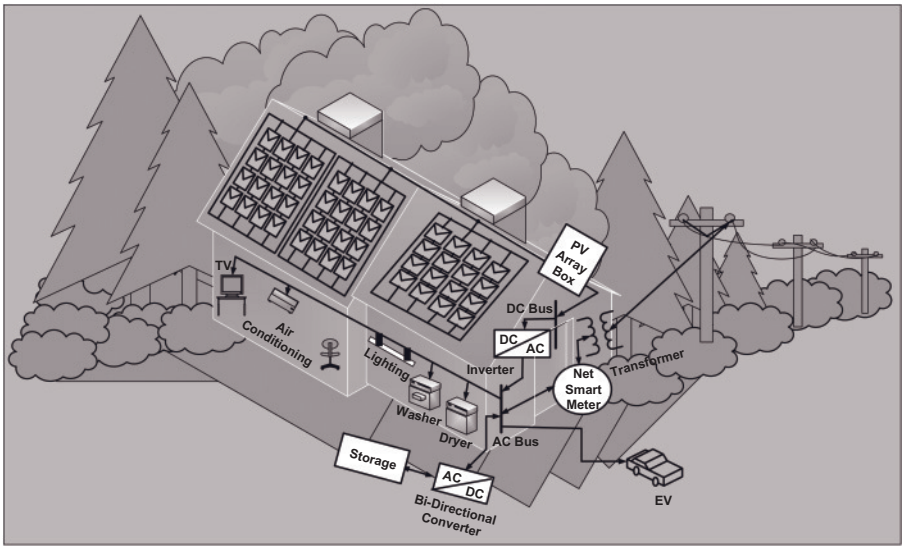

Figure 5.42 Figure for Problem 5.12.

ii) PV system for 500 kW at 460 V AC: Specify the inverter operating condition

iii) PV system for 50 kW at 120 V AC: Specify the inverter operating condition

5.12 Consider the residential home of Fig. 5.42. Perform the following:

i) Estimate the load consumption of the house.

ii) Plot the daily load cycle operation of the house's loads over 24 hours and calculate the total energy consumption.

iii) Search the Internet and select a PV module and design the PV array for the house. Compute cost, weight of PV array, and roof areas needed for the PV system. Search the Internet and select an inverter, battery storage, and bidirectional converter.

5.13 For Problem 5.11, if only 25% of the load is operated during the night, use the data of Problem 5.10 and specify a battery storage system to store the required energy for operating 25% of the load during the night.

5.14 If the price of kWh from a utility company is \$0.3 for buying or selling energy, estimate the net operating cost or revenue for the house of Problem 5.12.

5.15 Design a PV system rated 50 kW using a boost converter and a DC/AC inverter. The system operates as a standalone and supports a water pumping system with a rated load voltage of 120 V AC. Use the data given in Problem 5.10.

5.16 Design a residential PV system. The load cycle is 10 kW from 11 P.M. to 8 A.M. and 14 kW for the remaining 24 hours. Determine the following:

i) Total kWh energy consumption for 24 hours

ii) What is the roof space needed to generate adequate kWh for 24 hours operation?

iii) Assume the maximum kWh to be used during the night is 40% of the total daily load. Search the Internet to select a battery storage system and compute the required energy for nightly operation. Give your design data.

5.17 Design a microgrid for a PV system rated one MW of power at 220 V, 60 Hz with all the PV strings connected to the same DC bus. The transformer data are 220/460, V 250 kVA, and 5% reactance; and 460 V / 13.2 kV of 1 MVA, and 10% reactance. Use the data given in Tables 5.47 through 5.51.

Determine the following:

i) Number of modules in a string for each PV type, number of strings in an array for each PV type, number of arrays and surface area, weight and cost for each PV type.

ii) Boost converter and inverter specifications and the one-line diagram of this system

5.18 Assume a sample value for the global daily irradiation, G = [1900, 2690, 4070, 5050, 6240, 7040, 6840, 6040, 5270, 3730, 2410, 1800] for 12 months of the year. Assume a reflectivity of 0.25. Perform the following:

i) Write a MATLAB M-file program to (a) compute the irradiation on different inclination angles, (b) tabulate the irradiance for each month at different inclination angles, (c) tabulate the overall

irradiance per year for different inclination angles, and (d) find the optimum inclination angle for each month and a year.

ii) If the sun irradiance is 0.4 sun for 8 hours daily for this location what is the roof space needed to capture 20 kW at an optimal angle?

iii) If the sun irradiance is 0.3 sun on the average over a year for 5 hours daily for this location what total kW can be captured over 1500 square feet at the optimum inclination angle?

5.19 Assume the global daily irradiation (G) for the city of Columbus solar irradiation data, G, on the horizontal surface is as follows:

G = [1800, 2500, 3500, 4600, 5500, 6000, 5900, 5300, 4300, 3100, 1900, 1500] for 12 months of the year. The latitudinal location of Columbus is 40 degrees. Assume a reflectivity of 0.25. Perform the following:

i) Write a MATLAB M-file to (a) compute the irradiation on different inclination angles, (b) tabulate the irradiance for each month at different inclination angles, (c) tabulate the overall irradiance per year for different inclination angles, and (d) find the optimum inclination angle for each month and a year.

ii) If the sun irradiance is 0.4 sun for 8 hours daily for this location what is the roof space needed to capture 50 kW at an optimum inclination angle?

iii) If the sun irradiance is 0.3 sun on the average over a year for 5 hours daily for this location what total kW that can be captured over 1500 square feet at the optimum inclination angle?

5.20 For your city, search the Internet for solar irradiation data, G, on the horizontal surface and its latitudinal location. Perform the following:

i) Write a MATLAB M-file to (a) compute the irradiation on different inclination angles, (b) tabulate the irradiance for each month at different inclination angles, (c) tabulate the overall irradiance per year for different inclination angles, and (d) find the optimum inclination angle for each month and a year.

ii) If the sun irradiance is 0.3 sun on the average over a year for 5 hours daily for this location what is total kW that can be captured over 1500 square feet at the optimum inclination angle?

TABLE 5.52 Data for Problem 5.21.

a_1 (Isc)	3.87 A
a_2 (Voc)	42.1 V
a_3 (VMPP)	33.7 V
a_4 (IMPP)	3.56 A
a_5 (nc)	72

5.21 For a PV module given below (Table 5.52), write a MATLAB simulation testbed using Gauss–Seidel iterative approximation and estimate the module parameters (use Internet resources and learn about Gauss–Seidel iterative approximation).

REFERENCES

1. California Energy Commission. Energy quest, the energy story. Chapter 15: Solar energy. Available at www.energyquest.ca.gov/story. Accessed 2009 June 10.
2. Elmhurst College. Virtual Chembook. Energy from the sun. Available at http://www.elmhurst.edu/~chm/vchembook/320sunenergy.html. Accessed 2009 July 10.
3. Deutsche Gesellshaft fur Sonnenenergie. ebook on web: Planning and installing photovoltaic systems: a guide for installers, architects and engineers. Available at http://www.ebookee.net/Planning-and-Installing-Photovoltaic-Systems-A-Guide-for-Installers-Architects-and-Engineers_181296.html. Accessed 2009 July 2010.
4. British Petroleum. BP Solar. Available at http://www.bp.com/genericarticle.do?categoryId=3050421&contentId=7028816. Accessed 2009 July 20.
5. Cleveland CJ. 2006. The encyclopedia of earth. Mouchout, Auguste. Available at http://www.eoearth.org/article/Mouchout,_Auguste. Accessed 2010 Nov 9.
6. U.S. Department of Energy, Energy Information Administration. Official Energy Statistics from the US Government. Available at http://www.eia.doe.gov/. Accessed 2009 Sept 10.
7. Wikipedia. Augustin-Jean Fresnel. Available at http://en.wikipedia.org/. Accessed 2009 Oct 9.
8. Carlson DE, Wronski CR. Amorphous silicon solar cells. Applied Physics Letters 1976; 28: 671–673.
9. Markvart T, Castaner L. Practical handbook of photovoltaics, fundamentals and applications. Amsterdam: Elsevier; 2003.
10. Georgia State University. The doping of semiconductors. Available at http://hyperphysics.phy-astr.gsu.edu/hbase/solids/dope.html. Accessed 2010 Nov 26.
11. Energie Solar. Homepage. Available at http://www.energiesolar.com/energie/html/index.htm. Accessed 2010 Nov 26.
12. American Society for Testing and Materials (ASTM) Terrestrial. ASTM Standards and Digital Library. Available at http://www.astm.org/DIGITAL_LIBRARY/index.shtml. Accessed 2010 Nov 26.
13. Nourai A. Large-scale electricity storage technologies for energy management. In: Proceedings of the Power Engineering Society Summer Meeting. Vol. 1. Piscataway, NJ: IEEE; 2002. p 310–315.
14. Song C, Zhang J, Sharif H, Alahmad M. A novel design of adaptive reconfigurable multicell battery for poweraware embedded network sensing systems. In: Proceedings of Globecom. Piscataway, NJ: IEEE; 2007. p 1043–1047.
15. U.S. Department of Energy National Renewable Energy Laboratory. Available at http://www.nrel.gov/. Accessed 2010 Oct 10.

16. Siemens. Photovoltaic power plants. Available at http://www.energy.siemens.com/hq/en/power-generation/renewables/solar-power/photovoltaic-power-plants.htm. Accessed 2010 Oct 10.
17. Gow JA, Manning CM. Development of a photovoltaic array model for use in power-electronics simulation studies in electric power application. In: IEEE Proceedings. Vol. 146. Piscataway, NJ: IEEE; 1999. p 193–200.
18. Esram T, Chapman PL. Comparison of photovoltaic array maximum power point tracking techniques. IEEE Transactions on Energy Conversion 2007; 22(2):439–449.
19. Sera D, Teodorescu R, Rodriguez P. PV panel model based on datasheet values. In: Proceedings of the IEEE International Symposium on Industrial Electronics. Piscataway, NJ: IEEE; 2007. p 2392–2396.
20. Quaschning V. Understanding renewable energy systems. Available at http://theebooksbay.com/ebook/understanding-renewable-energy-systems/. Accessed 2009 Dec 20.

ADDITIONAL RESOURCES

Alahmad M, Hess HL. Reconfigurable topology for JPLs recharge able micro-scale batteries. Paper presented at: 12th NASA Symposium on VLSI Design; Oct 4–5, 2005; Coeur dAlene, ID.

Alahmad MA, Hess HL. Evaluation and analysis of a new solid-state rechargeable microscale lithium battery. IEEE Transactions on Industrial Electronics 2008; 55(9): 3391–3401.

ASTM International. Homepage. Available at http://www.astm.org/

Burke A. Energy storage in advanced vehicle systems. 2005. Available at http://gcep.stanford.edu/pdfs/ChEHeXOTnf3dHH5qjYRXMA/14_Burke_10_12_trans.pdf

Chan D, Phang J. Analytical methods for the extraction of solar-cell single- and double-diode model parameters from I-V characteristics. IEEE Transactions on Electronic Devices 1987; 34(2):286–293.

Davis A, Salameh ZM, Eaves SS. Evaluation of lithium-ion synergetic battery pack as battery charger. IEEE Transactions on Energy Conversion 1999; 14(3):830–835.

Delta Energy Systems. ESI 48/120V Inverter specifications. Available at http://www.delta.com.tw/product/ps/tps/us/download/ESI%20120V%20Inverter.pdf

Dzimano G. Modeling of photovoltaic systems [master's thesis]. Columbus: The Ohio State University; 2008.

Hahnsang K. On dynamic reconfiguration of a large-scale battery system. In: Proceedings of the 15th IEEE Real-Time and Embedded Technology and Applications Symposium. Piscataway, NJ: IEEE; 2009.

International Energy Agency. 2009. Trends in photovoltaic applications, survey report of selected IEA countries between 1992 and 2008. Report IEA-PVPS Task 1 IEA PVPS T1-18:2009. Available at http://www.ieapvps.org/products/download/rep1_18.pdf

Maui Solar Software. Homepage. Available at http://www.mauisolarsoftware.com.

National Renewable Energy Laboratory. Renewable Resource Data Center. Solar radiation for flat-rate collectors—Ohio. Available at http://rredc.nrel.gov/solar/pubs/redbook/PDFs/OH.PDF

Rodriguez P. PV panel model based on datasheet values. In: IEEE International Symposium on Industrial Electronics. Piscataway, NJ: IEEE; 2007.

Sandia National Laboratories. Photovoltaic research and development. Available at http://photovoltaics.sandia.gov

Siemens. Solar inverter systems. Available at http://www.automation.siemens.com/photovoltaik/sinvert/html_76/referenzen/

Taymur E. Photovoltaics systems sizing [master's thesis]. Columbus: The Ohio State University; 2009.

U.S. Department of Energy. Solar Energies Technologies Program. Available at http://www1.eere.energy.gov/solar/

U.S. General Services Administration. Homepage. Available at http://www.gsa.gov/

CHAPTER 6

MICROGRID WIND ENERGY SYSTEMS

6.1 INTRODUCTION

Historians estimate that wind energy has been utilized to sail ships since about 3200 BC.[1] The first windmills were developed in Iran (Persia) for pumping water and grinding grain.[1] Denmark developed the first wind turbine for electricity generation in 1891.[2] Today over 20% of Denmark's electricity comes from wind energy and Denmark's wind energy industry has a 27% share of the global market.

Wind energy is captured from the mechanical power of wind and converted to electric power using the classical process of Faraday's law of induction.[3]

Figure 6.1 depicts the distribution of energy consumption by energy source from 2004 to 2009 as determined by the U.S. Department of Energy (DOE).[4,5]

Although renewable energy production is small, the renewable electricity production in the United States (excluding hydropower) has nearly tripled since 2000. In 2009, about 10% of U.S. electricity was generated from renewable sources (http://www.eia.doe.gov/energyexplained/index.cfm?page=renewable_home).

The National Renewable Energy Laboratory (NREL) of the Department of Energy (DOE)[9] of the United States is dedicated to the research, development, commercialization, and deployment of renewable energy sources. The NREL provides wind data by U.S. location; students are encouraged to visit the NREL Web site to obtain data for wind power in their geographic area.

Design of Smart Power Grid Renewable Energy Systems, First Edition. Ali Keyhani.

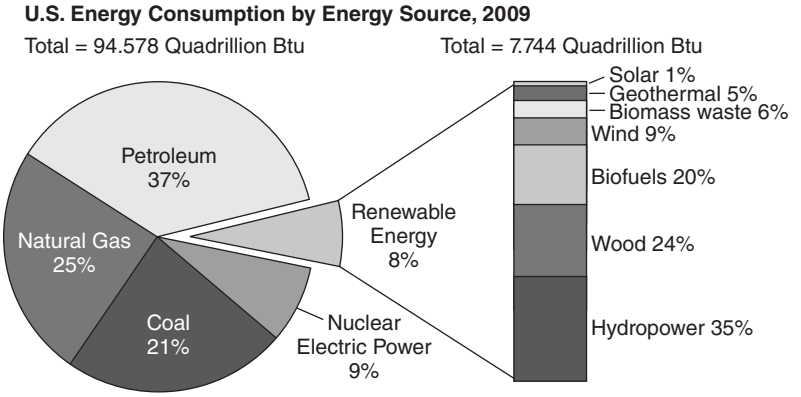

Note: Sum of components may not equal 100% due to independent rounding.
Source: U.S. Energy Information Administration, *Annual Energy Review 2009*, Table 1.3, Primary Energy Consumption by Energy Source, 1949-2009 (August 2010).

Figure 6.1 Energy Consumption in the United States by Energy Source, 2004–2009.[7]

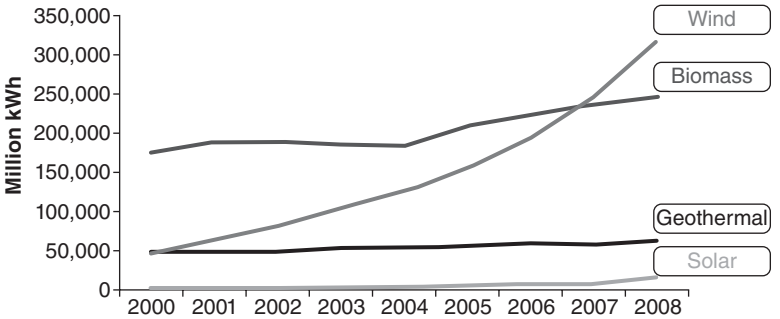

Figure 6.2 Worldwide Electricity Generation for Wind, Biomass, Geothermal, and Solar Resources, Years 2000–2008.[4]

6.2 WIND POWER

Wind energy,[7–15] as one of our most abundant resources, is the fastest growing renewable energy technology worldwide as shown in Fig. 6.2. Improved turbine and power converter designs have promoted a significant drop in wind energy generation cost making it the least-expensive source of electricity—from 37 cents/kWh in 1980 down to 4 cents/kWh in 2008. In 2008, wind energy systems worldwide generated 331,600 million kWh, which is 1.6% of total electricity generation—making wind the second highest resource after hydroelectric power (16.6%), while the photovoltaic (PV) technology contribution was only 0.1%.

The United States alone possesses more than 8,000 GW of land-based wind resources suitable for harnessing, and an extra 2,000 GW of shallow offshore resources. With U.S. total electricity generating capacity at 1,109 GW in 2008, the untapped wind sources in United States is almost 8 times as large.

Global wind movement is predicated on the earth's rotation, and regional and seasonal variations of sun irradiance and heating. Local effects on wind include the differential heating of the land and the sea, and topography such as mountains and valleys. We always describe wind by its speed and direction. The speed of the wind is determined by an anemometer, which measures the angular speed of rotation and translates it into its corresponding linear wind speed in meters per second or miles per hour. The average wind speed determines the wind energy potential at a particular site. Wind speed measurements are recorded for a 1-year period and then compared to a nearby site with available long-term data to forecast wind speed and the location's potential to supply wind energy.

A wind energy resource map for the contiguous United States from the NREL is shown in Fig. 6.3(a).[9] This map is based on a location's annual average wind speed and wind power density (in W/m^2) at 60-m (164 ft) tower height; it can be used for initial site assessment. The coastal areas have high wind energy potential; nevertheless, 90% of the U.S. usable wind resources lie in the wind belt spanning the 11 Great Plains states.[9]

As of September 30, 2009, 36,698 MW of wind power have been installed across the United States (http://www.windpoweringamerica.gov/pdfs/wind_maps/installed_capacity_current.pdf). A horizontal-axis wind turbine is made of the following subsystems.

1. Blades: Two or three blades are attached to the hub of the shaft (rotor) of the wind generator; they are made of high-density epoxy or fiberglass composites. Wind exerts a drag force perpendicular to the blades and produces lift forces on the blades that cause the rotor to turn. The blades' cross section is designed to minimize drag forces and boost lift forces to increase turbine output power at various speeds.
2. Rotor: The rotor transfers the mechanical power of wind and acts to power the generator.
3. Pitch control uses an electric motor or hydraulic mechanism. It is used to turn (or pitch) the blades to maximize the power capture of the turbine or to reduce the rotor's rotational speed in high winds.
4. A rotor brake system is used to stop the rotor for maintenance. Some advanced turbines use hydraulic brakes for the cut-in and the cut-out wind speeds when turbine power output is either too low or too high.
5. Low-speed shafts are designed to transfer mechanical power of the rotor at a speed of 30–60 rpm to the gearbox.
6. A gearbox is used to couple low-speed and high-speed shafts and steps-up the rotational speed to 1200–1600 rpm suitable for electric generators. Gearboxes have disadvantages such as noise, high cost,

frictional losses, and maintenance requirements, which preclude their use in some turbine designs.

7. Induction and permanent magnet generators are used for wind turbines.
8. Wind controllers are used to regulate and control the turbine's electrical and mechanical operation.
9. An anemometer is used to measure the wind speed and sends the measurements to the controller.
10. A weather vane is an instrument for showing the direction of the wind. The vane is used to determine wind direction and sends it to the controller, which in turn commands the yaw drive to aim the turbine nose cone in the proper orientation as the wind direction changes.
11. A nacelle is used as a weatherproof streamlined enclosure for housing shafts, a generator, a controller, and rotor brakes.
12. A high-speed shaft is used that mechanically couples the gearbox and rotor of the electric generator.
13. A yaw drive is used to orient the nacelle and the rotor using the yaw motor or hydraulic mechanism.
14. A yaw motor is used to move the nacelle with its components.
15. A tower is used to raise the turbine and hold the rotor blades and the nacelle. Turbine towers are tubular with heights approximately equal to the rotor diameter; however, a minimum height is 26 meters to avoid turbulence.

Appendix D gives a summary of estimating the mechanical power of wind.

6.3 WIND TURBINE GENERATORS

Wind turbine generators (WTG) are rapidly advancing in both technology and installed capacity.[6] Conventional geared wind generator systems have dominated the wind market for many years. Wind turbine technologies are classified based on their speed characteristics. They are either at fixed or variable speed. The speed of a wind turbine is usually low. The classical WTGs are of two types: (1) wound rotor winding, and (2) squirrel-cage induction. These systems use multistage gear systems coupled to a fixed-speed squirrel cage induction generator (SCIG), which are directly connected to the power grid.

Figure 6.5(a) depicts the distribution of stator and rotor windings. The concentrated representations of stator and rotor windings are represented in Fig. 6.5(a). However, in practice, the windings of a stator and rotor are approximately distributed sinusoidal windings. The axes of these windings are displaced by 120°. The sinusoidal distribution of stator windings are measured with angle ϕ_s and sinusoidal distribution of rotor windings are measured with angle ϕ_r. The angle θ_r represents the rotor angle as it rotates around the air gap.

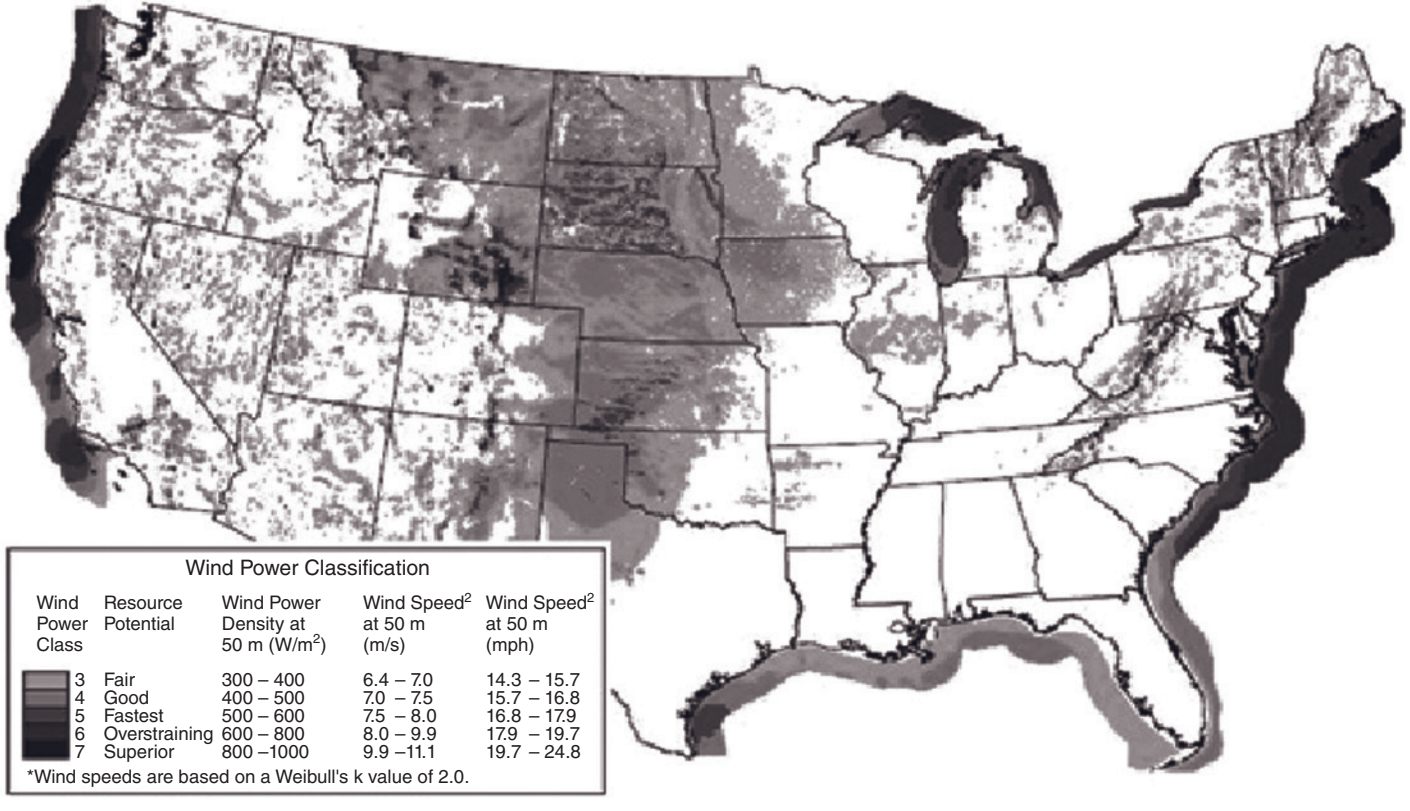

Wind Power Classification

Wind Power Class	Resource Potential	Wind Power Density at 50 m (W/m^2)	Wind Speed[2] at 50 m (m/s)	Wind Speed[2] at 50 m (mph)
3	Fair	300 – 400	6.4 – 7.0	14.3 – 15.7
4	Good	400 – 500	7.0 – 7.5	15.7 – 16.8
5	Fastest	500 – 600	7.5 – 8.0	16.8 – 17.9
6	Overstraining	600 – 800	8.0 – 9.9	17.9 – 19.7
7	Superior	800 –1000	9.9 –11.1	19.7 – 24.8

*Wind speeds are based on a Weibull's k value of 2.0.

(a)

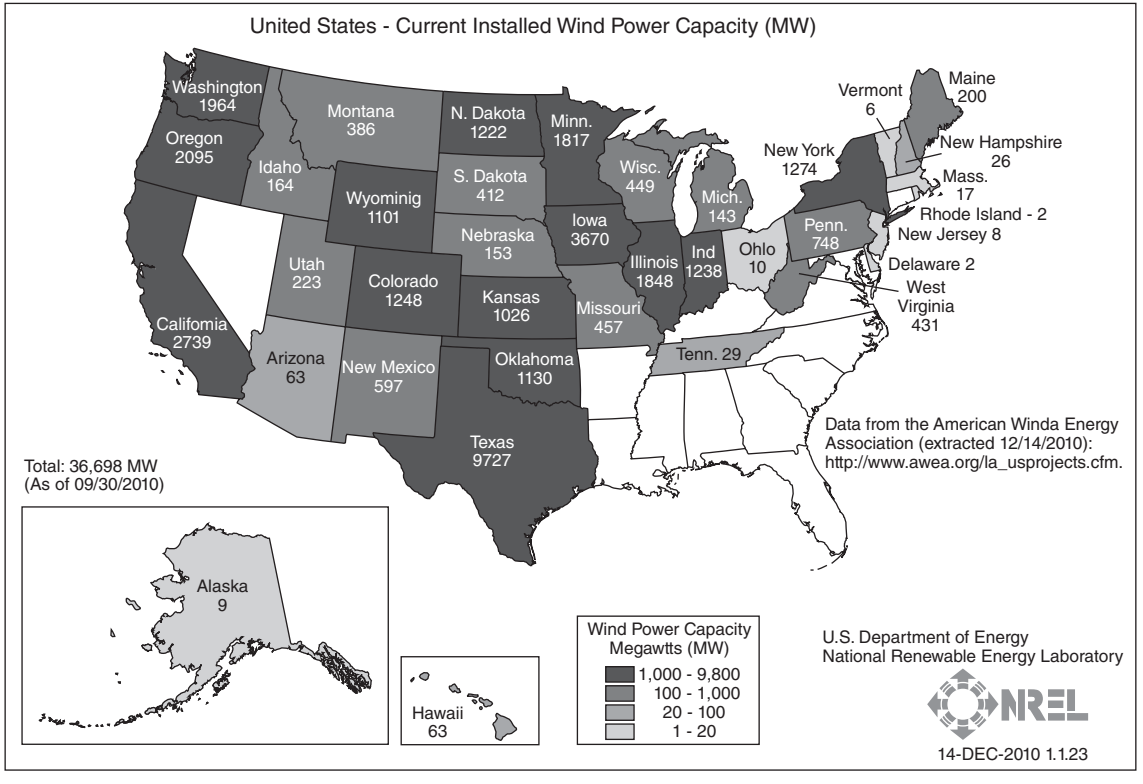

(b)

Figure 6.3 **(a)** Wind Resource Map of the Contiguous United States with Wind Power Classifications Indicated by Region.[6] **(b)** Installed Wind Power in the United States as of 2009 (http://www.windpoweringamerica.gov/pdfs/wind_maps/installed_capacity_current.pdf).

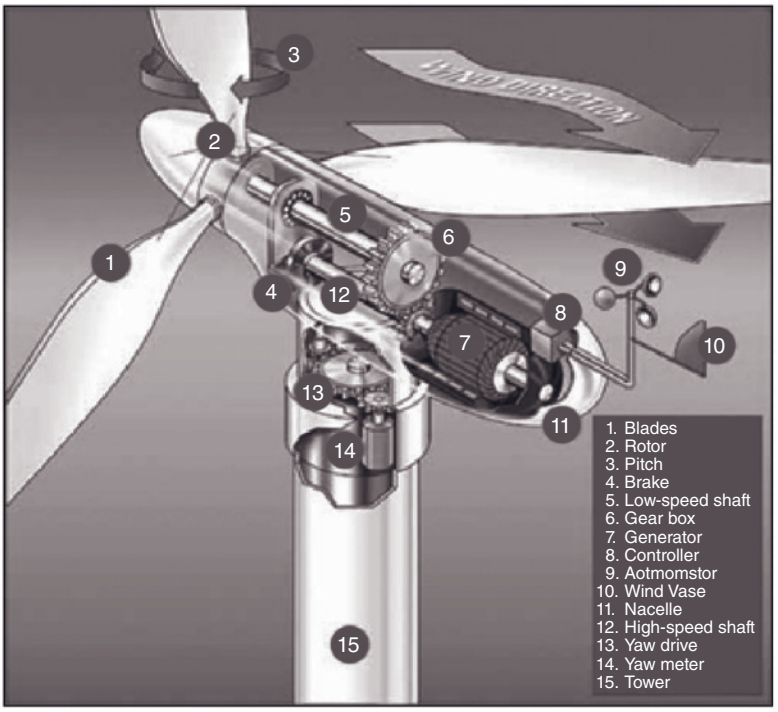

Figure 6.4 A Wind Turbine System (Photo from the National Renewable Energy Laboratory).[7–9]

When the stator windings are excited with balanced three-phase sinusoidal currents, each phase winding produces a pulsating sinusoidal vector field along the winding axis and pointing to where the field is maximum positive as shown in Fig. 6.5(a). The effect of the three-phase winding vector field distribution is equivalent to having a single sinusoidal distributed vector field. For a two-pole machine, if the stator winding are excited by a 60-Hz source, the synchronous speed of the two-pole vector field is 3600 rpm.

An electronic switch is used to provide a soft start to smooth the connection and disconnection of the generator to the grid by limiting the unwanted inrush current to about 1.6 times the nominal current. The circuit breaker can be automatically controlled by a microcontroller or manually controlled. A zero-crossing is the instantaneous point at which there is no voltage (current) present. In an AC alternating wave, this normally occurs twice during each cycle as shown in Fig. 6.7. Assuming the system operates at a lagging power factor, for example at a lagging power factor of 0.86, the current then lags the voltage as shown in Fig. 6.7.

The soft-switch circuit breaker is controlled by a microcontroller or a digital signal processor. The soft-switch circuit breaker is closed at a zero crossing of voltage and it is open at zero crossing of current. The soft switch is also

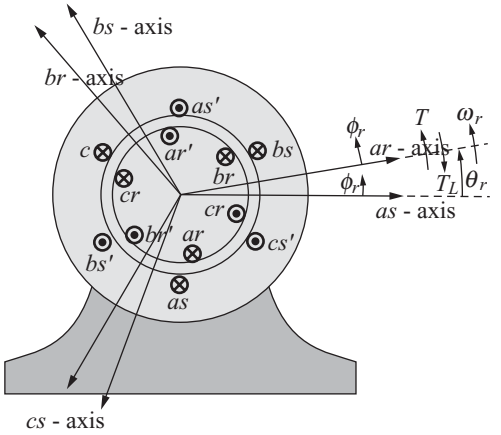
bs - axis
br - axis
as'
ar'
c
bs
br
cr
cr
bs'
br'
ar
cs'
as
cs - axis
ϕ_r
T
ω_r
ar - axis
ϕ_r
T_L
θ_r
as - axis

(a)

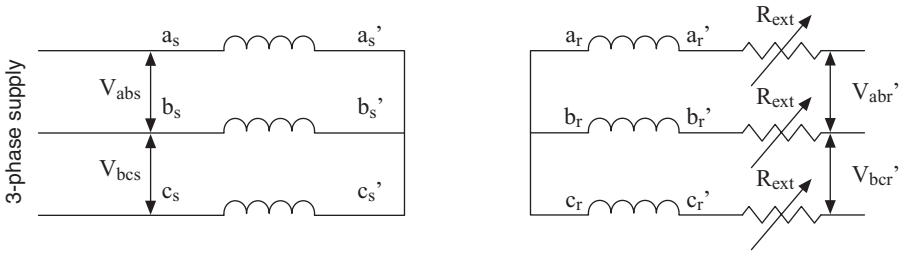
3-phase supply
a_s
a_s'
V_{abs}
b_s
b_s'
V_{bcs}
c_s
c_s'
a_r
a_r'
R_{ext}
R_{ext}
V_{abr}'
b_r
b_r'
R_{ext}
V_{bcr}'
c_r
c_r'

(b)

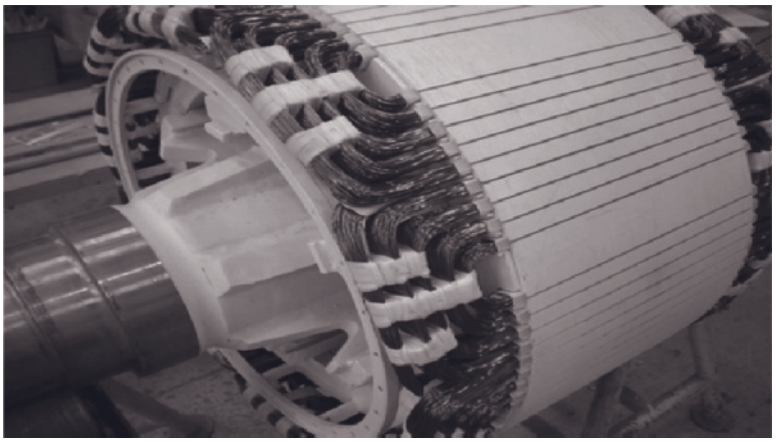

(c)

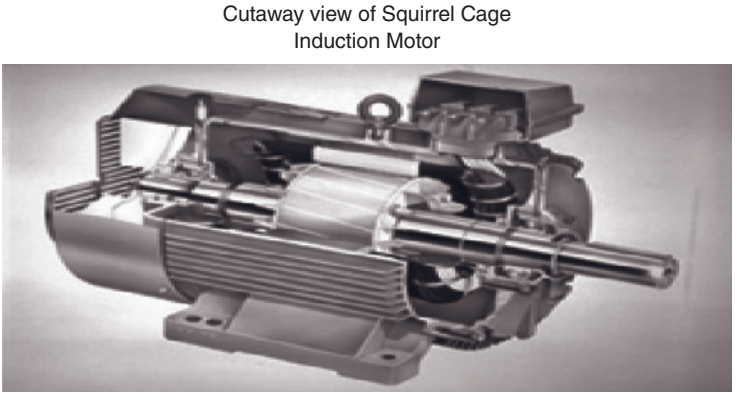

(d)

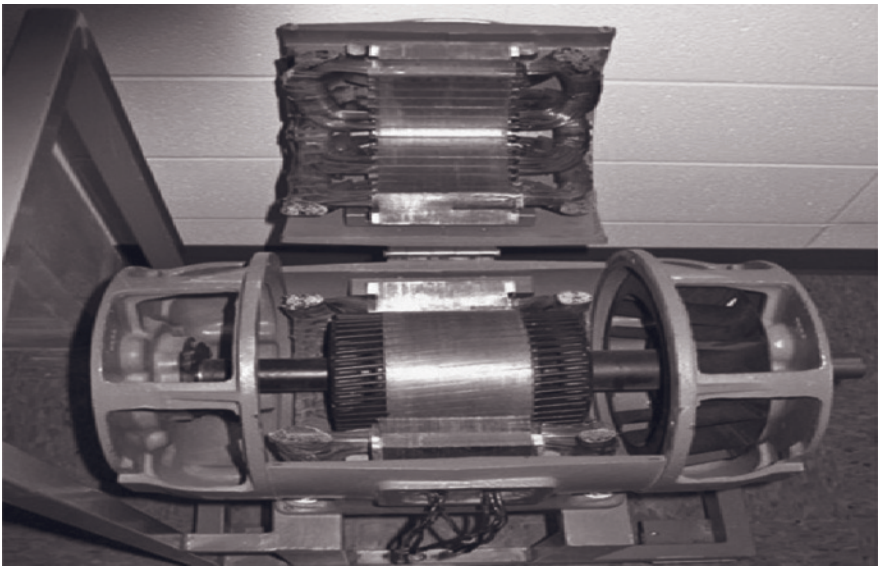

(e)

Figure 6.5 Induction Machine Types. (a) Wound Machine Stator and Rotor Windings. (b) Equivalent Circuit. (c) A View of Wound Rotor Winding. (d) A Cutaway View of a Squirrel Cage Induction Generator (SCIG). (e) A View of a Squirrel Cage Induction Generator.[15–16] Figures 6.5(c)–(e) are courtesy of ABB (http://www.abb.com/product/us/9AAC133417.aspx).

protecting the mechanical parts of the turbines such as a gearbox and shaft against high forces. The soft switch uses controllable thyristors to connect the generator to the induction generator at zero crossing of the sinusoidal voltage of the generator 2 seconds after the induction machine operates above the synchronous speed.

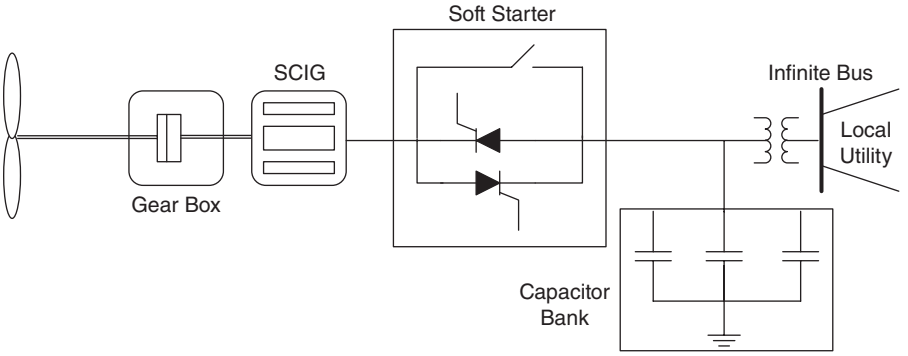

Figure 6.6 The Schematic of a Squirrel Cage Induction Generator (SCIG) System Microgrid.

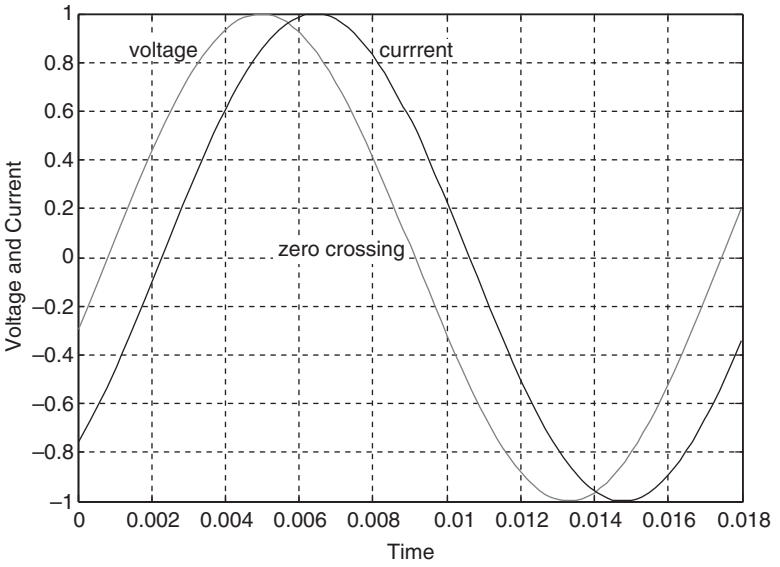

Figure 6.7 The Zero Crossing of an AC Source Supplying Power at 0.86 Power Factor Lagging.

6.4 THE MODELING OF INDUCTION MACHINES

In the three-phase round induction machines with wound windings on the rotor, the stator windings consist of three-phase windings. The rotor winding also consists of three-phase wound windings. For a squirrel cage induction machine, the rotor of the machine does not have winding; instead it has a cage that is normally constructed from aluminum.

For mathematical modeling of the machine's steady-state model,[17–18] it is assumed that the stator and rotor windings are balanced. In the case of a squirrel cage induction machine, it is assumed the rotor is represented by an equivalent winding. Each phase of the stator winding is designed using the same wire size and occupies the same space on the stator of the machine. The same is true for rotor winding. To understand the basic relationship between the current flowing in the windings and the resulting field distribution, we need to recall the relationship of field distribution in the machine stator and rotor and machine air gap. Let us first review the fundamentals of field distribution in a rectangular structure of an inductor depicted in Fig. 6.8. These discussions facilitate our understanding of the basic concept of inductance and induction, which is used later in this chapter.

According to the fundamentals of electromagnetics, the field intensity can be expressed as the product of H in A/m, times the mean length of the magnetic core is equal to number of turns, N times the current, I flowing in the winding as given below.

$$Hl = NI \tag{6.1}$$

From the fundamental relationship the field intensity, H and flux density, B in weber per square meter (Wb/m^2), and the permeability, μ of the core material are related as:

$$H = \frac{B}{\mu} \tag{6.2}$$

where $\mu = \mu_r\ \mu_o$; $\mu_o = 4\pi \times 10^{-7}$ (H / m), and μ_r is relative permeability. For example, the relative permeability is equal to one for air. For iron, the relative permeability is in the range of 26,000 to 360,000. Therefore, μ is the slope of the $B = \mu H$ and H is the field winding. The flux lines distribution in the rectangular structure of Fig. 6.8 can be computed by multiplying the field density by cross-sectional area of core, A expressed as:

$$\Phi = BA \tag{6.3}$$

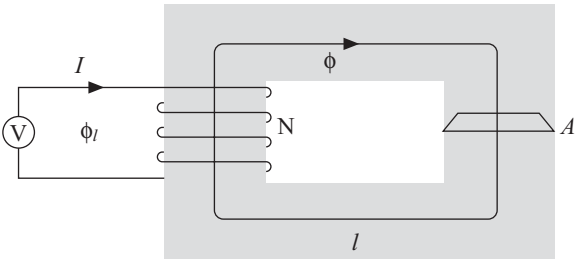

Figure 6.8 An Inductor Winding.

The flux linkage Φ represents the flux lines that link the winding; they are expressed in weber. The flux leakage, Φl represents the flux lines that are leaked in the surrounding medium and do not remain in the core structure.

If we assume the leakage flux lines are zero, then we can express the product of field intensity, H, and the mean length of the core to be equal to magnetomotive force, mmf, as shown by Equation 6.4.

$$Hl = mmf \tag{6.4}$$

Therefore, the magnetomotive force is the force of the number of turn times of the current flowing through the winding, NI, which creates the force that produces the magnetic flux that is the result of the field intensity H.

By substituting for H in Equation 6.4, we obtain the flux flow in the stator structure, rotor structure, and the air gap as:

$$\Phi \cdot \frac{l}{\mu.A} = mmf \tag{6.5}$$

$$\Re = \frac{l}{\mu \cdot A} \tag{6.6}$$

The Equation 6.6 is defined as reluctance. The reluctance is analogous to resistance. It is a function of the dimension of the medium through which the flux flows.

$$\Phi \cdot \Re = mmf \tag{6.7}$$

The reluctance is inversely proportional to inductance, which is directly proportional to the square of the number of turns. The inductance, L, represents the inductance of the inductor of Fig. 6.8

$$L = \frac{N^2}{\Re} \text{ or } L = \mu \frac{N^2 A}{l} \tag{6.8}$$

To understand the permeability, μ, we need to understand the hysteresis phenomena. A hysteresis loop shows the magnetic characterics of a ferromagnetic material under test. The relationship shows the relationship between the voltage applied to a winding with a core structure made from a ferromagnetic material and resulting current flow in the winding. The induced magnetic flux density (B) is calculated from the applied voltage and the magnetizing field intensity (H) from the current flow through the winding. It is often referred to as the B-H loop. An example of a hysteresis loop is shown in Fig. 6.9. The

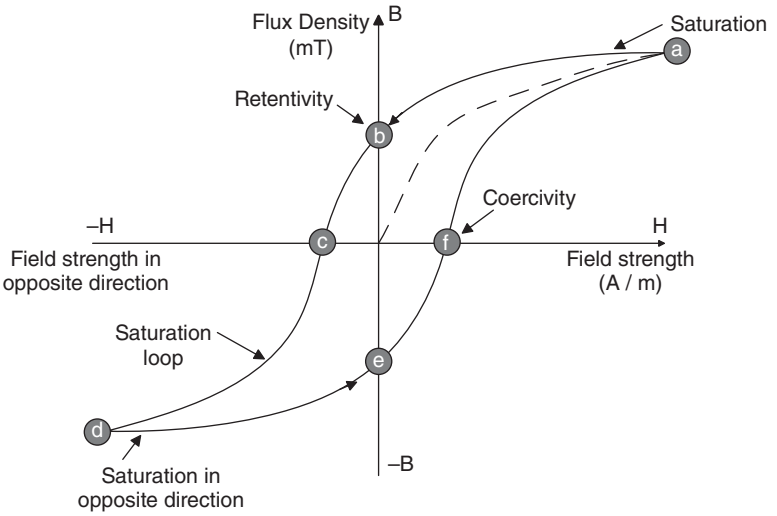

Figure 6.9 A Schematic of a Hysteresis Loop.[19]

loop is produced by measuring the magnetic flux of a ferromagnetic material while the applied voltage is changed.

A ferromagnetic core that has not been previously magnetized will follow the dashed line as the applied voltage is increased, resulting in higher current and higher magnetic intensity, H is increased. The greater the applied excitation current to produce, H+, the stronger is the magnetic field density, B+. For a Point a, depending on the type of magnetic material, however, a higher applied voltage will not produce an increased value in magnetic flux. At the point of magnetic saturation the process is changed in the opposite direction as shown in Fig. 6.9 and recorded voltage and current representing flux density and field intensity move from Point a to Point b. At this point, some residual flux remains in the material even after the applied voltage is reduced to zero. This point is called retentivity on the hysteresis loop and shows the residual magnetism (remanence) in the material. As the applied voltage direction is changed, the recorded flux density and field intensity moves to Point c. At this point the flux is reduced to zero. This is called the point of coercivity on the hysteresis loop. When the voltage is applied in a negative direction, the material is saturated magnetically in the opposite direction and reaches Point d. As the applied voltage is increased in positive direction, again H crosses zero at some value of the applied voltage and the hysteresis loop reaches the Point e. As the applied voltage is increased further, H is increased back in the positive direction, the flux density, B returns to zero. If the applied voltage repeats the same cycle, the process is repeated. If the process is reversed, the loop does not return to original position. Some force is required to remove the residual magnetism and to demagnetize the material.[19]

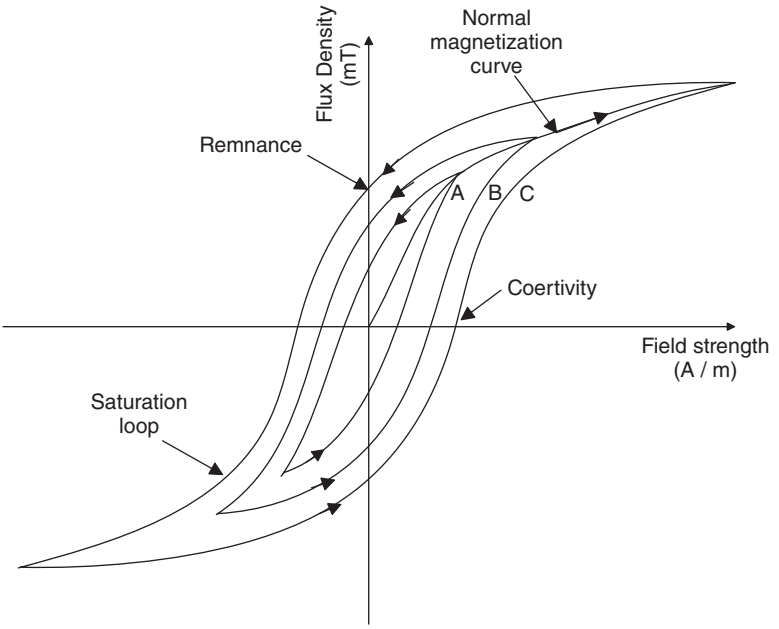

Figure 6.10 A Family of Hysteresis Loops as Applied Voltage to the Winding Is Varied.[19]

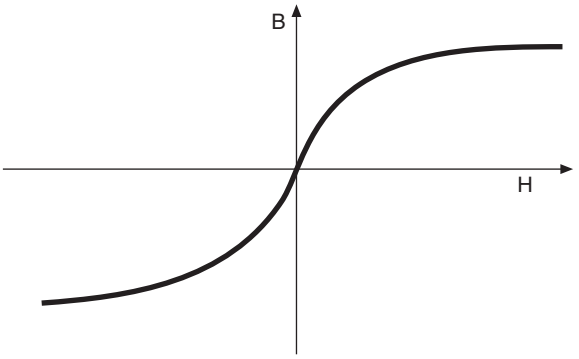

Figure 6.11 The Normalized Magnetization Curve.

Figure 6.10 shows the traces of a family of hysteresis loops as applied voltage to the winding is varied. When the tips of the hysteresis loops, A, B, C, and D are connected, the result is a normalized magnetizing curve.

Because $B = \mu H$, therefore, the permeability, μ is the slope of hysteresis as expressed by Equation 6.9.

$$\mu = \frac{B}{H} \tag{6.9}$$

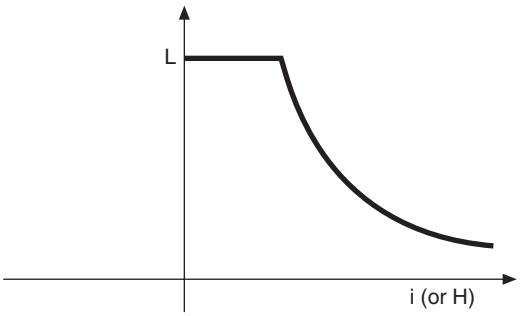

Figure 6.12 Schematic of Inductance as a Core Structure Saturated.

In the linear region of magnetization curve, the inductance is linear as given by Equation 6.8. Figure 6.12 shows the change in inductance of the rectangular core as the core is saturated.

Figure 6.8 represents a simple rectangular structure. However, a three-phase induction machine has three windings on the stator and three windings on the rotor as shown in Fig. 6.5(b). The three windings on the stator are placed on the circumference of the stators at 120° apart. The three-phase rotor windings are also located on the circumference of the rotor at 120° apart. As a motor operation, the stator is supplied from the three-phase AC voltage source. The time-varying AC source would magnetize the stator structure and give rise to time-varying flux density and time-varying inductance for each phase of the stator. Although the cylindrical structure is more complex to calculate these inductances, we can use an advanced finite element calculation and make discrete elements of the stator structure to calculate the flux in these elements. However, finite element calculation is an advanced topic that is not a subject in this book. From our study of the inductor, we can conclude that the inductances of the stator are a function of the diameter, number of turns, permeability of the stator material, and cross-sectional area and excitation current. Therefore, we recognize that the flux density variation in winding a-a′ when it is energized from the AC alternating source can be expressed as:

$$B_a(\theta_r, t) = B(t)\cos\left(\frac{P}{D}\theta_r\right) \tag{6.10}$$

where $B\ (t)$ is time-varying flux density produced by the phase a applied voltage, $v_a(t)$

$$B(t) = B_{\max}\cos\omega_s t \tag{6.11}$$

In Equation 6.11, the $\omega_s = 2\pi f$ is the source frequency and θ_r is the angle around the circumference of the stator; P is number of poles; D is diameter and $\frac{P}{D}\theta_r$ angle in radians.

For example, $B_a(x,t) = B_{\max}$ when $\theta_r = 0$.

And $\theta_r = \frac{2\pi D}{P}$, the Equation 6.10 can be expressed,

$$B_a(x,t) = B(t)\cos\left(\frac{P}{D}\frac{2\pi D}{P}\right) = B_{\max} \tag{6.12}$$

Substituting Equation 6.12 in Equation 6.10, we can obtain Equation 6.13.

$$B_a(x,t) = \hat{B}\cos\omega_s t\cos\left(\frac{P}{D}\theta_r\right) \tag{6.13}$$

Using the cosine identity in Equation 6.13, we can obtain Equation 6.14.

$$\cos\alpha\cos\beta = \frac{1}{2}[\cos(\alpha-\beta)+\cos(\alpha+\beta)]$$

$$B_a(x,t) = \frac{\hat{B}}{2}\cos\left(\frac{P\theta_r}{D}-\omega_s t\right)+\frac{\hat{B}}{2}\cos\left(\frac{P\theta_r}{D}+\omega_s t\right) \tag{6.14}$$

We can obtain the same expression for windings b-b′ and c-c′ as expressed by Equations 6.15 and 6.16.

$$B_b(x,t) = \hat{B}\cos\left(\omega_s t-\frac{2\pi}{3}\right)\cos\left(\frac{P\theta_r}{D}-\frac{2\pi}{3}\right) \tag{6.15}$$

$$B_c(x,t) = \hat{B}\cos\left(\omega_s t-\frac{4\pi}{3}\right)\cos\left(\frac{P\theta_r}{D}-\frac{4\pi}{3}\right) \tag{6.16}$$

Recall that the flux density is a vector quantity, we can add flux density generated by phase a, phase b, and phase c, and we can obtain the total flux generated as expressed by Equation 6.17.

$$B_{tot}(x,t) = B_a(\theta_r,t)+B_b(\theta_r,t)+B_c(\theta_r,t) \tag{6.17}$$

$$B_{tot}(x,t) = \frac{3}{2}\hat{B}\cos\left(\frac{P\theta_r}{D}-\omega_s t\right) \tag{6.18}$$

The peak value of flux density crossing the air gap of the machine is given by Equation 6.19.

$$B_{\max} = \frac{3}{2}\hat{B} \tag{6.19}$$

The rotor windings are distributed on the rotor structure. The total time-varying flux density of stator windings crossing the air gap links the rotor windings and induces voltage in the rotor windings. Let us analyze the rotor induced voltage assuming two conditions: (1) the rotor is at standstill, and (2) the rotor is free to rotate.

1. The rotor is at standstill.

$B_{tot}(\theta_r, t)$ is the total flux distribution in the machine and the frequency of flux wave is expressed as

$$\begin{aligned} \omega_s &= 2\pi \cdot f_s \\ f_s &= \text{stator frequency} \end{aligned} \tag{6.20}$$

This flux distribution can be regarded as a flux wave that is distributed in the air gap machine with the mechanical equivalent speed as

$$\omega_{mech}(equivalent) = \frac{2}{P} \cdot \omega_s \tag{6.21}$$

The mechanical speed expressed by Equation 6.21 is also called the synchronous speed.

$$\omega_{syn} = \frac{2}{P} \cdot \omega_s \tag{6.22}$$

Let us assume that we short the rotor windings and also assume that the rotor is restrained and remains at standstill. The stator flux wave distribution of the stator crosses the machine air gap and links the rotor windings and induces the voltage in phases a, b, and c of the rotor windings. The resulting current flow in rotor windings gives rise to the rotor flux of rotor windings. Adding flux waves produced by phases a, b, and c of rotor windings, we can obtain,

$$\begin{aligned} B_R(x,t) &= B_{aR}(x,t) + B_{bR}(x,t) + B_{cR}(x,t) \\ &= \frac{3}{2}\hat{B}\cos\left(\frac{P\theta_r}{D} - \omega_{stator}t\right) \end{aligned} \tag{6.23}$$

Because the rotor is at standstill, and shaft speed is zero, the rotor frequency is the same as stator frequency. In fact, the induction machine is acting like a three-phase transformer; however, in a cylindrical structure with the rotor supported on a bearing system that separates the stator from the rotor with a very small air gap, the stator and rotor windings are coupled.

2. The rotor is free to rotate.

Suppose the rotor is free to rotate. Let us assume the rotor is rotating at a speed of ω_m, then the rotor total flux wave distribution, $B_R(x,t)$ has the mechanical speed as expressed by Equation 6.24.

$$\omega_r(mech) = \omega_{syn} - \omega_m \tag{6.24}$$

$\omega_r(mech)$ is the rotor mechanical speed that is the difference between the synchronous speed and the shaft speed because the shaft is free to rotate. The electrical speed of the rotor flux wave is expressed as given by Equation 6.25.

$$\omega_r = \frac{P}{2}\omega_r(mech) = \frac{P}{2}(\omega_{syn} - \omega_m) \tag{6.25}$$
$$\omega_r = 2\pi f_r$$

f_r = frequency of induced voltage (current) in the rotor

The total flux distribution of stator flux, $B_s(\theta_r,t)$ has the equivalent mechanical speed of $\omega_{syn.}$ This flux distribution for a two-pole machine has two poles as shown in Fig. 6.13. The total flux distribution of the rotor, $B_R(\theta_r,t)$ of the rotor rotates at $\omega_{syn} - \omega_m$ for a two-pole machine with respect to the rotor structure and $B_R(\theta_r,t)$ of the rotor structure rotates at ω_m (mechanical speed) with respect to the stator.

The two flux waves are distributed in the machine at an angle as shown in Fig. 6.13. Motor action ω_{syn} and ω_m are rotating in the same direction and $\omega_{syn} > \omega_m$.

6.4.1 Calculation of Slip

$$\omega_r = \frac{P}{2}(\omega_{syn} - \omega_m) \tag{6.26}$$

Let us multiply and divide by ω_{syn} (stator electrical speed):

$$\omega_r = \frac{\omega_{syn} - \omega_m}{\frac{2}{P}\omega_{syn}}\omega_{syn} \tag{6.27}$$

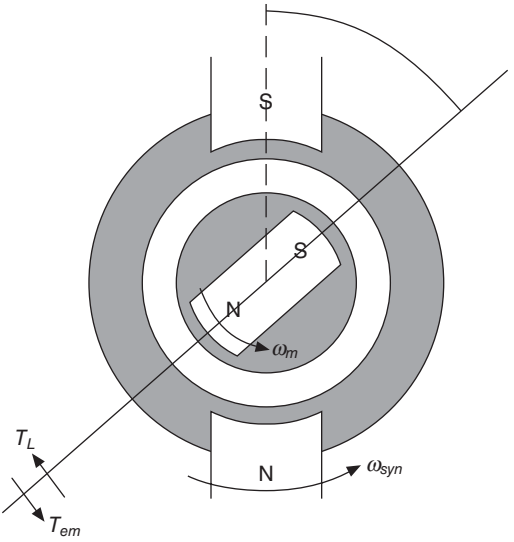

Figure 6.13 The Schematic Flux Distributions for Two-Pole Machines.

Let us define

$$s = \frac{\omega_{syn} - \omega_m}{\omega_{syn}} = \text{slip} \tag{6.28}$$

$$\omega_r = s\omega_{syn} \text{ or } f_r = sf \tag{6.29}$$

where ω_{syn} rad/sec, ω_m rad/sec. The slip can be calculated as presented in Equation 6.30.

$$s = \frac{n_{syn} - n_m}{n_{syn}} \tag{6.30}$$

$$n_{syn} = \frac{120 f_s}{P} \tag{6.31}$$

where n_{syn} is the synchronous speed in rpm and n_m is the rotor speed in rpm.

6.4.2 The Equivalent Circuit of an Induction Machine

Figure 6.14 depicts a three-phase Y-connected stator and rotor windings. As a motor operation, the stator is fed from a three-phase AC source or through a PWM inverter with a variable frequency. The rotor is short-circuited or connected to an external resistance. As a motor, the machine operates at a

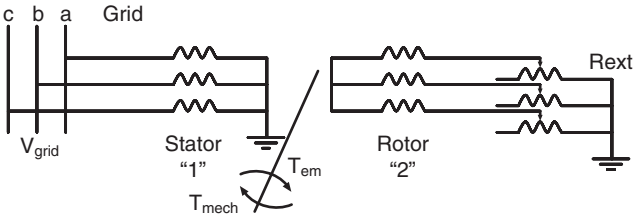

Figure 6.14 The Equivalent Circuit of a Wound Rotor Induction Machine with External Resistance, $R_{ext,}$ Inserted in the Rotor Circuit.

shaft speed below the synchronous frequency and supports a mechanical load. As a wind generator, the mechanical wind power is supplied and the generator operates above the synchronous speed. To describe how the machine operates, we need to develop an equivalent circuit model for the machine. In Fig. 6.16, we refer to stator winding with a subscript "1" and rotor as a subscript "2." We look at two operating conditions: (1) The rotor is at standstill, and (2) the rotor is free to rotate.

1. The rotor is at standstill.

Suppose the rotor is at standstill and the shaft speed is zero ($\omega_m = 0$). Using the approach used in modeling the coupled winding, the equivalent circuit for one phase to ground can be depicted by Fig. 6.15.

The machine is designed to use a small amount of current to magnetize it. Normally, the magnetizing current is less than 5% of the rated load current. This requires that magnetizing reactance, X_m, and resistance, R_m, which is net magnetizing impedance, acts as high impedance. Therefore, we can ignore the shunt elements. With this assumption, we can obtain the following:

$$I_1 = I_2' \tag{6.32}$$

$$\tilde{V}_{grid} = \tilde{I}_1(R_1 + j\omega_s L_1) + \tilde{E}_1 \tag{6.33}$$

$$\tilde{E}_2 = \tilde{I}_2(R_2 + R_{ext} + j\omega_s L_2) \tag{6.34}$$

2. The rotor is free to rotate.

Suppose rotor speed is running at ω_m. Let us express $R_2 = R_{2,rotor} + R_{ext}$

$$\tilde{V}_{grid} = \tilde{I}_1(R_1 + jX_1) + \tilde{E}_1 \tag{6.35}$$

$$\tilde{E}_2 = \tilde{I}_2(R_2 + j\omega_r L_2) \tag{6.36}$$

where, R_1 is stator resistance/phase and $X_1 = \omega_s L_1$ is stator reactance/phase, I_1 is stator current (line) and E_1 is induced emf/phase.

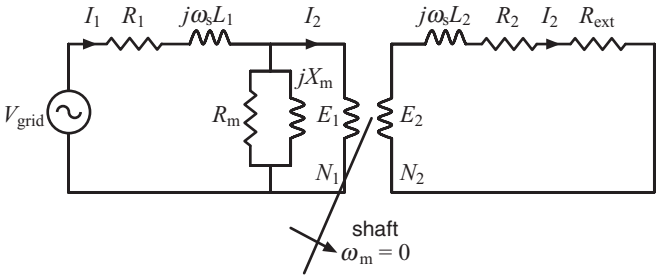

Figure 6.15 The Equivalent Circuit Model of an Induction Machine at Standstill.

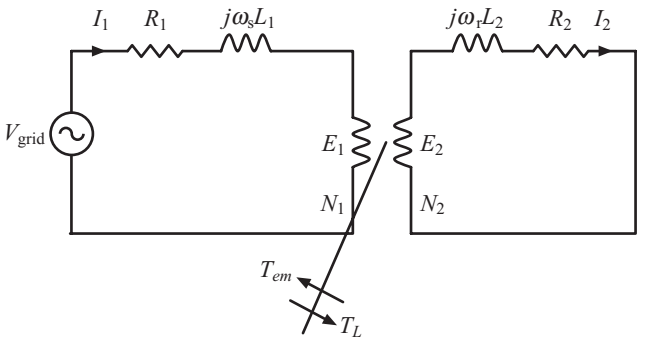

Figure 6.16 The Equivalent Circuit Model of an Induction Machine when the Rotor Is Free to Rotate.

Let us define

$$a = \frac{N_1}{N_2} \tag{6.37}$$

$$I_1 = \frac{I_2}{a} \tag{6.38}$$

Based on Faraday's law of induction, the following expression defines the induced voltage, e_1 and e_2.

$$e_1 = N_1 \frac{d\Phi}{dt} = N_1 \Phi_{max} \cos(\omega t + \theta_1) \tag{6.39}$$

$$e_2 = N_2 \frac{d\Phi}{dt} = sN_2 \Phi_{max} \cos(\omega t + \theta_2) \tag{6.40}$$

Then, the RMS values E_1 and E_2 can be expressed as

$$E_1 = \frac{N_1 \Phi_{max}}{\sqrt{2}} \text{ and } E_2 = \frac{sN_2 \Phi_{max}}{\sqrt{2}} \tag{6.41}$$

The ratio of E_1 and E_2 can be computed as

$$E_2 = sN_2 \frac{E_1}{N_1} = s\frac{E_1}{a} \tag{6.42}$$

And the I_2 and I_1 can be expressed as

$$\tilde{I}_2 = a\tilde{I}_1 \tag{6.43}$$

Using the above relationship, we can compute the equivalent model of an induction machine from the stator side by referring the rotor variables to the stator sides.

$$\tilde{E}_2 = \tilde{I}_2(R_2 + j\omega_r L_2) \tag{6.44}$$

$$s\frac{\tilde{E}_1}{a} = a\tilde{I}_1(R_2 + j\omega_r L_2) \tag{6.45}$$

The Equation 6.50 can by recomputed by multiplying by *a* and dividing by *s*.

$$s\tilde{E}_1 = \tilde{I}_1(a^2 R_2 + jsa^2 X_2) \tag{6.46}$$

$$\tilde{E}_1 = \tilde{I}_1\left(a^2\frac{R_2}{s} + ja^2 X_2\right) \tag{6.47}$$

Equation 6.47 represents the rotor variables from the stator side. The one-phase stator variables are given by Equation 6.48

$$\tilde{V}_{grid} = \tilde{I}_1(R_1 + jX_1) + \tilde{E}_1 \tag{6.48}$$

Combining Equation 6.47 with Equation 6.48, we obtain the following:

$$\tilde{V}_{grid} = \tilde{I}_1(R_1 + jX_1) + \tilde{I}_1\left(a^2\frac{R_2}{s} + ja^2 X_2\right) \tag{6.49}$$

We can rewrite Equation 6.49 as defined by Equation 6.50:

$$R_2' = a^2 R_2 \quad X_2' = a^2 X_2 \tag{6.50}$$

$$\tilde{V}_{grid} = \tilde{I}_1\left[\left(R_1 + \frac{R_2'}{s}\right) + j(X_1 + X_2')\right] \tag{6.51}$$

The induction motor equivalent circuit from the stator side is given in Figs. 6.17 and 6.18.

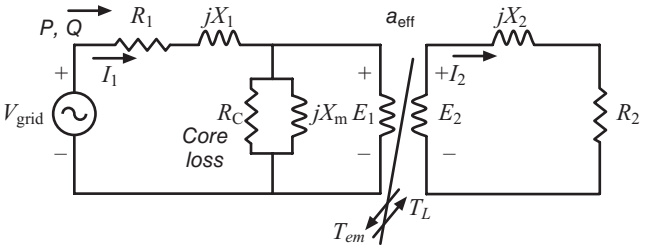

Figure 6.17 The Equivalent Circuit Model of an Induction Machine with Magnetizing Inductance Represented on the Stator Side.

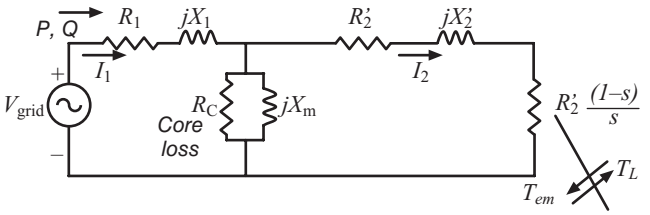

Figure 6.18 The Equivalent Circuit Model of an Induction Machine with Rotor Variables Referred to the Stator Side.

6.5 POWER FLOW ANALYSIS OF AN INDUCTION MACHINE

The input power can be calculated from the input voltage and current drawn by the machine as given by Equation 6.52.

$$P_i = 3\,\mathrm{Re}\left\{V_1 I_1^*\right\} \tag{6.52}$$

The power crossing the air gap of the machine (see Figs. 6.17 or 6.28) can be calculated by subtracting stator wire resistance losses and core losses as given by Equation 6.53.

$$P_{AG} = 3P_i - 3\left(I_1^2 R_1 + P_c\right) = 3|I_2|^2 \frac{R_2'}{s} \tag{6.53}$$

where P_c is the core loss shown by equivalent resistance R_c in Fig. 6.18.

As per Equation 6.53, the air gap power can also be computed by the square of rotor current, I_2 and $\dfrac{R_2'}{s}$.

When the machine is operating as a motor, the power delivered to the shaft can be calculated by accounting for rotor losses.

$$P_{em} = P_{AG} - 3I_2^2 R_2' \tag{6.54}$$

By substituting for the air gap power in Equation 6.54, we can obtain Equation 6.55.

$$P_{em} = 3I_2'^2 \frac{R_2'}{s} - 3I_2'^2 R_2' = 3I_2'^2 \left(\frac{R_2'}{s} - R_2' \right) \tag{6.55}$$

$$P_{conv} = P_{em} = 3I_2'^2 R_2' \left(\frac{1-s}{s} \right) \tag{6.56}$$

Therefore, the electromagnetic power delivered to the machine shaft can be expressed as a function of air gap power by Equation 6.59.

$$P_{em} = 3I_2'^2 \frac{R_2'}{s}(1-s) = P_{AG}(1-s) \tag{6.57}$$

The flow of power from the stator to the machine shaft is depicted by the power flow as shown in Fig. 6.19. The power flow is given from input power P_i, the air gap power, P_{AG}, electromagnetic power, P_{em}, and output power, P_o to the shaft of the machine.

An induction machine has three regions of operations. It can operate as a motor, as a generator, or as a brake. To describe these regions of operation, we need to study the machine torque as a function of speed.

Using Equation 6.58 and the machine model as shown in Fig. 6.15, we first need to calculate the machine torque as a function of input voltage.

$$P_{em} = T_{em}\omega_m \tag{6.58}$$

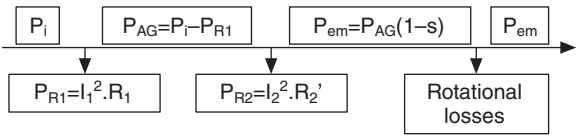

Figure 6.19 The Power Flow in Induction Machines.

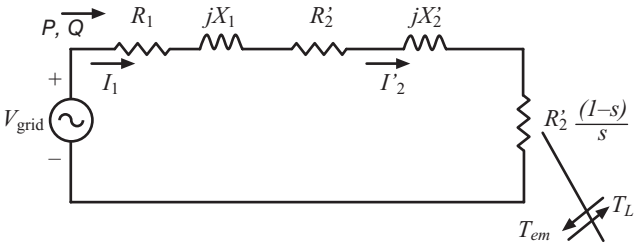

Figure 6.20 The Equivalent Circuit Model of an Induction Machine Operating as a Motor from Stator Terminals Omitting the Magnetizing Elements.

In Equation 6.58, ω_m is the shaft speed and T_{em} is torque driving the shaft and P_{em} is the power supplied to the machine. We can calculate P_{em} by calculating the current supplied to the machine from the grid. Because the magnetizing element is ignored, the current, I_1 is equal to I_2'.

$$V_{grid} = I_1\{(R_1 + R_2) + j(X_1 + X_2')\} \tag{6.59}$$

From the above equation, we can calculate the current I_1 as expressed by Equation 6.60.

$$|I_1|^2 = \frac{|V_{grid}|^2}{\left(R_1 + \frac{R_2'}{s}\right)^2 + (X_1 + X_2')^2} \tag{6.60}$$

The torque supplied to the rotor is expressed by Equation 6.61.

$$T_{em} = \frac{3}{\omega_m}\left(\frac{1-s}{s}\right)R_2'|I_1|^2 \tag{6.61}$$

The shaft speed can also be expressed as given by Equation 6.62.

$$\omega_m = \omega_{sync}(1-s) \tag{6.62}$$

By substituting Equations 6.61 and 6.62, we can express the shaft torque as a function of input voltage as given by Equation 6.63.

$$T_{em} = \frac{3}{\omega_{sync}}\frac{R_2'}{s}\frac{|V_{grid}|^2}{\left(R_1 + \frac{R_2'}{s}\right)^2 + (X_1 + X_2')^2} \tag{6.63}$$

It is instructive to study the machine performance for various values of external resistance for a constant input voltage. From careful examination of Equation 6.63, we can conclude the following:

a. When the slip is zero, the shaft speed, ω_m is equal the synchronous speed, ω_{sync} and the produced electromagnetic torque is zero.
b. When the slip, s is equal to one, i.e., the shaft speed is zero (starting), the standstill torque (starting torque) can be obtained.
c. As the external resistance is changed using a controller, the value of maximum torque occurs at different values of the shaft speed.

The control of shaft speed over a wide range would provide the capability to operate the machine at various speeds. When the machine is used as an induction generator, we can capture the wind power and inject the generated power into the local grid.

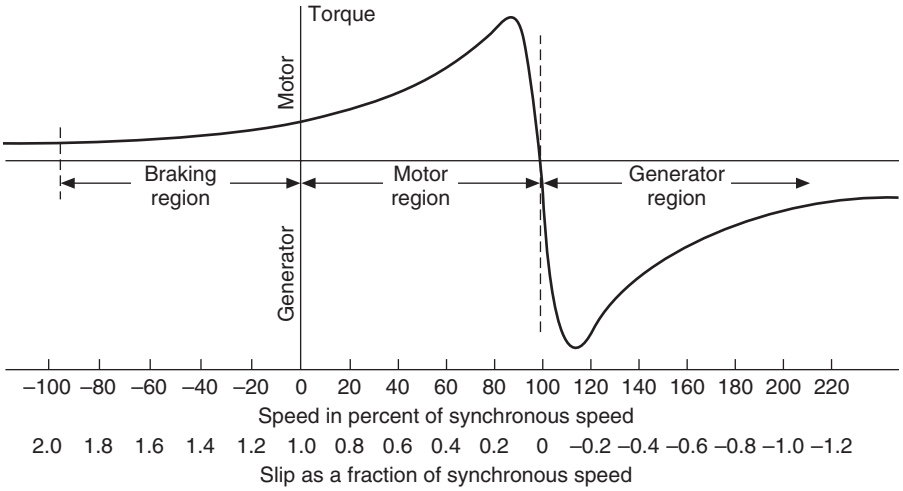

Figure 6.21 An Induction Machine's Various Regions of Operation.

There are three distinct points in an induction machine torque versus speed curve: (1) the starting torque when the shaft speed is zero; (2) when the shaft speed is equal the synchronous speed of the flux waves, the generated torque is zero (see Fig. 6.21); and (3) the point of maximum torque production. To calculate the maximum torque, we compute the derivative of torque expression as given by Equation 6.63, with respect to slip and set it to zero.

$$\frac{dT_m}{ds} = 0 \tag{6.64}$$

The maximum slip point is given by Equation 6.65.

$$s_{\max} = \pm \frac{R_2'}{\sqrt{R_1^2 + (X_1 + X_2')^2}} \tag{6.65}$$

The resulting maximum torque is given by Equation 6.66.

$$T_{\max} = \pm \frac{3}{2\omega_{sync}} \frac{|V_{grid}|^2}{\left[R_1 \pm \sqrt{R_1^2 + (X_1 + X_2')^2} \right]} \tag{6.66}$$

Equation 6.65 shows that the slip at which the maximum torque occurs is directly proportional to the rotor resistance. Equation 6.66 shows that the maximum torque is independent of the rotor resistance. However, it is directly proportional with the square of input voltage.

6.6 THE OPERATION OF AN INDUCTION GENERATOR

Wound rotor induction machines have stators like the squirrel cage machine. However, their rotors' winding terminals are brought out via slip rings and brushes for torque and speed control. For torque control no power is applied to the slip rings. External resistances are placed in series with the rotor windings during starting to limit the starting current. Without the external resistances, the starting currents are many times the rated currents. Depending on the size of the machine, it can draw 300% to over 900% of full-load current. The resistances are shorted out once a motor is started. The external resistances are also used to control the machine speed and its starting torque. The negative slip operation of an induction machine indicates that the machine is operating as a generator and power is injected into the local power grid.[20] Induction generators required reactive power for magnetizing the rotor, and this power is supplied by the following different methods.

1. The machine is magnetized and started as an induction. Then, the wind turbine is engaged to supply mechanical power and shaft speed is increased above synchronous speed. As a standalone, we can use any induction machine and by adding capacitors in parallel with the machine terminals, then driving it above synchronous speed, the machine would operate as an induction generator. The capacitance helps to induce currents into the rotor conductors and AC current is produced. The loads can be connected to the capacitor leads because the capacitors are in parallel. This method of starting a standalone machine is assured, if the residual magnetism in the rotor exits. However, the machine can be magnetized by using a direct current source such as a 12 V battery for a very short time.
2. Rotor resistance of the induction generator is varied instantly using a fast power electronics controller. Variable rotor speed (consequently variable slip) provides the capability to increase the power captured from the wind at different wind speeds. This can be achieved if rotor winding terminals can be accessed by changing slip via external resistors connected to the generator rotor winding. The external resistors will only be connected to produce the desired slip when the load on the wind turbine becomes high.

The relationships between the variation of external resistance and the location of maximum and standstill torques can be studied by varying the external resistance in the rotor circuit. We can study this relationship by writing a MATLAB M-file as described in Example 6.1.

The power from the rotation of the wind turbine rotor is transferred to the induction generator through a transmission train consisting of the main turbine shaft, the gearbox, and the high-speed generator shaft. The normal range of

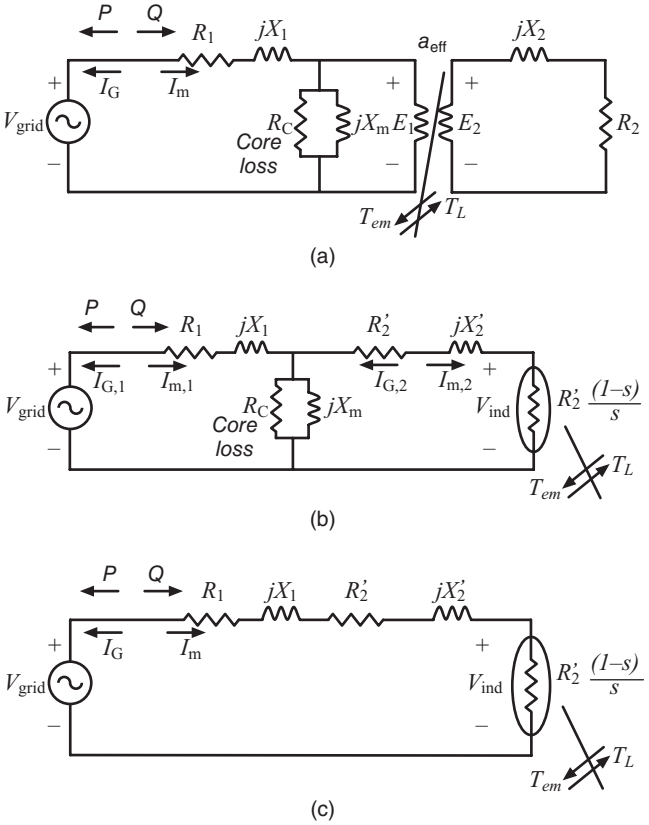

Figure 6.22 (a) Equivalent Circuit of an Induction Generator. (b) Equivalent Circuit of an Induction Generator with All Quantities Referred to the Stator Side. (c) Equivalent Circuit of an Induction Generator Referred to the Stator Neglecting Magnetizing and Loss Components.

wind speed is not high and changes during the day and with the seasons. For example, a three-phase generator with two poles directly connected to a local power grid operating at 60 Hz is running at 3600 rpm. We can reduce the speed of the generator rotor, if the generator has a higher number of poles. For example, if the number of poles is four, six, or eight, the shaft speed reduces to 1800, 1200, and 900 rpm, respectively. A power grid supplied by a wind generator requires much higher wind speed in the range of 900–3600 rpm. To reduce the speed of the generator rotor, we can increase the number of poles. However, designing a generator with a very high number of poles requires a large diameter and will result in high volume and weight. We can increase the low speed and high torque of the wind turbine to low torque and high speed using gear systems. Before discussing the gear concepts, we need to understand how to convert linear velocity to rotational velocity.

From fundamental physics, we know the linear velocity and rotational velocity can be expressed as

$$V = r \cdot \omega \tag{6.67}$$

where V is the linear velocity in meters per second, r is the radius in meter, and rotational velocity, ω is in radians per second.

We can convert the rotational velocity, ω to revolutions per minute as

$$\omega = N \frac{2\pi}{60}$$

In the above, N is in revolutions per minute. Equation 6.67 can be restated as

$$V = N \frac{2\pi}{60} \mathrm{r} \tag{6.68}$$

where V is in meters per second, N is in rotations per minute, and r is in meters. Conversely, we can rewrite the above as

$$N = V \cdot \frac{60}{2\pi \cdot r} \tag{6.69}$$

In Equation 6.69, V is in meters per second, r is meters, and N is in rotations per minute. Conversely, the unit in Equation 6.69 can be in feet per second for V, r in feet, and N is in rotations per minute.

If we want to express the velocity in miles per hour (mph), we rewrite Equation 6.69 as

$$\frac{5280}{3600} V = \frac{\pi r \cdot N}{30} \tag{6.70}$$

where V is in miles per hour, r is in feet, and N is in rotations per minute. In Equation 6.70, we have substituted the value of 5280 feet for one mile and 3600 seconds for an hour. Equation 6.70 can be restated as

$$N = \frac{14.01 \cdot V}{r} \tag{6.71}$$

The wind speed in the range of 10 miles per hour (14.67 ft/sec) will result in 124.2 rotations per minute.

The wind generators are designed to capture the wind power in the range of less than 120 rpm using a gear box transmission system. The gear box operates like a transformer. The gearbox provides speed and torque conversions

$$T_{input} \omega_{input} = T_{output} \omega_{output} \tag{6.72}$$

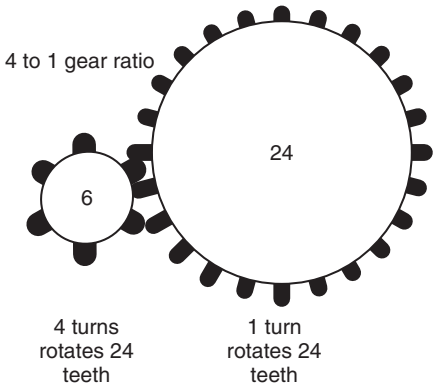

Figure 6.23 A Schematic of a Gear Mechanism.

where T_{input} and T_{output} are torque in newton-meter and ω_{input} and ω_{output} in radian per second. To provide torque speed conversion, a gearbox transmission is used. A gearbox is designed with a number of teeth.

$$Gear\ ratio = \frac{input\ number\ of\ teeth}{output\ number\ of\ teeth} = \frac{T_{input}}{T_{output}} \tag{6.73}$$

The gearbox converts low speed and high torque powers of a wind turbine rotor to low torque power and the high speed of the generator rotor. The gear ratio is in the range of 1 to 100 for a wind generator in the range of 600 kW to 1.5 MW.

Example 6.1 Consider a three-phase Y wound rotor-connected induction machine operating as a generator in parallel with a local power grid. The machine is rated at 220 V, 60 Hz, and 14 kW, with eight poles and the following parameters:

Stator resistance (R_1) of 0.2 ohms per phase (Ω/phase) and reactance of (X_1) of 0.8 Ω/phase

Rotor resistance R_2' of 0.13 Ω/phase and reactance (X_2) of 0.8 Ω/phase.

Ignore magnetizing reactance and core losses.
Perform the following:

i) Develop a one-line diagram and one-phase equivalent model.

ii) If the prime mover speed is 1000 rpm, determine the active and reactive power between the local grid and wind generator. How much capacitor must be placed at the machine stator terminal for unity power factor operation?

iii) Plot the torque speed characteristics of the machine at different values of external resistances.

Solution

The synchronous speed, $N_s = \dfrac{120f}{P} = \dfrac{120 \times 60}{8} = 900\ rpm$

The rotor speed, $N_r = 1000\ rpm$

The slip, $s = \dfrac{N_s - N_r}{N_s} = \dfrac{900 - 1000}{900} = -0.111$

Writing Kirchhoff's voltage law (KVL) for the circuit of Fig. 6.24(b), the current in motor convention,

$$I_m = \frac{V_{grid}}{R_1 + R_2'/s + j(X_1 + X_2')}$$

$$= \frac{220/\sqrt{3}}{0.2 - 0.13/0.111 + j(0.8 + 0.8)} = 67.88\angle -121.22°$$

For motor operation, the power flows from the grid to the induction machine. For generator operation, the direction of active power is reversed. Using motor convention and calculating the current, the angle of the current is greater than 90°. This means that the direction of current is opposite to the direction as shown by generator convention in Fig. 6.26(b).

With current following the generator convention and flowing from induction generator to the grid, the current $I_G = 67.88\angle 180 - 121.22° = 67.88\angle 58.77°$

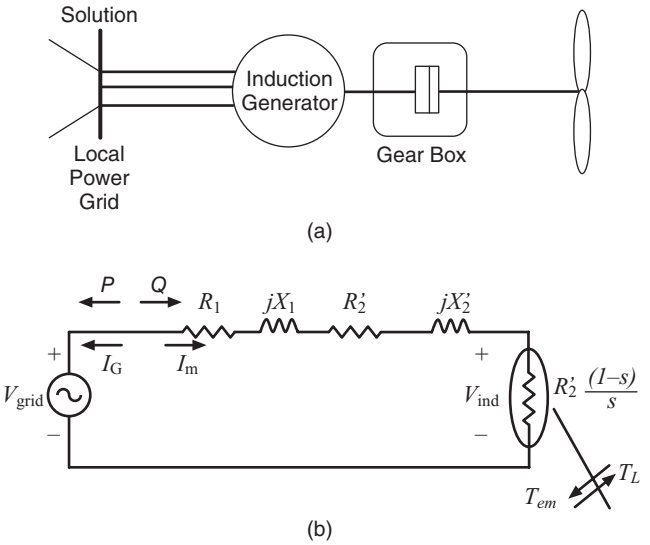

Figure 6.24 (a) A One-Line Diagram. (b) A One-Phase Equivalent Circuit of an Induction Generator.

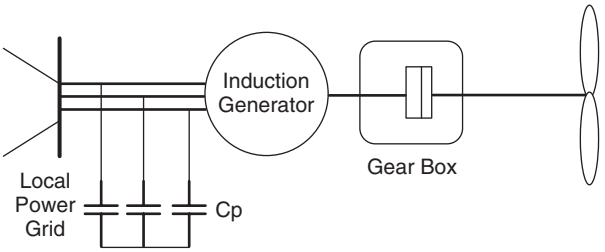

Figure 6.25 A Squirrel Cage Induction Generator with Reactive Power Supplied Locally by a Capacitor Bank.

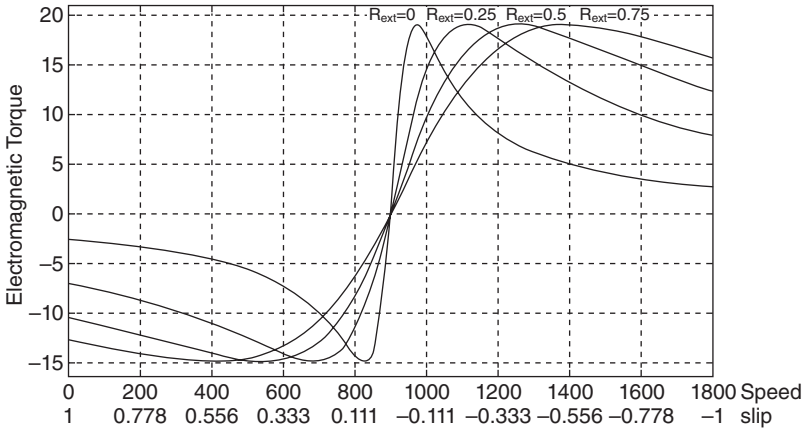

Figure 6.26 The Schematic Presentation of Torque as a Function of Various External Resistances with Generator Convention.

The induced voltage is given as

$$V_{ind} = \frac{1-s}{s} R_2' \cdot I_G$$

$$= \frac{1-(-0.111)}{-0.111} \times 0.13 \times 67.88\angle 58.77° = 88.25\angle 58.77°$$

Neglecting the mechanical losses, the electrical power generated from the supplied wind mechanical power is given as $S_{ind} = 3V_{ind} \cdot I_G^* = 3 \times 88.25\angle 58.77° \times 67.88\angle -58.77° = 17.93 + j0\ kVA$

From S_{ind}, it is seen that the induction generator produces active power. However, it does not produce any reactive power. The reactive power is supplied by the grid.

The power produced by the induction generator is injected to the local grid and some power is lost in stator and rotor resistance.

The complex power injected to the grid is given by

$$S_{grid} = 3V_{grid} \cdot I_G^* = 3 \times \frac{220}{\sqrt{3}} \angle 0° \times 67.88 \angle -58.77° = 13.41 - j22.12\ kVA$$

The induction generator feeds 13.41 kW of active power to the grid, but consumes 22.12 kVAr of reactive power from the grid.

Let a three-phase Y-connected capacitor bank be connected at the terminals of the induction generator. For unity power factor operation, the capacitor bank must supply the reactive power demand of the induction generator.

$$C_P = \frac{3V_{grid}^2}{2\pi f \cdot Q} = \frac{3 \times \left(220/\sqrt{3}\right)^2}{2\pi \times 60 \times 22.12 \times 10^3} = 5.8\ mF$$

Let us assume that the value of external resistance is varied from zero to 0.75 in steps of 0.25 and the speed of the machine is varied from zero to the synchronous speed. In the following MATLAB testbed, a plot is made for the different values of R_{ext}.

```
%TORQUE vs SPEED
clc; clear all;
v1=220/sqrt(3);
f=60;
P=8;
r1=0.2;
x1=0.8;
r2d=0.13;
x2d=0.8;                              % The electrical
                                      quantities are defined
ws=120*f/P;
Tmax=-(3/2/ws)*v1^2/(r1+sqrt(r1^2+(x1+x2d)^2))
Tmax_gen=-(3/2/ws)*v1^2/(r1-sqrt(r1^2+(x1+x2d)^2))
w=0:1:2*ws;
for r_ext=0:0.25:0.75                 % the value of external
                                      resistance is varied
  Tstart=-(3/ws)*((r2d+r_ext)/1)*v1^2/((r1+(r2d+r_ext)/
  1)^2+(x1+x2d)^2)
  smax=(r2d+r_ext)/sqrt(r1^2+(x1+x2d)^2)
  for j = 1:length(w)
    s(j)=(ws-w(j))/ws;
    Tem(j)=-(3/ws)*((r2d+r_ext)/s(j))*v1^2/((r1+(r2d+
    r_ext)/s(j))^2+(x1+x2d)^2);
  end
```

TABLE 6.1 The Results of Example 6.1.

External Resistance (Ω)	Starting Torque (N-m)	Slip at Maximum Torque (N-m)	Maximum Torque (N-m)
0.00	–2.62	0.08	
0.25	–7.06	0.24	–14.84 (Motor)
0.50	–10.43	0.39	19.04 (Generator)
0.75	–12.70	0.55	

```
  plot(w,Tem,'k','linewidth',2)
  hold on;
end
grid on;

xlabel('Speed')
ylabel('Electromagnetic Torque')
axis([0 2*ws 1.1*Tmax_gen 1.1*Tmax])
gtext('R_e_x_t=0')
gtext('R_e_x_t^,=0.25')
gtext('R_e_x_t^,^,=0.5')
gtext('R_e_x_t^,^,^,=0.75')
```

The results are tabulated in Table 6.1.

The operation of an induction generator is the same as an induction motor except the direction of power flow is from wind power driving the shaft of the machine. Therefore, an induction generator injects or supplies power to the local power grid. For motor convention, the positive current flows from the source to the motor. For generator convention, the positive current flows from the motor terminal voltage to the local power grid. This means the sign of the current with motor convention will be negative for generator operation.

Example 6.2 For the machine of Example 6.1 with the same supply voltage connected to the local utility, plot the torque-slip characteristics in the speed range of 1000 rpm to 2000 rpm with motor convention. Write a MATLAB M-file testbed and plot.

Solution
The MATLAB M-file testbed for Example 6.2 is given below.

```
%TORQUE vs SPEED
clc; clear all;
v1=220/sqrt(3);
f=60;
P=8;
```

```
r1=0.2;
x1=0.8;
r2d=0.13;
x2d=0.8;                    % The electrical quantities
                            are defined
ws=120*f/P;
w=-1000:0.2:2000;
for j = 1:length(w)
  s(j)=(ws-w(j))/ws;
  Tem(j)=(3/ws)*(r2d/s(j))*v1^2/((r1+r2d/s(j))^2+(x1+
  x2d)^2);
end
plot(w,Tem,'k','linewidth',2)
hold on;
grid on;
xlabel('Speed')
ylabel('Electromagnetic Torque')
```

The following observations can be made from the above examples:

When ω_{syn} and ω_m are rotating in the same direction and ω_{syn} is rotating faster than ω_m: this condition describes the normal operation of the induction machine as a motor.

In this region, the slip as given by Equation 6.70 is positive because both are rotating in the same direction.

$$s = \frac{\omega_{syn} - \omega_m}{\omega_{syn}} \tag{6.74}$$

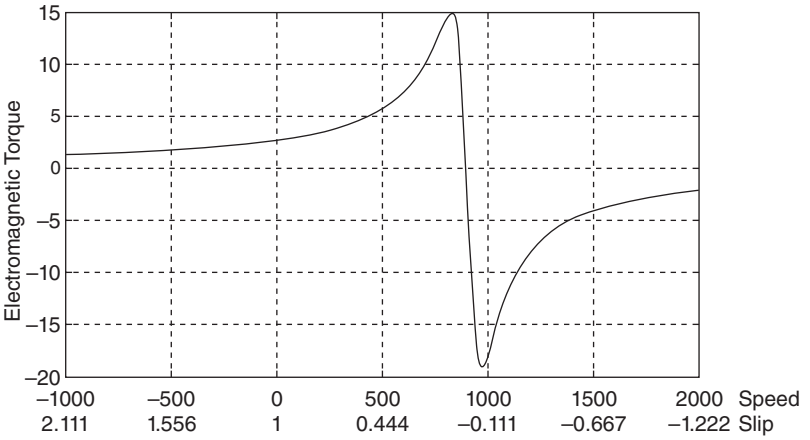

Figure 6.27 The Plot of Torque versus Speed of the Induction Machine of Example 6.2.

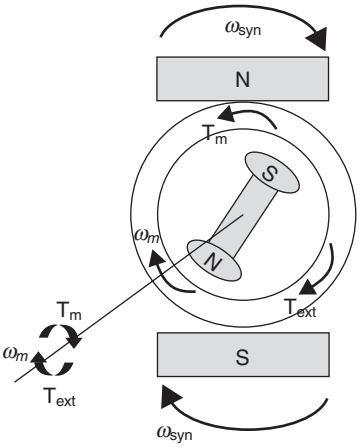

Figure 6.28 The Operation of an Induction Machine as a Generator.

$$R_{eff} = \frac{1-s}{s} R_2' \tag{6.75}$$

When ω_{syn} and ω_m are rotating in the same direction and ω_{syn} is rotating slower than ω_m, this operating condition describes the operation of a machine in generator mode. In this region, ω_{syn} and ω_m are rotating in the same direction. However ω_{syn} is rotating slower than ω_m. Therefore, in this region, mechanical power supplied to the shaft by an external source and ω_m is greater than ω_{syn} and slip is negative ($s < 0$). This region ($s < 0$) corresponds to the generator operation. For this region, the equivalent effective resistance as given by Equation 6.71 of the rotor is negative (see Fig. 6.22) and the corresponding power (torque) is also negative. This means that the mechanical power is driving the machine and the machine in turn delivers electric power at its stator terminals to the source. The generator operation can be summarized as follows:

1. $\omega_m > \omega_{syn}$
2. ω_m and ω_{syn} are rotating in the same direction.
3. Generator action: Electrical power is supplied to the network via stator terminals.
4. $s = \dfrac{\omega_{syn} - \omega_m}{\omega_{syn}} < 0$

The negative slip indicates generator action.

When ω_{syn} and ω_m are rotating in opposite directions, the machine is operating in the brake region. The brake mode of operation can be implemented when an induction motor is operating under normal conditions at some value

of positive slip in a stable region ($0 < s < s_{max}$); then we interchange any two terminals of the stator. This operation reverses the direction of the stator rotating field. The rotor speed ω_m may now be considered as negative with respect to that of the stator field. For this case, s > 1 and power loss is negative, indicating that mechanical energy is being converted to electric energy. The power fed from the stator and the power fed from the rotor are both lost as heat in the rotor resistance. This region is called the braking region.

Example 6.3 The air-gap power of an eight-pole 60-Hz induction machine, running at 1000 rpm is 3 kW. What are the rotor copper losses?

Solution
The air-gap power is

$$P(Input \cdot power \cdot to \cdot rotor) = P_{AG_\phi} = 3|I_2|^2 \frac{R_2'}{s}$$

The rotor copper loss is given by

$$P_{rotor\ loss} = 3|I_2|^2 R_2'$$

Therefore,

$$\frac{P_{rotor\ loss}}{P_{rotor\ in} = P_{AG}} = \frac{3|I_2|^2 R_2'}{3|I_2|^2 \dfrac{R_2'}{s}} = s$$

The rotor power loss, $P_{rotorloss}$, is slip times the air-gap power:

$$P_{rotorloss} = sP_{AG}$$

For motor convention, $P > 0$ indicates power is being consumed by the machine.

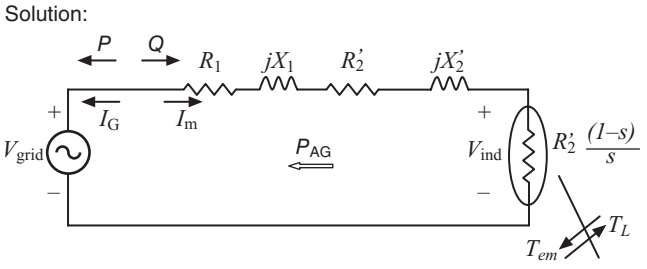

Figure 6.29 A Single-Phase Equivalent Circuit of an Induction Generator.

For generator convention, $P > 0$ indicates power is being generated by the machine.

Synchronous speed is given by $N_{syn} = 120\dfrac{f}{P} = 120\dfrac{60}{8} = 900\ rpm$

Slip is given by $s = \dfrac{N_{syn} - N_m}{N_{syn}} = \dfrac{900 - 1000}{900} = -0.11$

The machine is operating as an induction generator.

Therefore, following generator convention, reversing the direction of air-gap power, the rotor power loss is given by

$$P_{rotorloss} = -sP_{AG} = 0.111 \times 3000 = 333\ kW$$

Example 6.4 A three-phase, six-pole, Y-connected induction generator rated at 400 V, 60 Hz is running at 1500 rpm supplying a current of 60 A at a power factor of 0.866 leading. It is operating in parallel with a local power grid. The stator copper losses are 2700 W, rotational losses are 3600 W.

Perform the following:

i) Determine the active and reactive power flow between induction generator and the power grid

ii) Determine how much reactive power must be supplied at the induction generator to operate the induction generator at unity power factor.

iii) Calculate the efficiency of the generator

Solution:

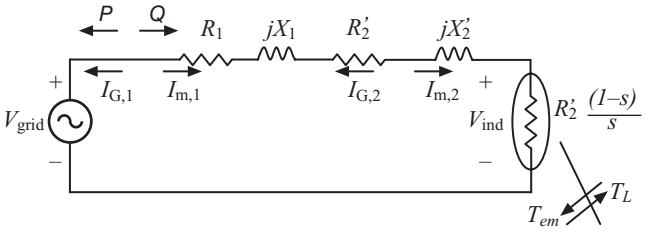

Figure 6.30 The Single-Phase Equivalent Circuit of Induction Generator.

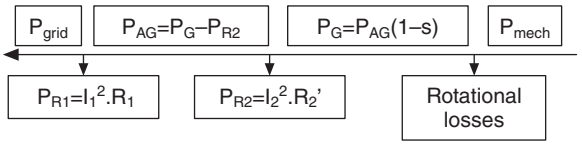

Figure 6.31 A Power Flow Diagram for the Generator Mode of the Operation of an Induction Machine.

iv) Find the value of stator resistance, rotor resistance, and the sum of the stator and rotor reactances

v) Compute the electromechanical power developed by the rotor

Solution

Synchronous speed is given by $N_{syn} = 120\frac{f}{P} = 120\frac{60}{6} = 1200\ rpm$

Slip is given by

$$s = \frac{N_{syn} - N_m}{N_{syn}} = \frac{1200 - 1500}{1500} = -0.25$$

The active power at the stator terminals is given by

$$P_{grid} = 3V_{L-N} \cdot I_s \cdot \cos\theta = 3 \times \frac{400}{\sqrt{3}} \times 60 \times 0.866 = 36,000\ W$$

The reactive power at the stator terminals is given by

$$Q_{grid} = 3V_{L-N} \cdot I_s \cdot \sin\left(\cos^{-1}\theta\right) = 3 \times \frac{400}{\sqrt{3}} \times 60 \times \sin\left(\cos^{-1} 0.866\right) = 20,786\ VAr$$

For unity power factor operation, the reactive power that needs to be supplied locally is the same as $Q_{grid} = 20,786\ VAr$

Stator copper loss, $P_{R1} = 2700\ W$

The air-gap power is

$$P_{AG} = P_{grid} + P_{R1} = 36000 + 2700 = 38700\ W\ (3\phi)$$

The fixed loss, $P_{rotational\ loss} = 3600\ W$

The mechanical power input,

Let P_G is the electromechanical power developed in the rotor

$$\begin{aligned} P_{mech} &= P_G + P_{rotational} = (1-s)P_{AG} + P_{rotational} \\ &= (1-(-0.25))38700 + 3600 = 51,975\ W \end{aligned}$$

The efficiency, $\eta = \frac{P_{elec}}{P_{mech}} = \frac{36,000}{51,975} = 0.6276 = 69.26\%$

The stator resistance is given by $R_1 = \frac{P_{R1}}{3I^2} = \frac{2700}{3 \times 60^2} = 0.25\ \Omega$

Following generator convention,

Rotor copper loss is given by $P_{R2} = -sP_{AG} = -(-0.25) \times 38700 = 9675\ W$

The rotor resistance is given by $R_2' = \frac{P_{R2}}{3I^2} = \frac{9675}{3 \times 60^2} = 0.90\ \Omega$

The sum of reactances of the rotor and the stator is given by

$$X = X_1 + X_2' = \frac{Q_{grid}}{3I^2} = \frac{20,786}{3\times 60^2} = 1.92\ \Omega$$

The electromechanical power developed by the rotor

$$= -3I^2 \frac{1-s}{s} R_2' = -3\times 60^2 \times \frac{1-(-0.25)}{-0.25} \times 0.9 = 48,600\ W$$

6.7 DYNAMIC PERFORMANCE

In the previous sections, we analyzed the steady state of induction machines. For a dynamic analysis, we must model the machines by a set of differential equations. For stator windings, we have three coupled windings that are sinusoidally distributed around the stator. When these coupled windings are represented in terms of self-inductances and mutual inductances, they give rise to a set of three time-varying differential equations. Similarly, we can obtain three time-varying differential equations for the rotor windings. The electromagnetic torque can be expressed by a nonlinear algebraic equation and the rotor s dynamic can be represented by a differential equation expensing the rotational speed of the motor. Therefore, the induction machine dynamic performance can be expressed by seven differential equations and one algebraic equation. The dynamic modeling of an induction machine is an advanced concept that students need to study with additional coursework.[17–18] Here it is instructive to study the results of a dynamic analysis as depicted in Figs 6.32 through 6.34.

Figure 6.32 depicts the start-up condition of an induction machine. As expected, the machine stator current has many cycles of transient oscillation

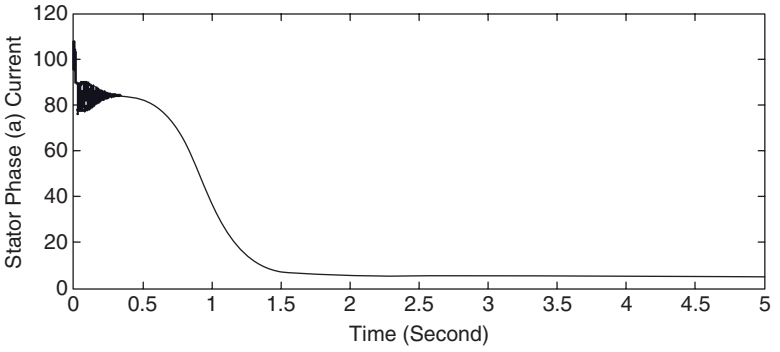

Figure 6.32 The Induction Machine Stator Current for a No Load Start-Up.

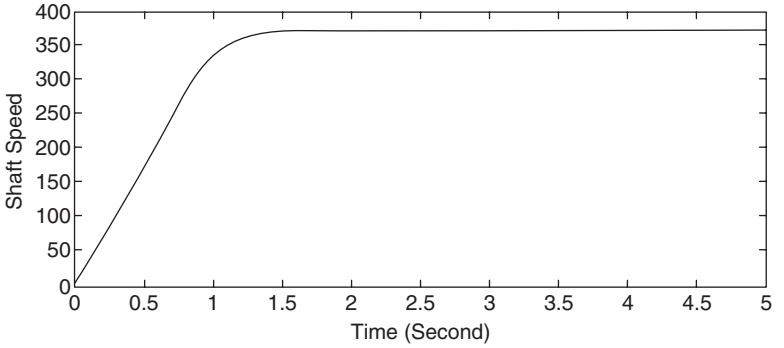

Figure 6.33 Induction Machine Shaft Speed for No Load Start-Up.

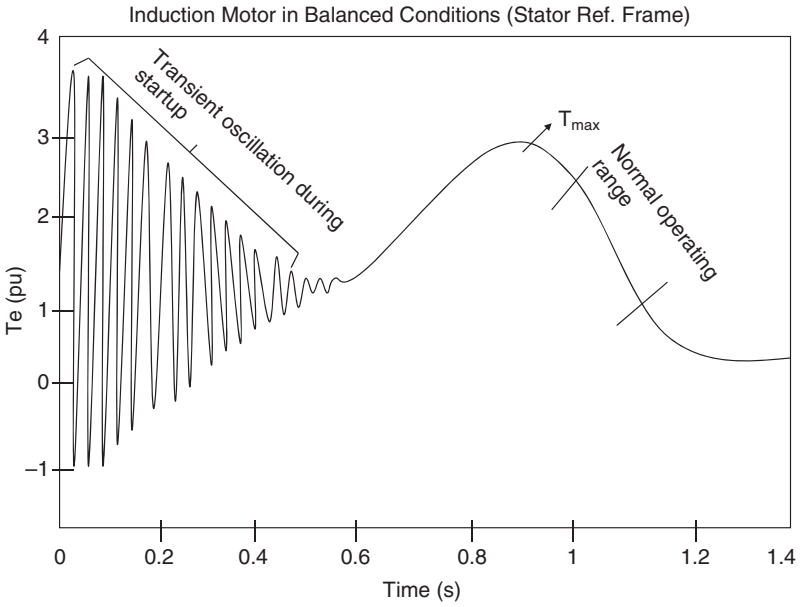

Figures 6.34 The Dynamic Performance of an Induction Machine.

before it reaches the steady-state current. The steady-state current supplied by the source magnetizes the machine and is lost as heat because the machine is operating at no load.

Figure 6.33 depicts the machine shaft speed from rest (start-up) to no load speed that is just below the synchronous speed.

Figure 6.34 depicts the transient oscillations of a machine. As can be seen from the Fig. 6.34, the machine goes through 0.4 seconds of oscillations and reaches it maximum torque. The normal region of the induction machine

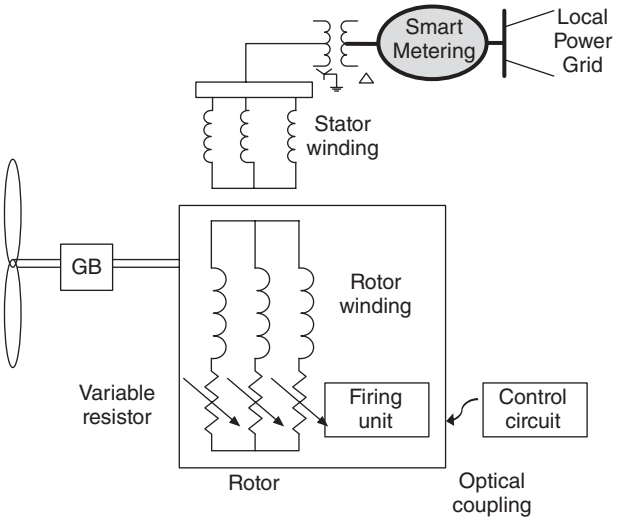

Figure 6.35 A Microgrid of an Induction Machine Controlled as an Induction Generator Supplying Power to the Local Power Grid.

operation is below maximum speed. In Fig. 6.34, the motor operation of the machine is presented. Because the machine is simulated at no load from rest, the machine develops enough torque to support the machine resistive and rotational losses.

The schematic of a microgrid of an induction machine controlled as a generator is presented in Fig. 6.35.

Example 6.5 Consider the microgrid given by Fig. 6.36 with the following data:

1. Transformer rated at 440 V/11 kV, with reactance of 0.16 Ω and resistance of 0.02 Ω, and rated 60 kVA
2. The induction machine rated at 440 V, 60 Hz, three-phase, eight-pole; 50 kVA, 440 V, 60 Hz; stator resistance of 0.2 Ω/phase; rotor referred resistance in the stator side of 0.2 Ω/phase, stator reactance of 1.6 Ω/phase; rotor referred reactance of 0.8 Ω/phase. The generator speed is 1200 rpm. Perform the following:
   i) Give the per unit (p.u) model of the system
   ii) Compute the power delivered to local power grid
   iii) Compute the reactive power flow between grid and induction generator. Assume base values equal to the rating of the induction machine.

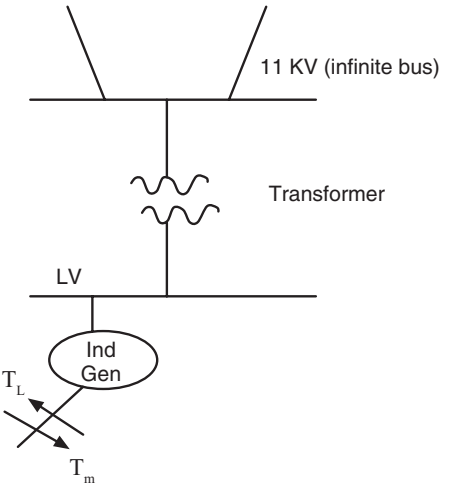

Figure 6.36 The Microgrid Connected to a Local Power Grid for Example 6.5.

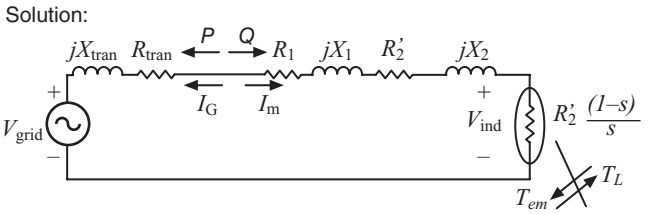

Figure 6.37 One-Phase Per Unit Equivalent Circuit for Example 6.5.

Solution

i) Selecting the induction machine's rating as base,

$$S_b = 50 \text{ KVA}$$

$$V_b = 440\ V$$

The base impedance of the system

$$Z_b = \frac{V_b^2}{S_b} = \frac{440^2}{50 \times 10^3} = 3.872$$

The p.u value of transformer resistance

$$R_{tran,pu} = \frac{R_{tran}}{Z_b} = \frac{0.02}{3.872} = 0.005$$

The p.u value of transformer reactance

$$X_{tran,pu} = \frac{X_{tran}}{Z_b} = \frac{0.15}{3.872} = 0.04$$

The p.u value of stator resistance

$$R_{s,pu} = \frac{R_s}{Z_b} = \frac{0.2}{3.872} = 0.052$$

The p.u value of rotor resistance referred to primary

$$R'_{r,pu} = \frac{R'_r}{Z_b} = \frac{0.2}{3.872} = 0.052$$

The p.u value of stator reactance

$$X_{s,pu} = \frac{X_s}{Z_b} = \frac{1.6}{3.572} = 0.413$$

The p.u value of rotor resistance referred to primary

$$X'_{r,pu} = \frac{X'_r}{Z_b} = \frac{0.8}{3.572} = 0.207$$

ii) Synchronous speed, N_s,

$$N_s = \frac{120f}{P} = \frac{120 \times 60}{8} = 900\ rpm$$

Slip, s is

$$s = \frac{N_s - N}{N_s} = \frac{900 - 1200}{900} = -0.333$$

where N is the motor shaft (rotor) speed in rpm.

The rotor voltage frequency

$$f_r = s \cdot f_s$$

$$f_r = 0.333 \times 60 = 20\ Hz$$

The supply voltage is 440 V = 1 p.u

The base current

$$I_b = \frac{VA_b}{\sqrt{3}V_b} = \frac{50 \times 10^3}{\sqrt{3} \times 440} = 65.61\ A$$

p.u impedance

$$Z_{pu} = \sqrt{\left(R_{s,pu} + R_{tran,pu} + R'_{r,pu}/s\right)^2 + \left(X_{s,pu} + X_{tran,pu} + X'_{r,pu}\right)^2}$$
$$= \sqrt{(0.052 + 0.005 - 0.052/0.333)^2 + (0.413 + 0.04 + 0.207)^2} = 0.667$$

The power factor angle

$$\tan^{-1}\left(\frac{X_{s,pu} + X_{tran,pu} + X_{r,pu}}{R_{s,pu} + R_{tran,pu} + R_{r,pu}/s}\right)$$
$$= \tan^{-1}\left(\frac{0.413 + 0.04 + 0.207}{0.052 + 0.005 - 0.052/0.333}\right) = 98.54°$$

$$Z_{pu} = |Z_{pu}| \angle\theta = 0.667 \angle 98.54°$$

The p.u stator current in motor convention is

$$I_{pu} = \frac{V_b}{Z_{pu}} = \frac{1}{0.667 \angle 98.54°} = 1.499 \angle -98.54°$$

The actual value of current in motor convention,

$$I_m = I_b \times I_{p.u} = 65.61 \times 1.499 = 98.35 \angle -98.54° A$$

Therefore, $I_m = 98.35 \angle -98.54° A$

Because this angle is more than 90°, the power flow is from the induction generator to the local power grid.

Using generator convention, the direction of current is reversed to represent I_G as in Fig. 6.38.

Therefore, the current in generator convention,

$$I_G = 98.35 \angle 180 - 98.54° = 98.35 \angle 81.46° A$$

The active power input to the grid,

$$P_{grid} = \sqrt{3} \cdot V_{grid} \cdot I_G \cdot \cos\theta = \sqrt{3} \times 440 \times 98.35 \times \cos 81.46 = 11{,}130\ W$$

Active power lost in the transformer $P_{loss} = 3I_G^2 R_{trans} = 3 \times 98.35^2 \times 0.02 = 580\ W$

Therefore, the active power injected by the induction generator to the transformer,

$$P = P_{grid} + P_{loss} = 11{,}130 + 580 = 11{,}710\ W$$

The reactive power input to the grid,

$$Q_{grid} = \sqrt{3} \cdot V_{grid} \cdot I_G \cdot \sin\theta = \sqrt{3} \times 440 \times 98.35 \times \sin 81.46 = 74121\ W$$

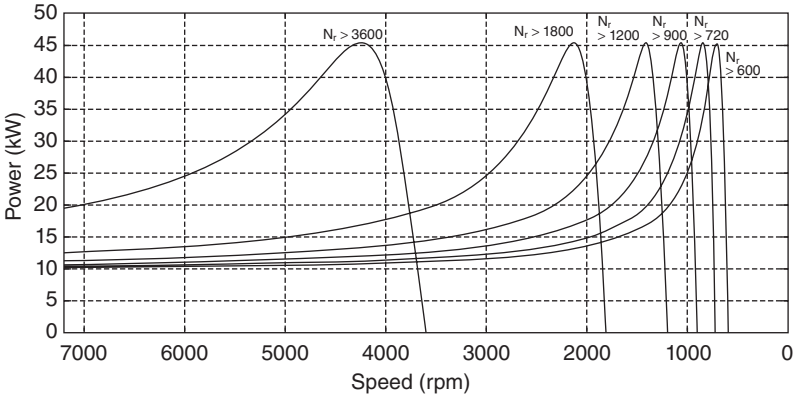

Figure 6.38 Power versus Speed of a Variable Pole Induction Generator for Various Rotor Speeds.

Reactive power lost in the transformer $Q_{loss} = 3I_G^2 X_{trans} = 3 \times 98.35^2 \times 0.15 = 4,355\ W$

Therefore, the reactive power consumed by the induction generator is given by

$$Q = Q_{grid} + Q_{loss} = 74121 - 4355 = 69,766\ W$$

Example 6.6 Consider a three-phase Y wound rotor-connected induction generator rated 220 V, 60 Hz, and 16 hp; the poles of the machine can be changed from 2 to 12 to control the wind speed. The machine has the following parameters:

$R_1 = 0.2\ \Omega$/phase and $X_1 = 0.4\ \Omega$/phase
$R_2' = 0.13\ \Omega$/phase and $X_2 = 0.4\ \Omega$/phase

Plot the power versus speed curve of the machine controlling the wind speed by changing the number of poles.

The following MATLAB M-file testbed depicts the operation of the machine.

```
%POWER vs SPEED
clc;
v1=220/sqrt(3);
f=60;
P=2;
r1=0.2;
x1=0.4;
r2d=0.13;
x2d=0.4;                              % The electrical
                                      quantities are defined
```

```
for P=2:2:12                          % The no. of poles is
                                      varied from 2 to 12
  ws=120*f/P;
  w=0:.2:7200;                        % The value of speed
                                      is varied till
                                      synchronous speed
  for i=1:length(w)
    s(i)=(ws-w(i))/ws;
    Tem(i)=(3/ws)*(r2d/s(i))*v1^2/((r1+r2d/s(i))^2+
    (x1+x2d)^2);
    Po(i)=-Tem(i)*w(i)/1000;   % Power in kW
  end
  plot(w,Po)
  hold on;
end
axis([0 7200 0 50])
grid on;
set(gca,'XDir','reverse')
xlabel('Speed (rpm)')
ylabel('Power (kW)')
```

Figure 6.38 depicts the power versus speed of a variable pole induction generator for various rotor speeds.

6.8 THE DOUBLY-FED INDUCTION GENERATOR

Electric machines are classified based on the number of windings in the conversion of mechanical power to electric power. A singly-fed machine has one winding. The SCIG-type machines have one winding, which contributes to the energy conversion process. Doubly-fed machines have two windings that likewise are instrumental in energy conversion. The wound-rotor doubly-fed induction generator (DFIG)[20] is the only electric machine that can operate with rated torque to twice synchronous speed for a given frequency of operation. In a DFIG, the current flowing in the magnetizing branch and torque current are orthogonal vectors. It is not desirable to design machines that are magnetized from the rotor because commutation[20] systems, supporting slip rings, and brushes are needed to inject current into the rotor winding. These types of machines have high maintenance costs. However, in these machines, the stators can have a unity power factor. The frequency and the magnitude of the rotor voltage are proportional to the slip as expressed by Equation 6.30. In principle, the DFIG is a transformer at standstill.

If the DFIG is producing torque and operating as a motor, the rotor is consuming power. At standstill all power fed into the stator is consumed as heat in the stator and the rotor. Therefore, at low speeds, the efficiency of the

DFIG is very low because the supplied current is mainly used to produce magnetizing current and the power conversion processes as a function of a motor or a generator do not take place. If the DFIG is operating at above the synchronous speed, the mechanical power is fed in both through the stator and rotor. Therefore, the machine has higher efficiency and the machine can produce twice the power as a singly-fed electric machine.

With the DFIG at below synchronous speeds, the stator winding is producing electric power and part of its power is fed back to the rotor. At speeds above synchronous speeds, the rotor winding and stator winding are supplying electric power to the grid. However, DFIGs do not produce higher torque per volume than singly-fed machines. The higher power rating can be obtained because of the higher speed and without weakening the magnetic flux.

A DFIG configuration system is depicted in Fig. 6.38. This DFIG is a wound rotor induction generator (WRIG) with the stator windings directly connected to the power grid. The DFIG has two parallel AC/DC converter units. Although these converters act together, they are not necessarily fully identical with regard to their power rating.

The rotor windings connected to an AC/DC power convert on the grid side and a DC/AC power converter on the rotor side. The back-to-back converter operates as a bidirectional power converter with a common DC-bus. The transformer in Fig. 6.39 has two secondary windings; one winding connecting the stator and the other connecting the rotor. The converter on the rotor side makes it possible to operate the rotor excitation at a lower DC bus voltage. This DFIG provides reactive power control through its power converter because it decouples active and reactive power control by independently controlling the rotor excitation current. A DFIG can supply (absorb) reactive power to and from the power grid. The control method is based on the variable speed/variable pitch wind. Two hierarchical control levels are used. These controllers are designed to track the wind turbine operation point, to

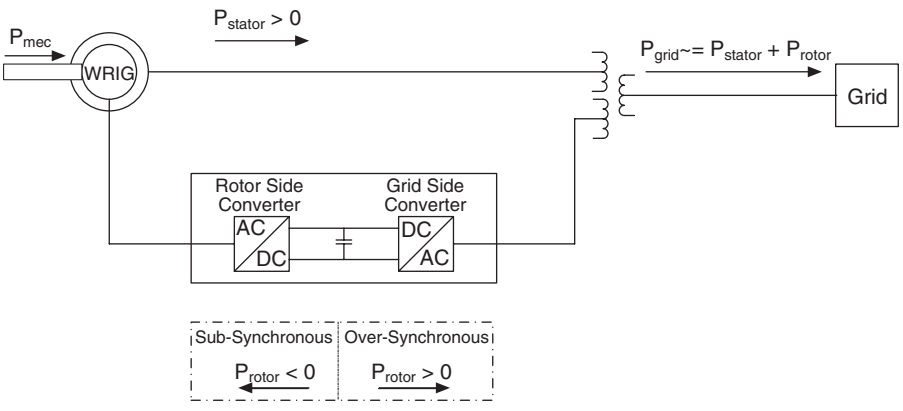

Figure 6.39 A Microgrid of a Doubly-Fed Wound Induction Generator.

limit the turbine operation in the case of high wind speeds. In addition, the controller controls the reactive power injected into the power grid and the reactive power consumed by the wind turbine generator. The power supervisory controller controls the pitch angle to keep the wind turbine operating at the rated power. At the same time, the speed controller controls the shaft speed of the generator to ensure that it remains within safe range. However, at low wind speeds, the speed controller attempts to maximize the generated power and generator efficiency. Therefore, the change in generator speed follows the slow change in wind speed.

As an inherent part of DFIG systems, the generator stator feeds up to 70% of the generated power directly into the grid, usually at low voltage, using a step-up transformer. A well-established disadvantage of DFIG systems is the occurrence of internal stray currents in the generator. These currents accelerate generator bearing failure. Protective counter-methods include the design of special generator bearings and/or seals that shield the bearings against the negative impact of stray currents.

A wound rotor DFIG has several advantages over a conventional induction generator. Because the rotor winding is actively controlled by a power converter, the induction generator can generate and consume reactive power. Therefore, the DFIG can support the power system stability during severe voltage disturbances by providing reactive power support. As an inherent part of DFIG systems, the generator stator feeds the remaining 70–76% of total power directly into the grid, usually for up to 690 V. The wind microgrid is connected to the local grid using a step-up transformer. The DFIG systems are designed for both a 60-Hz and 50-Hz system, but each grid situation requires a generator operation adapted to the specific operational circumstances. However, the control of DC/AC converters is an advanced topic that is not the subject of this book. Students who are interested in the control of converters in green energy systems should refer to reference 23. Squirrel cage induction generators have a lower cost of manufacturing than wound rotor induction generators and are relatively simple to design; they are robust, cost-effective, and widely used in wind microgrids.

6.9 BRUSHLESS DOUBLY-FED INDUCTION GENERATOR SYSTEMS

Brushless DFIG systems[21] are designed by placing two multiphase winding sets with a different number of pole-pairs on the stator structure. One of the stator winding sets is designated as power winding and is connected to the power grid. The second winding control is supplied from a converter and controls the energy conversion process. The generator is controlled by varying the frequency of the winding connected to the power converter. Because the pole-pairs of two windings are not identical, the low-frequency magnetic induction is created in the winding that connects to the power grid over a speed range that the rotor supplies by wind power. Brushless DFIGs do not utilize the

magnetic core efficiently. The dual winding set stator area is physically larger than that of other electric machines of comparable power rating.

6.10 VARIABLE-SPEED PERMANENT MAGNET GENERATORS

These types of wind generators operate with variable wind speed.[22] They use a "full" AC/DC and DC/AC power converter. The DC power is inverted using a DC/AC inverter and is connected to a step-up transformer, and then connected to the local power grid as shown in Fig. 6.41.

The variable-speed permanent magnet generator of Fig. 6.41 produces a variable AC voltage with a variable frequency. Because the power generated is not at the frequency of the local power grid, the output power of the variable frequency generator cannot be injected into local power grid as we have discussed in Chapter 4 (see section on automatic generation control). Therefore, the variable AC frequency voltage is rectified by the AC/DC rectifier (see Fig. 6.41). The DC bus of Fig. 6.40 can be used to charge a storage system using a boost–buck converter. Figure 6.42 depicts a variable-speed generator. This type of generator is studied in Chapter 4. The field winding of the generator of Fig. 6.42 is supplied from DC power using a AC/DC rectifier from an AC bus of the microgrid. Because the supplied wind mechanical power has a variable speed, the generator output power would also contain variable frequency. The DC/AC inverter is used to convert the DC power to AC power at the local power grid frequency and voltage as shown in Fig. 6.41 and

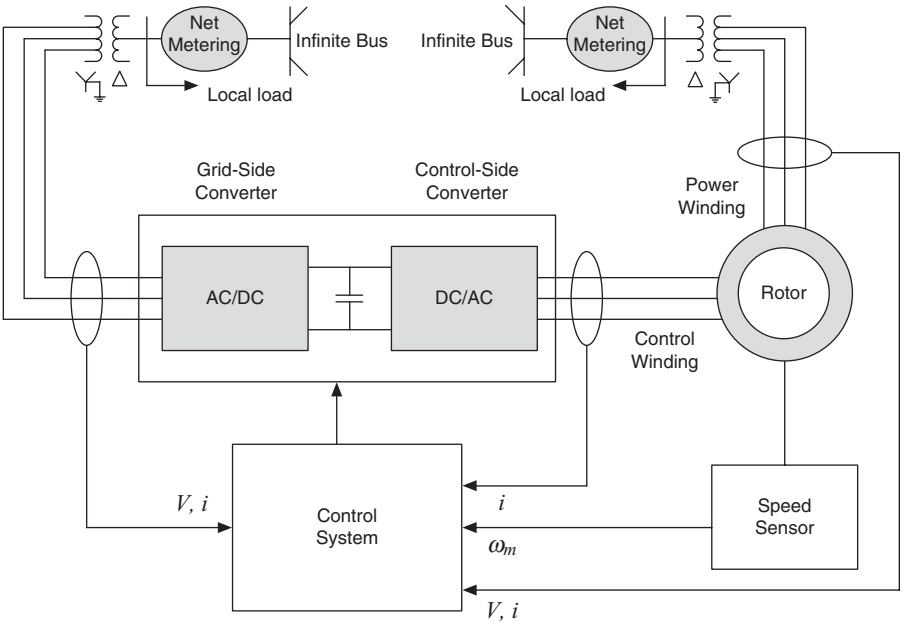

Figure 6.40 A Microgrid of Brushless Doubly-Fed Induction Generator.

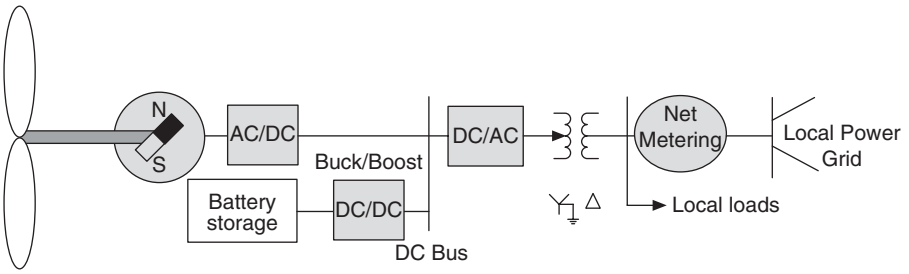

Figure 6.41 A Microgrid of a Variable-Speed Permanent Magnet for a Wind Generator.

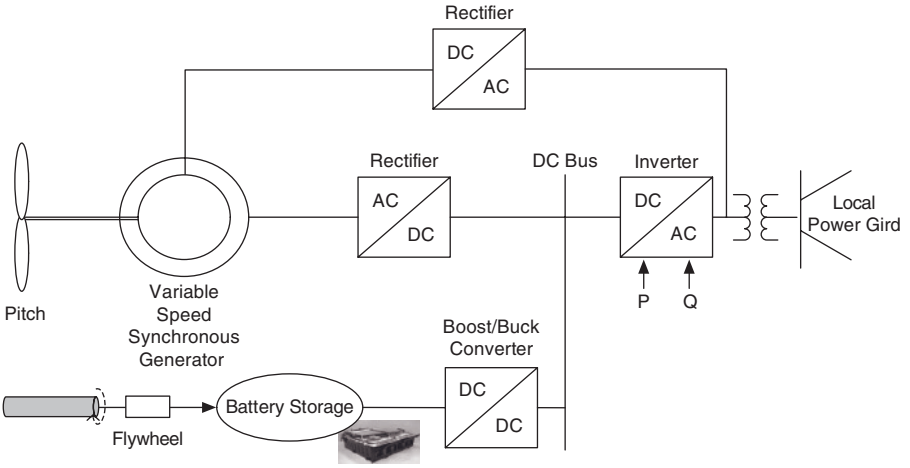

Figure 6.42 A Microgrid of a Multipole Synchronous Generator.

Fig. 6.42. The microgrid of wind power can be connected to the local power grid of an AC bus because it is operating at the frequency of the local power grid. However, the coordinated control of converters of Fig. 6.41and Fig. 6.42 is an advanced topic that is not addressed in this book. Students who are interested in the control of converters in green energy systems should refer to reference 23.

6.11 A VARIABLE-SPEED SYNCHRONOUS GENERATOR

The rotor of a synchronous generator rotates at synchronous speed. [19,21] For a synchronous generator, the frequency of the voltage induced in the stator windings is given by the expression below.

$$\omega_{syn} = \frac{2}{P}\omega_s$$

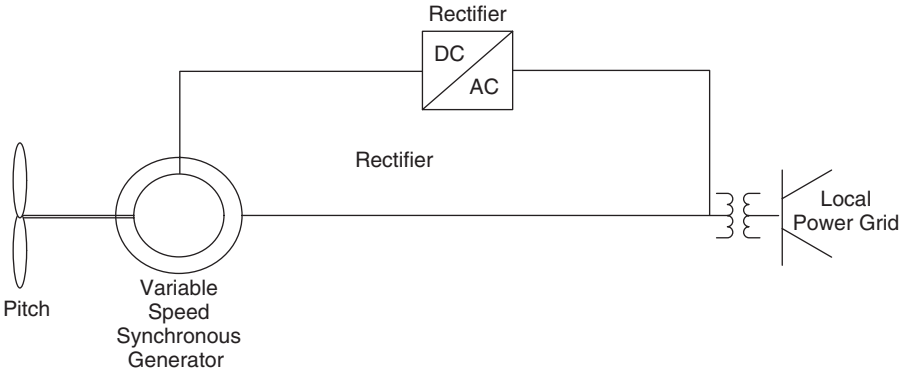

Figure 6.43 A Variable-Speed Synchronous Generator.

If $P = 2$, then $\omega_{syn} = \omega_s$

And the frequency of induced voltage is given by

$$\omega_s = 2 \cdot \pi \cdot f_e$$

If the wind speed is variable, the induced voltage will also be time varying, and it will be of multiple frequencies. Figure 6.43 depicts such a wind-based microgrid. However, before connecting the generator to the local power grid, we must operate the generator at the synchronous speed. Depending on the expected wind speed for a given location, the generator can be designed with a gear system. The gear ratio is adjusted such that the speed of the rotor of the generator is at synchronous speed. Therefore, the induced voltage of the stator of the generator is at the same frequency as the local power grid.

6.12 A VARIABLE-SPEED GENERATOR WITH A CONVERTER ISOLATED FROM THE GRID

Another type of wind turbine generator system consists of an electrical exciter machine together with a DFIG. In comparison to a normal DFIG system, this wind generator has one converter. By including the excitation machine, it is possible to isolate the power converter so it is not directly connected to the grid. That is, the stator is the only grid-connected output. This is a solution that is different from a normal DFIG grid-connection, in which the generator rotor power is fed into the grid via a power converter.

Figure 6.44 depicts a variable-speed wind turbine generator with a converter isolated from the grid. The first converter is a DC/AC inverter that feeds the rotor of DGIF. However, in this topology, the second converter unit is an AC/DC rectifier, which is supplied from the exciter machine (see Fig. 6.44).

Furthermore, in contrast to both synchronous and asynchronous generators, DFIGs are inherently incapable of acting as electric brakes for the sudden

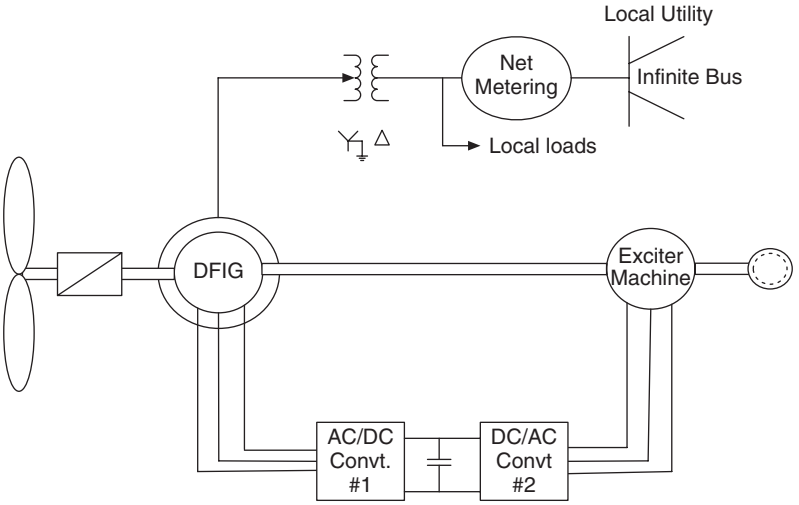

Figure 6.44 A Microgrid of Variable-Speed Wind Turbine Generator with the Converter Isolated from the Grid.

separation of a wind turbine from the grid or a sudden high wind speed. However, in the above topology, the exciter machine power can be used to drive an electric brake. The electric brake may also be used together with aerodynamic braking, minimizing peak torque loads.

These wind turbines are characterized by lower inertia than classical power plants; therefore, they cannot participate in power system load–frequency regulation. When the wind generators are equipped with a storage system, they can participate in load–frequency control. The variable speed turbines are designed based on the use of back-to-back power electronic converters. The intermediate DC voltage bus creates an electrical decoupling between the machine and the grid. Such decoupling creates a new opportunity to use these types of wind-generating systems for load–frequency control.

Example 6.7 Select AC/DC rectifiers and DC/AC inverters for a 600 kW variable-speed wind generator operating at 690 V AC. The utility-side voltage is 1000 V.

Solution
The peak value of the instantaneous line-to-line as voltage:

$$V_{L-L,peak} = \sqrt{2} \cdot V_{L-L,rms} = \sqrt{2} \times 690 = 975.8\ V$$

Therefore, the DC-side voltage rating of the rectifier is ≥976.8 V.

Let the voltage rating of the rectifier be 1000 V on the DC side and 690 V on the AC side. The inverter also can be selected with a rating of 1000 V on the AC side. Both the rectifier and the inverter should be rated 600 kW.

In this chapter, we have studied the modeling of induction machines and their operation as motors and generators. The use of induction generators as a source of power in microgrids requires an excitation current for generator operation to be provided from local microgrids. If the wind-based microgrids are connected to the local power grids, the power grids will provide the excitation currents (VAr). Therefore, the local power grids must be planned to provide the reactive power (VAr) requirements of the wind microgrids.

We have also reviewed doubly-fed induction generators, variable-speed induction generators, and variable-speed permanent magnet generators.[20–23] The coordinated control of converter is an advanced topic that is not the subject of this book. Students who are interested in control of converters in green energy systems should refer to reference 23.

PROBLEMS

6.1 Consider a wind microgrid given in Fig. 6.45. The system has a local load rated 100 kVA at a power factor rated 0.8 lagging.

The three-phase transformer is rated 11 kV/0.44 kV; 300 kVA; X = 0.06 p.u. The induction generator is rated as 440 V, 60 Hz, three-phase, eight-pole; stator resistance of 0.08 Ω/phase; rotor referred resistance in the stator side of 0.07 Ω/phase, stator reactance of 0.2 Ω/phase; rotor referred reactance of X_2 0.1 Ω/phase. Compute the following:

i) The p.u equivalent model based on a kVA base of 300 kVA and 440 V

ii) The shaft mechanical power if the shaft speed is at 1200 rpm

iii) The amount of power injected into the local utility

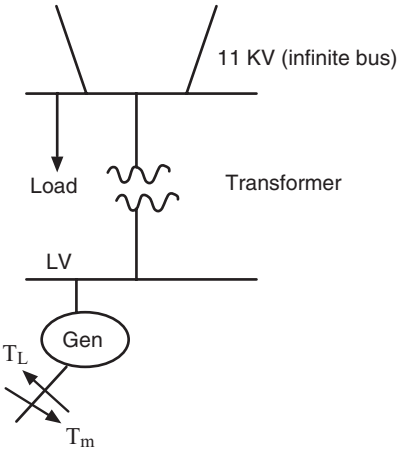

Figure 6.45 The Schematic of Problem 6.1.

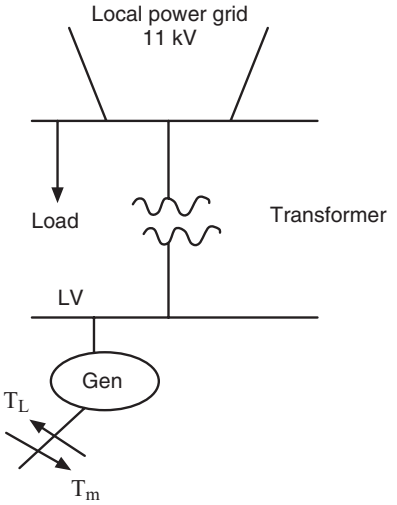

Figure 6.46 System of Problem 6.4.

iv) The flow of reactive power between grid and local microgrid

v) How much reactive power must be placed at the local grid to have unity power factor at the local power grid

6.2 The microgrid of Figure 6.46 is supplied by an induction generator. The system has a local load rated 100 kVA at power factor rated 0.8 lagging. The three-phase transformer is rated 11 kV/0.44 kV, 300 kVA, and reactance of 6%. The induction machine rated at 440 V, 60 hz, three-phase, eight-pole; 500 kVA, 440 V, 60 Hz; stator resistance of 0.1 Ω/phase; rotor referred resistance in the stator side of 0.1 Ω/phase, stator reactance of 0.8 Ω/phase; rotor referred reactance of 0.4 Ω/phase. Compute the following:

i) Compute the per unit power flow model and short-circuit model based on a base of 500 kVA and 440 V.

ii) If the speed of the induction generator is 1000 RPM, what is the rotor frequency?

iii) The flow of active and reactive power between microgrid and the local power grid.

6.3 A six-pole wound rotor induction machine is rated at 60 Hz, 380 V, 160 kVA. The induction machine has a stator and referred rotor resistance of 0.8 ohms per phase and stator and rotor reactance of 0.6 ohms per phase. The generator shaft speed is at 1500 rpm. Determine how much resistance the rotor circuit must have to operate the generator at 1800 rpm.

6.4 A 400 V, three-phase Y-connected induction generator has the following data.

$$\bar{Z}_1 = (0.6 + j1.2)\Omega / phase$$
$$\bar{Z}_2' = (0.5 + j1.3)\Omega / phase$$

The generator is connected to a local power grid. Perform the following:

i) The maximum active power that generator can supply.

ii) The reactive power flow between the induction generator and local power grid.

6.5 Design a 15 kW wind power generator that is supplied from a variable wind speed. The designed system must provide 220 V_{AC}, single-phase AC power. Compute the DC bus voltage.

6.6 The same as problem 6.7, except the wind generating system must provide three-phase AC nominal voltage of 210 V_{AC}. Compute the DC bus voltage.

6.7 Design a 2 MW wind system using a variable speed system. The DC bus voltage is to be at nominal value of 600 V_{DC}. The panels are located at 5 miles from the local utility. The utility voltage is three-phase AC rated at 34.5 kV. Assume the rated power factor is 0.8 leading.

The data for the transmission line is given by Table 6.2. The data for transformers are given as: 460 V/13.2 kV 250 kVA 10% impedance and 13.2 KV to 34.5 kV, 1 MVA 8.5% impedance.

Perform the following:

i) Give the one-line diagram

ii) Per unit model based on rated wind generator

6.8 A wound rotor six-pole 60 Hz induction generator has stator resistance of 1.1 ohms per phase and rotor resistance of 0.8 ohms and runs at 1350 rpm. The prime mover torque remains constant at all speeds. How much resistance must be inserted in the rotor circuit to change the speed to 1800 rpm. Neglect the motor leakage reactance, X_1 and X_2.

6.9 Consider a three-phase Y-wound rotor connected induction generator rated 220 V, 60 Hz, 16 hp, eight pole with the following parameters:

$R_1 = 1\ \Omega$/phase and $X_1 = 1.6\ \Omega$/phase

TABLE 6.2 13.2–132 kV Class One Phase–Neutral Return Line Model.

Conductor	DC Resistance (Ω/km)	Inductance (Ω/km) L	Susceptance (S/km) C	Current Ratings
Magpie	1.646	j 0.755	j 1.45e-7	100 Amp
Squirrel	1.3677	j 0.78	j 6.9e-7	130 Amp
Gopher	1.0933	j 0.711	j 7.7e-7	150 Amp

$R_2' = 0.36\ \Omega$/phase and $X_2 = 1.8\ \Omega$/phase

The generator is connected to the local power grid.

Write a MATLAB simulation testbed to plot slip and speed as a function of machine torque and various external inserted resistance in the rotor circuit. Make the plot for a value of external resistance of 0.0, 0.4, 0.8, and 1.2 Ω.

REFERENCES

1. Wikipedia. History of wind power. Available at http://en.wikipedia.org/wiki/Wind_Energy#History. Accessed 2009 Aug 10.
2. Technical University of Denmark. National Laboratory for Sustainable Energy. Wind Energy. Available at http://www.risoe.dk/Research/sustainable_energy/wind_energy.aspx Accessed 2009 July 11.
3. California Energy Commission. Energy Quest. Chapter 6: Wind energy. Available at http://www.energyquest.ca.gov/story/chapter16.html. Accessed 2009 June 10.
4. U.S. Department of Energy, Energy Information Administration. Official Energy Statistics from the US Government. Available at http://www.eia.doe.gov/energyexplained/index.cfm?page=us_energy._Accessed 2009 Sept 10.
5. U.S. Department of Energy. U.S. installed wind capacity and wind project locations. Available at http://www.windpoweringamerica.gov/wind_installed_capacity.asp. Accessed 2011 March 1.
6. U.S. Department of Energy, National Renewable Energy Laboratory. Available at http://www.nrel.gov/. Accessed 2011 March 1..
7. Jangamshetti SH, Guruprasada Rau V. Site matching of wind turbine generators: a case study. IEEE Transactions in Energy Conversion 1999; 14(4):1537–1543.
8. Jangamshetti SH, Guruprasada Rau V. Optimum siting of wind turbine generators. IEEE Transactions of Energy Conversion 2001; 16(1):8–13.
9. Justus CG, Hargraves WR, Mikhail A, Graber D. Methods of estimating wind speed frequency distribution. Journal of Applied Meteorology 1978; 17(3):350–353.
10. Quaschning V. Understanding renewable energy systems. London: Earthscan; 2006.
11. Freris L, Infield D. Renewable energy in power systems. Hoboken, NJ: Wiley; 2008.
12. Patel MK. Wind and solar power systems: design, analysis, and operation. Boca Raton, FL: CRC Press; 2006.
13. Hau E. Wind turbines: fundamentals, technologies, application and economics. Heidelberg: Springer; 2006.
14. Simoes MG, Farrat FA. Alternative energy systems: design and analysis with induction generators. Boca Raton, FL: CRC Press; 2008.
15. AC Motor Theory. Available at http://www.pdftop.com/ebook/ac+motor+theory/. Accessed 2010 Dec 5.
16. HSL Automation Ltd. Basic motor theory: squirrel cage induction motor. Available at http://www.hslautomation.com/downloads/tech_notes/HSL_Basic_Motor_Theory.pdf. Accessed 2010 Oct 10.

17. Krause P, Wasynczuk O. Electromechanical motion devices. New York: McGraw-Hill; 1989.
18. Majmudar H. Electromechanical energy converters. Reading, MA: Allyn & Bacon; 1966.
19. Sung SWF, Rudowicz C. A closer look at the hysteresis loop for ferromagnets Available at http://arxiv.org/ftp/cond-mat/papers/0210/0210657.pdf. Accessed 2010 Dec 5.
20. Pena R, Clare JC, Asher GM. Doubly fed induction generator using back-to-back PWM converters and its application to variable-speed wind-energy generation. IEEE Proceedings of Electric Power Applications 1996; 143(3):231–241.
21. 1999 European Wind Energy Conference: Wind energy for the next millenium. Proceedings of the European Wind Energy Conference, Nice, France, 1–5 March 1999. London: Earthscan; 1999.
22. Boldea I. The electric generators handbook. Variable speed generators. Boca Raton, FL: CRC Press; 2005.
23. Keyhani A, Marwali M, Dai M. Integration of green and renewable energy in electric power systems. Hoboken, NJ: Wiley; 2010.

CHAPTER 7

LOAD FLOW ANALYSIS OF POWER GRIDS AND MICROGRIDS

7.1 INTRODUCTION

We have established that the main objectives of electric energy distribution are to provide rated voltage and rated frequency at specified loads. In Chapter 4, we discussed load frequency control; here we will focus on voltage control. To ensure the rated voltage at each bus in a power grid, the system must be modeled in steady state. Hence, the integration of renewable energy sources as part of a microgrid that is connected to the local power grid is also examined as well as the asynchronous operation of a microgrid. The calculation of bus load voltage is formulated as a power flow problem. Once the load voltages are established—this includes the bus voltage magnitude and phase angle—the power flow on lines can be computed from line impedance and voltages on the two ends of a line. This takes us to the use of power flow analysis as an engineering tool. In the formulation of the power flow problem, we will study how interconnected transmission systems are modeled. Both the bus-admittance matrix and bus-impedance matrix models are presented in this chapter. At the end of the chapter, we will review three methods for solving power flow problems: the Gauss–Seidel, Newton–Raphson, and fast decoupled load flow solutions. Several solved examples and homework problems are provided to further students' understanding of microgrid design.

Design of Smart Power Grid Renewable Energy Systems, First Edition. Ali Keyhani.

7.2 VOLTAGE CALCULATION IN POWER GRID ANALYSIS

In a circuit problem, the impedance of loads and the source voltage are given, and the problem is to find the current flow in the circuit and calculate the voltage across each load. In voltage calculation in a power problem, the loads are given in terms of active and reactive power consumption. We can study this problem via two methods: (1) assume the voltage across the load and calculate the source voltage, and (2) assume the source voltage and compute the bus load voltage (this is known as a power flow or load flow problem). Example 7.1 illustrates the first method.

Example 7.1 A three-phase feeder is connected through two cables with equal impedance of 4 + j15 Ω in series to 2 three-phase loads. The first load is a Y-connected load rated 440 V, 8 KVA, p.f. = 0.9 (lagging) and the second load is a Δ-connected motor load rated 440 V, 6 KVA, p.f. = 0.85 (lagging). The motor requires a load voltage of 440 V at the end of the line on the Δ-connected loads. Perform the following:

i) Give the one-line diagram
ii) Find the required feeder voltage

Solution
The line voltage at bus 3 is equal to 440 V.

The rated current drawn by a motor on bus 3 is

$$I_3 = \frac{kVA_{r3}}{\sqrt{3}\cdot V_3} = \frac{6000}{\sqrt{3}\times 440}\angle -\cos^{-1}0.85 = 7.87\angle -31.77^\circ\ A$$

The voltage at bus 2 is given by

$$V_{2,ph} = V_{3,ph} + \mathcal{Z}_{2-3}\times I_3 = 440/\sqrt{3} + (4+j15)\times 7.87\angle -31.77 = 353.04\angle 13.7^\circ\ V$$

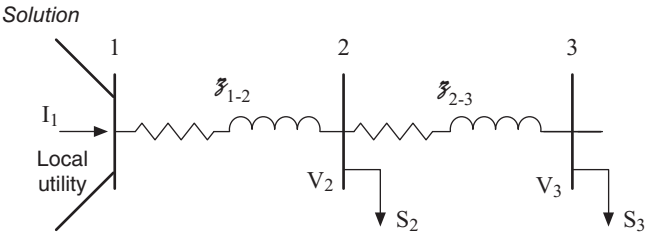

Figure 7.1 The One-Line Diagram of Example 7.1.

The rated current drawn by a load on bus 2 is

$$I_2 = \frac{kVA_{r2}}{3 \cdot V_2} = \frac{8000}{3 \times 353.04} \angle -\cos^{-1} 0.9 = 7.55 \angle -25.84^\circ \; A$$

The supply current of the generator is given by

$$I_1 = I_2 + I_3 = 7.55 \angle -25.84 + 7.87 \angle -31.77 = 15.39 \angle -28.87^\circ \; A$$

The generator phase voltage is given by

$$V_1 = V_2 + \mathcal{Z}_{1-2} \times I_1 = 353.04 \angle 13.7 + (4 + j15) \times 15.39 \angle -28.87 = 569.21 \angle 26.73^\circ \; V$$

The line voltage of the generator is given by

$$V_1 \sqrt{3} = 569.21 \times \sqrt{3} = 985.90 \; V$$

Example 7.1 is not a practical problem. The generator voltage is controlled by its excitation system. In practice, the field current is set to obtain the rated generator voltage. If the generator has two poles and the generator is operating at synchronous speed, that is, for a 60-Hz system, it operates at 3600 rpm.

Therefore, in a practical problem, we need to compute the voltage at load buses given the generator voltage and load power consumption. The solution to this latter problem—known as the power flow problem—is more complex.

Example 7.2 Consider a distributed feeder presented in Fig. 7.2.

Assume the following:

a. Feeder line impedances, that is $\mathcal{Z}_{1-2}$ and $\mathcal{Z}_{2-3}$, are known.
b. The active and reactive power consumed, that is S_2 and S_3, by loads are known.
c. The local power grid bus voltage V_1 is known and all data are in per unit.

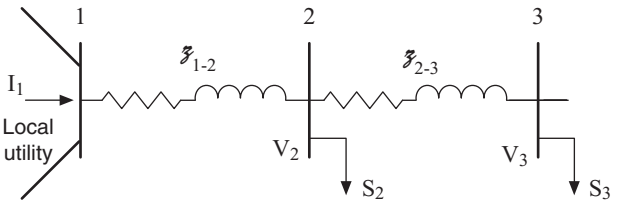

Figure 7.2 A Distribution Feeder.

Solution

Let us write the Kirchhoff's current law for each node (bus) of Fig. 7.2 and assume that the sum of the currents away from the bus is equal to zero. That is, for buses 1–3, we have

$$\begin{aligned}(v_1 - v_2)\, y_{12} - I_1 &= 0,\\ (v_2 - v_1)\, y_{12} + (v_2 - v_3)\, y_{23} + I_2 &= 0\\ (v_3 - v_2)\, y_{23} + I_3 &= 0\end{aligned} \tag{7.1}$$

where $y_{12} = 1/\mathcal{Z}_{1-2}$ and $y_{23} = 1/\mathcal{Z}_{2-3}$

$$I_1 = \left(\frac{S_1}{V_1}\right)^*, \quad I_2 = \left(\frac{S_2}{V_2}\right)^* \quad \text{and} \quad I_3 = \left(\frac{S_3}{V_3}\right)^* \tag{7.2}$$

We can rewrite Equation 7.1 as

$$\begin{aligned} y_{12}v_1 - y_{12}v_2 &= I_1\\ -y_{12}v_1 + (y_{12} + y_{23})\, v_2 - y_{23}v_3 &= -I_2\\ -y_{23}v_2 + y_{23}v_3 &= -I_3\end{aligned}$$

The above can be written as:

$$\begin{bmatrix} Y_{11} & Y_{12} & 0\\ Y_{21} & Y_{22} & Y_{23}\\ 0 & Y_{23} & Y_{33}\end{bmatrix} \cdot \begin{bmatrix} V_1\\ V_2\\ V_3\end{bmatrix} = \begin{bmatrix} I_1\\ -I_2\\ -I_3\end{bmatrix} \tag{7.3}$$

where $Y_{11} = y_{12}, Y_{12} = -y_{12}, Y_{21} = -y_{12}, Y_{22} = y_{12} + y_{23}, Y_{23} = -y_{23}, Y_{32} = -y_{23}, Y_{33} = y_{23}$

The matrix Equation 7.3 represents the bus admittance matrix; it is also the Y_{Bus} model for Example 7.2.

The Y_{Bus} matrix is described as

$$I_{Bus} = Y_{Bus} \cdot V_{Bus} \tag{7.4}$$

If the system has n buses, I_{Bus} is a vector of $n\times1$ current injection, V_{Bus} is a voltage vector of $n\times1$, and Y_{Bus} is a matrix of $n\times n$.

For Example 7.2, we have three buses. Therefore, the Y_{Bus} matrix is 3×3 as shown in Equation 7.3 or Equation 7.4.

Let us continue our discussion for a general case of a power grid with n buses. For each bus, k, we have

$$S_k = V_k I_k^* \qquad k = 1, 2, \ldots . n \tag{7.5}$$

And I_k is the current injection into the power grid at bus k. Therefore, from k row of Y_{Bus} matrix, we have

$$I_k = \sum_{j=1}^{n} Y_{kj} V_j \tag{7.6}$$

Substituting Equation 7.6 in Equation 7.5, we have

$$S_k = V_k \left(\sum_{j=1}^{n} Y_{kj} V_j \right)^* \qquad k = 1,2,\ldots..n \tag{7.7}$$

For each bus k, we have a complex equation of the form given by Equation 7.7. Therefore, we have n nonlinear complex equations.

$$\begin{aligned} P_k &= \mathrm{Re}\left\{ V_k \sum_{j=1}^{n} Y_{kj}^* V_j^* \right\} \\ Q_k &= \mathrm{Im}\left\{ V_k \sum_{j=1}^{n} Y_{kj}^* V_j^* \right\} \end{aligned} \tag{7.8}$$

$$\begin{aligned} P_k &= V_k \sum_{j=1}^{n} V_j \left(G_{kj} \cos\theta_{kj} + B_{kj} \sin\theta_{kj} \right) \\ Q_k &= V_k \sum_{j=1}^{n} V_j \left(G_{kj} \sin\theta_{kj} - B_{kj} \cos\theta_{kj} \right) \end{aligned} \tag{7.9}$$

where

$$\begin{aligned} Y_{kj} &= G_{kj} + jB_{kj}, \theta_{kj} = \theta_k - \theta_j \\ V_j &= V_j \left(\cos\theta_j + j \sin\theta_j \right) \\ V_k &= V_k \left(\cos\theta_k + j \sin\theta_k \right) \end{aligned}$$

For Example 7.2, $n = 3$, we have six nonlinear equations. However, because the power grid bus-voltage magnitude is given and used as a reference with a phase angle of zero, we have four nonlinear equations.

In Example 7.2, we are given the feeder impedances ($\mathcal{Z}_{1-2}$ and $\mathcal{Z}_{2-3}$) and loads (S_2 and S_3). To find the bus load voltages, we need to solve the four nonlinear equations for V_2, V_3, θ_2, and θ_3. After calculating the bus voltages, we can calculate the complex power ($S_1 = P_1 + jQ_1$) injected by the local power feeder. The four nonlinear equations are

$$P_2 = V_2 \sum_{j=1}^{n} V_j \left(G_{2j} \cos\theta_{2j} + B_{2j} \sin\theta_{2j} \right)$$

$$P_3 = V_3 \sum_{j=1}^{n} V_j \left(G_{3j} \cos\theta_{3j} + B_{3j} \sin\theta_{3j} \right)$$

$$Q_2 = V_2 \sum_{j=1}^{n} V_j (G_{2j} \sin\theta_{2j} - B_{2j} \cos\theta_{2j})$$

$$Q_3 = V_3 \sum_{j=1}^{n} V_j (G_{3j} \sin\theta_{3j} - B_{3j} \cos\theta_{3j})$$

The above expressions present the basic concepts of bus active and reactive power injections of a power grid. If we know the bus-injected power, then we can solve for the load bus voltages. Voltage calculation is an important step in the design of a power grid network.

We should understand that Example 7.2 is not the same as Example 7.1. Example 7.1 is not a realistic problem because we cannot expect the local power grid to provide the voltage at the point of interconnection of a microgrid or a feeder. However, in Example 7.2 we know the local power grid bus voltage and our objective is the design of a feeder to provide the rated voltage to its loads.

7.3 THE POWER FLOW PROBLEM

In the design of a power grid, a fundamental problem is the power flow analysis.[1–9] The solution of the power flow ensures that the designed power grid can deliver adequate electric energy to the power grid loads at acceptable voltage and frequency (acceptable voltage is defined as the rated load voltage). For example, for a light bulb rated at 50 W and 120 V, the voltage provided across the load should be 120, with deviation of no more than 5% under normal operating conditions and 10% under emergency operating conditions. In per unit (p.u) value, we seek to provide 1 p.u voltage to the loads within the range of 0.95 and 1.05 p.u. That is, once we have specified the schedule of generation to satisfy the system load demand, the solution for bus voltages must be 1 p.u ± 5%.

The acceptable frequency can be ensured if a balance between the system loads and generation is maintained on a second-by-second basis as controlled by load and frequency control and automatic generation control. In terms of loads, the frequency deviation from the rated frequency—60 Hz in the United States and 50 Hz in the rest of the world—affects the machinery loads such as that of the induction motors and pumps. If the frequency drops, the speed of the induction motors will drop and result in excessive heating and failure of the induction motors. For example, consider a power system supported by a few diesel generators. If the operating frequency drops due to heavy load demands on the system, the pumps of a diesel generating station slow down; as a result, the diesel generators are not cooled enough. The overheated diesel engines are then removed from service by the system's override control system, causing a cascade failure of that power system. Therefore, to maintain stable

operation, system bus load voltages are maintained at 1 p.u with a deviation of no more than 10% in emergency operating conditions.

The terms *power flow studies* and *load flow studies* are used interchangeably to refer to the flow of power from the generating units to the loads. To solve a power flow problem, the question is "Given the system model and the schedule of generation and loads, find the voltage of the load buses."

7.4 LOAD FLOW STUDY AS A POWER SYSTEM ENGINEERING TOOL

As we discussed in the preceding section, the power grid must be designed to provide rated voltage to the grid's loads. We need to calculate bus voltages from the scheduled transmission system, scheduled generation system, and scheduled bus loads. In power grid system planning, the grid is planned based on projected future loads. The main objective of a power flow study is to determine whether a specific system design with a lower cost can produce bus voltages within an acceptable limit. In general, power grid planning entails many studies addressing (1) power generation planning, (2) transmission system planning, and (3) reactive power supply planning. The objectives of planning studies are to ensure that all power grids are operating within their operating limits and bus load voltages are within acceptable limits.

In the operation of a power grid, the following questions are addressed. Over the next 24 hours, for all scheduled busloads, transmission systems, transformers, and generation will the bus voltages be within the limits of their rated values? If a transformer has oil leaks, can the transformer be taken out of service without affecting load voltages? In the sudden loss of a line, can the power grid load demand be satisfied without any lines being overloaded?

Load flow studies in power grid and operational planning, outage control, as well as power system optimization and stability studies are performed to provide the needed answers. In the following section, we present the power flow problem formulation by first introducing bus types in a power grid.

7.5 BUS TYPES

In a power flow problem, several bus types are defined. The three most important types are a load bus, a generator bus, and a swing bus. Figure 7.3 depicts a load bus.

A power system bus has four variables. These variables are (1) the active power at the bus, (2) the reactive power at the bus, (3) the voltage magnitude, and (4) the phase angle. For a load bus, the active and reactive power consumptions are given as a scheduled load for a given time. The time can be specified as the day ahead forecasted peak load. If the system is being planned for 10 years ahead, then the forecasted peak load is used at the bus.

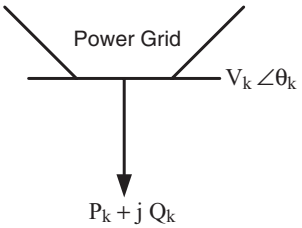

Figure 7.3 A Load Bus.

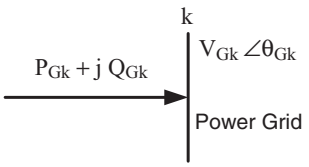

Figure 7.4 A Constant Voltage-Controlled (P-V) Bus.

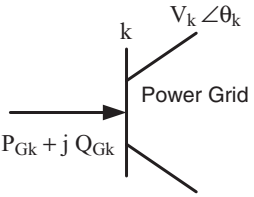

Figure 7.5 A Constant $P_G - Q_G$ Bus.

Figure 7.4 depicts a generator bus. This type of bus is referred to as a constant P-V bus.

A P-V (voltage-controlled) bus models a generator bus. For this bus type, the power injected into the bus by the connected generator is given in addition to the magnitude of bus voltage. The reactive power injected into the network and phase angle must be computed from the solution of the power flow problem. However, the reactive power must be within the limit (minimum and maximum) of what the P-V bus can provide.

Figure 7.5 depicts a constant $P_G - Q_G$ bus. This bus type represents a generator with known active and reactive power injection into the power system. However, the generator magnitude of the voltage and the phase angle must be computed from the solution of power flow problems.

Figure 7.6 defines a swing bus or slack bus. The swing bus is identical to a P-V bus except the bus voltage is set to 1 p.u and its phase angle to zero. For a swing bus, the net injected active power and reactive power into the network are not known. The generator connected to the swing bus is called a swing

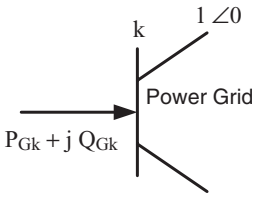

Figure 7.6 Swing Bus or Slack Bus.

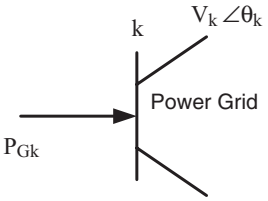

Figure 7.7 A Photovoltaic or Wind Generating Station Bus Model.

generator or slack generator. The function of a swing bus is to balance power consumption and power loss with net-injected generated power. The swing bus can also be considered as an infinite bus, i.e., it can theoretically provide an infinite amount of power. Hence, the swing bus is considered an ideal voltage source: it can provide an infinite amount of power and its voltage remains constant. Note that all the above definitions are identical and are used interchangeably.

Let us consider the bus type for microgrids of photovoltaic (PV) or wind generating stations. Because the energy captured from the sun or wind source is free, these types of generating units are operated to produce active power. This means that a PV or wind bus is operating at unity power factor. Therefore, the PV or wind bus can be modeled as given in Fig. 7.7.

Figure 7.7 depicts the modeling of a PV or wind generating station connected to a bus when a microgrid is connected to the local power grid. In this model, for the voltage analysis of the microgrid, the PV or wind bus active power generation is given and the reactive power generation is assumed to be zero. The bus voltage and phase angle is computed from the solution of the power flow problem subject to a minimum and maximum limitation as specified by the modulation index setting of a PV generating station. Therefore, we can summarize the PV generating bus model for bus k as P_{GK} and $V_{min} < V_k < V_{max}$ as specified. At the same time, the reactive power to be provided by a PV or wind generator must be within the limits (minimum and maximum) of the generating station.

Let us now consider the case when a microgrid is separated from the local power grid. In this case, the local microgrid must control its own frequency

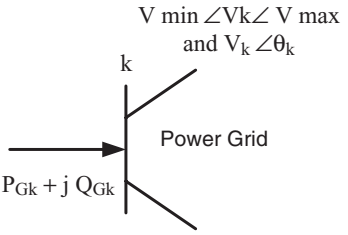

Figure 7.8 A Photovoltaic or Wind Generating Bus Model.

and bus voltages. When the microgrid of a PV and wind generating system is separated from the local power grid, the PV or wind generating bus can be modeled as given in Fig. 7.8.

In the above model, the magnitude of bus voltage is specified with a minimum and maximum as defined by the modulation index of the inverter; active power generation and reactive powers are also specified. The phase angle and voltage magnitude are to be computed from the power flow solution. However, a PV generating station without a storage system has very limited control over reactive power. To control an inverter power factor, a storage system is essential. To make an inverter with its supporting storage system operate like a steam unit and be able to provide active and reactive power is the subject of ongoing research on modeling and inverter control modeling. In case a wind generating station is connected to the microgrid directly, the reactive power injection control is limited within the acceptable voltage range of a connected wind bus.

For an isolated microgrid to operate at a stable frequency and voltage, it must be able to balance its loads and generation at all times. Because the load variation is continuous and renewable energy sources are intermittent, it is essential that a storage system and/or a fast-acting generating source such as high-speed microturbines, and/or a combined heat and power generating station be part of the generation mix of the microgrid.

Students are urged to read Chapter 4 again and study the factors that must be considered for the stable operation of a power grid.

In a load flow problem, all buses within the network have a designation. In general, the load buses are modeled as a constant P and Q model where the active power, P and reactive power, Q are given and bus voltages are to be calculated. It is assumed that power flowing toward loads is represented as a negative injection into the power system network. The generator buses can be modeled as a constant P_G and Q_G or as PV bus type. The generators inject algebraically positive active and reactive power into the power system network. For formulation of the power flow problem, we are interested in injected power into the power system network; the internal impedance of generators is not included in the power system model. However, for short-circuit studies, the internal impedance of the generators is included in the system model. The

internal impedance limits the fault current flow from the generators. For viable power flow, the balance of the system loads and generation must be maintained at all times. This balance can be expressed as

$$\sum_{k=1}^{n_1} P_{Gk} = \sum_{k=1}^{n_2} P_{Lk} + P_{losses} \tag{7.10}$$

where P_{Gk} is the active power generated by generator k, P_{Lk} is the active power consumed by the load k, n_1 is the number of the system generators, and n_2 is the number of the system loads. Similarly,

$$\sum_{k=1}^{n_1} Q_{Gk} = \sum_{k=1}^{n_2} Q_{Lk} + Q_{losses} \tag{7.11}$$

where Q_{Gk} is the reactive power generated by generator bus k, Q_{Lk} is the reactive power consumed by load k, n_1 is the number of system generators, and n_2 is the number of system loads.

Let us consider the system depicted in Fig. 7.9.

In the system given in Fig. 7.9, we need to balance the three-bus power system loads and generation.

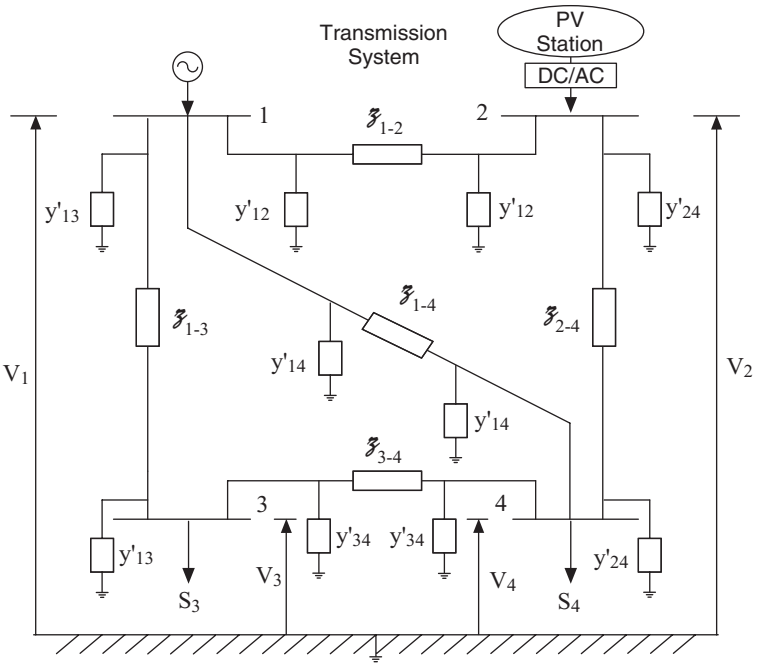

Figure 7.9 The Schematic Presentation of a Three-Bus Microgrid System.

$$\begin{aligned} P_{G1} + P_{G2} &= P_{L4} + P_{L3} + P_{losses} \\ P_{G1} + P_{G2} - P_{L4} - P_{L3} - P_{losses} &= 0 \end{aligned} \tag{7.12}$$

$$\begin{aligned} Q_{G1} + Q_{G2} &= Q_{L4} + Q_{L3} + Q_{losses} \\ Q_{G1} + Q_{G2} - Q_{L4} - Q_{L3} - Q_{losses} &= 0 \end{aligned} \tag{7.13}$$

In the above formulation, we assume inductive loads consume reactive power $Q_{Ind} > 0$ and capacitive loads supply reactive power $Q_{Cap} < 0$.

To ensure the balance between load and generation, we must calculate the active and reactive power losses. However, to calculate power losses, we need the bus voltages. The bus voltages are the unknown values to be calculated from the power flow formulation. This problem is resolved by defining a bus of the power grid—a swing bus and the generator behind it as a swing generator as defined earlier. By definition, the swing bus is an ideal voltage source. As an ideal voltage source, it provides both active and reactive power while the bus voltage remains constant. Therefore, a swing generator is a source of infinite active and reactive power in a power flow problem formulation. The swing bus voltage is set to 1 p.u and its phase angle as the reference angle set to zero degree, $V_s = 1 \angle 0$. With this assignment, the generator behind the swing bus can provide the required power to the loads of the power grid and its voltage will not be subject to fluctuations. Of course, in practice, such a constant voltage source with an infinite power source does not exist. However, if the connected loads are much smaller than the power behind a bus then it can be approximated as an ideal voltage source. The swing bus allows balancing the system loads plus system losses to the system's supply generation; thus, the balance of energy in the network is ensured.

7.6 GENERAL FORMULATION OF THE POWER FLOW PROBLEM

Let us now formulate the same problem, for a network of a power grid. We should keep in mind the following assumptions.

a. The generators are supplying balanced three-phase voltages.
b. The transmission lines are balanced.
c. The loads are assumed to be balanced.
d. The PV or wind generating stations are presented by a *PV* bus with the bus voltage having a minimum and maximum limit.

Consider the injection model of a power grid given in Fig. 7.10.

In Fig. 7.10, the current injections at each bus are presented based on the known power injection and the bus voltage that is calculated from the mathematical model of the system.

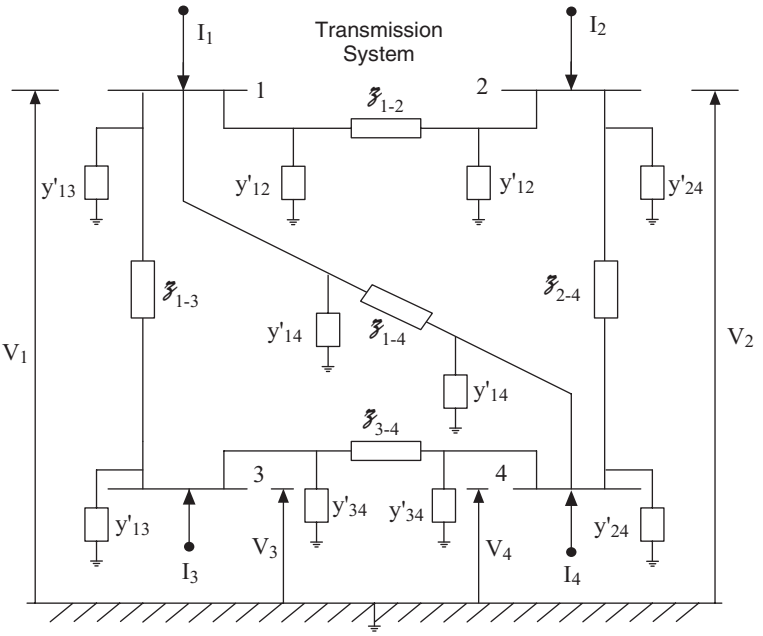

Figure 7.10 A Current Injection Model for Power Flow Studies.

In Fig. 7.10, the following definitions are implied:

- The bus voltages are actual bus-to-ground voltages in per unit.
- The bus currents are net injected currents in per unit flowing into the transmission system from generators and loads.
- All currents are assigned a positive direction into their respective buses. This means that all generators inject positive currents and all loads inject negative currents.
- The $\mathcal{Z}_{i\text{-}j}$ is the one-phase primitive impedance, also called the positive sequence impedance between bus i and j. We will study sequence impedances in the next chapter. However, the positive sequence impedance is the same balanced line impedance that we have been using in this book.
  - The y'_{ij} is the half of the shunt admittance between bus i and j.

Representing the series primitive impedance at the lines by their corresponding primitive admittance form where

$$y_{12} = 1/\mathcal{Z}_{1-2};\ y_{13} = 1/\mathcal{Z}_{1-3};\ y_{14} = 1/\mathcal{Z}_{1-4};\ y_{24} = 1/\mathcal{Z}_{2-4};\ y_{34} = 1/\mathcal{Z}_{3-4} \quad (7.14)$$

the power system shown in Fig. 7.10 can be redrawn as Fig. 7.11

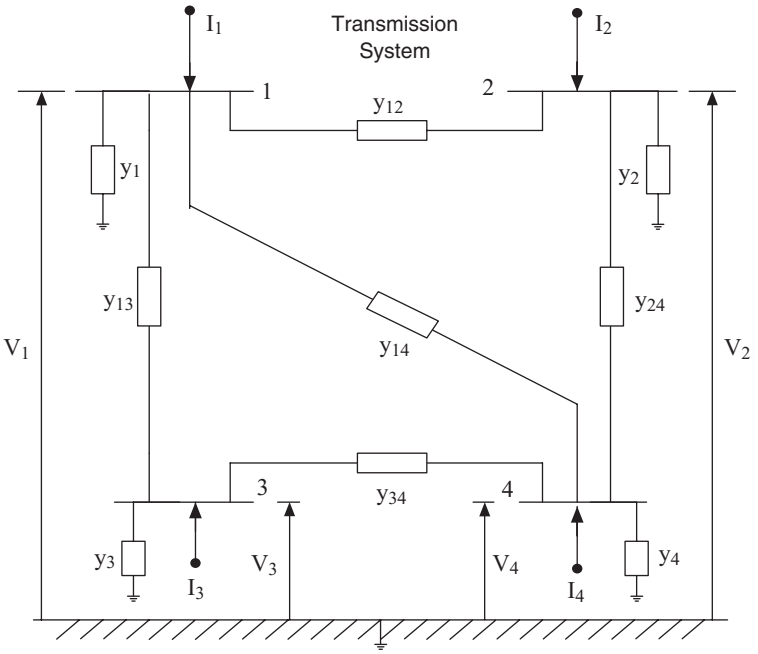

Figure 7.11 The Current Injection Model Using the Admittance Representation.

where

- $y_1 = y'_{12} + y'_{13} + y'_{14}$: Total shunt admittance connected to bus 1.
- $y_2 = y'_{12} + y'_{24}$: Total shunt admittance connected to bus 2.
- $y_3 = y'_{13} + y'_{34}$: Total shunt admittance connected to bus 3.
- $y_4 = y'_{14} + y'_{24} + y'_{34}$: Total shunt admittance connected to bus 4.

Assuming the ground bus as the reference bus, Kirchhoff's current law for each bus (node) gives:

$$\begin{aligned} I_1 &= V_1 y_1 + (V_1 - V_2) y_{12} + (V_1 - V_3) y_{13} + (V_1 - V_4) y_{14} \\ I_2 &= V_2 y_2 + (V_2 - V_1)\, y_{12} + (V_2 - V_4) y_{24} \\ I_3 &= V_3 y_3 + (V_3 - V_1)\, y_{13} + (V_3 - V_4) y_{34} \\ I_4 &= V_4 y_4 + (V_4 - V_1) y_{14} + (V_4 - V_2) y_{24} + (V_4 - V_3) y_{34} \end{aligned} \tag{7.15}$$

The above equations can be written as

$$\begin{aligned} I_1 &= V_1(y_1 + y_{12} + y_{13} + y_{14}) + V_2(-y_{12}) + V_3(-y_{13}) + V_4(-y_{14}) \\ I_2 &= V_1(-y_{12}) + V_2(y_2 + y_{12} + y_{24}) + V_3(0) + V_4(-y_{24}) \\ I_3 &= V_1(-y_{13}) + V_2(0) + V_3(y_3 + y_{13} + y_{34}) + V_4(-y_{34}) \\ I_4 &= V_1(-y_{14}) + V_2(-y_{24}) + V_3(-y_{34}) + V_4(y_4 + y_{14} + y_{24} + y_{34}) \end{aligned} \tag{7.16}$$

In matrix form

$$\begin{bmatrix} I_1 \\ I_2 \\ I_3 \\ I_4 \end{bmatrix} = \begin{bmatrix} Y_{11} & Y_{12} & Y_{13} & Y_{14} \\ Y_{21} & Y_{22} & Y_{23} & Y_{24} \\ Y_{31} & Y_{32} & Y_{33} & Y_{34} \\ Y_{41} & Y_{42} & Y_{43} & Y_{44} \end{bmatrix} \begin{bmatrix} V_1 \\ V_2 \\ V_3 \\ V_4 \end{bmatrix} \tag{7.17}$$

where

$$Y_{11} = y_1 + y_{12} + y_{13} + y_{14};\ Y_{12} = -y_{12};\ Y_{13} = -y_{13};\ Y_{14} = -y_{14}$$
$$Y_{21} = Y_{12};\ Y_{22} = y_2 + y_{12} + y_{24};\ Y_{23} = 0;\ Y_{24} = -y_{24};$$
$$Y_{31} = Y_{13};\ Y_{32} = Y_{23};\ Y_{33} = y_3 + y_{13} + y_{34};\ Y_{34} = -y_{34};$$
$$Y_{41} = Y_{14};\ Y_{42} = Y_{24};\ Y_{43} = Y_{34};\ Y_{44} = y_4 + y_{14} + y_{24} + y_{34}$$

7.7 THE BUS ADMITTANCE MODEL

We can formalize the formulation of a bus admittance matrix. This formulation is known as an "algorithm."[10] An algorithm is used to solve a problem using a finite sequence of steps. In 825 AD, Al-Khwārizmī, a Persian astronomer and mathematician wrote, *On Calculation with Hindu Numerals*. His work was translated into Latin as *Algoritmi de Numero Indorum* in the 12th century. The words, *algebra* and *algorithm* are derived from Al-Khwārizmī's treatise.[10] Later, Omar Khayyam (1048–1122)[11] the renowned poet, mathematician, and astronomer wrote *Demonstrations of Problems of Algebra* (1070), which laid down the principles of algebra. He also developed algorithms for the root extraction of arbitrarily high-degree polynomials.[10] Since 825 AD, the word algorithm has been used by mathematicians to formulate and solve complex problems. Here we formulate an algorithm for the determination of the Y_{Bus} matrix and solve a power flow problem.

The elements of Y_{Bus} matrix can be calculated from the following algorithm.

Step 1. If $i = j$, $Y_{ii} = \sum y$, i.e., the $\sum$ of admittances connected to bus i.

Step 2. If $i \neq j$, and bus i is not connected to bus j then the element $Y_{ij} = 0$.

Step 3. If $i \neq j$, and bus i is connected to bus j through the admittance y_{ij}, then the element is $Y_{ij} = -y_{ij}$

(7.18)

The above algorithm can be easily programmed for the solution of a power flow problem encompassing an eastern U.S. power grid.

In a more compact form, we can express the bus current injection vector into a power grid in terms of a bus admittance matrix and a bus voltage vector:

$$[I_{Bus}] = [Y_{Bus}][V_{Bus}]$$

I_{Bus}: Bus injected current vector
Y_{Bus}: Bus admittance matrix
V_{Bus}: Bus voltage profile vector

The Y_{Bus} matrix model of the power grid is a symmetric, complex, and sparse matrix. The row sum (or column sum) corresponding to each bus, is equal to the admittance to the reference bus. If there is no connection to a reference bus every row sum is zero. For this case, the Y_{Bus} matrix is singular and det $[Y_{Bus}] = 0$, and such a Y_{Bus} matrix cannot be inverted.

At this time, we should recall that if we formulate the Y_{Bus} matrix model for short-circuit studies, we will include the internal impedance of generators and motors. However, for power flow studies, we represent the power grid with injection models. We should also note that in general, a power grid is normally grounded through the capacitance of transmission lines.

7.8 THE BUS IMPEDANCE MATRIX MODEL

From Fig. 7.11, it can be seen that the bus current injections are related to bus voltages by the bus admittance matrix as given below:

$$\begin{aligned} [I_{Bus}] &= [Y_{Bus}][V_{Bus}] \\ [V_{Bus}] &= [Z_{Bus}][I_{Bus}] \end{aligned} \tag{7.19}$$

$$[Z_{Bus}] = [Y_{Bus}]^{-1} \tag{7.20}$$

Therefore, the Z_{Bus} matrix is the inverse of the Y_{Bus} matrix. Now the bus voltage vector is expressed in terms of Z_{Bus}, which is the bus impedance matrix and I_{Bus} is the bus injected current vector.

For the system of Fig. 7.11, the impedance matrix of Equation 7.20 can be expressed as

$$\begin{bmatrix} V_1 \\ V_2 \\ V_3 \\ V_4 \end{bmatrix} = \begin{bmatrix} Z_{11} & Z_{12} & Z_{13} & Z_{14} \\ Z_{21} & Z_{22} & Z_{23} & Z_{24} \\ Z_{31} & Z_{32} & Z_{33} & Z_{34} \\ Z_{41} & Z_{42} & Z_{43} & Z_{44} \end{bmatrix} \begin{bmatrix} I_1 \\ I_2 \\ I_3 \\ I_4 \end{bmatrix} \tag{7.21}$$

Example 7.3 For the power grid given below, compute the bus admittance and bus impedance models.

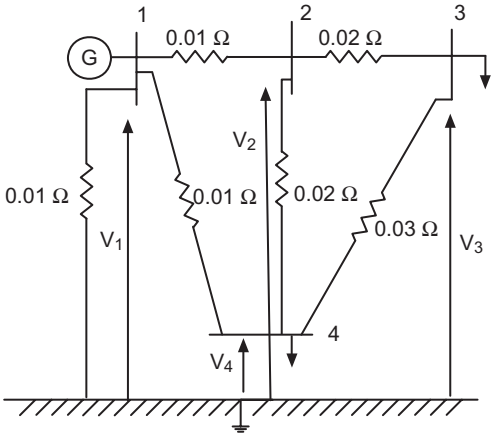

Figure 7.12 The Power Grid for Example 7.3.

Solution
The admittance matrix is calculated according to Equation 7.16.

$$Y_{11} = y_1 + y_{12} + y_{14} = \frac{1}{.01} + \frac{1}{.01} + \frac{1}{.01} = 300,\ Y_{12} = -y_{12} = -\frac{1}{.01} = -100,$$

$$Y_{14} = -y_{14} = -\frac{1}{.01} = -100,\ Y_{21} = -y_{21} = -\frac{1}{.01} = -100,$$

$$Y_{22} = y_{12} + y_{23} + y_{24} = \frac{1}{.01} + \frac{1}{.02} + \frac{1}{.02} = 200,\ Y_{23} = -y_{23} = -\frac{1}{.02} = -50,$$

$$Y_{24} = -y_{24} = -\frac{1}{.02} = -50,\ Y_{32} = -y_{23} = -\frac{1}{.02} = -50,$$

$$Y_{33} = y_{32} + y_{34} = \frac{1}{.02} + \frac{1}{.03} = 83.33,\ Y_{34} = -y_{34} = -\frac{1}{.03} = -33.33,$$

$$Y_{41} = -y_{14} = -\frac{1}{.01} = -100,\ Y_{42} = -y_{24} = -\frac{1}{.02} = -50,\ Y_{43} = -y_{34} = -\frac{1}{.03} = -33.33,$$

$$Y_{44} = y_{41} + y_{42} + y_{43} = \frac{1}{.01} + \frac{1}{.02} + \frac{1}{.03} = 183.33.$$

The admittance matrix elements are zero if there are no direct connections between the buses.

$$Y_{Bus} = \begin{bmatrix} Y_{11} & Y_{12} & Y_{13} & Y_{14} \\ Y_{21} & Y_{22} & Y_{23} & Y_{24} \\ Y_{31} & Y_{32} & Y_{33} & Y_{34} \\ Y_{41} & Y_{42} & Y_{43} & Y_{44} \end{bmatrix} = \begin{bmatrix} 300 & -100 & 0 & -100 \\ -100 & 200 & -50 & -50 \\ 0 & -50 & 83.33 & -33.33 \\ -100 & -50 & -33.33 & 183.33 \end{bmatrix}$$

$$Z_{Bus} = Y_{Bus}^{-1} = \begin{bmatrix} 0.010 & 0.010 & 0.010 & 0.010 \\ 0.010 & 0.017 & 0.015 & 0.013 \\ 0.010 & 0.015 & 0.027 & 0.015 \\ 0.010 & 0.013 & 0.015 & 0.017 \end{bmatrix}$$

Z_{Bus} is the bus impedance model for the power grid of Example 7.3.

7.9 FORMULATION OF THE LOAD FLOW PROBLEM

Consider the power grid presented by Fig. 7.11. The power flow problem can mathematically be stated as given by a bus admittance matrix.

$$[I_{Bus}] = [Y_{Bus}][V_{Bus}] \tag{7.22}$$

The vector of the current injection represents the net injection where the injected current is algebraically a positive injection for power generation and a negative injection for loads. Therefore, if the generation at a bus is larger than the load connected to the bus, then there is a positive net injection into the power grid. Otherwise, it will be negative if there are more loads connected to the bus than generating power. Therefore, for each bus k we have

$$S_k = V_k I_k^* \qquad k = 1,2,\ldots..n \tag{7.23}$$

and I_k is the current injection into the power grid at bus k. Therefore, from row k of Y_{Bus} matrix, we have

$$I_k = \sum_{j=1}^{n} Y_{kj} V_j \tag{7.24}$$

Substituting Equation 7.24 in 7.23, we have

$$S_k = V_k \left(\sum_{j=1}^{n} Y_{kj} V_k \right)^* \qquad k = 1,2,\ldots..n \tag{7.25}$$

For each bus k we have a complex equation of the form given by Equation 7.25. Therefore, we have n nonlinear complex equations

$$Y_{kj} = G_{kj} + jB_{kj},\ \theta_{kj} = \theta_k - \theta_j$$
$$V_j = V_j(\cos\theta_j + j\sin\theta_j)$$
$$V_k = V_k(\cos\theta_k + j\sin\theta_k)$$

$$I_k^* = \left(\frac{S_k}{V_k}\right)^* = \frac{(P_k + jQ_k)^*}{V_k^*} = \frac{P_k - jQ_k}{V_k \cdot \angle -\theta_k}$$

where n is the total number of buses in the power grid network.

From the Y_{Bus} model, we have the relationship of injected current into the power grid as it relates to the network admittance model, as well as how the power will flow in the transmission system based on the bus voltages. Therefore, for each bus k based on the bus admittance model, we have the following expressions.

$$\frac{P_1 - jQ_1}{V_1^*} = Y_{11}V_1 + Y_{12}V_2 + Y_{13}V_3 + Y_{14}V_4 \tag{7.26}$$

$$\frac{P_2 - jQ_2}{V_2^*} = Y_{21}V_1 + Y_{22}V_2 + Y_{23}V_3 + Y_{24}V_4 \tag{7.27}$$

$$\frac{P_3 - jQ_3}{V_3^*} = Y_{31}V_1 + Y_{32}V_2 + Y_{33}V_3 + Y_{34}V_4 \tag{7.28}$$

$$\frac{P_4 - jQ_4}{V_4^*} = Y_{41}V_1 + Y_{42}V_2 + Y_{43}V_3 + Y_{44}V_4 \tag{7.29}$$

We can rewrite the Equations 7.26 through 7.29 and express them as

$$\begin{aligned}
P_1 - jQ_1 &= Y_{11}V_1^2 + Y_{12}V_1^*V_2 + Y_{13}V_1^*V_3 + Y_{14}V_1^*V_4 \\
P_2 - jQ_2 &= Y_{21}V_1V_2^* + Y_{22}V_2^2 + Y_{23}V_2^*V_3 + Y_{24}V_2^*V_4 \\
P_3 - jQ_3 &= Y_{31}V_1V_3^* + Y_{32}V_2V_3^* + Y_{33}V_3^2 + Y_{34}V_3^*V_4 \\
P_4 - jQ_4 &= Y_{41}V_1V_4^* + Y_{42}V_2V_4^* + Y_{43}V_3V_4^* + Y_{44}V_{44}^2
\end{aligned} \tag{7.30}$$

The above systems of equations are complex and nonlinear. As we stated, one bus of the system is selected as a swing bus and its voltage magnitude is set to 1 p.u; its phase angle is set to zero as the reference phasor. The swing bus will ensure the balance of power between the system loads and the system generations. In a power flow problem, the load bus voltages are the unknown variables and all the injected powers are known variables. Here, there are three nonlinear complex equations to be solved for bus load voltages.

In general, as we discussed before, for each bus k a complex equation can be written as two equations in terms of real numbers. Using the above expressions in general formulation, we have

$$P_k = V_k \sum_{j=1}^{n} V_j (G_{kj}\cos\theta_{kj} + B_{kj}\sin\theta_{kj})$$

$$Q_k = V_k \sum_{j=1}^{n} V_j (G_{kj}\sin\theta_{kj} - B_{kj}\cos\theta_{kj})$$

where,

$$Y_{kj} = G_{kj} + jB_{kj}, \theta_{kj} = \theta_k - \theta_j$$
$$V_k = V_k(\cos\theta_k + j\sin\theta_k)$$
$$V_j = V_j(\cos\theta_j + j\sin\theta_j)$$
$$I_k = \left(\frac{S_k}{V_k}\right)^* = \frac{P_k - jQ_k}{V_k^*} = \frac{P_k - jQ_k}{V_k \cdot \angle -\theta_k}$$

If the system has n bus, the above equations can be expressed as $2n$ equations:

$$\begin{aligned} f_1(V_1 \ldots\ldots\ldots V_n, \theta_1 \ldots\ldots\ldots\ldots\ldots \theta_n) &= 0 \\ f_2(V_1 \ldots\ldots\ldots V_n, \theta_1 \ldots\ldots\ldots\ldots\ldots \theta_n) &= 0 \\ f_n(V_1 \ldots\ldots\ldots V_n, \theta_1 \ldots\ldots\ldots\ldots\ldots \theta_n) &= 0 \\ f_{2n}(V_1 \ldots\ldots\ldots V_n, \theta_1 \ldots\ldots\ldots\ldots\ldots \theta_n) &= 0 \end{aligned} \tag{7.31}$$

The above $2n$ equations can be expressed as

$$F(x) = \begin{bmatrix} f_1(x) \\ f_2(x) \\ . \\ . \\ . \\ . \\ f_{2n}(x) \end{bmatrix} \tag{7.32}$$

where the elements of vector X represent the magnitude of voltage and phase angle. In Equation 7.32, we have $2n$ nonlinear equations to be solved and vector X can be presented as

$$\begin{aligned} [X]^t &= [V_1, \ldots\ldots\ldots V_n, \ \theta_1 \ldots\ldots\ldots\ldots\ldots \theta_n] \\ &= [x_1, \ldots\ldots\ldots x_n, x_{n+1} \ldots\ldots\ldots\ldots\ldots x_{2n}] \end{aligned}$$

7.10 THE GAUSS–SEIDEL Y_{BUS} ALGORITHM

The Gauss–Seidel algorithm is an iterative process. In this method, the objective is to satisfy the set of nonlinear equations by repeated approximation. The solution is reached when all nonlinear equations are satisfied at an acceptable accuracy level. In the case of power flow problems, the solution is reached

when all bus voltages are converging to around 1 p.u within 5% of the rated voltage and all nonlinear equations are satisfied at an acceptable tolerance.

Let us now restate the main equations of power flow problems:

$$V_1 = 1\angle 0 \tag{7.33}$$

$$I_{Bus} = Y_{Bus} \cdot V_{Bus} \tag{7.34}$$

$$S_k = V_k I_k^* \tag{7.35}$$

where $k = 1, 2, 3, \ldots\ldots n$

Equation 7.33 is the model for the swing bus (also called a *slack bus*) that creates balance between the system loads and system generation by providing the system transmission losses. When a microgrid is connected to a local power grid, the power grid bus is selected as the swing bus; this ensures that the balance between loads and local generation and losses are maintained. If the microgrid has deficiencies in generation, the balance is maintained by the power grid bus. If the microgrid has excess generation, the balance is injected into the local power grid. Equation 7.34 describes the current flow or power flow through transmission lines for a set of bus voltages. Equation 7.35 presents the net injected power at each bus of the system.

The Gauss–Seidel Y_{Bus} algorithm is as depicted in Fig. 7.13.

In the Gauss–Seidel method, we repeatedly solve the fundamental load flow equation expressed by Equation 7.31.

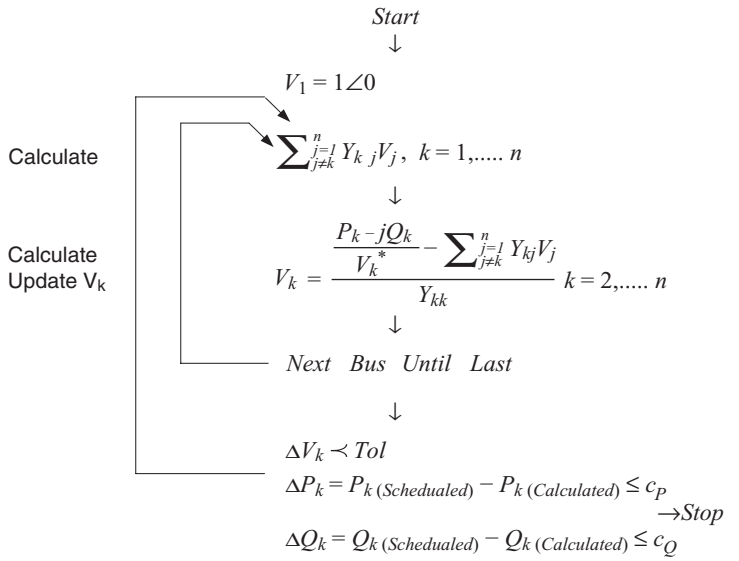

Figure 7.13 The Gauss–Seidel Algorithm for Iterative Approximation.

$$V_k = \frac{\dfrac{P_k - jQ_k}{V_k^*} - \sum_{\substack{j=1 \\ j \neq k}}^{n} Y_{kj} V_j}{Y_{kk}} \qquad k = 2, \ldots . n \tag{7.36}$$

Equation 7.36 represents the load bus voltages with the power grid depicted by the bus admittance matrix. The diagonal element for a bus for which a voltage approximation is being computed appears in the denominator. Because the diagonal elements of the bus admittance matrix are never zero, an approximation of bus voltages is assured. If the power grid is correctly designed, the convergence can be obtained.

In Equation 7.37, we check to see if the original nonlinear load flow equations are satisfied with the last approximated bus voltages.

$$\begin{aligned} \Delta P_k &= P_{k(Schedualed)} - P_{k(Calculated)} \leq c_P \\ \Delta Q_k &= Q_{k(Schedualed)} - Q_{k(Calculated)} \leq c_Q \end{aligned} \tag{7.37}$$

Example 7.4 For the system depicted in Fig. 7.14, use the Gauss–Seidel Y_{Bus} method and solve for the bus voltages.

For the example depicted in Fig. 7.14, bus 1 is the swing bus and its voltage is $V_1 = 1 \angle 0$. The scheduled power at bus 2 is 1.2 p.u. The load at bus 3 is 1.5 p.u. Compute the bus 2 and bus 3 voltages.

Solution

To solve the above problem, we need to formulate the bus admittance matrix.

$$Y_{Bus} = \begin{bmatrix} 14 & -4 & -10 \\ -4 & 9 & -5 \\ -10 & -5 & 15 \end{bmatrix}$$

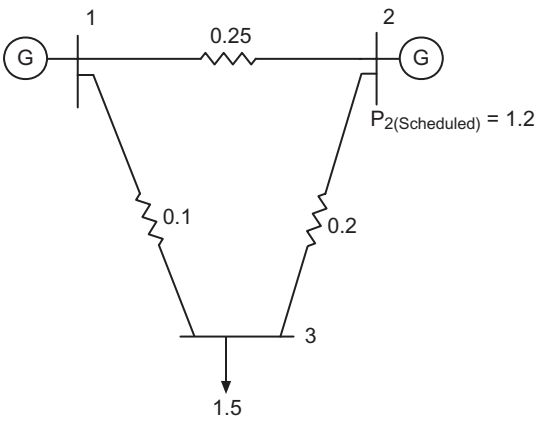

Figure 7.14 The One-Line Diagram of Example 7.4.

The power flow models are

$$V_1 = 1\angle 0$$
$$I_{Bus} = V_{Bus} \cdot Y_{Bus}$$

For a DC system, we only have active power flow.

$$I_k^* = I_k, V_k^* = V_k$$
$$S_k = V_k \cdot I_k^* = V_k I_k = P_k, \text{and } Q_k = 0$$

Therefore, for bus 2 we have

$$1.2 = V_2 I_2$$

For bus 3, we have

$$-1.5 = V_3 I_3$$

We can start the iterative approximation for $i = 0$ iteration by assuming bus 2 and bus 3 voltages are equal to 1 p.u

$$V_{Bus}^{(0)} = \begin{bmatrix} 1 \\ 1 \end{bmatrix}$$

For bus 2 we have

$$\sum_{\substack{j=1 \\ j\neq 2}}^{3} Y_{2j} V_j = Y_{21} V_1 + Y_{23} V_3 = (-4)(1) + (-5)(1)$$

Next, we update V_2

$$V_2 = \frac{\dfrac{P_2 - jQ_2}{V_2} - \sum_{\substack{j=1 \\ j\neq 2}}^{n} Y_{2j} V_j}{Y_{22}} \qquad i = 1, \ldots\ldots\ldots, j \neq i$$

$$V_2 = \frac{1}{Y_{22}} \left[\frac{1.2}{V_2} - \{(-4)(1.0) + (-5)(1)\} \right]$$

The updated bus 2 voltage is given as

$$V_2^{(1)} = \frac{1}{9} \left[\frac{1.2}{1} + 4 + 5 \right] = 1.1333 \; p.u$$

We continue the iterative process and update bus 3 voltage.

$$\sum_{\substack{j=1\\ j\neq 3}}^{3} Y_{3j}V_j = Y_{31}V_1 + Y_{32}V_2$$

We update the bus 3 voltage, V_3

$$V_3 = \frac{1}{Y_{33}}\left[\frac{-1.5}{V_3} - [Y_{31}V_1 + Y_{32}V_2]\right]$$

$$V_3 = \frac{1}{15}\left[\frac{-1.5}{1.0} - \{(-10)(1) + (-5)(1.1333)\}\right]$$

$$V_3^{(1)} = \frac{1}{15}[-1.5 + 10 + 5.666] = \frac{14.1666}{15} = 0.9444\ p.u$$

We continue the approximation by calculating the mismatch at bus 2 and bus 3. The mismatch at bus 2 is

$$P_{2(Calculated)} = \sum_{\substack{j=0\\ j\neq 2}}^{3} V_2 I_{2j}$$

$$P_{2(Calculated)} = V_2 I_{20} + V_2 I_{21} + V_2 I_{23}$$

$$P_{2(Calculated)} = 0 + 1.1333\left(\frac{V_2 - V_1}{0.25}\right) + 1.333\left(\frac{V_2 - V_3}{0.2}\right)$$

$$P_{2(calculated)} = 0 + 1.1333\left(\frac{1.1333 - 1.0}{0.25}\right) + 1.1333\left(\frac{1.1333 - 0.944}{0.2}\right) = 1.6769$$

$$\Delta P_2 = P_{2(Scheduled)} - P_{2(Calculated)} = 1.2 - 1.6769$$

$$\Delta P_2 = -0.4769\ p.u$$

The mismatch at bus 3 is

$$P_{3(Calculated)} = \sum_{\substack{j=0\\ j\neq 3}}^{3} V_3 I_{3j}$$

$$P_{3(Calculated)} = V_3 I_{30} + V_3 I_{31} + V_3 I_{32}$$

$$P_{3(Calculated)} = 0 + 0.944\left(\frac{V_3 - V_1}{0.1}\right) + 0.944\left(\frac{V_3 - V_2}{0.2}\right)$$

$$P_{3(Calculated)} = 0.944\left(\frac{0.944 - 1.0}{0.1}\right) + 0.944\left(\frac{0.944 - 1.1333}{0.2}\right) = -1.4221$$

$$\Delta P_3 = P_{3(Scheduled)} - P_{3(Calculated)} = -1.5 - (-1.4221)$$

$$\Delta P_3 = -0.0779\ p.u$$

TABLE 7.1 Example 7.4 Results.

Bus	p.u Voltage	p.u Power Mismatch
2	1.078	0.63×10^{-4}
3	0.917	0.28×10^{-4}

The process is continued until error reduces to a satisfactory value. The result is obtained after seven iterations with c_p of 1×10^{-4}. The results are given in Table 7.1.

The power supplied by bus 1, the swing bus is equal to the total load minus total generation by all other buses plus the losses.

$$P_1 = V_1 I_1 = V_1 \sum_{j=1}^{3} Y_{1j} V_j = V_1 (Y_{11} V_1 + Y_{12} V_2 + Y_{13} V_3)$$

The bus voltage of swing bus is $1\angle 0$ and the p.u power injected by bus is $P_1 = 0.522$ p.u.

The total power loss of the transmission lines is 0.223 p.u.

7.11 THE GAUSS–SEIDEL Z_{BUS} ALGORITHM

In the Gauss–Seidel Z_{Bus} algorithm method,[6] the power problem can be expressed as

$V_1 = 1\ \angle 0$ defines the swing bus voltage.

$$V_{Bus} = Z_{Bus} I_{Bus}$$

The Z_{Bus} defines the power flow through the transmission system.

$$S_k = V_k \cdot I_k^*$$

The Z_{Bus} defines the injection model.

The Gauss–Seidel Z_{Bus} algorithm is given in Fig. 7.15.

Example 7.5 Consider the system shown in Fig. 7.16. Find the bus voltages using the Gauss–Seidel Z_{Bus} algorithm.

Bus 1 is the swing bus and its voltage is set to $V_1 = 1\ \angle 0$.

Without the fictitious line to ground, the Z_{Bus} is not defined. The swing bus is grounded and power drawn by this bus will be accounted for when the problem is solved. The tie to ground is selected in the same order as the line impedances. The injected power is $S_2 = -½$, $S_3 = -1$, and $S_4 = -½$. All data is expressed in per unit.

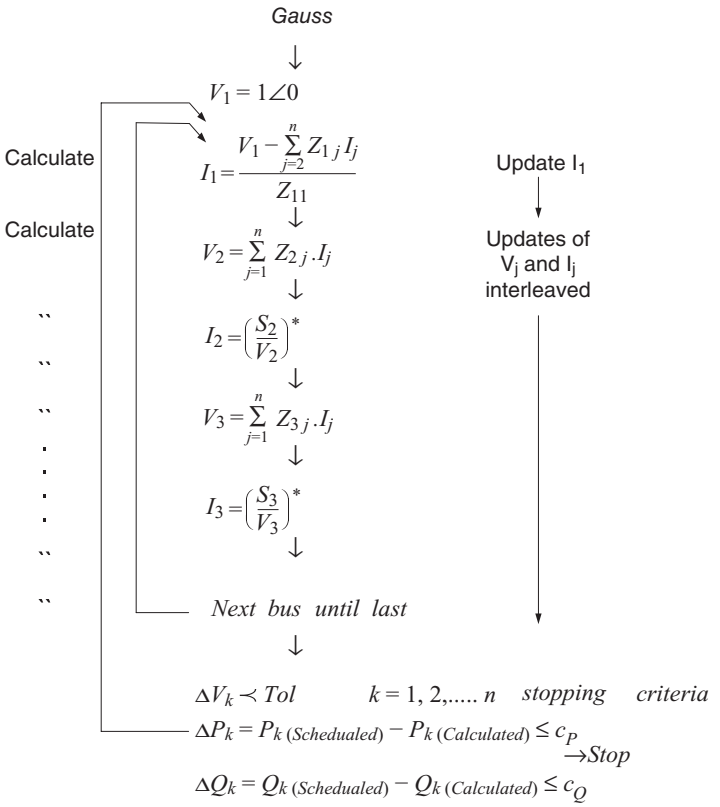

Figure 7.15 The Gauss–Seidel Z_{Bus} Algorithm.

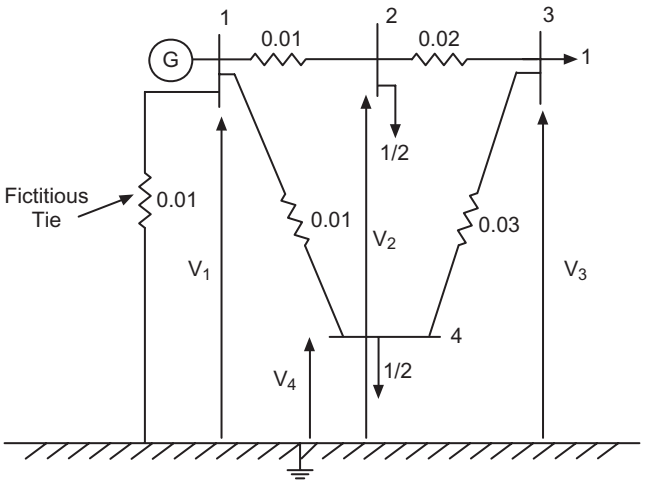

Figure 7.16 The One-Line Diagram of Example 7.5.

Solution

The Z_{Bus} with respect to the ground bus is

$$Z_{Bus} = \begin{bmatrix} 0.01 & 0.01 & 0.01 & 0.01 \\ 0.01 & 0.0186 & 0.0157 & 0.0114 \\ 0.01 & 0.0157 & 0.0271 & 0.0143 \\ 0.01 & 0.0114 & 0.0143 & 0.0186 \end{bmatrix}$$

The power flow problem can be expressed as

$$V_1 = 1\angle 0$$
$$V_{Bus} = Z_{Bus} I_{Bus}$$

For a DC system, we will only have active power flow.

$$S_k = V_k \cdot I_k^* = V_k I_k = P_k, \quad Q_k = 0$$

The busload and generation can be expressed as

$$-0.5 = V_2 I_2$$
$$-1.0 = V_3 I_3$$
$$-0.5 = V_4 I_4$$

The first step is to compute the gauss zero iteration (0) values for bus voltages and current as given below.

$$V_{Bus}^{(0)} = \begin{bmatrix} 1 \\ 0 \\ 0 \\ 0 \end{bmatrix}, I_{Bus}^{(0)} = \begin{bmatrix} 0 \\ 0 \\ 0 \\ 0 \end{bmatrix}$$

For the first row of $V_{Bus} = Z_{Bus}\, I_{Bus}$, we have the following:

Update I_1

$$I_1 = \frac{V_1 - \sum_{j=2}^{n} Z_{1j} I_j}{Z_{11}} = \frac{1-0}{0.01} = 100 \qquad n = 4$$

Update V_2

$$V_2 = \sum_{j=1}^{n} Z_{2j} I_j = (0.01)(100) + (0.0186)(0) + (0.0157)(0) + (0.0114)(0) = 1$$

Update I_2

$$I_2 = \left(\frac{S_2}{V_2}\right) = \left(\frac{-0.5}{1}\right) = -0.5$$

Update V_3

$$V_3 = \sum_{j=1}^{n} Z_{3j} I_j = (0.01)(100) + (0.0157)(-0.5) + (0.0271)(0) + (0.0143)(0)$$
$$= 1 - 0.0078 = 0.9922$$

Update I_3

$$I_3 = \left(\frac{S_3}{V_3}\right) = \left(\frac{-1}{0.9922}\right) = -1.0079$$

Update V_4

$$V_4 = \sum_{j=1}^{n} Z_{4j} I_j = (0.01)(100) + (0.0114)(-0.5) + (0.0143)(-1.0079) + (0.0186)(0)$$
$$= 1 - 0.0057 - 0.0144 = 0.9799$$

Update I_4

$$I_4 = \left(\frac{S_4}{V_4}\right) = \left(\frac{-0.5}{0.9799}\right) = -0.5102$$

From the above calculation, we have

$$V_{Bus}^{(1)} = \begin{bmatrix} 1 \\ 1 \\ 0.9922 \\ 0.9799 \end{bmatrix}, \quad I_{Bus}^{(1)} = \begin{bmatrix} 100 \\ -0.5 \\ -1.0079 \\ -0.5102 \end{bmatrix}$$

Update I_1

$$I_1 = \frac{1 - (0.01)(-0.5) - (0.01)(-1.0079) - (0.01)(-0.5102)}{0.01} = \frac{1.02019}{0.01} = 102.019$$

Update V_2

$$V_2 = (0.01)(102.019) + (0.0186)(-0.5) + (0.0157)(-1.0079) + (0.0114)(-0.5102)$$
$$= 0.9892$$

Update I_2

$$I_2 = \left(\frac{S_2}{V_2}\right) = \left(\frac{-0.5}{0.9892}\right) = -0.5055$$

Update V_3

$$V_3 = (0.01)(102.019) + (0.0157)(-0.5055) + (0.0271)(-1.0079) + (0.0143)(-0.5102)$$
$$= 0.9776$$

Update I_3

$$I_3 = \left(\frac{S_3}{V_3}\right) = \left(\frac{-1}{0.9776}\right) = -1.023$$

Update V_4

$$V_4 = \sum_{j=1}^{n} Z_{4j} I_j$$
$$= (0.01)(102.019) + (0.0114)(-0.5055) + (0.0143)(-1.023) + (0.0186)(-0.5102)$$
$$= 0.9903$$

Update I_4

$$I_4 = \left(\frac{S_4}{V_4}\right) = \left(\frac{-0.5}{0.9903}\right) = -0.5049$$

The mismatch at each bus k is given as

$$P_{(Calculated)k} = V_k\, I_k$$
$$\Delta P_k = P_{(Scheduled)k} - P_{(Calculated)k}$$

For bus 2:

$$P_{2(Calculated)} = V_2 I_2$$
$$\Delta P_2 = P_{2(scheduled)} - P_{2(Calculated)}$$

For bus 3:

$$P_{3(Calculated)} = V_3 I_3$$
$$\Delta P_3 = P_{3(scheduled)} - P_{3(Calculated)}$$

TABLE 7.2 Example 7.5 Results.

Bus	p.u Voltage	p.u Power Mismatch
2	0.99	0.1306×10^{-5}
3	0.98	0.2465×10^{-5}
4	0.99	0.6635×10^{-5}

The process is continued until error reduces to a satisfactory value. The results are obtained after four iterations with c_p of 1×10^{-4}. The results are provided in Table 7.2.

If the error is more than that for satisfactory performance, the next iteration is followed.

The MATLAB simulation testbed for the above problem is given below:

```
%Power Flow: Gauss-Seidel method
clc; clear all;
tolerance= 1e-4;
N=4;     % no. of buses
Y=[ 1/.01+1/.01+1/.01   -1/.01     0      -1/.01;
    -1/.01     1/.01+1/.02    -1/.02     0;
     0         -1/.02      1/.02+1/.03   -1/.03;
    -1/.01        0     -1/.03         1/.01+1/.03];
Z=inv(Y)

P_sch=[1 -.5 -1 -.5]'

I=[0 0 0 0]';
V=[1 0 0 0]';

iteration=0;

while (iteration <= 999)
iteration=iteration+1;
  VZ=0;
  for n=2:N
    VZ=VZ+Z(1,n)*I(n);
  end
  I(1)=(V(1)-VZ)/Z(1,1);
  for m=2:N
    V(m)=Z(m,:)*I;
    I(m)=P_sch(m)/V(m);
  end

  P_calc = V.*(Y*V);
  mismatch=[P_sch(2:N)-P_calc(2:N)];
```

```
  if (norm(mismatch,'inf') < tolerance)
    break;
  end
 end
P_calc(1)=P_calc(1)-V(1)^2/.01; % Subtracting the power
                                  of the fictitious branch
iteration
for i = 1:N
 fprintf(1, 'Bus %d:\n', i);
 fprintf(1, '  Voltage = %f p.u\n',V(i));
 fprintf(1, '  Injected P = %f p.u\n', P_calc(i));
end
```

The power supplied by bus 1, the swing bus is equal to the total load minus total generation by all other buses plus the losses.

$$P_1 = V_1 I_1 = V_1 \sum_{j=1}^{3} Y_{1j} V_j = V_1 (Y_{11} V_1 + Y_{12} V_2 + Y_{13} V_3)$$

The bus voltage of the swing bus is $1\angle 0$ and the p.u power is $P_1 = 102.033$.

The power loss in the fictitious line is $= \dfrac{V_1^2}{z_{fictitious,pu}} = \dfrac{1^2}{0.01} = 100$ p.u.

Therefore, the actual power injected by bus 1 is $P_1 = 102.033 - 100 = 2.033$ p.u.

The total power loss of the transmission lines is 0.033 p.u.

7.12 COMPARISON OF THE Y_{BUS} AND Z_{BUS} POWER FLOW SOLUTION METHODS

For a power grid with n number of buses, there are n nonlinear complex equations. The complete complex Y_{Bus} matrix or Z_{Bus} matrix has about $2n^2$ elements. If all elements were to be stored, for a system with 500 buses, the core requirements would be 500,000 words. However, because both Y_{Bus} and Z_{Bus} are symmetric matrices, the upper triangle is stored. Therefore, the storage requirement for a 500-bus system is 250,000 words. The Z_{Bus} matrix model is full because the elements of Z_{Bus} matrix are generally non-zero. The computation and storage requirement is astronomical for very large problems. On the other hand, the Y_{Bus} matrix is a sparse matrix because each element Y_{kj} will be non-zero only if there is a direct connection, that is, a transmission line or a transformer is located between buses k and j. The zero elements are not stored. Therefore, for large power system problems, by exploiting this natural sparsity, the storage and computation time are reduced substantially. The Y_{Bus} should possess strict diagonal dominance. This condition may not be satisfied for some practical power grids. The power grid with long-distance extra-high voltage (EHV) lines,

series and shunt compensation, an abnormally high impedance, or very low series impedances, and cable circuits with high charging capacitances may need a large number of iterations. These systems have a Y_{Bus} with weak diagonal elements. For a power flow solution, because the swing bus voltage is known, the corresponding row and column are deleted from Y_{Bus}. For power grids with the least diagonally dominant Y_{Bus}, the swing bus can be located on that bus thus ensuring convergence. The Z_{Bus} matrix method is not usually sensitive to the choice of a swing bus. The disadvantage of the Z_{Bus} matrix method is the need to obtain, store, and iterate the non-sparse Z_{Bus}. The advantage of the Y_{Bus} matrix method is that both the storage requirements for the network and the computation per iteration are small and roughly proportional to the number of buses. However, the disadvantages of the Y_{Bus} matrix are a slow convergence property and that at times it may not converge. On the other hand, the Z_{Bus} method has a fast convergence property and always will converge.

7.13 THE SYNCHRONOUS AND ASYNCHRONOUS OPERATION OF MICROGRIDS

Figure 7.17 depicts a typical microgrid connected to a local power grid. Depending on the size of the microgrid generation sources, the local network can be designed to operate in a 480 V to 20 kV voltage class. It is clear that in

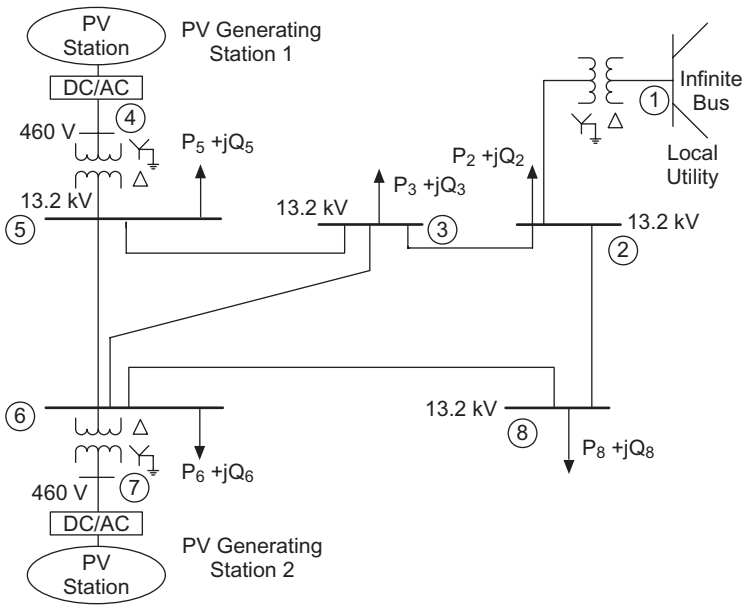

Figure 7.17 Microgrid of Distributed Generation as Part of the Local Power Grid.

this microgrid, bus 1 must be designated as a swing bus because the amount of power available at the local power grid is many times larger than the PV microgrid system of Fig. 7.17.

The operation of the microgrid of Fig. 7.17 can take two forms: (1) The microgrid can operate as part of the interconnected system, and (2) the microgrid can operate as a standalone once it is separated from the local network. When the microgrid is operating as part of the local power grid, the load and frequency control and voltage control are the responsibility of the local power-grid control center. As we discussed in Chapter 4, when a microgrid of PV or wind is connected to the local power grid, the entire system operates at a single frequency. The voltage of the power grid bus is also controlled by the local control center. However, the microgrid load buses can still have low voltages if adequate VAr support is not provided. However, the microgrid of PV or wind can be designed to operate asynchronously. Figure 7.18 depicts such a design.

The microgrid distributed generation system of Figure 7.18 is designed to operate both as a synchronous and asynchronous system. This distributed generation system has a variable-speed wind doubly-fed induction generator (DFIG) and a gas turbine synchronous generator. When this microgrid is operating as part of the local power grid, the frequency control and voltage control are the responsibility of the local power-grid control center. The local power grid operator monitors and controls the system frequency as discussed in Chapter 4. The system operator also controls the local power-grid bus voltages.

The gas turbine generator can be operated as a P-V bus: the bus voltage and active power injected into the microgrid are fixed and the reactive power and phase angle are computed in a load flow analysis. The DFIG generating station is modeled as a P-V bus that is injecting only active power at a constant voltage.

When the distributed generation section of a microgrid is separated from the local power grid, the gas turbine unit is responsible for both voltage control and load frequency control. In this case, the gas turbine unit should be modeled as a swing bus for power flow analysis. To ensure stable operation, the local load control of the distributed generation system is essential. If the load control is also provided, this independent microgrid is termed a smart microgrid because it can remain stable with control over its loads.

7.14 AN ADVANCED POWER FLOW SOLUTION METHOD: THE NEWTON–RAPHSON ALGORITHM

To formulate the Newton–Raphsonalgorithm,[8] the main equations of a power flow problem are restated as below:

$$V_1 = 1\angle 0 \tag{7.38}$$

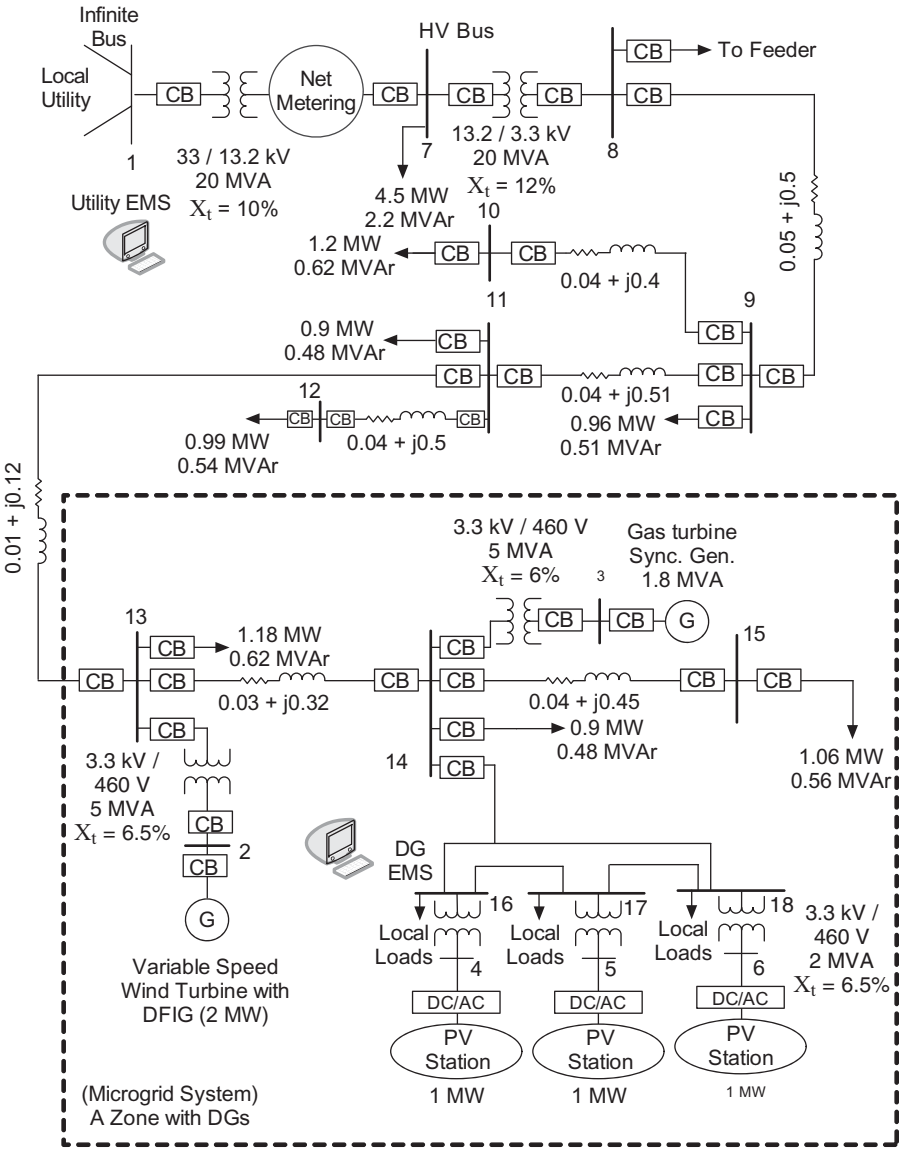

Figure 7.18 The Synchronous and Asynchronous Operation of a Microgrid.

The matrix bus admittance describes the flow of net injected current through the transmission systems as given below:

$$I_{Bus} = Y_{Bus} V_{Bus} \tag{7.39}$$

The bus injection is described as

$$S_k = V_k \cdot I_k^* \tag{7.40}$$

where S_k is the net injected complex power at bus k, V_k is the complex voltage of bus k and I_k is the net injected current at the bus k.

We can substitute for bus net injected current from Equation 7.39 in Equation 7.40 to obtain the residue form of the equation for each bus k as

$$S_k - V_k \sum_{j=1}^{n} Y_{kj}^* V_j^* = 0 \qquad k = 1, \ldots\ldots\ldots n. \tag{7.41}$$

For $k = 1$, we have

$$S_1 - V_1 \sum_{j=1}^{n} Y_{1j}^* V_j^* = 0 \qquad f_1(X) = 0 \tag{7.42}$$

$$\text{And } k = 2 \qquad S_2 - V_2 \sum_{j=1}^{n} Y_{2j}^* V_j^* = 0 \qquad f_2(X) = 0 \tag{7.43}$$

$$\text{And } k = n \qquad S_n - V_n \sum_{j=1}^{n} Y_{nj}^* V_j^* = 0 \qquad f_n(X) = 0 \tag{7.44}$$

The above can be expressed in a compact form as

$$F(x) = \begin{bmatrix} f_1(x) \\ f_2(x) \\ . \\ . \\ . \\ . \\ f_n(x) \end{bmatrix} = 0 \tag{7.45}$$

where

$$[X]^T = [x_1\ x_2\ x_3\ \ldots\ldots\ x_n]$$

In the above equation, the variable vector X represents the bus voltage vector.

Expanding row 1 of $F(x) = 0$ in a Taylor series, about a guess solution $X^{(o)}$, we have

$$f_1(X) = f_1(x_1, x_2 \ldots . x_n) = f_1(x_1^{(0)}, x_2^{(0)} \ldots . x_n^{(0)}) + \frac{\partial f_1}{\partial x_1}\Big|_{X^{(0)}} \Delta x_1 + \frac{\partial f_1}{\partial x_2}\Big|_{X^{(0)}} \Delta x_2$$

$$+ \ldots\ldots . \frac{\partial f_n}{\partial x_n}\Big|_{X^{(0)}} + \text{higher order terms.} \tag{7.46}$$

Equation 7.46 can be expressed in compact form as

$$f_1(X) = f_1(X^{(0)}) + \sum_{j=1}^{n} \frac{\partial f_1}{\partial x_j}\Big|_{X^{(0)}} \Delta x_j = 0 \tag{7.47}$$

$$f_2(X) = f_2(X^{(0)}) + \sum_{j=1}^{n} \frac{\partial f_2}{\partial x_j}\Big|_{X^{(0)}} \Delta x_j = 0 \tag{7.48}$$

$$f_n(X) = f_n(X^{(0)}) + \sum_{j=1}^{n} \frac{\partial f_n}{\partial x_j}\Big|_{X^{(0)}} \Delta x_j = 0 \tag{7.49}$$

where $\Delta x_j = x_j - x_j^{(0)}$. In compact matrix notation, we have

$$F(X) = F(X^{(0)}) + \begin{bmatrix} \frac{\partial f_1}{\partial x_1} & \frac{\partial f_1}{\partial x_2} & \ldots\ldots\ldots & \frac{\partial f_1}{\partial x_n} \\ \frac{\partial f_2}{\partial x_1} & \frac{\partial f_2}{\partial x_2} & \ldots\ldots\ldots & \frac{\partial f_2}{\partial x_n} \\ & & . & \\ \frac{\partial f_n}{\partial x_1} & \frac{\partial f_n}{\partial x_2} & \ldots\ldots\ldots & \frac{\partial f_n}{\partial x_n} \end{bmatrix}_{|X^{(0)}} \begin{bmatrix} \Delta x_1 \\ \Delta x_2 \\ . \\ . \\ \Delta x_n \end{bmatrix} = 0 \tag{7.50}$$

The matrix of Equation 7.50 is referred to as the Jacobian matrix. The above equation can be rewritten as

$$F(X^{(0)}) + [J]_{|X^{(0)}} [\Delta X] = 0 \tag{7.51}$$

$$f_k(X^0) = S_k - V_k \sum_{j=1}^{n} Y_{kj}^* V_j^* \text{ and } [X^0] = [V_1^{(0)} \ldots\ldots . V_i^{(0)} \ldots\ldots . V_n^{(0)}] \tag{7.52}$$

where S_k is the scheduled net injected (generator bus or load) complex power into bus k (positive for generation). Therefore, the term $F(X^{(0)})$ represents the power mismatch at each bus. When the term $F(X^{(0)})$ is very small the power flow solution has been obtained.

$$S_{k(Calculated)} = V_k \sum_{j=1}^{n} Y_{kj}^* V_j^* \tag{7.53}$$

Equation 7.53 represents the calculated power flowing away from bus k to all the other buses j.

Equation 7.51 can be solved for ΔX

$$[\Delta X] = -[J]^{-1}_{X^{(0)}} \cdot F(X^{(0)}) \tag{7.54}$$

$$F_k(X^0) = \Delta S_k = \Delta P_k + j\Delta Q_k = S_{k(Scheduled)} - S_{k(Calculated)} \tag{7.55}$$

$$\begin{aligned} \Delta P_k &= P_{k(Scheduled)} - P_{k(Calculated)} \\ \Delta Q_k &= Q_{k(Scheduled)} - Q_{k(Calculated)} \end{aligned} \tag{7.56}$$

7.14.1 The Newton–Raphson Algorithm

The solution steps are as follows:

1. Write load flow equations in residual form: $F(X) = 0$
2. Guess a solution vector, i.e., $X^{(0)}$ and evaluate $F(X^{(0)})$
3. Calculate J at $X^{(0)}$

$$J_{X^{(0)}} = \left[\begin{array}{cccc} \frac{\partial f_1}{\partial x_1} & \frac{\partial f_1}{\partial x_2} & \cdots\cdots & \frac{\partial f_1}{\partial x_n} \\ \frac{\partial f_2}{\partial x_1} & \frac{\partial f_2}{\partial x_2} & \cdots\cdots & \frac{\partial f_2}{\partial x_n} \\ & & \cdot & \\ \frac{\partial f_n}{\partial x_1} & \frac{\partial f_n}{\partial x_2} & \cdots\cdots & \frac{\partial f_n}{\partial x_n} \end{array} \right]_{X^{(0)}(or\_in\_general\_X^{(i)})} = J(X^{(0)})$$

The ΔX is computed from the equation below.

Initial computation: Use an initial guess for X.

Step 1. $[\Delta X] = -[J]^{-1}_{X^{(i)}} F(X^{(i)})$.

Step 2. Update $X^{(i+1)} = X^{(i)} + \Delta X$.

Step 3. Calculate $F(X)$ at $X^{(i+1)}$.

Step 4. Check if $F(X^{(i+1)}) < 10^{-6}$, then the solution has converged. Store the solution vector $X^{(i+1)}$.

Step 5. Update i to $i + 1$.

If not, go to Step 1.

Example 7.6 Consider the three-bus power system given in Fig. 7.19. The system data are as follows:

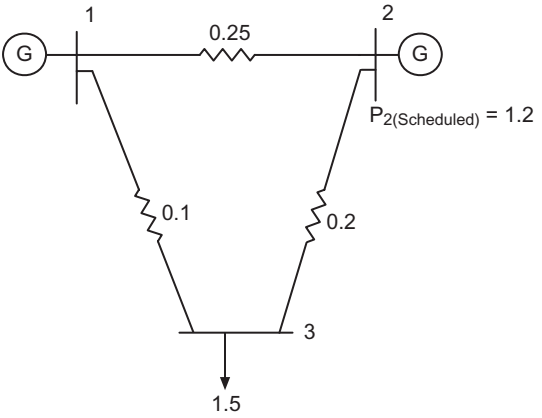

Figure 7.19 The One-Line Diagram of Example 7.6.

a. Bus 1 is a swing bus with $V_1 = 1 \angle 0$.
b. Scheduled injected power at bus 2 is 1.2 p.u.
c. Scheduled load (negative injection) at bus 3 is 1.5 p.u.

The bus admittance matrix of the system in Example 7.6 is

$$Y_{Bus} = \begin{bmatrix} 14 & -4 & -10 \\ -4 & 9 & -5 \\ -10 & -5 & 15 \end{bmatrix}$$

The bus powers can be expressed as nonlinear functions of bus voltages in residue form as

$$P_1(V_1, V_2, V_3) - V_1(Y_{11}V_1 + Y_{12}V_2 + Y_{13}V_3) = 0$$
$$P_2(V_1, V_2, V_3) - V_2(Y_{21}V_1 + Y_{22}V_2 + Y_{23}V_3) = 0$$
$$P_3(V_1, V_2, V_3) - V_3(Y_{31}V_1 + Y_{32}V_2 + Y_{33}V_3) = 0$$

Using a Taylor series expansion about a guess solution, i.e., $V_2^{(0)}$, $V_3^{(0)}$, and $V_1^{(0)} = 1\angle 0$

$$\begin{bmatrix} \Delta P_1 \\ \Delta P_2 \\ \Delta P_3 \end{bmatrix} = -\begin{bmatrix} \frac{\partial P_1}{\partial V_1} & \frac{\partial P_1}{\partial V_2} & \frac{\partial P_1}{\partial V_3} \\ \frac{\partial P_2}{\partial V_1} & \frac{\partial P_2}{\partial V_2} & \frac{\partial P_2}{\partial V_3} \\ \frac{\partial P_3}{\partial V_1} & \frac{\partial P_3}{\partial V_2} & \frac{\partial P_3}{\partial V_3} \end{bmatrix}_{V^{(0)}} \begin{bmatrix} \Delta V_1 \\ \Delta V_2 \\ \Delta V_3 \end{bmatrix}$$

In compact notation, we have

$$[\Delta V] = -[J]^{-1} \times [\Delta P]$$

where

$$P_{2(Calculated)} = V_2^{(0)}(Y_{21}V_1^{(0)} + Y_{22}V_2^{(0)} + Y_{23}V_3^{(0)})$$
$$\Delta P_2 = P_{2(Scheduled)} - P_{2(Calculated)} = 0$$
$$P_{3(Calculated)} = V_3^{(0)}(Y_{31}V_1^{(0)} + Y_{32}V_2^{(0)} + Y_{33}V_3^{(0)})$$
$$\Delta P_3 = P_{3(Scheduled)} - P_{3(Calculated)} = 0$$

since $V_1 = 1 \angle 0$ (slack bus). Therefore $\Delta V_1 = 0.0$. Hence, only bus 2 and bus 3 voltages are to be calculated. The Jacobian matrix is a 2×2 matrix as shown below.

$$\begin{bmatrix} \Delta P_2 \\ \Delta P_3 \end{bmatrix} = \begin{bmatrix} \dfrac{\partial P_2}{\partial V_2} & \dfrac{\partial P_2}{\partial V_3} \\ \dfrac{\partial P_3}{\partial V_2} & \dfrac{\partial P_3}{\partial V_3} \end{bmatrix}_{|V^{(0)}} \begin{bmatrix} \Delta V_2 \\ \Delta V_3 \end{bmatrix}$$

From the above equation, we can calculate ΔV_2 and ΔV_3.

$$\begin{bmatrix} \Delta V_2 \\ \Delta V_3 \end{bmatrix} = -[J]^{-1}_{|V^{(0)}} \begin{bmatrix} \Delta P_2 \\ \Delta P_3 \end{bmatrix}$$

The above solution can be restated as

$$\Delta V_2 = V_{2(\text{new})} - V_{2(\text{old})}$$
$$\Delta V_3 = V_{3(\text{new})} - V_{3(\text{old})}$$
$$\begin{bmatrix} V_2 \\ V_3 \end{bmatrix}_{|new} = \begin{bmatrix} V_2 \\ V_3 \end{bmatrix}_{|old} + [J]^{-1}_{|V^{(0)}} \begin{bmatrix} \Delta P_2 \\ \Delta P_3 \end{bmatrix}$$

The elements of the Jacobian matrix are

$$\frac{\partial P_2}{\partial V_2} = Y_{21}V_1 + 2Y_{22}V_2 + Y_{23}V_3$$

$$\frac{\partial P_2}{\partial V_3} = Y_{23}V_2$$

$$\frac{\partial P_3}{\partial V_2} = Y_{32}V_3$$

$$\frac{\partial P_3}{\partial V_3} = Y_{31}V_1 + Y_{32}V_2 + 2Y_{33}V_3$$

Assuming that $V_2^{(0)} = 1$, $V_3^{(0)} = 1$, the elements of the Jacobian matrix are

$$\frac{\partial P_2}{\partial V_2} = -4 + 2\times 9 - 5 = 9$$

$$\frac{\partial P_2}{\partial V_3} = -5$$

$$\frac{\partial P_3}{\partial V_2} = -5$$

$$\frac{\partial P_3}{\partial V_3} = -10 - 5 + 2\times 15 = 15$$

Therefore, the Jacobian matrix is given below as

$$[J] = \begin{bmatrix} 9 & -5 \\ -5 & 15 \end{bmatrix}$$

And, the $[J]^{-1}$ is

$$[J]^{-1} = \frac{1}{110}\begin{bmatrix} 15 & 5 \\ 5 & 9 \end{bmatrix}$$

The mismatch power at each bus k is

$$P_{2(Calculated)} = V_2^{(0)}(Y_{21}V_1^{(0)} + Y_{22}V_2^{(0)} + Y_{23}V_3^{(0)})$$

$$P_{2(Calculated)} = 1.0(-4.(1) + 9.(1) - 5.(1)) = 0$$

$$\Delta P_2 = P_{2(Scheduled)} - P_{2(Calculated)}$$

$$\Delta P_2 = 1.2 - 0 = 1.2$$

$$P_{3(Calculated)} = V_3^{(0)}(Y_{31}V_1^{(0)} + Y_{32}V_2^{(0)} + Y_{33}V_3^{(0)})$$

$$P_{3(Calculated)} = 1.0(-10.(1) - 5.(1) + 15.(1)) = 0$$

$$\Delta P_3 = P_{3(Scheduled)} - P_{3(Calculated)}$$

$$\Delta P_3 = -1.5 - 0 = -1.5$$

$$\begin{bmatrix} V_2 \\ V_3 \end{bmatrix} = \begin{bmatrix} 1.0 \\ 1.0 \end{bmatrix} + \frac{1}{110}\begin{bmatrix} 15 & 5 \\ 5 & 9 \end{bmatrix}\begin{bmatrix} 1.2 \\ -1.5 \end{bmatrix}$$

$$\begin{bmatrix} V_2 \\ V_3 \end{bmatrix} = \begin{bmatrix} 1.095 \\ 0.932 \end{bmatrix}$$

This new value is now used in the next iteration. The iteration is continued until error does not go below the satisfactory level. The MATLAB simulation testbed for solving the above problem is given below.

```
%Power Flow: Newton Raphson
clc; clear all;
mis_match=0.0001;
Y_bus=[ 1/.25+1/.1    -1/.25         -1/.1;
        -1/.25     1/.25+1/.2      -1/.2;
        -1/.1        -1/.2       1/.1+1/.2];

P_sch = [1; 1.2; -1.5];

N = 3; % no. of buses

% allocate storage for Jacobian
J = zeros(N-1,N-1);

% initial mispatch
V = [1 1 1]';

P_calc = V.*(Y_bus*V);
mismatch = [P_sch(2:N)-P_calc(2:N)];

iteration=0;
% Newton-Raphson iteration
while (iteration<10)
 iteration=iteration+1;
 % calculate Jacobian
 for i = 2:N
  for j = 2:N
   if (i == j)
    J(i-1,j-1)=Y_bus(i,:)*V+Y_bus(i,i)*V(i);
   else
    J(i-1,j-1)=Y_bus(i,j)*V(i);
   end
  end
 end
 % calculate correction
 correction =inv(J)*mismatch;
 V(2:N) = V(2:N)+correction(1:(N-1));

 % calculate mismatch and stop iterating
 % if the solution has converged
 P_calc = V.*(Y_bus*V);
 mismatch = [P_sch(2:N)-P_calc(2:N)];
```

TABLE 7.3 Example 7.6 Results.

Bus	p.u Voltage	p.u Power Mismatch
2	1.08	0.3036×10^{-6}
3	0.92	0.6994×10^{-6}

```
 if (norm(mismatch,'inf') < mis_match)
  break;
 end
end
iteration
% output solution data
for i = 1:N
 fprintf(1, 'Bus %d:\n', i);
 fprintf(1, ' Voltage = %f p.u\n', abs(V(i)));
 fprintf(1, ' Injected P = %f p.u \n', P_calc(i));
end
```

Results

The result is obtained after three iterations for $c_p = 1\times10^{-4}$.

The power supplied by bus 1, the swing bus is equal to the total load minus total generation by all other bus plus the losses.

The bus voltage of swing bus is $1\angle0$ and the p.u power is $P_1 = 0.522$.

The total power loss of the transmission lines is 0.223 p.u.

7.14.2 General Formulation of the Newton–Raphson Algorithm

In the above discussions, we presented the basic concepts of the Newton–Raphson algorithm. In the following, we present a general formulation of the Newton–Raphson method in calculating the element of the Jacobian matrix.[12] Let us start from a basic equation again.

$$I_{Bus} = Y_{Bus}V_{Bus}$$

For each bus k, $I_k = \sum_{j=1}^{n} Y_{kj}V_j$, where n is the number of buses and Y_{kj} is the element of Y_{Bus} matrix. For each bus k, we can also write:

$$P_k + jQ_k = V_k I_k^*$$

where P_k, and Q_k are real and the reactive power is entering node k (* is a complex conjugate and $j = \sqrt{-1}$).

Let,

$$P_k + jQ_k = V_k \sum_{j=1}^{n} Y_{kj}^* V_j^* \tag{7.57}$$

$$v_k = V_k \cdot e^{j\theta_k} = e_k + j \cdot f_k; \theta_k = \tan^{-1} \frac{f_k}{e_k} \tag{7.58}$$

$$Y_{kj} = Y_{kj} \cdot e^{j\alpha_{kj}} = G_{kj} + j \cdot B_{kj}; \alpha_{kj} = \tan^{-1} \frac{B_{kj}}{G_{kj}} \tag{7.59}$$

Using Equations 7.58 and 7.59 in 7.57, we have

$$P_k + jQ_k = V_k e^{j\theta_k} \sum_{j=1}^{n} Y_{kj} e^{-j\alpha_{kj}} V_j e^{-j\theta_j} \tag{7.60}$$

Using the Taylor–Series expansion, express the power flow problem as

$$\Delta P_k = \sum_{j=1}^{n} H_{kj} \Delta\theta_j + \sum_{j=1}^{n} N_{kj} \frac{\Delta V_j}{V_j} \tag{7.61}$$

$$\Delta Q_k = \sum_{j=1}^{n} J_{kj} \Delta\theta_j + \sum_{j=1}^{n} L_{kj} \frac{\Delta V_j}{V_j} \tag{7.62}$$

And in compact form as

$$\begin{bmatrix} \Delta P \\ \Delta Q \end{bmatrix} = \begin{bmatrix} \frac{\partial P}{\partial \theta} & \frac{\partial P}{\partial V} V \\ \frac{\partial Q}{\partial \theta} & \frac{\partial Q}{\partial V} V \end{bmatrix} \cdot \begin{bmatrix} \Delta\theta \\ \frac{\Delta V}{V} \end{bmatrix} \tag{7.63}$$

The basic load flow nonlinear equation in a complex domain is given by Equation 7.60. Students can take the derivative of Equation 7.60 and calculate for $j = k$ using the following diagonal elements of the Jacobian matrix:

$$\begin{aligned} H_{kk} &= \frac{\partial P_k}{\partial \theta_k} = -Q_k - V_k^2 B_{kk} \\ J_{kk} &= \frac{\partial Q_k}{\partial \theta_k} = P_k - V_k^2 G_{kk} \\ N_{kk} &= \frac{\partial P_k}{\partial V_k} V_k = P_k + V_k^2 G_{kk} \\ L_{kk} &= \frac{\partial Q_k}{\partial V_k} V_k = Q_k - V_k^2 B_{kk} \end{aligned} \tag{7.64}$$

So far, we have calculated (general equations) the diagonal elements of the Jacobian matrix. To calculate the off-diagonal elements of the Jacobian matrix, we first calculate the following:

$$I_j = a_j + j \cdot b_j = Y_{kj} \cdot V_j \tag{7.65}$$

$$\begin{aligned} Y_{kj} \cdot V_j &= (G_{kj} + j \cdot B_{kj}).(e_j + j \cdot f_j) \\ Y_{kj} \cdot V_j &= (G_{kj} \cdot e_j - B_{kj} f_j) + j(B_{kj} e_j + G_{kj} f_j) \\ Y_{kj} \cdot V_j &= a_j + jb_j \end{aligned} \tag{7.66}$$

where $a_j = G_{kj} \cdot e_j - B_{kj} f_j$ and $b_j = B_{kj} e_j + G_{kj} f_j$

For j ≠ k, we have the following off-diagonal elements for the Jacobian matrix:

$$\begin{aligned} H_{kj} &= \frac{\partial P_k}{\partial \theta_j} = a_j f_k - b_j e_k \\ J_{kj} &= \frac{\partial Q_k}{\partial \theta_j} = -a_j e_k - b_j f_k \\ N_{kj} &= \frac{\partial P_k}{\partial V_j} V_j = a_j e_k + b_j f_k \\ L_{kj} &= \frac{\partial Q_k}{\partial V_j} V_j = a_j f_k - b_j e_k \end{aligned} \tag{7.67}$$

$$\begin{bmatrix} \Delta P \\ \Delta Q \end{bmatrix} = \begin{bmatrix} H & N \\ J & L \end{bmatrix} \cdot \begin{bmatrix} \Delta \theta \\ \frac{\Delta V}{V} \end{bmatrix} \tag{7.68}$$

Power flow program software incorporates the following steps:

1. Renumber the system buses by creating an internal bus numbering system by bus types.
2. A swing bus is selected as bus 1 and followed by all P-V bus types.
3. Sparsity programming is used to eliminate storage requirements.
4. The Jacobian matrix is factored into upper and lower triangular matrices.
5. The diagonal and off-diagonal elements are computed as summarized below.

For $j = k$, the diagonal elements of the Jacobian matrix are

$$\left.\begin{aligned} H_{kk} &= -Q_k - B_{kk} V_k^2 \\ L_{kk} &= Q_k - B_{kk} V_k^2 \\ N_{kk} &= P_k + G_{kk} V_k^2 \\ J_{kk} &= P_k - G_{kk} V_k^2 \end{aligned}\right\} \text{For } j = k \tag{7.69}$$

For j ≠ k, the off-diagonal elements

$$\left.\begin{aligned} H_{kj} &= L_{kj} = a_j f_k - b_j e_k \\ N_{kj} &= -J_{kj} = a_j e_k + b_j f_k \end{aligned}\right\} j \neq k \tag{7.70}$$

6. The $P_{k(Calculated)}$ and $Q_{k(Calculated)}$ for each bus k are computed.

$$P_{k(calculated)} = \sum_{j=1}^{n} [e_k (e_j G_{kj} - f_j B_{kj}) + f_k (e_j B_{kj} + f_j G_{kj})] \tag{7.71}$$

$$Q_{k(Calculated)} = \sum_{j=1}^{n} [f_k (e_k G_{kj} - f_j B_{kj}) - e_k (e_j B_{kj} + f_j G_{kj})] \tag{7.72}$$

where $V_k = e_k + j \cdot f_k$; $Y_{kj}^* = G_{kj} - j \cdot B_{kj}$; $V_k^* == e_k - j \cdot f_k$

7. The power mismatch for active and reactive powers are calculated:

$$\Delta P_k^{(i)} = P_{k,(Scheduled)}^{(i)} - P_{k,(Calculated)}^{(i)} < c_P \tag{7.73}$$

$$\Delta Q_k^{(i)} = Q_{k,(Scheduled)}^{(i)} - Q_{k,(Calculated)}^{(i)} < c_Q \tag{7.74}$$

The Jacobian matrix is evaluated at each iterative approximation at the last computed solution.

$$V = V^{(i)} \text{ and } \theta = \theta^{(i)}$$

$$\Delta V^{(k)} = V^{(k+1)} - V^{(k)}$$

$$\Delta \theta^{(k)} = \theta^{(k+1)} - \theta^{(k)}$$

The power mismatch at each bus is calculated based on $P_{k,(Scheduled)}$ and $Q_{k,(Scheduled)}$ and the calculated power flow at the bus, $P_{k,(Calculated)}$, $Q_{k,(Calculated)}$. The calculated active and reactive powers are based on the voltage profile of the network and Y_{Bus} model using $V^{(i)}$ and $\theta^{(i)}$ computed bus voltages.

For P-V buses, the ΔV_k is set equal to zero. Notice that for a P-V bus, the reactive power generation has to be calculated and checked for violation of Q-limits. In case of limit violations, the bus type has to be switched from P-V to PQ type to maintain the reactive generation within the specified limits.

7.14.3 The Decoupled Newton–Raphson Algorithm

Numerical studies of many systems clearly indicate that the change in voltage magnitudes has little effect on power flows. In addition, the changes in voltage

angles have little effect on reactive power flows. These observations may not be true for cables and short lines. However, for bulk power flows they are generally true. Using the above assumptions facilitate a substantial reduction in the amount of computer memory required for a large-scale power grid load flow analysis.

We can restate the above assumptions as

1. The partial of $\frac{\partial P}{\partial V}$ is assumed to be zero.
2. The partial of $\frac{\partial Q}{\partial \theta}$ is assumed to be zero.

With the above assumptions, we can decouple the $\Delta P - \Delta\theta$ equations and $\Delta Q - \Delta V$ equations of the load flow problems.

$$\begin{bmatrix} \Delta P \\ \Delta Q \end{bmatrix} = \begin{bmatrix} \frac{\partial P}{\partial \theta} & 0 \\ 0 & \frac{\partial Q}{\partial V} V \end{bmatrix} \begin{bmatrix} \Delta\theta \\ \frac{\Delta V}{V} \end{bmatrix} \tag{7.75}$$

Therefore, Equation 7.75 will become two decoupled and independent equations.

$$\begin{aligned} [\Delta P] &= \left[\frac{\partial P}{\partial \theta}\right][\Delta\theta] \\ [\Delta Q] &= \left[\frac{\partial Q}{\partial V} V\right]\left[\frac{\Delta V}{V}\right] \end{aligned} \tag{7.76}$$

Therefore, Equation 7.75 can be rewritten as:

$$\begin{bmatrix} \Delta P \\ \Delta Q \end{bmatrix} = \begin{bmatrix} H & 0 \\ 0 & L \end{bmatrix} \begin{bmatrix} \Delta\theta \\ \frac{\Delta V}{V} \end{bmatrix} \tag{7.77}$$

where $[H] = \left[\frac{\partial P}{\partial \theta}\right]$ and $[L] = \left[\frac{\partial Q}{\partial V} V\right]$

Equation 7.77 presents the decoupled Newton–Raphson method.

7.15 THE FAST DECOUPLED LOAD FLOW ALGORITHM

The fast decoupled load flow (FDLF) algorithm is a modified version of the Newton–Raphson algorithm. The FDLF algorithm[9] takes advantage of the weak coupling between the real and reactive powers and uses two constant

matrices to approximate and decouple the Jacobian matrix.[8] We rewrite the H matrix as

$$[\Delta P] = [H][\Delta\theta]$$
$$[H] = \left[\frac{\partial P}{\partial \theta}\right] = [V][B'][V]$$
$$[\Delta P] = [V][B'][V][\Delta\theta]$$

Dividing both sides by V, we have

$$\left[\frac{\Delta P}{V}\right] = [B'][V][\Delta\theta]$$

To obtain a constant linear approximation with constant coefficient, we set the V in the above equation to 1 and we obtain:

$$\left[\frac{\Delta P}{V}\right] = [B'] \cdot [\Delta\theta] \tag{7.78}$$

Similarly, we can observe that the L matrix in the decoupled Newton–Raphson can be written as

$$[\Delta Q] = [L]\left[\frac{\Delta V}{V}\right]$$
$$[L] = \left[\frac{\partial Q}{\partial V} V\right] = [V][B'']$$

Then, we divide both sides by V and setting the second V to 1 p.u, we have

$$\left[\frac{\Delta Q}{V}\right] = [B''] \cdot [\Delta V] \tag{7.79}$$

Equations 7.78 and 7.79 present the FDLF algorithm.[13] The matrix B″ is the imaginary part of the Y matrix and B' is the same as B'' except for the line resistances and shunt elements that are neglected. The FDLF method reduces the memory requirement and converges in most problems to an acceptable solution. However, the number of iterations increases. When the power grid has short cables and has phase-shifting transformers, the FDLF can fail to converge. However, we should observe that even when the FDLF is constructed from approximation of the Jacobian matrix, the convergence of the power flow problem is still checked based on the original power flow mismatch of active and reactive power. Therefore, if FDLF converges, then the solution is as accurate as the full Newton–Raphson method.

7.16 ANALYSIS OF A POWER FLOW PROBLEM

Let us consider the case of the decoupled Newton–Raphson method and analyze the injection model of Fig. 7.20.

We will use the data in Tables 7.4 and 7.5 to show the linearized relationship of known variables in terms of the unknown variables. Bus 1, bus 2, and bus 3 voltages are specified at a fixed value; therefore, for these buses the change in voltage is zero and these voltages are not listed as unknowns in Table 7.5.

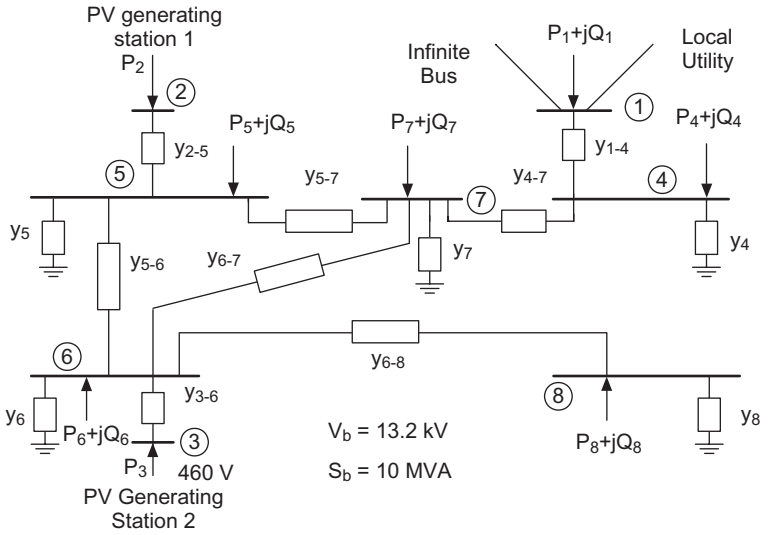

Figure 7.20 A One-Line Injection Model of a Microgrid.

TABLE 7.4 Active Power Injection as a Function of Bus Angle.

Knowns	Unknowns
P_2	θ_2
P_3	θ_3
P_4	θ_4
P_5	θ_5
P_6	θ_6
P_7	θ_7
P_8	θ_8

TABLE 7.5 Reactive Power Injection as a Function of Bus Voltage.

Knowns	Unknowns
Q_4	V_4
Q_5	V_5
Q_6	V_6
Q_7	V_7
Q_8	V_8

The same is true for the phase angle of bus 1.

$$
\begin{aligned}
\Delta P_2 &= \frac{\partial P_2}{\partial \theta_2}\Delta\theta_2 + \frac{\partial P_2}{\partial \theta_5}\Delta\theta_5 \\
\Delta P_3 &= \frac{\partial P_3}{\partial \theta_3}\Delta\theta_3 + \frac{\partial P_3}{\partial \theta_6}\Delta\theta_6 \\
\Delta P_4 &= \frac{\partial P_4}{\partial \theta_4}\Delta\theta_4 + \frac{\partial P_4}{\partial \theta_7}\Delta\theta_7 \\
\Delta P_5 &= \frac{\partial P_5}{\partial \theta_2}\Delta\theta_2 + \frac{\partial P_5}{\partial \theta_5}\Delta\theta_5 + \frac{\partial P_5}{\partial \theta_6}\Delta\theta_6 + \frac{\partial P_5}{\partial \theta_7}\Delta\theta_7 \\
\Delta P_6 &= \frac{\partial P_6}{\partial \theta_3}\Delta\theta_3 + \frac{\partial P_6}{\partial \theta_5}\Delta\theta_5 + \frac{\partial P_6}{\partial \theta_6}\Delta\theta_6 + \frac{\partial P_6}{\partial \theta_7}\Delta\theta_7 + \frac{\partial P_6}{\partial \theta_8}\Delta\theta_8 \\
\Delta P_7 &= \frac{\partial P_7}{\partial \theta_4}\Delta\theta_4 + \frac{\partial P_7}{\partial \theta_5}\Delta\theta_5 + \frac{\partial P_7}{\partial \theta_6}\Delta\theta_6 + \frac{\partial P_7}{\partial \theta_7}\Delta\theta_7 \\
\Delta P_8 &= \frac{\partial P_8}{\partial \theta_6}\Delta\theta_6 + \frac{\partial P_8}{\partial \theta_8}\Delta\theta_8
\end{aligned}
\tag{7.80}
$$

If you carefully evaluate the sets of equations given within Equation 7.80, you will observe that an injected power at each bus is only the function of the bus under consideration and the buses they are connected to in the network. For example, bus 4 is connected to bus 1 and bus 7. The injection at bus 4 changes the flow between bus 1 and bus 7. However, the bus 1 change in angle is zero because bus 1 is the swing bus. As we know, the swing bus injection is computed last when bus voltages are computed and the power flow problem has converged. Again, the same condition is true for all lines connecting buses in the network. For example, bus 7 is connected to buses 4, 5, and 6 and corresponding terms are given in the bus 7 injection model. As we have stated before, each active power mismatch is computed based on injected power and calculated active power based on the system Y_{Bus} and bus voltages.

$$\begin{bmatrix} \Delta P_2 \\ \Delta P_3 \\ \Delta P_4 \\ \Delta P_5 \\ \Delta P_6 \\ \Delta P_7 \\ \Delta P_8 \end{bmatrix} = \begin{array}{c} \begin{matrix} P_2 & P_3 & P_4 & P_5 & P_6 & P_7 & P_8 \end{matrix} \\ \begin{bmatrix} \frac{\partial P_2}{\partial \theta_2} & 0 & 0 & \frac{\partial P_2}{\partial \theta_5} & 0 & 0 & 0 \\ 0 & \frac{\partial P_3}{\partial \theta_3} & 0 & 0 & \frac{\partial P_3}{\partial \theta_6} & 0 & 0 \\ 0 & 0 & \frac{\partial P_4}{\partial \theta_4} & 0 & 0 & \frac{\partial P_4}{\partial \theta_7} & 0 \\ \frac{\partial P_5}{\partial \theta_2} & 0 & 0 & \frac{\partial P_5}{\partial \theta_5} & \frac{\partial P_5}{\partial \theta_6} & \frac{\partial P_5}{\partial \theta_7} & 0 \\ 0 & \frac{\partial P_6}{\partial \theta_3} & 0 & \frac{\partial P_6}{\partial \theta_5} & \frac{\partial P_6}{\partial \theta_6} & \frac{\partial P_6}{\partial \theta_7} & \frac{\partial P_6}{\partial \theta_8} \\ 0 & 0 & \frac{\partial P_7}{\partial \theta_4} & \frac{\partial P_7}{\partial \theta_5} & \frac{\partial P_7}{\partial \theta_6} & \frac{\partial P_7}{\partial \theta_7} & 0 \\ 0 & 0 & 0 & 0 & \frac{\partial P_8}{\partial \theta_6} & 0 & \frac{\partial P_8}{\partial \theta_8} \end{bmatrix} \end{array} \cdot \begin{bmatrix} \Delta\theta_2 \\ \Delta\theta_3 \\ \Delta\theta_4 \\ \Delta\theta_5 \\ \Delta\theta_6 \\ \Delta\theta_7 \\ \Delta\theta_8 \end{bmatrix} \tag{7.81}$$

Equation 7.81 presents the matrix formulation of Equation 7.80. As we described above, the elements of the Jacobian matrix are computed by taking the partial derivative of the general load flow equation. For each iteration, we use the voltages computed from the last iteration to compute the matrix H of Equation 7.82.

$$\begin{bmatrix} \Delta P_2 \\ \Delta P_3 \\ \Delta P_4 \\ \Delta P_5 \\ \Delta P_6 \\ \Delta P_7 \\ \Delta P_8 \end{bmatrix} = \begin{array}{c} \begin{matrix} P_2 & P_3 & P_4 & P_5 & P_6 & P_7 & P_8 \end{matrix} \\ \begin{bmatrix} H_{22} & 0 & 0 & H_{25} & 0 & 0 & 0 \\ 0 & H_{33} & 0 & 0 & H_{36} & 0 & 0 \\ 0 & 0 & H_{44} & 0 & 0 & H_{47} & 0 \\ H_{52} & 0 & 0 & H_{55} & H_{56} & H_{57} & 0 \\ 0 & H_{63} & 0 & H_{65} & H_{66} & H_{67} & H_{68} \\ 0 & 0 & H_{74} & H_{75} & H_{76} & H_{77} & 0 \\ 0 & 0 & 0 & 0 & H_{86} & 0 & H_{88} \end{bmatrix} \end{array} \cdot \begin{bmatrix} \Delta\theta_2 \\ \Delta\theta_3 \\ \Delta\theta_4 \\ \Delta\theta_5 \\ \Delta\theta_6 \\ \Delta\theta_7 \\ \Delta\theta_8 \end{bmatrix} \tag{7.82}$$

$$[\Delta P] = [H][\Delta\theta] \tag{7.83}$$

The linearized $\Delta Q - \Delta V$ equations are written using Table 7.5 and Fig. 7.20. Again, we recognize that the bus voltage is a function of the reactive power from other buses. For example, the voltage at bus 4 is a function of reactive power at bus 4 and bus 7 only because bus voltage is fixed.

$$\begin{matrix} & Q_4 & Q_5 & Q_6 & Q_7 & Q_8 & \\ \begin{bmatrix}\Delta Q_4\\ \Delta Q_5\\ \Delta Q_6\\ \Delta Q_7\\ \Delta Q_8\end{bmatrix} = & \begin{bmatrix} \frac{\partial Q_4}{\partial V_4}V_4 & 0 & 0 & \frac{\partial Q_4}{\partial V_7}V_7 & 0 \\ 0 & \frac{\partial Q_5}{\partial V_5}V_5 & \frac{\partial Q_5}{\partial V_6}V_6 & \frac{\partial Q_5}{\partial V_7}V_7 & 0 \\ 0 & \frac{\partial Q_6}{\partial V_5}V_5 & \frac{\partial Q_6}{\partial V_6}V_6 & \frac{\partial Q_6}{\partial V_7}V_7 & \frac{\partial Q_6}{\partial V_8}V_8 \\ \frac{\partial Q_7}{\partial V_4}V_4 & \frac{\partial Q_7}{\partial V_5}V_5 & \frac{\partial Q_7}{\partial V_6}V_6 & \frac{\partial Q_7}{\partial V_7}V_7 & 0 \\ 0 & 0 & \frac{\partial Q_8}{\partial V_6}V_6 & 0 & \frac{\partial Q_8}{\partial V_8}V_8 \end{bmatrix} \cdot \begin{bmatrix}\frac{\Delta V_4}{V_4}\\ \frac{\Delta V_5}{V_5}\\ \frac{\Delta V_6}{V_6}\\ \frac{\Delta V_7}{V_7}\\ \frac{\Delta V_8}{V_8}\end{bmatrix} \end{matrix} \tag{7.84}$$

$$\begin{matrix} & Q_4 & Q_5 & Q_6 & Q_7 & Q_8 & \\ \begin{bmatrix}\Delta Q_4\\ \Delta Q_5\\ \Delta Q_6\\ \Delta Q_7\\ \Delta Q_8\end{bmatrix} = & \begin{bmatrix} L_{44} & 0 & 0 & L_{47} & 0 \\ 0 & L_{55} & L_{56} & L_{57} & 0 \\ 0 & L_{65} & L_{66} & L_{67} & L_{68} \\ L_{74} & L_{75} & L_{76} & L_{77} & 0 \\ 0 & 0 & L_{86} & 0 & L_{88} \end{bmatrix} \cdot \begin{bmatrix}\frac{\Delta V_4}{V_4}\\ \frac{\Delta V_5}{V_5}\\ \frac{\Delta V_6}{V_6}\\ \frac{\Delta V_7}{V_7}\\ \frac{\Delta V_8}{V_8}\end{bmatrix} \end{matrix} \tag{7.85}$$

$$[\Delta Q] = [L]\left[\frac{\Delta V}{V}\right]$$

Example 7.7 Consider the microgrid given in Fig. 7.21.
Assume the following data:

a. Transformers connected to the PV generating station are rated at 460 V Y-grounded/13.2 kV Δ, have 10% reactance and 10 MVA capacity. The transformer connected to the power grid is 13.2 / 63 kV, 10 MVA, 10% reactance.
b. Assume the load on bus 4 is 1.5 MW, 0.9 p.f. lagging, on bus 5 is 2.5 MW, 0.9 p.f. lagging, on bus 6 is 1.0 MW, 0.95 p.f. lagging, on bus 7 is 2 MW, 0.95 p.f. leading, and on bus 8 is 1.0 MW, 0.9 p.f. lagging.
c. The transmission line has a resistance of 0.0685 Ω/mile, reactance of 0.40 Ω/mile, and half of line charging admittance (Y′/2) of 11×10^{-6} Ω^{-1}/mile. The line 4–7 is 5 miles, 5–6 is 3 miles, 5–7 is 2 miles, 6–7 is 2 miles, and 6–8 is 4 miles long.

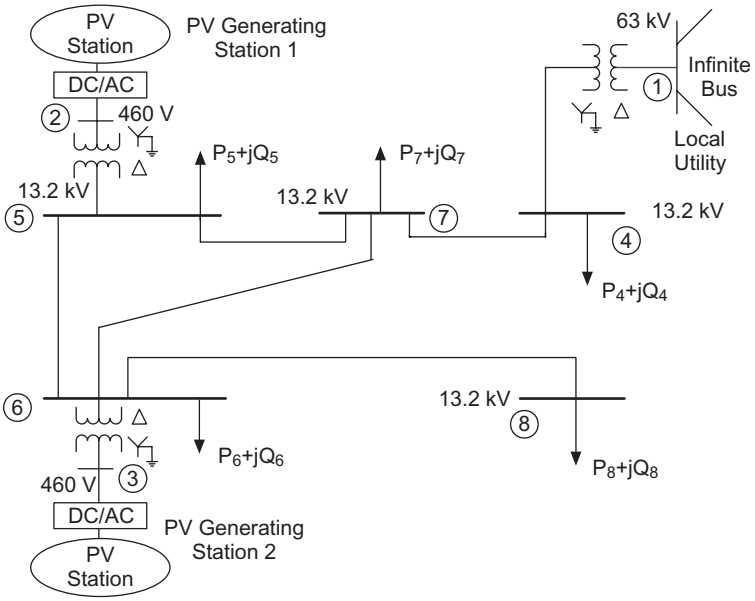

Figure 7.21 The Photovoltaic Microgrid of Example 7.7.

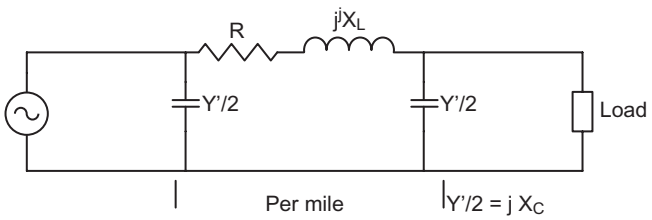

Figure 7.22 The Transmission-Line Pie Model.

d. Assume the PV generating station 1 is rated at 0.75 MW and PV generating station 2 is rated at 3 MW. Assume PV generating stations are operating at unity power factors.

Perform the following:

i) Assume an S_{base} of 10 MVA and a voltage base of 460 V in PV generator #1 and compute the p.u model.

ii) Compute the Y bus model

iii) Compute the load bus voltages using the Newtown–Raphson and Gauss–Seidel methods

iv) Compute the bus voltages and power flow of the microgrid.

v) How much green power is imported or exported to the local power grid?

Solution

The base value of the volt-amp is designated as $S_b = 10$ MVA; the voltage base on the PV generator side is specified as 460 V, and the voltage base on the transmission line side is specified as $V_b = 13.2$ kV.

The base impedance is

$$Z_b = \frac{V_b^2}{S_b} = \frac{\left(13.2\times10^3\right)^2}{10\times10^6} = 17.424\ \Omega$$

The base admittance is given by

$$Y_b = \frac{1}{Z_b} = \frac{1}{17.424} = 0.057$$

The current injection model of the PV system is shown in Fig. 7.23.

From transmission line data, the primitive impedance and admittance are calculated:

$$\begin{aligned}
\mathcal{Z}_{1-4\ \text{p.u}} &= \mathcal{Z}_{2-5\ \text{p.u}} = \mathcal{Z}_{3-6\ \text{p.u}} = j0.1,\\
y_{14,p.u} &= y_{25,p.u} = y_{36,p.u} = \frac{1}{j0.1} = -j10\\
\mathcal{Z}_{4-7} &= 5(0.0685 + j0.4)/Z_b = 0.020 + j0.115,\\
y_{47,p.u} &= \frac{1}{0.020 + j0.115} = 1.45 - j8.46\ \text{p.u}\ \Omega\\
\mathcal{Z}_{5-6} &= 3(0.0685 + j0.4)/Z_b = 0.012 + j0.069,\\
y_{56,p.u} &= \frac{1}{0.012 + j0.069} = 2.42 - j14.11\ \text{p.u}\ \Omega\\
\mathcal{Z}_{5-7} &= \mathcal{Z}_{6-7} = 2(0.0685 + j0.4)/Z_b = 0.008 + j0.046\ \text{p.u}\ \Omega\\
y_{57.} &= y_{67,p.u} = \frac{1}{0.008 + j0.046} = 3.62 - j21.16\\
\mathcal{Z}_{6-8} &= 4(0.0685 + j0.4)/Z_b = 0.016 + j0.092,\ \text{p.u}\ \Omega\\
y_{68,.} &= \frac{1}{0.016 + j0.092} = 1.18 - 10.57
\end{aligned} \tag{7.86}$$

The line-charging admittance is the same as the $\frac{Y'}{2}$ as shown in Fig. 7.22. The line-charging admittances in per unit are as follows:

$$y'_{47.} = 5\times\frac{j11\times10^{-6}}{Y_b} = j9.58\times10^{-4},\ y'_{56,p.u} = 3\times\frac{j11\times10^{-6}}{Y_b} = j5.75\times10^{-4},$$

$$y'_{57.} = y'_{67,} = 2\times\frac{j11\times10^{-6}}{Y_b} = j3.83\times10^{-4},\ y'_{68,.} = 4\times\frac{j11\times10^{-6}}{Y_b} = j7.67\times10^{-4}$$

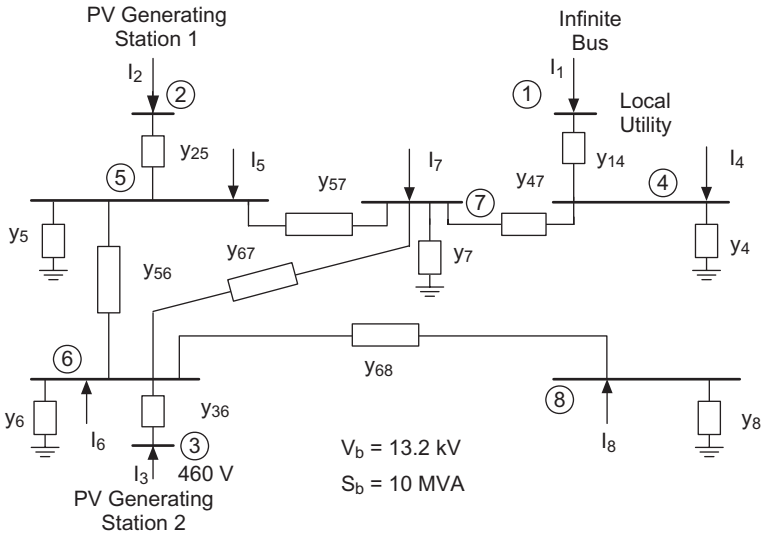

Figure 7.23 The Current Injection Model of Example 7.7.

The p.u admittance matrix, Y_{Bus} is calculated using Equation 7.18,

$$Y_{Bus} = \begin{bmatrix} -j10 & 0 & 0 & j10 & 0 & 0 & 0 & 0 \\ 0 & -j10 & 0 & 0 & j10 & 0 & 0 & 0 \\ 0 & 0 & -j10 & 0 & 0 & j10 & 0 & 0 \\ j10 & 0 & 0 & 1.45 - j18.46 & 0 & 0 & -1.45 + j8.46 & 0 \\ 0 & j10 & 0 & 0 & 6.04 - j45.26 & -2.42 + j14.11 & -3.62 + j21.16 & 0 \\ 0 & 0 & j10 & 0 & -2.42 + j14.11 & 7.85 - j55.84 & -3.62 + j21.16 & -1.81 + j10.58 \\ 0 & 0 & 0 & -1.45 + j8.46 & -3.62 + j21.16 & -3.62 + j21.16 & 8.69 - j50.78 & 0 \\ 0 & 0 & 0 & 0 & 0 & -1.81 + j10.58 & 0 & 1.81 - j10.58 \end{bmatrix}$$

A MATLAB program was written to perform the load flow analysis. The PV generator buses are treated as PV buses in the load flow problem. The voltage at the PV generator buses are fixed at 1 p.u. Table 7.6 provides the scheduled powers of each bus.

For this load flow problem, the tolerance of error chosen was 1×10^{-5}. The load flow problem was solved using the Newton–Raphson and Gauss–Seidel methods. Table 7.7 gives the results using the Newton–Raphson method, which converges in three iterations. The Gauss–Seidel converges in 392 iterations (Table 7.8).

To maintain PV bus 2 and PV bus 3 at 1 p.u, the required reactive power at bus 2 is 0.094 p.u. and at bus 3 is 0.085 p.u. The active power flow from the local power grid is 0.427 p.u. The reactive power flow from the local power grid is 0.065 p.u.

It can be seen from Tables 7.7 and 7.8 that the reactive power of 0.094 p.u and 0.085 p.u is needed from the PV generating station's connected buses 2 and 3 to maintain a voltage of 1 p.u at these buses. If the PV system has a local storage system, the control of the inverter can be set to provide the reactive power. The reactive power can also be provided by placing the required VAr support at the AC side of the PV generating stations. The scheduled reactive VAr support at bus 2 is 0.094 p.u and at bus 3 is 0.085 p.u. The power flow problem was solved with scheduled VAr support reactive power injected into the PV generating station buses. The results are shown in Table 7.9. The program converged in three iterations.

TABLE 7.6 The Scheduled Active and Reactive Power of Each Bus.

Bus	2	3	4	5	6	7	8
$P_{\text{scheduled}}$	0.075	0.3	–0.150	–0.250	–0.100	–0.200	–0.100
$Q_{\text{scheduled}}$	—	—	–0.073	–0.121	–0.033	0.066	–0.048

TABLE 7.7(a) The Voltages and Power of Each Bus Using the Newton–Raphson Method.

$S_b = 10$ MVA, $V_b = 13.2$ kV								
			Generation		Load			
Bus #	Volts (p.u)	Angle (°)	MW (p.u)	MVAr (p.u)	MW (p.u)	MVAr (p.u)	ΔP	ΔQ
1	1.000	0.0	0.427	0.065	0	0	0	0
2	1.000	–4.1	0.075	0.094	0	0	0.005×10^{-10}	0
3	1.000	–2.5	0.300	0.085	0	0	0.021×10^{-10}	0
4	0.994	–2.5	0	0	0.150	0.073	0.189×10^{-10}	0.424×10^{-10}
5	0.991	–4.6	0	0	0.250	0.121	0.127×10^{-10}	0.002×10^{-10}
6	0.992	–4.3	0	0	0.100	0.033	0.079×10^{-10}	0.071×10^{-10}
7	0.992	–4.3	0	0	0.200	–0.066	0.233×10^{-10}	0.110×10^{-10}
8	0.986	–4.8	0	0	0.100	0.048	0.074×10^{-10}	0.009×10^{-10}

TABLE 7.7(b) The Power Flow through Transmission Lines and Transformers Using the Newton–Raphson Method.

P_{loss} (p.u) = 0.002, Q_{loss} (p.u) = 0.035			
From Bus #	To Bus #	MW Flow (p.u)	MVAr Flow (p.u)
1	4	0.427	0.065
2	5	0.075	0.094
3	6	0.300	0.085
4	7	0.277	–0.025
5	6	–0.079	–0.006
5	7	–0.097	–0.021
6	7	0.021	–0.012
6	8	0.100	0.049

TABLE 7.8(a) The Voltages and Power of Each Bus Using the Gauss–Seidel Method.

$S_b = 10$ MVA, $V_b = 13.2$ kV								
			Generation		Load			
Bus #	Volts (p.u)	Angle (°)	MW (p.u)	MVAr (p.u)	MW (p.u)	MVAr (p.u)	ΔP	ΔQ
1	1.000	0.0	0.427	0.065	0	0	0	0
2	1.000	–4.1	0.075	0.094	0	0	0.179×10^{-5}	0
3	1.000	–2.5	0.300	0.085	0	0	0.181×10^{-5}	0
4	0.994	–2.5	0	0	0.150	0.073	0.141×10^{-5}	0.018×10^{-5}
5	0.991	–4.6	0	0	0.250	0.121	0.783×10^{-5}	0.100×10^{-5}
6	0.992	–4.3	0	0	0.100	0.033	0.979×10^{-5}	0.132×10^{-5}
7	0.992	–4.3	0	0	0.200	–0.066	0.822×10^{-5}	0.137×10^{-5}
8	0.986	–4.8	0	0	0.100	0.048	0.188×10^{-5}	0.031×10^{-5}

TABLE 7.8(b) The Power Flow through Transmission Lines and Transformers Using the Gauss–Seidel Method.

P_{loss} (p.u) = 0.002, Q_{loss} (p.u) = 0.035			
From Bus #	To Bus #	MW Flow (p.u)	MVAr Flow (p.u)
1	4	0.427	0.065
2	5	0.075	0.094
3	6	0.300	0.085
4	7	0.277	–0.025
5	6	–0.079	–0.006
5	7	–0.097	–0.021
6	7	0.021	–0.012
6	8	0.100	0.049

With the reactive power injected into the PV generator buses, the voltage of theses buses is maintained at 1 p.u. From Table 7.9, we see that the active power supplied by bus 1 is positive 0.427 p.u. This means, the power is being imported (bought) from the local power grid.

The base volt-amp is 10 MVA ($S_b = 10$ MVA); therefore, the power imported from the local power grid is $P_1 = 0.427 \times S_b = 4.27$ MW. The power generated by the PV generator 1 connected to bus 2 is $P_2 = 0.075 \times S_b = 0.75$ MW.

The power generated by the PV generator 2 connected to bus 3 is $P_3 = 0.300 \times S_b = 3.00$ MW.

TABLE 7.9(a) The Voltage and Power of Each Bus with Reactive Power Correction for the PV Generation Buses.

$S_b = 10$ MVA, $V_b = 13.2$ kV								
			Generation		Load			
Bus #	Volts (p.u)	Angle (°)	MW (p.u)	MVAr (p.u)	MW (p.u)	MVAr (p.u)	ΔP	ΔQ
1	1.000	0.0	0.427	0.065	0	0	0	0
2	1.000	–4.1	0.075	0.094	0	0	0.049×10^{-8}	0.003×10^{-8}
3	1.000	–2.5	0.300	0.085	0	0	0.196×10^{-8}	0.081×10^{-8}
4	0.994	–2.5	0	0	0.150	0.073	0.064×10^{-8}	0.086×10^{-8}
5	0.991	–4.6	0	0	0.250	0.121	0.230×10^{-8}	0.016×10^{-8}
6	0.992	–4.3	0	0	0.100	0.033	0.131×10^{-8}	0.148×10^{-8}
7	0.992	–4.3	0	0	0.200	–0.066	0.131×10^{-8}	0.042×10^{-8}
8	0.986	–4.8	0	0	0.100	0.048	0.146×10^{-8}	0.007×10^{-8}

TABLE 7.9(b) The Power through the Transmission Lines and Transformers with Reactive Power Correction for the PV Generation Buses.

P_{loss} (p.u) = 0.002, Q_{loss} (p.u) = 0.035			
From Bus #	To Bus #	MW Flow (p.u)	MVAr Flow (p.u)
1	4	0.427	0.065
2	5	0.075	0.094
3	6	0.300	0.085
4	7	0.277	–0.025
5	6	–0.079	–0.006
5	7	–0.097	–0.021
6	7	0.021	–0.012
6	8	0.100	0.049

Example 7.8 For Example 7.7, perform the following:

i) Compute the matrix of B'' and matrix B' of FDLF.
ii) Compute the load bus voltages and the mismatch using the FDLF method

Solution

i) From Example 7.7, the bus 1 is the swing bus and buses 2 and 3 are PV buses. Hence, out of eight buses, there are five PQ buses. The matrix B'' is, 5×5 and is equal to the imaginary part of the last five rows and columns of the Y_{Bus} matrix:

$$B''=\begin{bmatrix} -18.46 & 0 & 0 & 8.46 & 0 \\ 0 & -45.26 & 14.11 & 21.16 & 0 \\ 0 & 14.11 & -55.84 & 21.16 & 10.58 \\ 8.46 & 21.16 & 21.16 & -50.78 & 0 \\ 0 & 0 & 10.58 & 0 & -10.18 \end{bmatrix}$$

To calculate B', the resistance and shunt elements are neglected. The B' matrix is a 7×7 matrix. The diagonal elements of B':

$$B'_{22.} = -j10,\ B'_{33,p.u} = -j10,\ B'_{44,p.u} = -j10 - j8.71 = -j18.71,$$

$$B'_{55.} = -j10 - j14.52 - j21.78 = -j46.30,\ B'_{66.} = -j10 - j14.52 - j21.78 - j10.89 = -j57.19,$$

$$B'_{77.} = -j8.71 - j21.78 - j21.78 = -j52.27,\ B'_{88.} = -j10.89$$

The off-diagonal elements of B':

$$B'_{kj} = \frac{1}{x_{kj,p.u}},$$

where $x_{kj,p.u}$ is the per unit series reactance between bus k and j

The matrix is symmetric. The upper triangular elements are as follows:

$$B'_{25} = B'_{36.} = \frac{1}{x_{25,p.u}} = \frac{1}{x_{36,p.u}} = -\frac{1}{j0.1} = j10\ ,\ B'_{57.} = \frac{1}{x_{57,p.u}} = -\frac{1}{j0.0459} = j21.78\ ,$$

$$B'_{47.} = \frac{1}{x_{47,p.u}} = -\frac{1}{j0.1148} = j8.71\ ,\qquad B'_{56.} = \frac{1}{x_{56,p.u}} = -\frac{1}{j0.0689} = j14.52\ ,$$

$$B'_{68.} = \frac{1}{x_{68,p.u}} = -\frac{1}{j0.0918} = j10.89\ ,\qquad B'_{67.} = \frac{1}{x_{67,p.u}} = -\frac{1}{j0.0459} = j21.78$$

The elements of the matrix are the imaginary part of the above.

$$B' = \begin{array}{c} \begin{matrix} 2 & 3 & 4 & 5 & 6 & 7 & 8 \end{matrix} \\ \begin{bmatrix} -10 & 0 & 0 & 10 & 0 & 0 & 0 \\ 0 & -10 & 0 & 0 & 10 & 0 & 0 \\ 0 & 0 & -18.71 & 0 & 0 & 8.71 & 0 \\ 10 & 0 & 0 & -46.30 & 14.52 & 21.78 & 0 \\ 0 & 10 & 0 & 14.52 & -57.19 & 21.78 & 10.89 \\ 0 & 0 & 8.71 & 21.78 & 21.78 & -52.27 & 0 \\ 0 & 0 & 0 & 0 & 10.89 & 0 & -10.89 \end{bmatrix} \end{array} \begin{matrix} 2 \\ 3 \\ 4 \\ 5 \\ 6 \\ 7 \\ 8 \end{matrix}$$

ii) The problem was solved using the FDLF method with the tolerance of error chosen as 1×10^{-5}. The solution converged in six iterations. The results are given in Table 7.10.

TABLE 7.10(a) The Voltages and Power of Each Bus Using the Fast Decoupled Method.

$S_b = 10$ MVA, $V_b = 13.2$ kV

			Generation		Load			
Bus #	Volts (p.u)	Angle (°)	MW (p.u)	MVAr (p.u)	MW (p.u)	MVAr (p.u)	ΔP	ΔQ
1	1.000	0.0	0.427	0.065	0	0	0	0
2	1.000	–4.1	0.075	0.094	0	0	0.002×10^{-5}	0
3	1.000	–2.5	0.300	0.085	0	0	0.002×10^{-5}	0
4	0.994	–2.5	0	0	0.150	0.073	0.052×10^{-5}	0.086×10^{-5}
5	0.991	–4.6	0	0	0.250	0.121	0.063×10^{-5}	0.129×10^{-5}
6	0.992	–4.3	0	0	0.100	0.033	0.388×10^{-5}	0.295×10^{-5}
7	0.992	–4.3	0	0	0.200	–0.066	0.301×10^{-5}	0.504×10^{-5}
8	0.986	–4.8	0	0	0.100	0.048	0.190×10^{-5}	0.062×10^{-5}

TABLE 7.10(b) The Power Flow through Transmission Lines and Transformers Using the Fast Decoupled Method.

P_{loss} (p.u) = 0.002, Q_{loss} (p.u) = 0.035

From Bus #	To Bus #	MW Flow (p.u)	MVAr Flow (p.u)
1	4	0.427	0.065
2	5	0.075	0.094
3	6	0.300	0.085
4	7	0.277	–0.025
5	6	–0.079	–0.006
5	7	–0.097	–0.021
6	7	0.021	–0.012
6	8	0.100	0.049

In this chapter, we have used the bus admittance matrix and bus impedance matrix to formulate the power flow in power grids. Power flow problems must be solved during the system planning of large, interconnected power grids using the forecasted bus loads to ensure that planned generation and transmission systems are at acceptable bus load voltages so that the system lines, transformers, etc., are not overloaded. Power flow problems must also be solved during daily operations and for a PV or wind generating microgrid operating as an isolated system using the forecasted bus loads also to ensure that the microgrid can support its loads at acceptable bus load voltages and that cables, lines, transformers, etc., are not overloaded.

PROBLEMS

7.1 A three-phase generator rated 440 V, 20 kVA is connected by one cable with impedance of 1 + j0.012 Ω to a motor load rated 440 V, 15 kVA, 0.9 p.f. lagging. Assume the load voltage to be set at 5% above its rated value. Perform the following:

i) Give the three-phase circuit if the load is Y connected

ii) Give the three-phase circuit if the load Δ connected

iii) Give a one-line diagram

iv) Compute the generator voltage

7.2 A three-phase generator rated 440 V, 20 kVA is connected through one cable with impedance of 1 + j.012 Ω to a Δ-connected motor load rated 440 V, 10 kVA, 0.9 p.f. lagging. Assume the generator voltage is to be controlled at its rated voltage and its phase angle is used as the reference angle. Perform the following:

i) What is the number of unknown variables?

ii) How many equations are needed to solve for bus voltage? Give the expressions.

iii) Compute the load bus voltage

7.3 The radial feeder of Fig. 7.24 is connected to a local power grid rated at 11.3 kV distribution. Assume the base voltage of 10 kVA and a voltage base of 11.3 kV. Perform the following:

i) Compute the per unit model

ii) Write the number of equations that are needed to solve for the bus load voltages

iii) Use the Gauss–Seidel method and compute the bus voltages

iv) Compute the power at bus 1. Assume the power mismatch of 0.00001 per unit.

v) Compute the total active and reactive power losses

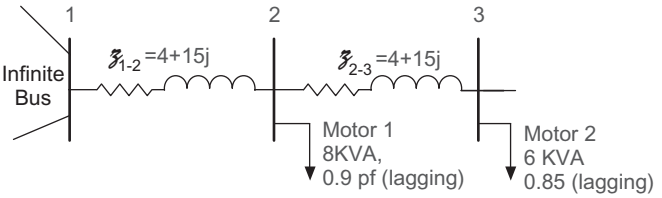

Figure 7.24 The Radial Feeder for Problem 7.3.

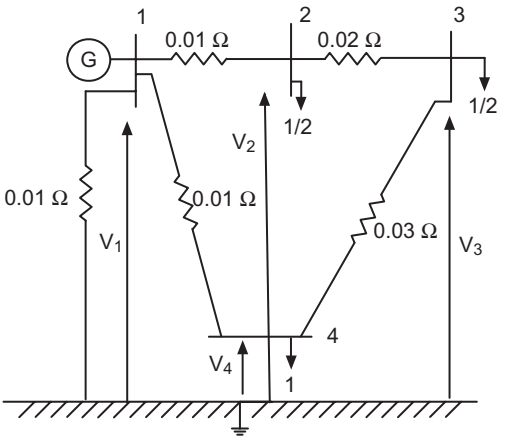

Figure 7.25 The Power Grid for Problem 7.5.

7.4 The radial feeder of Fig. 7.24 is connected to a local power grid rated at 11.3 kV distribution. Assume the base voltage of 15 kVA and a voltage base of 11.3 kV. Perform the following:

i) Compute the per unit model
ii) Write the number of equations that are needed to solve for the bus load voltages
iii) Compute the Y bus matrix
iv) Compute the matrix B′ and B″
v) Compute the bus voltages. Assume the power mismatch of 0.00001 per unit.
vi) Compute the power at bus 1
vii) Compute the total active and reactive power losses

7.5 For the power grid of Figure 7.25, perform the following:

i) Compute the bus admittance and bus impedance model for power flow studies
ii) Add a parallel line between bus 1 and bus 2 with the same impedance and compute the bus impedance model

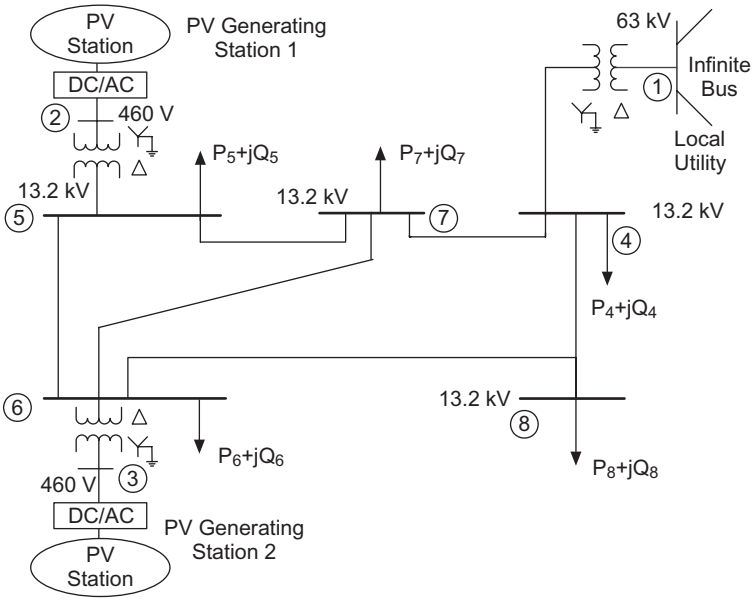

Figure 7.26 The System for Problem 7.6.

iii) What is the driving point impedance of bus 1 before and after adding the line?

iv) Remove the shunt element to ground and compute the bus admittance and bus impedance model

7.6 Consider the power grid depicted in Fig. 7.26.
Assume the following data:

a. The transformers connected to the PV generating station are rated at 460 V Y-grounded/13.2 kV Δ, have 10% reactance and 8 MVA capacity. The transformer connected to the power grid is 13.2 / 63 kV, 8 MVA, 10% reactance.

b. Assume the bus 5 load is 1.5 MW, 0.85 p.f lagging, the bus 6 load is 1.2 MW, 0.9 p.f. lagging, the bus 7 load is 2.4 MW, 0.9 p.f. leading, the bus 4 load is 1.5 MW, 0.85 p.f lagging, and the bus 8 load is 1.3 MW, 0.95 p.f. lagging.

c. Assume PV generating station 1 is rated at 0.95 MW and PV generating station 2 is rated at 3.5 MW.

d. Transmission line has a resistance of 0.0685 Ω/mile, reactance of 0.40 Ω/mile and half of line charging admittance (Y′/2) of 11×10^{-6} Ω^{-1}/mile. The line 4–7 is 4 miles, 4–8 is 2 miles, 5–6 is 4 miles, 5–7 is 1 mile, 6–7 is 3 miles, and 6–8 is 5 miles long.

Perform the following:

i) Find the per unit Y_{Bus} matrix

ii) Write a MATLAB program and compute the load bus voltages using FDLF

iii) If line 6–7 is out of service, compute the power flow through each transformer

iv) If 500 kVAr is added to bus 5, compute the bus load voltages

7.7 Consider a power grid where the system is modeled as $I_{Bus} = Y_{Bus} V_{Bus}$. For each bus k we have $I_k = \sum_{m=1}^{n} Y_{km} V_m$ and where m is the number of buses and Y_{km} is the element of Y_{Bus} matrix. For each bus k, we can also write:

$$P_k + jQ_k = V_k I_k^*$$

where P_k, and Q_k are real and reactive power is entering node k (* is a complex conjugate and $j = \sqrt{-1}$).

Let,

$$P_k + jQ_k = V_k \sum_{m=1}^{n} Y_{km}^* V_m^*$$

$$V_k = V_k e^{j\theta_k} = e_k + j f_k; \quad \theta_k = \tan^{-1} \frac{f_k}{e_k}$$

$$Y_{km} = Y_{km}\, e^{j\alpha_{km}} = G_{km} + j\, B_{km}; \alpha_{km} = \tan^{-1} \frac{B_{km}}{G_{km}}$$

Using the above in $P_k + jQ_k = V_k \sum_{m=1}^{n} Y_{km}^* V_m^*$

and obtain $P_k + jQ_k = V_k e^{j\theta_k} \sum_{m=1}^{n} Y_{km} e^{-j\alpha_{km}} V_m e^{-j\theta_m}$

Then using Taylor—Series expansion, express the power flow problem as

$$\Delta P_k = \sum_{m=1}^{n} H_{km} \Delta\theta_m + \sum_{m=1}^{n} N_{km} \frac{\Delta V_m}{V_m}$$

$$\Delta Q_k = \sum_{m=1}^{n} J_{km} \Delta\theta_m + \sum_{m=1}^{n} L_{km} \frac{\Delta V_m}{V_m}$$

And in compact form as

$$\begin{bmatrix}\Delta P\\ \Delta Q\end{bmatrix}=\begin{bmatrix}H & N\\ J & L\end{bmatrix}\cdot\begin{bmatrix}\Delta\theta\\ \dfrac{\Delta V}{V}\end{bmatrix}$$

$$\begin{bmatrix}\Delta P\\ \Delta Q\end{bmatrix}=\begin{bmatrix}\dfrac{\partial P}{\partial\theta} & \dfrac{\partial P}{\partial V}V\\ \dfrac{\partial Q}{\partial\theta} & \dfrac{\partial Q}{\partial V}V\end{bmatrix}\cdot\begin{bmatrix}\Delta\theta\\ \dfrac{\Delta V}{V}\end{bmatrix}$$

Show that for $m = k$, we have

$$H_{kk}=\frac{\partial P_k}{\partial\theta_k}=-Q_k-V_k^2B_{kk}$$

$$J_{kk}=\frac{\partial Q_k}{\partial\theta_k}=P_k-V_k^2G_{kk}$$

7.8 For the system given in Problem 7.7 show that for $m = k$, we have the following expressions

$$N_{kk}=\frac{\partial P_k}{\partial V_k}V_k=P_k+V_k^2G_{kk}$$

$$L_{kk}=\frac{\partial Q_k}{\partial V_k}V_k=Q_k-V_k^2B_{kk}$$

7.9 Consider the Problem 7.7, first let

$$I_m=a_m+jb_m=Y_{km}V_m$$

$$\text{and } Y_{km}V_m=(G_{km}+jB_{km})(e_m+jf_m)$$

$$Y_{km}V_m=(G_{km}e_m-B_{km}f_m)+j(B_{km}e_m+G_{km}f_m)$$

then using the following:

$$a_m=G_{km}\cdot e_m-B_{km}f_m$$

$$b_m=B_{km}\cdot e_m+G_{km}f_m$$

derive the following expressions:

$$H_{km}=\frac{\partial P_k}{\partial\theta_m}=a_mf_k-b_me_k$$

$$J_{km}=\frac{\partial Q_k}{\partial\theta_m}=-a_me_k-b_mf_k$$

7.10 For Problem 7.7 show that for m ≠ k, we have the following off-diagonal elements for the Jacobian matrix:

$$N_{km} = \frac{\partial P_k}{\partial V_m} V_m = a_m e_k + b_m f_k$$

$$L_{km} = \frac{\partial Q_k}{\partial V_m} V_m = a_m f_k - b_m e_k$$

7.11 For Problem 7.7 show that the off-diagonal elements of the Jacobian matrix for $m \neq k$ are:

$$\left.\begin{aligned} H_{km} &= L_{km} = a_m f_k - b_m e_k \\ N_{km} &= -j_{km} = a_m e_k + b_m f_k \end{aligned}\right\} Off - Diagonal\ Elements\ of\ Jacobian\ Matrix$$

And the diagonal elements of the Jacobian matrix for $m = k$ are:

$$\left.\begin{aligned} H_{kk} &= -Q_k - B_{kk} V_k^2 \\ L_{kk} &= Q_k - B_{kk} V_k^2 \\ N_{kk} &= P_k + G_{kk} V_k^2 \\ J_{kk} &= P_k - G_{kk} V_k^2 \end{aligned}\right\} Diagonal\ Elements\ of\ Jacobian\ Matrix$$

7.12 For Problem 7.7, compute the $P_{k(Calculated)}$ and $Q_{k(Calculated)}$ for each bus k as expressed below.

$$P_k = \sum_{m=1}^{n} [e_k (e_m G_{km} - f_m B_{km}) + f_k (e_m B_{km} + f_m G_{km})]$$

$$Q_k = \sum_{m=1}^{n} [f_k (e_k G_{km} - f_m B_{km}) - e_k (e_m B_{km} + f_m G_{km})]$$

where $V_k = e_k + j f_k$; $Y_{km}^* = G_{km} - j B_{km}$; $V_m^* = e_m - j f_m$

7.13 Assume that the power balance equation for a power system network can be written as

$$S = P + jQ = [V]^T [I^*] = [V]^T [YV]^*$$

where S is the complex power injection vector, P is the real power injection vector, Q is the reactive power injection vector, I is the current injection vector, V is the bus voltage vector, and $Y_{kj} = G_{kj} + j B_{kj}$ is the system admittance matrix.

Assume that in polar coordinate system, the complex voltage can be written as

$$V_k = V_k (\cos \theta_k + j \sin \theta_k)$$

Show that the calculated real and reactive powers can be expressed as

$$P_{k(Calculated)} = V_k \sum_{j=1}^{n} V_j (G_{kj} \cos\theta_{kj} + B_{kj} \sin\theta_{ij})$$

$$Q_{k(Calculated)} = V_k \sum_{j=1}^{n} V_j (G_{kj} \sin\theta_{kj} - B_{kj} \cos\theta_{ij})$$

where $\theta_{kj} \cong \theta_k - \theta_j$

And in the Cartesian coordinate system the calculated real and reactive powers can be expressed as

$$P_{k(Calculated)} = e_k \sum_{j=1}^{n} (G_{kj} e_j - B_{kj} f_j) + f_k \sum_{j=1}^{n} (G_{kj} f_j + B_{ik} e_j)$$

$$Q_{k(Calculated)} = f_k \sum_{j=1}^{n} (G_{kj} e_j - B_{kj} f_j) - e_k \sum_{j=1}^{n} (G_{kj} f_j + B_{kj} e_j)$$

where the bus voltage is given by

$$V_k = \mathrm{e}_k + j f_k$$

7.14 Consider the feeder given in Fig. 7.27.

System data: $V_1 = 1\angle 0$, $Z_{25} = 5 + j\ 10\ \Omega$, $Z_{34} = 2 + j\ 8\ \Omega$, $Z_{23} = 5.41 + j\ 3.34\ \Omega$, $S_2 = 3$ MVA, p.f. = 0.75 lagging; $S_3 = 3$ MVA, p.f. = 0.8 lagging; $S_4 = 4$ MVA, p.f. = 0.9 lagging; $S_5 = 2$ MVA, p.f. = 0.9 lagging; T_1; 63/20 kV, 10% reactance, 20 MVA; T_2 is the same as T_1

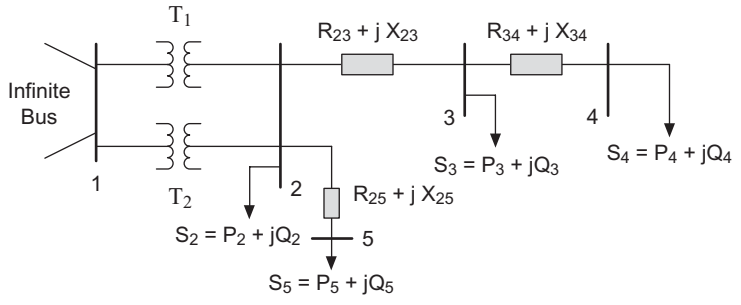

Figure 7.27 The Feeder of Problem 7.14.

Perform the following:

i) Calculate the per-unit equivalent circuit model. Use S_b equal to the MVA rating of transformer T_1.

ii) Let $V_1 = V_1\angle 0, V_K = V_{RK} + j\,V_{IK}, K = 2, 3, 4, 5$. Develop an equation in a Cartesian coordinate for $V_{RK} = f\,(V_{RK}, V_{IK})$, ΔP_K and ΔQ_K, $K = 2, 3, 4, 5$ for each bus. Use an iterative Gauss–Seidel approximation technique and compute bus voltages and system losses. Use five iterations and assume initial voltages are $V_K = 1\angle 0, K = 1, 2, 3, 4, 5$. Put your results in a table.

iii) Compute the Y_{Bus} B′ and B″ matrices and use the fast decoupled load flow technique to compute bus voltages. Make a table and compare your results with (ii) above. Use five iterations.

iv) Use the FDLF load flow technique and compute bus voltages after correcting the power factor of each bus to unity. Make a table and compare your results with (iii) above.

7.15 Consider the five-bus system depicted in Fig. 7.28.
Perform the following:

i) Calculate $Y_{Bus} = Y_r + j\,Y_i$ (internal Y bus), i.e., compute the Y_r and Y_i matrices

ii) Compute the Jacobian matrix [H, N, J, L]

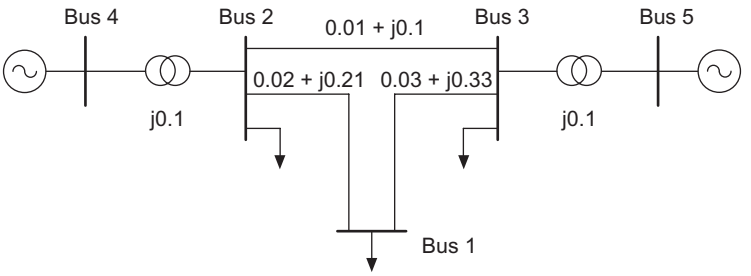

Figure 7.28 The System for Problem 7.15.

TABLE 7.11 Bus Data for a Five-Bus System.

Bus #	Bus Type	V_N (kV)	V (p.u)	θ (rad)	P_G (MW)	P_L (MW)	Q_L (MVAr)
Bus 1	PQ	138	—	—	—	160	80
Bus 2	PQ	138	—	—	—	200	100
Bus 3	PQ	138	—	—	—	370	130
Bus 4	PV	1	1.05	—	500	—	—
Bus 5	Swing	4	1.05	0.0	—	—	—

iii) Compute ΔP and ΔQ

iv) Solve the Newton–Raphson power flow for the five-bus system of Fig. 7.28

7.16 Consider the power grid given in Fig. 7.30.

a. Bus 1 is swing bus $V_1 = 1\angle 0$

b. Bus 2 is $P - V$ bus $|V_2| = 1.05$ and $P_{2(\text{Scheduled})} = 0.9$ p.u

c. Bus 2 Q_2 is assumed to be $-1 \leq Q_2 \leq 2$.

Compute:

i) The bus voltages using the decoupled Newton–Raphson method.

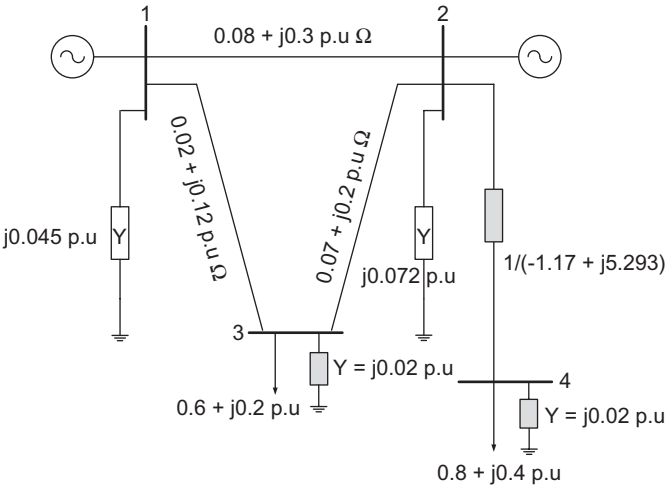

Figure 7.29 The System for Problem 7.16.

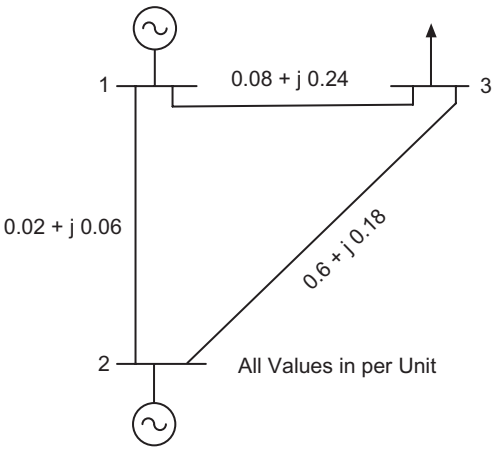

Figure 7.30 The Power Grid for Problem 7.17.

7.17 Consider the power grid given in Fig. 7.30.
Consider bus 1 as a swing bus with $1.05\angle 0$, bus 2 as $P - V$ with $P = 0.20$ and $|V_2| = 0.96$.
Compute:

i) The B′, B″, and Y_{Bus} matrices

ii) One iteration of a fast decoupled load flow. Assume the following starting voltages: $V_1 = 1.0\angle 0$, $V_2 = 0.9\angle 2°$, $V_3 = 0.9\angle -1.2°$. System losses are based on the computed voltages after the first iteration.

7.18 Consider the power system given in Fig. 7.30. Assume that bus 1 has a gas turbine generator. It has a load of 1 p.u; the bus voltage is fixed at 1 p.u and is the swing bus. Bus 2 has a number of PV generators with total injected power of 1.5 p.u into the bus. The transmission data is given in per unit as specified. Bus 3 has a number of loads with a total connected load of 2.0 p.u. Perform the following by writing a MATLAB simulation testbed. The maximum mismatch tolerance is 0.001. Perform the following:

i) Compute the system Y_{bus}

ii) Use the Gauss–Seidel Y_{bus} method and compute the bus 2 and 3 voltages

iii) Use the Gauss–Seidel Z_{Bus} method and compute the bus 2 and 3 voltages

iv) Use the Newton–Raphson method and compute the bus 2 and 3 voltages

v) Make a table and compare the above methods

vi) Determine the power provided by a swing generator

vii) Determine the total power losses

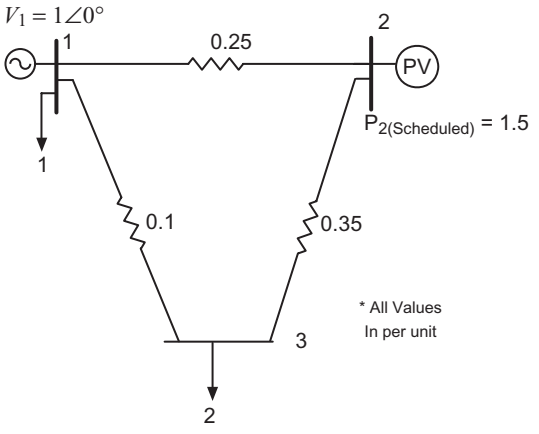

Figure 7.31 The One-Line Diagram of Problem 7.18.

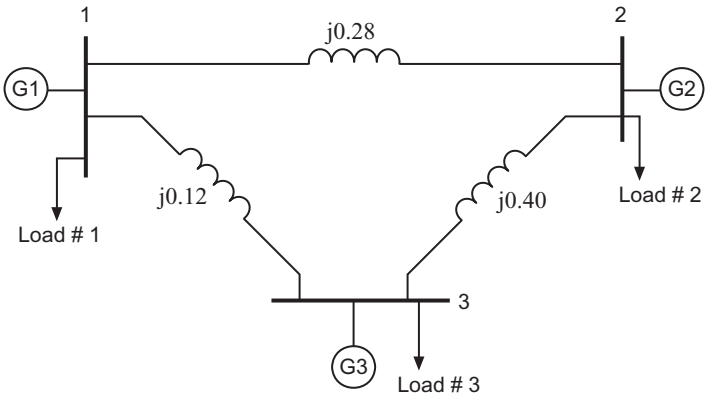

Figure 7.32 The Power Grid for Problem 7.19.

7.19 Consider the power system given in Fig. 7.32.
Assume $V_1 = 1\angle 0°$ *p.u* (*Swing Bus*). Also, assume transmission line impedances are given in per unit on 440 V, 100 MVA base ($S_b = 100\ MVA$ for the entire system)

Assume the generation and load schedules are as follows:

a. Bus 1: Load #1: 4 MVA, p.f. = 0.85 lagging
b. Bus 2: G2: 2 MW, p.f. = 0.95 lagging
   Load #2: 4 MVA, p.f. = 0.90 leading
c. Bus 3: G3: 1 MW, p.f. = 0.95 leading
   Load #3: 2 MVA, p.f. = 0.90 leading

Compute:

i) The bus voltages using the decoupled Newton–Raphson and Gauss–Seidel methods

7.20 Consider the system of Fig. 7.33.
Assume that generators internal reactance in p.u are 0.8. Assuming the load voltage is one p.u, compute the following:

i) The Y_{Bus} model for short-circuit studies.
ii) The Z_{Bus} model for short-circuit studies

7.21 For the radial power system given below, compute the following:

i) For the load of 500 W, which bus should be considered as an infinite bus?
ii) Assume the load voltage is to be maintained at its rated value. Which bus should be considered as an infinite bus?

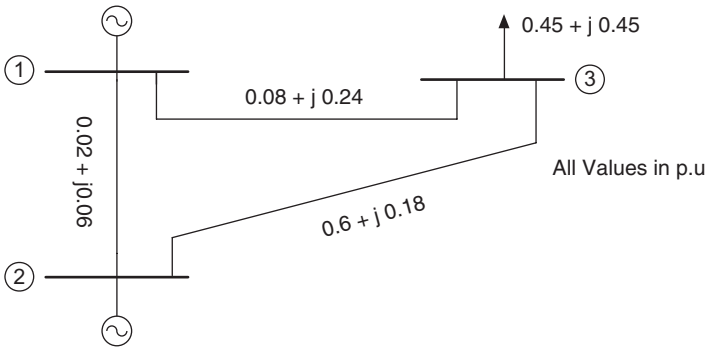

Figure 7.33 The System for Problem 7.20.

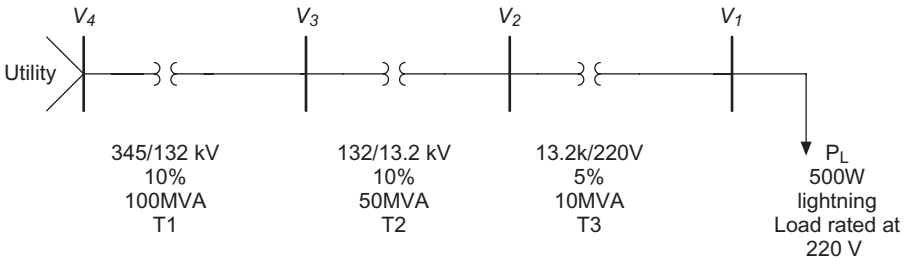

Figure 7.34 The System for Problem 7.21.

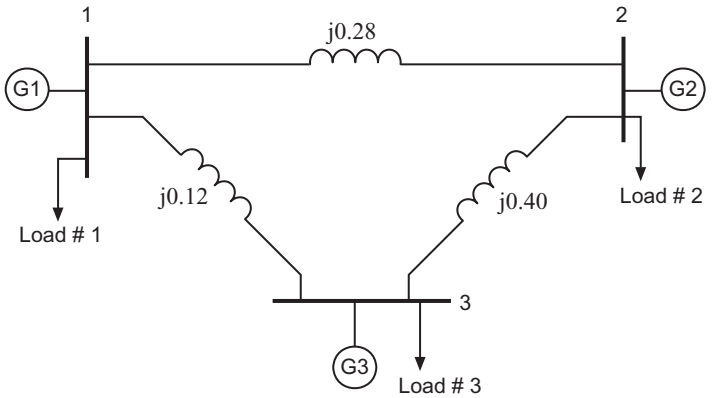

Figure 7.35 The System for Problem 7.22. All Values Are in Per Unit.

7.22 Consider the microgrid power system given in Fig. 7.35.
The transmission line impedances are given in per unit on 100 MVA base (S_b 100 MVA for the entire system.) The generation and load schedules are as follows:

a. Bus 1: Load #1: 4 MVA, p.f. = 0.85 lagging
b. Bus 2: G2: 2 MW, p.f. = 0.95 lagging, X = 10%
   Load #2: 4 MVA, p.f. = 0.90 leading
c. Bus 3: G3: 1 MW, p.f. = 0.95 leading, X = 25%
   Load #3: 2 MVA, p.f. = 0.90 leading

Compute the following:

i) Compute bus load voltages using the FDLF power flow method.
ii) Compute the load impedance of each load.

REFERENCES

1. Gross AC. Power system analysis. Hoboken, NJ: Wiley; 1986.
2. Grainger J, Stevenson WD. Power systems analysis. New York: McGraw Hill; 2008.
3. Dommel H, Tinny W. Optimal power flow solution. IEEE Transactions on Power Apparatus and Systems 1968; PAS-87(10):1866–1876.
4. Duncan Glover J, Sarma MS. Power system analysis and design. Pacific Grove, CA: Brooks/Cole Thomson Learning; 2002.
5. Weedy RM. Electric power systems. Hoboken, NJ: Wiley; 1970.
6. Heydt GT. Computer analysis methods for power systems. New York: Macmillan; 1986.
7. Stagg G, El-Abiad A. Computer methods in power system analysis. New York: McGraw Hill; 1968.
8. Tinney WF, Hart CE. Power flow solution by Newton's method. IEEE Transactions on Power Apparatus and Systems 1967; PAS-86:1449–1456.
9. Stott B. Review of load-flow calculation methods. Proceedings of the IEEE 1974; 62(7):916–929.
10. Chabert J-C, Barbin E. A history of algorithms: from the pebble to the microchip. New York/Heidelberg/ Berlin: Springer; 1999.
11. Khayyám, O. Rubáiyát of Omar Khayyám: A critical edition (FitzGerald E, Trans., Decker C, Ed.). Charlottesville, VA: University of Virginia Press; 1997.

ADDITIONAL RESOURCES

Adamiak M. Phasor measurement overview. Available at http://phasors.pnl.gov/Meetings/2004%20January/Phasor%20Measurement%20Overview.pdf. Accessed 2010 Oct 24.

Anderson PM, Fouad AA. Power system control and stability. 1st ed. Ames, IA: Iowa State University Press; 1977.

Bergen A, Vittal V. Power systems analysis. Englewood Cliffs, NJ: Prentice Hall; 2000.

Bohn R, Caramanis M, Schweppe F. Optimal pricing in electrical networks over space and time. Rand Journal on Economics 1984; 18(3):360–376.

Elgerd OI. Electric energy system theory: an introduction. 2d ed. New York: McGraw-Hill; 1982.

El-Hawary, Mohamed E. Electric power systems: design and analysis. Reston, VA: Reston Publishing; 1983.

Energy Information Administration, Official Energy Statistics from the US Government. Available at http://www.eia.doe.gov. Accessed 2010 Oct 7.

IEEE Brown Book. IEEE recommended practice for power system analysis. New York: Wiley-Interscience; 1980.

Institute for Electric Energy. Homepage. Available at http://www.edisonfoundation.net/IEE. Accessed 2010 Oct 7

Institute of Electrical and Electronics Engineers. IEEE Std 1451.1-1999, standard for a smart transducer interface for sensors and actuators–network capable application processor (NCAP) information model. Piscataway, NJ: IEEE; 1999.

Masters GM. Renewable and efficient electric power systems. New York: Wiley; 2004.

Midwest ISO. Available at http://toinfo.oasis.mapp.org/oasisinfo/MMTA_Transition_Plan_V2_3.pdf. Accessed 2010 Jan 12.

North American Electric Reliability Corp. (NERC). NERC 2008 Long-Term Reliability Assessment 2008–2017. Available at http://www.nerc.com/files/LTRA2008.pdf. Accessed 2010 Oct 8.

Nourai A, Schafer, C. Changing the electricity game. IEEE Power and Energy Magazine 2009; 7(4):42–47.

Phadke AG. Computer applications in power. IEEE Power & Energy Society 1993; 1(2):10–15.

Sauer P, Pai MA. Power systems dynamics and stability. Englewood Cliffs, NJ: Prentice Hall; 1998.

Schweppe FC, Wildes J. Power system static-state estimation, part I: exact model. IEEE Transactions on Power Apparatus and Systems 1970; PAS-89(1):120–125.

Shahidehpour M, Yamin H. Market operations in electric power systems: forecasting, scheduling, and risk management. New York/Piscataway, NJ: Wiley/IEEE; 2002.

Wood AJ, Wollenberg, BF. Power generation, operation, and control. New York: Wiley; 1996.

CHAPTER 8

POWER GRID AND MICROGRID FAULT STUDIES

8.1 INTRODUCTION

A fault in a power grid is any condition that results in abnormal operation. When energized parts of the system are accidently connected to the ground, two phase conductors are connected together, or a conductor is broken, the result is a faulted power grid. As an example, when a transmission line is accidentally grounded due to weather conditions, such as lightening from an electrical storm, the result is a flashover of the insulation and a flow of high fault currents.

When a fault or short-circuit occurs in a power grid, all synchronous generators contribute current directly to that fault until protective equipment acts to isolate the fault as quickly as possible. If the fault current is not isolated, the protective system of the power grid will trip (switch-off) the generators, and as a result, the balance between system loads and power generation is lost and the power grid is unstable. Most blackouts are the consequence of an unstable power grid. The power grid must be designed to operate successfully for the isolation of faults at the highest levels of current that can be anticipated for power grid operation. If the fault current exceeds the ability of breakers to extinguish the high fault current and to protect the grid, the result could be a catastrophic failure, fire, and permanent damage to significant portions of the power grid infrastructure. Therefore, before microgrids of distributed

Design of Smart Power Grid Renewable Energy Systems, First Edition. Ali Keyhani.

generation are connected to a local power grid, the fault current contribution must be calculated and mitigating measures must be taken prior to connection.

In fault studies of power grids, it is assumed that the power grids remain balanced except for the faulted point. Therefore, when a fault occurs, the power grid *must remain* balanced. As soon as a fault occurs, the faulted part of the power grid must be quickly isolated and removed from service. Therefore, in fault studies of power grids, we are working with an "if-then condition": if a point in a power grid is faulted, then we want to calculate the fault current and protect the power grid's equipment by isolating the faulted part of the system.[1–7]

The study of a faulted power grid is the topic of this chapter. In fault studies, we learn how a balanced three-phase network can be modeled as positive, negative, and zero sequence networks.

Most faults are a single line to ground or double lines that are faulted and then grounded. For any unbalanced fault current calculation that involves a ground, we use positive, negative, and zero sequence networks. Balanced three-phase faults are also used to size the circuit breakers. For balanced faults, we use the positive sequence network.

Solved examples and homework problems for symmetrical components; positive, negative, and zero sequence networks; and modeling balanced three-phase faults: single-line, double-line-to-ground faults, and double-line-to-line faults are given at the end of the chapter.

8.2 POWER GRID FAULT CURRENT CALCULATION

Figure 8.1 depicts a power grid and its circuit breakers. The elements of a power grid include generators, transformers, transmission lines, etc.—all of which must be protected so that if a fault occurs the fault currents can be isolated by the circuit breakers. For example, if a fault occurs because of a storm, e.g., a line between bus 3 and bus 4 are faulted, both circuit breakers will open by a control action issued from a ground relay fault current detection system. The main objective of the short-circuit study is to determine the power interruption capability of a circuit breaker at each switching location. To determine the required interrupting capability of breakers, a three-phase fault is assumed at each bus to calculate the maximum fault current. All breakers connected to the bus must be able to interrupt the fault current. For a protective relay system to issue control commands, the voltages and currents for balanced and unbalanced faults at many locations in the power grid must be determined.

To compute the short-circuit current flow through a power grid due to three-phase balanced and unbalanced faults, the power grid system must be modeled to reflect the intended study. The types of faults are a three-phase balanced fault and an unbalanced fault. Figure 8.2 depicts a balanced fault at

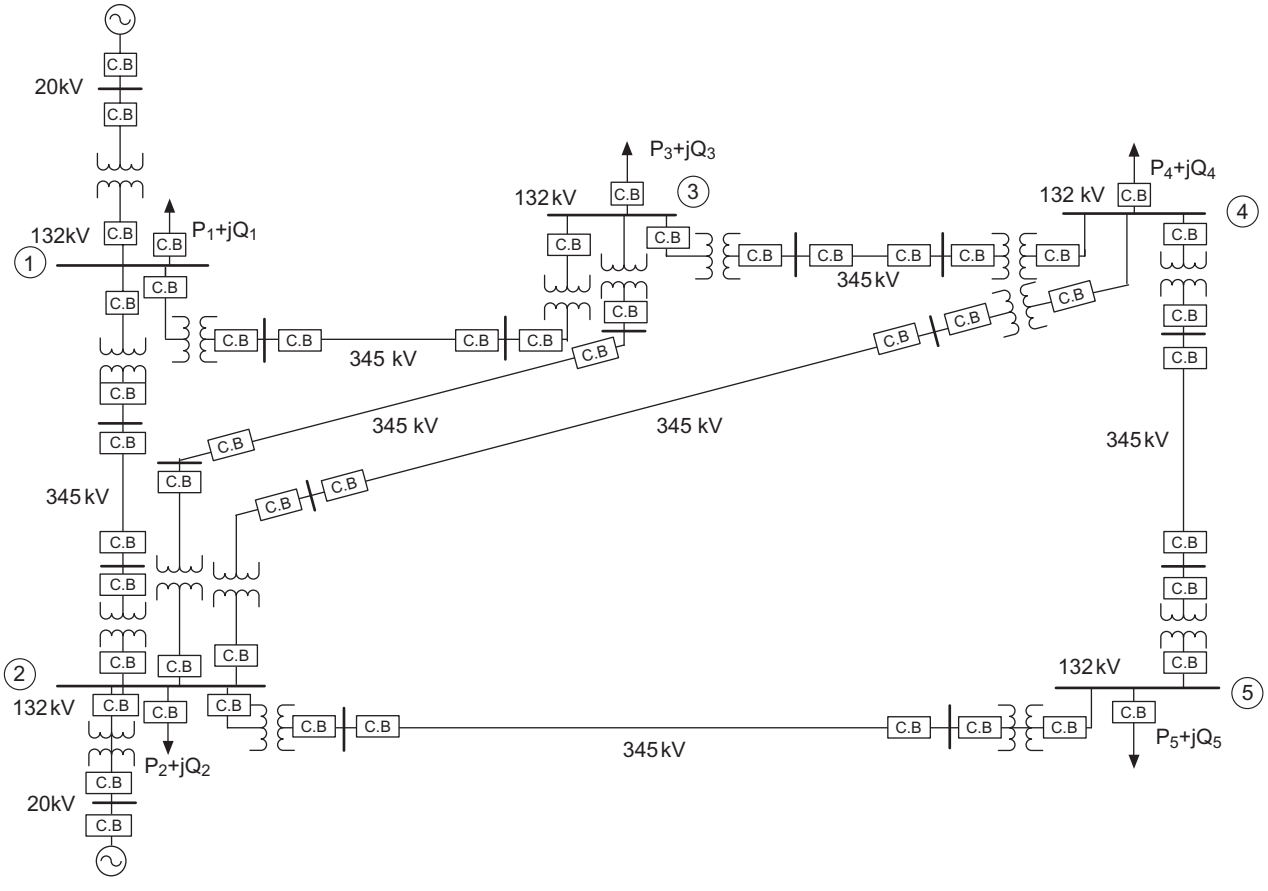

Figure 8.1 A Power Grid with Its Associated Circuit Breakers.

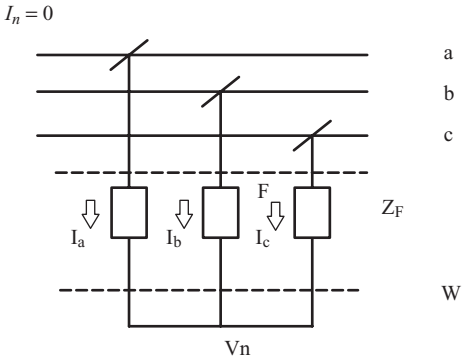

Figure 8.2 A Balanced Three-Phase Fault.

a bus of a power grid where the three phases, a, b, and c are shown. We know that in a balanced power grid, the sum of phase a, phase b, and phase c currents adds up to zero. Therefore, the neutral current is zero and

$$I_n = I_a + I_b + I_c$$

is noted as I_n. If the system is unbalanced, the neutral current will flow through the neutral conductor. However, if a balanced fault occurs in a balanced power grid, the neutral point where three phases are connected is at zero potential and neutral current will not flow.

$$I_n = 0$$

The dashed lines marked by "w" in Figure 8.2 delineate the section of a three-phase system that has a fault.

Figure 8.3 depicts a single line to ground fault. For an if-then study of a single line to ground fault, the phase designation is arbitrary. In single line to ground fault studies, it is customary to designate the faulted phase at phase a, with the two other phases operating as normal. The dashed lines marked by "w" depicted in Figure 8.3 delineate the faulted phase. Because phase a is faulted, the ground current flow is equal to the fault current of phase a.

Figure 8.4 depicts a double line to ground fault. For an if-then study of a double line to ground fault, again, the phase designation is arbitrary. In double line to ground fault studies, it is customary to designate the faulted phases as phases b and c, with phase a operating as normal. The dashed lines marked by "w" in Figure 8.4 delineate the section and the phases with faults in a three-phase system. Because phases b and c are faulted to ground, the ground current flow is equal to the sum of the fault currents of phases b and c.

Figure 8.5 depicts faulted double lines. For an if-then study of double lines, again, the phase designation is arbitrary. In double-line fault studies, it is customary to designate the faulted phases on phases b and c, with phase a

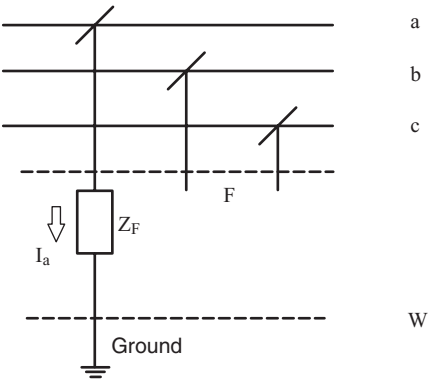

Figure 8.3 An Unbalanced Fault: One Line to Ground.

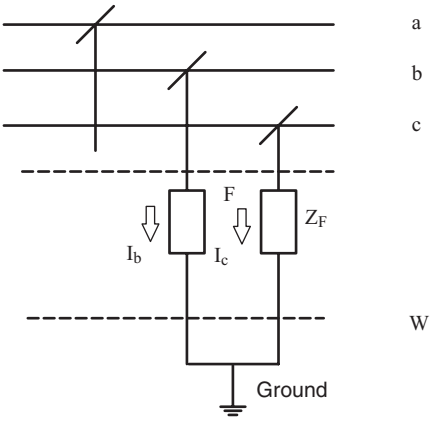

Figure 8.4 An Unbalanced Fault: Two Lines to Ground.

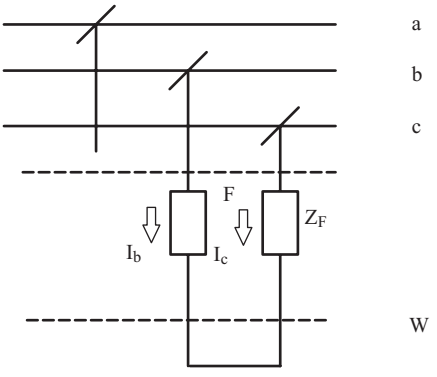

Figure 8.5 An Unbalanced Fault: Line to Line.

operating as normal. The dashed lines marked by "w" in Figure 8.5 delineate the section and the phases with faults in a three-phase system. Because phase a and the faulted phases are not connected to ground, the ground current will not flow. The fault current is equal to phase b current. The phase c current is the negative of phase b. To calculate fault currents, we must model the system using symmetrical components. We will study this topic next.

8.3 SYMMETRICAL COMPONENTS

In 1918, Charles Legeyt Fortescue[8] described how a set of three unbalanced phasors could be expressed as the sum of three symmetrical sets of balanced phasors. These three sets are defined as a positive sequence, a negative sequence, and a zero sequence. In essence, Fortescue's method converts three unbalanced phases into three independent balanced sets. Although in practice, power grids are not completely balanced, a balanced approximation is an acceptable engineering solution.

In a balanced system, it is assumed that every element of the power grid is balanced. Generators are designed to generate a balanced set of voltages: all phase voltages have the same magnitude and are 120 degrees apart. Similarly, the three-phase transmission lines are balanced: each line has the same impedance and admittance. However, in practice, the spacing of the lines may not be the same; hence, unbalanced inductances and therefore line impedances will result. However, the lines are transposed as they are hung on transmission line towers or poles, i.e., the positions of phases a, b, and c are changed every few miles. This results in approximately balanced spacing and balanced inductance per mile. Three-phase transformers and loads are also balanced. The transposition of three-phase transmission lines was discussed in Chapter 2.

The loads in secondary distribution systems are not balanced. However, as a first approximation, we can assume the loads are also balanced because power grids are designed as balanced systems. Therefore, as we discussed in the previous chapter, the balanced three-phase system can be analyzed by analyzing phase a with respect to ground. However, if a line in the system has been damaged during a storm and falls on the ground, the system will become unbalanced. The unbalanced systems are analyzed using the symmetrical components of the power grid. For example, on line to ground faults, we compute the ground current and then set the protection system to isolate the faults by opening the circuit breakers on both ends of the line. However, we need to isolate the faulted line in a very short time—within a few cycles—to prevent damage to any of the power grid equipment. This requirement dictates that the system must remain balanced during the faults; only the unbalanced part of the power grid is the faulted segment. This is a key concept in the calculation of fault current. First, we need to develop an impedance model of a balanced system and model the different fault types. Once that is done, we will better understand how to construct a model of faulted systems.

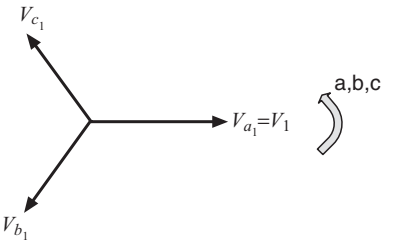

Figure 8.6 Three-Phase Voltage Presented in Terms of Positive Sequence Quantities.

The basic concepts of symmetrical components can be introduced by presenting the three-phase systems in terms of positive, negative, and zero sequences.[1–7] Normally, the designation of "1" or "+" is used to present the positive sequence variables of voltage, current, and impedance. The balanced three-phase voltages can be expressed as shown in Figure 8.6.

Figure 8.6 depicts a positive sequence voltage with phase a as the reference followed by phase b and then phase c. The phase voltages, a, b, and c are given by equations

$$V_a = V_{a_1} = V\angle 0° = V_1\angle 0° \tag{8.1}$$

$$V_b = V_{b_1} = V_1\angle 240° \tag{8.2}$$

$$V_c = V_{c_1} = V_1\angle 120° \tag{8.3}$$

Let $a = 1\angle 120°$ and $a^2 = 1\angle 240°$, then we have

$$V_{a_1} = V_1 \qquad V_{b_1} = a^2 V_1 \qquad V_{c_1} = aV_1 \tag{8.4}$$

Rearranging the above in matrix form, we have

$$\begin{bmatrix} V_{a_1} \\ V_{b_1} \\ V_{c_1} \end{bmatrix} = \begin{bmatrix} 1 \\ a^2 \\ a \end{bmatrix} V_1 \tag{8.5}$$

The negative sequence voltage is presented by designating "2" or a negative sign ("-") as a subscript or superscript. The negative sequence is depicted in Figure 8.7.

From Figure 8.7, we can write the following:

$$V_{a_2} = V_2 \tag{8.6}$$

$$V_{b_2} = aV_2 \tag{8.7}$$

$$V_{c_2} = a^2 V_2 \tag{8.8}$$

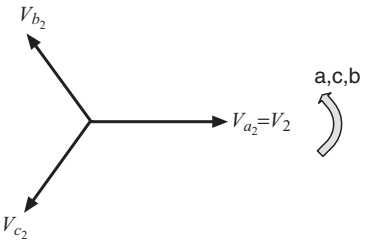

Figure 8.7 Three-Phase Voltage Presented in Terms of Negative Sequence Quantities.

When the above is expressed in matrix form, we have

$$\begin{bmatrix} V_{a_2} \\ V_{b_2} \\ V_{c_2} \end{bmatrix} = \begin{bmatrix} 1 \\ a \\ a^2 \end{bmatrix} V_2 \tag{8.9}$$

The zero sequence voltages are presented by a set of voltages that are in phase. The zero sequence voltages are designated by "0." The zero sequence voltages are

$$V_{a_o} = V_o \tag{8.10}$$

$$V_{b_o} = V_o \tag{8.11}$$

$$V_{c_o} = V_o \tag{8.12}$$

Using the above presentation, a set of three-phase voltages can be expressed in terms of its sequence voltages. In general, a set of unbalanced voltages, V_a, V_b, V_c can be written as

$$V_a = V_{a_o} + V_{a_1} + V_{a_2} \Rightarrow V_a = V_o + V_1 + V_2 \tag{8.13}$$

$$V_b = V_{b_o} + V_{b_1} + V_{b_2} \Rightarrow V_b = V_o + a^2 V_1 + aV_2 \tag{8.14}$$

$$V_c = V_{c_o} + V_{c_1} + V_{c_2} \Rightarrow V_c = V_o + a\ V_1 + a^2 V_2 \tag{8.15}$$

The above equations can be expressed in compact matrix form as

$$\begin{bmatrix} V_a \\ V_b \\ V_c \end{bmatrix} = \begin{bmatrix} 1 & 1 & 1 \\ 1 & a^2 & a \\ 1 & a & a^2 \end{bmatrix} \begin{bmatrix} V_o \\ V_1 \\ V_2 \end{bmatrix} \tag{8.16}$$

We can designate the matrix transformation by T and present as

$$T = \begin{bmatrix} 1 & 1 & 1 \\ 1 & a^2 & a \\ 1 & a & a^2 \end{bmatrix} \tag{8.17}$$

Therefore, the three-phase voltages can be expressed in terms of their sequence variables as given below:

$$[V_{abc}] = [T][V_{012}] \tag{8.18}$$

We can multiply the above by the inverse of matrix T.

$$\begin{aligned} [T]^{-1}[V_{abc}] &= [T]^{-1}[T][V_{012}] \\ [V_{012}] &= [T]^{-1}[V_{abc}] \\ [T]^{-1} &= \tfrac{1}{3}\begin{bmatrix} 1 & 1 & 1 \\ 1 & a & a^2 \\ 1 & a^2 & a \end{bmatrix} \end{aligned} \tag{8.19}$$

Therefore the sequence voltages are

$$\begin{aligned} V_o &= \tfrac{1}{3}(V_a + V_b + V_c) \\ V_1 &= \tfrac{1}{3}(V_a + aV_b + a^2V_c) \\ V_2 &= \tfrac{1}{3}(V_a + a^2V_b + aV_c) \end{aligned} \tag{8.20}$$

Similarly, we can compute the symmetrical components of current in terms of three-phase currents:

$$\begin{aligned} [I_{abc}] &= [T][I_{012}] \\ [I_{012}] &= [T]^{-1}[I_{abc}] \end{aligned} \tag{8.21}$$

Example 8.1 Consider a balanced, Y-connected, 460 V generator. Compute the positive, negative, and zero sequence voltages.

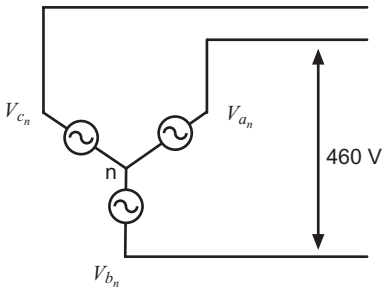

Figure 8.8 The Three-Phase Generator of Example 8.1.

Solution

Let us assume that phase a is selected as the reference phase. The phase a, b, and c voltages are

$$V_{a_n} = \frac{460}{\sqrt{3}}\angle 0° = 265.9\angle 0°$$
$$V_{b_n} = 265.9\angle 240° = 265.9\,a^2$$
$$V_{C_n} = 265.9\angle 120° = 265.9\,a$$

The sequence voltages can be computed as

$$\begin{bmatrix} V_o \\ V_1 \\ V_2 \end{bmatrix} = \frac{1}{3}\begin{bmatrix} 1 & 1 & 1 \\ 1 & a & a^2 \\ 1 & a^2 & a \end{bmatrix}\begin{bmatrix} V_{a_n} \\ V_{b_n} \\ V_{c_n} \end{bmatrix} \tag{8.22}$$

$$V_o = \frac{1}{3}\left(265.9 + 265.9\,a^2 + 265.9\,a\right)$$
$$= \frac{265.9}{3}\left(1 + a + a^2\right) = 0 \Rightarrow V_o = 0$$

Since $\left(1 + a + a^2\right) = 0$

$$V_1 = \frac{1}{3}\left(265.9 + 265.9a^3 + 265.9a^3\right)$$

Since $a^3 = 1\angle 0°$, therefore $V_1 = 265.9\angle 0°$

Since $a^4 = a = 1\angle 120°$, therefore, for the negative sequence voltages we have

$$V_2 = \frac{1}{3}\left(265.9 + 265.9\,a^4 + 265.9\,a^2\right)$$
$$V_2 = \frac{1}{3}\left[265.9\left(1 + a + a^2\right)\right] = 0$$

We can conclude that for three-phase balanced voltages, the positive voltage sequence is the only source of power to the grid.

The transformation of the three-phase system to a symmetrical component can be used to show the relationship between the two systems. The three-phase power expressed in terms of phase a, phase b, and phase c can be expressed as

$$S_{3\varphi} = \left[V_a I_a^* + V_b I_b^* + V_c I_c^*\right] \tag{8.23}$$

In matrix notation, we have

$$S_{3\varphi} = \left[V_{abc}\right]^T \left[I_{abc}\right]^*$$

We can use the symmetrical transformation for both voltage and current and obtain the power in a symmetrical system.

$$\begin{aligned} S_{3\varphi} &= [V_{012}]^T [T]^T [T]^* [I_{012}]^* \\ S_{3\varphi} &= 3\left[V_0 I_0^* + V_1 I_1^* + V_2 I_2^*\right] = 3[S_{012}] \end{aligned} \tag{8.24}$$

8.4 SEQUENCE NETWORKS FOR POWER GENERATORS

Figure 8.9 depicts an impedance model of a synchronous generator. The impedance, Z_n, is the grounding impedance. Its function is to limit the ground current fault if a ground fault occurs in the generator. The model depicts the steady-state operation of the generator. In this model, the shaft speed, ω_m and the field current I_f are constant. The generator supplies balanced three-phase voltages. Using the equivalent model depicted in Figure 8.9, we can write the following:

$$\begin{aligned} E_a &= (R_a + jX_s + Z_n) I_a + (jX_m + Z_n) I_b + (jX_m + Z_n) I_c + V_a \\ E_b &= (R_a + jX_s + Z_n) I_b + (jX_m + Z_n) I_a + (jX_m + Z_n) I_c + V_b \\ E_c &= (R_a + jX_s + Z_n) I_c + (jX_m + Z_n) I_a + (jX_m + Z_n) I_b + V_c \end{aligned} \tag{8.25}$$

Let us assume that the generator is supplying balanced three-phase voltages as depicted in Figure 8.10. The supply voltage of each phase can be expressed as

$$\begin{aligned} E_a &= E \\ E_b &= a^2 E \\ E_c &= aE \end{aligned} \tag{8.26}$$

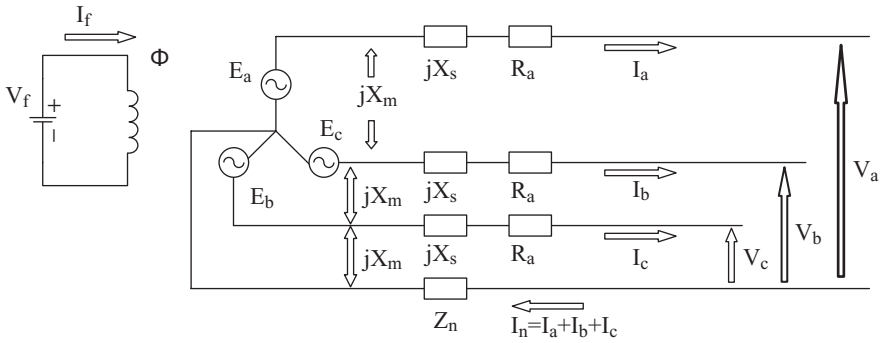

Figure 8.9 A Synchronous Generator Reactance Model.

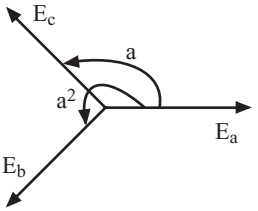

Figure 8.10 A Balanced Three-Phase Generator.

We can rewrite the Z_s and Z_m as

$$Z_s = R_a + jX_s + Z_n$$
$$Z_m = jX_m + Z_n$$

Then the set of equations given by Equation 8.25 can be written as

$$\begin{bmatrix} E_a \\ E_b \\ E_c \end{bmatrix} = \begin{bmatrix} Z_s & Z_m & Z_m \\ Z_m & Z_s & Z_m \\ Z_m & Z_m & Z_s \end{bmatrix} \begin{bmatrix} I_a \\ I_b \\ I_c \end{bmatrix} + \begin{bmatrix} V_a \\ V_b \\ V_c \end{bmatrix} \tag{8.27}$$

The set of equations presented by Equation 8.27 can be expressed in a matrix form

$$[E_{abc}] = [Z_{abc}][I_{abc}] + [V_{abc}] \tag{8.28}$$

Substituting $[I_{abc}] = [T_s][I_{012}]$ in Equation 8.28 and then pre-multiplying by $[T_s]^{-1}$, we have

$$[T_s]^{-1}[E_{abc}] = [T_s]^{-1}[Z_{abc}][T_s][I_{012}] + [T_s]^{-1}[V_{abc}] \tag{8.29}$$

Recall the transformation from abc to 012 as given below.

$$[T_s]^{-1} \cdot [E_{abc}] = [T_s]^{-1} \cdot [T_s] \cdot [E_{012}]$$
$$[E_{012}] = [T_s]^{-1} \cdot [E_{abc}]$$
$$[T_s]^{-1} = \frac{1}{3} \begin{bmatrix} 1 & 1 & 1 \\ 1 & a & a^2 \\ 1 & a^2 & a \end{bmatrix}$$

Because the generator is supplying balanced three-phase voltages, the right-hand side of Equation 8.29, can be written as the generator sequence voltages as given by Equation 8.30.

$$\begin{bmatrix} E_0 \\ E_1 \\ E_2 \end{bmatrix} = \frac{1}{3}\begin{bmatrix} 1 & 1 & 1 \\ 1 & a & a^2 \\ 1 & a^2 & a \end{bmatrix}\begin{bmatrix} E \\ a^2E \\ aE \end{bmatrix} = \frac{E}{3}\begin{bmatrix} 0 \\ 3 \\ 0 \end{bmatrix} = \begin{bmatrix} 0 \\ E \\ 0 \end{bmatrix} \tag{8.30}$$

We can rewrite the expression $[T]^{-1}[Z_{abc}][T] = [Z_{012}]$ as expressed by Equation 8.31

$$[T]^{-1}[Z_{abc}][T] = [Z_{012}] = \begin{bmatrix} Z_0 & 0 & 0 \\ 0 & Z_1 & 0 \\ 0 & 0 & Z_2 \end{bmatrix} \tag{8.31}$$

where $Z_0 = Z_{0,Gen} + 3Z_n$ and $Z_{0,Gen} = R_a + j(X_s + 2X_m)$ and

$$\begin{aligned} Z_0 &= R_a + j(X_s + 2X_m) + 3Z_n \\ Z_1 &= Z_s - Z_m = R_a + j(X_s - X_m) \\ Z_2 &= Z_s - Z_m = R_a + j(X_s - X_m) \end{aligned} \tag{8.32}$$

Now Equation 8.29 can be written as

$$\begin{bmatrix} 0 \\ E \\ 0 \end{bmatrix} = \begin{bmatrix} Z_0 & 0 & 0 \\ 0 & Z_1 & 0 \\ 0 & 0 & Z_2 \end{bmatrix}\begin{bmatrix} I_0 \\ I_1 \\ I_2 \end{bmatrix} + \begin{bmatrix} V_0 \\ V_1 \\ V_2 \end{bmatrix} \tag{8.33}$$

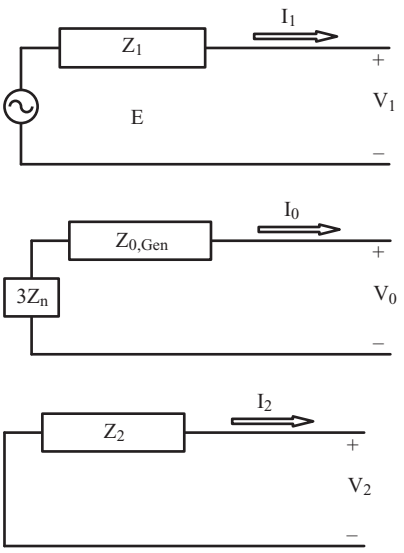

Figure 8.11 The Positive, Zero, and Negative Sequences of a Generator.

The above system of equations will result in the following sequence of zero, positive, and negative networks.

$$Z_0 I_0 + V_0 = 0$$
$$Z_1 I_1 + V_1 = E$$
$$Z_2 I_2 + V_2 = 0$$

Therefore, when the three-phase generator supplies balanced three-phase voltages, only the positive sequence network is excited by positive sequence voltage, that is the same as phase a of the three-phase system.

8.5 THE MODELING OF A PHOTOVOLTAIC GENERATING STATION

In Chapter 5, we studied the modeling of photovoltaic- (PV-) generating modules. We learned that the PV-module input impedance is purely resistive; it is a function of the input irradiance and temperature of the module. In Chapter 3, we studied the operation of DC/AC inverters. We modeled inverters using ideal power switches. Because inverters are operating at zero frequency on the DC side and at the power grid frequency on the AC side, the disturbance on the AC side has a limited propagation to the DC side. In fact, the DC/AC inverters block the propagation of disturbance. At the same time, because there is no inertia energy and the stored energy in PV arrays is limited to irradiance energy, the fault current contribution of PV is quite low. Therefore, the input impedance of PV-generating stations is high. Figures 8.12 and 8.13 depict PV-generating stations. For estimating the fault current contributions of PV-generating stations, we need to model the input impedance of PV-generating stations from measured operating data. The modeling of PV-generating stations is currently being investigated. Students can find updated models for PV and wind-generation systems from the National Renewable Energy Laboratory (NREL) website, *www.nrel.gov*. However, we can safely use a high impedance model using the model developed in Chapter

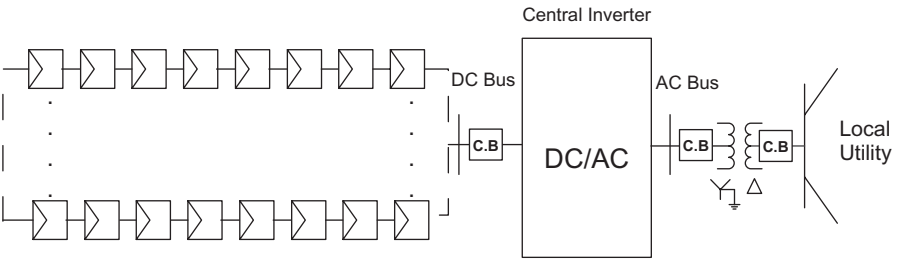

Figure 8.12 A Central DC/AC Inverter for a Large-Scale Photovoltaic Power Configuration.

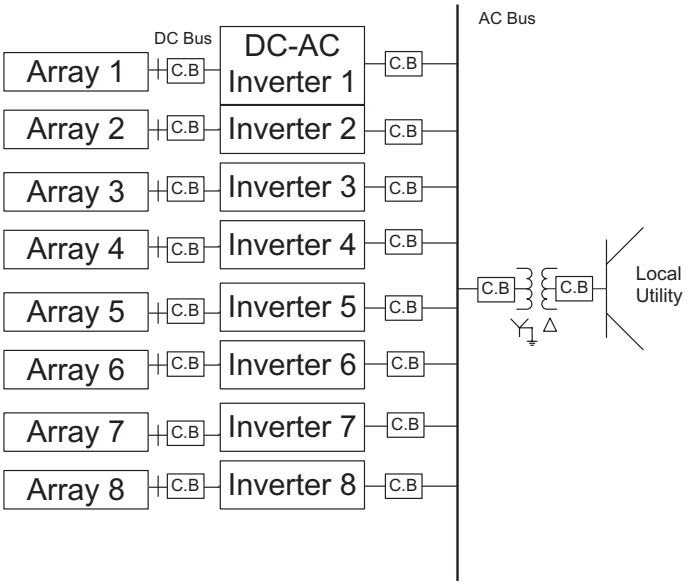

Figure 8.13 The General Structure of Photovoltaic Arrays with Inverters.

5 for the PV module operating at maximum PV-generating station voltage and current.

8.6 SEQUENCE NETWORKS FOR BALANCED THREE-PHASE TRANSMISSION LINES

Figure 8.14 depicts the balanced three-phase network model of a transmission line. The voltage equations expressing the voltage drop across the lines can be expressed as given by Equation 8.34.

$$\begin{aligned} V_a &= jX_sI_a + jX_mI_b + jX_mI_c + V_a' \\ V_b &= jX_sI_b + jX_mI_a + jX_mI_c + V_b' \\ V_c &= jX_sI_c + jX_mI_a + jX_mI_b + V_c' \end{aligned} \tag{8.34}$$

The set of equation can be expressed in a compact matrix as given below.

$$\begin{bmatrix} V_a \\ V_b \\ V_c \end{bmatrix} - \begin{bmatrix} V_a' \\ V_b' \\ V_c' \end{bmatrix} = j \begin{bmatrix} X_s & X_m & X_m \\ X_m & X_s & X_m \\ X_m & X_m & X_s \end{bmatrix} \begin{bmatrix} I_a \\ I_b \\ I_c \end{bmatrix} \tag{8.35}$$

$$[V_{abc}] - [V_{abc}'] = [Z_{abc}][I_{abc}] \tag{8.36}$$

$$[V_{abc}] = [T_s][V_{012}] \tag{8.37}$$

$$[I_{abc}] = [T_s][I_{012}] \tag{8.38}$$

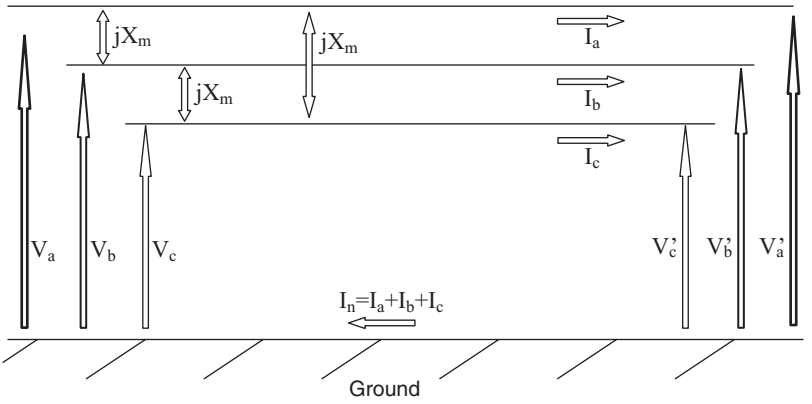

Figure 8.14 A Balanced Three-Phase Transmission Reactance Model.

Replace V_{abc} with Equation 8.37 and I_{abc} with Equation 8.38 to obtain:

$$[T_s][V_{012}]-[T_s][V'_{012}]=[Z_{abc}][T_s][I_{012}] \tag{8.39}$$

Multiplying Equation 8.39 by $[T_s]^{-1}$:

$$[T_s]^{-1}[T_s][V_{012}]-[T_s]^{-1}[T_s][V'_{012}]=[T_s]^{-1}[Z_{abc}][T_s][I_{012}]$$

Since $[Ts]^{-1}[Ts]=$ Identity Matrix
we obtain:

$$[V_{012}]-[V'_{012}]=[Z_{abc}][I_{012}] \tag{8.40}$$

$$[Z_{012}]=[T_s]^{-1}[Z_{abc}][T_s]$$

$$Z_{012}=\frac{1}{3}\begin{bmatrix}1 & 1 & 1\\ 1 & a & a^2\\ 1 & a^2 & a\end{bmatrix} j \begin{bmatrix}X_s & X_m & X_m\\ X_m & X_s & X_m\\ X_m & X_m & X_s\end{bmatrix}\begin{bmatrix}1 & 1 & 1\\ 1 & a^2 & a\\ 1 & a & a^2\end{bmatrix} \tag{8.41}$$

Equation 8.40 simplifies as

$$Z_{012}=\frac{j}{3}\begin{bmatrix}X_s+2X_m & X_s+2X_m & X_s+2X_m\\ X_s-X_m & aX_s+\left(1+a^2\right)X_m & a^2X_s+(1+a)X_m\\ X_s-X_m & a^2X_s+(1+a)X_m & aX_s+\left(1+a^2\right)X_m\end{bmatrix}\begin{bmatrix}1 & 1 & 1\\ 1 & a^2 & a\\ 1 & a & a^2\end{bmatrix}$$

After further simplification, we obtain:

$$Z_{012}=j\begin{bmatrix}X_s+2X_m & 0 & 0\\ 0 & X_s-X_m & 0\\ 0 & 0 & X_s-X_m\end{bmatrix} \tag{8.42}$$

Therefore, the symmetrical sequence network model of a transmission line can be expressed as

$$\begin{bmatrix} V_0 \\ V_1 \\ V_2 \end{bmatrix} - \begin{bmatrix} V_0' \\ V_1' \\ V_2' \end{bmatrix} = j \begin{bmatrix} X_s + 2X_m & 0 & 0 \\ 0 & X_s - X_m & 0 \\ 0 & 0 & X_s - X_m \end{bmatrix} \begin{bmatrix} I_0 \\ I_1 \\ I_2 \end{bmatrix} \tag{8.43}$$

And zero, positive, and negative sequence model networks are

$$Z_0 = \text{Zero Sequence Impedance} = j(X_s + 2X_m) \tag{8.44}$$

$$Z_1 = \text{Positive Sequence Impedance} = j(X_s - X_m) \tag{8.45}$$

$$Z_2 = \text{Negative Sequence Impedance} = j(X_s - X_m) \tag{8.46}$$

Figure 8.15 depicts the sequence networks for a transmission line's zero, positive, and negative circuit models.

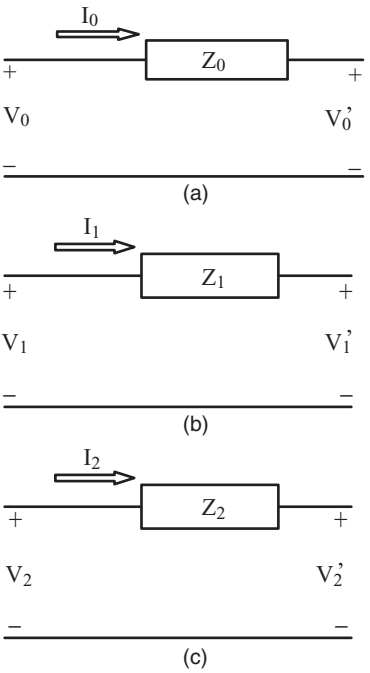

Figure 8.15 The Sequence Networks for a Transmission Line's **(a)** Zero, **(b)** Positive, and **(c)** Negative Circuit Models.

8.7 GROUND CURRENT FLOW IN BALANCED THREE-PHASE TRANSFORMERS

The neutral point of a power grid is often connected to earth ground. Often ground and neutral are the same electrical point if there is no ground impedance between neutral and the earth ground point. The conductor that connects the power grid's neutral point and ground will not carry load current; its function is to detect the ground fault current. If a power grid is faulted and the faulted bus is connected to ground, then the first question of interest is how ground current fault will flow through the power grid.

The transformers' high and low voltage sides are not electrically connected. The voltages induced in either side of the transformers are due to magnetic coupling of respective windings. Consider a Y-Y-connected transformer depicted in Fig. 8.16. Let us assume the three-phase voltages supplied to the three-phase transformers are not balanced.

Let us also assume that the transformer is grounded on the high voltage side and it is not grounded on the low voltage side as shown in Fig. 8.16. The question is whether ground current can flow in the transformer when it is grounded on the generator side (high voltage side) and its low voltage side is not grounded. To answer this question, we need to remember that in transformers, voltage is induced in the low voltage side by magnetic induction and resulting currents that are flowing must obey the Kirchhoff current law. This means the current must return to its generating source. Therefore, the ground current cannot flow in either the high voltage side or the low voltage side. If the ground current flows in the low voltage side, it must return to neutral on the low voltage side. However, if the low voltage side is not grounded, it cannot complete the flow path. Therefore, if there is no flow path for the ground current, then the low voltage side neutral will be at a value that will satisfy the following:

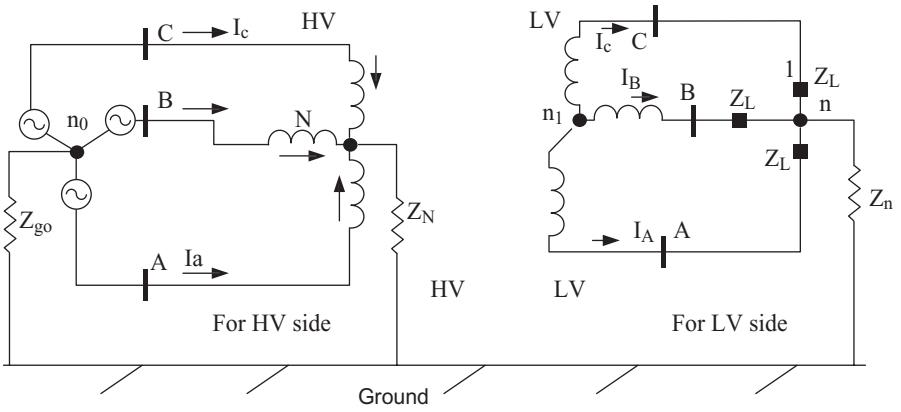

Figure 8.16 The Y-Y-Connected Transformer with High Voltage Side Grounded and Low Voltage Side Not Grounded.

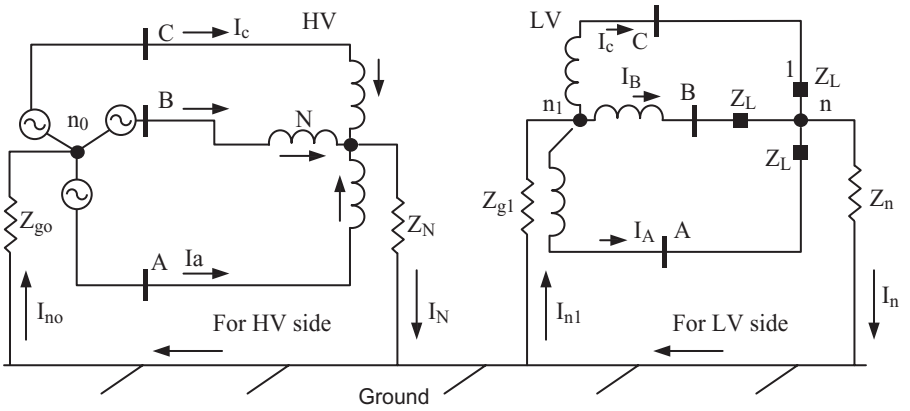

Figure 8.17 The Y-Y-Connected Transformer with the High Voltage Side and the Low Voltage Side Grounded.

$$V_n = V_{an} + V_{bn} + V_{cn} \tag{8.47}$$

By the same reasoning, the ground current cannot flow on the high voltage side. If there is ground current flowing on the high voltage side, the magnetic coupling must induce the three-phase voltages on the low side and have the low-side phase current flowing, which will add up and result in ground current flow on the low voltage side. However, the low voltage side is not grounded; therefore, the low-side voltages will add up as given in Equation 8.47.

Now consider a case where both high and low voltage sides are grounded, and ground current can flow on both sides as shown in Fig. 8.17.

8.8 ZERO SEQUENCE NETWORK

8.8.1 Transformers

We have concluded that for a Y-Y transformer with grounded neutral on one side and ungrounded neutral on the other side, the ground current cannot flow because there is no ground path on the ungrounded side as shown in Fig. 8.18(a). We have also stated that ground current can flow if the neutral point of both sides of a Y-Y-connected transformer is grounded as shown in Fig. 8.18(b). The arrows in Fig. 8.18(b) show the direction of the current flow and resulting ground current, I_n. Figure 8.18(b) displays a transformer that has been supplied with unbalanced voltages on one side that results in the current I_n because for the unbalanced three-phase currents, $I_n = I_a + I_b + I_c$. As shown in Fig. 8.18(b), the ground current I_n flows through the ground conductor; the arrow is pointing downward. On the other side of the transformer in Fig. 8.18(b), the unbalanced voltages result in a ground current flowing out of

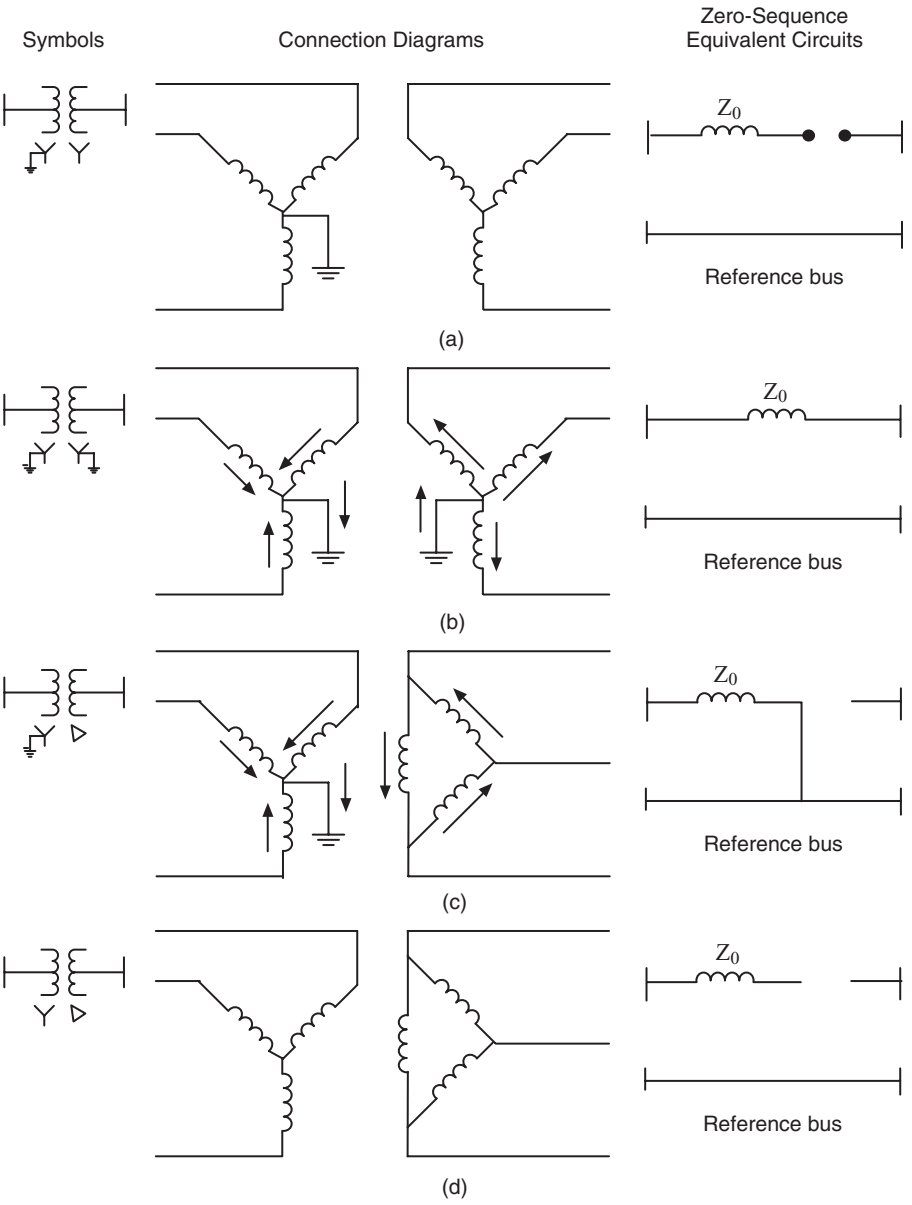

the ground so that $I_n = I_a + I_b + I_c$. Of course, the relationship of ground currents on both sides of the transformer is governed by the turn ratio of the transformer.

Figure 8.18(c) depicts a grounded Y-Δ transformer. In this case, the ground current flows on the grounded Y side because we have a circulating current on the Δ side of the transformer. Again, we should remember that if unbal-

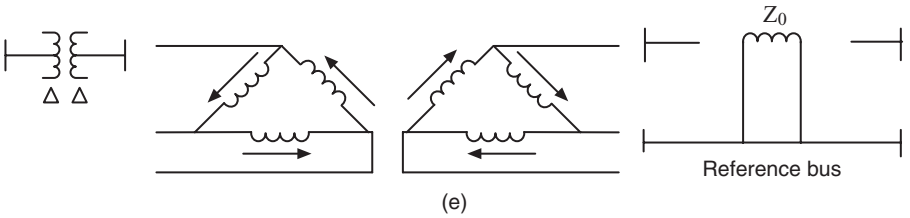

Figure 8.18 Zero-Sequence Equivalent Circuits of Three-Phase **(a)** Y-Y-Connected Transformer Banks with One Side Grounded, **(b)** Y-Y-Connected Transformer Banks with Both Sides Grounded, **(c)** Grounded Y-Δ-Connected Transformer Banks, **(d)** Ungrounded Y-Δ-Connected Transformer Banks, and **(e)** Δ-Δ-Connected Transformer Banks.

anced three-phase voltages are applied to the grounded Y side, we have created a ground path for ground current to flow as shown in Fig. 8.18(c). Figures 8.18(d) and 8.18(e) depict the conditions of an ungrounded Y-Δ connection and Δ-Δ connection.

Ground current flows if a path is established for it to flow; however, in a transformer, we must keep in mind Faraday's law of induction, the Kirchhoff current law, and the current laws for ground current flow.

8.8.2 Load Connections

Figure 8.19(a) depicts the zero sequence of a Y-connected load when the load is not grounded. As seen from the zero sequence of the ungrounded load, no ground current flows.

In Fig. 8.19(c), three times the value of the ground impedance Z_n appears in the zero sequence network for the grounded load because $I_n = 3\ I_0$. Finally, Fig. 8.19(d) depicts the Δ-connected load. In this case, the zero sequence current circulates as shown in Fig. 8.19(d).

8.8.3 Power Grid

As we have discussed in this chapter, when a fault occurs in a power grid that involves the ground, the ground current will flow. The ground current is three times the zero sequence current. Again, we must remember that in the calculation of fault current, it is assumed the power grid remains balanced, except for the faulted part. Finally, we study the if-then condition to calculate the faulted currents and set the protective relay to open the associated circuit breakers to isolate the fault before the power grid becomes unbalanced. Power grids are always designed and operated as balanced three-phase systems. To compute the ground fault current, we need to use a zero sequence network. In the preceding sections, we presented each element of a power grid zero sequence network. Now, we need to learn how to construct a zero sequence network for power grids to compute the unbalanced fault currents.

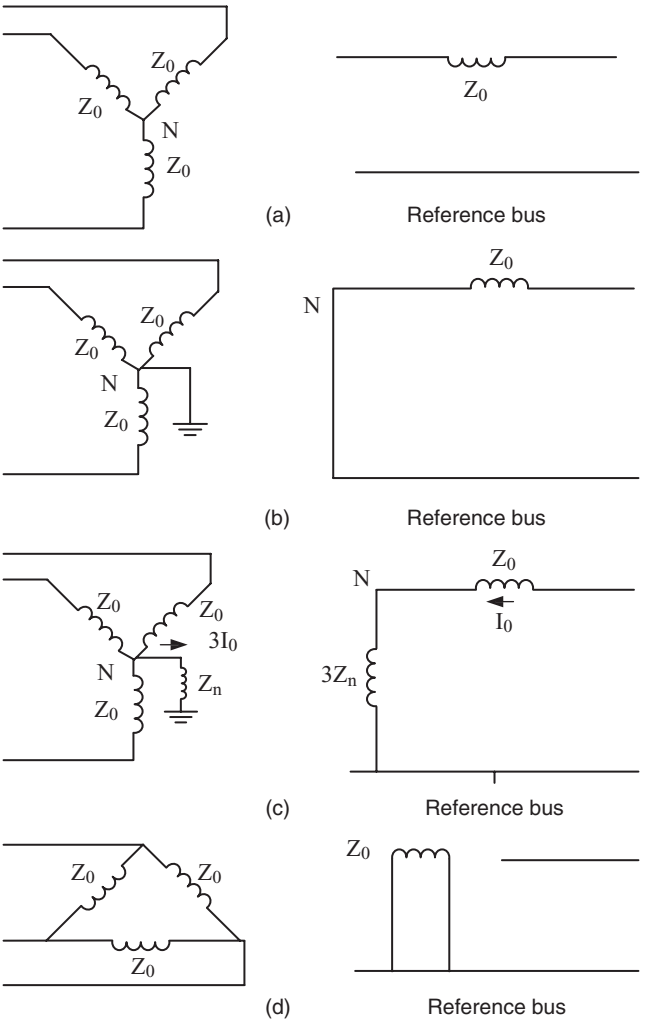

Figure 8.19 Zero Sequence Equivalent Circuit **(a)** for a Y-Connected Ungrounded Load, **(b)** for a Grounded Y-Connected Load, **(c)** for a Y-Connected Load with Grounding Impedance, and **(d)** for a Δ-Connected Load.

Figure 8.20 depicts a one-line diagram of a power microgrid with the designation of how the transformers in the power grid are connected. As we can see in Fig. 8.20, the generator connected to bus 6 is a gas turbine unit; its neutral point is grounded through impedance Z_G. Bus 6 is connected through an ungrounded Y-Δ transformer to bus 5.

Figure 8.21 depicts the zero sequence network of Fig. 8.20. In Fig. 8.21, we have replaced the gas turbine generator with its zero sequence impedance of gas turbine generator, Z_{Go}. However, we have placed Z_{Go} in series with three

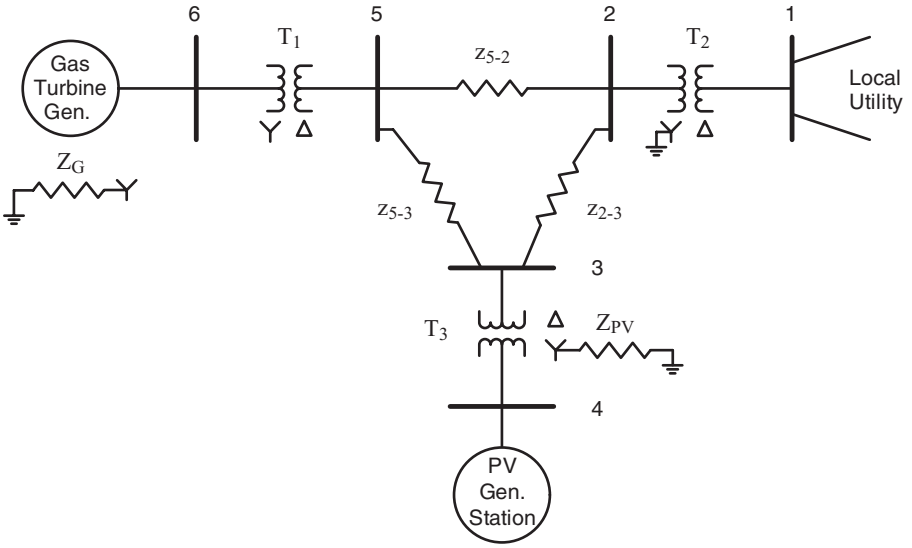

Figure 8.20 A Balanced Three-Phase Microgrid.

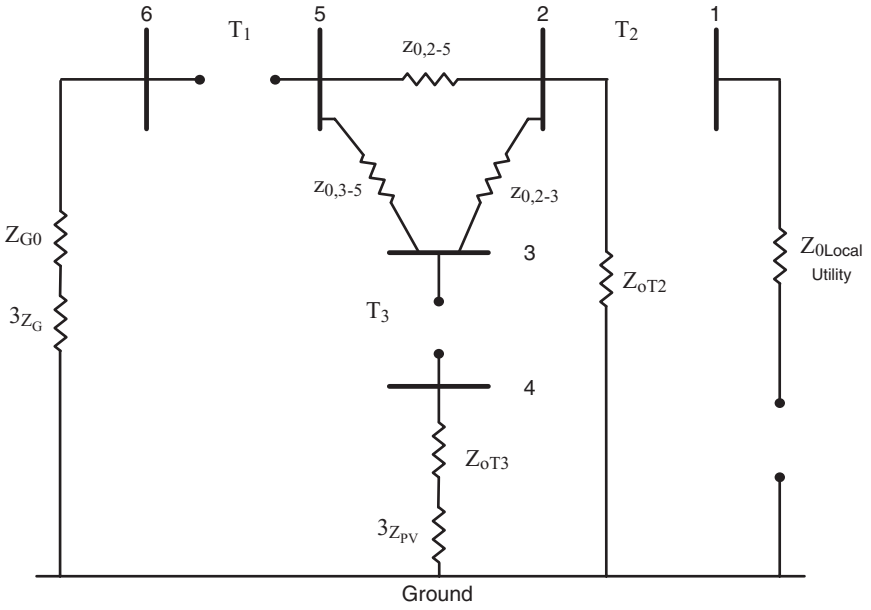

Figure 8.21 The Zero Sequence Network of Fig. 8.20.

times the Z_G because the ground current flowing into the ground reference is equal to three times the zero sequence current.

The transformer T_1 is Y-Δ-connected and the Y side is not grounded. Therefore, this transformer is not connected to ground through its neutral point and breaks the ground connection in the Y-Δ transformer. Therefore, this transformer is shown as an open circuit in the zero sequence network depicted in Fig. 8.21.

The three-bus power grid transmission network is connected to a PV-generating station and its local power grid. The zero sequence network of the transmission system is shown in Fig. 8.21. Through bus 2, the transformer T_2 is connected to bus 1, and then to the local power grid bus. The transformer T_2 is a grounded Y-Δ. Because grounded Y-Δ is connected to the ground on the Y side, bus 2 is connected to the ground reference through its zero sequence impedance as shown in Fig. 8.21.

Transformer T_3 connects bus 3 to bus 4 through a grounded Δ-Y transformer to a PV-generating station. Ground impedance, Z_{PV} is inserted in series from the neutral point of the Y side of the transformer to ground. Again, because the grounded Y is connected to bus 4, bus 4 is connected to the ground reference as shown in Fig. 8.21. However, bus 3 is shown as an open circuit. On the Δ side of the transformer T_2, the zero sequence current (ground current) does not flow and an open circuit reflects this condition as shown in Fig. 8.21.

As another illustration, the one-line diagram is given in Fig. 8.22. Figure 8.23 depicts the zero sequence network of the microgrid given in Fig. 8.22.

To construct zero sequence networks correctly, close observation of ground connections is essential. In addition, close attention should be paid to how the transformers are connected. Basically, ungrounded transformers break the ground current path as shown by the transformer connections in Figs. 8.22

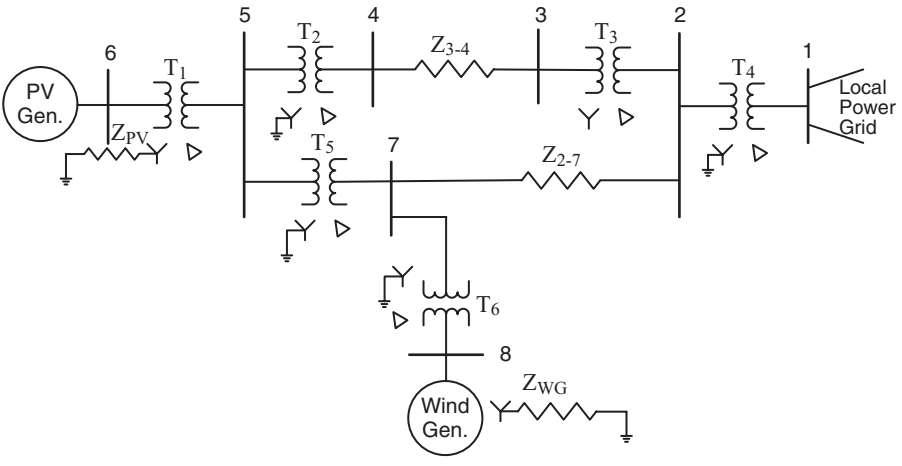

Figure 8.22 A Balanced Three-Phase Wind-Power Microgrid.

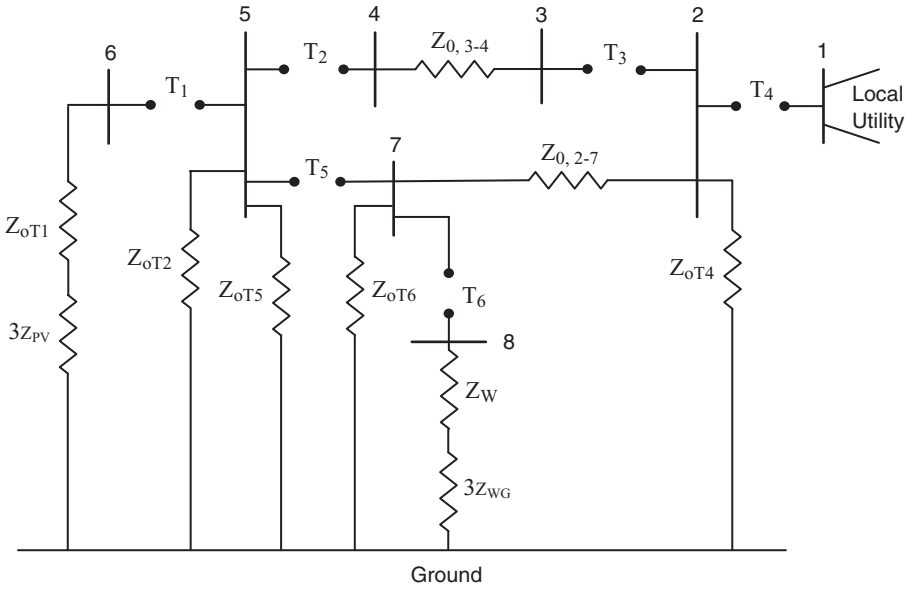

Figure 8.23 The Zero Sequence Network of Fig. 8.22.

and 8.23. However, particular attention should be paid to grounded Y-Y transformers. In these transformers, the path of zero sequence currents is maintained as can be seen in Fig. 8.18(b).

8.9 FAULT STUDIES

For a balanced three-phase fault, only the positive sequence network is excited. For unbalanced faults, all three sequence networks may be excited. If a fault involves a connection to ground, the ground current will flow. The back emf voltage behind the generator reactance is assumed equal in magnitude and phase angle; normally, it is assumed to be equal to 1 per unit.

For a faults study, normally, all shunt elements including loads and line charging are neglected. Loads may be represented with constant load impedance models. All tap changing transformers are assumed to be at their nominal tap settings and balanced transmission lines are assumed. The negative and positive sequence networks are assumed equal; coupling between adjacent circuits only is taken into account in a zero sequence network.

Power grid generators are maintained by a constant voltage behind the transient reactance. Normally, three reactances are used depending on when the faults are cleared. The subtransient reactance, X'', of a generator is estimated from tests performed on the generator and from recordings of the generator current response. The subtransient reactance is estimated from the

slope of the current response during the first quarter cycle. After the subtransient reactance, the transient reactance, X' is estimated from the slope of current response from the first half cycle and synchronous reactance, X, is estimated from the steady-state current. The value of $X'' < X' < X$. The lower value of reactance results in higher short-circuit current. The selection of reactance is a function of circuit breakers' timing. If the breakers are fast acting and can interrupt higher fault current, then the lower value of reactances is used in the fault calculation.

The study of unbalanced faults requires the modeling of the power grid using the symmetrical analysis of a power grid. Therefore, we use the sequence network of generators, transformers, transmission lines, and loads. Based on the type of unbalanced faults, one line to ground, two lines to ground, line to line faults, etc., the symmetrical models of the power grid are constructed. These sequence network models are used to construct the unbalanced fault models of the power grid.

The objectives of balanced fault studies are to determine the required circuit breaker short capacity in kVA or MVA. The objectives of unbalanced fault studies are to determine how to set the protective relay systems. It is important that close attention be paid to the representation of large motors in fault studies. The back emf of the motors can contribute substantially to the fault currents. Although the short-circuit capacity (SCC) of breakers in power grids are computed based on balanced faults, in some system single line to ground faults, the fault currents may be higher than balanced three-phase faults. Finally, a fault can happen anywhere in a power grid. For example, faults may occur in the middle of a transmission line. For these cases, we place a bus at that location in the if-then condition of the fault current calculations.

Example 8.2 Consider the power grid given below.

Assume the generator positive, negative, and zero sequence impedances are $Z_{gen,1}$, $Z_{gen,2}$, and $Z_{gen,0}$, the generator is grounded through the ground impedance Z_n. Also, assume the transmission line model as depicted in Fig. 8.25.

Perform the following:

i) If the supply generator is unbalanced and supplies three-phase unbalanced voltages, determine the positive, negative, and zero sequence networks for the one-line diagram in Fig. 8.24.

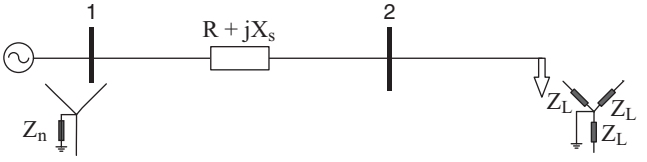

Figure 8.24 A One-Line Diagram of Example 8.2.

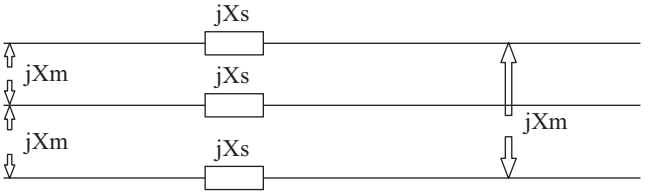

Figure 8.25 The Balanced Three-Phase Transmission Line of Fig. 8.24.

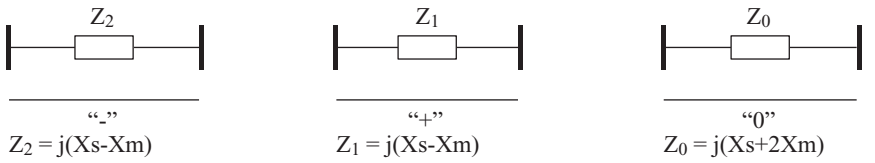

Figure 8.26 The Negative, Positive, and Zero Sequence Model of the Transmission Line of Example 8.2.

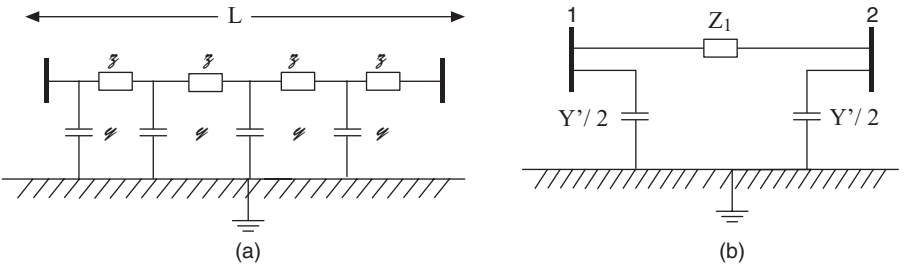

Figure 8.27 **(a)** The distributed model of the transmission line, and **(b)** the lumped model of the transmission line.

ii) If the supply generator is balanced and supplies three-phase balanced voltages, determine the positive, negative, and zero sequence networks for the one-line diagram in Fig. 8.24.

Solution

i) The positive, negative, and zero sequence of the transmission line of Example 8.2 is presented in Fig. 8.26.

If the transmission line has the total length of "L," the distributed line impedance and line charging capacitance are depicted in Fig. 8.27(a) and its lumped model is presented in Fig. 8.27(b).

$$\begin{aligned} z_1 &= L \times z \\ Y' &= L \times y \end{aligned} \tag{8.48}$$

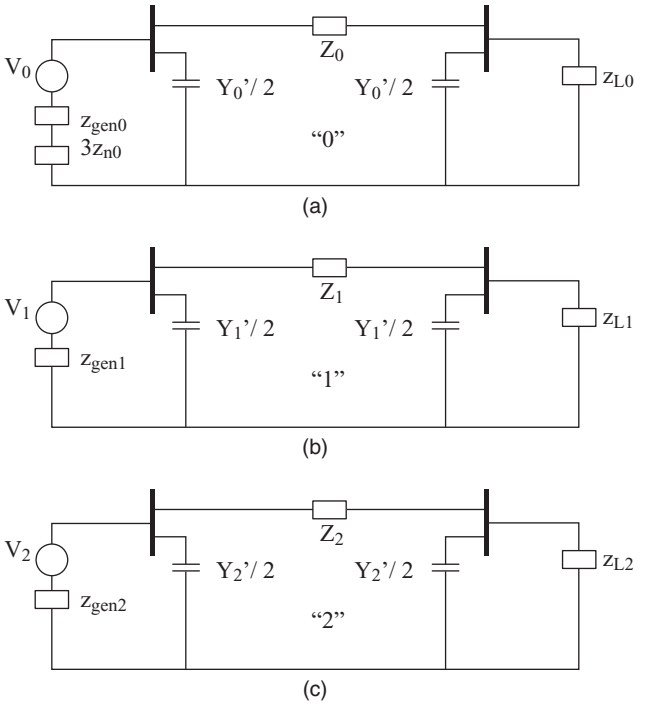

Figure 8.28 **(a)** The Zero Sequence, **(b)** Positive Sequence, and **(c)** Negative Sequence for Example 8.2 when the Power Supply Generator Voltages Are Unbalanced.

The zero, positive, and negative sequence networks for Example 8.2 are depicted in Fig. 8.28.

ii) If the supply generator is balanced, the zero, positive, and negative sequence networks are as depicted in Fig. 8.29.

8.9.1 Balanced Three-Phase Fault Analysis

For a balanced three-phase faults study, only the positive network model must be constructed. Figure 8.30 depicts a one-line diagram of a three-bus power grid. Figure 8.31 depicts the positive sequence network model for balanced fault studies.

Figure 8.31 depicts the complete model of a power system including the shunt elements and loads. In the figure, the load is represented by its equivalent impedance model

$$z_{load} = \frac{V_{load}^2}{P_{load} - jQ_{load}}. \tag{8.49}$$

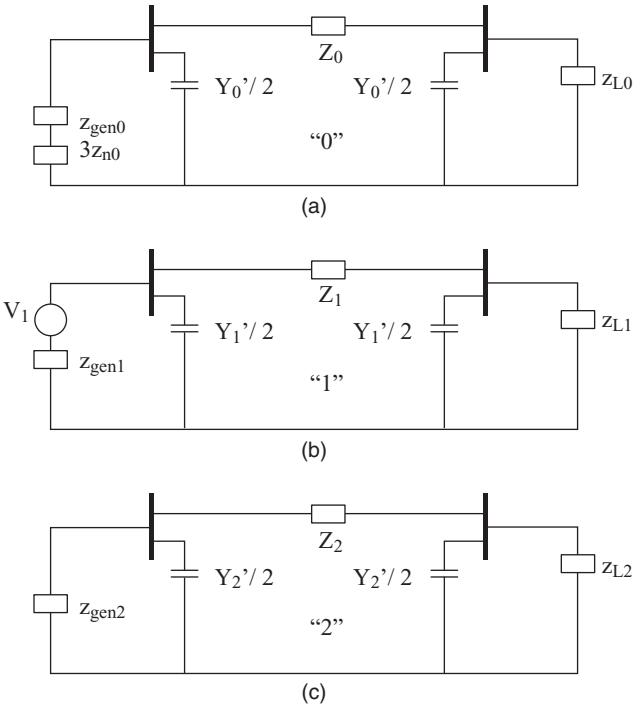

Figure 8.29 **(a)** The Zero Sequence, **(b)** Positive Sequence, and **(c)** Negative Sequence for Example 8.2 when the Power Supply Generator Voltages Are Balanced.

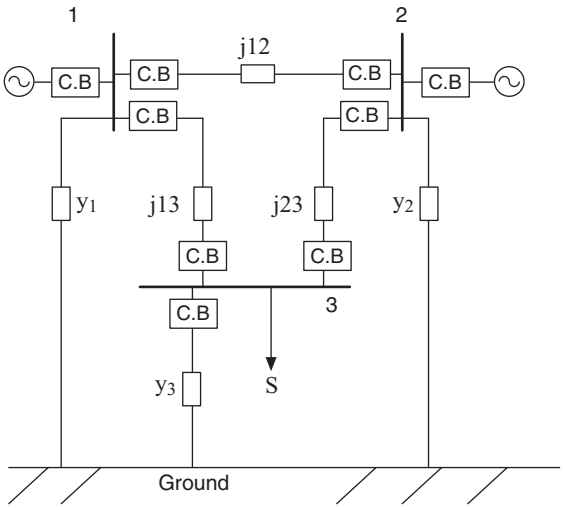

Figure 8.30 A One-Line Diagram of a Balanced Three-Bus Power Grid.

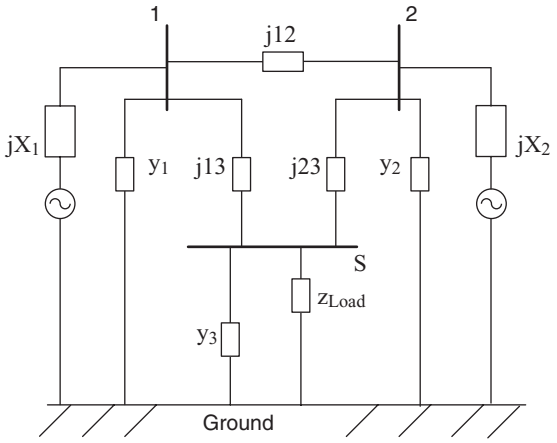

Figure 8.31 A Positive Sequence Network Model for Balanced Fault Studies.

The model given in Fig. 8.31 can be simplified by removing the shunt elements and load. This will result in a higher value for the fault currents.

In the design of power grids, the voltage calculation and power flow studies are performed before the short-circuit currents are calculated. Then, the calculated bus load voltages are used to determine the circuit breakers' interrupting capacities. Therefore, the pre-fault voltages are calculated from power flow studies and are known.

$$E_{Bus(0)} = Z_{Bus} I_{Bus(0)} \tag{8.50}$$

In Equation 8.50, $E_{Bus(0)}$ is the bus voltage vector before the fault and Z_{Bus} is the bus impedance matrix model with respect to the ground bus. $I_{Bus(0)}$ is the generator injected currents before the fault.

During the fault, the faulted network variables are designated by "F" and the bus voltage during a fault can be expressed as

$$E_{Bus(F)} = E_{Bus(0)} - Z_{Bus(F)} I_{Bus(F)} \tag{8.51}$$

where $E_{Bus(F)}$ is the bus voltage vector during the fault, $E_{Bus(0)}$ is the bus voltage before the fault, and $Z_{Bus(F)}$ is the bus impedance matrix, and $I_{Bus(F)}$ is the bus fault current during the fault.

For the bus system of Fig. 8.30 with a fault at bus 3, we have

$$\begin{bmatrix} E_{1(F)} \\ E_{2(F)} \\ E_{3(F)} \end{bmatrix} = \begin{bmatrix} E_{1(0)} \\ E_{2(0)} \\ E_{3(0)} \end{bmatrix} - \begin{bmatrix} Z_{11} & Z_{12} & Z_{13} \\ Z_{21} & Z_{22} & Z_{23} \\ Z_{31} & Z_{32} & Z_{33} \end{bmatrix} \begin{bmatrix} 0 \\ 0 \\ I_{3(F)} \end{bmatrix} \tag{8.52}$$

Therefore, the bus voltage at each bus during the fault can be expressed as

$$\begin{aligned} E_{1(F)} &= E_{1(0)} - Z_{13} I_{3(F)} \\ E_{2(F)} &= E_{2(0)} - Z_{23} I_{3(F)} \\ E_{3(F)} &= E_{3(0)} - Z_{33} I_{3(F)} \end{aligned} \tag{8.53}$$

If the fault has impedance Z_f, then the voltage across the fault impedance is given as

$$E_{3(F)} = Z_f I_{3(F)} \tag{8.54}$$

Substituting Equation 8.54 in Equation 8.53, we have

$$Z_f I_{3(F)} = E_{3(0)} - Z_{33} I_{3(F)} \tag{8.55}$$

Therefore, the fault current at bus 3 for a balanced three-phase fault can be calculated as

$$I_{3(F)} = \frac{E_{3(0)}}{Z_{33} + Z_f} \tag{8.56}$$

In Equation 8.56, $E_{3(0)}$ is pre-fault voltage and Z_{33} is the Thevenin impedance of bus 3 with respect to the ground bus.

For the general case with a balanced three-phase fault on a bus "i," we have

$$\begin{bmatrix} E_{1(F)} \\ E_{2(F)} \\ . \\ . \\ E_{i(F)} \\ . \\ . \\ E_{n(F)} \end{bmatrix} = \begin{bmatrix} E_{1(0)} \\ E_{2(0)} \\ . \\ . \\ E_{i(0)} \\ . \\ . \\ E_{n(0)} \end{bmatrix} - \begin{bmatrix} Z_{11} & Z_{12} & \ldots\ldots & Z_{1i} & \ldots\ldots & Z_{1n} \\ \ldots\ldots & & & & & \\ \ldots\ldots & & & & & \\ \ldots\ldots & & & & & \\ Z_{i1} & Z_{i2} & \ldots\ldots & Z_{ii} & \ldots\ldots & Z_{in} \\ \ldots\ldots & & & & & \\ \ldots\ldots & & & & & \\ Z_{n1} & Z_{n2} & \ldots\ldots & Z_{nP} & \ldots\ldots & Z_{nn} \end{bmatrix} \begin{bmatrix} 0 \\ 0 \\ . \\ . \\ I_{i(F)} \\ 0 \\ . \\ 0 \end{bmatrix} \tag{8.57}$$

From the above, we can express the fault at bus i as

$$E_{i(F)} = E_{i(0)} - Z_{ii} I_{P(F)} \tag{8.58}$$

And, $E_{i(F)} = Z_f I_{i(F)}$

Therefore, the fault current at bus i is

$$I_{i(F)} = \frac{E_{i(0)}}{Z_{ii} + Z_f} \tag{8.59}$$

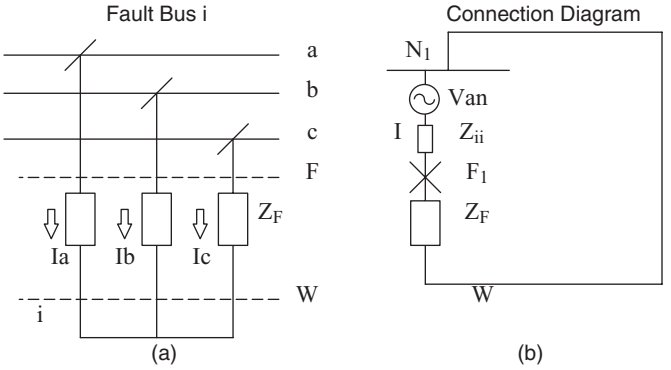

Figure 8.32 The Balanced Three-Phase **(a)** Fault, and **(b)** the Thevenin Equivalent Circuit.

In Equation 8.59, $E_{i(0)}$ is pre-fault voltage and Z_{ii} is the Thevenin impedance of bus "i" with respect to the ground bus.

$$Z_{Bus} = \begin{array}{c} \begin{matrix} 1 & & i & & n \end{matrix} \\ \begin{bmatrix} Z_{11} & \cdots & Z_{i1} & \cdots & Z_{1n} \\ . & \cdots & . & \cdots & . \\ Z_{i1} & \cdots & Z_{ii} & \cdots & Z_{in} \\ . & \cdots & . & \cdots & . \\ Z_{n1} & \cdots & Z_{ni} & \cdots & Z_{nn} \end{bmatrix} \begin{matrix} 1 \\ . \\ i \\ . \\ n \end{matrix} \end{array}$$

The elements of a Z_{Bus} positive sequence matrix are computed from the positive sequence network.

We can generalize an algorithm for a balanced three-phase fault calculation as

Step 1. Build the Z_{Bus} (matrix) for a positive impedance network

Step 2. Obtain the pre-fault bus voltage from load flow

Step 3. Compute: $I_{i(F)} = \dfrac{E_{i(0)}}{Z_{ii} + Z_f}$

Using the above algorithm, we can calculate the balance fault current for each bus i.

The SCC for breakers connected to each bus is computed based on the balanced three-phase fault at each bus. The SCC is defined as

$$SCC = \left|V_{prefault(p.u)}\right| \cdot \left|I_{fault(p.u)}\right| \tag{8.60}$$

If the pre-fault voltage and fault current are given in per unit (p.u), the SCC is also given in p.u of MVA. To obtain SCC in MVA, the p.u MVA is multiplied by S_b.

$$SCC = S_b \left|V_{prefault(p.u)}\right| \cdot \left|I_{fault(p.u)}\right| \tag{8.61}$$

$$SCC = \sqrt{3} \cdot \left|V_{prefault,line-line}\right| \cdot \left|I_{fault,line}\right| VA \tag{8.62}$$

In Equation 8.62, the voltage is in volts and current is in amperes. Therefore, at each bus, the fault level of the bus is determined by its Thevenin impedance to the ground. To explain this concept clearly, consider the system given in Fig. 8.33.

To calculate the fault current at bus 3, the Thevenin equivalent circuit is given in Fig. 8.34.

where V_{th} is the voltage at bus 3 before the fault.

$Z_{th} = Z_{33}$ is obtained from the Z_{bus} impedance matrix; the impedance between bus 3 and ground by looking into the system at bus 3.

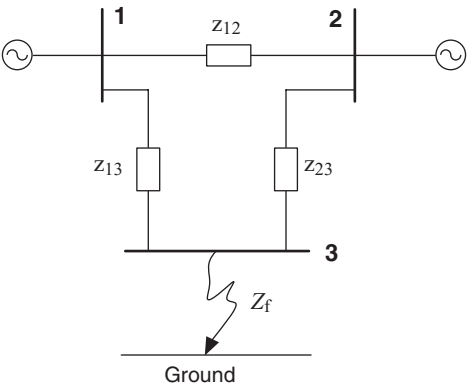

Figure 8.33 A Fault at Bus 3.

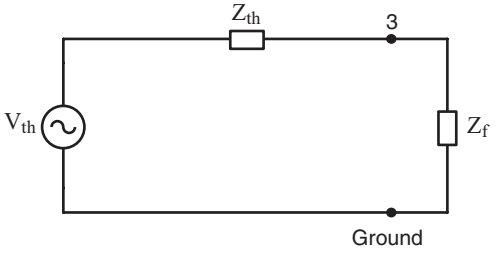

Figure 8.34 The Thevenin Equivalent Circuit for the Fault Current Calculation at Bus 3.

$$I_f = \frac{V_{th}}{Z_{th} + Z_f} \tag{8.63}$$

If the fault impedance is zero, that is we have a bolted fault, then the Equation 8.63 can be expressed as

$$I_f = \frac{V_{th}}{Z_{th}} \tag{8.64}$$

The power grid system is designed such that the voltage at each bus of the system is around one per unit. Therefore,

$$V_{th} \cong 1 \text{ p.u}$$

As a result, the fault current is

$$I_f = \frac{1}{Z_{th}} \tag{8.65}$$

Therefore, the Thevenin can be computed as

$$Z_{th} = \frac{1}{I_f} \tag{8.66}$$

Because the SCC in per unit is expressed as

$$SCC = |V_{prefault}|\,|I_{fault}|\,p.u$$

And $V_{prefault} \cong 1$ p.u; therefore,

$$SCC = I_{f(fault)}\ p.u \tag{8.67}$$

and

$$Z_{th} = \frac{1}{SCC} \tag{8.68}$$

Power companies calculate the SCC for each bus of their system. When a microgrid of a green energy system is connected to the local power grid, the SCC is provided to assess the fault current contribution from the local power grid to the microgrid. Therefore, SCC specifies the input Thevenin impedance that is needed for computing the interrupting capacities of the microgrid circuit breakers.

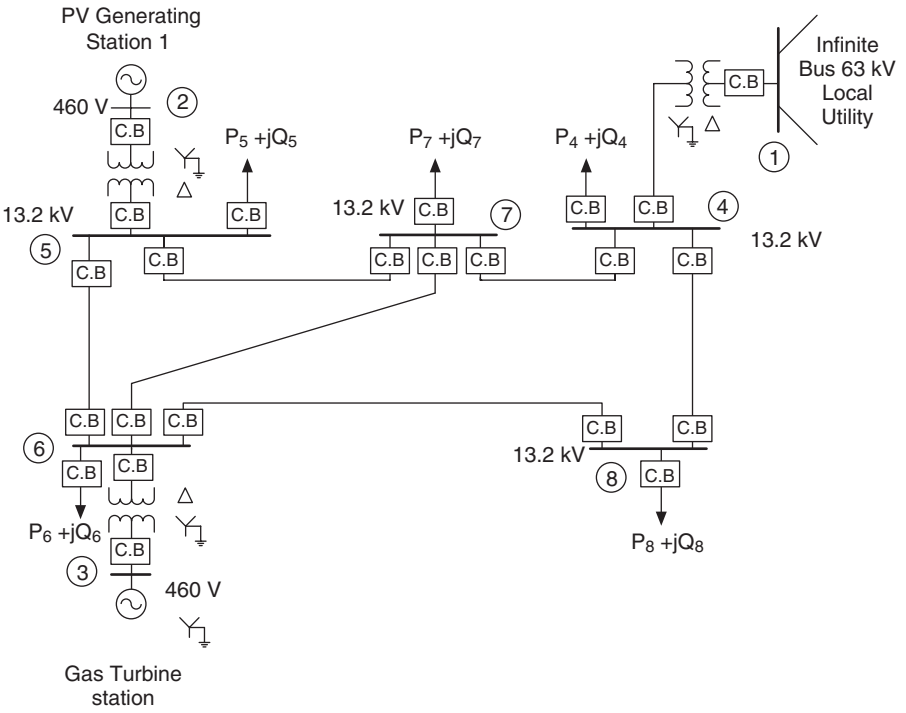

Figure 8.35 A Microgrid of Distributed Generation Connected to a Local Power Network.

Example 8.3 Consider a microgrid as part of an interconnected power grid. Assume the following data:

Local power grid short-circuit capacity = 320 MVA

PV-generating station #1: PV arrays = 2 MVA, internal impedance = highly resistive, 50% of its rating

Gas turbine station: combined heat and power (CHP) units = 10 MVA, internal reactance = 4%. Units are Y connected and grounded.

Transformers = 460 V Y grounded/13.2 kV Δ, 10% reactance, 10 MVA capacity

Power grid transformer: 20 MVA, 63 kV/13.2 kV, 7% reactance

Bus 4 load = 1.5 MW, power factor (p.f.) = 0.85 lagging; bus 5 load = 5.5 MW, p.f. = 0.9 lagging; bus 6 load = 4.0 MW, p.f. = 0.95 leading; bus 7 load = 5 MW, p.f. = 0.95 lagging; bus 8 load = 1.0 MW, p.f. = 0.9 lagging

Transmission line: resistance = 0.0685 Ω/mile, reactance = 0.40 Ω/mile, and half of line charging admittance (Y′/2) of 11×10^{-6} Ω^{-1}/mile. Line 4–7 = 5 miles, 4–8 = 1 mile, 5–6 = 3 miles, 5–7 = 2 miles, 6–7 = 2 miles, 6–8 = 4 miles

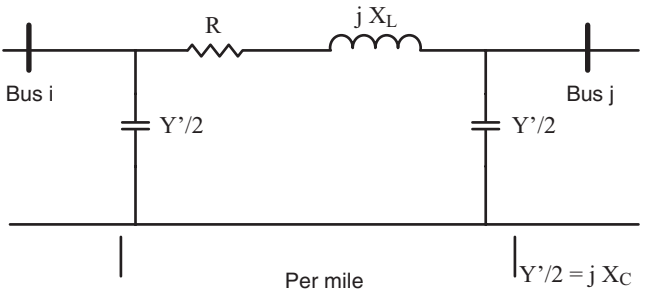

Figure 8.36 The Equivalent Impedance of the Transmission Line Model for Example 8.3.

Perform the following:

i) Develop a per unit equivalent model for balanced three-phase fault studies based on a 20 MVA base

ii) If the bus load voltages are at 1 per unit, compute the per impedance model of each load.

iii) For three-phase faults, compute the SCC of each distribution network bus

iv) To increase the security of the system two identical transformers are used at each distribution network and the interconnection to the local power grid. Compute the SCC of each bus.

Solution

i) The base value of the volt-amp is selected as $S_b = 20$ MVA. The voltage base selected on the PV generator and gas turbine side is selected to be 460 V. The voltage base on the transmission lines side is therefore $V_b = 13.2$ kV

The p.u SCC of the local power grid is given by

$$\frac{SCC}{S_b} = \frac{320}{20} = 16$$

Therefore, the internal p.u impedance of the local power grid is

$$Z_{th} = \frac{1}{SCC_{p.u}} = \frac{1}{16} = j0.063$$

The internal p.u impedance of the PV-generating station at 20 MVA base is given by

$$Z_{p.u(new)} = Z_{p.u(old)} \times \frac{VA_{b(new)}}{VA_{b(old)}} \times \left(\frac{V_{b(old)}}{V_{b(new)}}\right)^2$$

$$= 0.5 \times \frac{20 \times 10^6}{2 \times 10^6} \times \left(\frac{460}{460}\right)^2 = 5$$

The p.u impedance of the gas turbine is

$$z = j0.4 \times \frac{20 \times 10^6}{10 \times 10^6} \times \left(\frac{460}{460}\right)^2 = j0.8$$

The base impedance transmission system is

$$Z_b = \frac{V_b^2}{S_b} = \frac{\left(13.2 \times 10^3\right)^2}{20 \times 10^6} = 8.712\ \Omega$$

The base admittance given by

$$Y_b = \frac{1}{Z_b} = \frac{1}{8.712} = 0.115$$

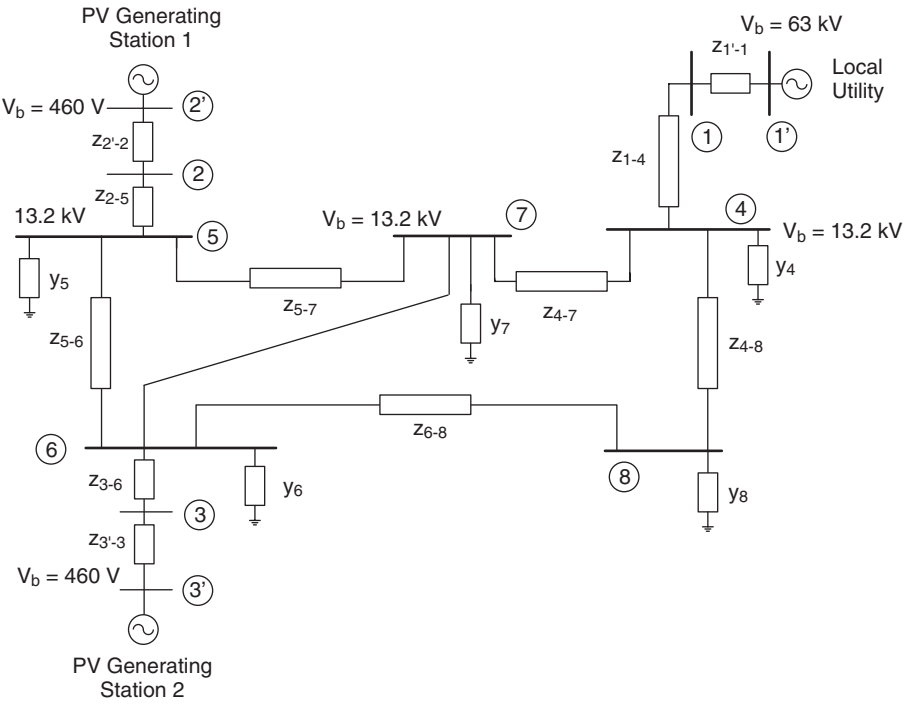

Figure 8.37 Impedance Model for Short-Circuit Studies.

The p.u impedance of the local power grid transformer is 7% based on 20 MVA.

ii) The loads represented by their equivalent impedance are calculated from the equation

$$z_{load} = \frac{V_{load}^2}{P_{load} - jQ_{load}}$$

iii) The per unit impedance of a line between bus i and j is given by

$$z_{i-j,p.u} = \frac{z_{i-j}}{Z_b}$$

Using the above equation, the transmission line p.u parameters are calculated and listed in Table 8.2(a).

TABLE 8.1 The Load of Each Bus and Its Equivalent Load Impedance.

Bus	Load	Complex Power (p.u)	Equivalent Load Impedance (p.u)
4	1.5 MW at 0.85 p.f. (lagging) $= 1.5 + j0.92$	$0.075 + j0.046$	$9.69 + j5.94$
5	5.5 MW at 0.9 p.f. (lagging) $= 5.5 + j2.66$	$0.275 + j0.133$	$2.95 + j1.43$
6	4.0 MW at 0.95 p.f. (leading) $= 4.0 - j1.31$	$0.20 - j0.066$	$4.51 - j1.49$
7	5 MW at 0.95 p.f. (lagging) $= 5.0 + j1.64$	$0.25 + j0.082$	$3.61 + j1.18$
8	1.0 MW at 0.9 p.f. (lagging) $1.0 + j0.48$	$0.05 + j0.024$	$16.25 + j7.80$

TABLE 8.2(a) Transformer Per Unit Impedance.

Line	Series Impedance (p.u)
1–4	$j0.07$
2–5	$j0.2$
3–6	$j0.2$

TABLE 8.2(b) Transmission Line Parameters.

Line	Series Impedance (p.u)	Line Charging Admittance (p.u)
4–7	$0.039 + j0.229$	$j479 \times 10^{-6}$
4–8	$0.008 + j0.046$	$j96 \times 10^{-6}$
5–6	$0.024 + j0.138$	$j287 \times 10^{-6}$
5–7	$0.016 + j0.092$	$j192 \times 10^{-6}$
6–7	$0.016 + j0.092$	$j192 \times 10^{-6}$
6–8	$0.031 + j0.184$	$j383 \times 10^{-6}$

The bus admittance matrix is calculated using the Y_{Bus} algorithm given by Equation 7.18. For short-circuit studies, it is industry practice to omit the line charging and the load impedances for calculating the balanced fault current for each bus. However, we can include the load impedance by using the bus load voltages from a power flow calculation.

$$z_{load} = \frac{V_{load}}{I_{load}} = \frac{V_{load}}{(V_{load} / I_{load})^*} = \frac{V_{load}^2}{S_{load}^*}$$

However, because in a designed power grid the load bus voltages are around 1 per unit with a tolerance of 5%, we can use 1 per unit for load voltages and compute the load impedance for use in short-circuit studies.

The Y_{Bus} matrix for short-circuit studies will include the internal impedance of the generator buses. For Example 8.3, the Y_{Bus} matrix will be 8×8 with the voltage sources replaced by their internal impedance to find the Thevenin's equivalent impedance.

$$Y_{Bus} = \begin{array}{c} \begin{array}{cccc} 1 & 2 & 3 & 4 \end{array} \\ \begin{bmatrix} -j30.2 & 0 & 0 & j14.3 \\ 0 & 0.2 - j5 & 0 & 0 \\ 0 & 0 & -j6.25 & 0 \\ j14.3 & 0 & 0 & 4.35 - j39.68 \\ 0 & j5.0 & 0 & 0 \\ 0 & 0 & j5.0 & 0 \\ 0 & 0 & 0 & -0.7 + j4.2 \\ 0 & 0 & 0 & -3.6 + j21.2 \end{bmatrix} \end{array}$$

$$\begin{array}{cccc} 5 & 6 & 7 & 8 \end{array}$$

$$\begin{bmatrix} 0 & 0 & 0 & 0 \\ j5.0 & 0 & 0 & 0 \\ 0 & j5.0 & 0 & 0 \\ 0 & 0 & -0.72 + j4.23 & -3.6 + j21.16 \\ 3.02 - j22.63 & -1.2 + j7.1 & -1.8 + j10.58 & 0 \\ -1.2 + j7.1 & 3.93 - j27.92 & -1.8 + j10.58 & -0.91 + j5.29 \\ -1.8 + j10.6 & -1.8 + j10.58 & 4.35 - j25.39 & 0 \\ 0 & -0.9 + j5.29 & 0 & 4.53 - j26.45 \end{bmatrix} \begin{array}{c} 1 \\ 2 \\ 3 \\ 4 \\ 5 \\ 6 \\ 7 \\ 8 \end{array}$$

The bus admittance matrix, Y_{Bus} is inverted to get the Z_{Bus} matrix. The diagonal elements of the Z_{Bus} matrix are the Thevenin's equivalent impedance of the bus looking back into the system. That is Z_{ii} is the Thevenin impedance of bus i with respect to ground.

TABLE 8.3 The Short-Circuit Capacity (SCC) of Each Bus.

Bus	SCC (p.u)
1	16.71
2	2.21
3	3.42
4	8.41
5	3.92
6	4.82
7	4.57
8	6.45

TABLE 8.4 The Short-Circuit Capacity (SCC) of Each Bus with Two Transformers.

Bus	SCC (p.u)
1	16.81
2	3.05
3	4.31
4	11.18
5	4.36
6	5.51
7	5.20
8	7.91

$$SCC_{p.u} = \frac{1}{Z_{ii}} \qquad i = 1, 2. \ldots 8$$

where Z_{ii} is the diagonal element of Z_{Bus} matrix. The SCC of each bus is given in Table 8.3.

iv) The SCC of each bus when two transformers are used for each generation bus is given in Table 8.4.

From the data in Tables 8.3 and 8.4 we find that when we parallel two transformers, we decrease the net Thevenin impedance of each bus and increase the short-circuit current. Therefore, when we make a change in a power grid, we must perform a short-circuit study of the grid to ensure that we have not exceeded the SCC of the breakers.

Example 8.4 Consider the power grid as given in Fig. 8.38 below.
Assume an MVA base of 100 MVA and compute the following:

i) The SCC of bus 5 (415 V) when all the transformers and the generator G_1 are in service.

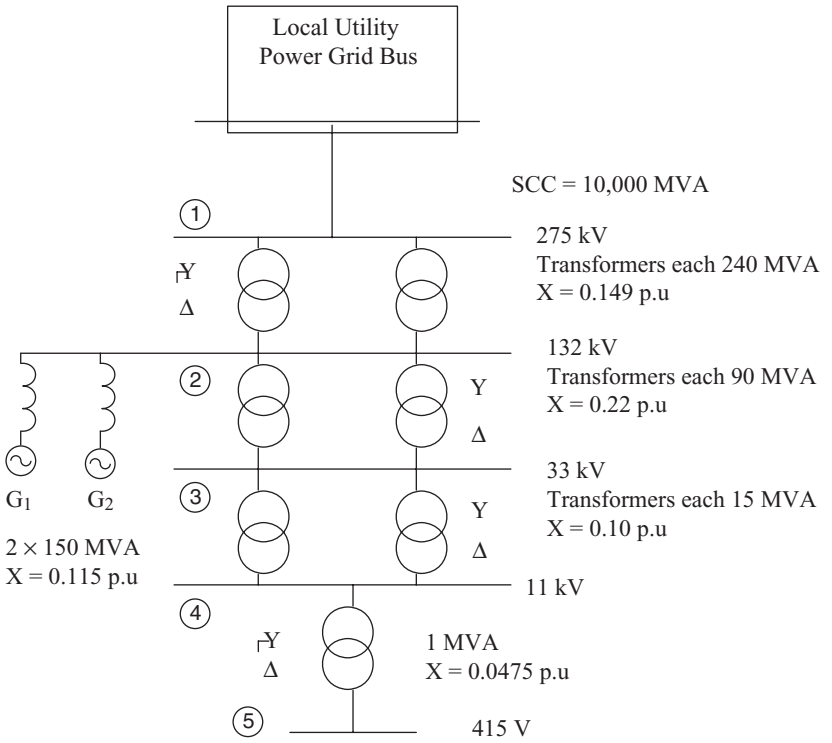

Figure 8.38 A One-Line Diagram of Example 8.4.

ii) The SCC of bus 5 (415 V) when all transformers are in service, but generator G_1 is not in service.

Solution

The base volt-amp is given as $S_b = 100$ MVA

The SCC of local power grid bus is given as SCC = 10,000 MVA

Therefore, p.u SCC is given

$$SSC_{p.u} = \frac{SSC}{S_b}$$

$$SSC_{p.u} = \frac{10,000}{100} = 100 \text{ p.u}$$

From Equation 8.68, the internal impedance of the power grid is

$$X_{th} = \frac{1}{100} = 0.01 \text{ p.u}$$

The p.u impedance of the transformers and generators at a new base is given by

$$Z_{p.u(new)} = Z_{p.u(old)} \times \frac{VA_{b(new)}}{VA_{b(old)}} \times \left(\frac{V_{b(old)}}{V_{b(new)}} \right)^2$$

Therefore, the p.u impedance of the transformers and generators at 100 MVA is as listed below.

For a 240 MVA transformer, $X_{Tr240} = 0.149\left(\frac{100}{240}\right) = 0.062$ p.u

For a 90 MVA transformer, $X_{Tr90} = 0.22\left(\frac{100}{90}\right) = 0.244$ p.u

For a 15 MVA transformer, $X_{Tr15} = 0.1\left(\frac{100}{15}\right) = 0.67$ p.u

For a 1 MVA transformer, $X_{Tr1} = 0.0475\left(\frac{100}{1}\right) = 4.75$ p.u

For the generators G_1 and $G_2 = X_G = 0.115\left(\frac{100}{150}\right) = 0.0766$ p.u

i) The equivalent circuit diagram for fault analysis when all the generators and transformers are in service is given in Fig. 8.39.

Figure 8.39(a) shows the equivalent circuit of Fig. 8.38 under fault conditions. The parallel impedances of Fig. 8.39(a) have been reduced to single equivalent impedances in Fig. 8.39(b), and in Fig. 8.39(c) the series impedances are combined together to form only three equivalent impedances. In Fig. 8.39(d) a simplified equivalent circuit is shown.

The p.u fault current from Equation 8.68 is given by

$$I_f = \frac{1}{Z_{th}}$$
$$= \frac{1}{j5.227} = 0.1913 \text{ p.u A}$$

It should be noted that the p.u fault current and the p.u *SCC* are equal at 1 p.u voltage.

$$SCC = SCC_{p.u} \times S_b$$
$$SCC = 0.1913 \times 100 = 19.13 \text{ MVA}$$

The fault current at bus 5 can also be calculated by finding the Thevenin impedance at bus 5 obtained from the Z^{+}_{Bus} matrix as shown below.

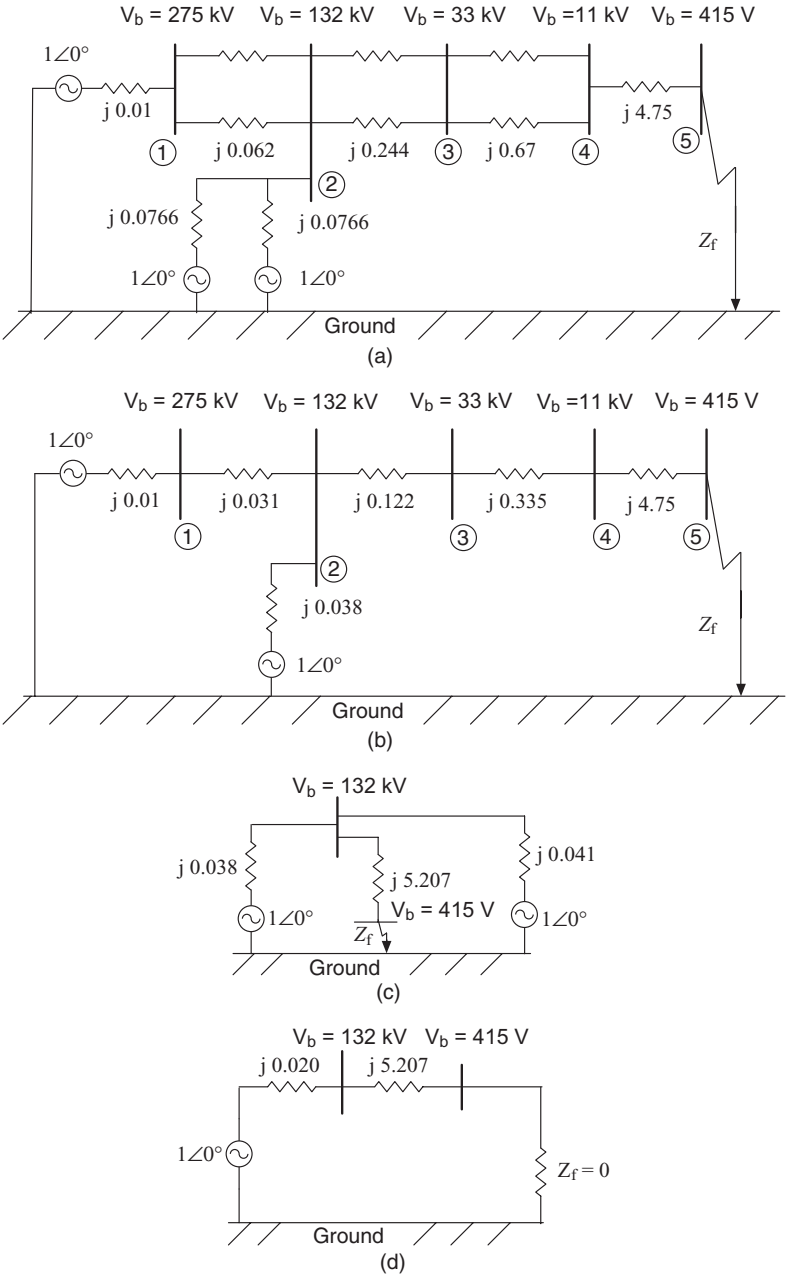

Figure 8.39 (a–d) The Impedance Diagram of Example 8.4.

$$Z^{+}_{Bus} = \begin{bmatrix} j0.009 & j0.005 & j0.005 & j0.005 & j0.005 \\ j0.005 & j0.020 & j0.020 & j0.020 & j0.020 \\ j0.005 & j0.020 & j0.142 & j0.142 & j0.142 \\ j0.005 & j0.020 & j0.142 & j0.477 & j0.477 \\ j0.005 & j0.020 & j0.142 & j0.477 & j5.227 \end{bmatrix}$$

The positive sequence Thevenin impedance for bus 5 is given by $Z^{+}_{Th,5} = Z^{+}_{55} = j5.227$.

This value obtained from the Z^{+}_{Bus} is the same as the value calculated from the circuit simplification as shown in Fig. 8.39. The fault current is calculated as shown before.

ii) The equivalent circuit for fault analysis with generator G_1 out of service is given in Fig. 8.40.

The simplification of the faulted network of Fig. 8.40(a) is shown in Fig. 8.40(b–d) following the same steps as explained in Part *i*.

The p.u fault current from Equation 8.68 is given by

$$I_f = \frac{1}{Z_{th}}$$

$$Z_{th} = \frac{1}{j5.233} = 0.1911 \text{ p.u}$$

It should be noted that the p.u fault current and the p.u. *SCC* are equal at 1 p.u voltage.

$$SCC = SCC_{p.u} \times S_b$$

$$SCC = 0.1911 \times 100 = 19.11 \text{ MVA}$$

The fault current at bus 5 can also be calculated by finding the Thevenin impedance at bus 5 obtained from the Z^{+}_{Bus} matrix as shown below.

$$Z^{+}_{Bus} = \begin{bmatrix} j0.009 & j0.007 & j0.007 & j0.007 & j0.007 \\ j0.007 & j0.027 & j0.027 & j0.027 & j0.027 \\ j0.007 & j0.027 & j0.149 & j0.149 & j0.149 \\ j0.007 & j0.027 & j0.149 & j0.484 & j0.484 \\ j0.007 & j0.027 & j0.149 & j0.484 & j5.233 \end{bmatrix}$$

The positive sequence Thevenin impedance for bus 5 is given by $Z^{+}_{Th,5} = Z^{+}_{55} = j5.233$.

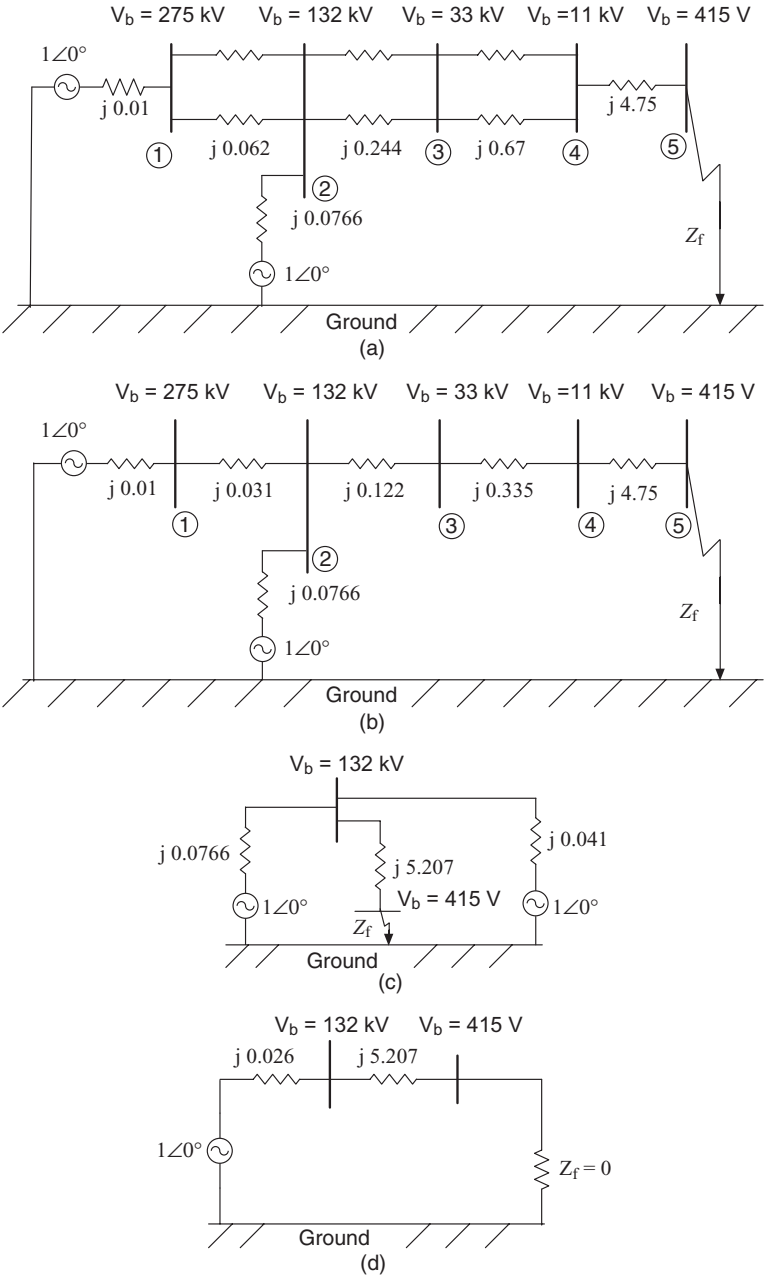

Figure 8.40 (a–d) The Impedance Diagram of Example 8.4, Part *ii*.

This value obtained from the Z^{+}_{Bus} is the same as the value calculated from the circuit simplification as shown above. The fault current is calculated as shown before.

8.9.2 Unbalanced Faults

Depending on the type of unbalanced faults, we need the positive, negative, and zero sequence networks. When a fault involves ground, the ground current will flow on part of the network if low impedance paths exist for the flow of ground current. The unbalanced fault currents are used to set the protection system relays. The most common fault is the single line to ground fault. For safety and for the protection of the power grid, a grounded grid is designed. When the ground current flow is detected, the relay system identifies the types of faults and isolates the faulted part of the systems by opening the circuit breakers as required.

Power grids are designed to operate as balanced three-phase systems. Again, as we discussed before, in an unbalanced fault analysis, the only part of the system that is unbalanced is the faulted part. For example, when one of the three-phase lines is faulted due to a passing storm, the faulted line is removed very quickly so that the power grid during fault still remains balanced.

8.9.3 Single Line to Ground Faults

To analyze the single line to ground fault, let us assume that a phase conductor of a transmission line of a power grid is broken due to a heavy storm and it has fallen on a tree and has an impedance Z_f. This is a typical single line to ground fault condition. It is customary to designate the faulted phase as phase a. Assume the faulted point is designated as bus *i*. Because phase b and phase c are not faulted the following condition holds at bus *i*.

$$I_{fb} = 0, I_{fc} = 0 \text{ and } V_{fa} = Z_f \cdot I_{fa}$$

where Z_f is the fault impedance to ground at phase a of bus *i*.

Recall from the symmetrical transformation of phase current a, b, and c to zero, positive, and negative current.

$$\begin{bmatrix} I^{0}_{fa} \\ I^{+}_{fa} \\ I^{-}_{fa} \end{bmatrix} = \frac{1}{3}\begin{bmatrix} 1 & 1 & 1 \\ 1 & a & a^2 \\ 1 & a^2 & a \end{bmatrix}\begin{bmatrix} I_{fa} \\ I_{fb} \\ I_{fc} \end{bmatrix} \tag{8.69}$$

When the conditions of a single line to ground fault are substituted for current, we have

$$\begin{bmatrix} I_{fa}^{0} \\ I_{fa}^{+} \\ I_{fa}^{-} \end{bmatrix} = \frac{1}{3}\begin{bmatrix} 1 & 1 & 1 \\ 1 & a & a^2 \\ 1 & a^2 & a \end{bmatrix}\begin{bmatrix} I_{fa} \\ 0 \\ 0 \end{bmatrix} \tag{8.70}$$

The above matrix simplifies to the following:

$$I_{fa}^{0} = I_{fa}^{+} = I_{fa}^{-} \tag{8.71}$$

The above equation clearly states that the zero, positive, and negative sequence network must be connected in series for a single line to ground fault calculation.

Again, we should remember that we are interested in an if-then condition at bus *i*. That is before bus *i* is faulted, the Thevenin voltage at bus *i* is the open-circuit voltage of bus *i*. Before the fault, the power grid is balanced and during the time of the fault, it is assumed it remains at the same voltage because the fault is isolated very quickly. The impedance in bus *i* is the Thevenin impedance. Therefore, we need to compute the Thevenin impedance by looking into bus *i* for its zero, positive, and negative sequence networks. Figure 8.41(b) depicts the sequence network connection for the single line to ground.

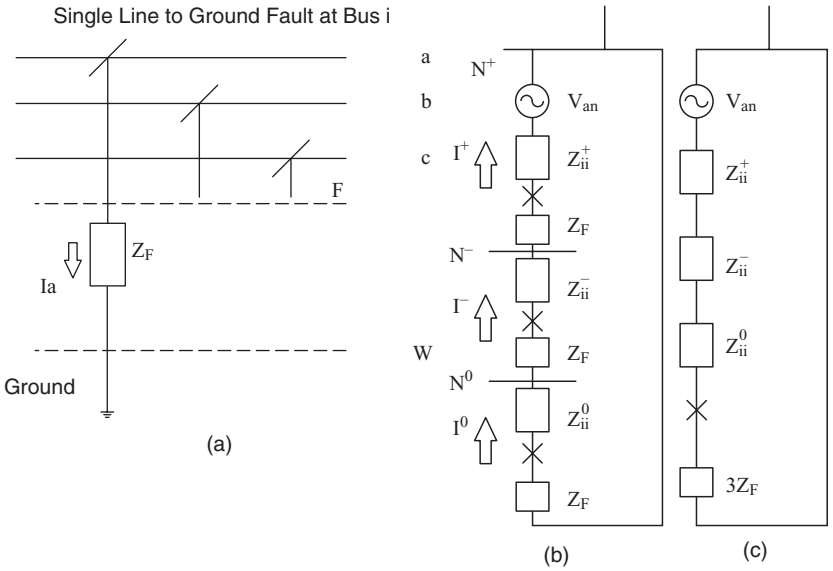

Figure 8.41 **(a)** A Single Line to Ground Fault, **(b)** The Connection of Sequence Networks for a Single Line to Ground Fault Calculation, and **(c)** The Simplified Connection of Sequence Networks for a Single Line to Ground Fault Calculation.

To compute the single line to ground fault, the positive, negative, and zero sequence networks of the power grid are constructed, and then Z^{+}_{Bus}, Z^{-}_{Bus}, and Z^{0}_{Bus} are computed as given in Equations 8.72–8.74.

$$Z^{+}_{Bus} = \begin{array}{c} \begin{matrix} 1 & & i & & n \end{matrix} \\ \begin{bmatrix} Z^{+}_{11} & \dots & Z^{+}_{i1} & \dots & Z^{+}_{1n} \\ . & \dots & . & \dots & . \\ Z^{+}_{i1} & \dots & Z^{+}_{ii} & \dots & Z^{+}_{in} \\ . & \dots & . & \dots & . \\ Z^{+}_{n1} & \dots & Z^{+}_{ni} & \dots & Z^{+}_{nn} \end{bmatrix} \begin{matrix} 1 \\ . \\ i \\ . \\ n \end{matrix} \end{array}, \tag{8.72}$$

$$Z^{-}_{Bus} = \begin{array}{c} \begin{matrix} 1 & & i & & n \end{matrix} \\ \begin{bmatrix} Z^{-}_{11} & \dots & Z^{-}_{i1} & \dots & Z^{-}_{1n} \\ . & \dots & . & \dots & . \\ Z^{-}_{i1} & \dots & Z^{-}_{ii} & \dots & Z^{-}_{in} \\ . & \dots & . & \dots & . \\ Z^{-}_{n1} & \dots & Z^{-}_{ni} & \dots & Z^{-}_{nn} \end{bmatrix} \begin{matrix} 1 \\ . \\ i \\ . \\ n \end{matrix} \end{array}, \tag{8.73}$$

$$Z^{0}_{Bus} = \begin{array}{c} \begin{matrix} 1 & & i & & n \end{matrix} \\ \begin{bmatrix} Z^{0}_{11} & \dots & Z^{0}_{i1} & \dots & Z^{0}_{1n} \\ . & \dots & . & \dots & . \\ Z^{0}_{i1} & \dots & Z^{0}_{ii} & \dots & Z^{0}_{in} \\ . & \dots & . & \dots & . \\ Z^{0}_{n1} & \dots & Z^{0}_{ni} & \dots & Z^{0}_{nn} \end{bmatrix} \begin{matrix} 1 \\ . \\ i \\ . \\ n \end{matrix} \end{array} \tag{8.74}$$

For the faulted bus, the driving point impedance, that is, the Thevenin impedance is selected from the diagonal elements of respective positive, negative and zero sequence networks. For a single line to ground fault, the Thevenin impedance of positive, negative, and zero sequence networks must be connected in series as shown in Fig. 8.41(b). The positive sequence voltage before the fault remains the same after the fault and excites the flow of current though the faulted network.

8.9.4 Double Line to Ground Faults

In a typical double line to ground fault, you can envision the following incident. Suppose the insulation of a one-phase conductor breaks and falls on another phase conductor, then the conductor falls on a tree. Because the tree is grounded, and we have two conductors that have made an accidental

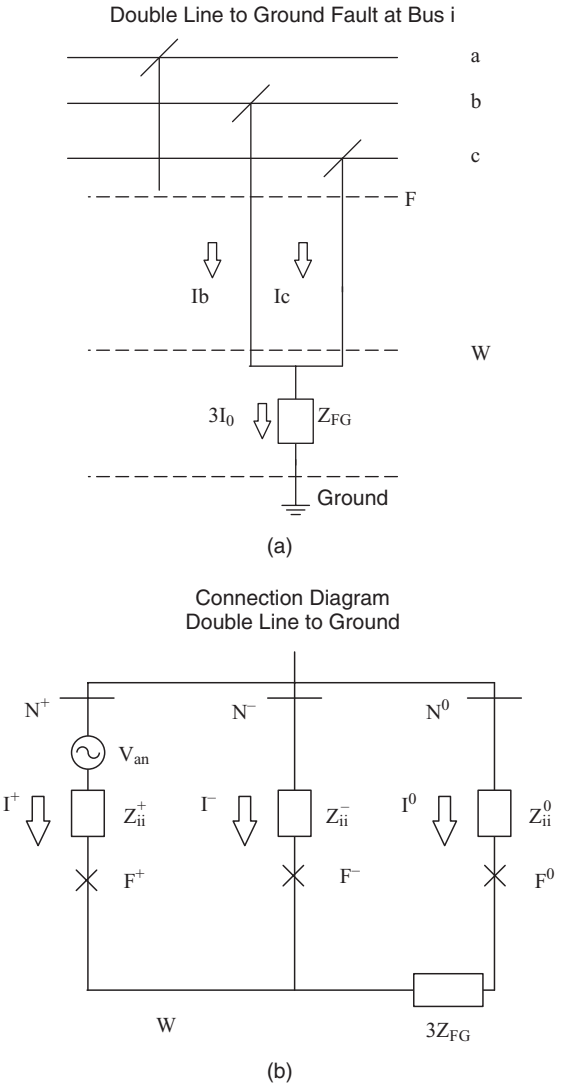

Figure 8.42 **(a)** A Double Line to Ground Fault, and **(b)** The Sequence Network Connection for a Double Line to Ground Fault.

connection, we have created a double line to ground fault condition. Figure 8.42(a) depicts a double line to ground fault.

It is customary to designate the faulted phases as b and c as shown in Fig. 8.42(a). The condition of the fault indicates that phase a in not faulted, $I_{fa} = 0$. We can calculate the sequence currents during the fault from the symmetrical transformation.

$$\begin{bmatrix} I_{fa}^{0} \\ I_{fa}^{+} \\ I_{fa}^{-} \end{bmatrix} = \frac{1}{3}\begin{bmatrix} 1 & 1 & 1 \\ 1 & a & a^2 \\ 1 & a^2 & a \end{bmatrix}\begin{bmatrix} 0 \\ I_{fb} \\ I_{fc} \end{bmatrix} \tag{8.75}$$

Therefore, the zero sequence current is given as

$$I_{fb} + I_{fc} = 3I_{fa}^{0} \tag{8.76}$$

Because the power grid is balanced and phase a, b, and c voltages at bus i remain balanced:

$$V_{fb} = V_{fc} = \left(I_{fb} + I_{fc}\right) Z_{FG} \tag{8.77}$$

Substituting for phase b and c current, $I_{fb} + I_{fc} = 3I_{fa}^{0}$, we have

$$V_{fb} = V_{fc} = 3 \cdot Z_{FG} \cdot I_{fa}^{0}$$

The above analysis clearly indicates that for computing a double line to ground fault, we need to use the sequence network connections given in Fig. 8.42(b).

Similar to the single line to ground fault in that the fault involves the ground connection, for the calculation of the double line to ground fault current, we need the Thevenin impedance from the fault point and the Thevenin voltage before the fault. Therefore, we need to construct the positive, negative, and zero sequence impedance matrices as given by Z_{Bus}^{+}, Z_{Bus}^{-}, and Z_{Bus}^{0} in Equations 8.78–8.80.

$$Z_{Bus}^{+} = \begin{array}{c} \begin{matrix} 1 & & i & & n \end{matrix} \\ \begin{bmatrix} Z_{11}^{+} & \cdots & Z_{i1}^{+} & \cdots & Z_{1n}^{+} \\ \cdot & \cdots & \cdot & \cdots & \cdot \\ Z_{i1}^{+} & \cdots & Z_{ii}^{+} & \cdots & Z_{in}^{+} \\ \cdot & \cdots & \cdot & \cdots & \cdot \\ Z_{n1}^{+} & \cdots & Z_{ni}^{+} & \cdots & Z_{nn}^{+} \end{bmatrix} \begin{matrix} 1 \\ \cdot \\ i \\ \cdot \\ n \end{matrix} \end{array}, \tag{8.78}$$

$$Z_{Bus}^{-} = \begin{array}{c} \begin{matrix} 1 & & i & & n \end{matrix} \\ \begin{bmatrix} Z_{11}^{-} & \cdots & Z_{i1}^{-} & \cdots & Z_{1n}^{-} \\ \cdot & \cdots & \cdot & \cdots & \cdot \\ Z_{i1}^{-} & \cdots & Z_{ii}^{-} & \cdots & Z_{in}^{-} \\ \cdot & \cdots & \cdot & \cdots & \cdot \\ Z_{n1}^{-} & \cdots & Z_{ni}^{-} & \cdots & Z_{nn}^{-} \end{bmatrix} \begin{matrix} 1 \\ \cdot \\ i \\ \cdot \\ n \end{matrix} \end{array}, \tag{8.79}$$

$$Z^0_{Bus} = \begin{array}{c} \begin{matrix} 1 & & i & & n \end{matrix} \\ \begin{bmatrix} Z^0_{11} & \cdots & Z^0_{i1} & \cdots & Z^0_{1n} \\ \cdot & \cdots & \cdot & \cdots & \cdot \\ Z^0_{i1} & \cdots & Z^0_{ii} & \cdots & Z^0_{in} \\ \cdot & \cdots & \cdot & \cdots & \cdot \\ Z^0_{n1} & \cdots & Z^0_{ni} & \cdots & Z^0_{nn} \end{bmatrix} \begin{matrix} 1 \\ \cdot \\ i \\ \cdot \\ n \end{matrix} \end{array} \tag{8.80}$$

Again, the diagonal elements of the Z bus matrices represent the corresponding Thevenin impedance.

8.9.5 Line to Line Faults

Figure 8.43(a) depicts a line to line fault. This type of fault can occur when a phasor conductor falls on another phasor conductor due to insulation failure caused by high wind. It is customary to designate the faulted phases on phase b and phase c. Therefore, the fault point can be expressed as

$$I_{fa} = 0, \qquad I_{fc} = -I_{fb} \tag{8.81}$$

The power grid before the fault and after the fault remains balanced because the fault is removed very quickly by opening the appropriative circuit breakers.

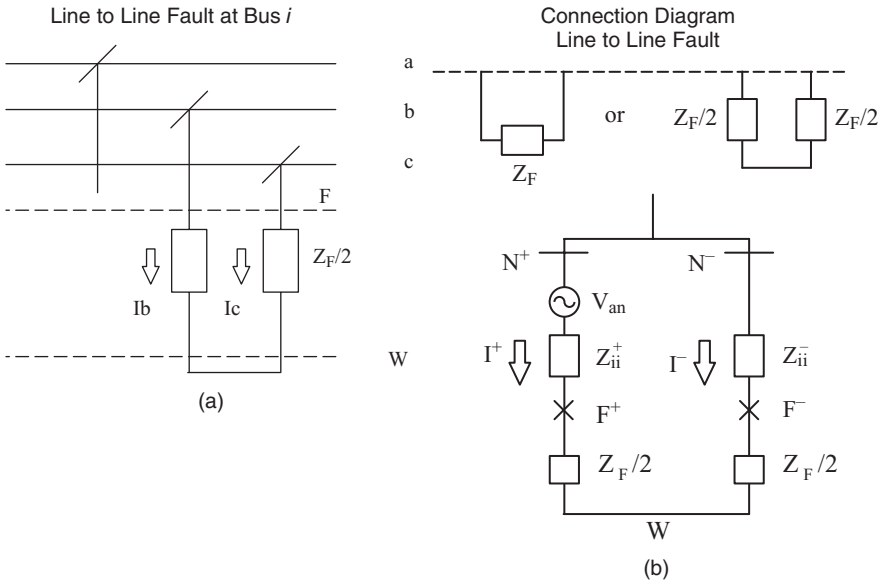

Figure 8.43 **(a)** A Line-to-Line Fault and **(b)** The Sequence Connection for a Line-to-Line Fault.

$$V_{fb} - V_{fc} = I_{fb} \cdot Z_f \tag{8.82}$$

$$\begin{bmatrix} I_{fa}^0 \\ I_{fa}^+ \\ I_{fa}^- \end{bmatrix} = \frac{1}{3}\begin{bmatrix} 1 & 1 & 1 \\ 1 & a & a^2 \\ 1 & a^2 & a \end{bmatrix}\begin{bmatrix} 0 \\ I_{fb} \\ -I_{fb} \end{bmatrix} \tag{8.83}$$

From the above, we have

$$I_{fa}^0 = 0 \tag{8.84}$$

$$I_{fa}^+ = -I_{fa}^- \tag{8.85}$$

The above results clearly indicate that we need to use the sequence network connection given by Fig. 8.43(b) to calculate the line to line fault.

To compute the Thevenin impedance of the faulted bus, we need to construct positive and negative sequence impedance matrices as given by Z_{Bus}^+ and Z_{Bus}^- in Equations 8.86 and 8.87. The diagonal elements of the Z bus matrix are equal to the Thevenin impedance. The Thevenin voltage is equal to the faulted bus before the fault.

$$Z_{Bus}^+ = \begin{array}{c} \begin{matrix} 1 & & i & & n \end{matrix} \\ \begin{bmatrix} Z_{11}^+ & \cdots & Z_{i1}^+ & \cdots & Z_{1n}^+ \\ \cdot & \cdots & \cdot & \cdots & \cdot \\ Z_{i1}^+ & \cdots & Z_{ii}^+ & \cdots & Z_{in}^+ \\ \cdot & \cdots & \cdot & \cdots & \cdot \\ Z_{n1}^+ & \cdots & Z_{ni}^+ & \cdots & Z_{nn}^+ \end{bmatrix} \begin{matrix} 1 \\ \cdot \\ i \\ \cdot \\ n \end{matrix} \end{array}, \tag{8.86}$$

$$Z_{Bus}^- = \begin{array}{c} \begin{matrix} 1 & & i & & n \end{matrix} \\ \begin{bmatrix} Z_{11}^- & \cdots & Z_{i1}^- & \cdots & Z_{1n}^- \\ \cdot & \cdots & \cdot & \cdots & \cdot \\ Z_{i1}^- & \cdots & Z_{ii}^- & \cdots & Z_{in}^- \\ \cdot & \cdots & \cdot & \cdots & \cdot \\ Z_{n1}^- & \cdots & Z_{ni}^- & \cdots & Z_{nn}^- \end{bmatrix} \begin{matrix} 1 \\ \cdot \\ i \\ \cdot \\ n \end{matrix} \end{array} \tag{8.87}$$

Example 8.5 Consider the power system given below.

The system data are given in per unit with a MVA base of 100.

Generator A: $X_G^+ = 0.25$, $X_G^- = 0.15$, $X_G^0 = 0.03$ p.u
Generator B: $X_G^+ = 0.2$, $X_G^- = 0.12$, $X_G^0 = 0.02$ p.u
Transmission line C–D: $Z^+ = Z^- = j0.08$, $Z^0 = j0.14$ p.u
Transmission line D–E: $Z^+ = Z^- = j0.06$, $Z^0 = j0.12$ p.u

Figure 8.44 A One-Line Diagram of Example 8.5.

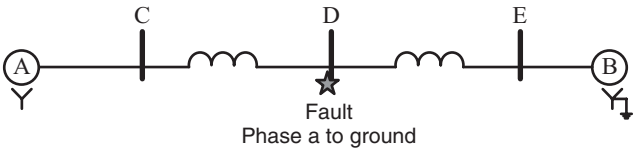

Figure 8.45 A Three-Phase Diagram of a Single Line to Ground Fault at Bus D.

Perform the following:

i) Assume generator A is Y connected and ungrounded and generator B is Y connected and grounded. Compute the single line to ground fault at bus D. Determine the sequence networks and show the flow of line to ground current in the faulted system at bus D.

Solution

The equivalent circuit for a single line to ground fault at bus D is shown in Fig. 8.46.

The sequence networks of Example 8.5 are calculated from the equivalent circuit of Fig. 8.46:

$$I = \frac{V}{Z} = \frac{1\angle 0^\circ}{j0.39} = 2.56\angle -90^\circ$$

$$I^0_{aCD} = 0$$

$$I^+_{aCD} = 2.56\angle -90^\circ \times \frac{j0.26}{j0.26 + j0.33} = 1.12\angle -90^\circ$$

$$I^-_{aCD} = 2.56\angle -90^\circ \times \frac{j0.18}{j0.18 + j0.23} = 1.12\angle -90^\circ$$

The actual line currents in line C–D are as follows:

$$\begin{bmatrix} I_{aCD} \\ I_{bCD} \\ I_{cCD} \end{bmatrix} = [T_s] \begin{bmatrix} I^0_{aCD} \\ I^+_{aCD} \\ I^-_{aCD} \end{bmatrix} = \begin{bmatrix} 1 & 1 & 1 \\ 1 & a^2 & a \\ 1 & a & a^2 \end{bmatrix} \begin{bmatrix} 0 \\ 1.12\angle -90^\circ \\ 1.12\angle -90^\circ \end{bmatrix} = \begin{bmatrix} -j2.24 \\ j1.12 \\ j1.12 \end{bmatrix}$$

The line currents in line E–D are as follows:

$$I^0_{aED} = I = 2.56\angle -90^\circ$$

$$I^+_{aED} = I - I^+_{aCD} = 1.44\angle -90^\circ$$

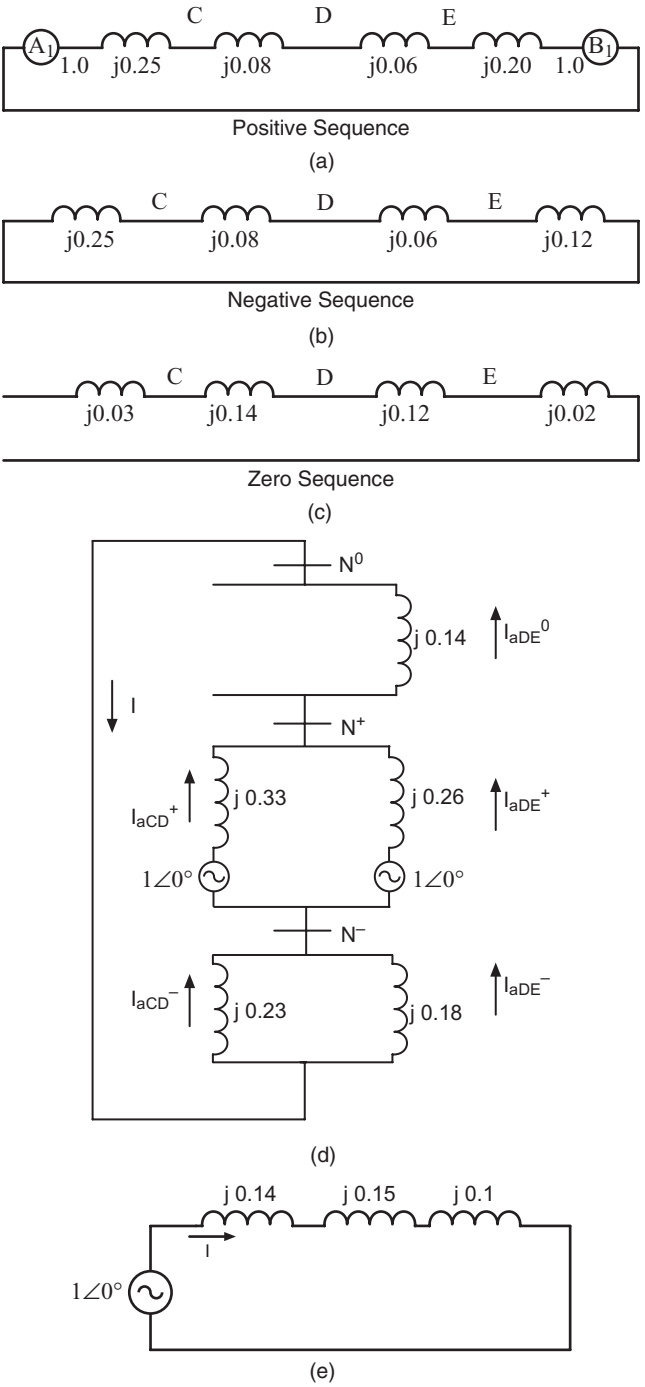

Figure 8.46 For Example 8.5: **(a)** Positive Sequence Network, **(b)** Negative Sequence Network, **(c)** Zero Sequence Network, **(d)** Connection Diagram of Sequence Networks for Single Line to Ground Fault at Bus D, and **(e)** Simplified Circuit of (d).

$$I_{aED}^{-} = I - I_{aCD}^{-} = 1.44\angle -90^\circ$$

$$\begin{bmatrix} I_{aED} \\ I_{bED} \\ I_{cED} \end{bmatrix} = [T_s] \begin{bmatrix} I_{aED}^{0} \\ I_{aED}^{+} \\ I_{aED}^{-} \end{bmatrix} = \begin{bmatrix} 1 & 1 & 1 \\ 1 & a^2 & a \\ 1 & a & a^2 \end{bmatrix} \begin{bmatrix} 2.56\angle -90^\circ \\ 1.44\angle -90^\circ \\ 1.44\angle -90^\circ \end{bmatrix} = \begin{bmatrix} -j5.44 \\ -j1.12 \\ -j1.12 \end{bmatrix}$$

Alternatively, the Z_{th} for bus D can also be computed from the Z_{Bus}^{+}, Z_{Bus}^{-}, and Z_{Bus}^{0}, which are shown below.

$$Z_{Bus}^{+} = \begin{matrix} \\ C \\ D \\ E \end{matrix} \begin{matrix} \begin{matrix} C & D & E \end{matrix} \\ \begin{bmatrix} j0.14 & j0.11 & j0.08 \\ j0.11 & j0.15 & j0.11 \\ j0.08 & j0.11 & j0.13 \end{bmatrix} \end{matrix}, \quad Z_{Bus}^{-} = \begin{matrix} \\ C \\ D \\ E \end{matrix} \begin{matrix} \begin{matrix} C & D & E \end{matrix} \\ \begin{bmatrix} j0.10 & j0.07 & j0.04 \\ j0.07 & j0.10 & j0.07 \\ j0.04 & j0.07 & j0.08 \end{bmatrix} \end{matrix},$$

$$Z_{Bus}^{0} = \begin{matrix} \\ C \\ D \\ E \end{matrix} \begin{matrix} \begin{matrix} C & D & E \end{matrix} \\ \begin{bmatrix} j0.28 & j0.14 & j0.02 \\ j0.14 & j0.14 & j0.02 \\ j0.02 & j0.02 & j0.02 \end{bmatrix} \end{matrix}$$

The positive sequence Thevenin impedance for bus D is given by $Z_{Th,D}^{+} = Z_{DD}^{+} = j0.15$.

The negative sequence Thevenin impedance for bus D is given by $Z_{Th,D}^{-} = Z_{DD}^{-} = j0.10$.

The zero sequence Thevenin impedance for bus D is given by $Z_{Th,D}^{0} = Z_{DD}^{0} = j0.14$.

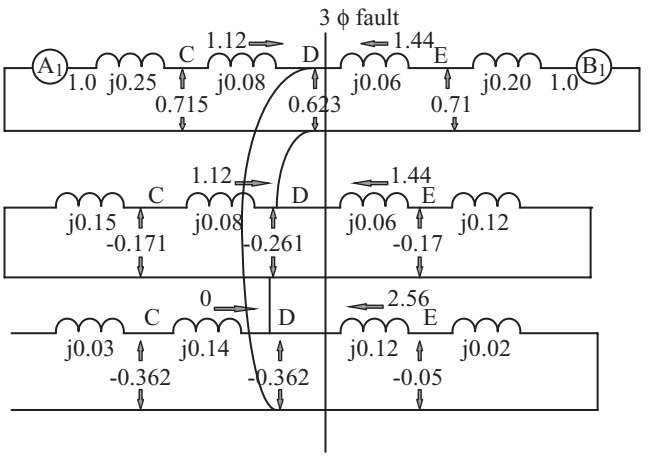

Figure 8.47 Current Flow in the Sequence Networks of Example 8.5.

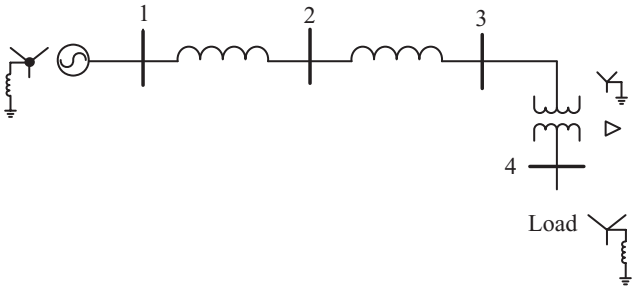

Figure 8.48 The System for Example 8.6.

The above values are same as those shown in Fig. 8.46(e) and the corresponding sequence currents can be calculated as shown before.

Example 8.6 Consider the power grid given in Fig. 8.48.
The sequence network data based on 100 MVA are

$$Z_G^+ = Z_G^- = j0.1 \text{ p.u}, \qquad Z_G^0 = j0.05 \text{ p.u}$$

$$Z_{12}^+ = Z_{12}^- = j0.3 \text{ p.u}, \qquad Z_{12}^0 = j0.6 \text{ p.u}$$

$$Z_{23}^+ = Z_{23}^- = j0.4 \text{ p.u}, \qquad Z_{23}^0 = j0.5 \text{ p.u}$$

$$Z_{Trans}^+ = Z_{Trans}^- = Z_{Trans}^0 = j0.08 \text{ p.u}$$

Assume the load is given as

$$S_{Load} = 1 + j0.5 \text{ p.u}$$

And the load voltage is

$$V_L = 0.9\angle -4.0 \text{ p.u};$$

The ground impedance in the generator is equal to j.01 p.u. For a single line to ground fault at bus 2, compute the following:

i) The fault currents flowing from bus 1 to bus 2 (faulted bus) and from bus 3 when the load is ignored
ii) The same as part *i*, but take the load into consideration
iii) The same as part *i*, but assume the generator is not grounded

Solution
i) The sequence circuits for a single line to ground fault at bus 2 without considering the loads is shown in Fig. 8.49.

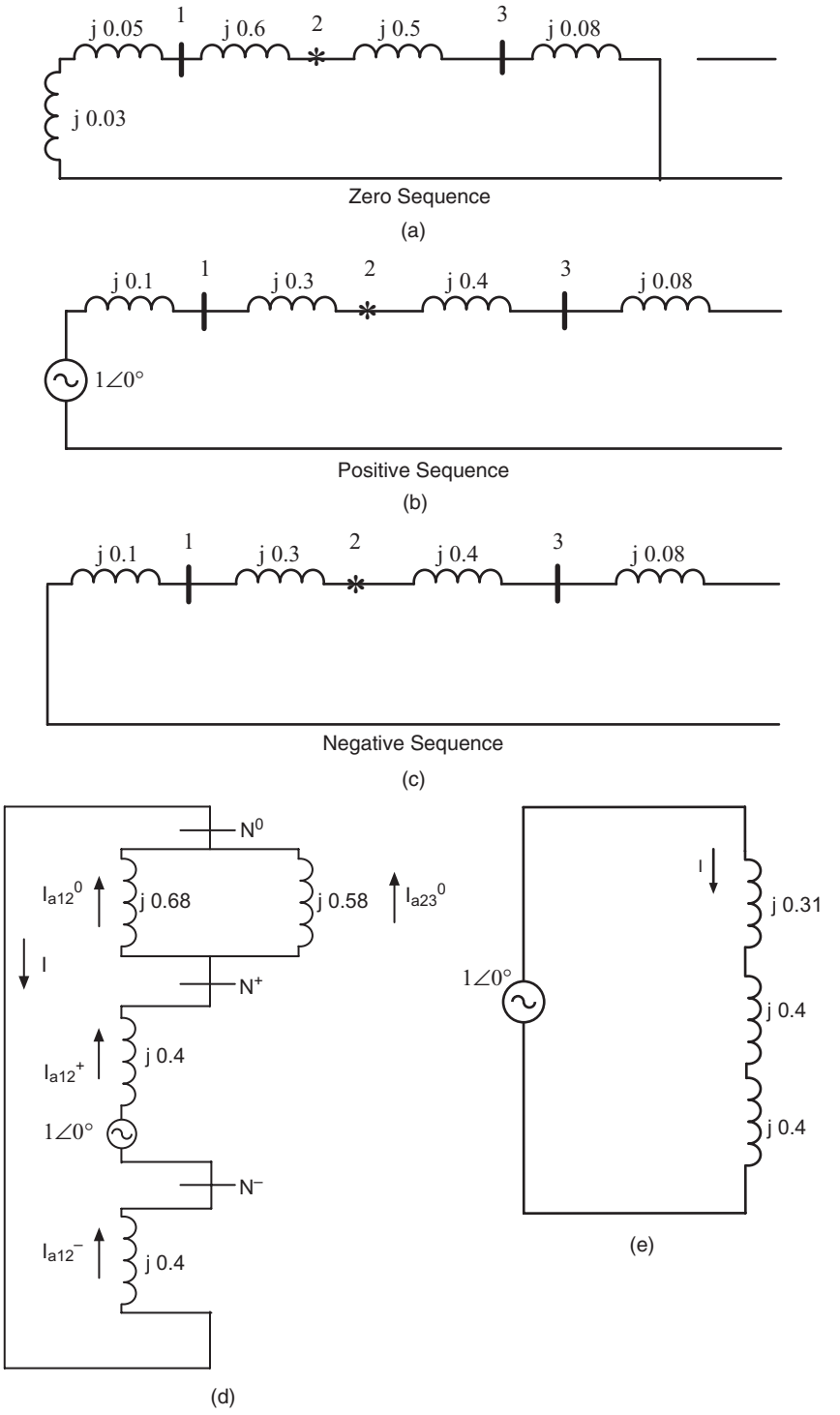

Figure 8.49 For Example 8.6, part *i*: **(a)** Zero Sequence Network, **(b)** Positive Sequence Network, **(c)** Negative Sequence Network, **(d)** Connection Diagram for Single Line to Ground Fault at Bus 2, and **(e)** Simplified Circuit of (d).

From Fig. 8.49, the sequence currents are calculated as follows:

$$I = \frac{V}{Z} = \frac{1\angle 0^\circ}{j1.11} = 0.9\angle -90^\circ$$

$$I_{a12}^0 = 0.9\angle -90^\circ \times \frac{j0.58}{j0.58 + j0.65} = 0.42\angle -90^\circ$$

$$I_{a12}^+ = I_{a12}^- = I = 0.9\angle -90^\circ$$

The actual currents in line 1–2 are given by

$$\begin{bmatrix} I_{a12} \\ I_{b12} \\ I_{c12} \end{bmatrix} = [T_s] \begin{bmatrix} I_{a12}^0 \\ I_{a12}^+ \\ I_{a12}^- \end{bmatrix} = \begin{bmatrix} 1 & 1 & 1 \\ 1 & a^2 & a \\ 1 & a & a^2 \end{bmatrix} \begin{bmatrix} 0.42\angle -90^\circ \\ 0.9\angle -90^\circ \\ 0.9\angle -90^\circ \end{bmatrix} = \begin{bmatrix} -j2.22 \\ j0.48 \\ j0.48 \end{bmatrix}$$

The sequence currents in line 3–2 are given by

$$I_{a32}^0 = I - I_{a12}^0 = 0.48\angle -90^\circ$$

$$I_{a32}^+ = I_{a32}^- = 0$$

The actual line currents in line 3–2 are given by

$$\begin{bmatrix} I_{a32} \\ I_{b32} \\ I_{c32} \end{bmatrix} = [T_s] \begin{bmatrix} I_{a32}^0 \\ I_{a32}^+ \\ I_{a32}^- \end{bmatrix} = \begin{bmatrix} 1 & 1 & 1 \\ 1 & a^2 & a \\ 1 & a & a^2 \end{bmatrix} \begin{bmatrix} 0.48\angle -90^\circ \\ 0 \\ 0 \end{bmatrix} = \begin{bmatrix} -j0.48 \\ -j0.48 \\ -j0.48 \end{bmatrix}$$

Alternatively, the Z_{th} for bus 2 can also be computed from the Z_{Bus}^+, Z_{Bus}^-, and Z_{Bus}^0, which are shown below.

$$Z_{Bus}^+ = Z_{Bus}^- = \begin{bmatrix} j0.1 & j0.1 & j0.1 \\ j0.1 & j0.4 & j0.4 \\ j0.1 & j0.4 & j0.8 \end{bmatrix}, \qquad Z_{Bus}^0 = \begin{bmatrix} j0.07 & j0.04 & j0.01 \\ j0.04 & j0.31 & j0.04 \\ j0.01 & j0.04 & j0.07 \end{bmatrix}$$

The positive sequence Thevenin impedance for bus 2 is given by $Z_{Th,2}^+ = Z_{22}^+ = j0.4$.

The negative sequence Thevenin impedance for bus 2 is given by $Z_{Th,2}^- = Z_{22}^- = j0.4$.

The zero sequence Thevenin impedance for bus 2 is given by $Z_{Th,2}^0 = Z_{22}^0 = j0.31$.

From Fig. 8.49(e) we see that the values of Thevenin impedance are the same as that calculated from the Z_{Bus} sequence matrices.

ii) Taking the load into consideration, the Δ equivalent load is given by

$$\bar{Z}_Y = \frac{V^2}{S^*} = \frac{(0.9/\sqrt{3})^2}{1 - j0.5} = 0.24\angle 26.6°$$

$$\bar{Z}_\Delta = 3\bar{Z}_Y = 0.72\angle 26.6°$$

$$Z_{load00} = Z_{load11} = Z_{load22} = 0.72\angle 26.6°$$

From Fig. 8.50, the sequence currents are calculated as follows:

$$Z_{th}^0 = \frac{(j0.68)(j0.58)}{(j0.68 + j0.58)} = j0.31$$

$$Z_{th}^+ = Z_{th}^- = \frac{(j0.4)(0.64 + j0.8)}{(j0.4) + (0.64 + j0.8)} = 0.06 + j0.3$$

$$V_{th}^+ = \frac{1\angle 0° \times (0.64 + j0.8)}{(j0.4) + (0.64 + j0.8)} = 0.75\angle -10.58°$$

$$I = \frac{0.75\angle -10.58°}{0.06 + j0.3 + 0.06 + j0.3 + j0.31} = 0.82\angle -93°$$

$$I_{12}^0 = \frac{0.82\angle -93° \times j0.58}{j0.58 + j0.68} = 0.38\angle -93°$$

$$I_{12}^+ = \frac{0.82\angle -93° \times (0.64 + j0.8) - 0.75\angle -10.88°}{j0.4 + 0.64 + j0.8} = 0.32\angle -167°$$

$$I_{12}^- = \frac{0.82\angle -93° \times (0.64 + j0.8)}{j0.4 + 0.64 + j0.8} = 0.62\angle -103°$$

The actual line currents in line 1–2 are as follows:

$$\begin{bmatrix} I_{a12} \\ I_{b12} \\ I_{c12} \end{bmatrix} = [T_s] \begin{bmatrix} I_{a12}^0 \\ I_{a12}^+ \\ I_{a12}^- \end{bmatrix} = \begin{bmatrix} 1 & 1 & 1 \\ 1 & a^2 & a \\ 1 & a & a^2 \end{bmatrix} \begin{bmatrix} 0.38\angle -93° \\ 0.32\angle -167° \\ 0.62\angle -103° \end{bmatrix} = \begin{bmatrix} 1.16\angle -114° \\ 0.67\angle 8° \\ 0.32\angle -142° \end{bmatrix}$$

The sequence currents in line 3–2 are as follows:

$$I_{32}^0 = I - I_{12}^0 = 0.44\angle -93°$$

$$I_{32}^+ = I - I_{12}^+ = 0.79\angle -70°$$

$$I_{32}^- = I - I_{12}^- = 0.24\angle -65°$$

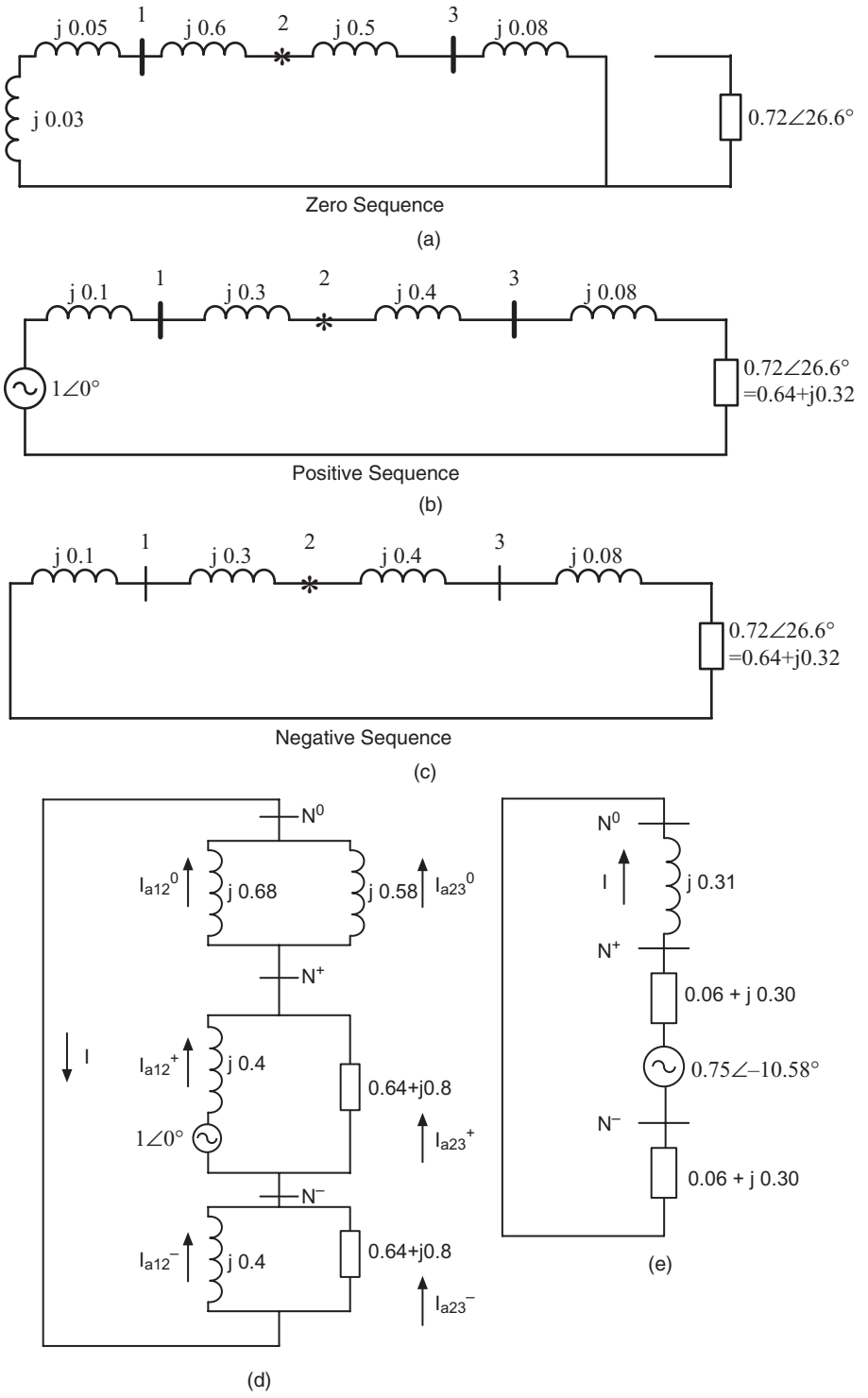

Figure 8.50 For Example 8.6, part *ii*: **(a)** Zero Sequence Network, **(b)** Positive Sequence Network, **(c)** Negative Sequence Network, **(d)** Connection Diagram for Single Line to Ground Fault at Bus 2, and **(e)** the Simplified Circuit of (d).

The actual line currents in the line 3–2 are given by

$$\begin{bmatrix} I_{a32} \\ I_{b32} \\ I_{c32} \end{bmatrix} = [T_s] \begin{bmatrix} I^0_{a32} \\ I^+_{a32} \\ I^-_{a32} \end{bmatrix} = \begin{bmatrix} 1 & 1 & 1 \\ 1 & a^2 & a \\ 1 & a & a^2 \end{bmatrix} \begin{bmatrix} 0.44\angle -93^\circ \\ 0.79\angle -70^\circ \\ 0.24\angle -65^\circ \end{bmatrix} = \begin{bmatrix} 1.44\angle -106^\circ \\ 0.35\angle -145^\circ \\ 0.62\angle -8.97^\circ \end{bmatrix}$$

Alternatively, the Z_{th} for bus 2 can also be computed from the Z^+_{Bus}, Z^-_{Bus}, and Z^0_{Bus}, which is shown below.

$$Z^+_{Bus} = Z^-_{Bus} = \begin{bmatrix} 0.004 + j0.094 & 0.014 + j0.074 & 0.028 + j0.048 \\ 0.014 + j0.074 & 0.06 + j0.30 & 0.111 + j0.192 \\ 0.028 + j0.048 & 0.111 + j0.192 & 0222 + j0.385 \end{bmatrix},$$

$$Z^0_{Bus} = \begin{bmatrix} j0.07 & j0.04 & j0.01 \\ j0.04 & j0.31 & j0.04 \\ j0.01 & j0.04 & j0.07 \end{bmatrix}$$

The positive sequence Thevenin impedance for bus 2 is given by $Z^+_{Th,2} = Z^+_{22} = 0.06 + j0.3$.

The negative sequence Thevenin impedance for bus 2 is given by $Z^-_{Th,2} = Z^-_{22} = 0.06 + j0.3$.

The zero sequence Thevenin impedance for bus 2 is given by $Z^0_{Th,2} = Z^0_{22} = j0.31$.

From Fig. 8.50(e) we see that the values of Thevenin impedance are the same as that calculated from the Z_{Bus} sequence matrices.

iii) The sequence circuits, at no load when the generator is not grounded, are given in Fig. 8.51.

The sequence currents, calculated from Fig. 8.51, are as follows:

$$I = \frac{V}{Z} = \frac{1\angle 0^\circ}{j1.38} = 0.72\angle -90^\circ$$

$$I^0_{a12} = 0$$

$$I^+_{a12} = I^-_{a12} = I = 0.72\angle -90^\circ$$

The actual line currents in line 1–2 are as follows:

$$\begin{bmatrix} I_{a12} \\ I_{b12} \\ I_{c12} \end{bmatrix} = [T_s] \begin{bmatrix} I^0_{a12} \\ I^+_{a12} \\ I^-_{a12} \end{bmatrix} = \begin{bmatrix} 1 & 1 & 1 \\ 1 & a^2 & a \\ 1 & a & a^2 \end{bmatrix} \begin{bmatrix} 0 \\ 0.72\angle -90^\circ \\ 0.72\angle -90^\circ \end{bmatrix} = \begin{bmatrix} -j1.44 \\ j0.72 \\ j0.72 \end{bmatrix}$$

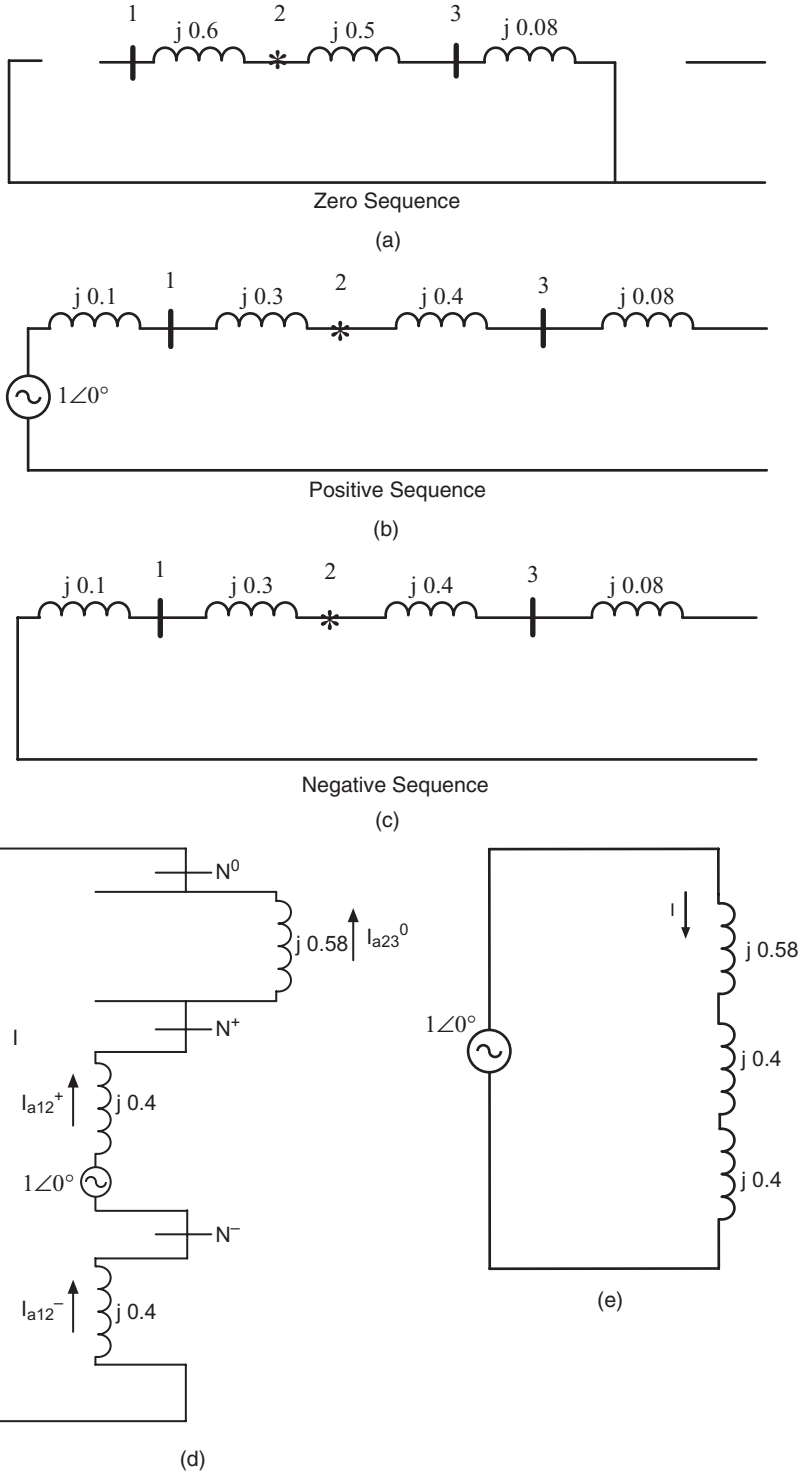

Figure 8.51 For Example 8.6, part *iii*: **(a)** Zero Sequence Network, **(b)** Positive Sequence Network, **(c)** Negative Sequence Network, **(d)** Connection Diagram for Single Line to Ground Fault at Bus 2, and **(e)** the Simplified Circuit of (d).

The sequence currents in the line 3–2 are as follows:

$$I_{a32}^{0} = I = 0.72\angle -90^\circ$$

$$I_{a32}^{+} = I_{a32}^{-} = 0$$

The actual line currents in 3–2 are given by:

$$\begin{bmatrix} I_{a32} \\ I_{b32} \\ I_{c32} \end{bmatrix} = [T_s] \begin{bmatrix} I_{a32}^{0} \\ I_{a32}^{+} \\ I_{a32}^{-} \end{bmatrix} = \begin{bmatrix} 1 & 1 & 1 \\ 1 & a^2 & a \\ 1 & a & a^2 \end{bmatrix} \begin{bmatrix} 0.72\angle -90^\circ \\ 0 \\ 0 \end{bmatrix} = \begin{bmatrix} -j0.72 \\ -j0.72 \\ -j0.72 \end{bmatrix}$$

Alternatively, the Z_{th} for bus 2 can also be computed from the Z_{Bus}^{+}, Z_{Bus}^{-}, and Z_{Bus}^{0}, which is shown below.

$$Z_{Bus}^{+} = Z_{Bus}^{-} = \begin{bmatrix} j0.1 & j0.1 & j0.1 \\ j0.1 & j0.4 & j0.4 \\ j0.1 & j0.4 & j0.8 \end{bmatrix}, \qquad Z_{Bus}^{0} = \begin{bmatrix} j1.18 & j0.58 & j0.08 \\ j0.58 & j0.58 & j0.08 \\ j0.08 & j0.08 & j0.08 \end{bmatrix}$$

The positive sequence Thevenin impedance for bus 2 is given by $Z_{Th,2}^{+} = Z_{22}^{+} = j0.4$.

The negative sequence Thevenin impedance for bus 2 is given by $Z_{Th,2}^{-} = Z_{22}^{-} = j0.4$.

The zero sequence Thevenin impedance for bus 2 is given by $Z_{Th,2}^{0} = Z_{22}^{0} = j0.58$.

From Fig. 8.51(e) we see that the values of Thevenin impedance are the same as that calculated from the ZBus sequence matrices.

Example 8.7 For Example 8.6, assume a double line fault at bus 2 and compute the currents in each line without considering the loads.

Solution

The equivalent sequence circuits for a double line fault are shown in Fig. 8.52.

The sequence currents for the double line fault at bus 2, calculated from Fig. 8.52, are as follows:

$$I = \frac{V}{Z} = \frac{1\angle 0^\circ}{j0.8} = 1.25\angle -90^\circ$$

$$I_{a12}^{0} = 0$$

$$I_{a12}^{+} = I = 1.25\angle -90^\circ$$

$$I_{a12}^{-} = -I = 1.25\angle 90^\circ$$

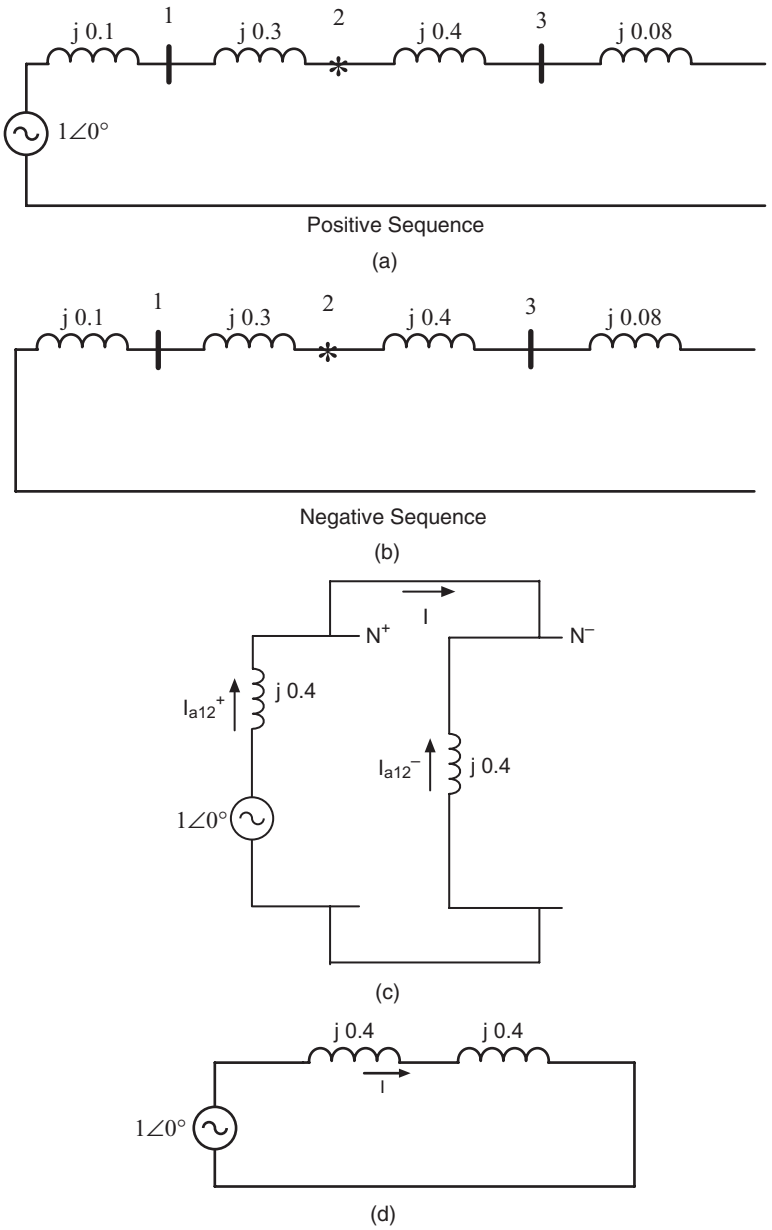

Figure 8.52 For Example 8.7: **(a)** Positive Sequence Network, **(b)** Negative Sequence Network, **(c)** Connection Diagram for Double Line Fault at Bus 2, and **(d)** the Simplified Circuit of (c).

The actual line currents in the line 1–2 are given by

$$\begin{bmatrix} I_{a12} \\ I_{b12} \\ I_{c12} \end{bmatrix} = [T_s] \begin{bmatrix} I^0_{a12} \\ I^+_{a12} \\ I^-_{a12} \end{bmatrix} = \begin{bmatrix} 1 & 1 & 1 \\ 1 & a^2 & a \\ 1 & a & a^2 \end{bmatrix} \begin{bmatrix} 0 \\ 1.25\angle -90^\circ \\ 1.25\angle 90^\circ \end{bmatrix} = \begin{bmatrix} 0 \\ 2.17\angle 180^\circ \\ 2.17\angle 0^\circ \end{bmatrix}$$

The sequence currents in line 3–2 are as follows:

$$I^0_{a32} = 0$$
$$I^+_{a32} = -I^-_{a32} = 0$$

The sequence curremts in 3–2 are given by

$$\begin{bmatrix} I_{a32} \\ I_{b32} \\ I_{c32} \end{bmatrix} = [T_s] \begin{bmatrix} I^0_{a32} \\ I^+_{a32} \\ I^-_{a32} \end{bmatrix} = \begin{bmatrix} 1 & 1 & 1 \\ 1 & a^2 & a \\ 1 & a & a^2 \end{bmatrix} \begin{bmatrix} 0 \\ 0 \\ 0 \end{bmatrix} = \begin{bmatrix} 0 \\ 0 \\ 0 \end{bmatrix}$$

Alternatively, the Z_{th} for bus 2 can also be computed from the Z^+_{Bus} and Z^-_{Bus}, which are shown below.

$$Z^+_{Bus} = Z^-_{Bus} = \begin{bmatrix} j0.1 & j0.1 & j0.1 \\ j0.1 & j0.4 & j0.4 \\ j0.1 & j0.4 & j0.8 \end{bmatrix}$$

The positive sequence Thevenin impedance for bus 2 is given by $Z^+_{Th,2} = Z^+_{22} = j0.4$.

The negative sequence Thevenin impedance for bus 2 is given by $Z^-_{Th,2} = Z^-_{22} = j0.4$.

From Fig. 8.52(d) we see that the values of Thevenin impedance are the same as that calculated from the Z_{Bus} sequence matrices.

PROBLEMS

8.1 Consider a typical power system given in Fig. 8.53.
All reactances are in p.u on a 100 MVA.

$X_{th} = 0.01$ when the maximum number of generators is in service
$X_{th} = 0.015$ when the minimum number of generators is in service

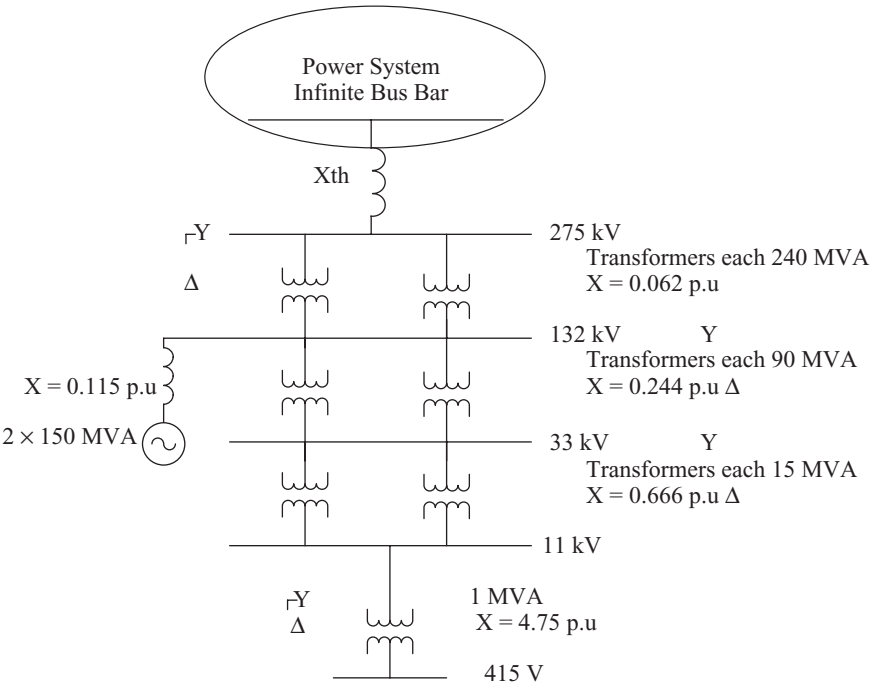

Figure 8.53 A Typical Power Grid System.

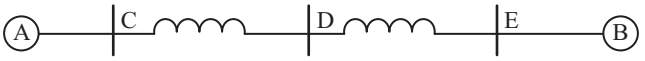

Figure 8.54 A One-Line Diagram for Problem 8.2.

Compute the following:

i) The SCC of the 415 V bus when all transformers are in service, but generator G_1 is not in service. Assume that the maximum numbers of generators are in service.

ii) The SCC of the 415 V bus when all the transformers and G_1 are in service. Assume one generator is in service.

8.2 Consider the power system given in Fig. 8.54.
Generator A:

$$X''_{G(1)} = 0.25,\ X''_{G(2)} = 0.15,\ X''_{G(0)} = 0.03 \text{ p.u}$$

Generator B:

$$X''_{G(1)} = 0.2,\ X''_{G(2)} = 0.12,\ X''_{G(0)} = 0.02 \text{ p.u}$$

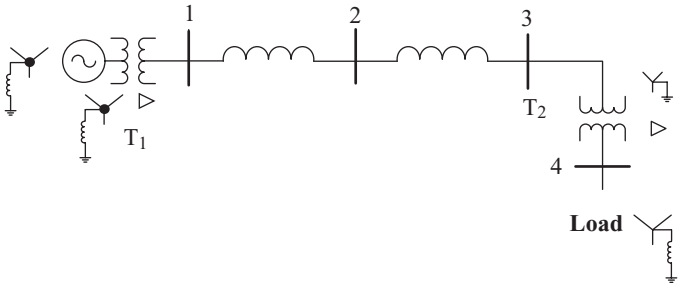

Figure 8.55 The System for Problem 8.3.

Transmission line C–D: $Z_1 = Z_2 = j0.08$, $Z_0 = j0.14$ p.u
Transmission line D–E: $Z_1 = Z_2 = j0.06$, $Z_0 = j0.12$ p.u

All values are given in per unit with a MVA base of 100.

Assume generator A is Y connected and ungrounded and generator B is Y connected and grounded, compute the single line to ground fault at bus D and the current and actual phase voltages (i.e., V_a, V_b, V_c in p.u) of buses C, D, and E.

8.3 Consider the power grid given below.
The sequence network data are

Generator: 20 kV, 100 MVA, 10% positive reactance, negative sequence network = positive sequence reactance, zero sequence reactance = 8% based on the generator's rating
Transmission line length: bus 1–2 = 50 km, reactance = 0.5 Ω/km
bus 2–3 = 100 km, reactance = 0.7 Ω/km
Transformer T_1 = 20 kV/138 kV, 8% reactance, 150 MVA
Transformer T_2 = 138 kV/13.8 kV, 10% reactance, 200 MVA
Transmission line sequence impedances: $Z_1 = Z_2 = j0.06$ p.u, Z_0 = j0.12 in p.u on a 100 MVA base
Transformers' sequence impedances: positive = negative = zero
Load: S_{Load} = 50 MVA, p.f. = 0.95 lagging
Generator ground impedance = j.01 p.u based on its rating

Perform the following:

i) Compute the per unit model for positive, negative, and zero sequence networks based on 100 MVA

8.4 For Problem 8.3, perform the following:

i) Compute the load voltage if the generator is set at 5% above its own rating

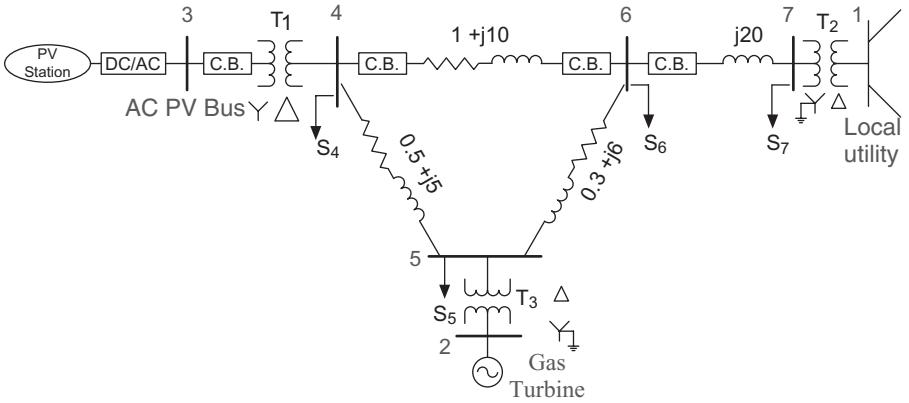

Figure 8.56 A One-Line Diagram for Problem 8.6.

ii) For a double line to ground fault at bus 3, find the fault currents flowing from bus 1 and bus 2 to bus 3 (faulted bus) when the load is ignored

8.5 For Problem 8.3, perform the following:

i) Compute the single line to ground fault at bus 2, but take the load into consideration

ii) The same as part *i*, but assume the generator is not grounded

8.6 Consider the microgrid given in Fig. 8.56.
The impedances of the transmission lines are given in the one-line diagram (Fig. 8.56).

The system data are

PV-generating station: 2 MW, 460 V AC; positive, negative, and zero sequence impedances = 10%.

Gas turbine generating station: positive sequence impedance = 10 MVA, 3.2 kV, 10% reactance

Sequence impedance: negative sequence = positive sequence, zero sequence = ½ positive sequence

Transformers' sequence impedances: positive = negative = zero

Transformer T_1: 10 MVA, 460 V/13.2 kV, 7% reactance

Transformer T_2: 25 MVA, 13.2 kV/69 kV, 9% reactance

Transformer T_3: 20 MVA, 13.2 kV/3.2 kV, 8% reactance

Loads: S_4 = 4 MW, p.f. = 0.9 lagging; S_5 = 8 MW, p.f. = 0.9 lagging;

S_6: 10 MVA, p.f. = 0.9 leading; S_7 = 5 MVA, p.f. = 0.85 lagging

Local power grid: positive, negative, and zero sequence internal reactance = 10 Ω; negligible internal reactance

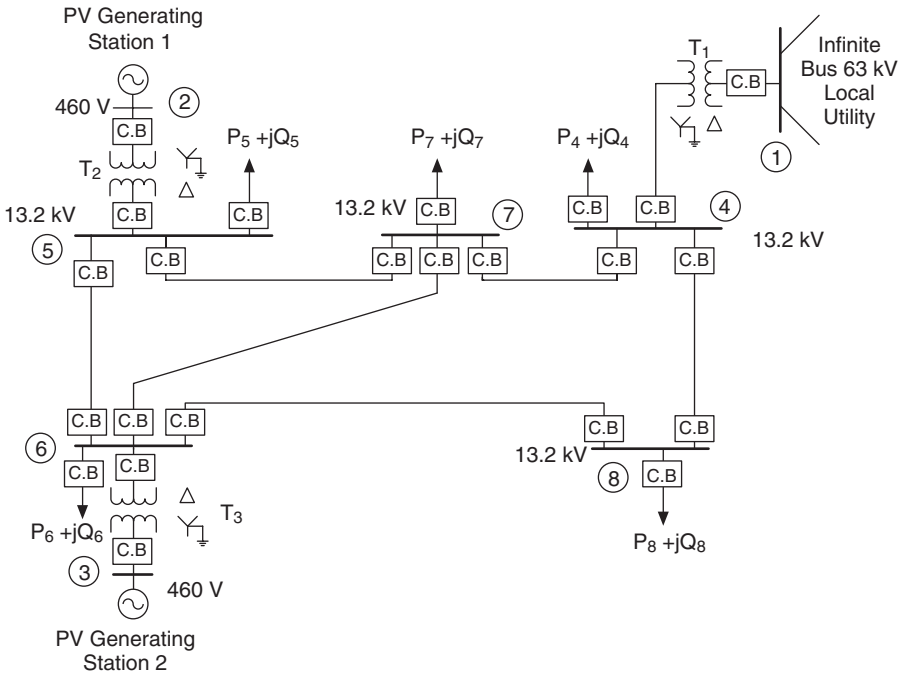

Figure 8.57 A Microgrid of Distributed Generation Connected to a Local Power Network.

Perform the following:

i) Per unit impedance model for positive, negative, and zero sequences

ii) Ignore the loads and compute a single line to ground fault at bus 4

iii) Compute the load voltages; use the load impedance models and compute the single line to ground fault at bus 4

8.7 Consider the microgrid given in Fig. 8.57.
The system data are

Local power grid SCC = 1600 MVA

PV-generating stations: ungrounded, approximate internal impedance (resistive only) = 50% for positive, negative, and zero sequence, 100 MVA

Transformers: 460 V Y grounded/13.2 kV Δ, 10% reactance, 10 MVA

Local power grid transformer: 20 MVA, 63 kV / 13.2 kV, 7% reactance

Transmission line: resistance = 0.0685 Ω/mile, reactance = 0.40 Ω/mile, half of line charging admittance (Y′/2) = 11 Ω/mile. Line 4–7 = 10 miles, 4–8 = 7 miles, 5–6 = 12 miles, 5–7 = 7 miles, 6–7 = 6 miles, 6–8 = 8 miles

Transmission line sequence impedance: positive = negative, zero sequence = 2 × positive sequence impedance

Perform the following:

i) Per unit equivalent model for positive, negative, and zero sequence impedances based on a 20 MVA base

ii) For a three-phase fault on bus 4, compute the bus 4 SCC

8.8 For Problem 8.7, for a single line to ground fault on bus 1, compute the ground fault current

8.9 For Problem 8.7, to increase the security of the system two identical transformers are used at each distribution network and at the interconnection to the local power grid. Compute the SCC of bus 4.

8.10 For Problem 8.7, assume that transformer T_1 is grounded Y-Y. Compute the line to ground fault current at bus 4.

8.11 For Problem 8.7, assume that transformer T_1 is grounded Y-Y. Compute the line to ground fault current at bus 4.

REFERENCES

1. Gross AC. Power system analysis. New York: Wiley; 1986.
2. El-Hawary ME. Electric power systems: design and analysis. Reston, VA: Reston Publishing; 1983.
3. IEEE Brown Book. IEEE recommended practice for power system analysis. New York: Wiley-Interscience; 1980.
4. Grainger J, Stevenson WD. Power systems analysis. New York: McGraw Hill; 2008.
5. Duncan Glover J, Sarma MS. Power system analysis and design. Pacific Grove, CA: Brooks/Cole Thomson Learning; 2002.
6. Stagg GW, El-Abiad AH. Computer methods in power system analysis. New York: McGraw Hill; 1968.
7. Bergen A, Vittal V. Power systems analysis. Englewood Cliffs, NJ: Prentice Hall; 2000.
8. Fortescue CL. Method of symmetrical co-ordinates applied to the solution of polyphase networks. AIEE Transactions 1918; 37(part II):1027–1140.

APPENDIX A

COMPLEX NUMBERS

Complex numbers operations are very important in the steady state of power systems. In this Appendix, we review the fundamentals of a complex number operation. A complex number is a quantity in the form of

$$z = a + jb \tag{A.1}$$

where a and b are real numbers, and $j = \sqrt{-1}$: a = real part; b = imaginary part.

Figure A.1 depicts a complex number plane where $z^* = a - jb$ is called the conjugate of z.

A complex number can also be written in phasor form:

$$z = |z|(\cos\theta + j\sin\theta) \tag{A.2}$$

$$z = |z|e^{j\theta} \tag{A.3}$$

$$z = |z|\angle\theta \tag{A.4}$$

where $|z|$: Modulus (or norm); θ: Argument (or phase)

Conversion between Cartesian and Polar coordinates can be expressed as:

$$z = a + jb \Rightarrow z = |z|\angle\theta$$

$$|z| = \sqrt{(a^2 + b^2)} \tag{A.5}$$

$$\theta = \tan^{-1}(b/a) \tag{A.6}$$

Design of Smart Power Grid Renewable Energy Systems, First Edition. Ali Keyhani.

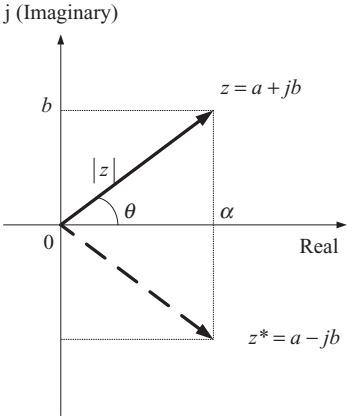

Figure A.1 The Complex Number Representation.

$$z = |z| \angle \theta \Rightarrow z = a + jb$$

$$a = |z| \cos\theta \tag{A.7}$$

$$b = |z| \sin\theta \tag{A.8}$$

We can add or subtract two complex numbers, z_1 and z_2, as shown:

$$z_1 = a + jb,\ z_2 = c + jd$$

Addition / Subtraction

$$z_1 \pm z_2 = (a \pm c) + j(b \pm d) \tag{A.9}$$

We can multiply two complex numbers, z_1 and z_2, in two ways.

$$z_1 \times z_2 = (ac - bd) + j(ad + bc) \tag{A.10}$$

We can obtain the multiplication of z_1 by itself as:

$$z_1 z_1^* = (a + jb)(a - jb) = (a^2 + b^2) \angle 0 = |z_1|^2 \angle 0 \tag{A.11}$$

where z_1^* is the conjugate of z_1.

We can divide two complex numbers in Cartesian form or Polar form.

$$z_1 = a + jb,\ z_2 = c + jd$$

$$\frac{z_1}{z_2} = \frac{(a + jb)}{(c + jd)} = \frac{(a + jb)(c - jd)}{(c + jd)(c - jd)},$$

The results are given below.

$$= \frac{ac+bd}{c^2+d^2} + j\frac{bc-ad}{c^2+d^2} \tag{A.12}$$

The addition and subtraction can be easily done in polar form, whereas multiplication and division have more computation if they are done in Cartesian form.

Let us use the polar form and multiply z_1 and z_2,

$$z_1 = |z_1|e^{j\theta_1},\ z_2 = |z_2|e^{j\theta_2}$$

To multiply, we simply, multiply the magnitude and add the phase angles.

$$z_1 \times z_2 = |z_1||z_2|e^{j(\theta_1+\theta_2)} \tag{A.13}$$

In general, we can take a complex number to the power of n as:

$$z_1^n = |z_1|^n e^{j(n\theta_1)} = |z_1|^n (\cos n\theta_1 + j\sin n\theta_1)$$

To divide two complex numbers, we can simply divide the magnitudes and subtract the angles:

$$\frac{z_1}{z_2} = \frac{|z_1|}{|z_2|}e^{j(\theta_1-\theta_2)} \tag{A.14}$$

Multiplication and division are easier to perform in phasor form.

APPENDIX B

TRANSMISSION LINE AND DISTRIBUTION TYPICAL DATA

TABLE B.1 Typical Characteristics of Copper Conductors, Hard Drawn, 97.3% Conductivity.[1]

Size of Conductor		Approximate Current Carrying Capacity* (A)	R_a Resistance (Ω/Conductor/Mi) at 60 Hz		X_a Inductive reactance (Ω/Conductor/Mi at 1-Ft Spacing)	X'_a Shunt Capacitive Reactance (MΩ/Conductor/Mi at 1-Ft Spacing)
Cmil	mm^2		25°C	50°C	60 Hz	60 Hz
1000000	506	1300	0.0634	0.0685	0.400	0.0901
900000	456	1220	0.0695	0.0752	0.406	0.0916
800000	405	1130	0.0772	0.0837	0.413	0.0934
750000	380	1090	0.0818	0.0888	0.417	0.0943
700000	354	1040	0.0871	0.0947	0.422	0.0954
600000	304	940	0.1006	0.1095	0.432	0.0977
500000	253	840	0.1196	0.1303	0.443	0.1004
500000	253	840	0.1196	0.1303	0.445	0.1005
450000	228	780	0.1323	0.1443	0.451	0.1020

Design of Smart Power Grid Renewable Energy Systems, First Edition. Ali Keyhani.

TABLE B.1 Continued

Size of Conductor		Approximate Current Carrying Capacity* (A)	R_a Resistance (Ω/Conductor/Mi) at 60 Hz		X_a Inductive reactance (Ω/Conductor/Mi at 1-Ft Spacing)	X'_a Shunt Capacitive Reactance (MΩ/Conductor/Mi at 1-Ft Spacing)
Cmil	mm^2		25°C	50°C	60 Hz	60 Hz
400000	202	730	0.1484	0.1619	0.458	0.1038
350000	177	670	0.1690	0.1845	0.466	0.1058
350000	177	670	0.1690	0.1845	0.460	0.1044
300000	152	610	0.1966	0.215	0.476	0.1080
300000	152	610	0.1966	0.215	0.470	0.1068
250000	126	540	0.235	0.257	0.487	0.1108
250000	126	540	0.235	0.257	0.481	0.1094
211600	107	480	0.278	0.303	0.497	0.1132
211600	107	490	0.278	0.303	0.491	0.1119
211600	107	480	0.278	0.303	0.503	0.1136
167800	85	420	0.350	0.382	0.505	0.1153
167800	85	420	0.350	0.382	0.518	0.1171
133100	67	360	0.440	0.481	0.532	0.1205
105500	53	310	0.555	0.607	0.546	0.1240
83690	42	270	0.699	0.765	0.560	0.1274
83690	42	270	0.692	0.757	0.557	0.1246
66370	33	230	0.882	0.964	0.574	0.1308
66370	33	240	0.873	0.955	0.571	0.1281
66370	33	220	0.864	0.945	0.581	0.1345
52630	26	200	1.112	1.216	0.588	0.1343
52630	26	200	1.101	1.204	0.585	0.1315
52630	26	190	1.090	1.192	0.595	0.1380
41740	21	180	1.388	1.518	0.599	0.1349
41740	21	170	1.374	1.503	0.609	0.1415
33100	16	150	1.750	1.914	0.613	0.1384
33100	16	140	1.733	1.895	0.623	0.1449
26250	13	130	2.21	2.41	0.628	0.1419
26250	13	120	2.18	2.39	0.637	0.1483
20820	10	110	2.75	3.01	0.651	0.1517
16510	8	90	3.47	3.80	0.665	0.1552

*For a conductor at 75°C, air temperature at 25°C , wind 1.4 mi/h (2 ft/sec), frequency = 60 Hz.

TABLE B.2 Typical Characteristics of Aluminum Cable, Steel, Reinforced (ACSR; Aluminum Company of America, http://www.alcoa.com/global/en/home.asp)[1]

Size of Conductor		Approximate Current Carrying Capacity* (A)	R_a Resistance (Ω/Conductor/Mi) at 60 Hz		X_a Inductive Reactance (Ω/Conductor/Mi at 1-Ft Spacing)	X'_a Shunt Capacitive Reactance (MΩ/Conductor/Mi at 1-Ft Spacing)
Cmil	mm^2		25°C	50°C (Current ~75% capacity†)	60 Hz	60 Hz
1590000	805	1380	0.0591	0.0684	0.359	0.0814
1510500	765	1340	0.0622	0.0720	0.362	0.0821
1431000	725	1300	0.0656	0.0760	0.363	0.0830
1351000	684	1250	0.0695	0.0803	0.369	0.0838
1272000	644	1200	0.0738	0.0851	0.372	0.0847
1192500	604	1160	0.0788	0.0906	0.376	0.0857
1113000	563	1110	0.0844	0.0969	0.380	0.0867
1033500	523	1060	0.0909	0.1035	0.385	0.0878
954000	483	1010	0.0982	0.1128	0.390	0.0890
900000	456	970	0.104	0.1185	0.393	0.0898
874500	443	950	0.108	0.1228	0.395	0.0903
795000	402	900	0.119	0.1378	0.401	0.0917
795000	402	900	0.117	0.1288	0.399	0.0912
795000	402	910	0.117	0.1288	0.393	0.0904
715500	362	830	0.132	0.1482	0.407	0.0932
715500	362	840	0.131	0.1442	0.405	0.0928
715500	362	840	0.131	0.1442	0.399	0.0920
666600	337	800	0.141	0.1601	0.412	0.0943
636000	322	770	0.148	0.1688	0.414	0.0950
636000	322	780	0.147	0.1618	0.412	0.0946
636000	322	780	0.147	0.1618	0.406	0.0937
605000	306	750	0.155	0.1775	0.417	0.0957
605000	306	760	0.154	0.1720	0.415	0.0953
556500	281	730	0.168	0.1859	0.420	0.0965
556500	281	730	0.168	0.1859	0.415	0.0957
477000	241	670	0.196	0.216	0.430	0.0988
477000	241	670	0.196	0.216	0.424	0.0980
397500	201	590	0.235	0.259	0.441	0.1015
397500	201	600	0.235	0.259	0.435	0.1006
336400	170	530	0.278	0.306	0.451	0.1039
336400	170	530	0.278	0.306	0.445	0.1032
300000	152	490	0.311	0.342	0.458	0.1057
300000	152	500	0.311	0.342	0.462	0.1049
266800	135	460	0.350	0.385	0.465	0.1074

*For a conductor at 75°C, air temperature at 25°C , wind 1.4 mi/h (2 ft/sec), frequency = 60 Hz.
†Current ~75% capacity is "75% of the approx current carrying capacity" and is approximately the current that will produce a conductor temperature of 50°C (25°C rise) with 25°C air temperature, wind 1.4 mi/h.

REFERENCE

1. Alcan Cable. Cable information. Available at http://www.cable.alcan.com/CablePublic/en-CA/Products/Energy+Cables/Bare+Overhead+Conductors/All+Aluminum+Conductor+AAC.htm. Accessed 2011 March 1.

APPENDIX C

ENERGY YIELD OF A PHOTOVOLTAIC MODULE AND ITS ANGLE OF INCIDENCE

The fundamental problems of solar power estimation are formulated in other sources.[1–9] Here we present a summary of solar power estimation as a function of the sun's position. Our objective is to provide an understanding of the sun's photovoltaic (PV) energy yield as input power injected into a microgrid, which is dependent on the location of a PV system. Students interested in a detailed analysis are urged to study references 1 and 2.

To estimate the energy yield of a PV module, the angle of inclination for a module with respect to the sun's position must be determined. The angle of inclination is defined by the position a magnetic needle takes when the horizontal plane is at a specific location. The magnetic inclination is 0 degrees at the magnetic equator and 90 degrees at each of the magnetic poles. The irradiance is defined as the density of radiation incident on a given surface expressed in watts per square meter or watts per square feet. When the sun rotates, the angle at which the rays of sun reach the PV module change. Figure C.1 depicts the inclination angle of a PV module.

In Fig. C.1, α_S is the solar azimuth angle, α is the azimuth angle of the PV module, β is the tilt angle of PV module, and γ_S is the solar elevation from the horizon. The reference angle is defined with respect to the south and is given by 0 degree, east is −90 degrees, and west is +90 degrees. The solar altitude determines the level of irradiance on the PV module. As the earth rotates, the

Design of Smart Power Grid Renewable Energy Systems, First Edition. Ali Keyhani.

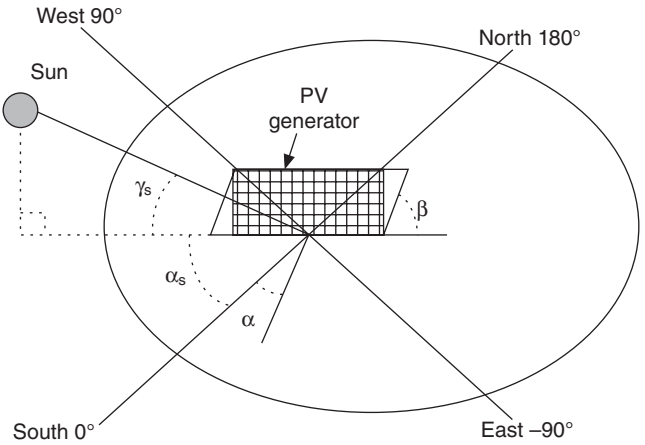

Figure C.1 A Schematic Presentation of the Inclination Angle of a Photovoltaic Module.[1]

elevation angle of the sun changes every month in the year, every day in the month, and every hour of the day. The air mass (AM) factor determines the total distance that the sunlight has to travel to reach the PV module as given by Equation C.1.

$$AM = \frac{1}{\sin(\gamma_S)} \tag{C.1}$$

Equation C.1 defines the relation between air mass and elevation angle. The energy flux incident reaching the atmosphere of earth is known as a solar constant, S. The solar constant, S is characterized in terms of incoming electromagnetic energy of an incident wave on a plane perpendicular at a distance of one astronomical unit (AU) in a per unit area. The AU defines the distance of the sun to the earth. The solar constant, S is equal to 1367 W/m^2. The total power falling on a unit area from the sun's radiation is called irradiance. When the solar radiation travels through the atmosphere to reach the surface of a PV module, a part of incident radiation is lost by air molecule scattering and pollution particles.

A direct beam of radiation is the radiation energy that is not dispersed and reaches the earth's surface directly. When a direct beam of radiation goes through the clouds, it creates diffused radiation. Albedo is the fraction of shortwave radiation that is dispersed from the earth back into space. The sum of these radiation sources—diffuse, direct, and albedo—is called global radiation. The air mass specifies the clearness of the atmosphere. The integration of the irradiance (w/m^2) over a time period gives us the solar energy production.

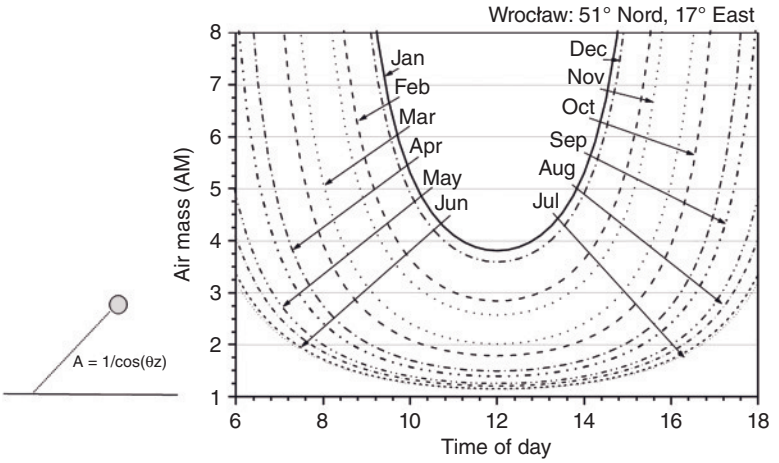

Figure C.2 Air Mass Calculated for a Specific Location.[9]

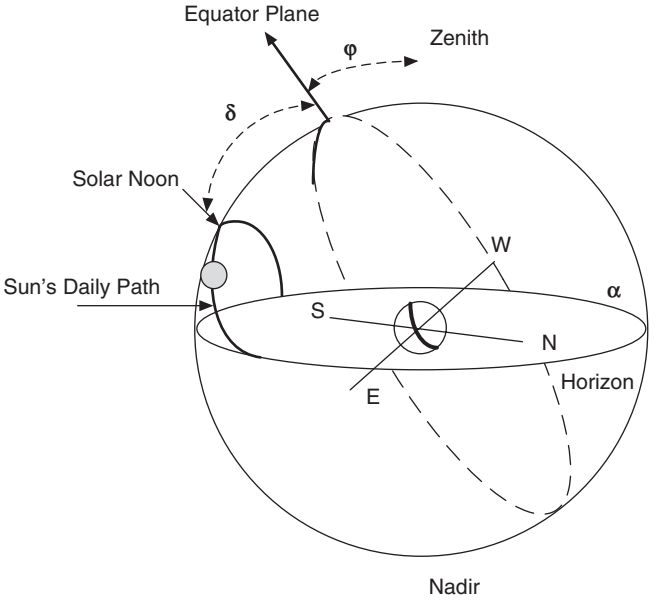

Figure C.3 Solar Noon and Definition of Angles.[9]

The earth rotates in an elliptical orbital plane around the sun. The earth rotates one cycle around the sun in one year. The angle between the equatorial plane and celestial plane is 23.45 degrees. The celestial sphere around the earth shows the relative position of the sun and earth. The angle between the line that connects the equatorial plane to the sun and earth is called a declination angle, δ. This angle will be at its reference point of zero on March 20/21

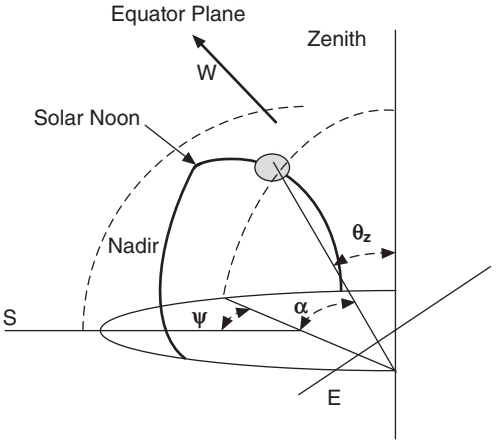

Figure C.4 Solar Noon and Equator Definition of Angles.[1]

(vernal) and on September 22/23 (autumnal) equinoxes. On these days, the sun rises exactly in the east and sets exactly in the west. At summer solstice, June 21/22, δ is 23.45 degrees; at winter solstice, December 21/22, it is –23.45 degrees.

In Fig. C.4, the nadir is the point on the celestial sphere directly beneath a given observer and entirely opposite the zenith.[1] The solar angle is the angle flanked by the meridian going through the sun and the meridian. The meridian is also known as a line of longitude. It is an imaginary arc on the surface of the earth from the North Pole to the South Pole. At solar noon, the angle is zero, and increases toward the east. In Fig. C.4, α defines the elevation angle and φ is the latitude for a given geographic location on the surface of the earth. During the daily earth rotation, the solar declination angle δ is assumed to be constant and equal to its value at midday. The irradiation on an inclined surface can be expressed as

$$\sin\alpha = \sin\delta \cdot \sin\varphi + \cos\delta \cdot \cos\varphi \cdot \cos w = \cos\theta_z \tag{C.2}$$

$$\cos\varphi = \frac{(\sin\alpha \cdot \sin\varphi - \sin\delta)}{(\cos\alpha \cdot \cos\varphi)} \tag{C.3}$$

From Equations C.2 and C.3, the solar hour angle can be found as

$$\omega_S = \cos^{-1}(-\tan\varphi \cdot \tan\delta) \tag{C.4}$$

where ω_S is the sunrise angle and $-\omega_S$ is the sunset angle for the day of the year.

The amount of solar energy is expressed in the form of global incident energy on a horizontal surface. Global daily irradiation energy is denoted by G.

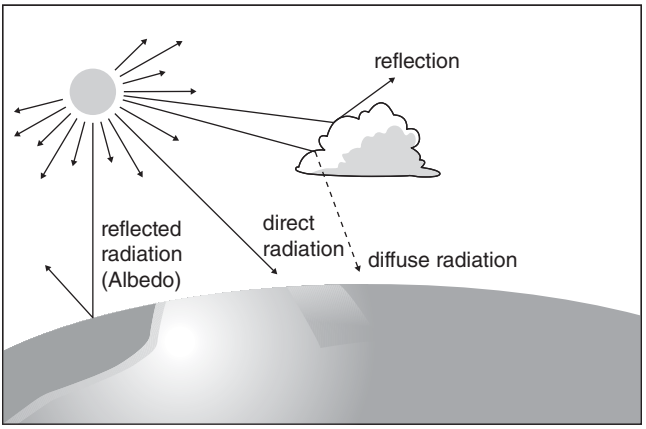

Figure C.5 Irradiation Components.[9]

The global daily irradiation (G) values are estimated for a typical day in any one month for a location on the earth's surface. B_o is the irradiation energy received over one day on a horizontal surface area above the atmosphere and is calculated using the expression below

$$B_o = 24/\pi \cdot S \cdot \{1 + 33 \cdot \cos(2 \cdot \pi \cdot d_n / 365)\} \cdot \{\cos\varphi \cdot \cos\delta \cdot \sin\omega_S + \omega_S \cdot \sin\varphi \cdot \sin\delta\} \quad \text{(C.5)}$$

where ω_S is the hour angle, d_n is the number of day starting from January 1, $d_n = 1$ and December 31, $d_n = 365$. By using B_o as a reference and value of G, the clearness index, KT can be estimated as

$$KT = G/B_o \quad \text{(C.6)}$$

In Equation C.5, B_o is calculated for the variation of extraterrestrial irradiance due to the eccentricity of the earth's orbit. The diffuse irradiation, D is calculated by using the diffuse fraction index D/G of the global irradiation. D/G is the universal function of clearness index, KT. $B = G - D$ gives the separate beam and diffuse radiation.

The angular dependent of each component will give the diffuse irradiation, D and beam irradiation, B on an inclined surface. The total albedo is calculated by using the reflectivity of the surrounding area. The total albedo is found by adding the albedo, beam, and diffuse irradiation.

For calculations of the average monthly irradiation, the daily global irradiation, G for a day, the middle of each month; the solar constant, S, which is 1367 W/m^2 the site's geographical latitude and the solar declination angle, δ for the day of the year can be used. Table C.1 depicts the typical albedo reflectivity coefficients.

TABLE C.1 Typical Reflectivity.

Ground Cover	Reflectivity
Dry bare ground	0.2
Dry grassland	0.3
Desert sand	0.4
Snow	0.5–0.8

From Equation C.6, *KT*, the clearance index can be calculated from the daily irradiation data, G.

The disuse irradiation, D can be calculated from Equation C.7.

$$D/G = 1 - 1.13 \cdot KT \tag{C.7}$$

The beam irradiation, *B* for the horizontal surface can also be found simply by subtracting *D* from *G*, *B* = *G* – *D*. The beam irradiation *B(β)* on a south-facing panel inclined at an angle β to the horizontal surface can be estimated in terms of the beam irradiation, *B* for the horizontal surface.

$$B(\beta) = B \cdot \frac{\cos(\phi - \beta) \cdot \cos\delta \cdot \sin[\omega_s(\phi - \beta)] + \omega_s(\phi - \beta) \cdot \sin(\phi - \beta)\sin\delta}{\cos\phi \cdot \cos\delta \cdot \sin\omega_s + \omega_s \cdot \sin\phi \cdot \sin\delta} \tag{C.8}$$

$$D(\beta) = \frac{1}{2} \cdot D \cdot (1 + \cos(\beta))$$

$$R(\beta) = \frac{1}{2} \cdot B \cdot \rho \cdot (1 + \cos(\beta))$$

where $D(\beta)$ is the diffuse radiation, and $R(\beta)$ is the albedo radiation. The global irradiation is estimated by summing up all three components.

$$G(\beta) = B(\beta) + D(\beta) + R(\beta) \tag{C.9}$$

The inclination angle, δ can be estimated from Equation C.10)

$$\delta = 23.45 \cdot \sin(360 \cdot (284 + n)/365) \tag{C.10}$$

The following steps can be used to estimate the irradiation on an inclined surface.

Step 1:

$$\delta = 23.45 \cdot \sin(360 \cdot (284 + n)/365) \tag{C.10}$$

The solar declination angle is estimated for the given day *n*.

Step 2:

$$\omega_s = \cos^{-1}(-\tan\varphi \cdot \tan\delta)$$
$$\omega_s' = \cos^{-1}(-\tan(\varphi - \beta) \cdot \tan\delta) \tag{C.11}$$

where ω_s is the solar declination angle and φ is the latitude of the location on the earth.

Because the earth rotates one revolution per day, this corresponds to 360° longitude = 24 hours. This means the day length is $2 \cdot \omega_s / 15$.

Step 3: The beam irradiation for the horizontal surface is

$$B_o = 24/\pi \cdot S \cdot \{1 + 33 \cdot \cos(2 \cdot \pi \cdot d_n / 365)\} \cdot \{\cos\varphi \cdot \cos\delta \cdot \sin\omega_S + \omega_S \cdot \sin\varphi \cdot \sin\delta\} \tag{C.12}$$

where n is the day of the year and $\omega_0 = \min\{\omega_S, \omega_S'\}$.

Step 4: Calculate clearance index

$$KT = G / B_o \tag{C.13}$$

KT is the clearness index, and G is the solar irradiation data of the area.

Step 5: Calculate the diffuse irradiation

$$D = G \cdot (1 - 1.13KT) \tag{C.14}$$

Step 6: Calculate the beam irradiation

$$B = G - D \tag{C.15}$$

Step 7: Calculate the beam irradiation at an angle

$$B(\beta) = B \cdot \frac{\cos(\phi - \beta) \cdot \cos\delta \cdot \sin\omega_0 + \omega_s(\phi - \beta) \cdot \sin(\phi - \beta)\sin\delta}{\cos\phi \cdot \cos\delta \cdot \sin\omega_s + \omega_s \cdot \sin\phi \cdot \sin\delta} \tag{C.16}$$

$$D(\beta) = \frac{1}{2} \cdot D \cdot (1 + \cos(\beta))$$

$$R(\beta) = \frac{1}{2} \cdot B \cdot \rho \cdot (1 + \cos(\beta))$$

$$G(\beta) = B(\beta) + D(\beta) + R(\beta)$$

The energy market regulatory authority of Turkey provides the irradiance data for different locations in Turkey. Example C.1 gives the global daily irradiance for Batman City, Turkey.

Example C.1 Assume a sample value for the global daily irradiation (G) given as G = [1900,2690,4070,5050,6240,7040,6840,6040,5270,3730,2410,1800] for each of the 12 months of the year, respectively. Assume a reflectivity of 0.25.

i) Compute the (a) irradiation on a different tilt angle, (b) tabulate the irradiance for each month at different tilt angles, (c) the overall irradiance per year for different tilt angles, and (d) find the optimum tilt angle for each month and a year.

ii) If the angle of the PV module is fixed at 24 degrees all year round, what is the average kWh generation of PV modules with 15% efficiency and spread over an area of 100 m^2, operating for 5 hours a day at 0.5 sun?

Solution

i) Steps 1–7 given above are used to calculate irradiance for each month. The tilt angle β is varied from zero to 90 degrees in steps of 12 degrees. Table C.2 presents the tabulated results.

TABLE C.2(a) Irradiation at Different Tilt Angles: Winter.

Tilt Angle	January W/m^2	February W/m^2	March W/m^2
0°	1900	2690	4070
12°	2194	3016	4414
24°	2425	3253	4616
36°	2582	3390	**4667**
48°	**2660**	**3421**	4567
60°	2653	3344	4316
72°	2563	3164	3929
84°	2393	2887	3421
90°	2281	2716	3129

TABLE C.2(b) Irradiation at Different Tilt Angles: Spring.

Tilt Angle	April W/m^2	May W/m^2	June W/m^2
0°	5050	**6240**	**7040**
12°	5237	6231	6851
24°	**5252**	6016	6433
36°	5093	5595	5787
48°	4768	4986	4940
60°	4288	4214	3928
72°	3678	3320	2807
84°	2965	2356	1653
90°	2582	1870	1099

TABLE C.2(c) Irradiation on Different Tilt Angles: Summer.

Tilt Angle	July W/m^2	August W/m^2	Sept. W/m^2
0°	**6840**	6040	5270
12°	6721	**6180**	5699
24°	6368	6095	**5915**
36°	5784	5784	5910
48°	4991	5259	5682
60°	4024	4542	5241
72°	2935	3671	4608
84°	1795	2689	3810
90°	1237	2175	3361

TABLE C.2(d) Irradiation on Different Tilt Angles: Autumn and Yearly Average.

Tilt Angle	Oct. W/m^2	Nov. W/m^2	Dec. W/m^2	Yearly Average W/m^2
0°	3730	2410	1800	4233
12°	4221	2803	2117	4640
24°	4570	3110	2371	**4702**
36°	4760	3316	2553	4602
48°	**4785**	**3415**	2653	4344
60°	4641	3398	**2667**	3938
72°	4337	3270	2595	3406
84°	3885	3035	2440	2778
90°	3609	2880	2333	2439

Table C.2 lists the irradiance in W/m^2 for tilt angles varying from 0 to 90 degrees with an interval of 12 degrees. The maximum irradiation occurs at a tilt angle of 24 degrees if the PV modules are fixed and not free to change tilt angles. At this angle, irradiance energy is 4702 Wh/m^2. This amount is almost 469 Wh/m^2 greater than the irradiation on a horizontal surface. If the angle of tilt can be changed every month of the year, the yield will be almost 4923.5 Wh/m^2. Using the optimum angle of irradiance, we can increase substantially the average of the maximum value of each month's irradiation in a PV system.

ii) The average irradiance at a 24-degree angle for 12 months from Table C.2 is 4702 kW/m^2. Therefore, the power received by a surface if 1 m^2 at 0.5 sun is given as

$$\text{Watts for } 0.5 \text{ sun} = 0.5 \times 4702 = 2{,}351 \text{ W/m}^2.$$

At an efficiency of 15%, the energy that the PV can generate when it is operating for 5 hours a day over a year is given by:

$$\text{Energy of PV at } 24° = 0.15 \times 2{,}351 \times 5 \times 365 = 644 \, kWh/m^2.$$

Therefore, the energy generated by 100 m^2 of PV modules is given by

$$\text{Energy produced for } 100\,\text{m}^2 = 100 \times 644 = 64.4\ MWh$$

The National Renewable Energy (NREL) Laboratory provides the global daily irradiation (G) values for all major cities in the United States for any given surface area. Students are urged to visit the NREL website to obtain data for PV systems.

Example C.2 Assume that the yearly global daily irradiation (G) for the city of Columbus, Ohio, on a horizontal surface is $G = [1800, 2500, 3500, 4600, 5500, 6000, 5900, 5300, 4300, 3100, 1900, 1500]$.

The latitude of Columbus is 40 degrees. Assume a reflectivity of 0.25.

i) Compute an irradiation table for Columbus, Ohio.

ii) For the month of June, if the tilt angle is 36 degrees and irradiance is 0.4 sun for 7 hours daily, compute the total kWh that can be captured over 1500 square feet assuming the efficiency of the PV module is 15%.

Solution

i) Following the same steps as given in Example C.1, we have the data as presented in Table C.3.

ii) From Table C.3(b), the irradiance at an angle of 36 degrees for the month of June for 1 sun is 5109 W/m^2.

Therefore, the power received by a surface if 1 m^2 at 0.4 sun is given by

$$\text{Watts generated at } 0.4 \text{ sun} = 0.4 \times 5109 = 2{,}044\ \text{W}/\text{m}^2$$

At an efficiency of 15%, the energy that the PV system can generate operating for 7 hours per day in the month of June is given by

$$\text{Energy produced} = 0.15 \times 2{,}044 \times 7 \times 30 = 64.38\ kWh/m^2$$

TABLE C.3(a) Irradiation Data for Columbus, Ohio: Winter.

Tilt Angle	January W/m^2	February W/m^2	March W/m^2
0°	1800	2500	3500
12°	2112	2822	3782
24°	2363	3061	3948
36°	2541	3206	**3992**
48°	2638	**3250**	3911
60°	**2650**	3193	3708
72°	2577	3035	3394
84°	2422	2784	2981
90°	2315	2627	2743

TABLE C.3(b) Irradiation Data for Columbus, Ohio: Spring.

Tilt Angle	April W/m^2	May W/m^2	June W/m^2
0°	4600	5500	**6000**
12°	4776	**5512**	5882
24°	**4802**	5353	5585
36°	4675	5022	5109
48°	4399	4534	4470
60°	3987	3908	3698
72°	3457	3176	2832
84°	2835	2378	1927
90°	2499	1971	1484

TABLE C.3(c) Irradiation Data for Columbus, Ohio: Summer.

Tilt Angle	July W/m^2	Aug W/m^2	Sept W/m^2
0°	**5900**	5300	4300
12°	5832	**5431**	4614
24°	5579	5378	**4772**
36°	5140	5138	4764
48°	4531	4720	4593
60°	3779	4143	4265
72°	2922	3434	3794
84°	2013	2630	3202
90°	1561	2206	2869

TABLE C.3(d) Irradiation Data for Columbus, Ohio: Autumn and Yearly Average.

Tilt Angle	Oct W/m^2	Nov W/m^2	Dec W/m^2	Yearly Average W/m^2
0°	3100	1900	1500	3825
12°	3479	2182	1762	4016
24°	3748	2400	1973	**4080**
36°	3895	2546	2125	4013
48°	**3912**	**2613**	2211	3815
60°	3800	2597	**2227**	3496
72°	3563	2500	2172	3071
84°	3211	2326	2049	2563
90°	2997	2212	1964	2287

$$1\,\text{m}^2 = 10.76\,\text{ft}^2.$$

$$\text{Energy produced in kWh/ft}^2 = \frac{64.38}{10.76} = 5.98\,\text{kWh/ft}^2$$

Therefore, the energy generated by 1500 sq ft of PV modules is given by

$$\text{Total Energy produced} = 1500 \times 5.98 = 8.97\ MWh$$

REFERENCES

1. Taymur E. Photovoltaics systems sizing [thesis]. Columbus: The Ohio State University; 2009.
2. California Energy Commission. Energy quest. Available at www.energyquest.ca.gov/story. Accessed 2009 June 10.
3. Markvart T, Castaner L. Practical handbook of photovoltaics, fundamentals and applications. Amsterdam: Elsevier; 2003.
4. Ophardt CE. The virtual chembook. Available at http://www.elmhurst.edu/~chm/vchembook/320sunenergy.html. Accessed 2009 July 10.
5. Photovoltaic Energy. U.S. Department of Energy. National Renewable Energy Laboratory. Available at http://www.nrel.gov/pv/news_hotline. Accessed 2010 Oct 10.
6. Wikipedia. Photovoltaic energy. Available at http://en.wikipedia.org/. Accessed 2009 Oct 9.
7. U.S. Department of Energy. Solar Energies Technologies Program. Available at http://www1.eere.energy.gov/solar/. Accessed 2009 Oct 22.
8. U.S. Department of Energy. Energy Information Administration. Official Energy Statistics from the US Government. Available at http://www.eia.doe.gov/. Accessed 2009 Sept 10.
9. Yogi Goswami JD. Principles of solar engineering. Boca Raton, FL: CRC Press; 2000.

APPENDIX D

WIND POWER

Fundamental problems in estimating wind power are reviewed in depth in other resources.[1–4] A brief overview is provided here. The annual available wind energy is determined by studying wind speed distribution. The Weibull reliability distribution function[5] is used to describe the variation in wind speed; it is given as

$$f(v) = \frac{k}{a}\left(\frac{v}{a}\right)^{k-1} \cdot e^{-\left(\frac{v}{a}\right)^{k}} \tag{D.1}$$

The variables of Equation D.1 are defined in Table D.1.

At most sites, wind speed has a Rayleigh distribution. When the time interval is equal to 2, the distribution is designated as a Rayleigh distribution. Therefore, a Rayleigh distribution is only a function of the scale parameter (a) and wind speed. The frequency of a particular wind speed band over a period of one year can be found from published wind speed data.[6]

$$f(v) = \frac{\textit{wind period in hours for } v \textit{ and } v + \Delta v}{\Delta v} \tag{D.2}$$

Mean wind speed over a time period is defined as the total area under the f–v curve integrated over a long period. Hence to estimate the mean speed, we

Design of Smart Power Grid Renewable Energy Systems, First Edition. Ali Keyhani.

TABLE D.1 Definition of Weibull Reliability Distribution Parameters.

Variable	Definition
k	Time interval
f	Relative probability distribution
v	Speed
a	Scale parameter

TABLE D.2 Definition of Parameters for the Estimation of Wind Mechanical Power.

Variable	Definition
ρ	Density of air
A	Rotor blades capturing wind power
v	Speed

need to divide by the total number of hours in that interval.[1] The approximate annual mean speed is given by

$$\overline{v} = 0.9a \tag{D.3}$$

Hence, given the mean wind speed for a site and assuming $a = \overline{v}$, the Rayleigh distribution[6] would be defined as

$$f(v) = \frac{2v}{\overline{v}^2} \cdot e^{-(v/\overline{v})^2} \tag{D.4}$$

The mechanical power generated by the wind passing an area of A with speed v can be estimated as

$$P = \frac{1}{2}\rho \cdot A \cdot v^3 \tag{D.5}$$

As the rotor blades capture the wind energy, the turbine slows the wind from speed v_1 to v_2. The wind speed at the exit of the rotor blades is as depicted in Fig. D.1 where $A_2 > A_1$ then $v_1 > v_2$.

The power of the wind is estimated as the air area swept by rotor blades and with the cube of wind speed as shown in Equation D.5.

Let the average speed be represented by v as shown in Equation D.6.

$$v = \frac{v_1 + v_2}{2} \tag{D.6}$$

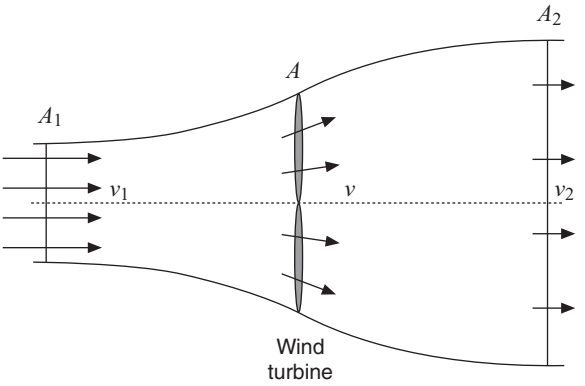

Figure D.1 Change of Wind Speed at a Wind Turbine.[1]

The mechanical power, P_T, extracted from the wind after passing through the turbine can be estimated as[1]

$$P_T = \frac{1}{2}\rho \cdot A \cdot \left(v_1^2 - v_2^2\right) \cdot \left(v_1 + v_2\right) \tag{D.7}$$

The mechanical power of wind passing through the area an A is given as

$$P = \frac{1}{2}\rho \cdot A \cdot v^3 \tag{D.8}$$

As expected, Equation D.8 is the same as Equation D.5. However, in Equation D.8, the cubic value of velocity representing the average velocity is used.

The power coefficient, c_p is the ratio between P_T and P.

$$c_p = \frac{P_T}{P} = \left(1 - \frac{{v_2}^2}{{v_1}^2}\right) \cdot \left(1 + \frac{v_2}{v_1}\right) \tag{D.9}$$

The maximum power coefficient, c_p, can be estimated as[2]

$$c_{p,\max} \approx 0.593$$

The maximum power coefficient is called the Betz Power Coefficient. It indicates that approximately 60% of the wind power is taken by the turbine. The practical modern high-speed turbines[1,2] have power coefficient values ranging from 0.4 to 0.6.[2-6] Low-speed turbines with more blades have a value ranging from 0.2 to 0.4. The efficiency of the wind turbine is the ratio of the power taken to the ideal usable power.

$$\eta = \frac{P_T}{c_{p,\max} \cdot P} = \frac{c_p \cdot P}{c_{p,\max} \cdot P} = \frac{c_p}{c_{p,\max}} \tag{D.10}$$

For a rotor coefficient equal to ½, the maximum power output of the turbine per square meter of rotor swept area can be expressed as

$$P_{T,\max} = \frac{\frac{1}{2}\cdot\frac{1}{2}\rho\cdot A\cdot v^3}{A} = \frac{1}{4}\rho\cdot v^3 \ \text{kW/m}^2 \tag{D.11}$$

To estimate annual energy production, a new variable representing the root mean cube of wind speed (RMC) is defined as

$$V_{RMC} = \sqrt[3]{\frac{\int_0^\infty f(v)\cdot v^3\cdot dv}{365\times 24}} \ \text{m/sec} \tag{D.12}$$

where the *f(v)* is the frequency distribution function for wind speed at that location. The empirical evidence has shown that a Rayleigh function with corresponding scale parameter *a* best fits wind speed frequency data for most sites. The annual average power generation in watts per square meter is given as

$$P_{T,\max} = \frac{1}{4}\rho\cdot V_{RMC}^3 \ \text{kW/m}^2 \tag{D.13}$$

The annual energy production can be expressed as

$$E = \frac{1}{4}\rho\cdot V_{RMC}^3\times 365\times 24 \ \text{MW/m}^2/\text{yr} \tag{D.14}$$

REFERENCES

1. Wikipedia. Wind turbines—technical aspects. Available at http://wiki.uiowa.edu/display/greenergy/Wind+Turbines. Accessed 2010 Oct 9.
2. Quaschning V. Understanding renewable energy systems. London: Earthscan: 2006.
3. Patel MK. Wind and solar power systems: design, analysis, and operation. Boca Raton, FL: CRC Press; 2006.
4. Abu-ham MS. Modeling of bi-directional converter for wind power generation [dissertation]. Columbus: The Ohio State University; 2009.
5. Fink DG, Beaty HW. Standard handbook of electrical engineering. New York: McGraw-Hill; 2006.
6. Justus CG, Hargraves WR, Mikhail A, Graber D. Methods of estimating wind speed frequency distribution. Journal of Applied Meteorology 1978, 17(3): 350–353.

INDEX

Design of Smart Power Grid Renewable Energy Systems, First Edition. Ali Keyhani.